

Materials Horizons: From Nature to Nanomaterials

Sunpreet Singh  
Chander Prakash  
Rupinder Singh *Editors*

# 3D Printing in Biomedical Engineering

 Springer

# **Materials Horizons: From Nature to Nanomaterials**

## **Series Editor**

Vijay Kumar Thakur, School of Aerospace, Transport and Manufacturing,  
Cranfield University, Cranfield, UK

Materials are an indispensable part of human civilization since the inception of life on earth. With the passage of time, innumerable new materials have been explored as well as developed and the search for new innovative materials continues briskly. Keeping in mind the immense perspectives of various classes of materials, this series aims at providing a comprehensive collection of works across the breadth of materials research at cutting-edge interface of materials science with physics, chemistry, biology and engineering.

This series covers a galaxy of materials ranging from natural materials to nanomaterials. Some of the topics include but not limited to: biological materials, biomimetic materials, ceramics, composites, coatings, functional materials, glasses, inorganic materials, inorganic-organic hybrids, metals, membranes, magnetic materials, manufacturing of materials, nanomaterials, organic materials and pigments to name a few. The series provides most timely and comprehensive information on advanced synthesis, processing, characterization, manufacturing and applications in a broad range of interdisciplinary fields in science, engineering and technology.

This series accepts both authored and edited works, including textbooks, monographs, reference works, and professional books. The books in this series will provide a deep insight into the state-of-art of Materials Horizons and serve students, academic, government and industrial scientists involved in all aspects of materials research.

More information about this series at <http://www.springer.com/series/16122>

Sunpreet Singh · Chander Prakash ·  
Rupinder Singh  
Editors

# 3D Printing in Biomedical Engineering

 Springer



*Editors*

Sunpreet Singh  
Department of Mechanical Engineering  
National University of Singapore  
Singapore, Singapore

Chander Prakash  
School of Mechanical Engineering  
Lovely Professional University  
Jalandhar, Punjab, India

Rupinder Singh  
Department of Mechanical Engineering  
National Institute of Technical Teachers  
Training & Research  
Chandigarh, India

ISSN 2524-5384

ISSN 2524-5392 (electronic)

Materials Horizons: From Nature to Nanomaterials

ISBN 978-981-15-5423-0

ISBN 978-981-15-5424-7 (eBook)

<https://doi.org/10.1007/978-981-15-5424-7>

© Springer Nature Singapore Pte Ltd. 2020

This work is subject to copyright. All rights are reserved by the Publisher, whether the whole or part of the material is concerned, specifically the rights of translation, reprinting, reuse of illustrations, recitation, broadcasting, reproduction on microfilms or in any other physical way, and transmission or information storage and retrieval, electronic adaptation, computer software, or by similar or dissimilar methodology now known or hereafter developed.

The use of general descriptive names, registered names, trademarks, service marks, etc. in this publication does not imply, even in the absence of a specific statement, that such names are exempt from the relevant protective laws and regulations and therefore free for general use.

The publisher, the authors and the editors are safe to assume that the advice and information in this book are believed to be true and accurate at the date of publication. Neither the publisher nor the authors or the editors give a warranty, expressed or implied, with respect to the material contained herein or for any errors or omissions that may have been made. The publisher remains neutral with regard to jurisdictional claims in published maps and institutional affiliations.

This Springer imprint is published by the registered company Springer Nature Singapore Pte Ltd. The registered company address is: 152 Beach Road, #21-01/04 Gateway East, Singapore 189721, Singapore

# Preface

The book titled *3D Printing in Biomedical Engineering* presents the emerging biomedical applications by clubbing the various aspects of the science and technology. Indeed, the content of this book has opened the various scientific horizons which are proved to be utmost beneficial for uplifting the standards of the day-to-day practices in biomedical domain. This edited book has been structured to not only discuss the current and emerging trends of 3D printing in biomedical sector, but also to provide the basic insights which could help the newcomers to understand the essential requirements. It has been witnessed while editing the book content that the prosthetic is the first biomedical area that has been revolutionized by 3D printing and, thereafter, transformed to more sophisticated products. Continued innovation has pushed 3D printing into new realms and has proved how far the technology has come since its invention. From dental products to prosthetics and tissue engineering, 3D printing is also helping address some of today's biomedical challenges. Additive manufacturing process has ability to manufacture highly complex engineered and customized components for specific biomedical applications. Furthermore, traditional feedstock materials of 3D printing have also been transformed in the last decade wherein different types of bio-inks, hydrogels, proteins, human cells and thereby combinations were used. Extensive research is being conducted in bioprinting and its potential as a future source for organ transplants. It is, however, much simpler to print in plastic than living cells. Noticeably, myriads of innovations of this class of manufacturing (including material, design and process iterations) are being transforming our day-to-day life in an extraordinary manner. This book has captured all aforementioned trends of the 3D printing in the area of biomedical science and engineering. With this, we are highly confident that this contribution will benefit all the readers in different ways.

Singapore, Singapore  
Jalandhar, India  
Chandigarh, India

Sunpreet Singh  
Chander Prakash  
Rupinder Singh

# Contents

<b>1</b>	<b>3D Printing: Challenges and Its Prospect in Futuristic Tissue Engineering Applications</b> .....	<b>1</b>
	Abir Dutta, Trina Roy, Preetam Guha Ray, Ragavi Rajasekaran, Mamoni Banerjee, Santanu Chattopadhyay, Sanjay Gupta, and Santanu Dhara	
<b>2</b>	<b>Fundamentals of 3D Printing and Its Applications in Biomedical Engineering</b> .....	<b>23</b>
	Hasan Kemal Surmen, Faruk Ortes, and Yunus Ziya Arslan	
<b>3</b>	<b>Thermal Effects in 3D Printed Parts</b> .....	<b>43</b>
	Prasansha Rastogi, Swaroop Gharde, and Balasubramanian Kandasubramanian	
<b>4</b>	<b>Role of Imaging Data in Additive Manufacturing for Biomedical Applications</b> .....	<b>69</b>
	Gurminder Singh and Pulak M. Pandey	
<b>5</b>	<b>Additive Manufacturing in Bone Tissue Engineering</b> .....	<b>95</b>
	Majid Fazlollahi, Yasaman Pooshidani, and Mahnaz Eskandari	
<b>6</b>	<b>FDM 3D Printing in Biomedical and Microfluidic Applications</b> .....	<b>127</b>
	Gabriel Gaal, Vladimir Gaal, Maria Luisa Braunger, Antonio Riul Jr, and Varlei Rodrigues	
<b>7</b>	<b>Integration of FDM and Indirect Rapid Tooling Technique for Fabrication of Low-Cost Hip Implant Replicas for Batch Production: A Case Study</b> .....	<b>147</b>
	Jaspreet Singh, Rupinder Singh, and Harwinder Singh	

<b>8</b>	<b>Biomaterials and Fabrication Methods of Scaffolds for Tissue Engineering Applications</b> . . . . .	167
	Atul Babbar, Vivek Jain, Dheeraj Gupta, Sunpreet Singh, Chander Prakash, and Catalin Pruncu	
<b>9</b>	<b>Rapid Prototyping Methods in Manufacturing of Biomedical Implants: A Review</b> . . . . .	187
	Ajjith Gopinath, Tobias Waclawczyk, Raman Bedi, Avinash Babu, Shijo Thomas, and Praise Tom	
<b>10</b>	<b>PLA-HAp-CS-Based Biocompatible Scaffolds Prepared Through Micro-Additive Manufacturing: A Review and Future Applications</b> . . . . .	209
	Nishant Ranjan, Rupinder Singh, I. P. S. Ahuja, Mustafizur Rahman, and Seeram Ramakrishna	
<b>11</b>	<b>Dental Crowns by FDM Assisted Vapour Smoothing and Silicon Moulding</b> . . . . .	231
	R. Singh, Rupinder Singh, and J. S. Dureja	
<b>12</b>	<b>Complex Shapes Prosthetics Process: An Application of Fused Deposition Modeling Technology</b> . . . . .	251
	Tan Thang Nguyen, Hoang Vu Nguyen, Minh Phung Dang, and Thanh-Phong Dao	
<b>13</b>	<b>Improvement of Human Gait in Foot Deformities Patients by 3D Printed Ankle–Foot Orthosis</b> . . . . .	269
	Harish Kumar Banga, Parveen Kalra, R. M. Belokar, and Rajesh Kumar	
<b>14</b>	<b>Influence of Laser Power and Scan Speed During Laser-Assisted Multi-layer Additive Manufacturing Using Finite Element Modeling</b> . . . . .	289
	Sapam Ningthemba Singh, Yadaiah Nirsanametla, Sohini Chowdhury, and M. Muralidhar	
<b>15</b>	<b>Novel and Emerging Materials Used in 3D Printing for Oral Health Care</b> . . . . .	317
	Anoop Kapoor, Priyanka Chopra, Komal Sehgal, Shaveta Sood, Ashish Jain, and Vishakha Grover	

# Editors and Contributors

## About the Editors

**Dr. Sunpreet Singh** is post-doc fellow in the School of Mechanical Engineering, National Univeristy of Singapore, Singapore. He has received Ph.D in Mechanical Engineering from Guru Nanak Dev Engineering College, Ludhiana, India. His area of research is additive manufacturing and application of 3D printing for development of new biomaterials for clinical applications. He has contributed extensively in additive manufacturing literature with publications appearing in *Journal of Manufacturing Processes*, *Composite Part: B*, *Rapid Prototyping Journal*, *Journal of Mechanical Science and Technology*, *Measurement*, *International Journal of Advance Manufacturing Technology*, and *Journal of Cleaner Production*. He is working in joint collaboration with Prof. Seeram Ramakrishna, NUS Nanoscience & Nanotechnology Initiative and Prof. Rupinder Singh, manufacturing research lab, GNDEC, Ludhiana. He is also editor of 3 books- “Current Trends in Bio-manufacturing”; “3D Printing in Biomedical Engineering”; and “Biomaterials in Orthopaedics and Bone Regeneration - Design and Synthesis”. He is also guest editor of 3 journals- special issue of “Functional Materials and Advanced Manufacturing”, *Facta Universitatis*, series: Mechanical Engineering (Scopus Indexed), *Materials Science Forum* (Scopus Indexed), and special issue on “Metrology in Materials and Advanced Manufacturing”, *Measurement and Control* (SCI indexed).

**Dr. Chander Prakash** is Associate Professor at the School of Mechanical Engineering, Lovely Professional University, Jalandhar, India. He has received Ph.D in mechanical engineering from Panjab University, Chandigarh, India. His area of research is biomaterials, rapid prototyping & 3-D printing, advanced manufacturing, modeling, simulation, and optimization. He has more than 11 years of teaching experience and 6 years’ of research experience. He has contributed extensively to the world in the titanium and magnesium based implant literature with publications appearing in *Surface and Coating Technology*, *Materials and Manufacturing Processes*, *Journal of Materials Engineering and Performance*,

*Journal of Mechanical Science and Technology, Nanoscience and Nanotechnology Letters, Proceedings of the Institution of Mechanical Engineers, Part B: Journal of Engineering Manufacture.* He has authored 60 research papers and 10 book chapters. He is also editor of 3 books: “Current Trends in Bio-manufacturing”; “3D Printing in Biomedical Engineering”; and “Biomaterials in Orthopaedics and Bone Regeneration - Design and Synthesis”. He is also guest editor of 3 journals: special issue of “Functional Materials and Advanced Manufacturing”, *Facta Universitatis, Series: Mechanical Engineering (Scopus Indexed)*, *Materials Science Forum (Scopus Indexed)*, and special issue on “Metrology in Materials and Advanced Manufacturing”, *Measurement and Control (SCI indexed)*.

**Prof. Rupinder Singh** is Professor in Department of Mechanical Engineering, National Institute of Technical Teachers Training and Research, Chandigarh, India. He has received Ph.D in Mechanical Engineering from Thapar Institute of Engineering & Technology, Patiala, India. His area of research is Non-traditional machining, Additive manufacturing and development of porous biomaterials using 3D printing and rapid prototyping techniques. He has more than 20 years of teaching and research experience. He has contributed extensively to the world in Additive Manufacturing literature with publications appearing in *Journal of Manufacturing Processes, Composite Part: B, Rapid Prototyping Journal, Journal of Mechanical Science and Technology, Measurement, International Journal of Advance Manufacturing Technology, and Journal of Cleaner Production.* He authored 21 books and 80 book chapters. He has received research grants from various funding agencies such as DST-SERB, AICTE.

## Contributors

**I. P. S. Ahuja** Department of Mechanical Engineering, Punjabi University, Patiala, India

**Yunus Ziya Arslan** Department of Mechanical Engineering, Faculty of Engineering, Istanbul University-Cerrahpasa, Avcilar, Istanbul, Turkey

**Atul Babbar** Department of Mechanical Engineering, Thapar Institute of Engineering and Technology, Patiala, India

**Avinash Babu** Christ Deemed to be University, Bengaluru, India

**Mamoni Banerjee** Rajendra Mishra School of Engineering Entrepreneurship, Indian Institute of Technology Kharagpur, Kharagpur, India

**Harish Kumar Banga** Production and Industrial Engineering Department, Punjab Engineering College (Deemed to Be University), Chandigarh, Punjab, India

**Raman Bedi** Christ Deemed to be University, Bengaluru, India

**R. M. Belokar** Production and Industrial Engineering Department, Punjab Engineering College (Deemed to Be University), Chandigarh, Punjab, India

**Maria Luisa Braunger** Department of Applied Physics, “Gleb Wataghin” Institute of Physics, University of Campinas (UNICAMP), Campinas, São Paulo, Brazil

**Santanu Chattopadhyay** Rubber Technology Centre, Indian Institute of Technology Kharagpur, Kharagpur, India

**Priyanka Chopra** Professor, Sri SGT Dental College and Hospital, SGT University, Gurugram, India

**Sohini Chowdhury** Department of Mechanical Engineering, North Eastern Regional Institute of Science and Technology (NERIST), Nirjuli, Arunachal Pradesh, India

**Minh Phung Dang** Ho Chi Minh City Industry and Trade College, Ho Chi Minh City, Vietnam

**Thanh-Phong Dao** Division of Computational Mechatronics, Faculty of Electrical & Electronics Engineering, Institute for Computational Science, Ton Duc Thang University, Ho Chi Minh City, Vietnam

**Santanu Dhara** School of Medical Science and Technology, Indian Institute of Technology Kharagpur, Kharagpur, India

**J. S. Dureja** Mechanical Engineering Department, Punjabi University Patiala, Patiala, India

**Abir Dutta** School of Medical Science and Technology, Indian Institute of Technology Kharagpur, Kharagpur, India

**Mahnaz Eskandari** Department of Biomedical Engineering, Amirkabir University of Technology (Tehran Polytechnic), Tehran, Iran

**Majid Fazlollahi** Mechanical Engineering Department, Amirkabir University of Technology (Tehran Polytechnic), Tehran, Iran

**Gabriel Gaal** Department of Applied Physics, “Gleb Wataghin” Institute of Physics, University of Campinas (UNICAMP), Campinas, São Paulo, Brazil

**Vladimir Gaal** Department of Applied Physics, “Gleb Wataghin” Institute of Physics, University of Campinas (UNICAMP), Campinas, São Paulo, Brazil

**Swaroop Gharde** Rapid Prototyping Laboratory, Department of Metallurgical and Materials Engineering, Defence Institute of Advanced Technology (DU), Ministry of Defence, Girinagar, Pune, India

**Ajith Gopinath** Christ Deemed to be University, Bengaluru, India

**Vishakha Grover** Associate Professor, Department of Periodontology and Oral Implantology, Dr. H.S.J. Institute of Dental Sciences, Panjab University, Chandigarh, India

**Dheeraj Gupta** Department of Mechanical Engineering, Thapar Institute of Engineering and Technology, Patiala, India

**Sanjay Gupta** Department of Mechanical Engineering, Indian Institute of Technology Kharagpur, Kharagpur, India

**Ashish Jain** Professor and Head, Department of Periodontology and Oral Implantology, Dr. H.S.J. Institute of Dental Sciences, Panjab University, Chandigarh, India

**Vivek Jain** Department of Mechanical Engineering, Thapar Institute of Engineering and Technology, Patiala, India

**Parveen Kalra** Production and Industrial Engineering Department, Punjab Engineering College (Deemed to Be University), Chandigarh, Punjab, India

**Balasubramanian Kandasubramanian** Rapid Prototyping Laboratory, Department of Metallurgical and Materials Engineering, Defence Institute of Advanced Technology (DU), Ministry of Defence, Girinagar, Pune, India

**Anoop Kapoor** Professor and Head, Sri Sukhmani Dental College and Hospital, Dera Bassi, Punjab, India

**Rajesh Kumar** Production and Industrial Engineering Department, Punjab Engineering College (Deemed to Be University), Chandigarh, Punjab, India

**M. Muralidhar** Department of Mechanical Engineering, North Eastern Regional Institute of Science and Technology (NERIST), Nirjuli, Arunachal Pradesh, India

**Hoang Vu Nguyen** Ho Chi Minh City Industry and Trade College, Ho Chi Minh City, Vietnam

**Tan Thang Nguyen** Ho Chi Minh City Industry and Trade College, Ho Chi Minh City, Vietnam

**Yadaiah Nirsanametla** Department of Mechanical Engineering, North Eastern Regional Institute of Science and Technology (NERIST), Nirjuli, Arunachal Pradesh, India

**Faruk Ortes** Department of Mechanical Engineering, Faculty of Engineering, Istanbul University-Cerrahpasa, Avcilar, Istanbul, Turkey

**Pulak M. Pandey** Mechanical Engineering Department, Indian Institute of Technology Delhi, New Delhi, Delhi, India

**Yasaman Pooshidani** Department of Biomedical Engineering, Amirkabir University of Technology (Tehran Polytechnic), Tehran, Iran



**Chander Prakash** Department of Mechanical Engineering, Lovely Professional University, Phagwara, India

**Catalin Pruncu** Department of Mechanical Engineering, Imperial College of London, London, UK

**Mustafizur Rahman** Department of Mechanical Engineering, Universiti Malaysia Pahang, Pekan, Malaysia

**Ragavi Rajasekaran** School of Medical Science and Technology, Indian Institute of Technology Kharagpur, Kharagpur, India

**Seeram Ramakrishna** Department of Mechanical Engineering, National University of Singapore, Sovereign, Singapore

**Nishant Ranjan** Department of Production Engineering, Guru Nanak Dev Engineering College, Ludhiana, India;  
Department of Mechanical Engineering, Punjabi University, Patiala, India

**Prasansha Rastogi** Rapid Prototyping Laboratory, Department of Metallurgical and Materials Engineering, Defence Institute of Advanced Technology (DU), Ministry of Defence, Girinagar, Pune, India

**Preetam Guha Ray** School of Medical Science and Technology, Indian Institute of Technology Kharagpur, Kharagpur, India

**Antonio Riul Jr** Department of Applied Physics, “Gleb Wataghin” Institute of Physics, University of Campinas (UNICAMP), Campinas, São Paulo, Brazil

**Varlei Rodrigues** Department of Applied Physics, “Gleb Wataghin” Institute of Physics, University of Campinas (UNICAMP), Campinas, São Paulo, Brazil

**Trina Roy** School of Medical Science and Technology, Indian Institute of Technology Kharagpur, Kharagpur, India

**Komal Sehgal** Associate Professor, Department of Prosthodontics, Dr. H.S.J. Institute of Dental Sciences, Panjab University, Chandigarh, India

**Gurminder Singh** Mechanical Engineering Department, Indian Institute of Technology Delhi, New Delhi, Delhi, India

**Harwinder Singh** Department of Mechanical Engineering, GNDEC, Ludhiana, India

**Jaspreet Singh** School of Mechanical Engineering, Lovely Professional University, Phagwara, India

**R. Singh** Punjabi University Patiala, Patiala, India;  
GNA University, Phagwara, Punjab, India

**Rupinder Singh** Department of Mechanical Engineering, National Institute of Technical Teachers Training and Research, Chandigarh, India;  
Department of Production Engineering, Guru Nanak Dev Engineering College, Ludhiana, India

**Sapam Ningthemba Singh** Department of Mechanical Engineering, North Eastern Regional Institute of Science and Technology (NERIST), Nirjuli, Arunachal Pradesh, India;  
Department of Mechanical Engineering, National Institute of Technology Silchar, Silchar, Assam, India

**Sunpreet Singh** Department of Mechanical Engineering, Lovely Professional University, Phagwara, India;  
Department of Mechanical Engineering, National University of Singapore, Singapore, Singapore

**Shaveta Sood** Assistant Professor, Department of Periodontology and Oral Implantology, Dr. H.S.J. Institute of Dental Sciences, Panjab University, Chandigarh, India

**Hasan Kemal Surmen** Department of Automotive Technology, Vocational School of Technical Sciences, Istanbul University-Cerrahpasa, Istanbul, Turkey

**Shijo Thomas** Christ Deemed to be University, Bengaluru, India

**Praise Tom** Christ Deemed to be University, Bengaluru, India

**Tobias Waclawczyk** University of Augsburg, Augsburg, Germany

# Chapter 1

## 3D Printing: Challenges and Its Prospect in Futuristic Tissue Engineering Applications



**Abir Dutta, Trina Roy, Preetam Guha Ray, Ragavi Rajasekaran,  
Mamoni Banerjee, Santanu Chattopadhyay, Sanjay Gupta,  
and Santanu Dhara**

### 1.1 Introduction

Recent developments in various critical diseases varying from dermal, musculoskeletal to internal organs and tissues, induced a steep increment in the surgical intervention of the patients [1]. The current condition in healthcare requires a quick diagnosis of the medical issue, followed by a pre-surgical analysis and further post-surgical care for the patients. In spite of a quick diagnosis of the issue in a patient, the medication in terms of surgery, or pre-surgical analysis, is delayed. There lies a spectrum of subtle issues which contribute to the delay and further burdening the patient with overloaded cost and critical conditions. Among many, pre-surgical analysis of the disease using computed tomography (CT) or magnetic resonance imaging (MRI) and preparation of the prototype of the implant plays a crucial role in the successful process from diagnosis to medication. The prototypes were used to be fabricated by conventional manufacturing processes such as milling, drilling, and

---

A. Dutta · T. Roy · P. G. Ray · R. Rajasekaran · S. Dhara (✉)  
School of Medical Science and Technology, Indian Institute of Technology Kharagpur,  
Kharagpur, India  
e-mail: [sdhara@smst.iitkgp.ernet.in](mailto:sdhara@smst.iitkgp.ernet.in)

M. Banerjee  
Rajendra Mishra School of Engineering Entrepreneurship, Indian Institute of Technology  
Kharagpur, Kharagpur, India

S. Chattopadhyay  
Rubber Technology Centre, Indian Institute of Technology Kharagpur, Kharagpur, India

S. Gupta  
Department of Mechanical Engineering, Indian Institute of Technology Kharagpur, Kharagpur,  
India

shaping. However, these processes were associated with many limitations. Manufacturing time and cost of the prototypes were very high. The failure rates were also very high due to poor manufacturing strategies. Moreover, the precise shape of the manufactured constructs was far from the actual contour and shapes of the targeted tissues and organs. The mass production of the implants was also hindered due to the long processing time associated with each fabrication unit. These issues raised a serious concern among the medical professionals to look forward to a type of manufacturing process which would decrease the manufacturing time as well as precisely tailor the actual shape and functionalization of the targeted tissues and implants.

Additive manufacturing is an approach which covers almost all the aforementioned drawbacks of the conventional manufacturing processes. Conceptually, 3D structures designed in a computer with the help of computer-aided modeling or image processing software are fabricated in a layerwise fashion, without any requirement of jigs or fixtures. The first 3D printing technology, developed and patented (US4575330) by C. W. Hull in 1984 [2], was called stereolithography (SLA). In this methodology, the ultraviolet (UV) lights are focused on the polymer layers according to the design of the structure, leading to fabrication of the structure by hardening the polymer layers. The main drawback to this system is the rigidity of the selection of materials. The only photo-curable-polymers and resins can be used for fabrication of the structures. In this regard, it is needless to mention that every polymer and resin are not photo-curable as well as applicable for the fabrication of implants and tissues. On the contrary, in many of the musculoskeletal disorders, the prototypes are required to endure high loads, which can be integrated using ceramics and metals as materials to prepare the implants and tissue analogs. In the year 1991, fused deposition modeling (FDM) was introduced in the manufacturing industry [3, 4]. In this process, high-density polymers are fed into the process as filament wires from a pool, and the material is deposited through a heated nozzle on the printing bed in layer by layer fashion. The process dealt with the issue of precision of the contours of the structures, but the diversity of materials was left unaddressed. The FDM process is limited to only thermoplastic materials such as polylactic acid (PLA), polyether-ether-ketone (PEEK), and acrylonitrile butadiene styrene (ABS) [5–7]. Moreover, in this process, if the requirement is to fabricate a structure of ceramic or metal powders, the metal powders have to be integrated with thermoplastic polymer in the form of a filament [6], else this process cannot be utilized to fabricate structures of ceramic or metal. However, this modification to use the ceramic or metal powders would amplify the time and cost of the final product, which is not intended. In the year 1992, selective laser sintering (SLS) was introduced to facilitate the path toward the additive manufacturing of the ceramics and metals [8–11].

The laser sintering process consists of a powder bed and a high-energy laser source. The high-energy laser source is focused on the powder layer to fuse the powder granules to build the 3D structures. Eventually, by repeating this process layerwise, the final structure is fabricated. This process builds the structure starting from the base layer. This is the reason that these processes are also called ‘bottom-up’ approach. The advantage of the laser sintering process is the availability of the final product with one step. However, there are few subtle, but strong disadvantages of this

process. The process is suitable for only the processing of ceramic or metal powders. The initial cost and maintenance cost of the machine are very high, leading to high cost of the patient-specific products. Moreover, a significant amount of powder is wasted while manufacturing using laser sintering. Cell-based printing for organs and soft tissues is not possible in this process.

Similarly, another additive manufacturing process evolved in the year 1997 known as laser engineered net shaping (LENS), which is also limited to produce metal and ceramic prototypes [12–14]. Around the same time as LENS was developed, electron beam melting (EBM) process was developed. The LENS is operated by high-energy laser source, whereas EBM is based on the shooting of electron beams on the powder layers [15]. However, as high energy is involved, both these processes lack the ability to process live cell constructs. Moreover, these high-energy sintering processes are limited to fabricate bone implants and grafts, excluding the soft tissue analogs and further live cell constructs. So, the requirement of a manufacturing process which is able to process versatile materials, with acceptable limitations, was always needed from both the medical professionals and engineers.

In the year 2000, an extrusion-based additive manufacturing of polymers and oligomers was reported by Landers et al. [16, 17]. The basic operation of the procedure [18, 19] can be explained in Fig. 1.1. A compressive load is applied at the entry section of a die, and the extruded material comes out of the die in the shape of the cross-section of the exit end. This particular system of additive manufacturing utilizing the conventional extrusion process is termed as 3D plotting. 3D plotting consists of one or a multiple numbers of cylindrical chambers, nozzles of varying diameters, and pressure control system. The printing bed is preferred to be

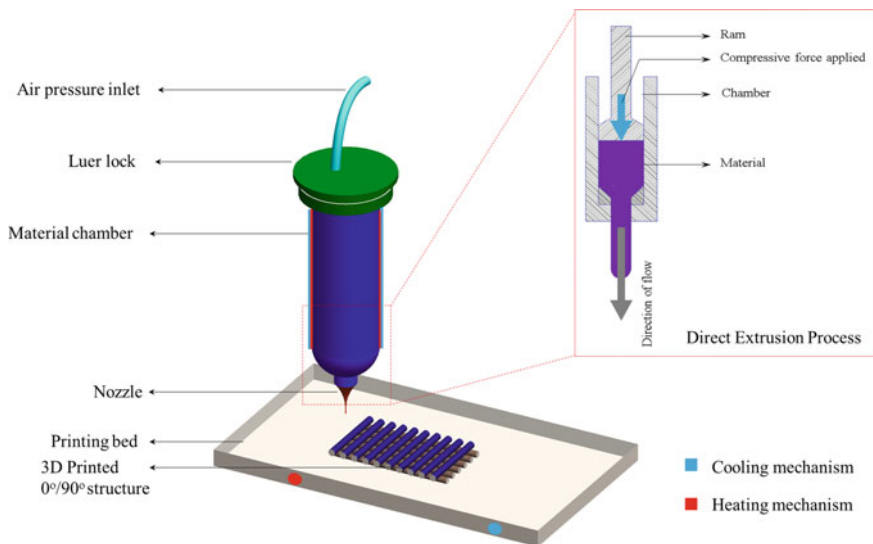


Fig. 1.1 Schematic representation of 3D printing process

equipped with a temperature control mechanism for precise and hassle-free printing. The major advantage of the 3D plotting, compared to other additive manufacturing processes, is the diversity of materials for printing structures. Precisely, polymers, ceramics, and metal powders can be printed to prepare prototypes for soft tissues, organs, musculoskeletal implants, and bone analogs [20]. Another distinct advantage of the 3D plotting is its capability to incorporate tailored porosity within the structures, which is a major limitation in the conventional manufacturing processes. Moreover, the various inter-fiber orientations such as  $+90^\circ/-90^\circ$  and  $+45^\circ/-45^\circ$  can be incorporated in the structures to increase the porosity, which may facilitate the communication between the analog and the host tissue.

A comprehensive literature is available to gain an insight into the genesis of the extrusion-based 3D plotting [21–25]. Polymers and metals have been extensively explored for fabrication of implants and tissue analogs using the 3D plotting. However, there are few critical issues, associated with this additive manufacturing process, which are rarely reported. Among several metal powders, steel (SS316), Co-Cr alloys, and Ti alloys (popularly Ti6Al4V) are extensively used to fabricate several hard tissue analogs and implants [25].

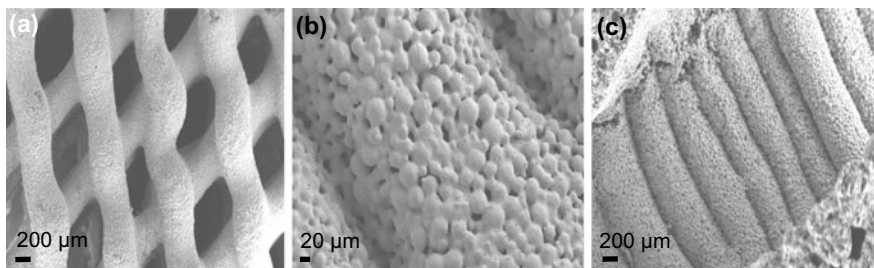
The crucial part of printing with metal powders is to prepare it in such a form which would be able to overcome the yield stress of the nozzle and flow, as well as would sustain its circular shape after deposition on the printing bed. The metal powders are required to be processed to a homogenized dough by mixing with a polymer. The inclusion of the polymers also leads to several critical issues which play an important role in determining the precision of the output structure. The ratio between the powder and polymer should be optimized to achieve an appropriate green stage structure after printing. The struts would suffer from waviness or microcracks if the ratio is not at its optimum composition. Moreover, the metal powder should be handled within a closed environment, preferably under a glove-box or vacuum hood, to protect the surfaces of metal particles from getting oxidized. Careful attention is required to optimize the flow behavior of the dough so that could overcome the yield stress of the internal wall of the nozzle. In this regard, the characterization of the rheological properties of the dough is necessary. However, there lies a limitation in the powder percentage in the composition. The range of maximum powder loading, which yielded to successful printing of circular fibers, was 80–85%. Low powder loading would result in sagging of the structures, and high powder loading would result in a high viscosity of the dough, which again adversely affect the printing parameters. The dough becomes highly viscous in cases of powder loading more than the allowed percentages, which loses its ability to flow through the nozzle. Inter-fiber contact is another issue which affects the integrity and mechanical strength of the printed structures. This issue is solved when the input parameters for slice thickness are prescribed. The optimum slice thickness should be 20% less than the nozzle diameter of the extrusion printer to achieve appropriate inter-connection between the fibers of two consecutive layers. However, the percentage of shrinkage, after drying in a vacuum oven and after the thermal treatment or sintering, should be considered while printing the green structures. Once the dough is prepared at its optimum composition, the pressure and printing speed are two major parameters to decide

the successful completion of the printing process. The pressure should be optimized within such a range, so that the deposition of the dough through the circular nozzle remains intact. Higher pressure leads to more material deposition and lower pressure leads to discontinuous extrusion of the fibers. However, the printing speed is also associated complementarily with the pressure range. High pressure ranges require high printing speed, so that the fast-moving nozzle would drag the over-extruded fiber in its continuous circular form. Though, high speed and pressure combination can affect the integrity of the inter-fiber connection. In a nutshell, material processing (i.e., preparation of the dough, specifically for metal and ceramic printing), printing pressure and printing speed are the key parameters which decide the final form of an extrusion-printed structure.

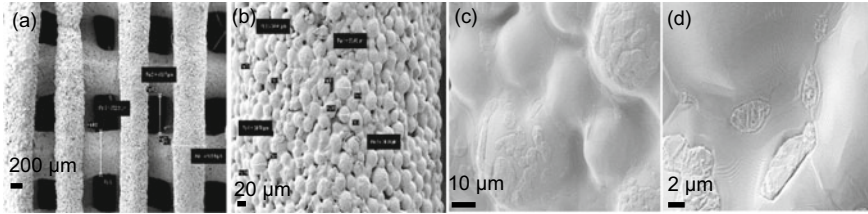
## 1.2 Case Study

The aforementioned critical issues regarding 3D printing should be associated with case studies to visualize the discussion. The extrusion printing is chosen to investigate the pros and cons of metal printing, because of its versatility of selection of matrix polymers according to the requirements, very less material processing time, low running cost, and absence of employing specialized operating professional. Moreover, these factors contribute to the reduction of the final cost for the implants and tissue analogs fabricated using this process.

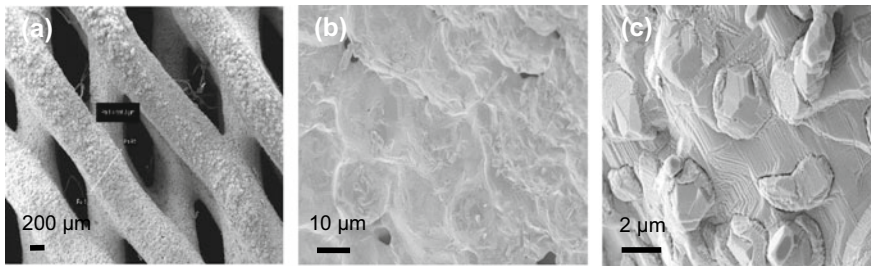
3D bioplotter manufactured by EnvisionTEC GmbH, Germany, has been used to fabricate the scaffolds. Titanium slurry was prepared with mixing titanium powders with a polymer matrix dissolved in 2% acetic acid. The viscosity of the slurry was optimized for flowability and stability of the particles in the suspended condition with minimum segregation. The slurry was further optimized in order to achieve structures without sagging. The green samples (Fig. 1.2) were air dried for half an hour and vacuum dried for 24 h in an oven (Rivotec, India) at 60 °C. The vacuum-dried samples were sintered in a controlled atmosphere tube furnace under Argon (99.9%) gas with a flow rate 50 ml/min followed by air cooling. The samples were



**Fig. 1.2** a Top view of green scaffold, b high magnification view of the morphology of the green sample with slurry prior to optimization and c fiber-to-fiber connection of dense samples



**Fig. 1.3** Morphology of **a** top view of the lattice structure with optimized slurry, **b** individual strut, **c** evidence of Oswald ripening during sintering, **d** grain growth of 0°/90° sintered Ti6Al4V scaffolds



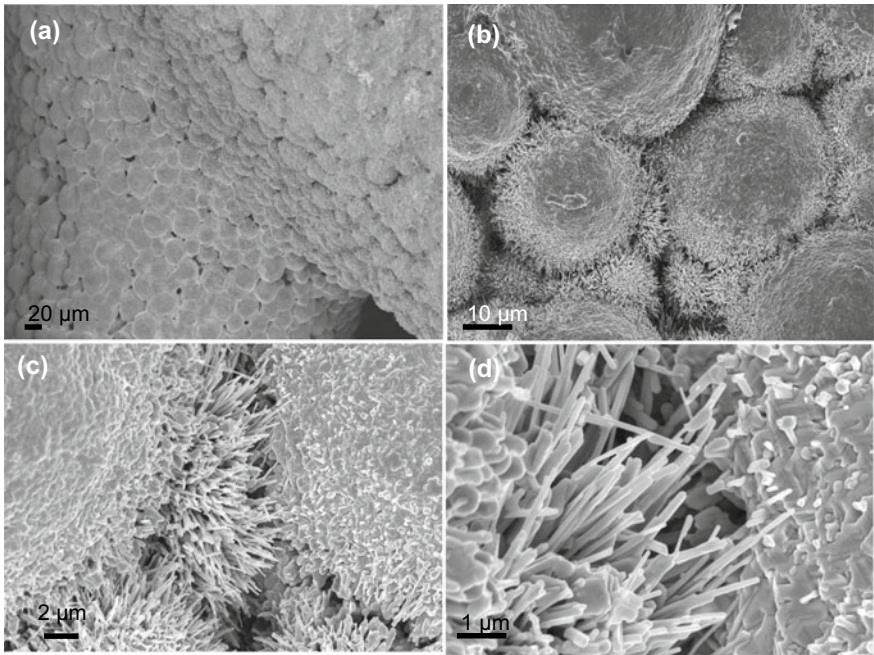
**Fig. 1.4** Morphology of **a** top view, **b** microstructure after sintering, **c** grain growth with roughening and resultant polygonal overlay of 0°/45° sintered Ti6Al4V scaffolds

ready for further characterization. 3D printed green (Fig. 1.2) and sintered samples (Figs. 1.3 and 1.4) were characterized under SEM (SEM, Zeiss EVO 60) to examine for powder distribution, scaffold structure, grain growth morphology, fiber diameter, and inter-fiber spacing.

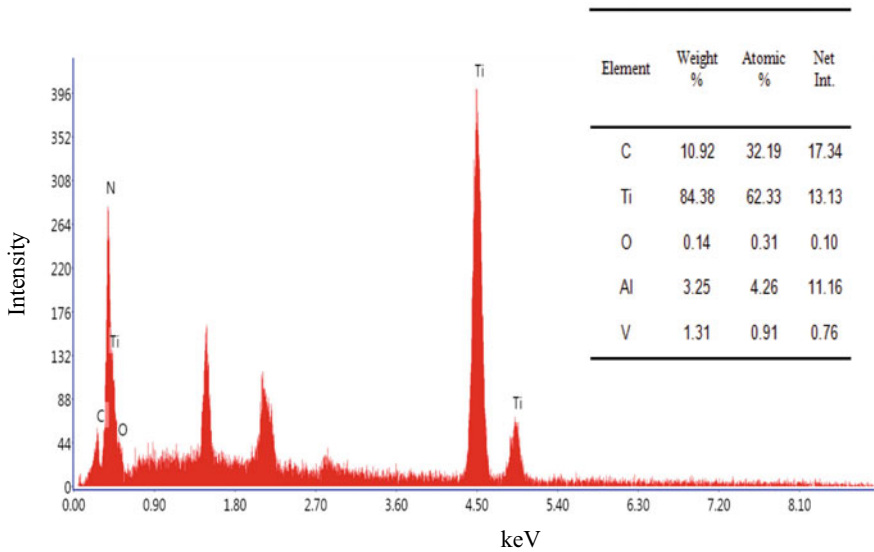
As titanium powder particles are prone to oxidation, the samples were primarily processed under controlled atmosphere. When the samples were air dried, the oxidized surface morphology is shown in Fig. 1.5. EDX (Zeiss EVO 60 scanning electron microscope with Oxford EDS detector) analysis (Fig. 1.6) was performed to know the percentage elemental composition present at the surface of the sintered samples. A very distinctive difference in the microstructure patterns between the oxidized and non-oxidized samples was found (Figs. 1.4 and 1.5).

Titanium powders are very sensitive to the moisture present in the air. It has a tendency to get oxidized very rapidly if it is allowed to remain in contact with the air for more than a few hours. The more oxidized the surface of the powder particles; the sintered structure will be more brittle. So, the powder processing while preparing the slurry is a crucial part of the fabrication. The samples were polished and examined with XRD (BRUKER, DISCOVER D8) analysis (Fig. 1.7) to know the phase information of titanium formed in the samples. It was revealed that the lattice structures contained both  $\alpha$  and  $\beta$  titanium structures.

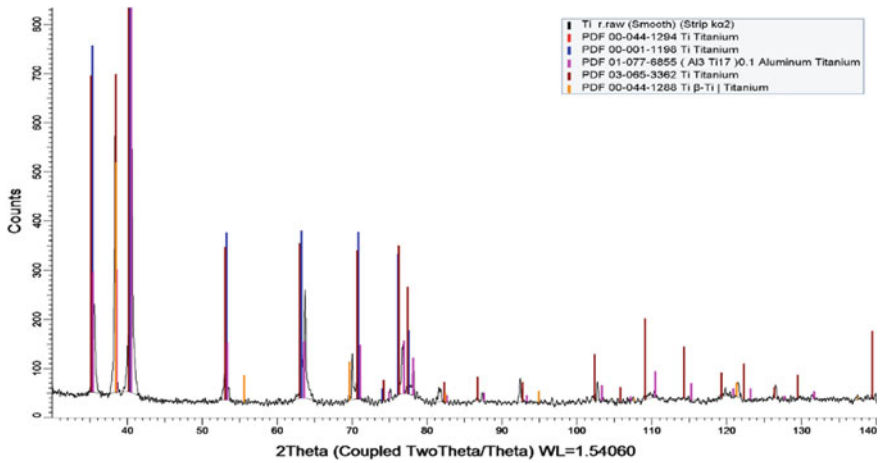




**Fig. 1.5** Surface morphology of oxidized Ti6Al4V scaffolds under SEM showing **a** junction between two struts, **b** oxidized titanium powder morphology after sintering, **c** oxidized titanium particle to particle junction in higher magnification, and **d** oxidized titanium particle surface structure



**Fig. 1.6** EDX analysis of the sintered Ti6Al4V 3D printed scaffolds



**Fig. 1.7** Results obtained by XRD analysis showing the titanium peaks and corresponding JCPDS files

### 1.3 Bioprinting

Bioprinting is a major breakthrough in 3D printing technology integrating live cells, ‘bioinks’ and high-precision robotic dispensing system to form complex biological structures *in vitro*. It involves additive manufacturing using layerwise assembly of living cells and biomaterials to fabricate structures mimicking native organs and tissues [20]. Bioprinting comprises of essentially three main components—(1) living cells, (2) bioinks which are mostly in the form of hydrogel or combination of hydrogel and cell culture medium along with some growth factors [26–29], and (3) robotic dispensing system in which structures are generated to the CAD file from CT data or other design software and prints the tissue structures [30, 31].

Different types of bioprinting techniques are available, and based on the mode of delivery on the target platform, they are classified into three main types—(a) laser-based bioprinting (b) jetting-based bioprinting, and (c) extrusion-based bioprinting [27, 30]. Other techniques involve magnetic printing and electrohydrodynamic printing in recent times.

#### 1.3.1 Laser-Based Bioprinting

This technique is further divided into following two types—laser-guided direct cell printing and laser-induced cell printing. In laser-guided direct cell printing, the laser pulse pools cells from the cell suspension based on the difference between the refractive index of the cells and cell media and guides the cells to the substrate. However, in the laser-induced cell printing, the laser power is utilized to heat up a donor

layer creating pressure change. The pressure change causes ejection of cell-laden hydrogel or droplet below the absorbing donor layer onto the substrate [32, 33]. Two-photon polymerization (2PP) or direct laser writing is also used to fabricate cell-laden photo-thermal sensitive hydrogels. In 2PP, the focal point of high-intensity femtosecond laser source generates two photons which are responsible for creating localized polymerization reaction within a photopolymer resin [34]. Stereolithography is a UV laser-based 3D printing technique which cures photopolymer moving from one point to another, on the surface of the resin and fabricates a 3D structure layer by layer [35].

### ***1.3.2 Jetting-Based Bioprinting***

The most potent and well-established jetting-based bioprinting is an inkjet-based bioprinting which is further categorized into two types—piezoelectric- and thermal-based bioprinting. In piezoelectric-based bioprinting, the shape distortion of piezoelectric transducer results in an air bubble which expands resulting in pushing the liquid out of the nozzle. In thermal inkjet bioprinting, a heater is used to heat up the resistor for expansion of the bubble which results in ejection of the droplet [32, 36]. Inkjet-based bioprinting is explored in *in vivo* printing [37]. More recently, new jetting-based bioprinting has been developed in the form of—valve-based jetting printer and acoustic-based jetting printer. The flow rate of valve-based printing system is controlled by the opening and closing of the valve resulting in a tunable precise number of cells and size of droplets [38, 39]. In acoustic bioprinting, the material is ejected by the generation of the acoustic wave. Heat is generated in this process which might hinder in the printing of thermoresponsive hydrogel [38, 40].

### ***1.3.3 Extrusion-Based Bioprinting***

Extrusion-based bioprinting is one of the popular versatile techniques involving deposition of cells and hydrogels. Extrusion is incorporated by either pneumatic force (air pressure) or mechanical force (through screw and piston) for extruding cell-laden hydrogels [33, 41]. In this technique, hydrogels having a wide range of viscosity (from 30 mPa s to  $6 \times 10^7$  mPa s) could be printed and from photo-crosslinkable to thermoresponsive hydrogels could be extruded efficiently yielding higher cell density structures [42]. Thermoresponsive hydrogels like gelatin, methyl-cellulose, agarose, pluronic (Lutrol F127), and poly-N-isopropylacrylamide (PNIPAAm) have been reported for extrusion-based printing with better response [43, 44] (Table 1.1).

**Table 1.1** Overview of existing bioprinting technology

Bioprinting technique	Advantages	Disadvantages
<i>Laser-based bioprinting</i>		
Laser-guided direct cell printing	High resolution and cell viability, non-clogging of nozzles	High printing cost and slow fabrication process
Laser-induced cell printing	High resolution and cell viability, multi-materials fabrication, non-clogging	High printing cost and limited scalability, metallic residuals contamination
Stereolithography (SLA) Two-photon polymerization (2PP)	High resolution, higher shape holding capacity in vertical 3D structure	Cell viability affected by laser source, hydrogel needs to be UV-photocrosslinked
<i>Jetting-based bioprinting</i>		
Piezo inkjet printing	High resolution, faster process	Nozzle clogging, lower cell density, low shape fidelity and complexity in 3D structure, limited bioink viscosity, droplets drying
Thermal inkjet printing	High resolution, faster process and low cost	Lower cell density, low shape fidelity, hydrogel properties affected by heat, non-uniform droplets
Valve-based printing	Medium-to-high resolution, good cell viability, less clogging, jetting ability from droplet to strand	Low shape fidelity in 3D structure, time delay
Acoustic printing	High resolution, uniform droplets size, lesser clogging	Low shape fidelity in 3D, lower cell density, limited bioink viscosity
<i>Extrusion-based bioprinting</i>		
Pneumatic extrusion printing	Versatile process, wide ranges of bioink could be used, high cell density	Low resolution, effect of shear stress on cell viability, time delay
Mechanic extrusion printing	Versatile with wide spectrum of bioinks, high shape sustaining ability in 3D structure, high cell density, direct control of material flow rate	Low resolution, effect of shear stress on cell viability
<i>Recent techniques in bioprinting</i>		
Magnetic printing	High resolution, support material free, high cell density	Toxicity of nanomaterials, high system cost
Electrohydrodynamic jetting	High resolution, precision control, better cell viability	High voltage and special setup, low shape fidelity in 3D form

### **1.3.4 4D Bioprinting**

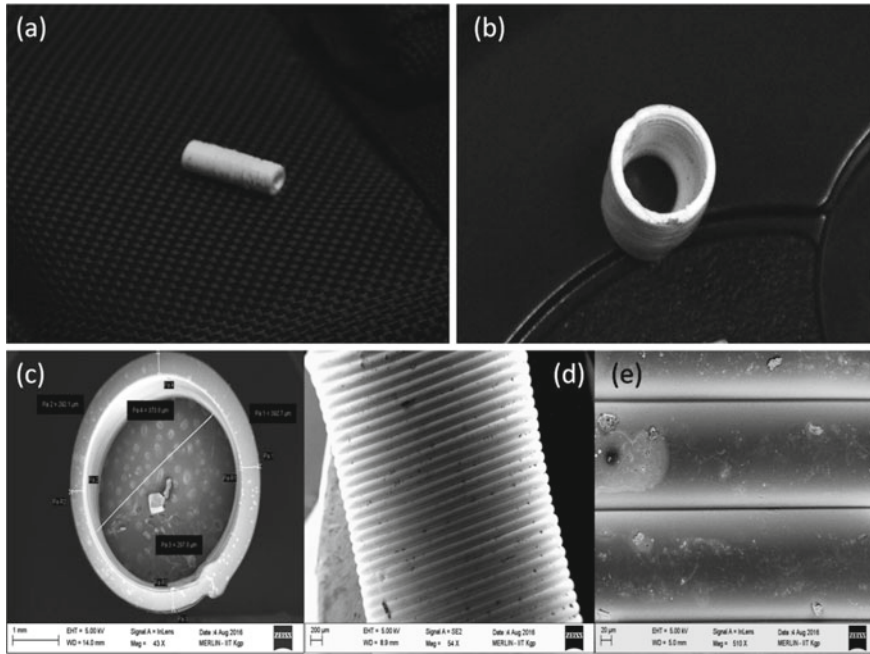
Profound advancement in 3D printing technology has resulted in new research area of 4D bioprinting technology. Researchers have incorporated stimuli-responsive dynamic environment which results in shape-morphing effects (SME) to the fabricated scaffolds. The external stimulus is given in the form of temperature, light, humidity, and using smart biomaterials which converts stimulus changes to produce dynamic environment [45]. Shape-morphing effects (SME) can be categorized into— (1) one-way shape morphing, (2) two-way shape morphing, and (3) multi-way shape morphing [46, 47]. Along with external stimulus application, smart biomaterials mimicking tissue geometry and physiological functions are being explored extensively, so that the printed tissue/organ can change its shape and form as per native tissue structure [48–50].

### **1.3.5 Case Study**

The versatility of 3D printing is one of the most prominent features that it is being explored in various domains ranging from aerospace, concrete printing to electronics, biomaterials, and tissue engineering applications [25, 32, 51, 52]. However, during 3D printing, certain critical issues could be encountered which might be deviating from the previously reported information. Herein, we have chosen an FDA approved synthetic polyester polycaprolactone (PCL) for 3D printing. The low glass transition temperature ( $T_g$ ) of 60 °C makes PCL a preferred polymer for melt extrusion 3D printing [53–56] in tissue engineering applications (Fig. 1.8).

In our study, however, we found quite a deviation from the previously reported articles. 3D bioplotter manufactured by EnvisionTEC GmbH, Germany, had been used to print PCL (Molecular weight ~80,000 Da, Sigma Aldrich, USA). The particular 3D printer comprises low-temperature (LT) head and high-temperature (HT) head. PCL was loaded into the HT head made of stainless steel cartridges. It was observed that even after keeping PCL granules at 60 °C for an approximately a long time, the polymer could not be extruded with precision strands. The pressure was maintained at 5 bars for extrusion. Following some trials, it was observed that raising the temperature to about 150–160 °C, and air pressure being kept at 8–9 bars yielded melt extruded PCL strands with precision structures.

The reason for such deviation could be hypothesized due to the influence of ambient conditions for 3D printing. While the steel cartridges were heated to 60 °C, it might have reduced the heat transferred to the PCL pellets owing to the thickness of the cartridge itself. Moreover, molecular weight being very high, it might have resulted in highly viscous polymer melts, difficult to be extruded with 5 bars pressure. Alongside, the distance between the nozzle mouth from where the polymer melt is being extruded, and the platform to be printed plays a major role in efficient 3D printing of polymer melts.



**Fig. 1.8** **a** 3D printed PCL tube (longitudinal view), **b** cross-sectional view of PCL tube, **c** cross-sectional view of 3D printed tube (scale bar—1 mm)

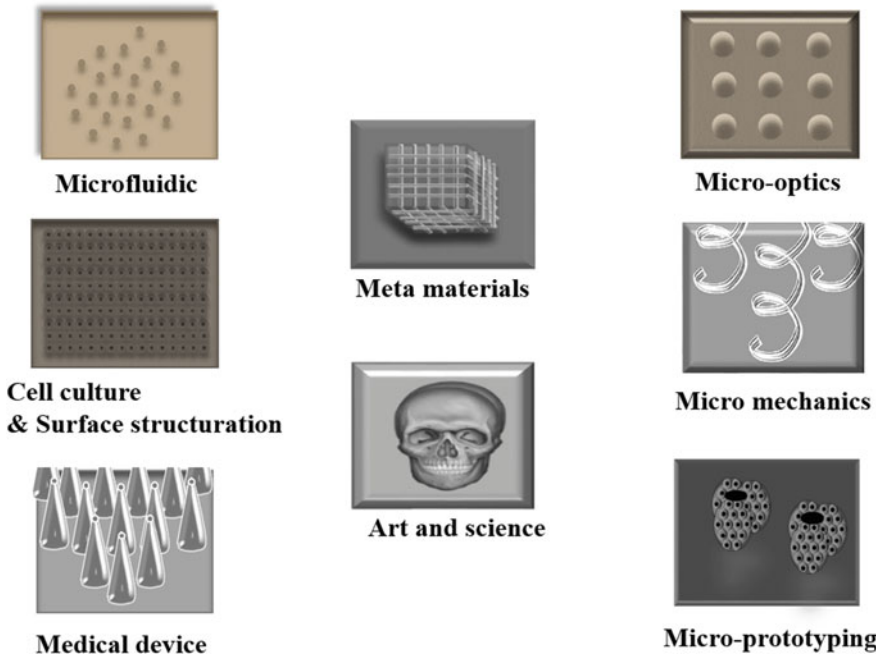
#### 1.4 3D Micro/Nanostructures—Directional Propagation of Cellular Viability

The *in vivo* periphery of cells in any tissue or organ system constitutes of a complex three-dimensional (3D), multifunctional microenvironment surrounded by multifunctional extracellular matrix components along with other cellular populations or ECM-trapped cellular signaling factors. It is often observed that cells undergo directional migration or restructure its microenvironment especially when triggered by the concentration gradient of one or more bioactive signaling molecules [57, 58]. A perfect example of such chemotactic migration of cells is the movement of immune cells to their specific target site. Furthermore, site-directed migration of cells take place within tissues in pathological conditions like cancer cell metastasis or chronic inflammation [59–61]. For example, the malignancy of cancerous condition is determined by the efficiency of tumor cells to migrate to either distant organs or neighboring tissues [61, 62]. It is apparent that not only biochemical constitution of the surrounding environment but the 3D or spatial distribution of ECM proteins need to be recapitulated in order to decode and understand the interaction between cellular components in any pathological or immunological conditions [63].

An array of various methods had been deployed in the last decade for achieving structurally stable 3D microstructures trying to mimic the *in vivo* microenvironment that has strongly influenced the tissue engineering fraternity. As explained earlier, these approaches depend on printing technologies like extrusion-based bioprinting [64, 65], inkjet-based bioprinting [32, 66], digital light processing (DLP)-based bioprinting [67], laser-induced forward transfer (LIFT)-centered bioprinting [68], or electrospinning [25, 69]. The biofunctionalization of microenvironment created based on the above technologies is often executed using either synthetic peptides or model compounds [70]. However, the above-narrated fabrication procedures either lack the possibility to construct true 3D free-standing microarchitectures without sacrificial support or are unable to reach micronanometric feature resolution desired for the above application. More recently, studies revealed fabrication of micro-nanostructures containing full-length bioactive proteins had been proposed [71]. The microfabrication of such structures are often based on light-assisted photopolymerization techniques which include stereolithography (SLA), digital light projection (DLP), or selective laser sintering (SLS), wherein the concept of 3D microstructures are often realized by a layerwise approach evolving from series of transverse-plane images as slices [72]. The above techniques can easily print microstructures possessing dimensions in the range of few micrometers, although spontaneous applications of such techniques are limited by the fact that there are only a few materials that feature biocompatibility and photosensitive properties at the same time. Another developing technique that is gaining much attention is two-photon polymerization-based direct laser writing technique (2P-DLW) that possesses the capability to write structures in the submicrometer range. Direct laser writing is a process, wherein a photoresist containing a radical photo-initiator and crosslinkable monomer moiety is polymerized using two- or multi-photon-based technique. Till date, an extensive array of complex and submicron-sized microstructures has been fabricated using the above technique (Fig. 1.9). However, only a few 2P-DLW based printable materials are considered biocompatible and could be used for cell culture activities.

One such material was reported by Accardo et al., wherein direct laser writing of PEGDA (poly (ethylene glycol)diacrylate) was carried out to prepare a 3D scaffold for neuronal tissue engineering [73]. PEGDA is an FDA approved biocompatible hydrogel, and the physical phenomena highlighting the fabrication is similar to the one narrated above. An appropriate photo-initiator in the form of phenylbis (2,4,6-trimethylbenzoyl) phosphine oxide was mixed with the hydrogel to facilitate the writing procedure, as it has a high absorption property in the UV range. The photo-initiator was considered to provide a very high writing speed, thus aiding in the rapid fabrication of submicron-sized scaffolds. After fabrication, the architecture was functionalized with poly-L-lysine and laminin to promote cellular adhesion. The porous architecture of as-fabricated scaffold allowed excellent growth and proliferation of neuronal cells with ramified neuronal network penetrating the 3D microstructure, thus forming multiple neuritic extensions possessing a length between 10 and 60  $\mu\text{m}$  per cell. Moreover, PEGDA hydrogel demonstrated low intrinsic fluorescent emission [74], thus allowing multi-staining immunofluorescence evaluation of neuronal cells in the 3D matrix. Further, it was also observed that PEGDA demonstrated



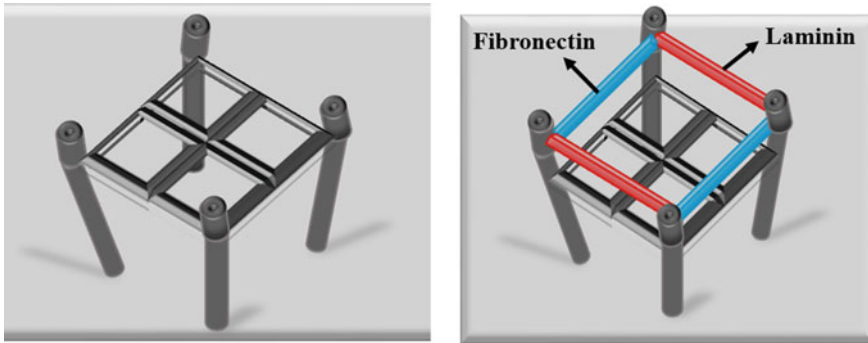


**Fig. 1.9** 3D microstructures which were printed using 2P-DLW fabrication technique

low stiffness (Y-modulus  $\sim 200$  kPa) which is comparable or close to that of brain's stiffness (Y-modulus  $\sim 600$  Pa), thus ratifying the excellent growth and proliferation of neural cells on the 3D architecture. It was apparent to conclude that the 3D hydrogel-based architecture can be further explored as a futuristic platform for neural tissue engineering or as a tissue model for studying the interaction between various biochemical compounds (including potential drugs or neurodegenerative proteins) and neural cell cultures.

The second approach is to make this 3D microstructure biocompatible which could be achieved by either functionalizing or coating the same with necessary proteins which could aid in particular cell proliferation. In a report by Martin Bastmeyer group, a 3D scaffold was constructed and bifunctionalized with two different extracellular matrix (ECM) proteins in a spatially resolved manner, as represented in Fig. 1.10, in an effort to specifically control cell adhesion [63]. A sequential DLW technique combined with three photoresists were deployed to attain the same. The square-shaped microstructures consist of four pillars with beams bridging the pillars on the edges on the top. While other set of beams present in the middle, not only bridge the pillars but also form square-shaped net-like structure. The beams on the top were used for the functionalization process, and beams facing each other were only functionalized with similar proteins. Fibronectin or laminin proteins were used to functionalize the upper beams of the microstructure in a spatial arrangement while the bottom ones were left bare. Epithelial A549 and NIH 3T3 fibroblast cell lines were





**Fig. 1.10** 3D microstructures which were printed using 2P-DLW fabrication technique by Martin Bastmeyer group to fabricate a cell instructive 3D microscaffolds for guided cell propagation

cultured on these dual-functionalized 3D matrices to understand the proliferation of each cell line in the presence of above two proteins. In case of the epithelial A549 cell line, it was observed that it adhered to both surfaces irrespective of the protein it constituted; however, the proliferation was restricted only to the functionalized beams while no migration was observed on the lower beams. This suggested that the adhesion of A549 cells did not depend on the kind of protein attached, but proliferation was restricted only to the functionalized surface. Further, NIH 3T3 fibroblast cell line was introduced, and it was observed that owing to the presence of a different set of integrin proteins, it only adhered and proliferated along the presence of a laminin protein. In another set of experiments, epithelial A549 cells were seeded onto a 3D matrix containing laminin and biotinylated vitronectin as the two proteins, and it was observed that the cells only proliferated on the beams containing the laminin protein.

The above experiment proves the epithelial nature of the two cell lines as they prefer the basal lamina adhesion protein, laminin which is the main component of natural ECM. It was clear that the group was able to fabricate a cell instructive 3D microscaffolds capable of guided cell propagation and could be used as an excellent alternative for investigating cell–matrix or cell–cell interactions. Also, the as-fabricated powerful platform can be used to evaluate cell response to multiple extracellular cues in the near future.

## 1.5 3D Printing as a Tool for Lab-on-Chip or Microbioreactor Applications

Recently, additive manufacturing has significantly producing Lab-on-chip (LOC) platform, which impacts on mostly biomedical science field. The microfluidic platform using 3D printing is the only existing technique delivered to create a complete

three-dimensional devices in one step with high portability, a fraction of time, cost, simple, and relatively required a lesser amount of resources [75]. Such 3D printed devices supported various medical purposes such as fabricating scaffolds, implants, LOC based cellular study, diagnostic of toxicity, genomic study, drug screening, metabolism studies, and microfluidic bioreactor for cell culturing [76, 77]. The widely used 3D printing approach for creating microfluidic channel are inkjet 3D printing, stereolithography, two-photon polymerization, and extrusion printing.

*Microfluidic bioreactor:* Lee et al. presented a comparative study between the widely used 3D printing such as inkjet and fused deposition modeling technique to fabricate microfluidic device [78]. Several characterizations such as microchannel accuracy, surface roughness, surface contact angle, biocompatibility, printer accuracy, and repeatability have studied. The result proved that inkjet printing showed high resolution in all the dimension with accuracy and smooth microchannel surface than FDM. Similarly, Ong et al. designed a microfluidic device using both stereolithography (SLA) (Proto Labs, USA) (material polycarbonate mixture) and polyjet [like Inkjet 3D (Objet260 Connex3 Printer) (Stratasys, USA)] (material photopolymer VeroClear-RGD810) printing technique to evaluate the multicellular spheroids immobilization, viability, and functionality in microstructure [77]. A comparative study showed similar output, but SLA printed microfluidic device was designated due to its high resolution resulted with clean-cut microstructure array providing better accuracy and surface smoothness on microchannel (200  $\mu\text{m}$  depth) and culture chamber (750  $\mu\text{m}$  diameter). The microfluidic device is carried out using a pump-free perfusion culture system, whereas computational fluid dynamic (CFD) simulation was employed to calculate the media inlet and outlet flow and culture chambers shear stress. Therefore, the microstructure array designed in the microchannel was seeded with cells (parental metastatic OSCC tumor derived from patient and human HepG2 hepatocyte spheroids) showed to immobilize at cell culture chamber supported with microstructure array and perfusion channel designed maintained good viability and functionality up to 72 h.

Takenaga et al. fabricated microfluidic chip using 3D printing (Asiga, PicoPlus 27) (resin-based photopolymer material) and prepared light-addressable potentiometric sensor (LAPS) as a sensor surface to attain a semiconductor-based new biochip [76]. LAPS which is an electrolyte–insulator–semiconductor structure (EIS) is composed of bilayers such as Ta<sub>2</sub>O<sub>5</sub> (60 nm) (pH-sensitive layer) and SiO<sub>2</sub> (30 nm) above the p-doped silicon substrate with an Al contact at its back side. With a photocurrent depending principle, light-emitting diode (LED 4 × 4 infrared) setup has been used with data acquisition card (DAQ) (from NI—National Instruments) to record the ion concentration on the LAPS surface, and 3D printed microfluidic channel was attached above. The LAPS chip and microfluidic channel were assembled using silicone adhesive sealant and photo-resin, and comparative study with Chinese hamster ovary (CHO) cells was studied. Photo-resin-based adhesion showed cell morphology and functionality similar to culture flask outstanding with its biocompatibility while silicon sealant with unhealthy cells.

Gowers et al. designed and fabricated robust microfluidic analysis system to continuously monitor human tissue metabolism level by measuring glucose and lactate in cyclist at the real time [79]. The 3D printed (ULTRA 3SP) microfluidic device incorporated with commercially available clinical microdialysis probe through a removable biosensor and monitored the glucose and lactate level in real time. Comina et al. [80] demonstrated the fabrication of LOC on PDMS-glass using template fabrication by microstereolithography 3D printer with 50  $\mu\text{m}$  resolution and smooth surface for sealing (PDMS-glass). The process is cost-effective, requires less time, and fabricated a reusable template with independent multilevel fluidics with functionalized surface and micromixers for detecting glucose. The functionalized surface with glucose oxidase (GOx), horseradish peroxidase (HRP), and a non-colored substrate (Ampliflu Red) as a result were tested with glucose solution at different concentration (2.5, 5 and 10 mM). The quantitative detection by quicker resorufin production for 10 mM glucose concentration resulted faster than others due to the hydrogen peroxide by GOx catalytic reaction and consequently resorufin consumed by HRP.

Kitson et al. demonstrated milli- and microfluidic reactionware LOC device using the 3DTouchTM printer with polypropylene (PP) material [81]. The designed reactor using such inert, robust, cost-effective, and reliable material with one, two, and three inlets performs organic, inorganic, and material synthesis successfully. Peris et al. validated 3D printed bioreactor with continuous flow and efficiently immobilizing the enzyme [82]. The microfluidic is printed using FDM printer with nylon 6; hence, to immobilize the enzyme, the surface was functionalized using glutaraldehyde after treating with HCL (5 ml). Additionally, treating with polyethylenimine (PEI) multiplied the free amines on the surface. and reaction with glutaraldehyde enhanced the C=O band resulting with surface functionality. The biocatalytic reactor with continuous flow showed stability for approximately 100 h and good activity of the enzyme by comparing reaction thru converting (R)-methyl-benzylamine into acetophenone. The kinetic resolution with the production of  $20.5 \mu\text{mol h}^{-1} \text{mg}_{\text{enz}}$  in 20 min was presented. In future by tailoring, the geometries of microchannel and chamber with continuous flow could present a rapid testing device with different immobilization.

## 1.6 Conclusions

In the realm of the current state of art for medical implants as well as for wide varieties of tissue analogs, 3D extrusion printing technology has provided a comfortable, feasible, economically viable, and medically corrigible platform in tissue engineering. Extrusion-based 3D printing has provided a much awaited process which would enable the researchers to fabricate scaffolds of a wide spectrum of materials with tailorable mechanical as well as *physicochemical* properties. On the contrary, the successful completion of the process is potentially dependent on the material processing compared to the other additive manufacturing processes. However, in

laser-based and fused deposition modeling, in spite of lacking the flexibility in material selection, the final product is produced with very less pre- and post-processing. However, the current demand of printing tissue analogs or organ with live cells has swayed off this drawback, because cell-based bioinks are needed significant attention to pre-processing along with the material selection. Further, future studies are required with novel biomaterial/bioink printed tissue which could pave the way to design an artificial tissue that would support, function, and replace the damaged tissue.

## References

1. Ferlay J et al (2012) Cancer incidence and mortality worldwide: IARC CancerBase. GLOBOCAN 2012 v10, 11
2. Hull CW (1986) Apparatus for production of three-dimensional objects by stereolithography. Google Patents
3. Hutmacher DW (2000) Scaffolds in tissue engineering bone and cartilage. In: *The biomaterials: Silver Jubilee Compendium*. Elsevier, pp 175–189
4. Naghieh S et al (2016) Numerical investigation of the mechanical properties of the additive manufactured bone scaffolds fabricated by FDM: the effect of layer penetration and post-heating. *J Mech Behav Biomed Mater* 59:241–250
5. Singh S et al (2019) Mechanical feasibility of ABS/HIPS-based multi-material structures primed by low-cost polymer printer. *Rapid Prototyping J* 25(1):152–161
6. Singh S et al (2019) Optimization and reliability analysis to improve surface quality and mechanical characteristics of heat-treated fused filament fabricated parts. *Int J Adv Manuf Technol* 1–16
7. Singh S, Prakash C, Ramakrishna S (2019) 3D printing of polyether-ether-ketone for biomedical applications. *Eur Polym J*
8. Fischer P et al (2003) Sintering of commercially pure titanium powder with a Nd: YAG laser source. *Acta Mater* 51(6):1651–1662
9. Kruth J-P et al (2005) Binding mechanisms in selective laser sintering and selective laser melting. *Rapid Prototyping J* 11(1):26–36
10. Shishkovsky I et al (2008) Porous biocompatible implants and tissue scaffolds synthesized by selective laser sintering from Ti and NiTi. *J Mater Chem* 18(12):1309–1317
11. Van der Stok J et al (2013) Selective laser melting-produced porous titanium scaffolds regenerate bone in critical size cortical bone defects. *J Orthop Res* 31(5):792–799
12. Roy S et al (2016) Understanding compressive deformation behavior of porous Ti using finite element analysis. *Mater Sci Eng C* 64:436–443
13. Atwood C et al (1998) Laser engineered net shaping (LENS™): a tool for direct fabrication of metal parts. In: *International congress on applications of lasers & electro-Optics*. LIA
14. Balla VK, Bose S, Bandyopadhyay A (2008) Processing of bulk alumina ceramics using laser engineered net shaping. *Int J Appl Ceram Technol* 5(3):234–242
15. Murr LE et al (2012) Metal fabrication by additive manufacturing using laser and electron beam melting technologies. *J Mater Sci Technol* 28(1):1–14
16. Landers R, Mülhaupt R (2000) Desktop manufacturing of complex objects, prototypes and biomedical scaffolds by means of computer-assisted design combined with computer-guided 3D plotting of polymers and reactive oligomers. *Macromol Mater Eng* 282(1):17–21
17. Carvalho C et al (2005) Fabrication of soft and hard biocompatible scaffolds using 3D-Bioplotting™. *Virtual Model Rapid Manuf Adv Res Virtual Rapid Prototyping* 97–102
18. Kalpakjian S, Schmid SR, Sekar K (2014) *Manufacturing engineering and technology*

19. Park S-I et al (2014) Effective mechanical properties of lattice material fabricated by material extrusion additive manufacturing. *Addit Manuf* 1:12–23
20. Poomathi N et al (2019) Bioprinting in ophthalmology: current advances and future pathways. *Rapid Prototyping J* 25(3):496–514
21. Wang X et al (2017) 3D printing of polymer matrix composites: a review and prospective. *Compos B Eng* 110:442–458
22. Peltola SM et al (2008) A review of rapid prototyping techniques for tissue engineering purposes. *Ann Med* 40(4):268–280
23. Moroni L, De Wijn J, Van Blitterswijk C (2006) 3D fiber-deposited scaffolds for tissue engineering: influence of pores geometry and architecture on dynamic mechanical properties. *Biomaterials* 27(7):974–985
24. Li JP et al (2007) Bone ingrowth in porous titanium implants produced by 3D fiber deposition. *Biomaterials* 28(18):2810–2820
25. Singh H, Singh S, Prakash C (2019) Current trends in biomaterials and bio-manufacturing. In: *Biomanufacturing*. Springer, pp. 1–34
26. Knowlton S et al (2015) Bioprinting for cancer research. *Trends Biotechnol* 33(9):504–513
27. Pereira RF, Bártolo PJ (2015) 3D bioprinting of photocrosslinkable hydrogel constructs. *J Appl Polym Sci* 132(48)
28. Ker ED et al (2011) Bioprinting of growth factors onto aligned sub-micron fibrous scaffolds for simultaneous control of cell differentiation and alignment. *Biomaterials* 32(32):8097–8107
29. Gough NR (2014) Bioprinting cartilage scaffolds. *Sci Sig* 7(356):ec347
30. Wang S, Lee JM, Yeong WY (2015) Smart hydrogels for 3D bioprinting. *Int J Bioprinting* 1(1)
31. Fantini M, Curto M, De Crescenzo F (2016) A method to design biomimetic scaffolds for bone tissue engineering based on Voronoi lattices. *Virtual Phys Prototyping* 11(2):77–90
32. Murphy SV, Atala A (2014) 3D bioprinting of tissues and organs. *Nat Biotechnol* 32(8):773
33. Zhang X, Zhang Y (2015) Tissue engineering applications of three-dimensional bioprinting. *Cell Biochem Biophys* 72(3):777–782
34. Ovsianikov A et al (2013) Laser photofabrication of cell-containing hydrogel constructs. *Langmuir* 30(13):3787–3794
35. Chia HN, Wu BM (2015) Recent advances in 3D printing of biomaterials. *J Biol Eng* 9(1):4
36. Tasoglu S et al (2013) Manipulating biological agents and cells in micro-scale volumes for applications in medicine. *Chem Soc Rev* 42(13):5788–5808
37. Ozbolat IT (2015) Bioprinting scale-up tissue and organ constructs for transplantation. *Trends Biotechnol* 33(7):395–400
38. Faulkner-Jones A et al (2013) Development of a valve-based cell printer for the formation of human embryonic stem cell spheroid aggregates. *Biofabrication* 5(1):015013
39. Duarte Campos DF et al (2016) Bioprinting organotypic hydrogels with improved mesenchymal stem cell remodeling and mineralization properties for bone tissue engineering. *Adv Healthc Mater* 5(11):1336–1345
40. Demirci U, Montesano G (2007) Single cell epitaxy by acoustic picolitre droplets. *Lab Chip* 7(9):1139–1145
41. Billiet T et al (2014) The 3D printing of gelatin methacrylamide cell-laden tissue-engineered constructs with high cell viability. *Biomaterials* 35(1):49–62
42. Lee JM, Yeong WY (2015) A preliminary model of time-pressure dispensing system for bioprinting based on printing and material parameters: this paper reports a method to predict and control the width of hydrogel filament for bioprinting applications. *Virtual Phys Prototyping* 10(1):3–8
43. Skardal A et al (2010) Photocrosslinkable hyaluronan-gelatin hydrogels for two-step bioprinting. *Tissue Eng Part A* 16(8):2675–2685
44. Fedorovich N et al (2010) 3D-fiber deposition for tissue engineering and organ printing applications. In *Cell and organ printing*. Springer, pp. 225–239
45. Zhou Y et al (2015) From 3D to 4D printing: approaches and typical applications. *J Mech Sci Technol* 29(10):4281–4288

46. Liu X et al (2014) Delivery of growth factors using a smart porous nanocomposite scaffold to repair a mandibular bone defect. *Biomacromolecules* 15(3):1019–1030
47. Kuksenok O, Balazs AC (2016) Stimuli-responsive behavior of composites integrating thermo-responsive gels with photo-responsive fibers. *Mater Horiz* 3(1):53–62
48. Villar G, Heron AJ, Bayley H (2011) Formation of droplet networks that function in aqueous environments. *Nat Nanotechnol* 6(12):803
49. Elani Y et al (2016) Microfluidic generation of encapsulated droplet interface bilayer networks (multisomes) and their use as cell-like reactors. *Chem Commun* 52(35):5961–5964
50. Villar G, Graham AD, Bayley H (2013) A tissue-like printed material. *Science* 340(6128):48–52
51. Kroll E, Artzi D (2011) Enhancing aerospace engineering students' learning with 3D printing wind-tunnel models. *Rapid Prototyping J* 17(5):393–402
52. Wong KV, Hernandez A (2012) A review of additive manufacturing. *ISRN Mech Eng* 2012
53. Temple JP et al (2014) Engineering anatomically shaped vascularized bone grafts with hASCs and 3D-printed PCL scaffolds. *J Biomed Mater Res Part A* 102(12):4317–4325
54. Rindone AN, Nyberg E, Grayson WL (2017) 3D-Printing composite polycaprolactone-decellularized bone matrix scaffolds for bone tissue engineering applications
55. Kolan KC et al (2018) Solvent and melt based extrusion 3D printing of polycaprolactone bioactive glass composite for tissue engineering
56. Pati F et al (2014) Printing three-dimensional tissue analogues with decellularized extracellular matrix bioink. *Nat Commun* 5:3935
57. Jin T, Xu X, Hereld D (2008) Chemotaxis, chemokine receptors and human disease. *Cytokine* 44(1):1–8
58. Weiner OD (2002) Regulation of cell polarity during eukaryotic chemotaxis: the chemotactic compass. *Curr Opin Cell Biol* 14(2):196–202
59. Gardel ML et al (2010) Mechanical integration of actin and adhesion dynamics in cell migration. *Annu Rev Cell Dev Biol* 26:315–333
60. Petrie RJ, Doyle AD, Yamada KM (2009) Random versus directionally persistent cell migration. *Nat Rev Mol Cell Biol* 10(8):538
61. Greiner AM et al (2014) Multifunctional polymer scaffolds with adjustable pore size and chemoattractant gradients for studying cell matrix invasion. *Biomaterials* 35(2):611–619
62. Friedl P, Alexander S (2011) Cancer invasion and the microenvironment: plasticity and reciprocity. *Cell* 147(5):992–1009
63. Richter B et al (2017) Guiding cell attachment in 3D microscaffolds selectively functionalized with two distinct adhesion proteins. *Adv Mater* 29(5):1604342
64. Stanton M, Samitier J, Sanchez S (2015) Bioprinting of 3D hydrogels. *Lab Chip* 15(15):3111–3115
65. Jakus AE, Rutz AL, Shah RN (2016) Advancing the field of 3D biomaterial printing. *Biomed Mater* 11(1):014102
66. Skardal A, Atala A (2015) Biomaterials for integration with 3-D bioprinting. *Ann Biomed Eng* 43(3):730–746
67. Zhang AP et al (2012) Rapid fabrication of complex 3D extracellular microenvironments by dynamic optical projection stereolithography. *Adv Mater* 24(31):4266–4270
68. Barron JA et al (2004) Application of laser printing to mammalian cells. *Thin Solid Films* 453:383–387
69. Guha Ray P et al (2018) Surface modification of eggshell membrane with electrospun chitosan/polycaprolactone nanofibers for enhanced dermal wound healing. *ACS Appl Bio Mater* 1(4):985–998
70. Pauloehrl T et al (2012) Adding spatial control to click chemistry: phototriggered Diels-Alder surface (bio) functionalization at ambient temperature. *Angew Chem Int Ed* 51(4):1071–1074
71. DeForest CA, Tirrell DA (2015) A photoreversible protein-patterning approach for guiding stem cell fate in three-dimensional gels. *Nat Mater* 14(5):523
72. Guvendiren M et al (2016) Designing biomaterials for 3D printing. *ACS Biomater Sci Eng* 2(10):1679–1693

73. Accardo A et al (2018) Direct laser fabrication of free-standing PEGDA-hydrogel scaffolds for neuronal cell growth. *Mater Today* 21(3):315–316
74. Meza LR et al (2015) Resilient 3D hierarchical architected metamaterials. *Proc Natl Acad Sci* 112(37):11502–11507
75. Waheed S et al (2016) 3D printed microfluidic devices: enablers and barriers. *Lab Chip* 16(11):1993–2013
76. Takenaga S et al (2015) Fabrication of biocompatible lab-on-chip devices for biomedical applications by means of a 3D-printing process. *Phys Status Solidi A* 212(6):1347–1352
77. Ong LJY et al (2017) A 3D printed microfluidic perfusion device for multicellular spheroid cultures. *Biofabrication* 9(4):045005
78. Lee JM, Zhang M, Yeong WY (2016) Characterization and evaluation of 3D printed microfluidic chip for cell processing. *Microfluid Nanofluid* 20(1):5
79. Gowers SA et al (2015) 3D printed microfluidic device with integrated biosensors for online analysis of subcutaneous human microdialysate. *Anal Chem* 87(15):7763–7770
80. Comina G, Suska A, Filippini D (2014) PDMS lab-on-a-chip fabrication using 3D printed templates. *Lab Chip* 14(2):424–430
81. Kitson PJ et al (2012) Configurable 3D-Printed millifluidic and microfluidic ‘lab on a chip’ reactionware devices. *Lab Chip* 12(18):3267–3271
82. Peris E et al (2017) Tuneable 3D printed bioreactors for transaminations under continuous-flow. *Green Chem* 19(22):5345–5349

**Abir Dutta** is pursuing doctoral research in Biomaterials and Biomechanics at Advanced Technology Development Centre, Indian Institute of Technology Kharagpur. He is also working in School of Medical Science and Technology in the domain of 3D printing of biomaterials.

**Ms. Trina Roy** is Ph.D. Research Scholar, School of Medical Science and Technology (SMST), Indian Institute of Technology Kharagpur. Her research area is focused on 3D printing of thermo-plastic polymers for vascular tissue engineering applications.

**Preetam Guha Ray** is working as Research Associate at the School of Medical Science and Technology, Indian Institute of Technology Kharagpur, India. His research interest is focused on fabrication and surface engineering of multimodel platforms and scaffolds for biosensing and tissue engineering applications.

**Ms. Ragavi Rajasekaran** is pursuing her doctoral program in Rajendra Mishra School of Engineering Entrepreneurship (RMSoEE), Indian Institute of Technology Kharagpur. She is working in the areas of stem cell-based tissue regeneration and its in vitro study in micro-environment.

**Prof. Mamoni Banerjee** is working on product development using phytochemicals and is currently an Assistant Professor of Rajendra Mishra School of Engineering Entrepreneurship, Indian Institute of Technology Kharagpur.

**Santanu Chattopadhyay** is a professor in Rubber Technology Centre, IIT Kharagpur and an expert in the field of synthesis and characterization of block copolymers by controlled polymerization, smart rubber composites, biomaterials, and polymers for health care and energy harvesting.

**Prof. Sanjay Gupta** Ph.D. (TU Delft), has 20 years of research experience in orthopaedic biomechanics and is currently a Professor of Mechanical Engineering, Indian Institute of Technology Kharagpur.

**Prof. Santanu Dhara** Ph.D. (IIT Kharagpur), has expertise in biomaterials and tissue engineering and is currently a Professor of School of Medical Science and Technology, Indian Institute of Technology Kharagpur.



# Chapter 2

## Fundamentals of 3D Printing and Its Applications in Biomedical Engineering



Hasan Kemal Surmen, Faruk Ortes, and Yunus Ziya Arslan

### 2.1 Introduction

Three-dimensional (3D) printing is a practical manufacturing method that allows us to transform objects designed in the digital environment into physical objects using layered manufacturing methods. The terms of *rapid prototyping* and *additive manufacturing* are also used to express the manufacturing process using 3D printers. Unlike the subtractive manufacturing (machining) approach in which 3D objects are constructed by successively cutting material away from a solid block of material, additive manufacturing processes produce parts by adding material one layer at a time.

In 3D printing technology, parts with complex geometries can be manufactured using less material compared to conventional manufacturing techniques. There is no need for molding in 3D printing, and the production of a part with different geometry can be quickly adapted. Objects designed in a digital environment can be directed to the production process immediately. Three-dimensional printing, which is very suitable for the production of objects with free-form surfaces, has been widely used in the medical sector, especially in the production of patient-specific biomedical devices [1].

Three-dimensional printing applications are spreading rapidly in many areas of the medical sector. Nowadays, orthopedic implants, prostheses, orthoses, dental products, anatomical models, customized tablets for personalized medicine, and many

---

H. K. Surmen

Department of Automotive Technology, Vocational School of Technical Sciences, Istanbul University-Cerrahpasa, Hadimkoy, Istanbul 34555, Turkey

F. Ortes · Y. Z. Arslan (✉)

Department of Mechanical Engineering, Faculty of Engineering, Istanbul University-Cerrahpasa, Avcilar, Istanbul 34320, Turkey

e-mail: [yzarslan@istanbul.edu.tr](mailto:yzarslan@istanbul.edu.tr)

© Springer Nature Singapore Pte Ltd. 2020

S. Singh et al. (eds.), *3D Printing in Biomedical Engineering*,

Materials Horizons: From Nature to Nanomaterials,

[https://doi.org/10.1007/978-981-15-5424-7\\_2](https://doi.org/10.1007/978-981-15-5424-7_2)

surgical instruments can be produced using 3D printers [2–5]. Three-dimensional printing allows significant flexibility for the fabrication of biomedical devices, offering geometric freedom without limitations experienced in traditional manufacturing methods. By using the 3D printing method, we are able to print complex-shaped functional parts with detailed internal features and adjust the material density to produce lighter biomedical devices with fewer parts.

Since the biomedical devices and implants must be compatible with the patient's anatomy, the production of such devices by traditional manufacturing methods is a challenging task. In addition, because these devices are supposed to be designed for patient-specific purposes, the design of each item should be independently carried out for each patient [6]. Three-dimensional printing technology does not require additional production stages such as production line installation and mold design, thereby having the advantage of manufacturing the parts immediately, which makes the 3D printing method very suitable for the production of biomedical devices. Three-dimensional printing has been one of the widely preferred approaches in the biomedical sector because of its high geometrical accuracy and resolution. In addition, the ability to print complex body implants by taking into account the magnetic resonance image (MRI) [7] and computed tomography (CT) [8] data further increased the functionality of this technology.

Three-dimensional bioprinting is another application area of the 3D printing technology in which the complex 3D living tissues and artificial organs are constructed [9]. It is possible to produce 3D functional and living tissues using 3D bioprinting [10]. These printers generally use materials such as hydrogel, silicon, and protein solutions. The major aim in this field is to produce functional and transplantable human organs in the near future [11].

Some disadvantages of the 3D printing method are (i) it is not economically feasible for mass production, (ii) size of the part to be manufactured is limited to the dimensions of the 3D printer, and (iii) production speed is relatively low. Furthermore, the variety of materials used in 3D printing is also limited. On the other hand, new strategies are being developed that allow different types of materials to be used in the 3D printing technology [12–15]. Thanks to these novel technologies, many types of metal [16], plastic [17], composite [18], and organic materials [19] can be used in 3D printing.

In biomedical applications, post-processing is of particular importance. For example, stair-stepped surface, which is a result of layer-by-layer manufacturing, may lead to undesirable surface conditions for implants required biocompatibility [20]. In such cases, surface finish operations should be done carefully and precisely. Moreover, clean and sterile manufacturing environments are required in the manufacture of medical products such as implants. In this context, precautions against contamination should be carefully taken for printing platform and other 3D printer equipment [21].

In this chapter, the general working principle of 3D printers, commonly used 3D printing technologies, and types of materials used in 3D printers were addressed. In addition, scientific studies focusing on 3D printing technology in the biomedical field have been discussed.

## 2.2 Stages of the 3D Printing Process

In the 3D printing process, the 3D model of the target object is divided into layers in a 3D slicer software by considering the desired surface precision, and the related G-codes are produced. The data obtained in this stage are digitally transmitted to the 3D printer, and the first layer of the object is created according to these data. The next layer is built on the previous layer so that all layers are created and the object is constructed.

In general, a 3D printing process consists of (i) obtaining the 3D model of the target object in the digital environment, (ii) converting the model file of the desired object into a digital file format compatible with 3D printer such as STL, (iii) slicing the model into layers by means of a 3D printer slicer software and producing the G-codes, (iv) transmission of the G-codes to the 3D printer, and (v) printing the object (Fig. 2.1).

### 2.2.1 3D Modeling

In the first step, the 3D printing process requires a 3D model of the object to be printed. The model can be obtained by using many different computer-aided design (CAD) programs, as well as a 3D scanning system (optical, MRI, CT, or image-based). More efficient printing results can be achieved if the design is made by taking into consideration the technology and sensitivity of the 3D printer. Moreover,

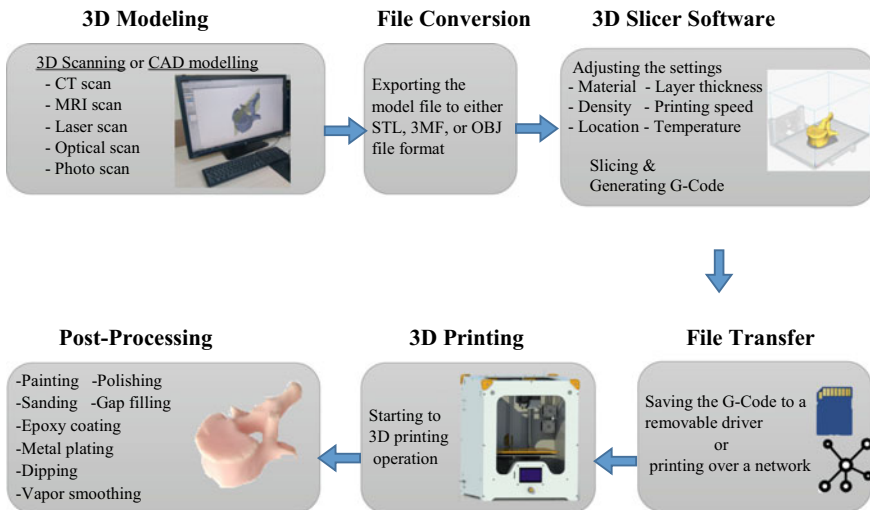


Fig. 2.1 Stages of the manufacturing process by using 3D printing technology

the capabilities of the 3D printer should be compatible with the assembly parts intended for printing at once and the intended clearance between moving parts.

### ***2.2.2 File Conversion***

Once the 3D model has been acquired, the model should be converted to a file format that a slicer software would recognize. The most common file format for 3D printing is STL. Other formats such as obj and 3MF are also recognized by many software. The model geometry cannot be changed after conversion of the file format, but the size and orientation of the model can be modified.

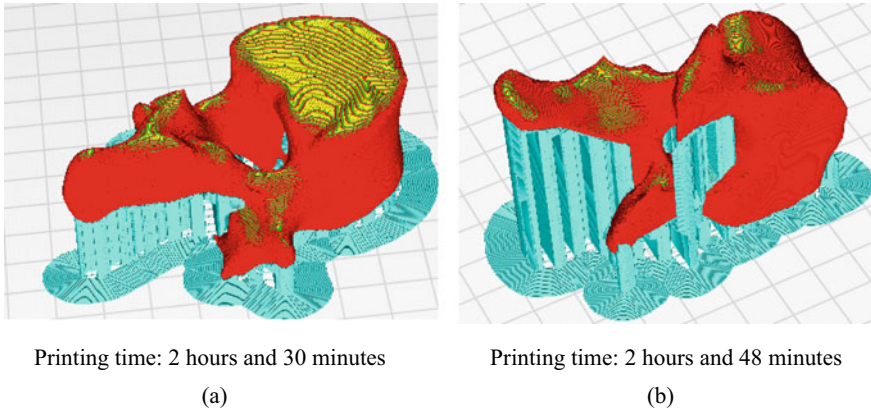
### ***2.2.3 3D Slicer Software***

Models saved in an appropriate format are transferred to a 3D slicer software before 3D printing. The purpose of the use of this software is to slice the model into layers and generate G-codes required to be fed into the 3D printer. The position of the object on the 3D printer table, layer thickness, type of the material to be used, temperature, material density, and printing speed can be adjusted using the software. According to the specified parameters, the model is sliced and G-codes are generated. Moreover, the construction of the model can be simulated and monitored by means of the slicer software just like in a computer-aided manufacturing (CAM) program. In this way, the errors that may occur during 3D printing can be detected and eliminated in a timely manner. Many open-source and open-access 3D slicer software such as Ultimaker Cura (Ultimaker B.V., The Netherlands), CraftWare (Craftunique, Hungary), and Z-Suite (Zortrax, Poland) are available for users. The resulting G-codes can be transferred to the printer via a memory card or through a wired/wireless network.

### ***2.2.4 3D Printing***

Once the file transfer has been completed, the 3D printer recognizing the G-codes starts printing after reaching the required temperature value. Before printing, the printer should be placed on a level surface, calibration operations should be performed, and the material should be prepared properly for printing. Printing duration varies according to the technology of the 3D printer, material density, geometry and size of the model, amount of support to be used, and the desired level of resolution.

In 3D printing, the geometry of the object directly affects the printing time. Since the software fills the support structures between the object and the printing tray in the order of the printing process to be carried out successfully, it is important to position the object appropriately on the printing tray (Fig. 2.2). If the objects are



**Fig. 2.2** Sample representation of the effect of the positioning of objects on the formation of the support structures. Printing time for the same object located horizontally (**a**) is less than that for located laterally (**b**)

positioned so that the minimum support structure is required, the printing and post-processing time, which require for isolating the model from the support structures, can be minimized.

### 2.2.5 Post-processing

When printing is finished, the part is taken from the 3D printer tray and cleaned from the support structures. Support structures are two types: standard and dissolvable. Standard support structures are removed from the workpiece using suitable hand tools. Dissolvable support structures are removed by immersing the workpiece in water or specific solutions developed for the material. After removal of the support structures, post-processing operations such as painting, polishing, sanding, gap filling, metal plating, epoxy coating, dipping, and vapor smoothing can be applied.

## 2.3 Types of 3D Printing Technologies

### 2.3.1 Stereolithography (SLA)

The SLA technique is based on the principle of curing the photopolymer resin layer, which is in a liquid state at room temperature, by an ultraviolet laser beam according to geometric data of the target object [22]. Curing is based on the additive manufacturing

approach, which forms the basis of 3D printer technologies. Each layer is obtained by G-code previously generated using a 3D slicer software. The laser beam scans the resin layer and performs the curing process. After the first layer is solidified, the building platform moves up to a layer height, a new resin layer is plastered on top, and the curing process is repeated. The layers are added to each other, and the entire object is produced. Thus, 3D objects having very detailed geometries can be obtained from the liquid resin which is filled in the pool and which does not have certain geometry. This 3D printing technology, with a high degree of accuracy and smooth surfaces, is highly suitable for the production of objects with detailed geometries in many areas. SLA printing technology has proven to be suitable for the production of 3D ceramic parts with desirable mechanical properties, as well as the production of 3D polymer parts in the biomedical device sector [23]. By adding ceramic powder suspensions into the photopolymer and by laser polymerization of the ceramic-resin mixture, complex shapes can be obtained.

### ***2.3.2 Digital Light Processing (DLP)***

DLP and SLA technologies are quite similar. The main difference is the source of the light to be used. DLP printing technology has a projector located in the bottom of the resin pool instead of the ultraviolet laser [24]. In the SLA, the laser beam scans the layer, while the projector in the DLP acts on the entire layer surface at one time, resulting in faster print speeds. However, SLA is more suitable for the parts requiring high resolution. In DLP technology, since projected images of each layer are composed of pixels, small quadratic volumes form at the layer edges. In DLP, the projector's resolution is directly related to print quality and print volume.

### ***2.3.3 Binder Jetting***

In this technology, a liquid binding agent is used to bond the materials together. Binder is added on the powder material, and a solid layer is obtained [25]. The printer platform is lowered by one layer, and the powder material is laid on the previously formed layer. This process is repeated in a loop, and the production of the object is completed. Metallic, ceramic, and sand materials can be used in this technology and are suitable for the production of large parts. Since there is no heating operation in this technology, dimensional distortions due to thermal effect do not occur. As in the SLS technology, metal powders serve as support and therefore no support structures are needed. Binder jetting also allows for the production of colored parts and offers low cost. The parts printed by metal binder jetting show high porosity, which adversely affects the mechanical properties of the parts. Compared to other 3D printer methods, binder jetting allows fewer material types to be used, which is another limitation of this technology.

### **2.3.4 Polyjet**

Another 3D printing technology used in the production of 3D objects with photopolymer resin material is polyjet. In addition to being used to produce colored parts, it is a printing technique with high speed that can print more than one material at the same time. Thus, parts having different mechanical properties can be manufactured in one piece. This technology, which is ideal for the production of parts with smooth surfaces and detailed geometries, can be considered as a combination of the 2D inkjet and SLA printing technologies. Thanks to polyjet technology, which allows the use of different materials at the same time, the support materials can be easily removable, even in a water-soluble form [26]. Thus, removing the support structures is effortless, and no marks/residuals remain on the surface of the fabricated part at the end of the removing process.

### **2.3.5 Fused Deposition Modeling (FDM)**

FDM is the most common 3D printer technology for fabricating prototypes and functional parts among many different desktop-type models [27]. This technology, also known as fused filament fabrication, generally uses filaments made from PLA and ABS materials. In the FDM process, one end of the filament is placed in the nozzle, and it is waited until the printing temperature is reached. The thermoplastic filament is then extruded and pressed into the printing table. The nozzle moves and forms the object layer by layer according to the G-codes [28]. The process ends with removing the support structures as in the most of the 3D printer technologies. Multicolor printing can be done by multiple-nozzle FDM printers, and the support structures can be printed using a dissolvable material, which makes removing the support structures easier. In some parts printed with this technology, layer traces can be seen on the outer surface of the object (stair effect). Surface roughness can be reduced by hand sanding at the post-processing stage. Robust and functional parts can be obtained by this technology. FDM, which has a lower printing speed compared to SLA, has become very popular thanks to its ease of use, environmental friendliness, relatively low cost, and high mechanical, thermal, and chemical properties.

### **2.3.6 Selective Laser Sintering (SLS)**

SLS technology is based on the principle of binding the powdered material by sintering with a laser beam. In SLS technology, the material powders are fused together without being completely dissolved [29]. The non-sintered powders serve as a support structure and are removed from the part at the end of the process. SLS technology allows the use of a wide variety of materials such as metal, nylon,

ceramic, and glass. Internal stresses can occur on the parts produced by SLS so that the stress relief annealing can be made [30]. This technology, which is popular in the 3D printing industry, requires a powerful laser source, which makes it costly. Direct metal laser sintering technology has been developed with some changes in SLS technology [31]. With this technology, successful results can be obtained in the fusing of the materials with micro dimensions and in the production of thin structures.

### ***2.3.7 Selective Laser Melting (SLM)***

SLM technology is very similar to SLS technology, but in SLM, a complete melting process is performed instead of sintering [32]. This technology, which is popular in the aviation and medical sectors, is not suitable for home users because of its high cost. Titanium material with high biocompatibility and corrosion resistance that can be used in SLM technology is suitable for many biomedical applications. Apart from titanium, metals such as stainless steel and aluminum can also be used in SLM. However, materials such as plastic, glass, and ceramic used in SLS cannot be used in SLM. Process control of the SLM in which high-power laser is used is not easy and requires good temperature control during the process.

### ***2.3.8 Electron Beam Melting (EBM)***

EBM technology is based on the principle of fusing metal powders or filaments under a high-pressure atmosphere by a focused electron beam providing high energy and temperature [33]. A layer of fused powder is obtained according to the geometric data, and once the current layer has been exposed to the laser, the build platform lowers. At each step, the top of the layer is covered with metal powders, the fusion process is repeated, and new layers are obtained. By combining all layers, 3D objects are obtained. In EBM technology, the vacuum environment prevents collisions of electrons with the gas molecules, thus providing a positive effect on the process of reactive metals. At the same time, significant energy consumption is avoided. EBM is a highly preferred technology in the production of high-strength parts. It is possible to reduce residual stresses by preheating the material and the print bed and adjust the porosity of the part by adjusting the beam parameters.

### ***2.3.9 3D Bioprinting***

Three-dimensional bioprinting is the adaptation of 3D printing technology to print the tissues of living cells. Three-dimensional bioprinting is being developed for use



in tissue and organ transplantation in regenerative medicine applications. Technologies commonly used for this purpose are thermal inkjet [34], microextrusion [35], and laser-assisted printing [36]. The type of technology to be selected is determined according to the material type, cell viability, and surface resolution. Each technology has different advantages and constraints. The printers with thermal inkjet technology have low cost, high resolution, and fast printing capability. However, the materials must be in liquid form. In addition, low printing density is another limitation of this technology. Printers using microextrusion technology have the ability to deposit a very high cell density [37]. Also, it is the most common technology used for scaffold-free tissue spheroid bioprinting. However, the cell viability ratio, which is inversely proportional to the applied extrusion pressure, is lower than that of inkjet technology. The studies are underway to increase the printing speed and resolution in this technology [37]. It is possible to print materials within different viscosity ranges by laser-assisted printing technology. In addition, the problem of nozzle clogging encountered in other technologies is not seen in this technology. However, this technology requires rapid gelation kinetics for obtaining high resolution [38].

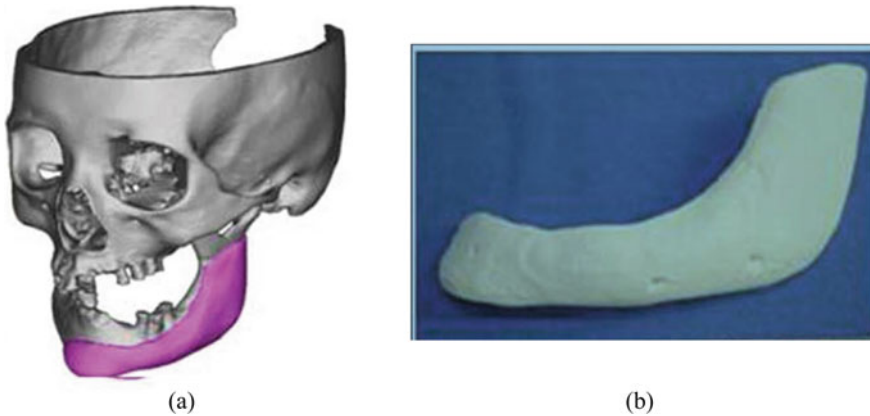
## 2.4 Biomedical Applications of 3D Printing Technology

Three-dimensional printing technology has a wide range of application field in the biomedical engineering such as tissue and organ fabrication [38], implants and prostheses production [39–41], drug formation in pharmaceutical research [42], and production of anatomical models for education and training purposes [43]. In this chapter, we focused on the products built by additive manufacturing technology, especially used in maxillofacial surgery, orthopedic surgery, and human arm prosthetics.

### 2.4.1 *Applications in Maxillofacial Surgery*

In maxillofacial surgery, maxillary and face defects are corrected by employing various surgical techniques and implants [44, 45]. It has been shown that a series of midface defects can be corrected by anterolateral thigh flap which is produced by rapid prototyping [46]. These implants have been reported to provide successful esthetic outcomes, and reduction in operation time and postoperative complications [46].

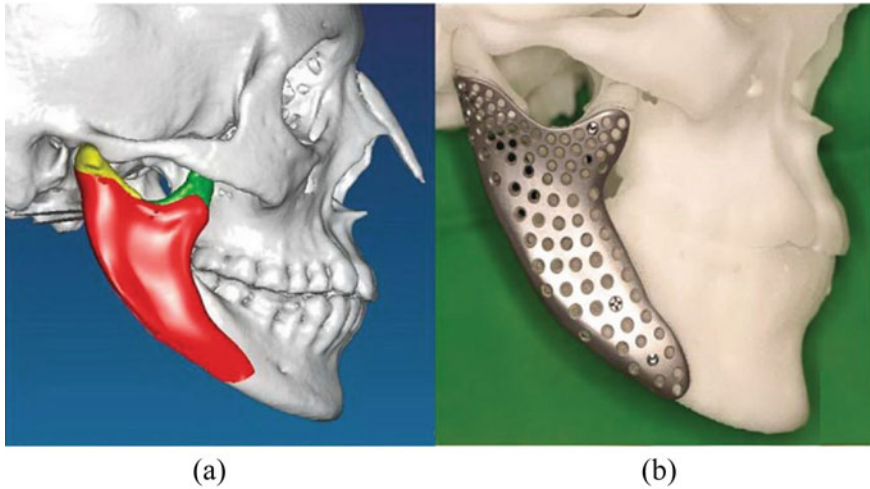
Saijo et al. treated several patients with mandibular deformity using the artificial bones manufactured by 3D printing technology [47]. They implanted custom-made inkjet-printed mandibular artificial bones into lower jaw area (Fig. 2.3). The authors also used rapid prototyping to produce a plaster model for surgery planning. They concluded that artificial bones had dimensional compatibility in all patients and partial union occurred between the artificial bones and host bone tissues without



**Fig. 2.3** Modeling and production of artificial mandibular bone. **a** The CAD model of the target area and **b** inkjet-printed custom-made artificial bone [This figure is reprinted from *J Artif Organs*. (2009; 12: 200–205) with permission] [47]

serious adverse reactions. They acquired reduced operational time ensured by the minimal need for size adjustment and fixing manipulation [47]. Three-dimensional printing technology is also utilized in the production of intermediate and final splints for maxillofacial surgeries. Sun et al. studied the computer-assisted surgical planning and splint fabrication using 3D printing [48]. In order to manufacture the splints, which can be considered as a surgical guide, 3D mandible models were created using CT and optical dental scanning data for patients undergone bimaxillary orthognathic surgery [48]. Splints were used for identifying the final position of the maxilla and mandible after re-positioning of split maxillofacial bones. The authors reported that they obtained acceptable accuracy and satisfactory aesthetics outcomes by using 3D printing techniques to produce intermediate splints [48]. Rapid prototyping is also used to produce bone implants in the treatment of mandible fractures or defects, which requires a precise reconstruction. Wang et al. reported a case of a patient with a square-shaped face and a bunch of symptoms such as the asymmetric face, collapse of the right face, and deviation in mouth opening, who had undergone mandibular outer cortex split osteotomy [49]. In the surgical intervention, the authors used a titanium mesh implant, which was designed based on the patient's mandibular anatomy, to replace a part of the mandible including ramus (Fig. 2.4). The implant was manufactured by means of a rapid prototyping method. After surgery, titanium implant ensured the complete accordance with the original bone. It was reported that the 3D printing technology facilitated the intervention for correcting the defects or fractures of the ramus in the mandible, which is commonly accepted as a critical complication of mandibular reduction and a challenging task because some surgeons have trouble in the formation of the original morphologic symmetry [49].

The 3D printing technique is also used to obtain 3D models of the skull or mandibula with various abnormalities. The models enable to plan surgery in which



**Fig. 2.4** Reconstruction of bone defects by the custom-specific implant. **a** The CAD model of the craniofacial structure and implant. **b** Custom-made implant [49]

pathological or traumatic deformities can be evaluated in 3D space, various treatment scenarios can be assessed, and clinical outputs can be predicted. Design and manufacture of the implants to be used in surgery can also be modified according to findings obtained from the models [50, 51].

Mehra et al. reported a series of case studies regarding the use of models in the correction of maxillofacial deformities [52]. Authors reported that a 16-year-old female patient had a progressive pathological lesion of the mandible (juvenile ossifying fibroma). Since there was significant destruction in the original mandible and its normal anatomic shape, the treatment and surgery decision had been made benefitting from 3D printing models. The models were also used as base geometries for bending of fixation plates [52].

### 2.4.2 Applications in Orthopedic Surgery

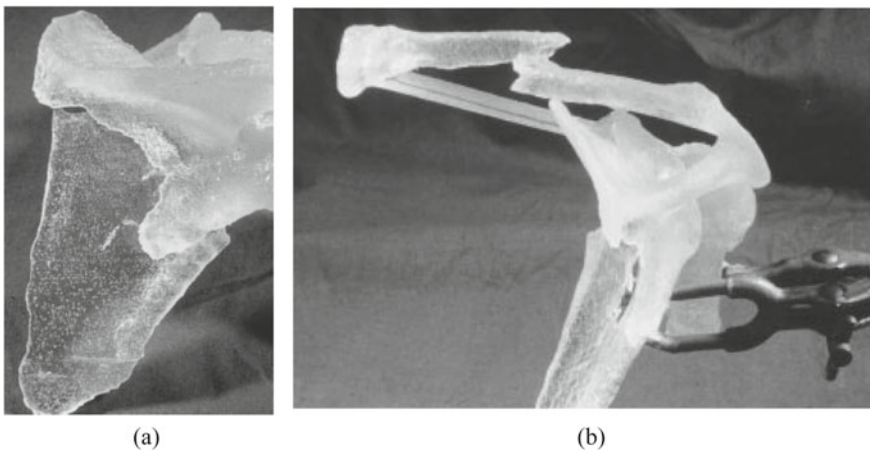
Three-dimensional printing technology is a useful tool for orthopedic surgical procedures in which the injuries with multiple bone fragmentation or bone deformities are treated. It was reported that although FDM or SLS provides reasonable manufacturing outcomes in terms of material properties, accuracy, and production time, SLA is the most widely used rapid prototyping technique in the field of orthopedic surgery [53].

Potamianos et al. reported a case study of a patient with a shoulder injury consisted of a double fracture of the clavicle and scapula [54]. Such an injury required surgical stabilization with plate and screw fixation. CT data of the bony parts of the shoulder were processed by fragmentation and segmentation. The solid model of the shoulder

was produced by a SLA machine. The reconstructed model showed that the fracture was not a floating shoulder type, clavicle had a complete transverse fracture, and scapula remained partially attached (Fig. 2.5). According to the evaluation made on the anatomical model, the researchers decided that the surgery is not essential, which enabled the patient was spared an unnecessary surgery [55]. This preoperative assessment based on the 3D model of shoulder fabricated by 3D printing saved time, cost, and labor.

Jeong et al. reported a case study of a patient with a midshaft fracture in the clavicle. Three-dimensional CT scans of both clavicles were obtained, and plastic models of fractured and intact clavicles were fabricated by a 3D printer [55]. A clavicular locking plate was contoured to the plastic model of the contralateral intact clavicle of the patient. Internal fixation of the fractured clavicle with the plate was implemented through surgical intervention. The authors reported that 3D printing techniques allowed for printing the contralateral mirror images and providing accurate prebent plates for a wide range of clavicular shapes besides the advantages of short surgery time and low cost [55].

Chareancholvanich et al. employed the additive manufacturing technique to produce an assistive guide for a total knee replacement task [56]. In their clinical study, they performed total knee replacement surgeries for around 80 patients for the treatment of knee osteoarthritis. A patient-specific splitting guide produced by rapid prototyping and conventional instrumentation was used in surgery. The patient-specific guide was designed based on preoperative MRI scans of the patients. These surgical guides were employed to improve the accuracy of alignment of the



**Fig. 2.5** Three-dimensional printed model of the shoulder. Oblique posterior view (a) and medial view (b) which show the fracture [This figure is reprinted from Proc. Inst. Mech. Eng. (Part H). (1998; 212: 383–393) with permission] [54]

total knee replacement. The authors reported that alignment results were satisfactory using the patient-specific guide and accuracy was comparable to that of the conventional instrumentation [57].

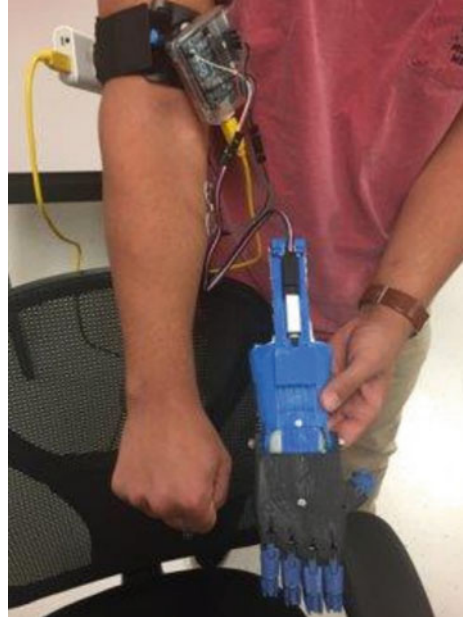
Surgical guide production using additive manufacturing in hip surgery is also becoming a common technique. Hananouchi et al. tested a surgical guide fabricated by rapid prototyping for insertion of the cup in total hip arthroplasty [57]. As the first step of work, the authors obtained CT scans of the pelvis of 24 patients with osteoarthritis, osteonecrosis, and rheumatoid arthritis and designed the surgical guide preoperatively. Rapid prototyping was utilized to fabricate the guide. The authors stated that the cup accuracy sustained throughout the surgery was acceptable using the 3D printed guide [57].

Additive manufacturing technology is also used in hand surgery. Fuller et al. presented a step-by-step description for the design of bone reduction clamp which was manufactured by 3D printing technology [58]. The authors changed the design of traditional bone reduction forceps so that it provided multiple points of contact at the fracture site and stabilized the fracture by multiple force vectors. They also considered the new design as an assembly of a series of smaller parts that could be connected to each other to reduce the exposure of clamping forces of the tissues. Following a few adaptations in the design, the authors produced the model by FDM 3D acrylic printer to obtain a plastic prototype of design. The prototype was tested on bony practice models and found to be not sufficiently rigid for clinical purposes. Another prototype, which had three components, was printed using stainless steel and the components assembled to each other after manufacturing. The authors highlighted that the main goals of these kinds of attempts were to increase patient safety and decrease operation time [58].

### ***2.4.3 Applications in Upper Limb Prosthetics***

Upper limb prosthetics are artificial devices that are built to regain functions of missing limbs. These kinds of mechanical devices allow amputated people to handle and manipulate objects with varying shapes to help the user perform fundamental daily tasks. The factors including mechanical structure, actuation method, sensing capability, and control features are the main determinants in the functionality and performance of prosthetics devices. Novel technologies such as 3D printing and other additive manufacturing techniques are improving the design and manufacturing features of prosthetics [59–61]. Hetherington and his colleagues designed and produced a prosthetic limb utilizing additive manufacturing technology [62] (Fig. 2.6). The mechanically operated prosthetic hand was produced by 3D printing and controlled by muscle activation recorded from electromyography (EMG) sensors. The actuation of the automated prosthetic hand was stimulated by forearm muscles [62]. These kinds of assistive devices made by new generation production techniques are mostly light, affordable, customizable, and replaceable.

**Fig. 2.6** Three-dimensional printed EMG-driven prosthesis developed and built by SenseTech [This figure is reprinted from Senior Theses 255, 2018 with permission] [62]



Another study based on a 3D printing implementation in human arm prosthetics was carried out by Low et al. [63]. The authors built a soft finger actuator which was driven by pneumatic means in the order of enabling the user to grasp objects. The actuators were fabricated by the 3D printing technique. The authors showed that by using this technique, lightweight actuators could be produced and a compliant gripping with acceptable stress could be achieved. Arjun et al. employed 3D printing technique in the manufacturing of a low-cost and functional prosthetic hand to have the ability to separately manipulate the fingers and grasp a variety of objects [64]. The authors considered that the technique allowed reducing the cost of customizable parts. According to the study, the prosthesis was able to grasp various structures with different shapes such as the cube, sphere, and cylinder. The authors also reported repeatable grip times with low standard deviations [64].

Prosthetics for children require frequent modifications and adaptations due to constant anthropometric changes. Zuniga et al. developed a 3D printed prosthetic hand for children with upper limb reductions called “Cyborg Beast” [65]. They reported that they were able to produce a low-cost prosthetic device that may produce a significant positive impact on the quality of life of children with upper limb reductions, especially from low-income, uninsured families. Although such low-cost and rapidly producible devices show promising outcomes, Ten Kate et al. stated in their review paper that the lack of evidence with respect to the user acceptance, functionality and durability of the 3D-printed hands are a major drawback of the 3D printed upper limb prosthetics [66]. Moreover, they claimed that 3D printing is not

necessarily cheap compared to injection molding, which can be seen as another disadvantage of the 3D printed prosthetics. Individualization of the prosthetic designs is seen as a major advantage of such medical devices.

## 2.5 Conclusions

Biomedical devices and medical products usually have free-form surfaces and patient-specific design features. Three-dimensional printing technologies, which enable the production of objects with complex geometries and do not require the installation of the production line and mold manufacturing, are an effective approach for biomedical applications. In the 3D printing sector, continuous progress has been observed in the area of printer technology, material type, maintenance, software, and methods. The market value of this developing area is expected to be almost 27 million dollars by 2019 [67].

Three-dimensional printing technology has been effectively used to fabricate customized implants, anatomical models, and surgical guides. Reduction of operation time and hospitalization duration, improvement of the surgery planning and education, allowing for the production of patient-specific complex-shaped devices consistent with the anatomical structure are some of the merits of the technique.

In clinical applications, high-resolution 3D printers are preferred to print biomaterials although high prices of these printers limit the use of this technology [68, 69]. Furthermore, post-processing applied after the printing process negatively affects the cost and production speed. This is another factor that restricts the use of 3D printing technology in the medical field.

## 2.6 Future Research Directions

The decrease in cost and fabrication duration and printing control for remote implementations might be improved in the near future. Production of the functional human body tissues would also be improved in future studies. Interaction of living and printed tissues would affect the developments of the technique. More complex and heterogeneous structures produced by improved bio-fabrication method are candidates for the next applications. In addition, novel design concepts are being developed in order to reduce post-processing stages, and also, the studies on support structures, which can be dissolved in aqueous solutions, are continued [70, 71].

The future research attempts are anticipated to focus on acceptable standardization of testing to enhance the commercialization of the products besides the attempts for reduction of manufacturing costs of biomedical devices [72, 73]. In addition, in the biomedical industry, as well as automotive, aerospace, and other manufacturing areas, the fabricated multi-material components might likely be developed [74]. The improvement of compatibility between workable materials and printing conditions



is another potential future trend in order for the lifelong survival of the printed devices. Academics and industrial enterprises should also work on the improvement of feasibility and accuracy of fabrication of the microstructures especially for the surgical implementations [75].

## References

1. Mohammed MI, Fitzpatrick AP, Gibson I (2017) Customised design of a patient specific 3D printed whole mandible implant. *KnE Eng* 2(2):104–111
2. Dombroski CE, Balsdon ME, Froats A (2014) The use of a low cost 3D scanning and printing tool in the manufacture of custom-made foot orthoses: a preliminary study. *BMC Res Notes* 7(1):443
3. Dawood A, Marti BM, Sauret-Jackson V, Darwood A (2015) 3D printing in dentistry. *Br Dent J* 219(11):521
4. Malik HH, Darwood AR, Shaunak S, Kulatilake P, Abdulrahman A, Mulki O, Baskaradas A (2015) Three-dimensional printing in surgery: a review of current surgical applications. *J Surg Res* 199(2):512–522
5. Khan FA, Narasimhan K, Swathi C, Mustak S, Mustafa G, Ahmad MZ, Akhter S (2019) 3D printing technology in customized drug delivery system: current state of the art, prospective and the challenges. *Curr Pharm Des* 561:1–8
6. Surmen K, Ortes F, Arslan YZ (2016) Design and production of subject specific insole using reverse engineering and 3D printing technology. *Int J Eng Sci Invent* 5(12):11–15
7. Damianou C, Giannakou M, Yiallouras C, Menikou G (2018) The role of three-dimensional printing in magnetic resonance imaging-guided focused ultrasound surgery. *Digit Med* 4:1–22
8. Canzi P, Marconi S, Manfrin M et al (2018) From CT scanning to 3D printing technology: a new method for the preoperative planning of a transcutaneous bone-conduction hearing device. *Acta Otorhinolaryngol Ital* 38:251–256
9. Zhang B, Luo Y, Ma L et al (2018) 3D bioprinting: an emerging technology full of opportunities and challenges. *Bio-Des Manuf* 1–12
10. Levato R, Visser J, Planell JA, Engel E, Malda J, Mateos-Timoneda MA (2014) Biofabrication of tissue constructs by 3D bioprinting of cell-laden microcarriers. *Biofabrication* 6(3):035020
11. Morris S (2018) Future of 3D printing: How 3D bioprinting technology can revolutionize healthcare? *Birth Defects Res* 110(13):1098–1101
12. Han Y, Wang F, Wang H, Jiao X, Chen D (2018) High-strength boehmite-acrylate composites for 3D printing: reinforced filler-matrix interactions. *Compos Sci Technol* 154:104–109
13. Eckel ZC, Zhou C, Martin JH, Jacobsen AJ, Carter WB, Schaedler TA (2016) Additive manufacturing of polymer-derived ceramics. *Science* 351:58–62
14. Garcia-Gonzalez D, Garzon-Hernandez S, Arias A (2018) A new constitutive model for polymeric matrices: application to biomedical materials. *Compos B Eng* 139:117–129
15. Suntornnond R, An J, Chua CK (2017) Bioprinting of thermoresponsive hydrogels for next generation tissue engineering: a review. *Macromol Mater Eng* 302:1600266
16. Martin JH, Yahata BD, Hundley JM, Mayer JA, Schaedler TA, Pollock TM (2017) 3D printing of high-strength aluminium alloys. *Nature* 549(7672):365
17. Cantrell JT, Rohde S, Damiani D, Gurnani R, DiSandro L, Anton J, Ifju PG (2017) Experimental characterization of the mechanical properties of 3D-printed ABS and polycarbonate parts. *Rapid Prototyping J* 23(4):811–824
18. Ho CMB, Mishra A, Lin PTP, Ng SH, Yeong WY, Kim YJ, Yoon YJ (2017) 3D printed polycaprolactone carbon nanotube composite scaffolds for cardiac tissue engineering. *Macromol Biosci* 17(4):1600250



19. Bas O, D'Angella D, Baldwin JG, Castro NJ, Wunner FM, Saïdy NT, Hutmacher DW (2017) An integrated design, material, and fabrication platform for engineering biomechanically and biologically functional soft tissues. *ACS Appl Mater Interfaces* 9(35):29430–29437
20. Asaoka K, Kuwayama N, Okuno O, Miura I (1985) Mechanical properties and biomechanical compatibility of porous titanium for dental implants. *J Biomed Mater Res* 19:699–713
21. Bandyopadhyay A, Bose S, Das S (2015) 3D printing of biomaterials. *MRS Bull* 40(2):108–115
22. Hull CW (1986) Apparatus for production of three-dimensional objects by stereolithography, 11 Mar. U.S. Patent No. 4,575,330
23. Chaput C, Chartier T (2007) Fabrication of ceramics by stereolithography. *RTejournal-Forum für Rapid Technologie* 4(1)
24. Hornbeck LJ (1987) Spatial light modulator and method, 5 May. U.S. Patent No. 4,662,746
25. Hanssen J, Moe ZH, Tan D, Chien OY (2013) Rapid prototyping in manufacturing. In: *Handbook of manufacturing engineering and technology*, pp 1–16
26. Adamidis O, Alber S, Anastasopoulos I (2018) Investigation into 3D printing of granular media. In: *Physical modelling in geotechnics, Volume 1: Proceedings of the 9th International Conference on Physical Modelling in Geotechnics (ICPMG 2018)*, 17–20 July 2018. CRC Press, London, United Kingdom
27. Masood SH (2014) Advances in fused deposition modeling. In: *Comprehensive materials processing*, pp 69–91
28. Crump SS (1992) Apparatus and method for creating three-dimensional objects, 9 June. U.S. Patent No. 5,121,329
29. Beaman JJ, Carl RD (1990) Selective laser sintering with assisted powder handling, 3 July. U.S. Patent No. 4,938,816
30. Cansiz E, Arslan YZ, Turan F, Atalay B (2014) Computer-assisted design of patient-specific sagittal split osteotomy guide and soft tissue retractor. *J Med Biol Eng* 34(4):363–367
31. Agarwala M, Bourell D, Beaman J, Marcus H, Barlow J (1995) Direct selective laser sintering of metals. *Rapid Prototyping J* 1(1):26–36
32. Meiners W, Wissenbach K, Gasser A (2001) Selective laser sintering at melting temperature, 10 Apr. U.S. Patent No. 6,215,093
33. Chua CK, Leong, KF (2014) 3D printing and additive manufacturing: principles and applications (with companion media pack) of rapid prototyping, 4th edn. World Scientific Publishing Company
34. Cui X, Boland T, DD'Lima D, Lotz M (2012) Thermal inkjet printing in tissue engineering and regenerative medicine. *Recent Pat Drug Deliv Formulation* 6(2):149–155
35. Panwar A, Tan LP (2016) Current status of bioinks for micro-extrusion-based 3D bioprinting. *Molecules* 21(6):685
36. Guillotin B et al (2010) Laser assisted bioprinting of engineered tissue with high cell density and microscale organization. *Biomaterials* 31(28):7250–7256
37. Rashidi H, Hay DC (2016) Generation and application of 3D culture systems in human drug discovery and medicine. *Stem Cells Toxicol Med* 265–287
38. Murphy SV, Atala A (2014) 3D bioprinting of tissues and organs. *Nat Biotechnol* 32:773–785
39. Mavroidis C, Ranky RG, Sivak ML, Patriiti BL, Dipisa J, Caddle A, Gilhooly K, Govoni L, Sivak S, Lancia M (2011) Patient specific ankle-foot orthoses using rapid prototyping. *J Neuroeng Rehabil* 8(1):1–11
40. Li H, Qu X, Mao Y, Dai K, Zhu Z (2015) Custom acetabular cages offer stable fixation and improved hip scores for revision THA with severe bone defects. *Clin Orthop Relat Res* 473(3):731–740
41. Boileau P, Watkinson DJ, Hatzidakis AM, Balg F (2005) Grammont reverse prosthesis: design, rationale, and biomechanics. *J Shoulder Elbow Surg* 14(1):147–161
42. Alhnan MA, Okwuosa TC, Sadia M, Wan K-W, Ahmed W, Arafat B (2016) Emergence of 3D printed dosage forms: opportunities and challenges. *Pharm Res* 33(8):1817–1832
43. McGurk M, Amis A, Potamianos P, Goodger N (1997) Rapid prototyping techniques for anatomical modelling in medicine. *Ann R Coll Surg Engl* 79:169–174

44. Ortes F, Cansiz E, Arslan YZ (2019) Computer-aided design of subject-specific dental instruments for preoperative virtual planning in orthognathic surgery. In: *Biomufacturing*. Springer, Cham, pp 89–102
45. Cansiz E, Turan F, Arslan YZ (2016) Computer-aided design and manufacturing of a novel maxillofacial surgery instrument: application in the sagittal split osteotomy. *J Med Devices* 10(4):044505
46. Han SW, Wang ZY, Hu QG, Han W (2014) Combined use of an anterolateral thigh lap and rapid prototype modeling to reconstruct maxillary oncologic resections and midface defects. *J Cranio-Maxillofac Surg* 25(4):1147–1149
47. Saijo H, Igawa K, Kanno Y et al (2009) Maxillofacial reconstruction using custom-made artificial bones fabricated by inkjet printing technology. *J Artif Organs* 12:200–205
48. Sun Y, Luebbbers HT, Agbaje JO et al (2013) Accuracy of upper jaw positioning with intermediate splint fabrication after virtual planning in bimaxillary orthognathic surgery. *J Craniofac Surg* 24(6):1871–1876
49. Wang G, Li J, Khadka A et al (2012) CAD/CAM and rapid prototyped titanium for reconstruction of ramus defect and condylar fracture caused by mandibular reduction. *Oral Surg Oral Med Oral Pathol Oral Radiol* 113(3):356–361
50. Azuma M, Yanagawa T, Ishibashi-Kanno N, Uchida F, Ito T, Yamagata K et al (2014) Mandibular reconstruction using plates prebent to fit rapid prototyping 3-dimensional printing models ameliorates contour deformity. *Head Face Med* 10:45
51. Park SW, Choi JW, Koh KS, Oh TS (2015) Mirror-imaged rapid prototype skull model and pre-molded synthetic scaffold to achieve optimal orbital cavity reconstruction. *J Oral Maxillofac Surg* 73(8):1540–1553
52. Mehra P, Miner J, D’Innocenzo R et al (2011) Use of 3-D stereolithographic models in oral and maxillofacial surgery. *J Maxillofac Oral Surg* 10(1):6–13
53. Popescu D, Laptoiu D (2016) Rapid prototyping for patient-specific surgical orthopaedics guides: a systematic literature review. *Proc Inst Mech Eng Part H J Eng Med* 230(6):495–515
54. Potamianos P, Amis AA, Forester AJ, McGurk M, Bircher M (1998) Rapid prototyping for orthopaedic surgery. *Proc Inst Mech Eng Part H* 212:383–393
55. Jeong HS, Park KJ, Kil KM et al (2014) Minimally invasive plate osteosynthesis using 3D printing for shaft fractures of clavicles: technical note. *Arch Orthop Trauma Surg* 134:1551–1555
56. Chareancholvanich K, Narkbunnam R, Pornrattanameewong C (2013) A prospective randomised controlled study of patient-specific cutting guides compared with conventional instrumentation in total knee replacement. *Bone Joint J* 95:354–359
57. Hananouchi T, Saito M, Koyama T, Hagio K, Murase T, Sugano N et al (2009) Tailor-made surgical guide based on rapid prototyping technique for cup insertion in total hip arthroplasty. *Int J Med Robot* 5(2):164–169
58. Fuller SM, Butz DR, Vevang CB, Makhlof MV (2014) Application of 3-dimensional printing in hand surgery for production of a novel bone reduction clamp. *J Hand Surg Am* 39:1840–1845
59. Dollar AM, Howe RD (2006) A robust compliant grasper via shape deposition manufacturing. *IEEE/ASME Trans Mechatron* 11:154–161
60. Hofmann M, Harris J, Hudson SE, Mankoff J (2016) Helping hands: requirements for a prototyping methodology for upper-limb prosthetics users. In: *Proceedings of the 2016 CHI conference on human factors in computing systems (CHI ’16)*. ACM, New York, NY, USA, pp 1769–1780
61. Gafford J, Ding Y, Harris A, McKenna T, Polygerinos P, Holland D et al (2014) Shape deposition manufacturing of a soft, atraumatic, deployable surgical grasper. *J Med Devices* 8:030927
62. Hetherington AT (2018) Integration of a sensory driven model for hand grasp function in 3D printed prostheses. Senior theses, 255
63. Low JH, Ang MH, Yeow CH (2015) Customizable soft pneumatic finger actuators for hand orthotic and prosthetic applications. In: *Proceedings of IEEE ICORR, Singapore*, pp 380–385
64. Arjun A, Saharan L, Tadesse Y (2016) Design of a 3D printed hand prosthesis actuated by nylon 6-6 polymer based artificial muscles. In: *IEEE international conference on automation science and engineering (CASE)*, pp 910–915

65. Zuniga J, Katsavelis D, Peck J, Stollberg J, Petrykowski M, Carson A, Fernandez C (2015) Cyborg beast: a low-cost 3d-printed prosthetic hand for children with upper-limb differences. *BMC Res Notes* 8(1):10
66. Ten Kate J, Smit G, Breedveld P (2017) 3D-printed upper limb prostheses: a review. *Disabil Rehabil Assistive Technol* 12(3):300–314
67. Kim H (2018) Market analysis and the future of sustainable design using 3D printing technology. *Arch Des Res* 31:23–35
68. Singh S, Singh G, Prakash C, Ramakrishna S (2020) Current status and future directions of fused filament fabrication. *J Manuf Proc*, 55: 288–306
69. Pandey A, Singh G, Singh S, Jha K, Prakash C (2020) 3D printed biodegradable functional temperature-stimuli shape memory polymer for customized scaffoldings. *J Mech Behav Biomed Mater*, 103781
70. Kim M-K et al (2018) Ink composition for 3D printing support and 3D printing manufacturing method using the same. U.S. Patent Application No. 15/745, 736
71. Swanson WJ, Mannella DF, Schloesser RG. Support structure removal system. U.S. Patent Application No. 10/016, 945
72. Singh S, Singh M, Prakash C, Gupta MK, Mia M, Singh R (2019) Optimization and reliability analysis to improve surface quality and mechanical characteristics of heat-treated fused filament fabricated parts. *Int J Adv Manuf Technol* 1–16
73. Singh S, Prakash C, Ramakrishna S (2019) 3D printing of polyether-ether-ketone for biomedical applications. *Eur Polym J* 114:234–248
74. Singh S, Singh N, Gupta M, Prakash C, Singh R (2019) Mechanical feasibility of ABS/HIPS-based multi-material structures primed by low-cost polymer printer. *Rapid Prototyping J* 25(1):152–161
75. Poomathi N, Singh S, Prakash C, Patil R, Perumal PT, Barathi VA, Balasubramanian KK, Ramakrishna S, Maheshwari NU (2018) Bioprinting in ophthalmology: current advances and future pathways. *Rapid Prototyping J* 1–20

**Dr. Hasan Kemal Surmen** is an Assistant Professor in the Vocational School of Technical Sciences, Istanbul University-Cerrahpasa, Istanbul, Turkey. He has received his Ph.D. in Mechanical Engineering Department from Istanbul University, Istanbul, Turkey. His research areas are computer-aided design and engineering, orthosis design, additive manufacturing, and 3D scanning. He has authored more than 10 journal and conference papers, one book and two chapters.

**Faruk Ortes** is a Ph.D. candidate and working as Research Assistant in the Department of Mechanical Engineering, Istanbul University-Cerrahpasa, Turkey. His research interests span muscle mechanics, computational biomechanics, applied mechanics, finite element analysis, as well as design and production of surgical instruments. He has authored more than five research papers in various journals and authored five chapters. He also reviewed many scientific papers from a wide variety of international journals.

**Dr. Yunus Ziya Arslan** is working as Associate Professor in the Department of Mechanical Engineering, Istanbul University-Cerrahpasa, Turkey. He received his B.Sc. degree in 2002, M.Sc. degree in 2005, and Ph.D. degree in 2009 all from the Mechanical Engineering Department, Istanbul University, Turkey. He spent six months at the Human Performance Laboratory of the University of Calgary as a visiting Ph.D. student (2008) and one year at the BioMotion Center of Karlsruhe Institute of Technology as a visiting professor (2018–2019). He is working in the areas of musculoskeletal biomechanics, computational modeling and simulation of human movement, computer-aided analysis of movement disorders, mechanical design and production of biomedical devices. He has six patents in his name and authored more than 35 research papers in various journals and authored eight chapters. He is a reviewer of various international journals.

# Chapter 3

## Thermal Effects in 3D Printed Parts



Prasansha Rastogi, Swaroop Gharde,  
and Balasubramanian Kandasubramanian

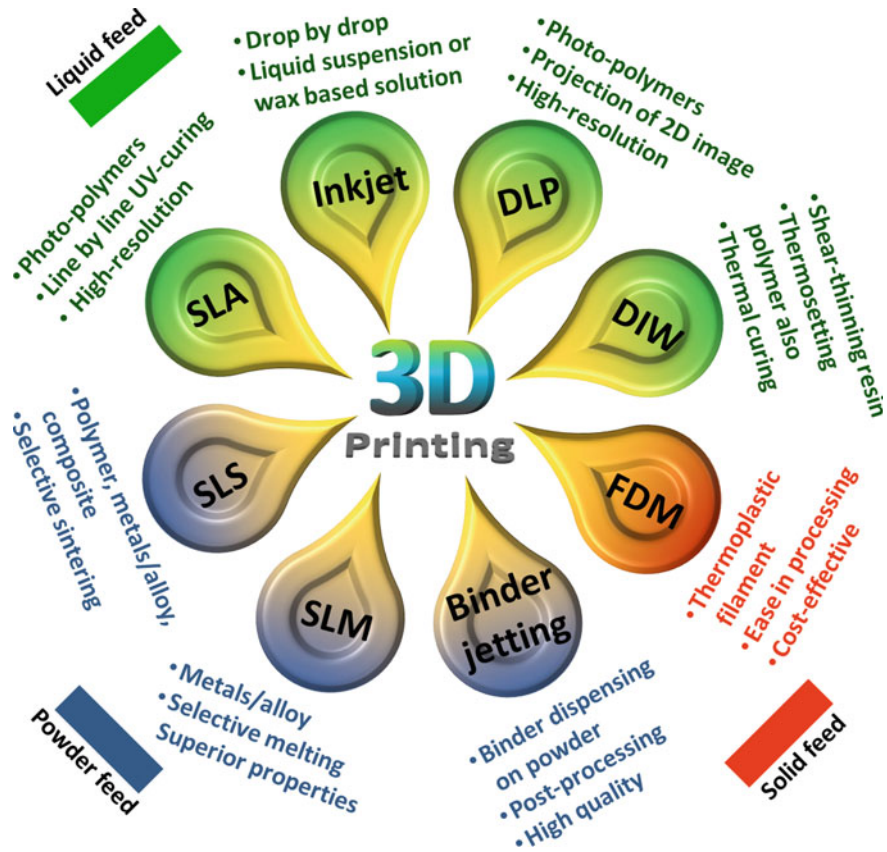
### 3.1 Introduction

Idiosyncrasy, intricacy, precise architecture, and caricatures of nature's beauty have always been a subject of curiosity for the world's ingenious minds and thus pilot the futuristic growth of technology. Same inquisitiveness by Charles Hulls in 1986 might have led to the invention of printing-based manufacturing of products. It has marked the onset of revolution in manufacturing tactics and proficiency in intricate designing, on-demand printing, controllable patterning, customize products in finite time boundary [1, 2]. According to MarketsandMarkets assessment, 3D printing will burgeon to occupy US \$32.78 billion market in forthcoming years (i.e., by 2023) witnessing 25.76% growth from 2017 [3]. Central to 3D printing manufacturing lies in its successive layering of materials—powders, liquids, or solids followed by crosslinking or coalescence steered solidification. Selective laser melting (SLM), binder jetting, and selective laser sintering (SLS) are the subset of powders-built entities which are thereupon sintered for densification (Fig. 3.1). Moreover, stereolithography (SLA), multi-material [4] printing, direct ink writing (DIW), and digital light processing (DLP) are labeled under liquid-feed printing (Fig. 3.1). However, fused deposition modeling (FDM) is typecast within solid-supplied printing on account of its filament-feed which then melts by heater coils around nozzle and raster dispensing follows for three-dimensional product [5, 6] (Fig. 3.1). Input materials for feed in above-categorized techniques are polylactic acid (PLA), polyamide (nylon, PA), polycarbonate (PC), polyurethane (PU), acrylonitrile butadiene styrene (ABS), polydimethylsiloxane (PDMS), copper (Cu), gold (Au), aluminum (Al), silver (Ag), polymethyl methacrylate (PMMA), gelatin, lutrol

---

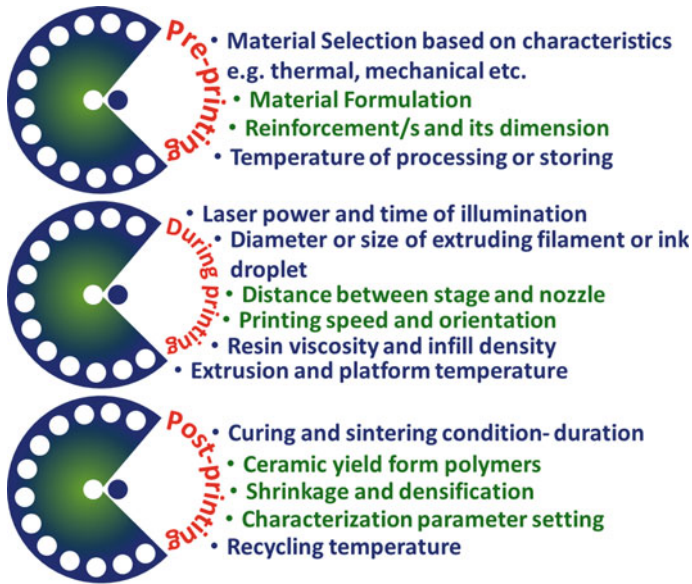
P. Rastogi · S. Gharde · B. Kandasubramanian (✉)

Rapid Prototyping Laboratory, Department of Metallurgical and Materials Engineering, Defence Institute of Advanced Technology (DU), Ministry of Defence, Girinagar, Pune 411025, India  
e-mail: [meetkbs@gmail.com](mailto:meetkbs@gmail.com)



**Fig. 3.1** Classification of 3D printed technique based on feed material, i.e., solid (filament), liquid (resin, solution), and powder

F127, chitosan, alginate, fibrinogen, collagen, polyether ether ketone (PEEK), polyimide (PI), polyester acrylate, composites and continued [7–17]. Materials utilized during printing have been subjected to varied parameters whose change in magnitude alters design output (**parameters depicted in Fig. 3.2**). Yadav et al. studied the effect of varied pattern structure (foliated complex cross-lamellar, nacre, and cross-lamellar on the mechanical properties where lastly defined design (owing to its orientational morphology) obtained improved toughness and wear rate ( $1.2 \times 10^{-4} \text{ mm}^3/\text{N m}$ ) [18]. Kuo et al. had recorded the effect of alteration in reinforcement (steric maleic anhydride copolymer, carbon black, titanium oxide, methacrylate butadiene styrene) in starch-ABS composite for enhancement in associated properties (heat distortion  $T$ , impact strength, flexural strength and modulus, thermal resistance, stability, tensile strength) owing to change in interactions [19]. Geng et al. had differed extrusion speed and characterized its effect on material after solidification (i.e., low speed  $\rightarrow$  pressure dropped  $\rightarrow$  improper flow of filament mismatch between feed rate and melt



**Fig. 3.2** Parameters (pre-, during, post-printing) investigated for determining the effect on final properties of entity

outlet rate  $\rightarrow$  porosity) [20]. Jayanth and Senthil had investigated variation in the thickness and width of printed sensor on capacitance performance. They reported proportionality relation between variables and outcome due to dependency of area in capacitance calculation which was further enhanced with carbon black additions [21]. These are some few variables that attune the performance of printed entity related to mechanical, electrical, thermal, and other related features.

3D printing is increasingly infiltrating into daily routine where custom-built designs have extensively been preferred for end-user utilization. Low  $T$  workability, convoluted (micro-) patterning ease in control over designing, and other variegated specialities, 3D printing has secured its prominence in electronics industry [22–24]. Utilization is burgeoning toward industry, e.g., in aerospace (aircrafts), consumer items (hearing aids, visual aids), vehicles, etc., due to materials (composites or alloys mechanical performance, etc.) [25–27]. The fascination of imitating nature synthetically has always thrilled scientists from all over the world to invest their time and money in bio-mimicking application from 3D printing due to fine engineering, e.g., nacre structure, molluscan construction, crustaceans, bones, fish scales, etc. [28–32]. Adding to it, biomedical utilization of 3D printing cannot remain untouched and research is extensively progressing in its every aspects. Multifarious bioink composition has been experimented for developing scaffolds for tissue engineering (eyes, heart, brain, cartilage, bones, etc.), drug delivery, transplantation, constructing proximity environment for studying various types of cancer, tumor, and other diseases (to develop treatment) along with various functions [12, 33–35]. The innovation

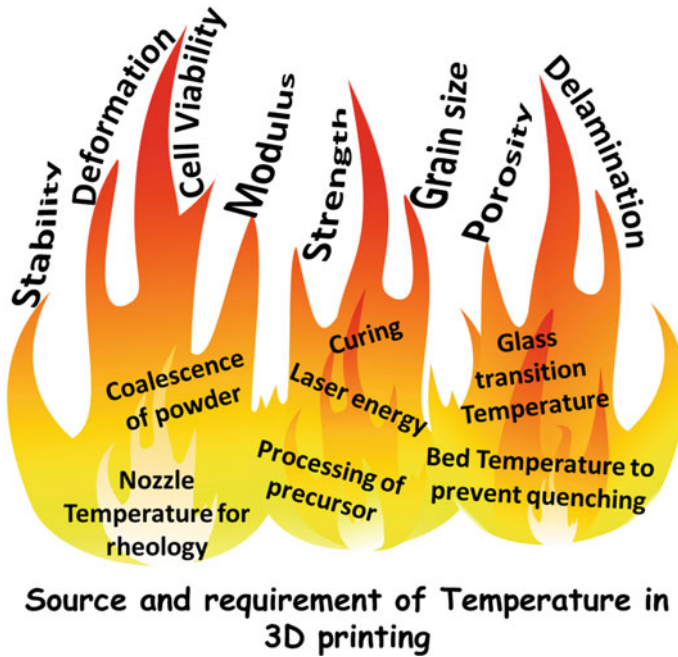
of additive manufacturing has not been restricted to aforesaid but expanding into other domains of space technology, textiles, jewelry, robotics, sensors, etc. [36, 37]. Though 3D printing bestows customized products, ease of production in small lots, high resolution, accommodating wide range of materials, multi-hues, multiple materials, multi-combinations of properties, cost-effective, etc., still the techniques have been challenged in certain aspects. Photopolymers in SLA have posed a limit in usability owing to their degrading, brittleness, intolerance toward heat, etc., along with compulsion of incorporating photosensitive groups for photocuring [7, 10]. FDM restricts to only filaments feeding and also the production defect, i.e., staircase effect (rough surface), low resolution printing, etc., that can contribute to interfacial weakness, distortion, etc. [38]. In addition, powder-feed techniques, i.e., SLS, SLM, binder jetting, have to confront densification complication (as adjacent particles necks down by laser rendering porosity or binder evaporation) along with post-processing like sintering, heat treatment, etc.; hence, pre-requisition of materials stability is exhorted [10, 38]. In general, 3D printing equips with user-designed product but necessitates amelioration in precision, time management (layer-by-layer print), support structures, and post-processing for further enhancement in its caliber.

This chapter scrutinizes pivotal aspect of 3D printing, i.e., temperature or thermal outlines practiced over from its cradle to finished product. Since temperature is scaled as one of the many influential parameters driving the course of printing, therefore, taking the stimulus of variable, concomitant effects of same has been categorized in pre-, during, post-printing operation. Furthermore, it also briefly elucidates on some extended temperature functions, e.g., in recycling, etc. The chapter in addition delves into fundamental features of temperature in bioprinting which engineer cells onto scaffolds for variety applications. Optimal magnitude setting of temperature while formulation, stage control, and post-treatments renders printed structure its efficient output.

## 3.2 Thermal Parameters in 3D Printing

Multifarious end-user applications of 3D printing products in either domain are engineered with an aspiration to attain long-lasting and steadfast performance. These properties are ensured in design, during different stages of printing which consists of pre-printing stage, printing stage, and post-printing stage. Further, these stages are governed by distinct parameters which are pivotal for any design and property optimization (Fig. 3.3). In myriads of parameters that are specific to material, printer setup, or during printing operation, temperature has significant influence in modulating characteristics of printed entity.

### Temperature impact on the post-printing characteristics of the 3D structure



### Source and requirement of Temperature in 3D printing

**Fig. 3.3** Some sources and requirement of temperature which governs end properties of printed product

#### 3.2.1 Pre-printing Thermal Characteristics

This section encloses features related to the selection of material, their innate properties, pre-printing processing, and printing stage conditions which pilot thermal or temperature attributes.

Considering innate thermal characteristics, e.g., glass transition temperature ( $T_g$ ), decomposition  $T$ , etc., of material during its selection has profound impact on final temperature stability of printed entity. As an instance, homogenization of carbon black, which can relatively endure high magnitudes of  $T$ , furnishes thermal stability in its composite. Temperature pertained to onset and accomplishment of composite decomposition also experiences proportional enhancement with the filler when investigated with thermogravimetric analysis (TGA) [7]. Correspondingly, graphene ascribed to its  $\pi$ -bond delocalization endows conductivity and  $T$  stability during printing of graphene–polylactic acid (Gr-PLA) composite. Studies also revealed that increasing graphene concentration (conc.) had lowered the resistance path to  $\sim 47 \Omega$  from  $\sim 2217 \Omega$ . Therefore, as a resultant minor heating/ $T$  upsurge in composite displayed distortion resistance when voltage up to 20 V was applied manifesting



its accessibility in electronics mobile for faster heat dissipation [39]. Furthermore, thermal stability of precursor for energy storage applications in printed batteries can mitigate flammability-related issues (fire accidents) of conventional non-printed electrolytes or electrodes (cell). In addition, it also augments and maintains ionic conductivity of gel electrolyte at significantly high- $T$  (vs. conventional) for an extended period of time while enduring thermal shock which boosts its life predictability [40]. Similarly, powder-state intermixing of copper, iron, or metal in polymer/s bridges resistive pathways engendering conductivity to composite as a consequence of the propagation of electrons and vibrations [41]. Another parameter is  $T_g$  which facilitates the selection of  $T$  environment for precursor material printing as low  $T_g$  enables room- $T$  designing. Moreover, the later also vindicate dimensional stability which otherwise prompts shrinkage when cooled as a result of water evaporation from gel network pertaining to its  $T$  gradient existence [42]. Geometrical soundness of printed material is also a function of thermal expansion coefficient (CTE), a measure of shrinkage or expansion during heat flow. Precursors with large CTE are susceptible to greater shrinkages while cooling which can engender delaminations, warpages or distortion printed interest, therefore, intermixing of hard or thermally stable phase contributes to minimization in CTE-related defects [43, 44]. Wei et al. reported CTE of graphene composite with ABS and mere ABS to be comparable, i.e., 75 ppm/°C and 78 ppm/°C, respectively, which otherwise would have seeded thermal stress in the printed part progressing to distortion [45].

$T$  has also been utilized while formulating materials to be used with respective printing equipment. Nikzad et al. had employed cryogrinder to produce acrylobutadiene-styrene (ABS) powder in which  $T$  was lowered to  $<T_g$  ceasing chain motion (glassy state—brittle), and subsequently, reduced molecular energy had favored crushing for later composite extrusion printing [41]. However, freeze-drying could also be functioned to prevent clustering and yield powder particles owing to its locking-in and low energy state [44]. Alternatively, ABS could also be blended with another polymer in pellets form which was dried (40 and 60 °C, respectively) [46] before being extruded to eliminate water which sources voids and improper filament in FDM; process is also practiced in general before printing commences [44]. Thence,  $T$  selection is momentous for material drying or other intended function over it as instance, ABS + PC  $T$  endurance limit  $<110$  °C and therefore printing conductive inks wherein drying  $T$  belongs within threshold [47]. Following the selection of precursor formulation, reinforcement, and drying, it is fed in screw extruder (SE) [48, 49]) to homogenize its conc. Barrel  $T$  is predetermined based on material to be extruded out, e.g., polylactic acid (PLA) was intermingled with carbon black (CB) and carbon nanotube (CNT) separately in batches and filled in extruder.  $T$  of progressing zones ranges between 160 and 175 °C, and the resultant extrudate was dried again to dehumidify for later extrusion into filament for printing [48]. Correspondingly, filaments of varied polymers or composites can be extruded with different  $T$  range suitable in accord with respective properties for FDM dispensing.

Nevertheless, for SLA where liquid resin layers are laid on platform for UV curing, a prerequisite for precursor material is viscosity which determines flowability and also crosslinkability [50]. As extreme magnitudes of viscosities can render SLA

printing in vain, therefore apposite  $T$  can be determined by heating and measuring its viscosity at intervals. Optimum viscosity for SLA printing ranges  $<1$  Pa s [51] and requisite heat (or  $T$ ) is catered with light intensity, e.g., in modified polycaprolactone (PCL),  $T < 46$  °C was apt to obtain viscosity around 0.66 Pa s [52]. DLP, which is bottom-up version of SLA, had similarly processed methacrylated functionalized polyimide which employed multiple heating and cooling cycles followed by drying (e.g., at 40 °C) (apposite for photocuring) [53].

SLM printing is exercised majorly in metals, ceramics, and alloys, attributable to their  $T$  tolerance and high-energy melting wherefore implementation is restricted in polymeric particles, ascertained to their  $T$ -related softness [5].

SLS printing entails densification by sintering of powder (polymeric-low melting  $T$ , ceramics, metals and composite-high melting  $T$ ) precursor particles, e.g., polyamide (PA), polystyrene (PS), polyether ether ketone (as PEEK), copper (Cu), aluminum (Al), etc. [5]. Precursors are manufactured by atomizing metals or alloys from their molten state which solidifies with highly pressured unreactive air, water, or rotary disk along with other processes. While for polymers, Dechet et al. had employed conc.- $T$  diagram-derived phase separation in liquid medium to precipitate beads (PA11) which were sintered at 170 °C for the densified product. Mechanism commenced with precursor solution heated to  $\sim 190$  °C, stabilized and cooled 0.5–3 K/min rate to 50 °C and instant when  $T < \text{solution } T$  (differed with conc.), PA11 precipitated out which were dried before being directed by laser for sintering [54].

In powder production mechanisms, the resultant due to  $T$  gradient, laser penetration, or solidification irregularity may have entrapped bubbles, satellite particles-rough finish, non-uniform size which ensued melting heterogeneity, deprived interface bonding, and truncated mechanical performance [55]. After solidification of 3D printed entities, volumetric shrinkage and residual stress prevail which guide emergence of delamination, cracks, or other interfacial defects that are accredited to constraints (previously built layers),  $T$ , solvent evaporation, and other parametric gradients [56].

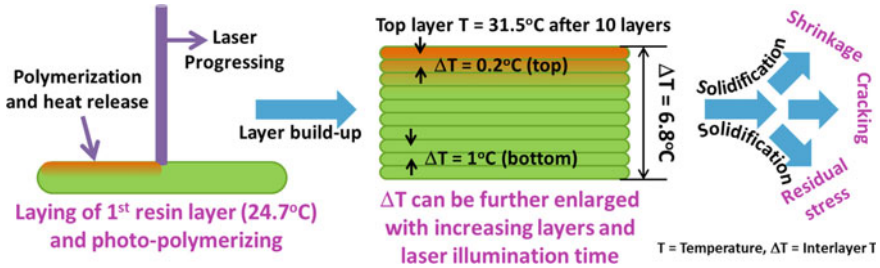
Optimization of pre-printing parameters in accordance with printing technique is followed by preheating of precursor materials before being patterned on platform to acclimatize it to the printing environment and reduce thermal variation (magnitudes), e.g., PA12 heated to 178 °C for printing with SLS [57].

### 3.2.2 Thermal Effects During Printing Process

Following the material preparations, temperature characteristics needs to be controlled in printer setups for stable production in user-controlled design. FDM dispensing is governed by nozzle- $T$  (which dispenses melt in printable viscosity) and bed/platform- $T$  (which controls thermal gradient for layer bonding and end performance). Optimum nozzle- $T$  steers solidification and mechanical behavior, e.g., in ABS-carbon fiber composite, the variable was tuned between 200 and 240°C

in intervals of 10 °C. Experiments employed 220 °C as optimal  $T$  because inter-layer energy was efficient in bonding as opposed to 200 °C which lacked requisite energy to bond adjacent layers in full and 240 °C where complete merging seeds porosity in structure. Therefore, superlative 220 °C peaked in mechanical strength (tensile and yield), toughness, and modulus ( $E$ ) [58]. Similarly, ABS–montmorillonite was extruded at 190 °C [44], nylon6–graphite, etc., blend at 250 °C [49], polymethyl methacrylate–graphene, etc., composite at 280 °C [59], and other formulation with varied filament extrusion  $T$  can be produced governed by their composition and innate characteristics. Emphasis is due to the observation that alteration of 5 °C could generate perceivable contrast mechanically and qualitatively [60]. Composite/polymer dispensing from extruder (FDM) nozzle experiences solidification immediately after being extruded and continued on platform. Nonetheless, prior to resting of filament on platform, minor amendments in  $T$  can bestow drastic property difference which was portrayed by Gantenbian et al. Authors had employed liquid crystalline polyesters which are FDM extruded in isotropic phase with room- $T$  cooling but while in air, ample  $T$  gradient engineered core–shell filament with dimensions determined by nozzle diameter. Circumference of filament was exposed to room- $T$  and therefore, got ordered in nematic configuration while central retained the thermal energy and thereby, slow orientation. Furthermore, authors explained that performance escalation due to core–shell solidification went substantial when nozzle- $T$  was in close proximation to  $T_{\text{melting}}$  (polymer). Additionally, post-thermal treatment assisted crosslinking had maneuvered the mechanical magnitudes (toughening, strength, crack-arresting, modulus, etc.) positively [61]. Idiosyncratically, FDM displays parallelism with acoustoplastic metal direct-write (AMDW) in the geometry of material feeding as filament. Inter-filament bonding in AMDW thrives with the application of ultrasonically generated energy; e.g., printed aluminum (Al) filaments were affixed with 60 kHz frequency horn. Incoming energy induces huge localized heat which macroscopically contributed to minimal change, unlike in FDM or ultrasonic processing. As Al experienced merely 50C divergence which was attributed to huge disparity between radial and lateral dimensions (aspect ratio to 0.001) [62–64]. Platform- $T$  in extrusion derived printing not only functions to lessen the gradient carried amendment but also boosts recrystallization process (e.g., for PLA and ABS, temperatures were 70 and 80 °C, respectively [65]). Along with the prior, hot dispensing on formerly printed layers aid in heat and fluid flow across dimension which corroborates evaporation of moisture which consequently revitalizes the interface interaction for densification and defect averting [66].

As aforementioned in Sect. 2.1, the viscosity in SLA is pivotal for printing and later curing commences with UV (majorly) light owing to photorezin incorporation at room- $T$  [50]. Contrarily, slight modulation in formulation, e.g., hybridizing Silicone-epoxy-acrylate resin evinced curing from two energy sources, i.e., heat (epoxy curing) and light (acrylate curing). First step curing by UV flooding had lifted-up  $T$  which further assisted in second step thermal crosslinking at 90 °C and thus elevated  $T_g$  (interpenetrating network (IPN) formation) empowering the thermosets with amplified performance [51, 67]. But, UV curing is also followed by entity’s geometrical disfigurement (curling or shrinkage) endowed to it by  $T$ .



**Fig. 3.4** Illustration of temperature build-up during SLA printing of resin layers owing to photopolymerization (release of thermal/internal energy).  $\Delta T$  later at top layers (e.g., 10th layer) < bottom layer due to temperature increment (heat liberation) from lower but overall  $\Delta T$  tends to enlarge with layers and laser scanning time

Photocuring reaction-instigated solidification liberate thermal energy which accrues with layer thickness (for ~10 layers,  $T = 31.5\text{ }^\circ\text{C}$ , resin  $T = 24.7\text{ }^\circ\text{C}$ ) and exposure time. Though interlayer change ( $\Delta T$ ) dwindles with thickness, inclusive (overall entity)  $T$  upsurges which induces thermal residual stress and shrinkage [68], thereby cracking [50] (Fig. 3.4). This  $\Delta T$  or minimum  $T$  before next layer deposition had also been witnessed in FDM printing, and results were modeled with various design and dimension (1D, 2D, etc.). Amico et al. demonstrated square and line modeling which exhibited conduction heat transfer (Eq. 3.1) but only former manifested convection (Eq. 3.2) owing to geometry and area. Though radiation energy interaction of filaments with circumambient or with their adjacent (owing to geometry) had been neglected, it could surpass convection when  $h$  was quantitatively small [69].

$$\text{Conduction: } Q = V' * \rho * c_p * (T_{\text{nozzle}} - T_{\text{ambient}}) \tag{3.1}$$

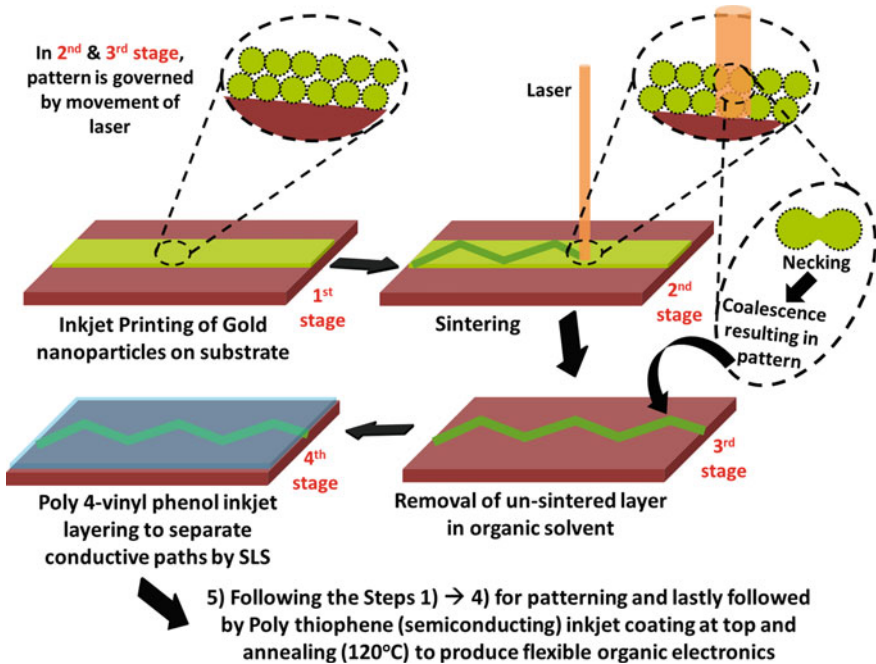
$$\text{Convection: } Q = h * (T - T_{\text{ambient}}) \tag{3.2}$$

where  $Q$  = conductive or convective heat,  $V'$  = deposition rate (volumetric),  $\rho$  = density,  $c_p$  = specific heat,  $h$  = heat transfer coefficient.

Finite element (FE) analysis outcomes displayed printing speed dependency on heat transfer and overall  $T$  enhancement with deposition of layers. Slower cooling rate except for (printing speed) 10 and 30 mm/s as lesser speed renders extended contact of hot source (filament) while higher quantity caused dwindling in time for next deposition (preventing heat transfer and thermal piling up). In other words,  $T$  rejection from bottom layers increased and therefore  $\Delta T$  lowered with layers stacking. Nevertheless, when time gap between depositing adjacent layers was uncontrolled, delamination (owing to improper bonding), cracking warping, etc., defects were evidenced, e.g., minimum layer  $T = \sim 72\text{--}65\text{ }^\circ\text{C}$ , maximum  $T = \sim 85\text{--}103\text{ }^\circ\text{C}$  when in-between layer duration varied from 3280 to 760 s. Additionally, layers  $\geq \sim 20$  rendered thermal transfer from sidewalls due to high gradient with central section of filament and therefore necessitated  $T$  optimization or side insulation to mitigate

warping, cracking, etc. (also vanquished when  $T_{\text{toplayer}} > T_g$ ). Furthermore, experimental (ABS material) and modeled results delineated that platform- $T$  and thermal conductivity of material influenced the cooling rate for few initial layers as quenching effect diminished with further built-up [70–72].

SLS in similarity with FDM and other techniques entails bed preheating as substantial  $T$  variation arises while scanning powder layers. Laser scanning on cooled former layers stems residual stress in sintered layer which continue accruing with gradual scanning of further layers and contribute to warping and mechanical impairment (modeled for PA12) [57]. Therefore, subsequent layering of powders necessitates above crystallization ( $T > 300\text{ }^\circ\text{C}$  for PEEK) heating to equalize rate of cooling of underneath sintered layers which also ensured densification and enhanced relative bending stress (0.15–0.35) [73]. This re-stimulation of sintered metal layers interrupt oxide formation and thence encourages interfacial bonding due to improved wetting [74]. Additionally, SLS had also aided in sintering of inkjet-printed self-assembled gold (Au) nanoparticles at  $150\text{ }^\circ\text{C}$  (melting  $T$  of Au due to nano-size-effect) with Argon laser which made pathways for conduction. Different Au patterns were spaced with poly 4-vinyl phenol (polymerized at  $150\text{ }^\circ\text{C}$ ) and finally walled with annealed ( $120\text{ }^\circ\text{C}$ ) conductive polythiophene inkjet-printed layer for flexible electronics applications (Fig. 3.5) [75].



**Fig. 3.5** Illustrating conductive patterned gold layer on polymer substrate for flexible organic electronics application

SLM printing is impeded by solidification ( $10^3$ – $10^8$  K/s rate of cooling) route as high-power laser pierce deep-down several layers depreciating  $T$  gradient (also dependent on interaction time) between underneath layers and promotes grain growth, atoms mobility inducing segregation, undesirable phases, stresses, etc., but attenuate voids geometry and formation [76]. Shrinkage as in SLM also involves in SLS due to thermal energy interference but the latter is more sensitive to melting or crystallization  $T$  which may initiate curling, dimensional instability or polymer flow, thus deviating from efficacious printing [77]. Wudy and Drummer had experimented PA12 with 50 W laser and to evade gradient (ranging to 10 K)-followed curling damage, build  $T$  was fluctuated between 164 and 172 °C which assisted in  $T$  distribution homogeneity and coalescence prevention in end product [78]. Succinctly, when the metal powder is impinged by laser beam, it coalesces and necks down to produce metallurgical bond followed by solidification which is governed by flow of heat energy. This flow pilots microstructural and macrostructural features in cooling material and the most critical section sustaining this is heat-affected zone (in short as HAZ—adjacent to region of laser focus).  $T$  gradient in these regions administer solidifying structure (columnar or dendritic) and thereby final properties. In addition, preponderated difference in  $T$  accompanies swift cooling  $\rightarrow$  small grain size or precipitate size, large residual stress, crack generation, coring phenomenon  $\rightarrow$  depletion in properties. Therefore, printed metal necessitates post-heat treatment to avert coring, coarsening (high- $T$  for extended period), segregation and therefore crack impediment [79].

In addition to other cracks, damages, etc., owing to laser (intrinsic heat) raster patterning on powder, SLM and SLS evinced heat-affected zone [80]. Ouyang et al. had formulated iron-based alloy powder for SLM printing and observed that high laser power (e.g., 350 W) coupled with low scanning speed (e.g., 200 mm/s) nucleated crystallinity to the solidifying structure in HAZ, i.e., crystallinity fraction  $\propto$  laser power, but  $\propto$  (scanning speed) $^{-1}$ . Authors had also verified the reliance with FE-modeling in which they implied susceptibility of HAZ to heat reflow due to high laser power and that duration (e.g., 7.29 s at HAZ) if exceed incubation period, bestowed intermetallic precipitation and crystallization. Further, the formation was also reasoned that heat reflow had directed the zone to above crystallization  $T$ , and thus, HAZ was governed by cooling time irrespective of cooling rate (which was  $\sim 8.07 \times 10^4$  °C/s  $\ggg$  11 °C/s for amorphous structure formation) [81]. Not only HAZ results in structural variation but also challenges mechanical performance and roots residual stress, distortion, etc. [82]. Analogous to SLM, SLS also employs laser for sintering phenomenon in metals along with polymers and thus are susceptible to HAZ which in addition subsist laser characteristic. Time and intensity of input energy are optimized so as to raise  $T$  below decomposition which otherwise can ablate the polymers, thus deflecting from requisite output. Lasers (e.g., CO<sub>2</sub>, Nd:YAG, etc.) penetrate to a depth and partially or fully melts the interacted material (polymer), adjacent to it lies HAZ whose width is controlled by incident fluence and other material innate properties, e.g., thermal conductivity and diffusivity  $T$  in HAZ, in similar to laser interaction zone, elevates to exceed  $T_g$ , and therefore also steers crystallinity in polymers which has direct influence on mechanical performance



[78, 83–86]. Another fact in sintering is boundaries of HAZ, and agglomeration (of powders appertained to heating) is dependent on again laser energy, e.g., Franco and Romoli had defined that  $>0.10 \text{ J/mm}^2$  was effective in making a clear distinction among them. Moreover, they also reported that sinter depth was a factor of melting and vaporization of polymer material (PA12) but HAZ could elongate deeper based on energy available [87]. Though laser is also utilized in SLA photocuring, HAZ ceases to exist appertained to (1) intensity is quite low to lift  $T$  to sufficient as resin is already in semi-molten form (2) UV light is used which prevents any HAZ formation [83]. In reference to above-mentioned facts, quantifying the gradient in HAZ zone is complex and therefore necessitates more in-depth study in relation to 3D printing processes.

### 3.2.3 *Post-printing Thermal Effects*

During thermal analysis of printed entity, temperature is pivotal as it determines product's feasibility, i.e., with  $T$  stiffness diminishes due to high mobility of chains which abate network formation and also strengthening which prepare the designs for functional application.

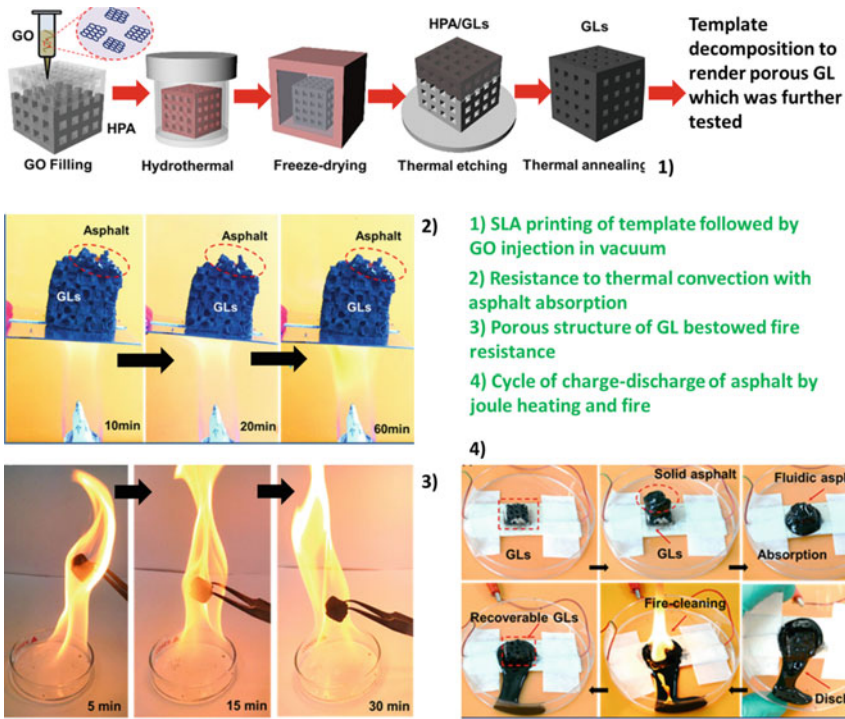
Though FDM furnish printing ease, cost-effectiveness, material efficiency, etc., the process is confronted with resolution and surface step-case (visible pathways) [38]. Roughness of print can be subdued by thermal assistance after complete manufacturing of entity, i.e., heating to  $T$  ( $160 \text{ }^\circ\text{C}$  for PLA)  $> T_g$  for thermoplastics melting. In printing of Braille letters, molecular chains-prompted mobilization had not only smoothens the pattern but also aided in interfacial bonding augmentation with cellulose paper (reduced viscosity empowered interdiffusion) [88]. Above-stated staircase-free smooth surface at upraised  $T$  also ameliorates reflectivity (but within limits) owing to its curtailed scattering. These features are showcased by PLA,  $T$ -glase, ABS, moldlay, high impact polystyrene (HIPS), thermoplastic elastomer (TE), etc., as an exemplary in which TE achieves the peak reflectivity at high- $T$  while HIPS and PLA emanates fumes but  $T$ -glase unveils suitability with printing among all. HIPS exhibits average roughness of  $0.523 \text{ }\mu\text{m}$  at  $\sim 123.5 \text{ }^\circ\text{C}$ ,  $T$ -glase =  $0.597 \text{ }\mu\text{m}$  at  $113.6 \text{ }^\circ\text{C}$ , ABS =  $0.592 \text{ }\mu\text{m}$  at  $126.6 \text{ }^\circ\text{C}$ , due to distinct tolerance of material toward  $T$  [89]. Apart from polymers, ceramics are high- $T$  workable materials and printing of suspensions (ceramics directly added [90] or derived from polymer [91]) rendered production of green body. This resultant is dehumidified at  $T$  slightly greater ( $50 \text{ }^\circ\text{C}$ ) than room- $T$  or at room- $T$  ( $25 \text{ }^\circ\text{C}$ ) to eliminate liquid (water) content which is ultimately sintered. Extortionate sintering  $T$  ( $\geq 1300 \text{ }^\circ\text{C}$ ) in conjunction with the period of holding at the same is significantly controlled and optimized to circumvent formation of defects. Expulsion of organic molecules with the application of heat energy ensured densification (can be  $\sim 97\%$ ) and strength building but also renders dimensional variation in the form of shrinkage which can also source pores. In addition, porosity defect is a function of sintering  $T$  and thus can be variegated positively ( $T$ ) to lessen the quantity and dimension of pores which

is accompanied by increased packing density of entity [90–92]. As an instance, Peng et al. sintered  $\text{Al}_2\text{O}_3$  green body at three distinct  $T$  of 1350, 1450, and 1550 °C and reported that for any printing path followed, porosity curtailed while an upsurge was recorded in bulk density (1550 °C  $\rightarrow$  3.71 g/cm<sup>3</sup>  $\rightarrow$  10.8% porosity). Additionally, authors also witnessed that contraction due to the densification had primarily affected the radial dimension and then height, i.e., diametrically 2.62% and height 0.98% [90]. In contrary, Li et al. had printed acrylate-modified polyborosilazane polymer by DLP and obtained SiBCN after pyrolysing at  $T$  up to 1500 °C. Pyrolysis at 900, 1200, and 1500 °C individually witnessed increasing percentage of shrinkage, crystallization, and densification, however, later slowed down (density,  $\rho_{900} - \rho_{1200} = 11$  g/cm<sup>3</sup> and  $\rho_{1200} - \rho_{1500} = 2$  g/cm<sup>3</sup>) due to the ceramic conversion which was approximately 58% at all  $T$ . organics were burnt endowing the design its black color and thermal stability and oxidation resistance coupled with anticipated mechanical enhancement (toughness and modulus) [91]. This sintering-assisted densification had also furnished thermoelectric application in waste to electricity generation with enhanced Seebeck coefficient for p- (199  $\mu\text{V/K}$ ) and n- (145  $\mu\text{V/K}$ )-type materials at around  $\sim$ 200 °C [93]. In addition to aforementioned pyrolysis and sintering which aids in functional improvement, mere heat treatment also delivers upgradation. Wang et al. had inkjet-printed VeroClear material with heat treatment to 150 from 60 °C at intervals of 30 °C and evidenced >20% increment for either of compressive/tensile strength, strain, and modulus at highest  $T$  of 150 °C. These achieved results were ascribed to internal energy increase in terms of chain mobility which engenders conversion efficiency and sites for crosslinking, therefore stiffness [94].

Zhang et al. had designed graphene oxide (GO) aerogel within printed template by hydrothermal reaction and freeze-drying equipping flowability of graphene in structure and locked the network, both relied on  $T$  optimization. This steep  $T$  gradient in freeze-drying had directionalized and positioned GO sheets to construct conductive bridge and a porous network. Later decomposition of template at 1000 °C rendered porous graphene construction water hydrophobicity and organics hydrophilicity which could be discharged by heating. This facilitated aerogel in remediation of organics (oils) (e.g., asphalt) by thermal (Joule) energization followed by recovery. Furthermore, the conductivity of constructs can be modulated with  $T$  in a proportional relation as low  $T \rightarrow$  high resistance to electrons flow and conversely for high- $T$ . Amidst the process, aerogel construction and thermal stability were preserved conferring multi-applications in electrical heater, absorbent, sensors, and thermal insulator (Fig. 3.6) [95, 96]. Moreover, GO nanocomposites were also sensitive to  $T$  as annealing at 50 °C could not overcome the wrinkling and dispersion (GO) barrier which thereby conferred drop in tensile strength with fillers but converse was discerned with 100 °C.

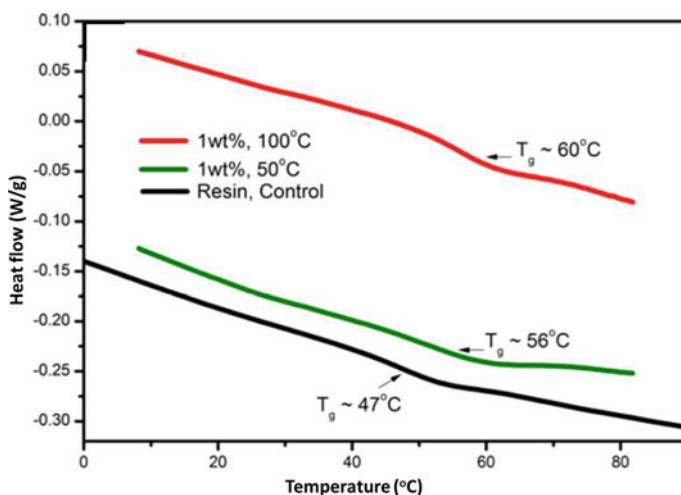
Corresponding to aforesaid nozzle or nozzle-free maneuvering of precursor metals, binder jetting employs binding agent (can be water-based), thus fabricating green body which is accompanied by curing and sintering in steps. In particular, iron, magnesium, and calcium powders were slightly cured at 200 °C and subsequently thermally treated at 430, 620, and 1200 °C for binder burnt-out and densification [97]. In contrast to treatment at elevated  $T$ , when quantification progress in freezing





**Fig. 3.6** Representing (1) the processing of graphene porous structure (or graphene lattice, GL) by decomposition of SLA printed template, (2) inhibiting convection of thermal energy by asphalt absorbed GL rendering it in application of insulator, (3) thermal stability of GL when tested ~30 min permitting GL for fireproof conditions, (4) asphalt is absorbed in GL by modulating its viscosity (by thermal energy) to overcome surface tension and filling the pores which can be discharged with aid of joule heating, subsequently by fire (which loosen asphalt consequently flowed out) thus leading to the recovery of GL to be utilized for further recycling (environment remediation, e.g., oil leakage, etc.) [95]

ranges, thermal characteristics may differ from its high- $T$  counterpart. For instance, thermal expansion of FDM printed ABS and polyjet printed PLA dropped down to around 15,000 and 12,500  $\mu\text{m}/\text{m}$  in negative at 4.2 K from to 0  $\mu\text{m}/\text{m}$  when tested in 290 K. Corresponding results were also reported for thermal conductivity which descended to  $\sim 0.04$  W/m K from  $\sim 0.2$  W/m K for both, therefore, advocating the material for cryogenic utilization [98], e.g., an auxiliary accessory for 77 K operable magnetic concentrator [99]. Laser intervention ( $T$ ) on metallic green body can also be led to the modification in composition owing to evaporation of highly volatile metals (if present) which further manages to alter the solidification, mechanical, microstructural, corrosion, and thermal properties. In addition, inadequate laser raster and coalescence of powder particles also engender fusion irregularity (contraction  $\rightarrow$  cracking) along with rough outer surface [55].



**Fig. 3.7** DSC thermogram (at 10 °C/min ramp rate) for  $T_g$  determination for acrylate-based resin and graphene oxides composites (green and red) after annealing (1 wt% at varied temperature for annealing 50 and 100 °C). Black line indicates for resin with  $T_g$  of 47 °C which climb-up (to 56 and 60 °C) with increasing annealing temperature owing to GO restraint to polymer motion (chain) and dwindling in flakes (GO) wrinkles for augmented adhesion [101]

Irrespective to printing stage, i.e., pre-, during, or post-printing characterization tools like differential scanning microscopy (DSC), thermogravimetric analysis (TGA), are exercised for explicit understanding of  $T_g$  and decomposition  $T$ . TGA analyses facilitate detection of thermal stability by weight loss that transpires when the sample is heated to requisite  $T$  (up to 800 °C, etc.) at a specific rate, e.g., 10, 20 °C/min, etc. It is determined within  $N_2$  or argon environment by onset weight loss of 5% following the sharp descend in weight of sample owing to the exclusion of organic content [100–103]. Dynamic mechanical analysis (DMA) assess loss factor (given by  $\tan\delta$ ) at 1 Hz which is a fraction of loss to storage modulus of the sample after being heated to predetermined  $T$  and the peak ascertains viscous/elastic nature for onset/offset of deformation [45, 46]. Similarly, DSC studies are performed to analyze heat absorption/release perceptible through endotherms and exotherms in the graph. Furthermore, these calculations aid in determination of transition  $T$  (melting, crystallization,  $T_g$ ), enthalpy, curing reactions, etc., at stable rate, e.g., 5, 10 °C/min (Fig. 3.7) [101, 104, 105].

### 3.3 Auxiliary Functions for Extended Application

Tailoring of precursor material during its processing can foster some adjunct features which transcends principle purpose and broaden the performance window. As an

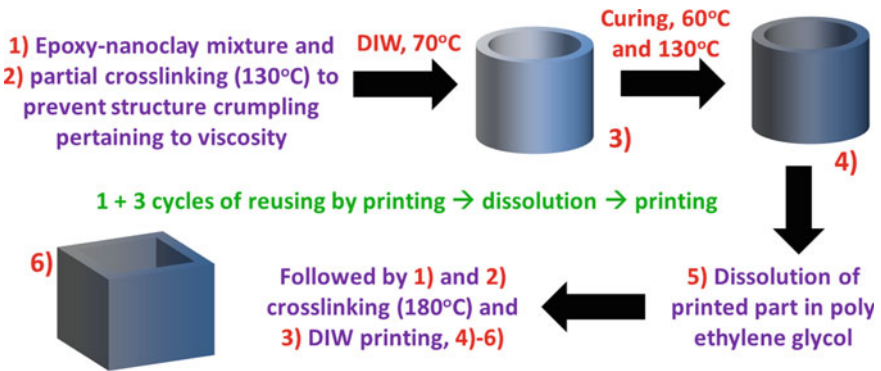
instance, ester-hydroxyl transesterification reaction was availed at elevated temperature (around 180 °C) which advocated bond dynamicity for exchange reactions (at interface) and stress curtailment ( $T$  dependency—Eq. 3.3) bestowing reprocessability to thermosets. These features facilitated repairment and recycling using exchange reaction; moreover,  $T_g$  of material was shifted to higher-end conferring increased modulus (~900 from 7.4 MPa), extended functioning, strength, and stiffness [106].

$$\ln t = \ln t_0 + \frac{E_a}{RT} \quad (3.3)$$

where  $t$  = time of relaxation at  $T$  of interest,  $t_0$  = time of relaxation at infinite  $T$ ,  $E_a$  = energy of activation for transesterification reaction,  $T$  = temperature,  $R$  = universal gas constant.

Analogous bond reaction course had been defined by Shi et al. with vitrimer epoxy through DIW approach where it had been processed over three cycles of printing, dissolving (ethylene glycol), and again printing (Fig. 3.8) with intact design to the endmost cycle of print.  $T$  had portrayed a pivotal role of attuning viscosity (by building flow), partial crosslinking (130 °C, strengthening a safeguarding printing geometry), dissolution of print (180 °C, for recycling), pre-curing (securing print at 60 °C), and post-curing (180 °C). Staircase challenge of printing had been subdued by coating of same epoxy (surface mending) by  $T$ -steered fluidity and curing for glossy finish in addition to repairing. Authors had also observed the enhancement of interfacial linkages and fracture energy when  $T$ -aided heating persists for an extended period [107].

Wang et al. had recycled un-scanned PA12 SLS powder (because adjacent laser sintering had enhanced powder weight and reusing could deteriorate surface integrity)



**Fig. 3.8** Thermoset vitrimer epoxy being printed and recycled (3 cycles in addition to original) (1) and (2) involves formulating and pre-crosslinking followed by (3) DIW printing which is (4) cured (in 2 steps) which also lead to darkening of color due to oxidation and curing (5) printed entity being dissolved in polyethylene glycol (PEG) followed by subsequent printing (6) and again following the loop {(2)–(6)}. However, the content of PEG is higher recycling (e.g., 3rd) > former (1st or 2nd)

into FDM processed filament with reinforcements (carbon fiber). PA12 filament was produced in twin-SE with zones varying 175–190 °C (die  $T$ ) → pelletized → dried at 60 °C to be re-extruded (174–199 °C in single-SE) as a composite. Authors printed the outcome at 240 °C nozzle- $T$  and 90 °C platform- $T$  and observed that though printed entity had not amplified thermal performance due to short fibers, mechanical magnitudes of elastic/flexural strength and modulus had outstripped the precursor [108]. Xu et al. had engineered scaffolds on petroleum jelly-coated substrate with reusable ink comprising of alloyed steel with kinetically jetting out chitosan–acetic acid (room- $T$  evaporation) binder endowing a green body which was thereupon sintered at 1165 °C. Furthermore, acidic solution-aided dissolution of wasted-out parts for re-formulating in prerequisite ratio and re-printing accompanied by heat treatment for carbon diffusion-assisted strengthening [109].

Before advancing as final product, post-processing of precursor materials enhances the utility but is also associated with certain challenges, mitigation of which can optimize product's functioning. Printing techniques where post-densification or sintering is progressed, material shrinks but its non-uniform change bestowed the entity with numerous cracks and wastage or non-serviceable especially, in medial where uniform porosity render effective circulation of fluids. With sintering in-progression, high intensity of laser or presence of humidity on material can encourage ablation, degradation, or vaporization of material and continuing can impair the part with unintentional porosity, thus attenuating practical workability and therefore necessitating optimal tuning of laser power and time of interaction. Yet another is allied with the employment of support materials in which post-sintering or support removal can close or destroy (large pore size generates) the interconnection between pores. Additionally, while erasure of support structures required part can also be damaged conferring inappropriate surface (or its incomplete removal) and thus necessity arises in controlling the precision or accuracy of elimination [87, 110, 111].

### 3.4 Thermal Features in Biomedical Application

Realization of 3D printing in biological has diversified the tactics of treatment and implantation as scientists or biologists can envision the criticality of design, its functioning, allied challenges, etc., by modeling/simulation bestowing user-specific medications. This enticing technology executes its strategy by counterfeiting nature to trick physiological systems in working, in vitro culturing or proliferating cells or tissue for organ generations, and scaffold-free therapeutics [1]. Implementation of material through printing thrives with extrusion, inkjet, laser-assisted, or SLA to yield scaffolds, organs, or drug carriers for treatment. For efficacious printing of biomaterials (e.g., hydrogels, etc.), parameters like  $T$ , pressure, environment, time, humidity, biocompatibility along with material properties are indispensable and therefore necessitate for optimization in cell viability [112]. Printing of cell-bearing ink, e.g., biodegradable PLA, imposes a challenge as it fluids out at  $T$  which are beyond the tolerance of biological cells [113]. Inkjet printing requisites the

controlled dispensing of successive drops on predetermined sites for 3D build-up in  $z$ -axis. Two analogues of inkjet printing comprise of thermal and piezoelectric in which either differs in driving force of dispensing, i.e.,  $T$  and acoustics energy, respectively. Outcome of localized invigoration in thermal inkjet is the concomitant increase in bulk- $T$  ( $\sim 4$  to  $10$  °C) but bestows user with speedy printing [1]. Other alternative is extrusion which is characterized by robotic-driven continuous dispensing of shear-thinning materials (hydrogels) at physiological  $T$ . This technique is propitious for high density of cell loadings but viability is compromised owing to stress dispensing at nozzle [1, 114]. Laser-assisted printing avails ink coating (highly viscous— $<30$  mPa/s) on laser absorbing layer which effectively sacrifices itself in bubble form (vaporize due to heat) to propel ink toward the platform in user-defined pattern controlled by laser position. This process is adapted by virtue of its high cell viability (no nozzle stress on the ink in contrast to pre-mentioned extrusion) and intricate/complex printing but confronts expensive manufacturing [114]. Yet another printing process is SLA, although similar to non-biological applications printing but is contrasted by the utilization of visible energy as a crosslinking medium due to the inimical nature of UV [115].

Analogous to above-mentioned pre- and during printing in Sects. 3.2.2 and 3.2.3, bioprinting also elicits features in  $T$ -controlled environment. As an instance, He et al. constructed alginate–gelatin scaffolds where the viscosity of the mixture was preserved to optimum ( $0.3$ – $3$  Pa s) at  $37$  °C by nozzle heating (as gelatin is inordinately sensitive to  $T$ , gel at room- $T$  while liquid at  $37$  °C [116]). This variable magnitude also expedited flow, thus mitigating nozzle occlusion; meanwhile, platform- $T$  was attuned to  $\sim 5$  °C which ushered in crosslinking of gelatin structure, additionally, also efficacious diffusion [117]. Tan et al. had also employed freezing platform- $T$  ( $\circ$ ) for polyvinyl alcohol (PVA) to establish hydrogen bonding-networked structure which also aided in soft gel engineering (e.g., in brain) [116]. Goyanes et al. had investigated three different polymeric materials (drug-carried) through FDM printing at different nozzle- $T$  determined by innate characteristics, e.g.,  $230$  °C for PLA,  $170$  °C for PCL, and  $220$ – $230$  °C for PU. While extruding drug-loaded polymer–salicylic acid, authors realized degradation of acid as well as drug at  $T$  of  $170$ ,  $190$ ,  $60$  °C for either of them due to modified functionality governed by modulated interactions. Moreover, improper solidification, cooling, and nozzle blockage had also been obtained with drug incorporation and also  $T$  selection (heat) [104]. Owing to miscellaneous incidents (disease or accidents), quantification in patients is burgeoning every year followed by anticipation for treatment (implantation). Correspondingly, bone implantation (craniomaxillofacial) cases in market will also envisage a financial inclination at  $6.9\%$  rate to  $2.49$  billion USD from  $1.79$  billion USD by the year 2021 [118]. These are customarily formulated with calcium phosphate (by virtue of natural presence) at  $1400$  °C, subsequently quenched and crushed for later printing [119]. Nevertheless, they (bones) are prone to  $T$  sensitivity (due to tissue's vulnerability toward it) and hence optimized not only to replicate the physiological environment but also to examine heat emanated during surgical piercing. On that account, specific heat, thermal diffusivity, and conductivity are reckoned while prototyping

artificial bones. Tai et al. attained parametric magnitudes which are in approximation to natural bones as thermal diffusivity = 0.31 and 0.25 mm<sup>2</sup>/s, Specific heat = 1.23 and 1.29 kJ/Kg K, thermal conductivity = 0.65 and 0.59 W/m K for artificial (VisiJet PXL Core) & bovine bones, respectively [120]. Another exploration for Bone tissue engineering was appraised by Rasoulianboroujeni et al. with poly lactic-co-glycolic acid/TiO<sub>2</sub>. Print initiated at nozzle- $T$  of 160 °C and results validated enhancement of  $T_g$  by 2 °C/10 wt% TiO<sub>2</sub> with decomposition/degradation onset shifted to 269.75 °C/352 °C (by DSC/TGA) (porosity augmentation) owing to thermal energy sinking (absorption) by TiO<sub>2</sub> [121]. In reference to above all literatures, cell proliferation is principally progressed at body  $T$  to mimic it for in vitro evaluation of materials and also as consequence of cell damage at high- $T$  [116, 122]. Rheologically also, numeric of loss modulus and storage modulus in relation to experimental  $T$  was an indicative of viscoelastic or solid-like state accompanied by spreading phenomenon (proportional with  $T$  by virtue of its brisk solidification at gelling  $T$  which aided in the upkeep of geometry) [123].

Thus, formulation prerequisites  $T$  (above ambient) mixing which are oftentimes followed by cooling and storing of precursors of printing at  $T < 10$  °C. The resultant when printed also demands physiological  $T$  for flow-out viscosity and retrenched  $T$  on ink or filament collecting surface for cell vitality. For cells to proliferate and be viable, the culture approximates at bodily  $T$  to simulate its working in vitro as they are exceedingly susceptible to external environment predominantly, temperature.

### 3.5 Conclusion

This chapter delineates  $T$  and thermal parametric variations and their resultant effect on overall performance of printed body. Preeminence of  $T$  is widespread across all stages of printing, compositions, material selection, and even after-treatments to manipulate properties to desired output; in pre-printing stage,  $T$  is influential for homogenization of additives, drying to eliminate humidity interference during printing which can also engender defects. Second stage employs build platform- $T$ , laser-generated heat, nozzle- $T$ , etc., that intervene in solidification and cooling of the material, thereby impacting the interfacial properties. Last stage involves sintering, various treatments, and other characterization tools which involve ramping up and down  $T$  rate for characterizing decomposition, weight loss, and other for concluding product's stability and resistance in external environments. Lastly, this document explores about the physiological  $T$ -driven bioprinting processes to mitigate vulnerability of cells and to mimic the bodily nature in vitro. Optimizing the fundamental features attributes to utmost accomplishment of workable efficiency in three dimensions and also explores material's utility in full.

## References

1. Murphy SV, Atala A (2014) 3D bioprinting of tissues and organs. *Nat Biotechnol* 32(8):773–785
2. Yadav R, Naebe M, Wang X, Kandasubramanian B (2017) Review on 3D prototyping of damage tolerant interdigitating brick arrays of nacre. *Ind Eng Chem Res* 56(38):10516–10525
3. MarketsandMarkets (2017) 3D printing market by offering (printer, material, software, service), process (binder jetting, direct energy deposition, material extrusion, material jetting, powder bed fusion), application, vertical, and geography—global forecast to 2023. [MarketsandMarkets.com](http://MarketsandMarkets.com)
4. Magisetty R, Shukla A, Kandasubramanian B (2018) Dielectric, hydrophobic investigation of ABS/NiFe<sub>2</sub>O<sub>4</sub> nanocomposites fabricated by atomized spray assisted and solution casted techniques for miniaturized electronic applications. *J Electron Mater* 47(9):5640–5656
5. Chen Z et al (2018) 3D printing of ceramics: a review. *J Eur Ceram Soc* 39(4):661–687
6. Chua CK, Leong KF (2015) 3D printing and additive manufacturing: principles and applications, Fourth edition of Rapid prototyping. World Scientific, Hackensack, New Jersey
7. Chiu S-H, Wicaksono ST, Chen K-T, Chen C-Y, Pong S-H (2015) Mechanical and thermal properties of photopolymer/CB (carbon black) nanocomposite for rapid prototyping. *Rapid Prototyping J* 21(3):262–269
8. Deoray N, Kandasubramanian B (2018) Review on three-dimensionally emulated fiber-embedded lactic acid polymer composites: opportunities in engineering sector. *Polym-Plast Technol Eng* 57(9):860–874
9. Giannopoulos AA, Mitsouras D, Yoo S-J, Liu PP, Chatzizisis YS, Rybicki FJ (2016) Applications of 3D printing in cardiovascular diseases. *Nat Rev Cardiol* 13(12):701–718
10. Kitson PJ, Glatzel S, Chen W, Lin C-G, Song Y-F, Cronin L (2016) 3D printing of versatile reactionware for chemical synthesis. *Nat Protoc* 11(5):920–936
11. Lind JU et al (2017) Instrumented cardiac microphysiological devices via multimaterial three-dimensional printing. *Nat Mater* 16(3):303–308
12. Pati F et al (2014) Printing three-dimensional tissue analogues with decellularized extracellular matrix bioink. *Nat Commun* 5(1):1–11
13. Wünscher S, Abbel R, Perelaer J, Schubert US (2014) Progress of alternative sintering approaches of inkjet-printed metal inks and their application for manufacturing of flexible electronic devices. *J Mater Chem C* 2(48):10232–10261
14. Gore PM, Zachariah S, Gupta P, Kandasubramanian B (2016) Multifunctional nano-engineered and bio-mimicking smart superhydrophobic reticulated ABS/fumed silica composite thin films with heat-sinking applications. *RSC Adv* 6(107):105180–105191
15. Gore PM, Kandasubramanian B (2018) Heterogeneous wettable cotton based superhydrophobic Janus biofabric engineered with PLA/functionalized-organoclay microfibers for efficient oil–water separation. *J Mater Chem A* 6(17):7457–7479
16. Yadav R, Naebe M, Wang X, Kandasubramanian B (2019) Thermomechanical characteristics of h-BN- and POSS-based bisphenol A polycarbonate nanocomposites. *Polym-Plast Technol Mater*, pp 1–15
17. Gore PM, Khurana L, Siddique S, Panicker A, Kandasubramanian B (2018) Ion-imprinted electrospun nanofibers of chitosan/1-butyl-3-methylimidazolium tetrafluoroborate for the dynamic expulsion of thorium (IV) ions from mimicked effluents. *Environ Sci Pollut Res* 25(4):3320–3334
18. Yadav R, Goud R, Dutta A, Wang X, Naebe M, Kandasubramanian B (2018) Biomimicking of hierarchal molluscan shell structure via layer by layer 3D printing. *Ind Eng Chem Res* 57(32):10832–10840
19. Kuo C-C et al (2016) Preparation of starch/acrylonitrile-butadiene-styrene copolymers (ABS) biomass alloys and their feasible evaluation for 3D printing applications. *Compos B Eng* 86:36–39
20. Geng P et al (2019) Effects of extrusion speed and printing speed on the 3D printing stability of extruded PEEK filament. *J Manuf Process* 37:266–273

21. Jayanth N, Senthil P (2019) Application of 3D printed ABS based conductive carbon black composite sensor in void fraction measurement. *Compos Part B Eng* 15(159):224–230
22. Malik A, Kandasubramanian B (2018) Flexible polymeric substrates for electronic applications. *Polym Rev*, pp 1–38
23. Raut NC, Al-Shamery K (2018) Inkjet printing metals on flexible materials for plastic and paper electronics. *J Mater Chem C* 6(7):1618–1641
24. Tahalyani J, Khanale M, Kandasubramanian B (2018) Dielectric polymeric compositions for improved electrical properties of flexible electronics. In: *Handbook of nanomaterials for industrial applications*, Elsevier, p. 430–467
25. Ligon SC, Liska R, Stampf J, Gurr M, Mülhaupt R (2017) Polymers for 3D printing and customized additive manufacturing. *Chem Rev* 117(15):10212–10290
26. Balasubramanian K, Tirumali M, Badhe Y, Mahajan YR (2017) Nano-enabled multifunctional materials for aerospace applications. In: Prasad NE, Wanhill RJH (eds) *Aerospace materials and material technologies*. Springer Singapore, Singapore, pp 439–453
27. Sanoj P, Kandasubramanian B (2014) Hybrid carbon-carbon ablative composites for thermal protection in aerospace. *J Compos* 2014:1–15
28. Korde JM, Shaikh M, Kandasubramanian B (2018) Bionic prototyping of honeycomb patterned polymer composite and its engineering application. *Polym-Plast Technol Eng*, pp 1–17
29. Mishra N, Kandasubramanian B (2017) Biomimetic design of artificial materials inspired by iridescent nacre structure and its growth mechanism. *Polym-Plast Technol Eng*, pp 1–15
30. Studart AR (2016) Additive manufacturing of biologically-inspired materials. *Chem Soc Rev* 45(2):359–376
31. Yadav R, Naebe M, Wang X, Kandasubramanian B (2016) Body armour materials: from steel to contemporary biomimetic systems. *RSC Adv* 6(116):115145–115174
32. Sahoo BN, Kandasubramanian B (2014) Recent progress in fabrication and characterisation of hierarchical biomimetic superhydrophobic structures. *RSC Adv* 4(42):22053
33. Ikegami T, Maehara Y (2013) Transplantation: 3D printing of the liver in living donor liver transplantation. *Nat Rev Gastroenterol Hepatol* 10(12):697–698
34. Melchels FPW, Domingos MAN, Klein TJ, Malda J, Bartolo PJ, Huttmacher DW (2012) Additive manufacturing of tissues and organs. *Prog Polym Sci* 37(8):1079–1104
35. Zhu W, Holmes B, Glazer RI, Zhang LG (2016) 3D printed nanocomposite matrix for the study of breast cancer bone metastasis. *Nanomed Nanotechnol Biol Med* 12(1):69–79
36. Wallin TJ, Pikul J, Shepherd RF (2018) 3D printing of soft robotic systems. *Nat Rev Mater* 3(6):84–100
37. Yap YL, Yeong WY (2014) Additive manufacture of fashion and jewellery products: a mini review: this paper provides an insight into the future of 3D printing industries for fashion and jewellery products. *Virtual Phys Prototyp* 9(3):195–201
38. Ngo TD, Kashani A, Imbalzano G, Nguyen KTQ, Hui D (2018) Additive manufacturing (3D printing): a review of materials, methods, applications and challenges. *Compos B Eng* 143:172–196
39. Zhuang Y et al (2017) 3D-printing of materials with anisotropic heat distribution using conductive polylactic acid composites. *Mater Des* 126:135–140
40. Kim S-H, Choi K-H, Cho S-J, Yoo J, Lee S-S, Lee S-Y (2018) Flexible/shape-versatile, bipolar all-solid-state lithium-ion batteries prepared by multistage printing. *Energy Environ Sci* 11(2):321–330
41. Nikzad M, Masood SH, Sbarski I (2011) Thermo-mechanical properties of a highly filled polymeric composites for fused deposition modeling. *Mater Des* 32(6):3448–3456
42. Govindarajan SR, Jain T, Choi J-W, Joy A, Isayeva I, Vorvolakos K (2018) A hydrophilic coumarin-based polyester for ambient-temperature initiator-free 3D printing: chemistry, rheology and interface formation. *Polymer* 152:9–17
43. Hwang S, Reyes EI, Moon K, Rumpf RC, Kim NS (2015) Thermo-mechanical characterization of metal/polymer composite filaments and printing parameter study for fused deposition modeling in the 3D printing process. *J Electron Mater* 44(3):771–777



44. Weng Z, Wang J, Senthil T, Wu L (2016) Mechanical and thermal properties of ABS/montmorillonite nanocomposites for fused deposition modeling 3D printing. *Mater Des* 102:276–283
45. Wei X et al (2015) 3D printable graphene composite. *Sci Rep* 5(1):11181
46. Andrade Chávez F, Siqueiros JG, Carrete IA, Delgado IL, Ritter GW, Roberson DA (2018) Characterisation of phases and deformation temperature for additively manufactured shape memory polymer components fabricated from rubberised acrylonitrile butadiene styrene. *Virtual Phys Prototyping*, pp 1–15
47. Tricot F et al (2018) Fabrication of 3D conductive circuits: print quality evaluation of a direct ink writing process. *RSC Adv* 8(46):26036–26046
48. Sanatgar RH, Campagne C, Nierstrasz V (2017) Investigation of the adhesion properties of direct 3D printing of polymers and nanocomposites on textiles: effect of FDM printing process parameters. *Appl Surface Sci* 1(403):551–563
49. Jia Y, He H, Geng Y, Huang B, Peng X (2017) High through-plane thermal conductivity of polymer based product with vertical alignment of graphite flakes achieved via 3D printing. *Compos Sci Technol* 145:55–61
50. Voet VSD et al (2018) Biobased acrylate photocurable resin formulation for stereolithography 3D printing. *ACS Omega* 3(2):1403–1408
51. Zhao T et al (2018) Silicone-epoxy-based hybrid photopolymers for 3D printing. *Macromol Chem Phys* 219(10):1700530
52. Elomaa L, Teixeira S, Hakala R, Korhonen H, Grijpma DW, Seppälä JV (2011) Preparation of poly( $\epsilon$ -caprolactone)-based tissue engineering scaffolds by stereolithography. *Acta Biomater* 7(11):3850–3856
53. Guo Y, Ji Z, Zhang Y, Wang X, Zhou F (2017) Solvent-free and photocurable polyimide inks for 3D printing. *J Mater Chem A* 5(31):16307–16314
54. Dechet MA et al (2019) Production of polyamide 11 microparticles for Additive Manufacturing by liquid-liquid phase separation and precipitation. *Chem Eng Sci* 197:11–25
55. DebRoy T et al (2018) Additive manufacturing of metallic components—process, structure and properties. *Prog Mater Sci* 92:112–224
56. Mu Q et al (2018) Intense pulsed light sintering of thick conductive wires on elastomeric dark substrate for hybrid 3D printing applications. *Smart Mater Struct* 27(11):115007
57. Manshoori Yeganeh A, Movahhedy MR, Khodaygan S (2019) An efficient scanning algorithm for improving accuracy based on minimising part warping in selected laser sintering process. *Virtual Phys Prototyping* 14(1):59–78
58. Ning F, Cong W, Qiu J, Wei J, Wang S (2015) Additive manufacturing of carbon fiber reinforced thermoplastic composites using fused deposition modeling. *Compos B Eng* 80:369–378
59. Mohan VB, Krebs BJ, Bhattacharyya D (2018) Development of novel highly conductive 3D printable hybrid polymer-graphene composites. *Mater Today Commun* 17:554–561
60. Tymrak BM, Kreiger M, Pearce JM (2014) Mechanical properties of components fabricated with open-source 3-D printers under realistic environmental conditions. *Mater Des* 58:242–246
61. Gantenbein S, Masania K, Woigk W, Sesseg JPW, Tervoort TA, Studart AR (2018) Three-dimensional printing of hierarchical liquid-crystal-polymer structures. *Nature* 561(7722):226–230
62. Deshpande A, Hsu K (2018) Acoustoplastic metal direct-write: Towards solid aluminum 3D printing in ambient conditions. *Addit Manuf* 19:73–80
63. Prasad A, Kandasubramanian B (2019) Fused deposition processing polycaprolactone of composites for biomedical applications. *Polym-Plast Technol Mater*, pp 1–34
64. Shabana S, Prasansha R, Kalinina I, Potoroko I, Bagale U, Shirish SH (2019) Ultrasound assisted acid hydrolyzed structure modification and loading of antioxidants on potato starch nanoparticles. *Ultrason Sonochem* 51:444–450
65. James S, Contractor R (2018) Study on nature-inspired fractal design-based flexible counter electrodes for dye-sensitized solar cells fabricated using additive manufacturing. *Sci Rep* 8(1):1–12

66. Väättäjä M, Kähäri H, Ohenoja K, Sobocinski M, Juuti J, Jantunen H (2018) 3D printed dielectric ceramic without a sintering stage. *Sci Rep* 8(1):1–8
67. Zhao T et al (2019) A comparative study on 3D printed silicone-epoxy/acrylate hybrid polymers via pure photopolymerization and dual-curing mechanisms. *J Mater Sci* 54(6):5101–5111
68. Xu K, Chen Y (2016) Photocuring temperature study for curl distortion control in projection-based stereolithography. *J Manuf Sci Eng* 139(2):021002
69. Costa SF, Duarte FM, Covas JA (2015) Thermal conditions affecting heat transfer in FDM/FFE: a contribution towards the numerical modelling of the process: This paper investigates convection, conduction and radiation phenomena in the filament deposition process. *Virtual Phys Prototyping* 10(1):35–46
70. Compton BG, Post BK, Duty CE, Love L, Kunc V (2017) Thermal analysis of additive manufacturing of large-scale thermoplastic polymer composites. *Addit Manuf* 17:77–86
71. D'Amico A, Peterson AM (2018) An adaptable FEA simulation of material extrusion additive manufacturing heat transfer in 3D. *Addit Manuf* 21:422–430
72. Kousiatza C, Chatzidai N, Karalekas D (2017) Temperature mapping of 3D printed polymer plates: experimental and numerical study. *Sensors* 17(3):456
73. Schmidt M, Pohle D, Rechtenwald T (2007) Selective laser sintering of PEEK. *CIRP Ann* 56(1):205–208
74. Das S (2003) Physical aspects of process control in selective laser sintering of metals. *Adv Eng Mater* 5(10):701–711
75. Ko SH, Pan H, Grigoropoulos CP, Luscombe CK, Fréchet JMJ, Poulidakos D (2007) All-inkjet-printed flexible electronics fabrication on a polymer substrate by low-temperature high-resolution selective laser sintering of metal nanoparticles. *Nanotechnology* 18(34):345202
76. Kong D et al (2018) Bio-functional and anti-corrosive 3D printing 316L stainless steel fabricated by selective laser melting. *Mater Des* 152:88–101
77. Thomas N, Sreedhar N, Al-Ketan O, Rowshan R, Al-Rub RK, Arafat H (2018) 3D printed triply periodic minimal surfaces as spacers for enhanced heat and mass transfer in membrane distillation. *Desalination* 1(443):256–271
78. Wudy K, Drummer D (2019) Aging effects of polyamide 12 in selective laser sintering: molecular weight distribution and thermal properties. *Addit Manuf* 25:1–9
79. Li Y, Chen K, Tamura N (2018) Mechanism of heat affected zone cracking in Ni-based superalloy DZ125L fabricated by laser 3D printing technique. *Mater Des* 150:171–181
80. Guerra AJ, Ciurana J (2018) 3D-printed bioabsorbable polycaprolactone stent: the effect of process parameters on its physical features. *Mater Des* 137:430–437
81. Ouyang D, Xing W, Li N, Li Y, Liu L (2018) Structural evolutions in 3D-printed Fe-based metallic glass fabricated by selective laser melting. *Addit Manuf* 23:246–252
82. Szost BA et al (2016) A comparative study of additive manufacturing techniques: residual stress and microstructural analysis of CLAD and WAAM printed Ti–6Al–4 V components. *Mater Des* 89:559–567
83. Sępak B, Antończak AJ, Bartkowiak-Jowska M, Filipiak J, Pezowicz C, Abramski KM (2014) Fabrication of a polymer-based biodegradable stent using a CO<sub>2</sub> laser. *Arch Civ Mech Eng* 14(2):317–326
84. Kruth JP, Wang X, Laoui T, Froyen L (2003) Lasers and materials in selective laser sintering. *Assembly Autom* 23(4):357–371
85. Duley WW, Mueller RE (1992) CO<sub>2</sub> laser welding of polymers. *Polym Eng Sci* 32(9):582–585
86. Ravi AK, Deshpande A, Hsu KH (2016) An in-process laser localized pre-deposition heating approach to inter-layer bond strengthening in extrusion based polymer additive manufacturing. *J Manuf Process* 24:179–185
87. Franco A, Romoli L (2012) Characterization of laser energy consumption in sintering of polymer based powders. *J Mater Process Technol* 212(4):917–926
88. Jo W, Kim DH, Lee JS, Lee HJ, Moon M-W (2014) 3D printed tactile pattern formation on paper with thermal reflow method. *RSC Adv* 4(60):31764–31770

89. Chen Y-F, Wang Y-H, Tsai J (2019) Enhancement of surface reflectivity of fused deposition modeling parts by post-processing. *Opt Commun* 430:479–485
90. Peng Z, Luo X, Xie Z, An D, Yang M (2018) Effect of print path process on sintering behavior and thermal shock resistance of  $Al_2O_3$  ceramics fabricated by 3D inkjet-printing. *Ceram Int* 44(14):16766–16772
91. Li S et al (2018) The fabrication of SiBCN ceramic components from preceramic polymers by digital light processing (DLP) 3D printing technology. *J Eur Ceram Soc* 38(14):4597–4603
92. Yang F, Zhang X, Guo Z, Volinsky AA (2018) 3D gel-printing of Sr ferrite parts. *Ceram Int* 44(18):22370–22377
93. Kim F et al (2018) 3D printing of shape-conformable thermoelectric materials using all-inorganic  $Bi_2Te_3$ -based inks. *Nat Energy* 3(4):301–309
94. Wang L, Ju Y, Xie H, Ma G, Mao L, He K (2017) The mechanical and photoelastic properties of 3D printable stress-visualized materials. *Scientific reports*. 7(1):1–9
95. Zhang Q, Zhang F, Xu X, Zhou C, Lin D (2018) Three-dimensional printing hollow polymer template-mediated graphene lattices with tailorable architectures and multifunctional properties. *ACS Nano* 12(2):1096–1106
96. Zhang Q, Zhang F, Medarametla SP, Li H, Zhou C, Lin D (2016) 3D printing of graphene aerogels. *Small* 12(13):1702–1708
97. Hong D et al (2016) Binder-jetting 3D printing and alloy development of new biodegradable Fe-Mn-Ca/Mg alloys. *Acta Biomater* 45:375–386
98. Weiss K-P, Bagrets N, Lange C, Goldacker W, Wohlgemuth J (2015) Thermal and mechanical properties of selected 3D printed thermoplastics in the cryogenic temperature regime. *IOP Conf Ser Mater Sci Eng* 102:012022
99. Bartolomé E, Bozzo B, Sevilla P, Martínez-Pasarell O, Puig T, Granados X (2017) ABS 3D printed solutions for cryogenic applications. *Cryogenics* 82:30–37
100. Guo Y et al (2017) Engineering flame retardant biodegradable polymer nanocomposites and their application in 3D printing. *Polym Degrad Stab* 137:205–215
101. Manapat JZ, Mangadlao JD, Tiu BDB, Tritchler GC, Advincola RC (2017) High-strength stereolithographic 3D printed nanocomposites: graphene oxide metastability. *ACS Appl Mater Interfaces* 9(11):10085–10093
102. Sanchez-Romaguera V et al (2015) Inkjet printed paper based frequency selective surfaces and skin mounted RFID tags: the interrelation between silver nanoparticle ink, paper substrate and low temperature sintering technique. *J Mater Chem C* 3(9):2132–2140
103. Zhang X, Guo Z, Chen C, Yang W (2018) Additive manufacturing of WC-20Co components by 3D gel-printing. *Int J Refract Metal Hard Mater* 70:215–223
104. Goyanes A, Det-Amornrat U, Wang J, Basit AW, Gaisford S (2016) 3D scanning and 3D printing as innovative technologies for fabricating personalized topical drug delivery systems. *J Controlled Release* 234:41–48
105. Ippolito F, Rentsch S, Hübner G, Claypole T, Gane P (2019) Influence of calcium carbonate on polyamide 12 regarding melting, formability and crystallization properties. *Compos B Eng* 164:158–167
106. Zhang B, Kowsari K, Serjouei A, Dunn ML, Ge Q (2018) Reprocessable thermosets for sustainable three-dimensional printing. *Nat Commun* 9(1):1–7
107. Shi Q et al (2017) Recyclable 3D printing of vitrimer epoxy. *Mater Horiz* 4(4):598–607
108. Wang L, Kiziltas A, Mielewski DF, Lee EC, Gardner DJ (2018) Closed-loop recycling of polyamide12 powder from selective laser sintering into sustainable composites. *J Clean Prod* 195:765–772
109. Xu C, Wu Q, L'Espérance G, Lebel LL, Therriault D (2018) Environment-friendly and reusable ink for 3D printing of metallic structures. *Mater Des* 160:262–269
110. Oropallo W, Piegil LA (2016) Ten challenges in 3D printing. *Eng Comput* 32(1):135–148
111. Bose S, Vahabzadeh S, Bandyopadhyay A (2013) Bone tissue engineering using 3D printing. *Mater Today* 16(12):496–504
112. Garreta E et al (2017) Tissue engineering by decellularization and 3D bioprinting. *Mater Today* 20(4):166–178

113. Jose RR, Brown JE, Polido KE, Omenetto FG, Kaplan DL (2015) Polyol-Silk bioink formulations as two-part room-temperature curable materials for 3D printing. *ACS Biomater Sci Eng* 1(9):780–788
114. Irvine S, Venkatraman S (2016) Bioprinting and differentiation of stem cells. *Molecules* 21(9):1188
115. Sakai S et al (2018) Visible light-induced hydrogelation of an alginate derivative and application to stereolithographic bioprinting using a visible light projector and acid red. *Biomacromolecules* 19(2):672–679
116. Tan Z, Parisi C, Di Silvio L, Dini D, Forte AE (2017) Cryogenic 3D printing of super soft hydrogels. *Sci Rep* 7(1):1–1
117. He Y, Yang F, Zhao H, Gao Q, Xia B, Fu J (2016) Research on the printability of hydrogels in 3D bioprinting. *Scientific reports*. 20(6):29977
118. MarketsandMarkets (2019) Craniomaxillofacial implants market worth 2.49 Billion USD by 2021. Craniomaxillofacial implants market. [Online]. <https://www.marketsandmarkets.com/PressReleases/craniomaxillofacial-implant.asp>. Accessed 23 Jan 2019
119. Habibovic P, Gbureck U, Doillon C, Bassett D, Vanblitterswijk C, Barralet J (2008) Osteoconduction and osteoinduction of low-temperature 3D printed bioceramic implants. *Biomaterials* 29(7):944–953
120. Tai BL, Kao Y-T, Payne N, Zheng Y, Chen L, Shih AJ (2018) 3D Printed composite for simulating thermal and mechanical responses of the cortical bone in orthopaedic surgery. *Med Eng Phys* 61:61–68
121. Rasoulianboroujeni M et al (2019) Development of 3D-printed PLGA/TiO<sub>2</sub> nanocomposite scaffolds for bone tissue engineering applications. *Mater Sci Eng, C* 96:105–113
122. Wang L, Xu ME, Luo L, Zhou Y, Si P (2018) Iterative feedback bio-printing-derived cell-laden hydrogel scaffolds with optimal geometrical fidelity and cellular controllability. *Sci Rep* 8(1):1–3
123. Warner EL, Norton IT, Mills TB (2019) Comparing the viscoelastic properties of gelatin and different concentrations of kappa-carrageenan mixtures for additive manufacturing applications. *J Food Eng* 246:58–66

**Prasansha Rastogi** has completed her Master's in Materials Science and Technology from Defence Institute of Advanced Technology (DIAT), Pune, India in 2019. For Master's thesis, she has worked on 4D printing, which utilized smart materials having property of stimuli responsiveness and shape memory. Presently, she is doing PhD on 3D printing of foams, at the University of Twente, Enschede, The Netherlands.

**Mr. Swaroop Gharde** is currently working as a Junior Research Fellow (JRF) in DIAT, Pune, and holds Master's degree in Computer-Aided Analysis and Design (CAAD) from Manipal University, Jaipur. His research interests include design and analysis of composite structures, 3D printing, vacuum casting, polymer composite for different applications.

**Prof. Balasubramanian Kandasubramanian** is highly acclaimed for his contribution towards the polymer processing and fabrication for various applications including antibacterial, smart textiles, hydrophobic coatings, ablative materials, fire retardant fabrics waste water treatment, biomimicking and polymer nanocomposite for defence applications and has 14 Indian patents with more than 200 papers in peer-reviewed journals. He is the Head of the Department of Metallurgical and Materials Engineering, associated with DIAT (DU) from 2010 till date. He was actively involved in the development of various research laboratory including polymer processing laboratory, characterization laboratories (FESEM, HRTEM, SAXS). His contribution towards the waste water management was acknowledged and perceived by the National Water Academy, Pune, and Board of Research in Nuclear Science (BRNS), Mumbai. Prof. Balasubramanian K. has been

recognized by the Royal Society of Chemistry (RSC) for one of the most cited authors of the year for his erudite work on super-hydrophobicity. They have gleaned the attention of Naval Post-graduate School California, USA, and Naval Material and Research Laboratory (NMRL), DRDO Ambarnath, Ministry of Defence, India, for the development of hydrophobic, antifungal and anti-corrosive coating for ship hulls. He is recently awarded with the prestigious award “Technology Innovation in Petrochemicals and Downstream Plastic Processing Industry” from the Ministry of Chemical and Fertilizers, Government of India for his contribution in polymer technology.

# Chapter 4

## Role of Imaging Data in Additive Manufacturing for Biomedical Applications



Gurminder Singh and Pulak M. Pandey

### 4.1 Introduction

Additive manufacturing (AM) has made a significant effect in several application fields, especially in the biomedical applications. The ability to fabricate customized or patient-specific scaffolds, prosthesis, or other implants has made a huge impact of AM in the present era. The combination of digital image processing (DIP) tools and other computer-aided design (CAD) techniques gives advantage to AM to fabricate implants, organs, tissues, vascular structures, fixation devices, etc., for transplantation and also as well for pre-surgery planning. AM has shown time- and cost-saving potential during surgery in the present time [1]. The fabricated 3D model gives idea and practice to the doctors to understand the complications of the operation.

Development of image scanning techniques has also rapidly increased the demand of AM in the medical field. Generally, computerized tomography (CT) or magnetic resonance imaging (MRI) scanning data is used to make 3D CAD model. There are also other scanning methods such as ultrasound, laser scanning, and positron emission tomography which are used to obtain patient data. The data presents exact density, colour, or other features of the human body parts as of real-time parts. Each slice of the data is joined to make 3D model by interpolation means. These scanning methods are discussed in detail in the further sections. The developed 3D models by image processing are further fabricated by AM techniques.

Generally, AM application has been classified in five different areas as shown in Fig. 4.1. Medical model fabricated by using AM techniques has made the medical learning more versatile and provided ease to the medical students. The development

---

G. Singh · P. M. Pandey (✉)

Mechanical Engineering Department, Indian Institute of Technology Delhi, New Delhi, Delhi 110016, India

e-mail: [pmpandey@mech.iitd.ac.in](mailto:pmpandey@mech.iitd.ac.in)

G. Singh

e-mail: [gurmindersingh2012@gmail.com](mailto:gurmindersingh2012@gmail.com)

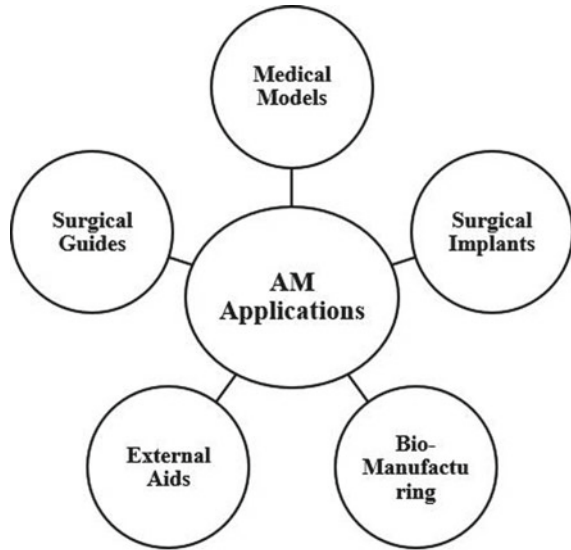
© Springer Nature Singapore Pte Ltd. 2020

S. Singh et al. (eds.), *3D Printing in Biomedical Engineering*,

Materials Horizons: From Nature to Nanomaterials,

[https://doi.org/10.1007/978-981-15-5424-7\\_4](https://doi.org/10.1007/978-981-15-5424-7_4)

**Fig. 4.1** Additive manufacturing application in the medical field



in AM for the metal printing techniques such as direct metal laser printing (DMLS), selective laser melting (SLM), and electron beam machining (EBM) provides facility to fabricate topological optimized implants or prosthesis for load-bearing applications. These patient-specific fabricated implants fit easily during surgical operations. AM provided not only the ability to fabricate implants for surgery transplantations; it also provides facility to fabricate organs or body part structures from the scanned data. The fabricated part gave information to doctors for better understanding and practice over the prototypes to reduce the surgery complications and time. Bio-manufacturing or bio-printing is the upgrowing area in the AM field. In bio-printing, the organs are printed with different types of cells using bio-inks [2]. The detail description of the bio-printing is given in the next sections of the present chapter.

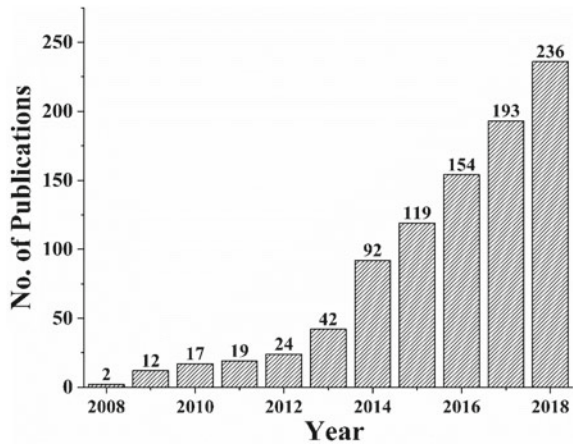
Apart from the above-mentioned major applications, other developments in the biomedical area due to the AM are summarized in the following points:

- Strength and surface quality enhancements in the implants or prosthetics.
- Production of topological optimized and lightweight implants.
- Reconstruction of soft tissues such as nose and cartilages.
- Development of surgical customized tools.
- Improved overall efficiency and reduced surgery time.

## 4.2 Motivation for Study

In current era, highly customized and precise implants, prosthetics, scaffolds, etc., are required for successful and productive medical studies both laboratory or clinically

**Fig. 4.2** Number of publications year-wise in medical applications of AM.  
Source Scopus



[3–5]. AM is a unique way of manufacturing to fulfil customization and precision in the medical sector. In the last decade, more than 900 papers have been published in the medical applications of the AM. Figure 4.2 depicts the yearwise number of publications of AM in the medical applications. The number of research outcomes in the present filed is increased rapidly in past five years with establishment and development in the AM to utilize the digital image processing data for the customized fabrications.

A study is required to understand the role of digital image processing in AM for biomedical applications. In the present chapter, specific concentration has been made to review the different image processing techniques used in the biomedical studies with the combination of additive manufacturing techniques.

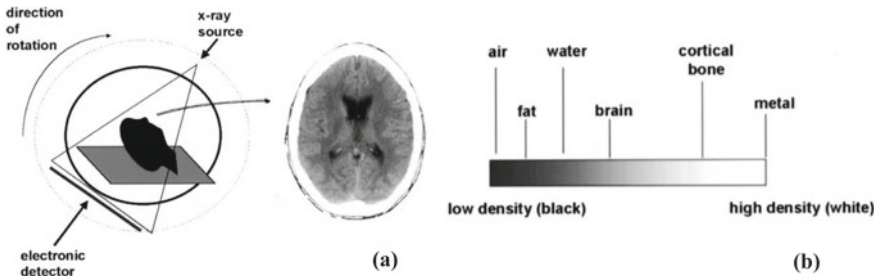
### 4.3 Image Capturing Techniques in Biomedical Area

There are different image capturing techniques available in the biomedical area to scan the human body organs, tissues, bones, etc. The generally used techniques with their principle, applications, advantages, and disadvantages are discussed in the following subsections.

#### 4.3.1 CT Scan

CT scan (earlier named as computerized axial tomography scan or CAT scan) gives the inside organ information and to the depth of different density levels of a human body. The X-ray intensity beam is used to capture different body parts such as shoulders, bones, eyes, spinal cord, heart and also other inner parts. CT scan records





**Fig. 4.3** a Basic principle of CT scan and b CT image shade variation with density variation [9]

different patterns of densities with the help of multi X-rays and electronic detectors to create images of the tissues or other body organs (ref. Fig. 4.3a). The multi X-rays pass through the patient at a time from different axis [6]. The bright/dark image quality depends upon the attenuation of X-rays. The higher attenuation of X-rays gives brighter or whitish CT image; lower attenuation of X-rays gives darker or blackish CT image. The variation or shades of CT scan image from lower to higher-density specimens are shown in Fig. 4.3). The fast scanning provided in this technology helps to improve patient comfort and easiness. Especially, CT scan provided visualization of different types of tumours or other small nodules to help doctors to diagnose, otherwise difficult or cannot be seen by other technologies [7]. CT scan bypasses the invasive angiography to provide clear 3D images (using different software's) to a surgeon [8]. It provides clear 3D images of the heart to a cardiologist without using any invasive angiography. The demerits of the scanning technique are it gives the risk of cancer by high dosage of radiation to the patient.

### 4.3.2 MRI Scan

In MRI scan (formerly known as nuclear magnetic resonance imaging or NMRI), powerful magnetic field and radio frequencies are used to capture the detail structures of the human body like heart, bones, liver, especially soft tissues, etc. The advantage of an MRI scan is to provide details regarding normal and abnormal tissues [10]. In MRI, radiofrequency signals are generated from hydrogen atoms and absorbed by the antennas after passing from the human body part [11]. The detected signals by antennas are further converted into layers segments. Furthermore, the collective layers present the different views of the scanned organ. The typical flow chart of the MRI scan processing is shown in Fig. 4.4. As the human body consists of hydrogen in different forms, it provides information regarding water and fat contents. The blood circulation information is easy to access using an MRI scanner, which helps to detect blood clots or blockages in cardiovascular or endovascular surgeries [12]. The technology is an accurate and safest method to detect different types of disease without any pain to the patient. Also, it provides alternative information about curing

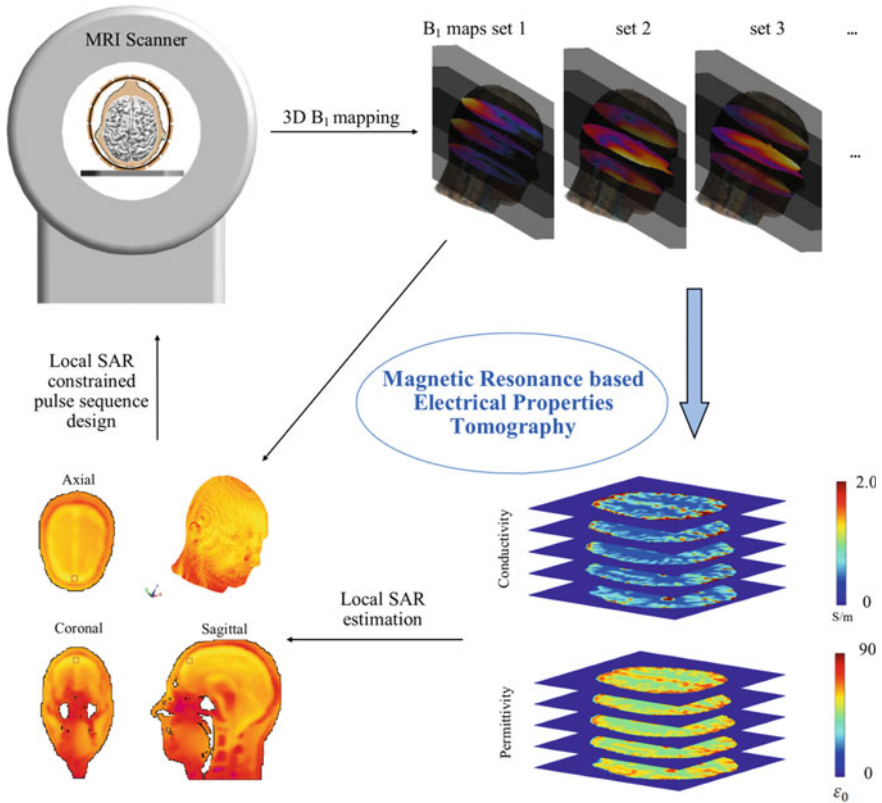


Fig. 4.4 Flow chart of MRI scan processing [15]

the disease. The advantage of the MRI scan is that it provides typical information such as swelling or bleeding in the organ, tumours in the brain, and inflammation of the spine [13, 14]. It easily provides information about blood circulation, which makes it different from other scanning techniques. The limitations are it involves loud noises during the scan, and generally, scan is performed in an enclosed chamber.

### 4.3.3 X-Rays

X-rays are the ray lights like visible rays with a different wavelength. X-rays are commonly used to capture dense parts of the human body. The rays easily pass through the low dense tissues such as skin, organs and absorbed by the dense parts such as bones [9]. The status of the dense parts is captured on X-ray films. These films are similar to the film of a camera. These types of scanning facility are generally used by dentists to diagnoses and for different broad variety treatments [16]. The

limitation of X-rays is it gives the risk of cancer on the prolonged use, can cause cell damage, and also can cause mutation disturbance in the DNA. This scanning information has application to treat malign tumours, identify cracks, infections, and also bone cancer.

### **4.3.4 *Ultrasound***

Sound waves are used to produce inside body pictures in the case of ultrasound. This kind of scanning images is generally used to diagnose the cause of internal organs infections, pain, and sometimes swelling [17]. It does not require any ionizing radiations and is safe and non-invasive. This imaging is also known as sonography or cardio-graphy. In this technique, an ultrasonic transducer is placed directly on the patient skin with the help of a gel. The high-frequency ultrasonic sound waves are transmitted through the skin to create images of the internal part. This is also helpful to guide bypass surgeries and heart conditions after the heart attack. As it is the safest capturing technique, the extensive research is going on to address the limitation of the technique. The ultrasound scanning failed to capture large images and created difficulty to capture the inside bone structure.

### **4.3.5 *3D Scanning***

In this type of scanning, cloud point data is collected to create a three-dimensional model. A standard reference data is used to format the collected data for the merging process to make models called as alignment. The structured light is falling on the object in a series of patterns by a projector, and a camera captures the images of the object in a cloud data form [18]. The basic difference of the 3D scanning from other developed scanning technologies is that it captures the outer surface of the body, whereas other technologies capture internal information such as tissues, different organs, and bones. For a single scan, 3D scanning takes only a few seconds and analyses the part quickly as compared to other techniques [19]. Three-dimensional scanning major application in the medical industry is to ensure the fit of the implant before surgery.

## **4.4 *Software's for Data Analysis***

The different software packages are available to create a 3D model from the scanned images by CT or MRI data. These software packages are helpful to make a virtual surgery simulation platform consisted of anatomical structures, volume, size, and complex shapes of tissues. Different companies have developed software to data

analysis from DICOM or other format files. The important steps carried out to obtain a 3D model from scanned data are briefly discussed in the coming sections. Generally used or recommended software packages advantages, disadvantages, and cost analysis are shown in Table 4.1.

**Table 4.1** Overview of established software packages used in the medical applications of AM

Software	User-friendly	Cost	Advantages	Disadvantages
Mimics	+++	\$\$	<ul style="list-style-type: none"> <li>• Most reliable and ISO-based software</li> <li>• Provision to analyse the 3D model with finite element study</li> <li>• Virtual surgery access is available for surgery planning</li> </ul>	<ul style="list-style-type: none"> <li>• Highly recommended PC specifications required for installation and working</li> </ul>
3D doctor	+	\$\$\$	<ul style="list-style-type: none"> <li>• FDA (US Food and Drug Administration) approved software for medical practices</li> <li>• Can access more than 2000 sliced data with 256 MB RAM</li> <li>• Detailed analysis tools are available in the parent package (no additional charges required for other modules)</li> </ul>	<ul style="list-style-type: none"> <li>• Software working environment is difficult to understand</li> <li>• A trained person is required to use the software</li> </ul>
3D slicer	+	Free	<ul style="list-style-type: none"> <li>• Diffusion tensor data analysis and visualization available</li> <li>• Image-tracking module available for device tracking</li> </ul>	<ul style="list-style-type: none"> <li>• Not approved for clinical uses</li> <li>• Subroutine programs required for analysis</li> </ul>
InVesalius	++	Free	<ul style="list-style-type: none"> <li>• Open-source and free software</li> <li>• Required low PC specifications</li> </ul>	<ul style="list-style-type: none"> <li>• Must write codes for the development</li> </ul>
OsiriX imaging	++	\$\$\$	<ul style="list-style-type: none"> <li>• Desktop and mobile versions available</li> <li>• Provision to access PET-CT and SPECT-CT data for 3D and 4D navigation</li> </ul>	<ul style="list-style-type: none"> <li>• Not advanced in post-processing functions or measurement analysis</li> </ul>
Gimias	+	Free	<ul style="list-style-type: none"> <li>• Movie control provision available for better visualization</li> <li>• Open-source framework for dynamic analysis</li> </ul>	<ul style="list-style-type: none"> <li>• Difficult to use</li> <li>• Required lot of plugins for different modules access</li> </ul>

## 4.5 Additive Manufacturing

Additive manufacturing (AM) is a layer-by-layer manufacturing process to fabricate 3D realistic prototypes from a 3D designed model. Generally, models are designed using CAD software or reverse engineering scanned model or model generated from medical scanning method CT or MRI scan [20]. AM techniques give the advantage to fabricate complex shape geometries at a reasonable cost and without the use of any additional machining or tooling. The complex shapes bones, heart, custom implants, and prosthetics can be easily fabricated within a few hours. AM is rapidly advancing in the field of medical to manufacture patient-specific custom implants [21–23]. AM provides ease to manufacture the customized shapes as per the patient requirement. There are different types of AM techniques available in the market based on different types of manufacturing principles. Several types of materials can be used in different AM techniques. Many authors [24–35] have reviewed the different types of AM techniques with their merits and demerits in literature. Apart from the present additive manufacturing techniques (having high capital cost), different rapid tooling or indirect additive manufacturing methods are also reported in the literature which required low capital and manufacturing cost [36–46]. Generally used AM techniques (in the present medical industry) based on different materials are shown in Fig. 4.5.

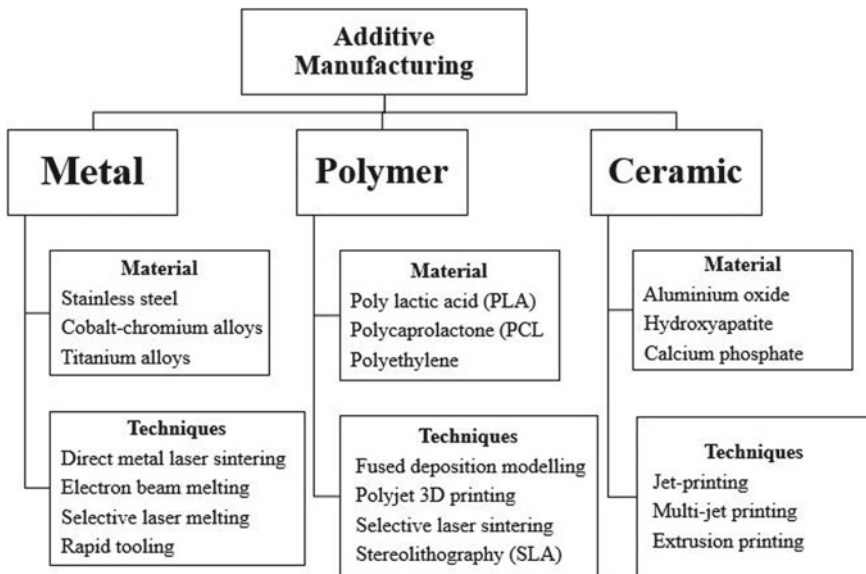


Fig. 4.5 Classification of AM techniques based on materials used in present medical industry

## 4.6 Scan to 3D Model: Steps

The steps used to convert the scanning data to a three-dimensional prototype or model are shown in Fig. 4.6. The description of the process stepwise is described in the following sections.

### 4.6.1 Image Acquisition

Image acquisition is a crucial step in the creation of a 3D model from the scanned images. Generally, CT and MRI scan data are used for image acquisition as these files consist of hidden information of the organs such as skin, tissues, and bone. The scanned data is saved in the DICOM or other compatible format and further used in the image processing tools for segmentation.

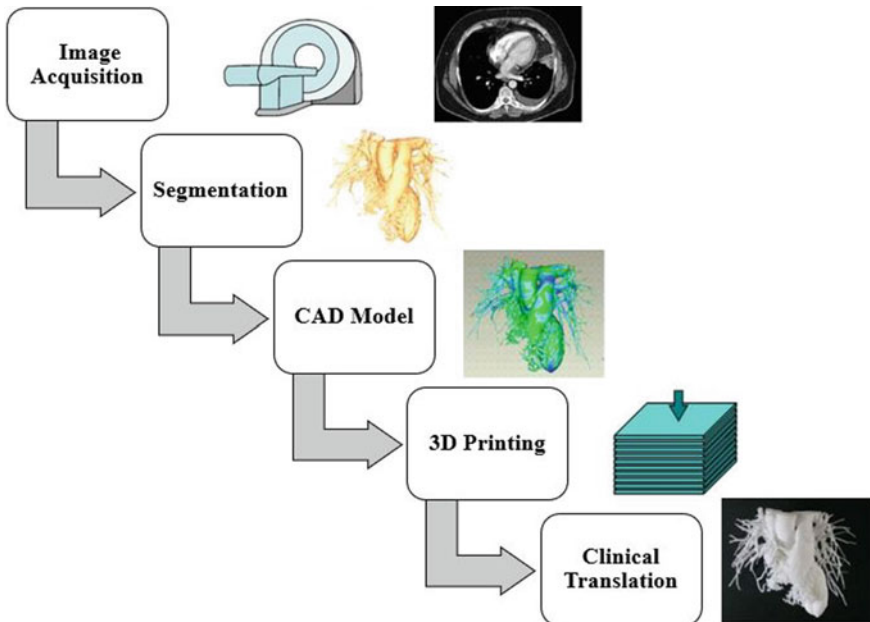


Fig. 4.6 Steps to convert scanning data into a clinically used 3D model

### **4.6.2 Segmentation**

In the scanned data, different types of information are stored in a DICOM file. Some of the data is of interest and some are useless. Therefore, the extraction of useful data is required from the scanned data. Segmentation steps come into the picture in the data processing. In segmentation, thresholding of the images is employed to extract the region of interest. Thresholding is done layer by layer to check the data in the form of voxel density. The required data is filtered by the selection of the desired density range. Therefore, the high-density structure such as cortical bone is easy to exclude or include during thresholding. In the case of thin structures such as scanning data of cancellous bone, high accuracy and practice experience are required during thresholding. Otherwise, it resulted in shrinkage of structure dimensions. The selection of thresholding range is a crucial part of the data segmentation.

Interpolation is included during the segmentation to increase the resolution of the contour data. Generally, CT-modeller software package is used to interpolate the threshold sliced data with mathematical interpolation algorithms. Two types of interpolation techniques (Bi-linear and C-spline) are used to increase the contour resolution and to minimize the staircase effect. Bi-linear interpolation is used for the liner or plane surfaces, and on the other side, c-spline is used for the curve or circular surfaces. After thresholding and interpolation in the segmentation step, further data is processed to make a CAD model.

### **4.6.3 Computer-Aided Design**

The segmented part developed from the patient CT or MRI data is exported to stereolithography (STL) format. The STL file is imported to a computer-aided design (CAD) package for editing. Further, the file is sliced using recommended slicer software for the printer. The sliced data is saved as G-code file for the 3D printing fabrication. CAD packages give facility to manipulate the STL file such as repair of triangulation error and any other design feature. Several CAD packages exist in the market, namely Solid-works, CREO or Pro-E, CATIA, Inventor, Unigraphics, etc. The different CAD packages have their own demerits and merits that depend upon the application requirement. The different types of CAD entities such as a circle, sphere, cylinder, B-spline curves, and surfaces are used to repair and to change the design feature of the STL file. Many CAD packages consisted of the interface of finite element analysis (FEA) or other analysis modules for segmented model design analysis. The analysis modules have used to analyse the material or design capability by applying different types of stresses as per the application requirement. These modules provide the ability to check the material and design implant capability virtually before the 3D printing process. It is done to prevent any failure after the fabrication of the implant. After the required changes and analyses, the STL file is used for the 3D printing fabrication.

### 4.6.4 3D Printing

The recommended steps for the 3D printing process after obtaining the STL file are shown in Fig. 4.7. The initial steps for the 3D printing process are too optimized orientation and slicing of the STL file. The optimized orientation reduced the fabrication time and also supported material requirement for the overhanging parts [47]. Traditionally, the optimized orientation was carried out by optimized algorithms by minimizing the use of support material and reducing time in a code compiler. However, with advancement in technology, the optimized orientation modules are available in the software provided by the AM companies. Support for hanging is minimized to acquire fine surface finish on the fabricated part. Further, the optimized oriented part is sliced with the help of slicing algorithms. Slicing step is crucial with respect to the fabricated part surface finish and the fabricating time also.

The thin layer thickness minimized the cusp height phenomena and improved the fabricated part surface finish and increased the fabrication time. As the surface finish is directly related to the fabricated part outer surface, a different combination of layer thickness can be used to acquire less fabrication time and better surface finish, known as adaptive slicing [48]. In the developed AM software packages, the different variation of the layer thickness is available which is selected as the application requirement. Generally, for medical implant, 50 or 100  $\mu\text{m}$  layer thickness is used for the fabrication to acquire a high surface finish. Further after slicing, the file is saved as the G-code (computer-aided manufacturing codes) file. The G-code file is used to fabricate the extracted part from the scanned data on the 3D printing machine. Different types of AM techniques are available depending upon the fabricated part requirements (material, strength, etc.). These techniques are already discussed earlier.

A post-processing step is carried out after the fabrication of the part. Several types of post-processing techniques such as acetone-vapour treatment shot blasting process, high-jet power treatment were used in literature to improve the part surface finish. Finally, the 3D printing part is transferred to the clinical or other application use.

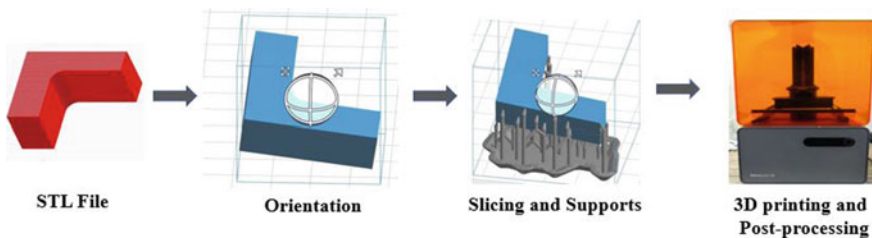


Fig. 4.7 Three-dimensional printing fabrication process steps



### 4.6.5 *Clinical Translation*

Three-dimensional implants fabricated by AM techniques help in different treatments and diagnoses of the diseases. It provides a better understanding between the doctors and patients for addressing the treatments [49, 50]. The case studies discussing the use of AM in the clinical trials are given in the next section.

## 4.7 Case Studies

AM process has shown enormous potential in the biomedical field. The advancement in scanning techniques and digital image processing tools has provided a unique way for the solid modelling of patient-specific human organs, bones, tissues, etc. The extracted model from the scanned data was used with AM processes for the fabrication with different materials for the applications. The use of AM techniques has made an impact on both in vitro (carried outside the body) and in vivo (carried inside the body) medical studies. The significant case studies from the literature are discussed in the following subsections.

### 4.7.1 *In Vitro*

Several researchers [51–53] have reported successful attempts to use AM fabricated in in vivo studies such as surgical planning and medical education. Different AM techniques contribution towards different types of disease treatments are summarized in Table 4.2. Significant contributions from the literature regarding improvement in in vitro studies are elaborated below.

Wake et al. [49] demonstrated the role of AM using fused deposition modelling (Stratasys) in the study of kidney tumour of a patient. The 3D model of the kidney was extracted from the patient MRI scan data. Further, the kidney model was printed by splitting to view the relationship of the renal tumour to the renal artery. Different colour materials were used to 3D print to distinguish the parts. The process from segmentation to 3D printing is shown in Fig. 4.8. It was revealed that the 3D printed parts gave proper understanding for radiologists and enhanced the patient care.

Bernhard et al. [54] reported the 3D printing of kidney tumour models from seven patient data. The object base stereolithography technique was used for fabrication with different colours. Patient's understanding was noted before and after the model presentation on the visualization scale. It was revealed that the understanding improvement was noticed in the patients for basic kidney physiology by 16.7%, kidney anatomy by 50%, tumour characteristics by 39.3%, and the planned surgical procedure by 44.6% after watching their own personal kidney's 3D printed models. The study helps for the better pre-surgical understanding of patients.

**Table 4.2** Contributions of different types of AM techniques in in vitro studies of biomedical applications

S. No.	Application	3D printing technique	Summary	References
1	Temporal bone prototype	Fused deposition modelling	<ul style="list-style-type: none"> <li>• The prototype was fabricated for the educational training quickly and at a cheaper cost</li> <li>• The prototype failed to replicate bone density and middle ear structures</li> </ul>	[57]
2	Transcatheter aortic valve prototype for replacement study	Stereolithography	<ul style="list-style-type: none"> <li>• The prototype was fabricated with a dimensional accuracy of 0.1 mm from the CAD model generated from CT scan</li> <li>• Nine patients designed were examined and correctly predicted in six of nine patients</li> </ul>	[58]
3	Segmented bone prototype dimensional analysis	Fused deposition modelling	<ul style="list-style-type: none"> <li>• The CT reconstruction parameters such as surface extraction, segmentation, and post-processing extraction effects were studied on the dimensional accuracy of the 3D model</li> <li>• The study helps to fabricate accurate dimensions prototypes</li> </ul>	[59]
4	Face bone tissue	Extrusion base printing	<ul style="list-style-type: none"> <li>• The topological study was carried out from the DICOM files</li> <li>• The 4% less volume difference was noted with surrounding less than 0.1 mm as compared to the STL mode</li> <li>• Fabricated implant successfully used in the surgical planning</li> </ul>	[60]

(continued)

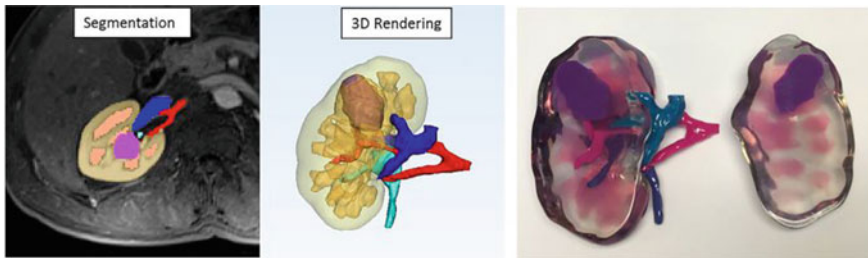
**Table 4.2** (continued)

S. No.	Application	3D printing technique	Summary	References
5	Cadaveric temporal bone for operation study	Fused deposition modelling	<ul style="list-style-type: none"> <li>• The prototype was fabricated for an operation planning study</li> <li>• Drilling was carried out on a prototype for operation training which minimized the risk during operation</li> </ul>	[61]
6	Thoracic aorta	Polyjet 3D printing	<ul style="list-style-type: none"> <li>• Rapid vessel prototyping permits the creation of a concrete solid replica of a patient's vascular anatomy</li> </ul>	[62]
7	Orthopaedic product	Selective laser sintering	<ul style="list-style-type: none"> <li>• AM reduced the product development time and fabricated patient-specific surgical accurately</li> </ul>	[63]
8	Shoulder, hip, knee, mandible, radiotherapy face mask, wrist, spine vertebrae, artery bypass graft models	Fused deposition modelling	<ul style="list-style-type: none"> <li>• Patient-specific models were fabricated to give surgeons a better understanding of the realistic problem</li> </ul>	[64]
9	Cranioplasty implant	Different method compared	<ul style="list-style-type: none"> <li>• Reverse engineering and CT data were used to design patient-specific implant by using CAD techniques</li> <li>• The technique will be helped to fabricate smooth fit implants</li> </ul>	[65]
10	Femur segment and customized scaffold	Selective laser sintering	<ul style="list-style-type: none"> <li>• The study was carried out to fabricate patient-specific scaffolds for the femur bone</li> <li>• AM is able to fabricate topologically ordered scaffold based on the CT scan data</li> </ul>	[66]

(continued)

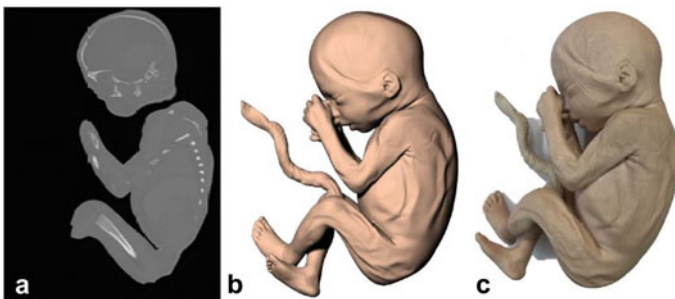
**Table 4.2** (continued)

S. No.	Application	3D printing technique	Summary	References
11	Laparoscopic splenectomy	Polyjet 3D printing	<ul style="list-style-type: none"> <li>• Complex anatomy structure was 3D printed for educational purposes</li> <li>• The printer was successfully able to reproduce even the small vessels and the finest details</li> </ul>	[67]

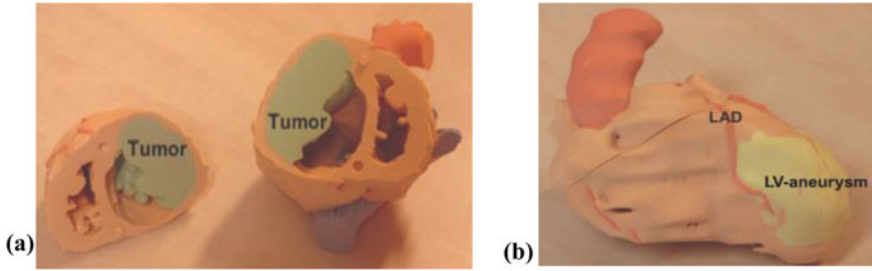


**Fig. 4.8** Different steps carried out to the 3D print patient kidney with tumour [49]

Young et al. [55] studied the practical aspect of human developmental using AM technique for biology education. The CT scan data of human embryonic and foetal for different weeks was used to make 3D CAD models. Further, these models were fabricated using stereolithography process for education purpose. The extracted CAD model from 20-week foetal CT scan data and its 3D printed part are shown in Fig. 4.9. It was noticed that the adopted approach improved the understanding of the students about human gestational.



**Fig. 4.9** a CT scan, b 3D CAD model, and c 3D printed model of 20-week foetus [55]



**Fig. 4.10** Three-dimensional printed model **a** with massive cardiac-tumour and **b** enlarged LV with an aneurysm [21]

Yang et al. [56] evaluated the role of AM in trimalleolar fracture treatment. Fused deposition modelling technique was used to fabricate thirty patients' feet by using their CT scan data. The effectiveness of the use of 3D printed parts was studied by the questionnaire among the doctors and the patients. It was revealed that patient satisfaction from doctor communication was around 9.3 out of 10. The 3D printed prototypes effectively help the doctors for the operation plan and acted as an effective tool for physician–patient communication.

Jacobs et al. [21] reported a case study about surgery planning to treat complex heart disease. Left ventricular aneurysm and the right ventricular tumour were 3D printed using CT and MRI scan data (ref. Figure 4.10). The surgeon was able to identify risk structures, assess the ideal resection lines, and determine the residual shape after a reconstructive procedure. Using a 3D print of the LV aneurysm, reshaping of the left ventricle ensuring sufficient LV volume was easily accomplished.

### 4.7.2 *In Vivo*

The use of AM in in vivo studies has shown a revolutionary change in medical history. The in vivo studies using AM are difficult to carry out as it directly deals with living beings. Few studies have been successfully reported in the literature for clinical implantation of AM fabricated implants. The different AM techniques used for in vivo studies are summarized in Table 4.3. A significant contribution of AM for in vivo case studies is elaborated below.

Popov et al. [68] have discussed the fabrication of patient-specific titanium implant for the foot surgery. The implant design, fabrication using EBM process, and implant surgery are shown in Fig. 4.11. It was studied that the AM manufactured implants were easy to fit and handle during the surgery. However, the manufacturing cost of the customized implants was relatively expensive as compared to the traditional process.

Khan et al. [69] reported the first in vivo case study of spinal prosthesis implantation fabricated by the 3D titanium printing machine. The customized prosthesis

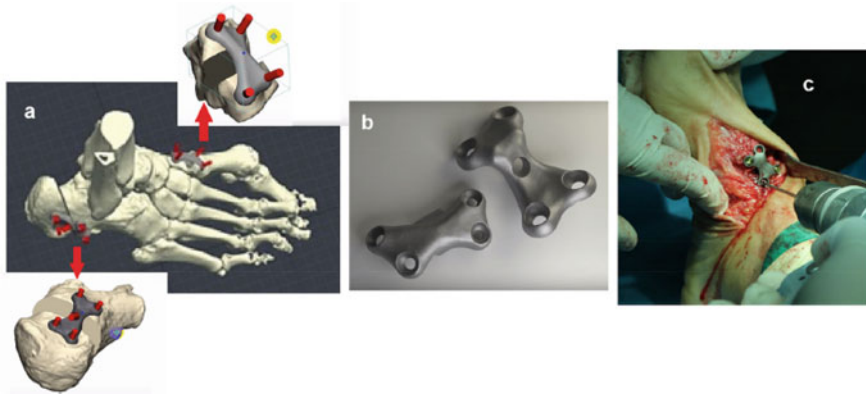
**Table 4.3** Contributions of different types of AM techniques in in vivo studies of biomedical applications

S. No.	Application	3D printing technique	Summary	References
1	Calvarial graft surgical planning and implantation	Stereolithography	<ul style="list-style-type: none"> <li>Physical prototype saved time and cost during surgery and gave a better idea to doctors for performing surgery</li> <li>The less-dimensional deviation was observed during implantation</li> </ul>	[73]
2	Prosthetic sockets implantation	Fused deposition modelling	<ul style="list-style-type: none"> <li>Patient-specific prosthetic socket was fabricated</li> <li>AM reduced the design problem and time for fabrication and provided better comfort and fit as compared to the traditional process</li> </ul>	[74]
3	Hemi-knee joint substitute	Stereolithography and rapid tooling	<ul style="list-style-type: none"> <li>A customized implant designed and implanted in a dog for trials</li> <li>The model was fabricated with a maximum tolerance of 0.206 mm</li> <li>The implanted joint was able to regenerate the damaged knee functions</li> </ul>	[1]
4	Maxillofacial prosthesis	Stereolithography and rapid tooling	<ul style="list-style-type: none"> <li>Patient-specific prosthesis was designed and fabricated to match the human mandible</li> <li>The implanted prosthesis has shown remarkable changes in the chewing function of the patient</li> </ul>	[75]

(continued)

Table 4.3 (continued)

S. No.	Application	3D printing technique	Summary	References
5	Chin implant	Stereolithography and rapid tooling	<ul style="list-style-type: none"> <li>• Better aesthetic form and fitting of the implant as compared traditional processing implant</li> <li>• Reduced the surgery time by pre-planning on the physical model</li> <li>• AM implant is accurate and provides easy insertion of the prosthesis into the defective site</li> </ul>	[76]
6	Maxillofacial prosthesis	Stereolithography and rapid tooling	<ul style="list-style-type: none"> <li>• Tremendous potential to fabricate lightweight custom prosthesis</li> </ul>	[77]
7	Osteotomy treatment for tibial plateau fracture	Fused deposition modelling	<ul style="list-style-type: none"> <li>• Three-dimensional printing technology was helpful to accurately design osteotomy operation and reduce the risk of postoperative deformity</li> <li>• It decreased intraoperative blood loss, shorten the operation time, and can effectively improve the treatment effect</li> </ul>	[78]
8	Treatment of cubitus varus deformity	Stereolithography	<ul style="list-style-type: none"> <li>• Twelve male and six female cases were treated using 3D printed osteotomy</li> <li>• The correction was confirmed with radiographs and surgery found successfully carried out</li> </ul>	[79]

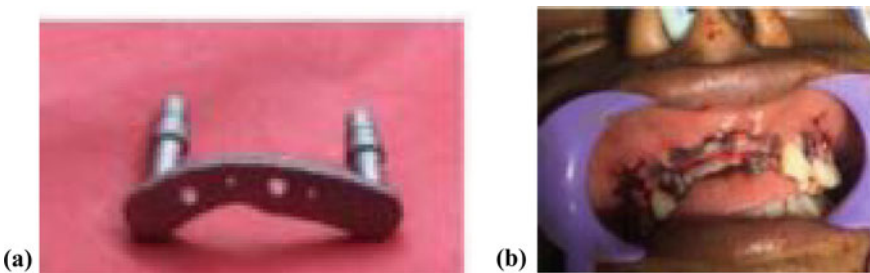


**Fig. 4.11** a Patient-specific implant design, b fabricated implant using the EBM process, and c implant surgery [68]

was designed from the CT scan data of a 65-year-old patient. After implantation, the patient responded uneventful recovery and pain reduction in occipital neuralgia.

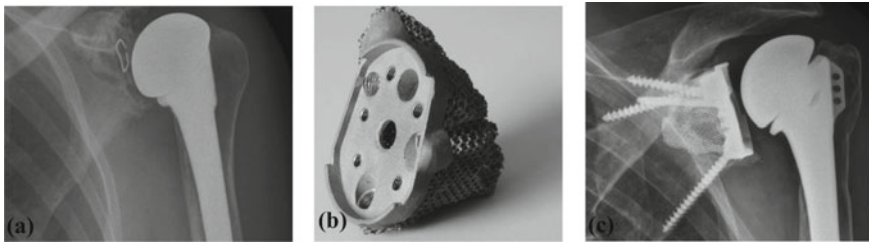
Malyala et al. [70] investigated the implantation of the 3D printed basal osseointegrated implant for maxillofacial surgery. CAD model was segmented from the accidental patient CT scan data. Then, the implant was designed for repair of denture jaws. Two-step printing was carried for surgical planning. First, designed implant and patients damaged jaw were 3D printed using FSM technique, and mock surgery was performed. After successful mock surgery, FEA analysis was performed in CAD software to check stress concentration with titanium as an implant material. Laser sintering technique was used to fabricate customized implant prosthesis with titanium material. The fabricated implants using laser sintering technique and surgery for implantation are shown in Fig. 4.12. The surgery was performed to implant the prosthesis and carried out in less time as compared to conventional surgery times.

Mohammed et al. [71] used selective laser melting process to fabricate patient-specific mandible implant. The titanium material was used for the fabrication of the implant. The size and geometric precision of the final implant were also evaluated



**Fig. 4.12** a Fabricated implant using laser sintering and b implant surgery [70]





**Fig. 4.13** a Radiograph demonstrating loosening of the glenoid component, b 3D-printed custom-made metal backing with porous structure filling, and c radiograph of stable glenoid component [72]

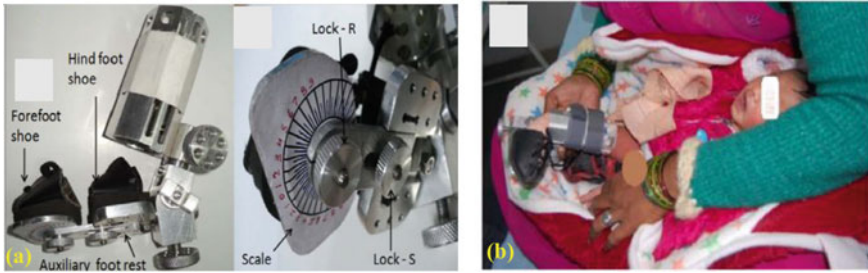
by reference to an FDM fabricated representative model of the patients surrounding skeletal anatomy and found to be an excellent fit. This device will address many of the shortcomings of current practice such as complications resulting from mandibular fractures, mismatching fixation plates, and general plate failures.

Stoffelen et al. [72] reported a case study of glenoid implant surgery on a 56-year-old woman. The radiograph images were taken to observe the destruction of the glenoid. The CT scan data was used for the repairing of the bone. It was noticed that the  $22 \text{ cm}^3$  bone was a loss from the joint. The porous implant was designed using CT data and fabricated with titanium material using metal printing technique. The fabricated part easily fitted to the bone and joint was observed over different time periods. The radiograph image of defected glenoid, fabricated porous implant, and radiograph of glenoid after surgery are shown in Fig. 4.13. It was observed that the functional and radiologic results, in this case, remained excellent even after 2 years of surgery.

Singh and Pandey [22, 80, 81] designed orthosis to address the problem of club foot deformity. Patient-specific and adjustable orthosis was designed and fabricated with help of selective laser sintering and rapid tooling to solve clubfoot problems of newborn babies. The orthosis was developed rotation of three mutually perpendicular planes and was subsequently tested on five patients over the duration of one week. Clinical trials confirmed the reliability of the product to reduce the deformities within short period of time (Fig. 4.14).

## 4.8 Conclusions and Future Scope

Additive manufacturing (AM) technology gives an advantage to fabricate 3D complex shapes directly from the CAD models. In medical applications, AM has been made a huge impact in different areas such as surgical planning, medical education and training, fabricating patient-specific implants, surgical tools, prosthesis, orthotics, scaffolding, and tissue engineering. The combination of scanning techniques, such as computerized tomography (CT), magnetic resonance imaging



**Fig. 4.14** a Fabricated and b applied orthosis for correction of clubfoot deformity [81]

(MRI), and ultrasound and image process tools such as MIMICS and 3D doctor, helps to model the patient-specific implants, organs, surgery models, etc. The scanning techniques and image process techniques have been discussed in detail in the present chapter. It was revealed that the scanning techniques have shown potential to capture in-depth images from the outer surface to inner parts of the human body. Renowned data conversion software's were discussed and compared on the basis of cost, advantages, and disadvantages. Few software's are available freeware and presently in the development stage with limitations. The important steps for conversion of scanned data to 3D printed parts were also given with step's description. Significant contribution of AM in vivo and in vitro case studies has been discussed. It was revealed that the AM techniques have played an important role in the biomedical field.

Due to different limitations such as high capital and fabrication cost, AM is difficult to use in everyday clinical practice yet. In the future, AM will have a better product customization and fabrication at a low or reasonable cost. The enormous potential in the technique promises development of new application in the fields of individual patient care, research activities, etc. It minimized the unkind side effects and has shown its capability to justify numerous challenges in the biomedical research and development sector.

## References

1. He J, Li D, Lu B et al (2007) Custom fabrication of a composite hemi-knee joint based on rapid prototyping. *Rapid Prototyping* 12:198–205. <https://doi.org/10.1108/13552540610682705>
2. Dababneh AB, Ozbolat IT (2014) Bioprinting technology: a current state-of-the-art review. *J Manuf Sci Eng* 136:061016. <https://doi.org/10.1115/1.4028512>
3. Singla A, Singh G, Virk GS (2016) Matlab/simMechanics based control of four-bar passive lower-body mechanism for rehabilitation. *Perspectives in Science* 8:351–354. <https://doi.org/10.1016/j.pisc.2016.04.072>
4. Singh S, Ramakrishna S (2017) Biomedical applications of additive manufacturing: present and future. *Curr Opin Biomed Eng* 2:105–115. <https://doi.org/10.1016/j.cobme.2017.05.006>

5. Hong D, Chou DT, Velikokhatnyi OI et al (2016) Binder-jetting 3D printing and alloy development of new biodegradable Fe-Mn-Ca/Mg alloys. *Acta Biomater* 45:375–386. <https://doi.org/10.1016/j.actbio.2016.08.032>
6. Goldman LW (2009) Principles of CT and CT Technology. *J Nuclear Med Technol* 35:115–129. <https://doi.org/10.2967/jnmt.107.042978>
7. Thompson A, McNally D, Maskery I, Leach RK (2017) X-ray computed tomography and additive manufacturing in medicine: a review. *Int J Metrol Qual Eng* 8:1–15. <https://doi.org/10.1051/ijmqe/2017015>
8. Vaishya R, Lal H (2018) Three common orthopaedic surgical procedures of the lower limb. *J Clin Orthop Trauma* 9:101–102. <https://doi.org/10.1016/j.jcot.2018.04.013>
9. Caldemeyer KS, Buckwalter KA (1999) The basic principles of computed tomography and magnetic resonance imaging. *J Am Acad Dermatol* 41:768–771
10. Ballyns JJ, Gleghorn JP, Niebrzydowski V, Rawlinson JJ, Potter HG, Maher SA, Wright TM, Bonassar LJ (2008) Implants via MRI and micro-CT using injection molding. *Tissue Eng Part A* 14(7):1195–1202. <https://doi.org/10.1089/ten.tea.2007.0186>
11. Brown MA, Richard SC (2011) MRI: basic principles and applications. John Wiley & Sons
12. Bernick C, Kuller L, Dulberg C et al (2001) Silent MRI infarcts and the risk of future stroke. *Neurology* 57:1222–1229
13. Mitsouras D, Lee TC, Liacouras P et al (2017) Three-dimensional printing of MRI-visible phantoms and MR Image-Guided Therapy simulation. *Magn Reson Med* 622:613–622. <https://doi.org/10.1002/mrm.26136>
14. Lal H, Kumar L, Kumar R et al (2017) Inserting pedicle screws in lumbar spondylolisthesis—The easy bone conserving way. *J Clin Orthop Trauma* 8:156–164. <https://doi.org/10.1016/j.jcot.2016.11.010>
15. Liu J, Wang Y, Katscher U, He B (2017) Electrical properties tomography based on B 1 maps in MRI: principles, applications, and challenges. *IEEE Trans Biomed Eng* 64:2515–2530. <https://doi.org/10.1109/TBME.2017.2725140>
16. Levine LE, Long GG (2004) X-ray imaging with ultra-small-angle X-ray scattering as a contrast mechanism. *J Appl Crystallogr* 37:757–765. <https://doi.org/10.1107/s0021889804016073>
17. Vaezi M, Chua CK, Chou SM (2012) Improving the process of making rapid prototyping models from medical ultrasound images. *Rapid Prototyping J* 18:287–298. <https://doi.org/10.1108/13552541211231716>
18. Bye E, McKinney E (2010) Fit analysis using live and 3D scan models. *Int J Clothing Sci Technol* 22:88–100. <https://doi.org/10.1108/09556221011018586>
19. Choi JW, Wicker RB, Cho SH et al (2009) Cure depth control for complex 3D microstructure fabrication in dynamic mask projection microstereolithography. *Rapid Prototyping J* 15:59–70. <https://doi.org/10.1108/13552540910925072>
20. Singh S, Ramakrishna S, Singh R (2017) Material issues in additive manufacturing: A review. *J Manuf Process* 25:185–200. <https://doi.org/10.1016/j.jmapro.2016.11.006>
21. Jacobs S, Grunert R, Mohr FW, Falk V (2008) 3D-Imaging of cardiac structures using 3D heart models for planning in heart surgery: a preliminary study. *Interact CardioVasc Thorac Surg* 7:6–9. <https://doi.org/10.1510/icvts.2007.156588>
22. Khas KS, Pandey PM, Ray AR (2015) Design and development of a device to measure the deformities of clubfoot. *Proc Inst Mech Eng [H]* 229:194–204. <https://doi.org/10.1177/0954411915574758>
23. Bose S, Vahabzadeh S, Bandyopadhyay A (2013) Bone tissue engineering using 3D printing. *Biochem Pharmacol* 16:496–504. <https://doi.org/10.1016/j.mattod.2013.11.017>
24. Ngo TD, Kashani A, Imbalzano G et al (2018) Additive manufacturing (3D printing): A review of materials, methods, applications and challenges. *Compos B* 143:172–196. <https://doi.org/10.1016/j.compositesb.2018.02.012>
25. Wong KV, Hernandez A (2012) A review of additive manufacturing. *Int Sch Res Netw* 2012:1–10. <https://doi.org/10.5402/2012/208760>
26. Chong L, Ramakrishna S, Singh S (2018) A review of digital manufacturing-based hybrid additive manufacturing processes. *Int J Adv Manuf Technol* 95:2281–2300

27. Patra S, Young V (2016) A review of 3D printing techniques and the future in biofabrication of bioprinted tissue. *Cell Biochem Biophys* 74:93–98. <https://doi.org/10.1007/s12013-016-0730-0>
28. Tack P, Victor J, Gemmel P, Annemans L (2016) 3D-printing techniques in a medical setting : a systematic literature review. *BioMed Eng OnLine*, pp 1–21. <https://doi.org/10.1186/s12938-016-0236-4>
29. Farid S, Shirazi S, Gharekhani S et al (2015) A review on powder-based additive manufacturing for tissue engineering: selective laser sintering and inkjet 3D printing. *Sci Technol Adv Mater* 16:1–20. <https://doi.org/10.1088/1468-6996/16/3/033502>
30. Singh S, Singh R (2016) Fused deposition modelling based rapid patterns for investment casting applications: a review. *Rapid Prototyping J* 22:123–143. <https://doi.org/10.1108/RPJ-02-2014-0017>
31. Wang X, Jiang M, Zhou Z et al (2017) 3D printing of polymer matrix composites: a review and prospective. *Compos B* 110:442–458. <https://doi.org/10.1016/j.compositesb.2016.11.034>
32. Poomathi N, Singh S, Prakash C et al (2018) Bioprinting in ophthalmology: current advances and future pathways. *Rapid Prototyping J*. <https://doi.org/10.1108/RPJ-06-2018-0144>
33. Prakash C, Singh S, Pabla BS et al (2018) Bio-inspired low elastic biodegradable Mg-Zn-Mn-Si-HA alloy fabricated by spark plasma sintering. *Mater Manuf Processes* 00:1–12. <https://doi.org/10.1080/10426914.2018.1512117>
34. Singh S, Prakash C, Ramakrishna S (2019) 3D printing of polyether-ether-ketone for biomedical applications. *Eur Polym J* 114:234–248. <https://doi.org/10.1016/j.eurpolymj.2019.02.035>
35. Singh S, Singh N, Gupta M et al (2019) Mechanical feasibility of ABS/HIPS-based multi-material structures primed by low-cost polymer printer. *Rapid Prototyping J* 25:152–161. <https://doi.org/10.1108/RPJ-01-2018-0028>
36. Singh G, Pandey PM (2019) Ultrasonic Assisted Pressureless Sintering for rapid manufacturing of complex copper components. *Mater Lett* 236:276–280. <https://doi.org/10.1016/j.matlet.2018.10.123>
37. Gill SS, Kaplas M (2009) Comparative study of 3D printing technologies for rapid casting of aluminium alloy. *Mater Manuf Process* 24:1405–1411. <https://doi.org/10.1080/10426910902997571>
38. Singh S, Singh R (2015) Wear modelling of Al-Al<sub>2</sub>O<sub>3</sub> functionally graded material prepared by FDM assisted investment castings using dimensionless analysis. *J Manuf Process* 20:507–514. <https://doi.org/10.1016/j.jmapro.2015.01.007>
39. Singh JP, Pandey PM (2018) Fabrication and assessment of mechanical properties of open cell porous regular interconnected metallic structure through rapid manufacturing route. *Rapid Prototyping J* 24:138–149. <https://doi.org/10.1108/RPJ-04-2015-0043>
40. Mun J, Yun BG, Ju J, Chang BM (2015) Indirect additive manufacturing based casting of a periodic 3D cellular metal - Flow simulation of molten aluminum alloy. *J Manuf Process* 17:28–40. <https://doi.org/10.1016/j.jmapro.2014.11.001>
41. Singh G, Pandey PM (2018) Design and analysis of long-stepped horn for ultrasonic assisted sintering. In: 21st International conference on advances in materials and processing technology (AMPT). Dublin, Ireland
42. Sharma P, Pandey PM (2018) Morphological and mechanical characterization of topologically ordered open cell porous iron foam fabricated using 3D printing and pressureless microwave sintering. *Mater Des* 160:442–454. <https://doi.org/10.1016/j.matdes.2018.09.029>
43. Sharma P, Pandey PM (2018) A novel manufacturing route for the fabrication of topologically-ordered open-cell porous iron scaffold. *Mater Lett* 222:160–163. <https://doi.org/10.1016/j.matlet.2018.03.206>
44. Sharma P, Pandey PM (2018) Rapid manufacturing of biodegradable pure iron scaffold using amalgamation of three-dimensional printing and pressureless microwave sintering. *Proc Inst Mech Eng Part C J Mech Eng Sci*, 0:1–20. <https://doi.org/10.1177/0954406218778304>
45. Singh G, Pandey PM (2019) Uniform and graded copper open cell ordered foams fabricated by rapid manufacturing: surface morphology, mechanical properties and energy absorption capacity. *Mater Sci Eng, A* 761:138035. <https://doi.org/10.1016/j.msea.2019.138035>

46. Singh G, Pandey PM (2019) Rapid manufacturing of copper components using 3D printing and ultrasonic assisted pressureless sintering: experimental investigations and process optimization. *J Manuf Process* 43:253–269. <https://doi.org/10.1016/j.jmapro.2019.05.010>
47. Thrimurthulu K, Pandey PM, Reddy NV (2004) Optimum part deposition orientation in fused deposition modeling. *Int J Mach Tools Manuf* 44:585–594. <https://doi.org/10.1016/j.ijmachtools.2003.12.004>
48. Pandey PM, Reddy NV, Dhande SG (2003) Real time adaptive slicing for fused deposition modelling. *Int J Mach Tools Manuf* 43:61–71. [https://doi.org/10.1016/S0890-6955\(02\)00164-5](https://doi.org/10.1016/S0890-6955(02)00164-5)
49. Wake N, Chandarana H, Huang WC et al (2016) Application of anatomically accurate, patient-specific 3D printed models from MRI data in urological oncology. *Clin Radiol* 71:610–614. <https://doi.org/10.1016/j.crad.2016.02.012>
50. Starosolski ZA, Kan JH, Rosenfeld SD et al (2014) Application of 3-D printing (rapid prototyping) for creating physical models of pediatric orthopedic disorders. *Pediatr Radiol* 44:216–221. <https://doi.org/10.1007/s00247-013-2788-9>
51. Haleem A, Javaid M (2018) Role of CT and MRI in the design and development of orthopaedic model using additive manufacturing. *J Clin Orthop Trauma* 9:213–217. <https://doi.org/10.1016/j.jcot.2018.07.002>
52. Javaid M, Haleem A (2018) Additive manufacturing applications in orthopaedics: a review. *J Clin Orthop Trauma* 9:202–206. <https://doi.org/10.1016/j.jcot.2018.04.008>
53. Rengier F, Mehndiratta A, Von Tengg-Kobligk H, Zechmann CM, Unterhinninghofen R, Kauczor HU, Giesel FL (2010) 3D printing based on imaging data: review of medical applications. *International journal of computer assisted radiology and surgery*. 5(4):335–341. <https://doi.org/10.1007/s11548-010-0476-x>
54. Bernhard JC, Isotani S, Matsugasumi T et al (2016) Personalized 3D printed model of kidney and tumor anatomy: a useful tool for patient education. *World J Urol* 34:337–345. <https://doi.org/10.1007/s00345-015-1632-2>
55. Young JC, Quayle MR, Adams JW et al (2019) Three-dimensional printing of archived human fetal material for teaching purposes. *Anat Sci Educ* 12:90–96. <https://doi.org/10.1002/ase.1805>
56. Yang L, Shang X, Fan J et al (2016) Application of 3D printing in the surgical planning of trimalleolar fracture and doctor-patient communication. *BioMed Res Int Table* 2016:1–5
57. Cohen J, Reyes SA (2016) Creation of a 3D printed temporal bone model from clinical CT data. *Am J Otolaryngol-Head Neck Med Surg* 36:619–624. <https://doi.org/10.1016/j.amjoto.2015.02.012>
58. Ripley B, Kelil T, Cheezum MK et al (2016) 3D printing based on cardiac CT assists anatomic visualization prior to transcatheter aortic valve replacement. *J Cardiovasc Computed Tomogr* 10:28–36. <https://doi.org/10.1016/j.jcct.2015.12.004>
59. Ogden KM, Aslan C, Ordway N et al (2015) Factors affecting dimensional accuracy of 3-D printed anatomical structures derived from CT data. *J Digit Imaging* 28:654–663. <https://doi.org/10.1007/s10278-015-9803-7>
60. Cai T, Rybicki FJ, Giannopoulos AA, et al (2015) The residual STL volume as a metric to evaluate accuracy and reproducibility of anatomic models for 3D printing : application in the validation of 3D-printable models of maxillofacial bone from reduced radiation dose CT images. *3D Printing Med* 2:1–9. <https://doi.org/10.1186/s41205-015-0003-3>
61. Hochman JB, Rhodes C, Wong D et al (2015) Comparison of cadaveric and isomorphic three-dimensional printed models in temporal bone education. *The Laryngoscope* 125:2353–2357. <https://doi.org/10.1002/lary.24919>
62. Markl M, Schumacher R (2005) Rapid vessel prototyping: vascular modeling using 3t magnetic resonance angiography and rapid prototyping technology. *Magma* 18:288–292. <https://doi.org/10.1007/s10334-005-0019-6>
63. Holmer B, Ashby A (2005) How rapid prototyping can assist in the development of new orthopaedic products—a case study. *Rapid Prototyping* 1:38–41
64. Sanghera B, Naique S, Papaharilaou Y, Amis A (2006) Preliminary study of rapid prototype medical models. *Rapid Prototyping* 7:275–284

65. Hieu LC, Bohez E, Vatcharaporn E et al (2003) Design for medical rapid prototyping of cranioplasty implants. *Rapid Prototyping* 9:175–186. <https://doi.org/10.1108/13552540310477481>
66. Naing MW, Chua CK, Leong KF, Wang Y (2006) Fabrication of customised scaffolds using computer-aided design and rapid prototyping techniques. *Rapid Prototyping* 11:249–259. <https://doi.org/10.1108/13552540510612938>
67. Pietrabissa A, Marconi S, Peri A et al (2016) From CT scanning to 3-D printing technology for the preoperative planning in laparoscopic splenectomy. *Surg Endosc* 30:366–371. <https://doi.org/10.1007/s00464-015-4185-y>
68. Popov VV, Gary J, Kovalevsky MA et al (2018) Design and 3D-printing of titanium bone implants: brief review of approach and clinical cases. *Biomed Eng Lett* 8:337–344. <https://doi.org/10.1007/s13534-018-0080-5>
69. Phan K, Sgro A, Maharaj MM et al (2016) Application of a 3D custom printed patient specific spinal implant for C1/2 arthrodesis. *J Spine Surg* 2:314–318. <https://doi.org/10.21037/jss.2016.12.06>
70. Kumar Malyala S, Kumar RY, Alwala AM (2017) A 3D-printed osseointegrated combined jaw and dental implant prosthesis—a case study. *Rapid Prototyping J* 23:1164–1169. <https://doi.org/10.1108/RPJ-10-2016-0166>
71. Mohammed MI, Fitzpatrick AP, Gibson I (2017) Customised design of a patient specific 3D printed whole mandible implant. *KnE Engineering* 2:104. <https://doi.org/10.18502/keg.v2i2.602>
72. Stoffelen DVC, Eraly K, Debeer P (2015) The use of 3D printing technology in reconstruction of a severe glenoid defect: a case report with 2.5 years of follow-up. *J Shoulder Elbow Surg* 24:e218–e222. <https://doi.org/10.1016/j.jse.2015.04.006>
73. James W, Slabbekoorn MA (1998) Correction of Congenital malar hypoplasia using stereolithography for presurgical planning. *Journal of oral and maxillofacial surgery* 56:512–517
74. Ng P, Lee PSV, Goh JCH (2011) Prosthetic sockets fabrication using rapid prototyping technology. *Rapid Prototyping* 8:53–59. <https://doi.org/10.1108/13552540210413310>
75. Yaxiong L, Dichen L, Bingheng L et al (2014) The customized mandible substitute based on rapid prototyping. *Rapid Prototyping* 9:167–174. <https://doi.org/10.1108/13552540310477472>
76. Singare S, Dichen L, Bingheng L et al (2009) Customized design and manufacturing of chin implant based on rapid prototyping. *Rapid Prototyping* 11:113–118. <https://doi.org/10.1108/13552540510589485>
77. Singare S, Yaxiong L, Bingheng L et al (2006) Fabrication of customised maxillo-facial prosthesis using computer-aided design and rapid prototyping techniques. *Rapid Prototyping* 12:206–213. <https://doi.org/10.1108/13552540610682714>
78. Ma J, Du D, Zhao L et al (2016) 3D printing-assisted osteotomy treatment for the malunion of lateral tibial plateau fracture. *Injury* 47:2816–2821. <https://doi.org/10.1016/j.injury.2016.09.025>
79. Zhang YZ, Lu S, Chen B et al (2011) Application of computer-aided design osteotomy template for treatment of cubitus varus deformity in teenagers: a pilot study. *J Shoulder Elbow Surg* 20:51–56. <https://doi.org/10.1016/j.jse.2010.08.029>
80. Khas KS, Pandey PM, Ray AR (2013) Rapid manufacturing of a clubfoot model imitating soft tissue and bones rapid manufacturing of a clubfoot model imitating soft tissue and bones This paper reports an exploration of fabricating a composite clubfoot model consisting of both soft and hard ti. *Virtual Phys Prototyping* 8:187–192. <https://doi.org/10.1080/17452759.2013.836455>
81. Khas KS, Pandey PM, Ray AR (2018) Development of an orthosis for simultaneous three-dimensional correction of clubfoot deformity. *Clin Biomech* 51:67–75. <https://doi.org/10.1016/j.clinbiomech.2017.12.002>

**Dr. Gurminder Singh** has completed his PhD from mechanical engineering department of Indian Institute of Technology Delhi, India. He is currently working in the area of 3D printing combined with ultrasonic-assisted sintering. He is a young scientist having two patents and five journal publication. His research interests are 3D printing, material development for biomedical applications, powder metallurgy, CAD/CAM and mechatronics.

**Prof. Pulak Mohan Pandey** is professor in the mechanical engineering department of Indian Institute of Technology Delhi, India. He joined IIT Delhi as a faculty member in 2004 and is presently serving as Professor. In IIT Delhi, Dr. Pandey diversified his research areas in the field of micro- and nano-finishing, micro-deposition and also continued working in the area of 3D printing. He supervised 30 PhDs and more than 34 M.Tech theses in last 10 years and also filed 17 Indian patent applications. He has approximately 154 international journal papers and 45 international/national refereed conference papers to his credit. These papers have been cited for more than 4403 times with h-index as 33. He received Highly Commended Paper Award by Rapid Prototyping Journal for the paper “Fabrication of three-dimensional open porous regular structure of PA 2200 for enhanced strength of scaffold using selective laser sintering” published in 2017. Many of his B.Tech. and M.Tech. supervised projects have been awarded by IIT Delhi. He is recipient of Outstanding Young Faculty Fellowship (IIT Delhi) sponsored by Kusuma Trust, Gibraltar and J. M. Mahajan outstanding teacher award of IIT Delhi. His students have won Gandhian Young Technological Innovation Award (GYTI) in 2013, 2015, 2017 and 2018.



# Chapter 5

## Additive Manufacturing in Bone Tissue Engineering



Majid Fazlollahi, Yasaman Pooshidani, and Mahnaz Eskandari

### 5.1 Introduction

The human skeleton helps the body to maintain its form and provides mechanical backing for the system included inside. It also plays a crucial role in the musculoskeletal system that provides us the ability of movement. Bone is a complex composite material that differs from other tissues in the body. This composite structure owes its hardness and strength the hydroxyapatite crystals, and collagen fibers provide the flexibility of this structure to avoid being fragile. Thanks to its unique structure, the bone is simultaneously durable and comparatively lightweight. The bone marrow forms the inner part of the bone. Two primary kinds of bone tissue surround it: cortical bone as the tough, exterior crust, and trabecular bone as the spongy center. Having a porosity less than 10%, the compact bone (cortical bone) is highly dense and also has orthotropic properties due to the rounded osteons. The inner layer of the bone is spongy bone (cancellous bone) that has a trabecular structure which contains osteocytes within the lacuna. Spongy bone has a porosity of 50–90%, which reduces bone weight, while due to the growth of trabecula in the direction of imposed tension, it has high anisotropic strength so shows a high load-carrying capacity in the direction of trabeculae.

Four different types of cells form the bone tissue: osteogenic, osteoblast, osteocyte, and osteoclast, each of which has its own function and characteristics. The primary cells are osteogenic cells which have not yet been differentiated. These cells turn into

---

M. Fazlollahi (✉)

Mechanical Engineering Department, Amirkabir University of Technology (Tehran Polytechnic),  
Tehran, Iran

e-mail: [majid.fazlollahi@aut.ac.ir](mailto:majid.fazlollahi@aut.ac.ir)

Y. Pooshidani · M. Eskandari

Department of Biomedical Engineering, Amirkabir University of Technology (Tehran  
Polytechnic), Tehran, Iran

© Springer Nature Singapore Pte Ltd. 2020

S. Singh et al. (eds.), *3D Printing in Biomedical Engineering*,

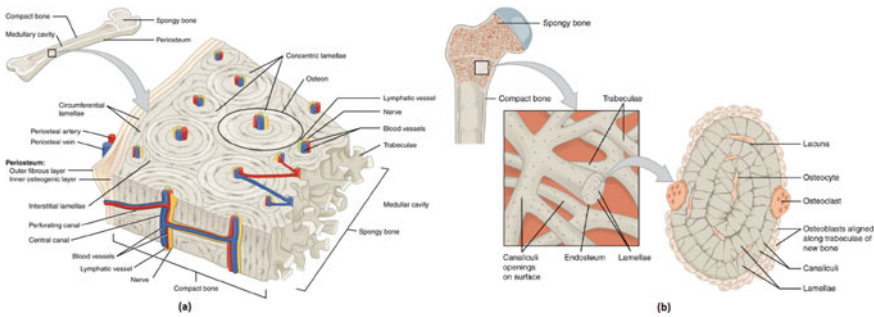
Materials Horizons: From Nature to Nanomaterials,

[https://doi.org/10.1007/978-981-15-5424-7\\_5](https://doi.org/10.1007/978-981-15-5424-7_5)



osteoblast cells after differentiation. The osteoblast is the main cell for the production of new bone, and when this cell becomes embedded in the material it has secreted, it becomes osteocyte, the most prevalent kind of cell observed in bone tissue. The osteoclast cells function is absorbing the old or damaged bone. The balance between the osteoblast and osteoclast cells results in the destruction of the old bone and the formation of a new bone that is essential for proper bone function. Figure 5.1 depicts the structure, cells, and layers of bone [1]. Also, the function and location of bone cells can be found in Table 5.1 [1].

Bone damage is a common injury, so much so that about 6 million people suffer from this injury each year in the USA, of which about 500,000 people need bone grafts [2]. These numbers indicate that while most bone defects are healed spontaneously due to the bone self-healing properties, but still a large number of injuries require implants and surgery for bone remodeling. The demand for joint and bone replacement is increasing rapidly [3]. The bone remodeling process can be viewed as five different stages: resting, activation, resorption, reversal, and formation [4]. Osteoclast cells (for absorbing damage bone) and osteoblast cells (for the production of new bone) have an essential part in these steps. During the formation of new bones,



**Fig. 5.1** Structure of bone; **a** cortical bone, **b** cancellous bone [1]

**Table 5.1** Bone cells [1]

Cell type	Function	Location
Osteogenic cells	Develop into osteoblasts	Deep layers of the periosteum and the marrow
Osteoblasts	Bone formation	Growing portions of bone, including periosteum and endosteum
Osteocytes	Maintain mineral concentration of matrix	Entrapped in matrix
Osteoclasts	Bone resorption	Bone surfaces and at sites of old, injured, or unneeded bone

trabeculae grow along the direction of imposed stress due to the property of mechanotransduction while osteocytes act as mechanical sensors to sense this mechanical stimulation (tension).

Today, still autograft and allograft are employed to treat a large-scale bone defect. In these methods, the bone is extracted from the part of the body of patient or donor which is not a load-bearing bone, and it is implanted in the defect site. But in the recent years, limiting factors such as the lack of donated organs, the transmission of certain diseases, and the insufficient integration into the damaged bone have made scientists keen to use bone tissue engineering (BTE) to form a new bone and implant it in the defective area [5].

BTE involves the employment of bio-scaffolds to create a supportive structure as a basis for the growth of the new tissue. Scaffolds are porous structures which act as a temporary template to guide and support osseous regeneration. Cell culture can be carried out in scaffolds under laboratory conditions, and then the created tissue be placed in the defect site to continue to grow and incorporate into the body. Scaffolds can also be planted directly on the defect area, and the tissue is grown using the body's own system. For this purpose, BTE scaffolds should provide the desired mechanical and biological properties. More precisely, a BTE scaffold must have the following properties [6, 7]:

1. Similar mechanical properties to the adjacent bone
2. Biocompatibility
3. Biodegradability
4. Suitable porosity and geometry for cell infiltration and growth
5. Proper stimulation of cells to growth (osteoconductivity and osteoinductivity).

Various materials are used to make BTE scaffolds depending on the advantages and disadvantages of each material. Most BTE scaffolds are made of ceramics, but these materials do not fully meet the mechanical properties requirements due to their fragility. Natural and synthetic polymers are also used for BTE scaffolds. Although producing polymeric scaffolds is much easier than other materials processing, most polymer scaffolds break down rapidly in the body and create an acidic environment that is hazardous to the body's tissue. Scaffolds made of metals and alloys show outstanding mechanical characteristics, but biodegradability remains a major challenge for them. Therefore, considering the pros and cons, different materials are used for the construction of scaffolds [8, 9].

The fabricating method is a criterion for designing BTE scaffolds that can affect all of the scaffold properties. There are several methods for making scaffolds that can be referred to as freeze-drying, solvent casting, gas forming, thermally induced phase separation, sol-gel method, and electrospinning. These methods do not provide satisfying controllability regarding the characteristics of pores such as geometry, size, and interconnectivity of pores, which results in loss of desired mechanical and fatigue life properties. Consequently, there was a need for a better method with higher control capabilities, and additive manufacturing (AM) method was the most suitable option to fulfill this goal [10].

In the AM or 3D printing method, the scaffold is created layer by layer to create a three-dimensional structure employing a CAD model [11]. By using this method, complex structures can be created without the need for molds and tools, which makes it ideal for producing patient-specific implants. Due to its unique advantages, the usage of 3D printing in the industry has been dramatically increased during the recent decade [12, 13]. Powder-bed-based and powder-fed-based 3D printing methods have been widely studied for the production of BTE scaffolds from metals and alloys. The results show that these scaffolds have excellent mechanical and biological features, biocompatibility and also biodegradability (in case of using proper alloy) [14–16].

## 5.2 AM and Its Application in the Fabricating of BTE Scaffolds

As mentioned, the AM process requires no tools and mold to produce complex shapes and also has a very good control capability that makes this technology suitable for BTE scaffold manufacturing. Using the CAD file and extracting the STL output, the printer builds the desired structure as a successive layer print. Depending on the material or method on which the materials are laid down, scaffolds with different properties can be made. Therefore, two important parameters in the scaffold production process are the type of materials and the technology adopted.

### 5.2.1 Different AM Methods

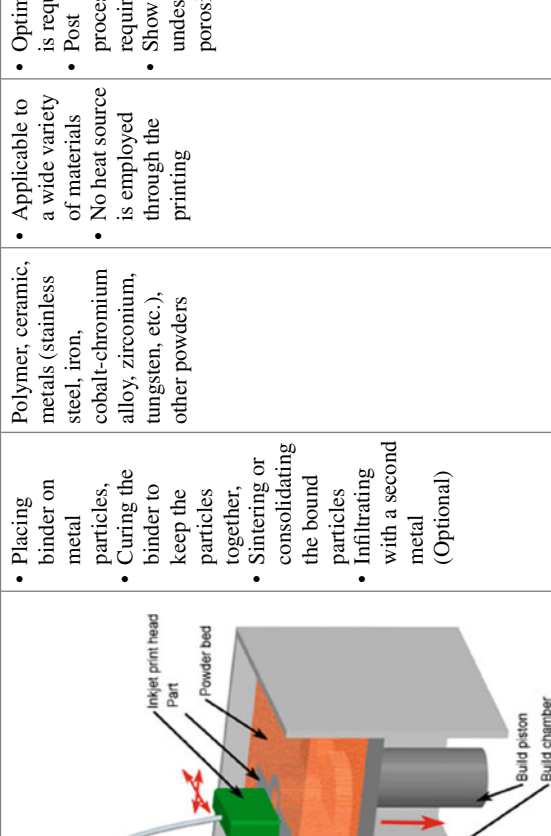
AM methods are divided into different categories, depending on whether they are powder-bed, powder-fed, or wire-fed, and also depending on whether their energy source is laser, electron beam, or plasma arc. Table 5.2 shows seven types of this technology and their features, which are divided by the American Society for Testing and Materials (ASTM) [5, 17].

Table 5.3 also compares these methods in a qualitative way [17]. In most of the new studies on BTE scaffolds, SLM and EBM methods have been used for their high accuracy and controllability.

### 5.2.2 Biomaterials

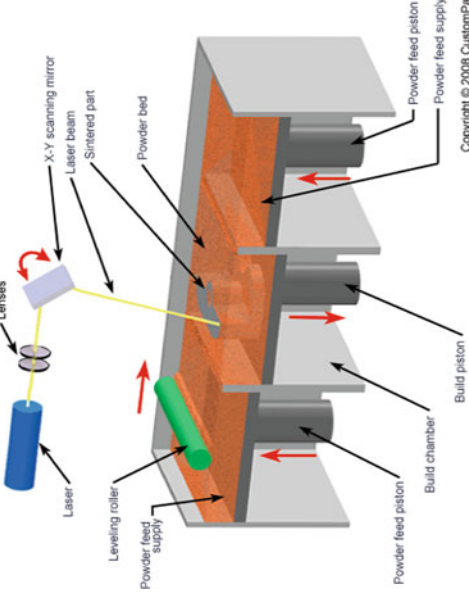
In general, the biomaterials employed in BTE scaffolds are divided into four categories: ceramics, metals, polymers, and composites, which are a combination of the three previous types. Depending on the required properties, one of these four types is selected.

**Table 5.2** Different AM methods

AM technology	Brief description	Applicable materials	Advantages	Disadvantages	Reference
<p>Powder bed and inkjet 3D Printing or binder jetting (3DP)</p> 	<ul style="list-style-type: none"> <li>Placing binder on metal particles,</li> <li>Curing the binder to keep the particles together,</li> <li>Sintering or consolidating the bound particles</li> <li>Infiltrating with a second metal (Optional)</li> </ul>	<p>Polymer, ceramic, metals (stainless steel, iron, cobalt-chromium alloy, zirconium, tungsten, etc.), other powders</p>	<ul style="list-style-type: none"> <li>Applicable to a wide variety of materials</li> <li>No heat source is employed through the printing</li> </ul>	<ul style="list-style-type: none"> <li>Optimization is required</li> <li>Post processing is required</li> <li>Shows undesirable porosity</li> </ul>	<p>[18, 19]</p>


(continued)

**Table 5.2** (continued)

AM technology	Brief description	Applicable materials	Advantages	Disadvantages	Reference
<p data-bbox="244 1289 268 1566">Selective laser sintering (SLS)</p> 	<ul style="list-style-type: none"> <li>Use of laser to sinter the 2D cross section layer according to the CAD model</li> <li>Layer by layer addition of particles</li> </ul>	<p>Thermoplastics, ceramic powders and metal powders (stainless steel, cobalt-chromium alloy, titanium, etc.)</p>	<ul style="list-style-type: none"> <li>Applicable to a wide variety of materials</li> <li>No support design required</li> </ul>	<ul style="list-style-type: none"> <li>Post processing required</li> </ul>	<p>[20]</p>

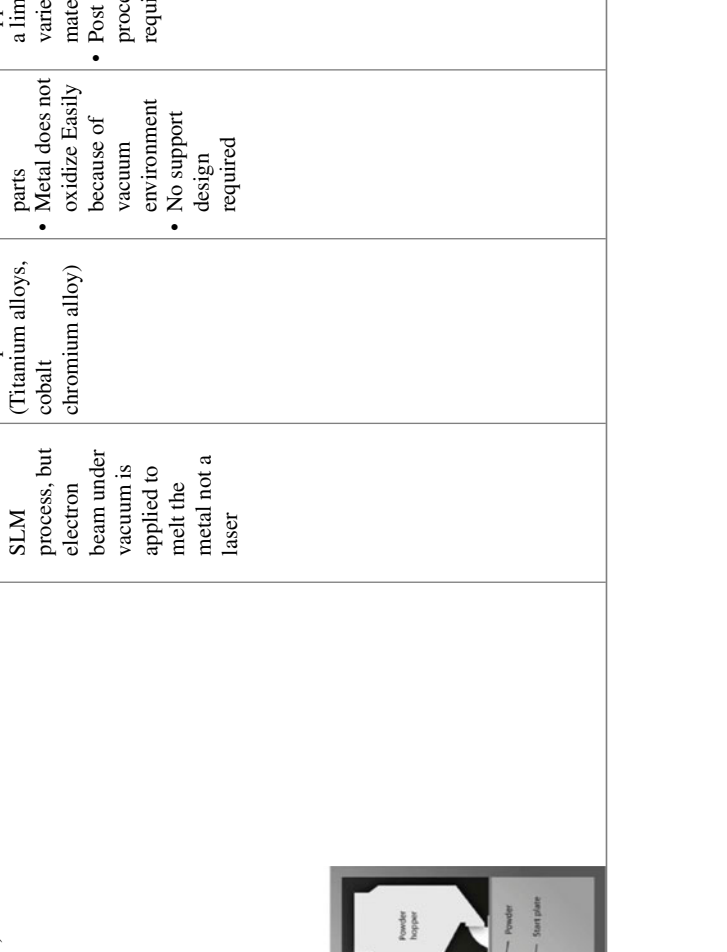
(continued)

**Table 5.2** (continued)

AM technology	Brief description	Applicable materials	Advantages	Disadvantages	Reference
<p>Selective laser melting (SLM)</p>  <p>The diagram illustrates the SLM process. A blue laser source emits a beam through a lens and an X-Y scanning mirror. The laser beam is focused onto a powder bed. A recoater arm, which includes a metal powder supply and a powder dispenser platform, moves across the powder bed. The powder dispenser piston is used to dispense the powder. The laser beam sinters the powder, creating a sintered part. The powder dispenser piston is also shown moving across the powder bed.</p>	<ul style="list-style-type: none"> <li>Similar to the SLS process, expect for melting powder instead of sintering powder to adhere material together</li> </ul>	<p>Metal alloys powders (Stainless steel, iron based alloys, titanium, gold, silver, etc.), ceramic powders</p>	<p>-High processing resolution</p> <ul style="list-style-type: none"> <li>High strength; Full dense parts</li> </ul>	<ul style="list-style-type: none"> <li>Post processing is required</li> <li>High quality requirements for metal particles and restricted piece size</li> </ul>	<p>[7, 21]</p>

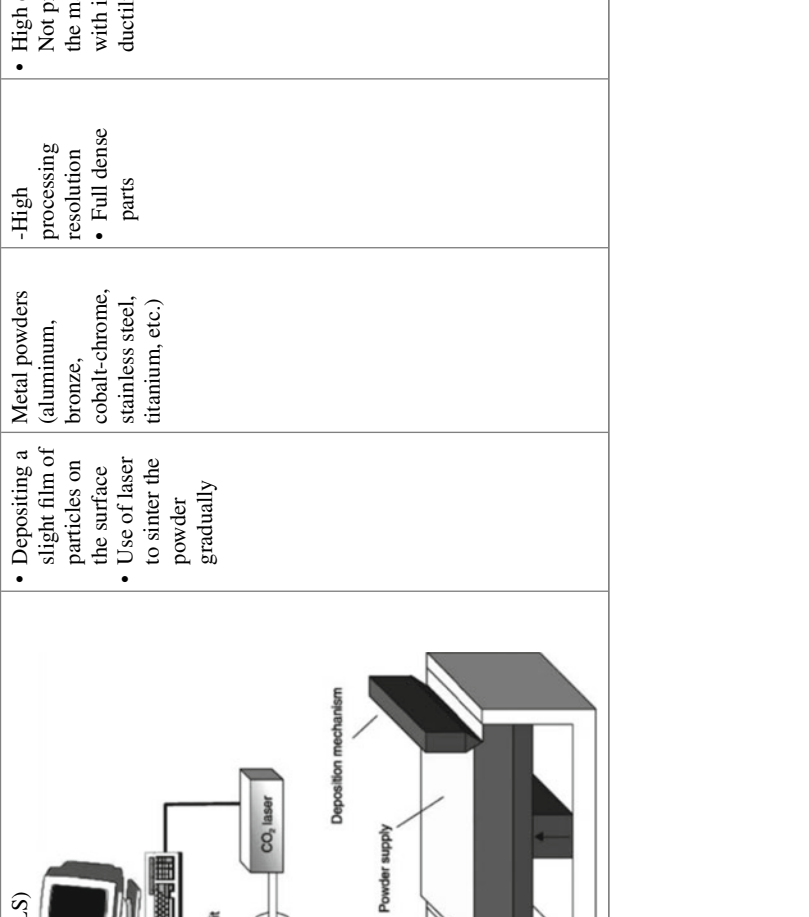
(continued)

**Table 5.2** (continued)

AM technology	Brief description	Applicable materials	Advantages	Disadvantages	Reference
<p data-bbox="241 1284 264 1561">Electron beam melting (EBM)</p> 	<ul style="list-style-type: none"> <li>Like the SLM process, but electron beam under vacuum is applied to melt the metal not a laser</li> </ul>	<p>Metal powders (Titanium alloys, cobalt chromium alloy)</p>	<ul style="list-style-type: none"> <li>Full dense parts</li> <li>Metal does not oxidize Easily because of vacuum environment</li> <li>No support design required</li> </ul>	<ul style="list-style-type: none"> <li>Applicable to a limited variety of materials</li> <li>Post processing required</li> </ul>	<p>[19, 22]</p>

(continued)

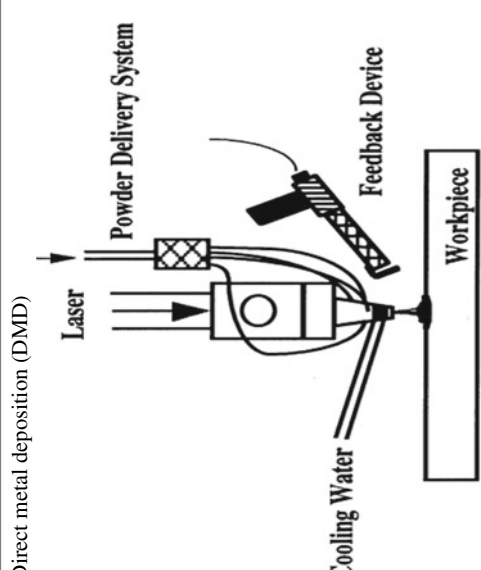
**Table 5.2** (continued)

AM technology	Brief description	Applicable materials	Advantages	Disadvantages	Reference
<p>Direct metal laser sintering (DMLS)</p> 	<ul style="list-style-type: none"> <li>• Depositing a slight film of particles on the surface</li> <li>• Use of laser to sinter the powder gradually</li> </ul>	<p>Metal powders (aluminum, bronze, cobalt-chrome, stainless steel, titanium, etc.)</p>	<p>-High processing resolution</p> <ul style="list-style-type: none"> <li>• Full dense parts</li> </ul>	<ul style="list-style-type: none"> <li>• High costs</li> <li>• Not proper for the materials with inferior ductility</li> </ul>	<p>[23]</p>

(continued)



**Table 5.2** (continued)

AM technology	Brief description	Applicable materials	Advantages	Disadvantages	Reference
<p>Direct metal deposition (DMD)</p>  <p>The diagram illustrates the Direct Metal Deposition (DMD) process. A laser beam is directed at a powder delivery system. The powder delivery system consists of a container of powder and a nozzle that deposits the powder onto a workpiece. A feedback device is used to monitor the process. Cooling water is also applied to the workpiece.</p>	<ul style="list-style-type: none"> <li>• A melt pool is formed on the underneath material by using Laser</li> <li>• Then the other particle (or wire) is transferred into the melt pool</li> </ul>	<p>Ceramics, Metal powders (Iron, titanium, etc.)</p>	<ul style="list-style-type: none"> <li>• Fully dense meta</li> <li>• Controllable microstructure</li> </ul>	<ul style="list-style-type: none"> <li>-Not repeatable enough</li> <li>• Post processing required</li> </ul>	<p>[24]</p>

(continued)

Table 5.2 (continued)

AM technology	Brief description	Applicable materials	Advantages	Disadvantages	Reference
<p>Electron beam additive manufacturing (EBAM)</p> 	<ul style="list-style-type: none"> <li>• Electron beam melts the metal layers (as particles or wire) successively to obtain the final configuration</li> </ul>	<p>Metals (Titanium alloys, cobalt chromium alloy)</p>	<ul style="list-style-type: none"> <li>• No support design required</li> <li>• Prevents metal oxidation due to vacuum condition</li> </ul>	<ul style="list-style-type: none"> <li>• Not sufficiently fine texture</li> <li>• Low precision</li> </ul>	<p>[19, 25]</p>

**Table 5.3** Qualitative comparison of different AM methods [17]

AM process	Resolution	Build speed	Surface roughness	Power efficiency	Build volume	Residual stress	Cost
3DP	Poor	Fast	Poor	–	Big	Low	Low
SLS	Good	Slow	Excellent	Poor	Small	High	High
SLM	Good	Slow	Excellent	Poor	Small	High	High
EBM	Moderate	Fast	Good	Good	Small	Moderate	High
DMLS	Good	Slow	Excellent	Poor	Small	Low	High
DMD	Poor	Fast	Poor	Poor	Big	High	Moderate
EBAM	Moderate	Moderate	Good	Good	Small	Moderate	High

### 5.2.2.1 Ceramics

Calcium phosphate (CaP) ceramics have composition characteristics near to the bone properties. This feature makes them extremely popular in using as BTE scaffolds material. For example, hydroxyapatite (HA) powder was one of the first materials used to make BTE scaffolds through AM. Tricalcium phosphate (TCP) is also highly regarded due to its better biodegradability than HA. Having good bioactivity bioglass ceramics are also used in BTE scaffolds, for example 45S5 bioglass. However, they do have not suitable capacity to withstand loads [26].

### 5.2.2.2 Metals

Having excellent strength, metallic biomaterials are of great importance in the fabricating of BTE scaffolds, especially with the advent of AM technology that allows controlling the structure of scaffolds. Ti-based biomaterials have high corrosion and fatigue resistance and also excellent biocompatibility. Additionally, iron-based alloys and cobalt-based alloys are highly regarded due to their excellent strength and good corrosion resistance.

### 5.2.2.3 Polymers

Polymers are the first materials used by the AM process and are highly regarded for their excellent processability. Polymers divide into two general classes: natural and synthetic. One of the most important natural polymers is collagen, which is known as the “extracellular matrix” (ECM). This polymer has many uses in the AM process of BTE structures. Other natural polymers like cellulose, chitosan, and starch have also been scrutinized for this work.

Synthetic polymers have interesting properties, such as physical, chemical, and mechanical properties that make them attractive. Polycaprolactone (PCL) is one of the most generally utilized synthetic polymers for making BTE structures. Other

synthetic polymers as for example polyglycolic acid (PGA) and polylactic acid (PLA) are likewise commonly used. Another example is polyether-ether-ketone (PEEK) in which its mechanical properties is near to bone, as well as excellent chemical resistance, and radiolucency [27].

#### 5.2.2.4 Composites

The combination of the three types of previous biomaterials can provide the desired properties, which has directed to the improvement of composite biomaterials for BTE scaffolds. Ceramic composites, such as biphasic calcium phosphate (BCP), which combines HA and TCP, have good properties like biocompatibility and biodegradability which make them ideal for utilization in the BTE scaffolds. Also, additives such as MgO, ZnO, and SiO<sub>2</sub> are promising to improve CaP scaffolds. For example, studies have shown that adding ZnO and SiO<sub>2</sub> particles to TCP can improve bone growth [28].

The combination of brittle ceramics and flexible polymers can provide extraordinary properties. Collagen–calcium phosphate scaffolds are an example of these composites which are widely used in AM of BTE. Other polymer–ceramic composites are also used in BTE scaffolds. For example, PLG A/β-TCP/HA nanocomposite scaffolds exhibited interesting biocompatibility and drug delivery properties [29].

Metal composites, like titanium alloys with TCP coating, showed an increase in cell adhesion as well as cell proliferation.

### 5.3 Architectural Design of BTE Scaffolds

Architecture design affects all properties of the BTE scaffold. The size and shape of the pores as well as the interconnectivity of porosities have a notable impact on the growth of the cells. In addition, metal scaffolds have wide variety of applications in BTE, but as they have more strength compared to the adjacent bones, they cause flaws like implant loosening and bone resorption. Therefore, fabricating porous structures can be the golden standard to use metal and alloy scaffolds for BTE. Using the AM method, the shape and size of pores can be controlled unlike most other methods that result in a stochastic structure.

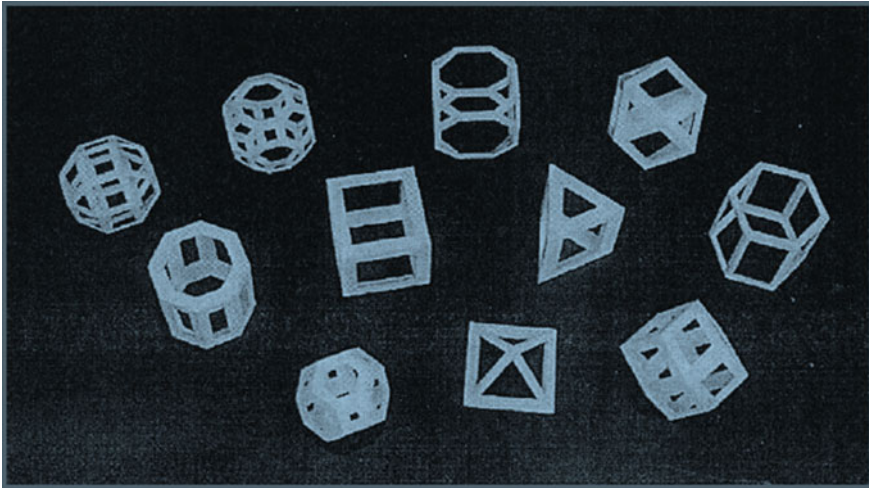
#### 5.3.1 Scaffold Library

Designing a suitable unit cell and repeating it as a pattern, will result in a structure with desired porosity. These unit cells can be truss, polyhedron, or triply periodic minimal surface (TPMS). Design methods for these unit cells are based on

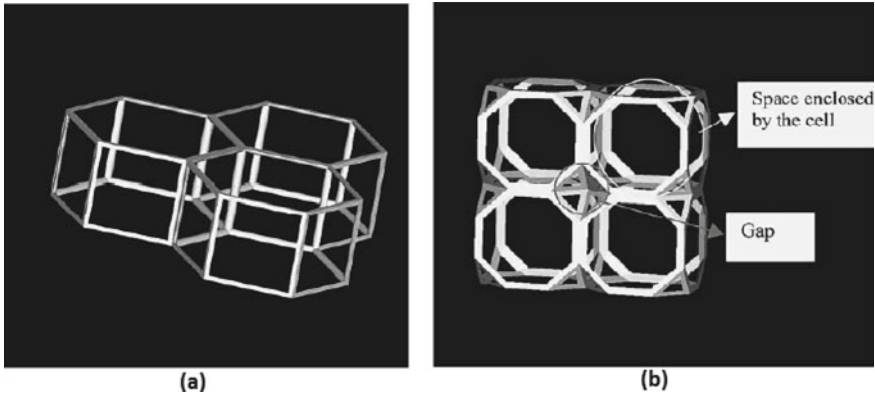
CAD modeling, medical image such as CT and MRI, implicit surface modeling, and topology optimization.

### 5.3.1.1 Polyhedron

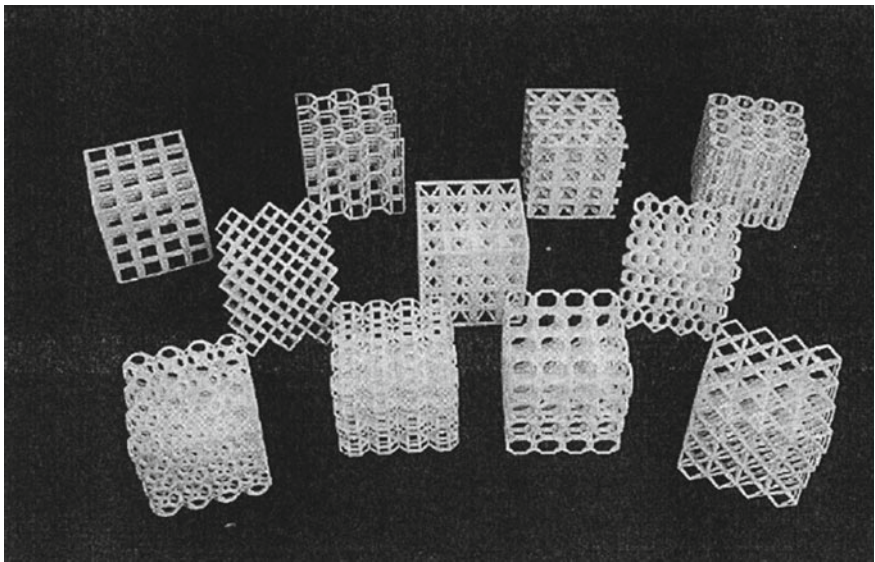
There are two criteria for designing a unit cell: 1. only by connecting vertices and edges it can be repeated in three-dimensional space, 2. it should be producible. A unit cell with many small surfaces would have a complex shape which makes it virtually impossible to produce. Based on these two criteria, there are 11 types of polyhedron unit cells [30]. They are, namely the cube, truncated octahedron, cuboctahedron, truncated cube, rhombicuboctahedron, truncated cuboctahedron, triangular prism, hexagonal prism, rectangular prism, octagonal prism, and rhombic dodecahedron. Figure 5.2 shows these 11 types of polyhedron unit cells. These 11 types of cells are divided into two groups, based on the fact that after being placed together, an empty space is created between them or not. Figure 5.3 shows an illustration of two types of assembly of cells. In Fig. 5.4, scaffolds created by repeating these 11 types of unit cells can be seen. Analytical solutions have been studied extensively for obtaining mechanical properties related to the various unit cell geometry.



**Fig. 5.2** 11 polyhedron assembly of cells (scale 50:1). *Forward row (L–R):* truncated octahedron, square pyramid, rhombic dodecahedron; *middle row (L–R):* octagonal prism, square prism, triangular prism, hexagonal prism; *back row (L–R):* truncated cuboctahedron, rhombicuboctahedron, truncated cube, cuboctahedron [31]



**Fig. 5.3** Examples of cells that: **a** occupy space without leaving holes (three hexagonal prisms), and **b** span 3D space by creating holes (four truncated cubes) [30]



**Fig. 5.4** 11 sample scaffold arrangements (scale 10:1). *Forward row(L-R):* rhombicuboctehedron, truncated cuboctetradron, truncated cube, cuboctetradron; *Middle row (L-R):* rhombic dodecahedron, square pyramid, truncated octahedron; *Back row (L-R):* square prism, hexagonal prism, triangular prism, and octagonal prism [31]

**5.3.1.2 TPMS**

Surface shape also has a critical influence on the growth of bone cells. Studies show that the concave surface of the scaffold is more useful for cell attachment and proliferation than the smooth or curved surfaces [32]. But since the natural trabecula

curvature is almost zero, a novel unit cell was developed, called TPMS. The TPMS shows an unlimited structure in three free directions, with an average curvature of zero. The TPMS porous structure is made with repeating the unit cells with the least possible area [33]. There are four types of TPMS, each of which can be expressed with implicit functions as follows [34]:

**Gyroid surface:**

$$F(x, y, z) = \cos(x) \cdot \sin(y) + \cos(y) \sin(z) + \cos(z) \cdot \sin(x) + \alpha \quad (1)$$

**Schwarz diamond:**

$$F(x, y, z) = \sin(x) \sin(y) \cdot \sin(z) + \sin(x) \cdot \cos(y) \cdot \cos(z) + \cos(x) \cdot \sin(y) \cdot \cos(z) + \cos(x) \cdot \cos(y) \cdot \sin(z) + \alpha \quad (2)$$

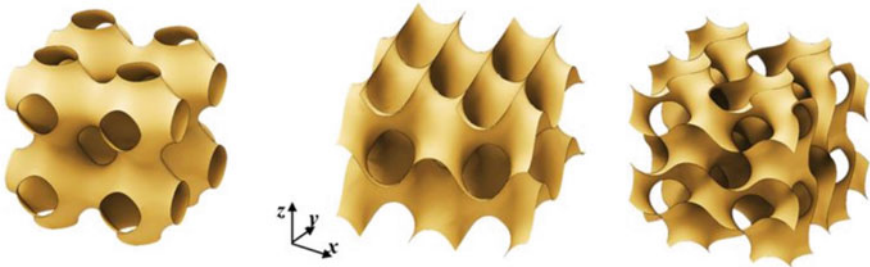
**Neovius surface:**

$$F(x, y, z) = 3(\cos(x) + \cos(y) + \cos(z)) + 4(\cos(x) \cdot \cos(y) \cdot \cos(z)) + \alpha \quad (3)$$

**D-prime surface:**

$$F(x, y, z) = 0.5(\sin(x) \cdot \sin(y) \cdot \sin(z) + \cos(x) \cdot \cos(y) \cdot \cos(z)) - 0.5(\cos(2x) \cdot \cos(2y) + \cos(2y) \cdot \cos(2z)) + \cos(2z)\cos(2x) + \alpha \quad (4)$$

$x$ ,  $y$ , and  $z$  are Cartesian coordinates, and  $\alpha$  is offset value, which can be used to control the porosity of the structure. Figure 5.5 shows some examples of TPMS. The



**Fig. 5.5** Some examples of the triply periodic minimal surfaces (TPMSs) [36]

most popular TPMS structure for BTE scaffolds is gyroid. Comparison of mechanical features of gyroid TPMS with stochastic scaffolds produced through particle-leaching with the same porosity percentage showed that scaffold permeability and tissue growth were significantly higher in gyroid TPMS scaffolds [35]. The gyroid TPMS scaffolds have two types of morphology, minimal surface network solids, and minimal surface sheet solids. Albeit sheet solid gyroid structure has better mechanical properties, and it does not have pores interconnectivity, which is a major drawback for cells penetration and tissue growth. On the other hand, network solid gyroid structure has good mechanical characteristics as well as good pores interconnectivity, which make it suitable for use in BTE scaffolds.

### 5.3.1.3 Truss

Trusses are also another form of unit cells that are created by connecting the points with struts. The truss unit cells can be elementary cubic truss, elementary non-cubic truss, complex truss, or compound truss, which are derived from the combination of two trusses in a spatial network [37]. Figure 5.6 shows some examples of these truss unit cells.

## 5.3.2 *Functionally Graded Scaffolds (FGSs)*

In order to mimic the mechanical properties, morphology, and physiology of the human body bone, it is necessary to have scaffolds that have gradient porosity and even gradient type of unit cell. Simply, a uniform porous structure cannot be suitable for the regeneration of a large-scale segmental bone damage with complex mechanical and biological function. There are four types of FGS for different applications [38]:

1. FGS with different strut diameters: Changing the strut diameter can result in desired changes in the pore size.
2. FGS with different cells sizes: Pore size and strut diameter can be changed by changing the cell size
3. FGS with various kinds of unit cells: By this method, desired pore size and strut diameter, in addition to the optimal porosity can be achieved in each section.
4. FGS with different chemical compositions: A porous construction which has a favorable gradient in mechanical properties can be obtained by changing the composition of the scaffold through the use of various materials.

Among these structures, varying strut diameter is more widely used because of its simplicity and lack of flaws, such as mismatching nodes. Figure 5.7 shows these four strategies.

Also, various kinds of porous structures can be found on the basis of the types of unit cells in Fig. 5.8.



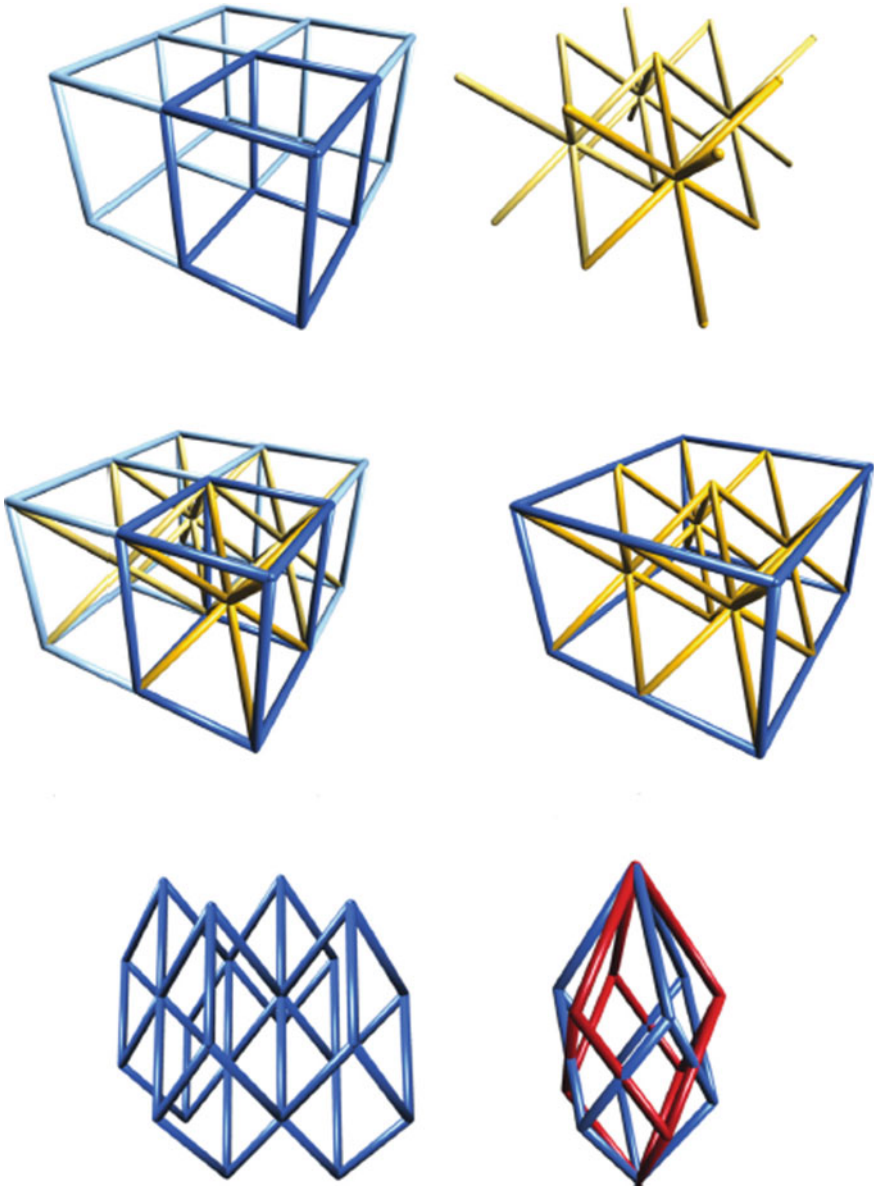


Fig. 5.6 Some examples of the truss unit cells [37]

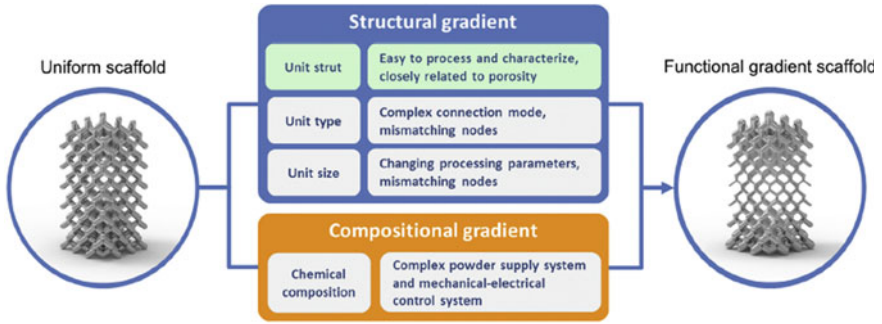


Fig. 5.7 Schematic picture of different designs of FGS and their qualities [38]

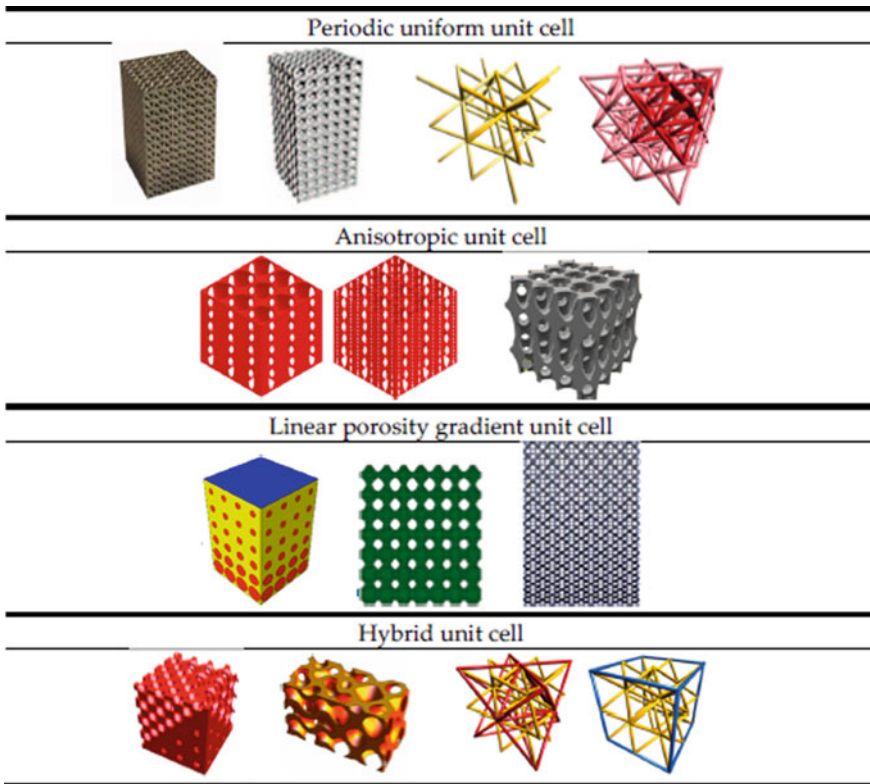


Fig. 5.8 Various designs of scaffolds on the basis of different types of unit cells [17]

## 5.4 Experimental Studies on the Additively Manufactured BTE Scaffolds

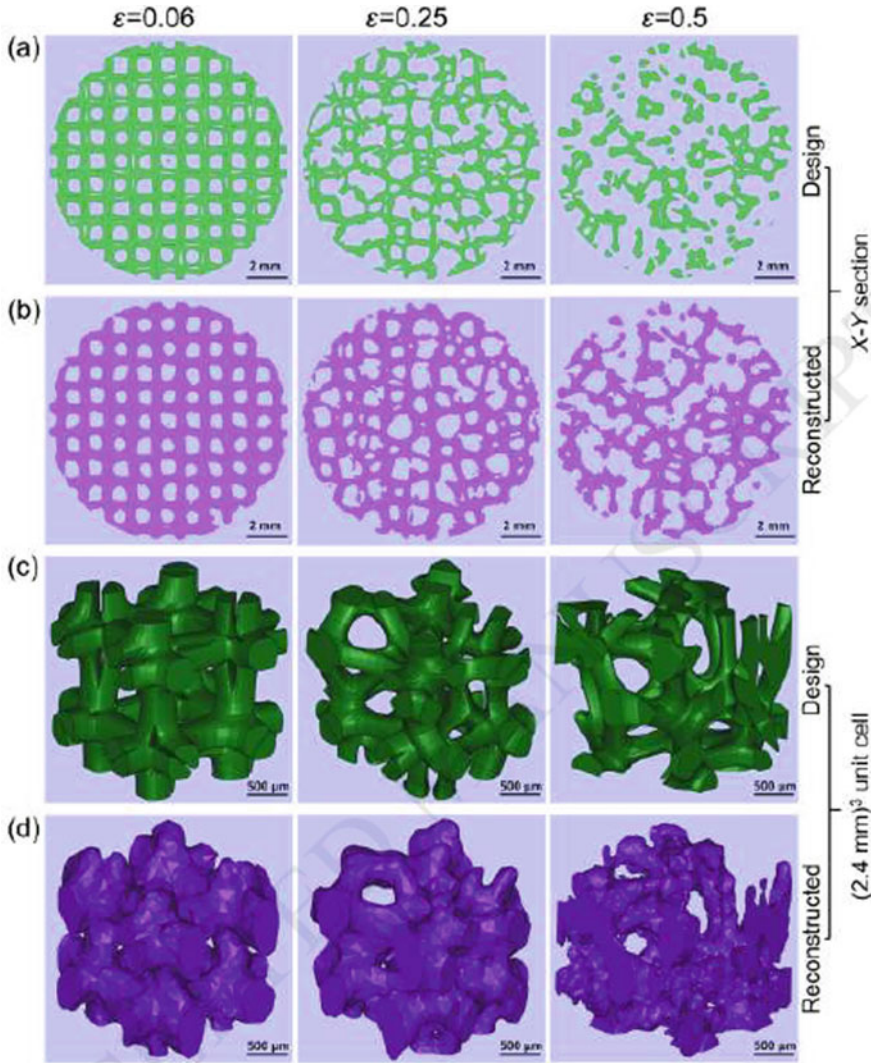
Since the additively manufactured BTE scaffolds do not match exactly with the theoretical models and are so complex, many empirical studies have been done to understand the behavior of these scaffolds in different conditions. The prediction of mechanical behavior of scaffolds through finite element (FE) simulation is a very effective tool for studying these scaffolds. Conducting mechanical tests is the most accurate way to get mechanical properties, failure mechanism, and fatigue behavior of the BTE scaffolds. Also, many empirical studies concentrate on the mechanical properties of FGS and comparing them with the uniform structures.

### 5.4.1 *FE Modeling to Predict Mechanical Behavior of Scaffolds*

FE simulation is employed to predict the mechanical response of scaffolds in the human body. It has been determined that FE modeling is an effective impediment for this purpose. It is possible to predict the properties of whole porous structure by modeling a unit cell and by using suitable boundary conditions. The FE model has been developed in two ways: 1. using micro-computed tomography (micro-CT) and 2. using the CAD model (with or without implementing the manufacturing defects).

Micro-CT imaging is a method to create a high-resolution 3D model from the real sample. This method of imaging can be used to obtain a 3D model of body organs and bones with micro-scale precision. In this method, after the fabrication of the scaffold by AM technology, an image is obtained from the scaffold through the micro-CT. Then, through the FE simulation, the mechanical behavior of scaffold is studied. Since, there is often some discrepancies between the produced AM parts and the CAD model, using micro-CT is a promising method to obtain a precise model of the scaffolds. In previous studies, the results of this simulation method have shown good compatibility with experimental data [39].

The second method is to use the CAD model for FE modeling. In this method, due to the differences between the produced sample and the original CAD model, there is usually no precise results. Figure 5.9 shows some of these irregularities. In order to solve this problem, manufacturing defects such as structural changes and cross-sectional changes of struts are also implemented in the model using statistical methods. The concept of equivalent diameter or Gaussian distribution can be used to insert the effect of variations in the diameter of struts in the FE model. For example, in a study on FE modeling of titanium alloy scaffolds, irregularities of the manufacturing process, such as changes in the cross section of struts, in addition to material flaws were inserted in the FE model. The results showed that the implementation of manufacturing weaknesses in the FE model significantly reduces the error to predict the mechanical properties [40].



**Fig. 5.9** Comparison between design and production of scaffolds with different irregular structures: **a, b** sections from the same location; **c, d** unit cells of  $2.4 \text{ mm} \times 2.4 \text{ mm} \times 2.4 \text{ mm}$  [41]

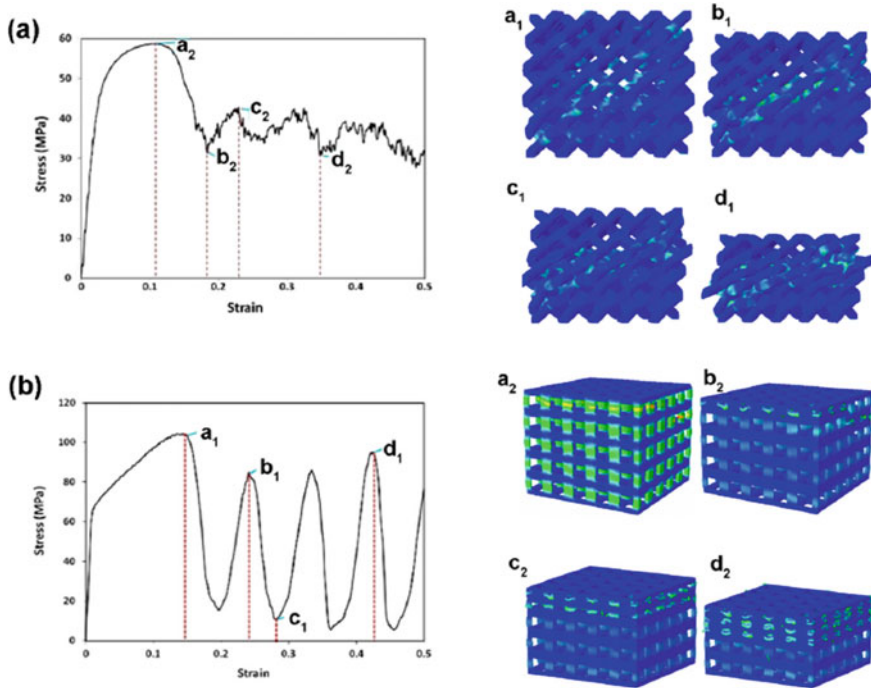
### 5.4.2 Failure Mechanisms of Lattice Structures

An examination of the failure mechanisms of the scaffolds at the micro-level indicates that the manufacturing imperfections are the main reason of the failure. In fact, during the fabrication process of a porous structure using AM methods, an imperfection is created in the microstructure of the scaffold, which results in stress concentration

and strain localization under the loading condition and ultimately followed by the failure of the entire structure [42].

The failure mechanism at the macro-level depends on the unit cell topology. In the stretch-dominant unit cell, the failure occurs in a layer-by-layer manner. In the bending-dominant unit cell, shearing at an angle of approximately  $45^\circ$  is the main mechanism of failure. In some cases, buckling can also be the main mechanism of failure that indicates a brittle mechanical behavior [42].

In general, the micro-strut orientation has a crucial impact on the mechanical behavior of scaffolds. When the micro-strut is oriented in the loading direction, the structure undergoes stretch-dominant loading. The higher the micro-strut angle, the more the bending-dominant mechanical behavior [43]. In a study conducted on the scaffolds with cubic and diamond unit cells, it was perceived that in the cubic scaffolds, as a structure with a stretch-dominant deformation, more specific mechanical properties are expected than the diamond structure with bending-dominant deformation [43]. Figure 5.10 shows the results of this study.



**Fig. 5.10** Failure mechanism of **a** diamond lattice structure at 22% volume fraction; continuous sharing band of  $45^\circ$ , because of breaking diagonal layers, is investigated. Shearing of layers and the bending failure of tying struts perpendicular to the diagonal plates is obvious; **b** cubic lattice structure; stretch in result of deformation in scaling laws shows the layer-by-layer deformation mechanism [43]



### 5.4.3 Mechanical Properties of Scaffolds

An ideal BTE scaffold should have properties comparable to the properties of the adjacent bone, as far as possible, to prevent stress shielding. Structure with the desired mechanical properties can be achieved by changing the porosity, the strut diameter, and the porosity of the scaffold through AM process, as well as taking into account the inevitable imperfections, such as material and production process defects. Also, the unit cell type plays a crucial role in the stress–strain curve of the scaffold. To obtain this curve, the uniaxial compression tests are usually employed.

The stress–strain curve of the scaffolds vary with different unit cells. Also, relative density (porosity) has a great influence on this curve. But in general, this chart contains a linear elastic segment. Then there is a plateau area of stress, and then the stress–strain curve fluctuations are observed. The final stage is usually accompanied by the stiffening of the scaffold. Generally, the fluctuations of this graph are reduced by increasing the relative density of the scaffold [44]. Figure 5.11 shows the variation of this graph for a unit cell type (cube) by changing the relative density. In Fig. 5.12, the effect of changing the unit cell type on the stress–strain curve of the porous scaffold, in a constant relative density, can be observed. Researches have shown that for different types of unit cells, increasing relative density increases the mechanical properties such as elastic gradient, first maximum stress, plateau stress, yield

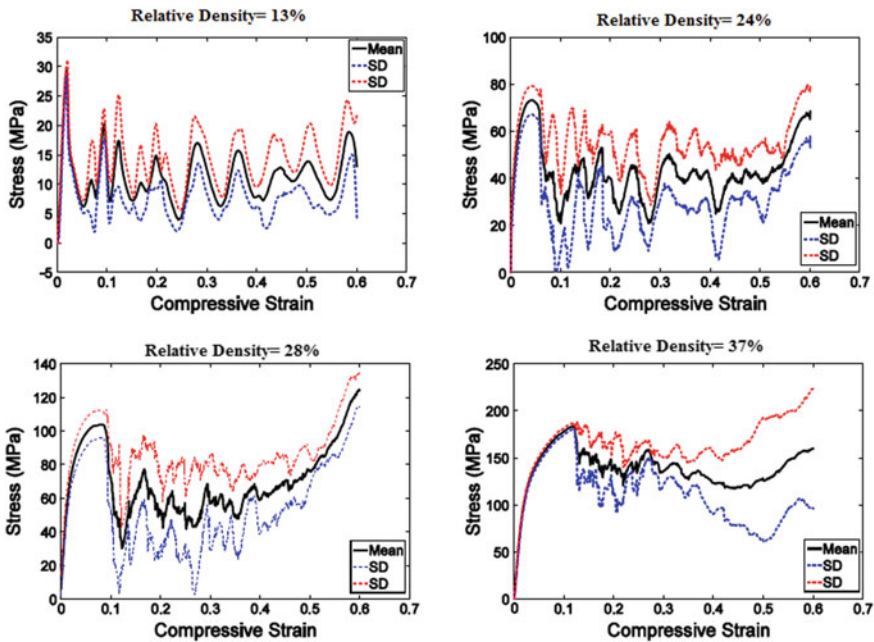
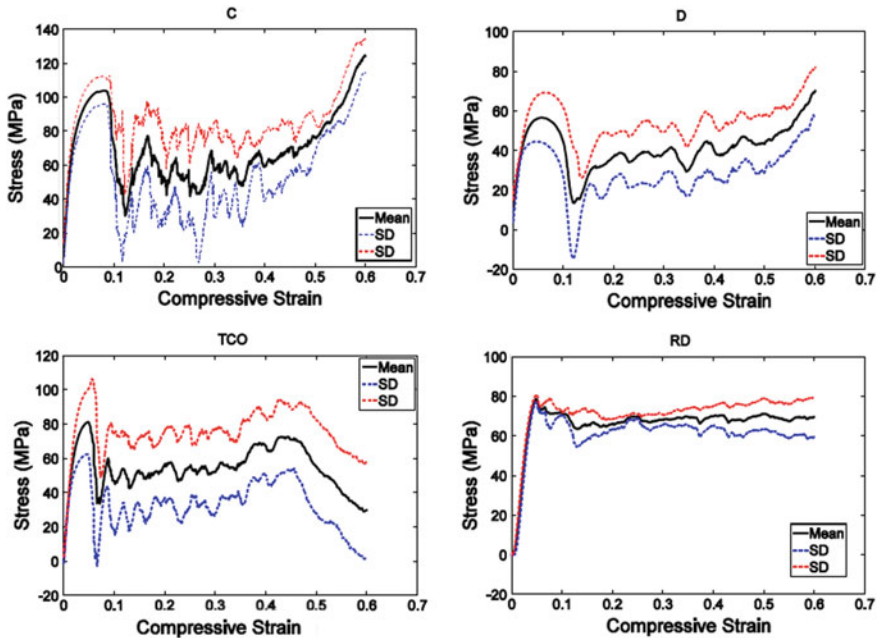


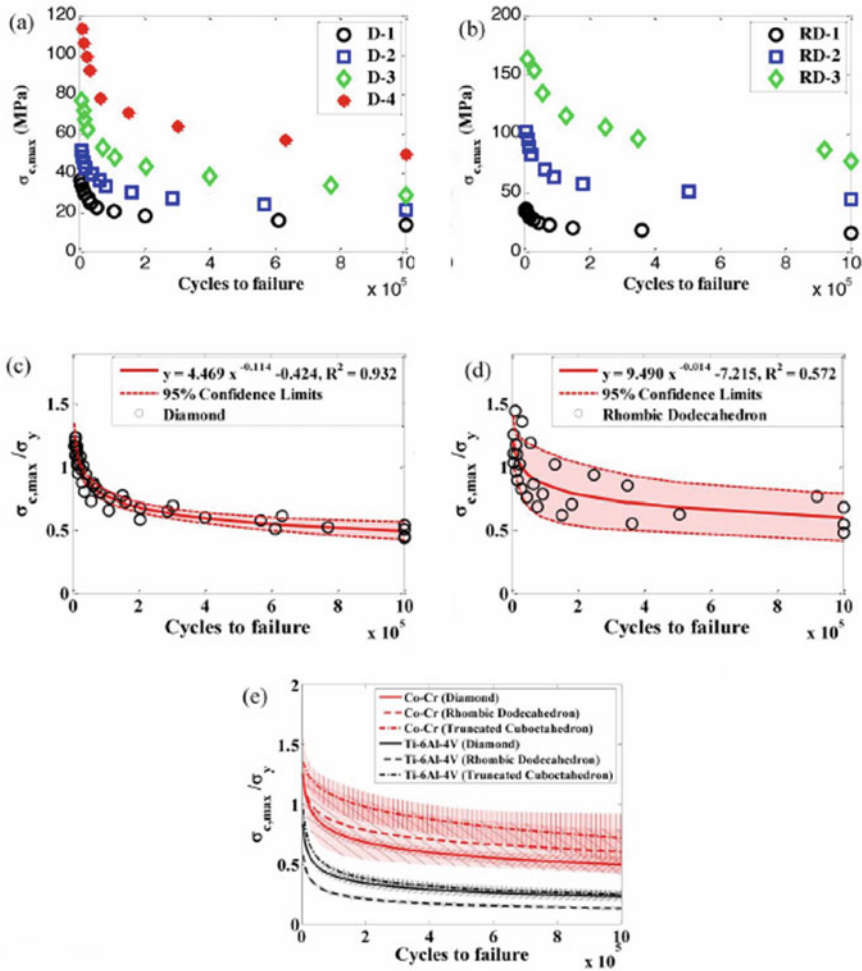
Fig. 5.11 Stress-compressive strain curves for samples with cube unit cell and different porosities [44]



**Fig. 5.12** Stress-compressive strain curves for samples with the same porosity (relative density of 28%) and with different types of unit cells: cube (C), diamond (D), truncated cubeoctahedron (TCO), rhombic dodecahedron (RD) [44]

stress, and energy absorption [44]. In most cases, a post-processing treatment is also performed on the additively manufactured scaffolds. Researches have shown that an appropriate annealing process can increase the ductility of the structure without any significant change in its strength [41].

Due to the movement of the body, implants in the human body experience cyclic musculoskeletal loads. Therefore, the evaluation of the fatigue behavior of these implants is also important. Most of these cyclic bone loads are compression loading. Figure 5.13 shows the S-N curves for fatigue life of Ti-6Al-4 V and Co-Cr biomaterials with two structures of diamond (D) and rhombic dodecahedron (RD). As can be seen, the scaffolds with more porosities have better fatigue life [42]. In the fatigue loading, the adjacent area of unit cell nodes is critical places for initiation and growth of cracks. Studies show that performing appropriate post-processing, such as hot isostatic pressing, stress relieving, and chemical etching, can increase the fatigue life of scaffolds by reducing the stress concentration in these nodes [45].



**Fig. 5.13** S-N curves for fatigue life of Ti-6Al-4 V and Co-Cr biomaterials with two structures of diamond **a** and rhombic dodecahedron **b** normalized S-N curves with respect to the yield stress ( $\sigma_y$ ) of the structures **c**, **d** it can be seen that biomaterial type affects fatigue life much more than the type of unit cell **e** [42]

### 5.4.4 FGSs

The most important challenge for FGSs is the stress concentration due to a sudden change in geometry, which often results in structural failure. But if the smooth gradient of stress can be achieved, significant results would be obtained. One study showed that the strength of a homogeneous structure increased from 47 MPa up to 90 MPa and the elastic modulus also increased from 2GPa to 3GPa, by changing the structure to a gradient structure [39].



## 5.5 In Vitro and In Vivo Studies on the Additively Manufactured BTE Scaffolds

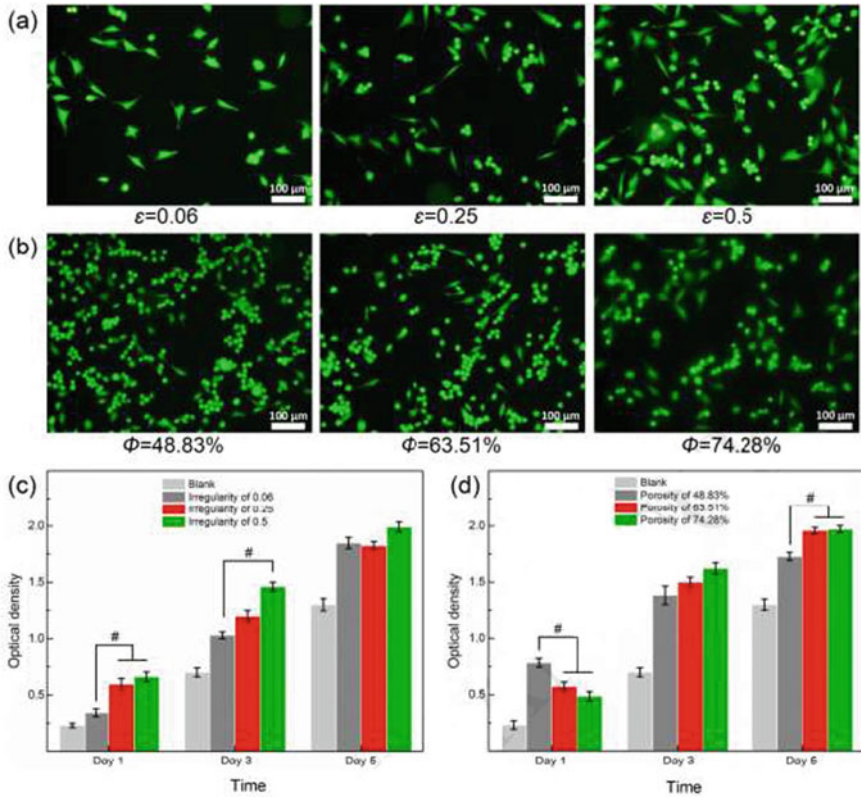
Many studies have been done *in vivo* and *in vitro* to evaluate the mechanical and biological performance of the scaffold during the service. It has been shown that cellular activity is considerably affected by the morphology of scaffolds and the growth factors. For example, in an *in vitro* study, MG63 cells were used on Ti-6Al-4 V scaffolds made by the SLM process. The results showed that micro-scale cavities and ravines on the original surface of scaffolds facilitate the attachment and migration of osteoblast cells. Due to the combination of large and small pores, increasing of irregularities facilitated cell proliferation and osteoblast differentiation. Although the scaffold with less porosity showed more cell density on the first day, but gradually cell density increased in the scaffold with more porosity, so much so that in the fifth day more cell density had been observed in the scaffold with more porosity than other scaffolds, indicating that more porosity is beneficial for cell growth [41]. Figure 5.14 shows the results of fluorescent microscopic images of cell proliferation. It has also been shown that curvature of the geometric shape can remarkably enhance cell attachment and also increase the growth of bone cells [46].

In another study, an *in vitro* study of Ti-6Al-4 V scaffolds made by the EBM method was performed to evaluate cytocompatibility using human bone mesenchymal stem cells (hBMSCs). Cell proliferation and osteogenic differentiation was higher in scaffolds with larger pores. *In vivo* study of these scaffolds was performed by implantation in a 30-mm segmental defect of goat metatarsus to examine osseointegration. The results showed good performance of these scaffolds and proper bone growth [47]. Figure 5.15 shows the samples with inserted scaffold at different times.

The effect of adding growth factors has also been widely studied. Researchers placed bioactive gels containing various growth factors in AM scaffolds. *In vivo* study showed that the inclusion of colloidal gelatin gel, which is capable of controlled releasing of BMP-2 and FGF-2, within the additive manufactured titanium scaffold is a successful approach for the recovery and reconstruction of damaged bones [48].

## 5.6 Conclusion

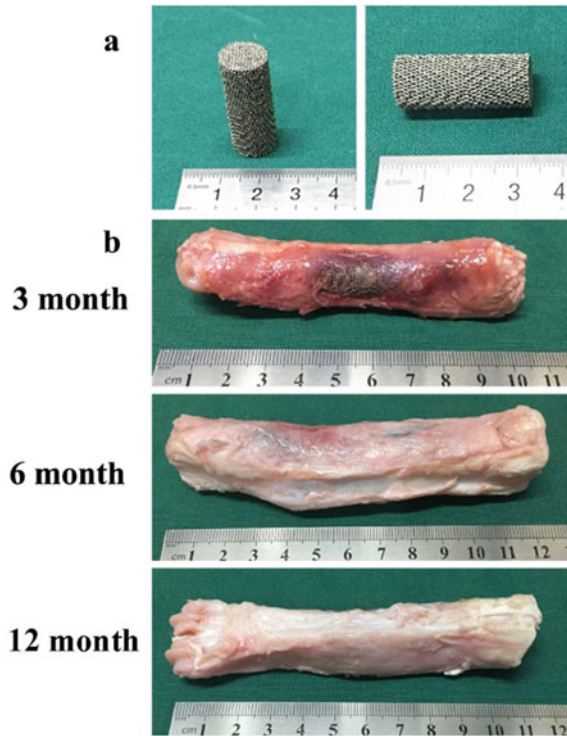
Having conspicuous advantages, additive manufacturing technology has attracted a great deal of attentions in recent years, to implement in the production of bone tissue engineering scaffolds. Scaffolds fabricated by AM technology have unique properties which cannot be obtained through other manufacturing methods. In this chapter, various AM methods used for BTE scaffold production were examined and the advantages and disadvantages of each method were presented. All of these methods print layers in a successive way based on the STL output from the CAD file. Depending on the energy source and whether it is powder-bed, powder-fed, or



**Fig. 5.14** Viability and proliferation of MG63 cells cultured on the Ti-6Al-4V scaffolds with different irregularities(0.06,0.25,0.5) and porosities(48.83%,63.51%,74.28%): **a, b** fluorescence microscopy images after being cultured for 1 d (live cells are in green color); **c, d** CCK-8 test results after being cultured for 1, 3, and 5 d [41]

wire-fed, AM methods are divided into seven categories, among which EBM and SLM are more used in the construction of BTE scaffolds. Also, various materials and powders employed in this method such as ceramics, metal, synthetic and natural polymers, and composites as well as their pros and cons were discussed. Then, the architecture design of the additively manufactured BTE scaffolds was studied and the evaluation of their mechanical properties was presented. It was observed that the unit cells give a pattern for the construction of scaffolds. These cells can be polyhedron, TPMS, or truss. It was found that FGS are also very promising structures for obtaining the desired properties of the scaffold. Depending on the requirements, the geometry and chemical composition of the FGS are different in every section of the scaffolds. Experimental and FEM investigations showed that when the micro-strut is oriented in the direction of loading, the loading would be stretch-dominant that results in better mechanical properties. By increasing the micro-strut angle, the mechanical properties are reduced. The strain curve of the scaffold is changed by

**Fig. 5.15** Scaffold used in the in vivo procedure (height and diameter of 30 and 10 mm) **a** tissue regeneration for 3 months, 6 months, and 12 months **b** [47]



changing the cell type and porosity. In addition, it was found that more porosity and appropriate post-processing could increase the fatigue life of the additively manufactured BTE scaffolds. Finally, in vitro and in vivo studies on these scaffolds showed that the presence of micro-scale cavities and ravines on the scaffold surface improves the adhesion and migration of osteoblast cells. Furthermore, porosity and addition of growth factor have a significant effect on cell growth. Consequently, with all these taken into account, additively manufactured BTE scaffolds offer a promising approach for the treatment of graft requiring bone defects.

## References

1. OpenStax AP, OpenStax CNX (2016). <http://cnx.org/contents/14fb4ad7-39a1-4eee-ab6e-3ef2482e3e22@8.24>
2. Mehta M, Schmidt-Bleek K, Duda GN, Mooney DJ (2012) Biomaterial delivery of morphogens to mimic the natural healing cascade in bone. *Adv Drug Deliv Rev* 64:1257–1276
3. Singh H, Singh S, Prakash C (2019) Current trends in biomaterials and bio-manufacturing. In: *Biomanufacturing*, Springer, pp 1–34
4. Sikavitsas VI, Temenoff JS, Mikos AG (2001) Biomaterials and bone mechanotransduction. *Biomaterials* 22:2581–2593

5. Ho CMB, Ng SH, Yoon Y-J (2015) A review on 3D printed bioimplants. *International Journal of Precision Engineering and Manufacturing* 16:1035–1046
6. Reichert JC, Cipitria A, Epari DR, Saifzadeh S, Krishnakanth P, Berner A, Woodruff MA, Schell H, Mehta M, Schuetz MA (2012) A tissue engineering solution for segmental defect regeneration in load-bearing long bones. *Science translational medicine*, 4:141ra193–141ra193
7. Guarino V, Gloria A, Raucci MG, De Santis R, Ambrosio L (2012) Bio-inspired composite and cell instructive platforms for bone regeneration. *Int Mater Rev* 57:256–275
8. Kohn DH, Sarmadi M, Helman JI, Krebsbach PH (2002) Effects of pH on human bone marrow stromal cells in vitro: implications for tissue engineering of bone. *J Biomed Mater Res Official J Soc Biomater, Japan Soc Biomater Aust Soc Biomater Korean Soc Biomater* 60:292–299
9. Cheung H-Y, Lau K-T, Lu T-P, Hui D (2007) A critical review on polymer-based bio-engineered materials for scaffold development. *Compos B Eng* 38:291–300
10. Soundarya SP, Menon AH, Chandran SV, Selvamurugan N (2018) Bone tissue engineering: Scaffold preparation using chitosan and other biomaterials with different design and fabrication techniques. *Int J Biol Macromol*
11. Singh S, Singh M, Prakash C, Gupta MK, Mia M, Singh R (2019) Optimization and reliability analysis to improve surface quality and mechanical characteristics of heat-treated fused filament fabricated parts. *Int J Adv Manuf Technol* 1–16
12. Poomathi N, Singh S, Prakash C, Patil RV, Perumal P, Barathi VA, Balasubramanian KK, Ramakrishna S, Maheshwari N (2019) Bioprinting in ophthalmology: current advances and future pathways. *Rapid Prototyping J* 25:496–514
13. Singh S, Singh N, Gupta M, Prakash C, Singh R (2019) Mechanical feasibility of ABS/HIPS-based multi-material structures primed by low-cost polymer printer. *Rapid Prototyping J* 25:152–161
14. Murr L, Gaytan S, Medina F, Lopez H, Martinez E, Machado B, Hernandez D, Martinez L, Lopez M, Wicker R (2010) Next-generation biomedical implants using additive manufacturing of complex, cellular and functional mesh arrays. *Philos Trans R Soc A Math Phys Eng Sci* 368:1999–2032
15. Hong D, Chou D-T, Velikokhatnyi OI, Roy A, Lee B, Swink I, Issaev I, Kuhn HA, Kumta PN (2016) Binder-jetting 3D printing and alloy development of new biodegradable Fe-Mn-Ca/Mg alloys. *Acta Biomater* 45:375–386
16. Wauthle R, Van Der Stok J, Yavari SA, Van Humbeeck J, Kruth J-P, Zadpoor AA, Weinans H, Mulier M, Schrooten J (2015) Additively manufactured porous tantalum implants. *Acta Biomater* 14:217–225
17. Zhang X-Y, Fang G, Zhou J (2017) Additively manufactured scaffolds for bone tissue engineering and the prediction of their mechanical behavior: A review. *Materials* 10:50
18. Prakash KS, Nancharaih T, Rao VS (2018) Additive Manufacturing Techniques in Manufacturing-An Overview. *Mater Today Proc* 5:3873–3882
19. Sames WJ, List F, Pannala S, Dehoff RR, Babu SS (2016) The metallurgy and processing science of metal additive manufacturing. *Int Mater Rev* 61:315–360
20. Lü L, Fuh J, Wong Y-S (2013) Laser-induced materials and processes for rapid prototyping. *Springer Science & Business Media*
21. Yap CY, Chua CK, Dong ZL, Liu ZH, Zhang DQ, Loh LE, Sing SL (2015) Review of selective laser melting: Materials and applications. *Appl Phys Rev* 2:041101
22. Heintl P, Müller L, Körner C, Singer RF, Müller FA (2008) Cellular Ti–6Al–4 V structures with interconnected macro porosity for bone implants fabricated by selective electron beam melting. *Acta Biomater* 4:1536–1544
23. Simchi A, Petzoldt F, Pohl H (2003) On the development of direct metal laser sintering for rapid tooling. *J Mater Process Technol* 141:319–328
24. Mazumder J, Dutta D, Kikuchi N, Ghosh A (2000) Closed loop direct metal deposition: art to part. *Opt Lasers Eng* 34:397–414
25. Ge W, Guo C, Lin F (2014) Effect of process parameters on microstructure of TiAl alloy produced by electron beam selective melting. *Procedia Engineering* 81:1192–1197

26. Oonishi H, Kushitani S, Yasukawa E, Iwaki H, Hench LL, Wilson J, Tsuji E, Sugihara T (1997) Particulate bioglass compared with hydroxyapatite as a bone graft substitute. *Clin Orthopaedics Relat Res* 316–325
27. Singh S, Prakash C, Ramakrishna S (2019) 3D printing of polyether-ether-ketone for biomedical applications. *Eur Polym J*
28. Fielding G, Bose S (2013) SiO<sub>2</sub> and ZnO dopants in three-dimensionally printed tricalcium phosphate bone tissue engineering scaffolds enhance osteogenesis and angiogenesis in vivo. *Acta Biomater* 9:9137–9148
29. Kim J, McBride S, Tellis B, Alvarez-Urena P, Song Y-H, Dean DD, Sylvia VL, Elgendy H, Ong J, Hollinger JO (2012) Rapid-prototyped PLGA/β-TCP/hydroxyapatite nanocomposite scaffolds in a rabbit femoral defect model. *Biofabrication* 4:025003
30. Cheah C, Chua C, Leong K, Chua S (2003) Development of a tissue engineering scaffold structure library for rapid prototyping. Part 1: investigation and classification. *Int J Adv Manuf Technol* 21:291–301
31. Cheah C, Chua C, Leong K, Chua S (2003) Development of a tissue engineering scaffold structure library for rapid prototyping. Part 2: parametric library and assembly program. *Int J Adv Manuf Technol* 21:302–312
32. Lee SJ, Yang S (2012) Micro glass ball embedded gels to study cell mechanobiological responses to substrate curvatures. *Rev Sci Instrum* 83:094302
33. Yuan L, Ding S, Wen C (2019) Additive manufacturing technology for porous metal implant applications and triple minimal surface structures: a review. *Bioactive Mater* 4:56–70
34. Sychov M, Lebedev L, Dyachenko S, Nefedova L (2018) Mechanical properties of energy-absorbing structures with triply periodic minimal surface topology. *Acta Astronaut* 150:81–84
35. Melchels FP, Bertoldi K, Gabbriellini R, Velders AH, Feijen J, Grijpma DW (2010) Mathematically defined tissue engineering scaffold architectures prepared by stereolithography. *Biomaterials* 31:6909–6916
36. Han SC, Choi JM, Liu G, Kang K (2017) A microscopic shell structure with schwarz's d-surface. *Scientific Rep* 7:13405
37. Zok FW, Latture RM, Begley MR (2016) Periodic truss structures. *J Mech Phys Solids* 96:184–203
38. Zhang X-Y, Fang G, Xing L-L, Liu W, Zhou J (2018) Effect of porosity variation strategy on the performance of functionally graded Ti-6Al-4 V scaffolds for bone tissue engineering. *Mater Des* 157:523–538
39. Barui S, Chatterjee S, Mandal S, Kumar A, Basu B (2017) Microstructure and compression properties of 3D powder printed Ti-6Al-4 V scaffolds with designed porosity: experimental and computational analysis. *Mater Sci Eng C* 70:812–823
40. Campoli G, Borleffs M, Yavari SA, Wauthle R, Weinans H, Zadpoor AA (2013) Mechanical properties of open-cell metallic biomaterials manufactured using additive manufacturing. *Mater Des* 49:957–965
41. Liang H, Yang Y, Xie D, Li L, Mao N, Wang C, Tian Z, Jiang Q, Shen L (2019) Trabecular-like Ti-6Al-4 V scaffolds for orthopedic: fabrication by selective laser melting and in vitro biocompatibility. *J Mater Sci Technol*
42. Zadpoor AA (2018) Mechanical performance of additively manufactured meta-biomaterials. *Acta Biomaterialia*
43. Kadkhodapour J, Montazerian H, Darabi AC, Anaraki A, Ahmadi S, Zadpoor A, Schmauder S (2015) Failure mechanisms of additively manufactured porous biomaterials: effects of porosity and type of unit cell. *J Mech Behav Biomed Mater* 50:180–191
44. Ahmadi S, Yavari S, Wauthle R, Pouran B, Schrooten J, Weinans H, Zadpoor A (2015) Additively manufactured open-cell porous biomaterials made from six different space-filling unit cells: the mechanical and morphological properties. *Materials* 8:1871–1896
45. Van Hooreweder B, Apers Y, Lietaert K, Kruth J-P (2017) Improving the fatigue performance of porous metallic biomaterials produced by selective laser melting. *Acta Biomater* 47:193–202
46. Hosseini V, Kollmannsberger P, Ahadian S, Ostrovidov S, Kaji H, Vogel V, Khademhosseini A (2014) Fiber-assisted molding (FAM) of surfaces with tunable curvature to guide cell alignment and complex tissue architecture. *Small* 10:4851–4857

47. Li G, Wang L, Pan W, Yang F, Jiang W, Wu X, Kong X, Dai K, Hao Y (2016) In vitro and in vivo study of additive manufactured porous Ti6Al4V scaffolds for repairing bone defects. *Sci Rep* 6:34072
48. van der Stok J, Wang H, Amin Yavari S, Siebelt M, Sandker M, Waarsing JH, Verhaar JA, Jahr H, Zadpoor AA, Leeuwenburgh SC (2013) Enhanced bone regeneration of cortical segmental bone defects using porous titanium scaffolds incorporated with colloidal gelatin gels for time- and dose-controlled delivery of dual growth factors. *Tissue Eng Part A* 19:2605–2614

**Mr. Majid Fazlollahi** M.Sc. Research Scholar, Mechanical Engineering Department, Amirkabir University of Technology (Tehran Polytechnic), Tehran, Iran. He has been working on advanced manufacturing methods and mechanics of materials. His core research area is mechanical behavior of biomaterials and advanced manufacturing methods such as additive manufacturing.

**Ms. Yasaman Pooshidani** M.Sc. Research Scholar, Biomedical Engineering Department, Amirkabir University of Technology (Tehran Polytechnic), Tehran, Iran. She has been working on biomaterials, tissue engineering, and drug delivery systems. Her core research area is investigating the scaffolds properties for tissue engineering and in vivo and in vitro studies of scaffolds. Also, she is working on drug delivery in the retina tissue.

**Dr. Mahnaz Eskandari** is Assistant Professor in the Biomedical Engineering Department, Amirkabir University of Technology (Tehran Polytechnic), Tehran, Iran. She has received Ph.D. in Chemical Engineering from Illinois Institute of Technology, Chicago, IL, USA. Her area of research is retina tissue engineering, neuron tissue engineering, bioink, cancer–laser interaction, and bioreactor design. She has more than 10 years of teaching and research experience. She has contributed extensively to the world in tissue engineering literature with publications appearing in *Journal of Materials Science and Engineering: C*, *Powder Technology*, *Reactive and Functional Polymers*, *BioNanoScience*, *Biotechnology* and *bioengineering*, etc.

# Chapter 6

## FDM 3D Printing in Biomedical and Microfluidic Applications



Gabriel Gaal, Vladimir Gaal, Maria Luisa Braunger, Antonio Riul Jr, and Varlei Rodrigues

### 6.1 Introduction

3D printing has attracted great attention due to its unique capacity of customization and rapid prototyping, consuming less resources and generating less residues than traditional subtraction techniques. It is a promising additive manufacturing (AM) technology because it can build 3D parts designed for highly specific prototyping of complex geometries. Despite the limited construct dimensions and low scalability achieved by this technique, there have been strong efforts to apply it in science, technology, education, and sustainable development [1].

3D printing features two main branches: cutting-edge technologies and rapid prototyping. The first requires trained personnel and complex infrastructures, being used in specific applications with high added value constructs, such as automobile industries and aerospace technologies. The second is used for the rapid design and prototyping of ideas and concepts and does not require experts. Overall, 3D printers offer user-friendly interfaces to enable a more versatile manufacturing process [2]. Among them, fused deposition modeling (FDM) 3D printers have been widely exploited as they are cheap, table-top printers. Despite the variety of commercial models, FDM printers have also innumerable open projects available on the Internet allowing common users to build their own setups. Moreover, this open-source technology allows constant improvements by the 3D printing community for FDM, sharing and discussing new ideas and projects.

---

G. Gaal · V. Gaal · M. L. Braunger · A. Riul Jr · V. Rodrigues (✉)  
Department of Applied Physics, “Gleb Wataghin” Institute of Physics, University of Campinas (UNICAMP), Campinas, São Paulo, Brazil  
e-mail: [varlei@ifi.unicamp.br](mailto:varlei@ifi.unicamp.br)

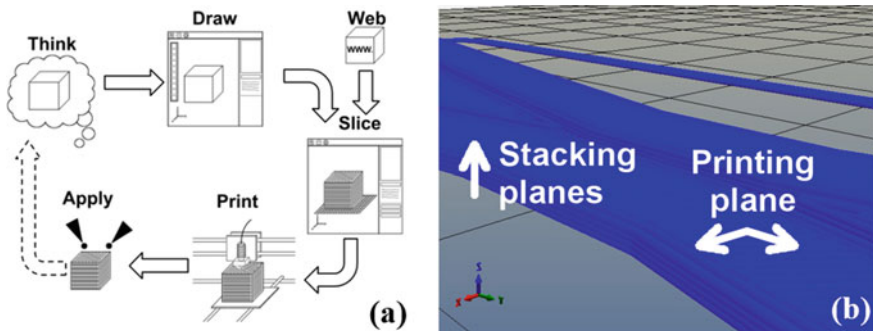
In this chapter, we will describe the FDM printing process, from the 3D digital model to a final printed prototype, reviewing the main available commercial filaments. Moreover, we will highlight current FDM technology in science, focusing on chemical and biomedical applications.

## 6.2 Printing Process

3D printing is an additive manufacturing process used by stereolithography (SLA), selective laser sintering (SLS), and fused deposition modeling (FDM) [1, 3–5]. Each one has its own specificity using different materials to fabricate the 3D model, but they all follow the same layer-by-layer printing process. In particular, the FDM technique uses thermoplastics having a specific property for an intended application. In this section, we will detail the FDM printing process, discussing the digital model design and its digital file format, the slicer software, GCODE basics, and FDM printer setups.

### 6.2.1 From Digital Model to GCODE

The AM creation process follows the steps presented on Fig. 6.1. The first delineates the needs of the project, outlining the filament material, the AM technique, and post-printing processes, in order to tune up specific properties of the printed part [6, 7]. Then, you have to translate your ideas into 3D computer models using computer-aided design (CAD) applications. The main CAD softwares are AutoCAD, OpenSCAD, Autodesk Inventor, and SolidWorks. Each CAD program stores information from the digital model in a particular native draw file format (DWG, IPT, PRT, among others). However, the drawing file must be translated into another format containing only the



**Fig. 6.1** **a** Schematic flowchart of prototyping process in FDM printing technique. **b** Lines to be printed, generated based on the GCODE instructions



necessary information of the model external surface. This process usually tessellates the digital model surface into a series of small triangles (facets), with each facet described by a perpendicular direction (labeling the external side) and three points representing the vertices (corners) of the triangle [8]. This shell representation of the 3D surface geometry is called STL (“StereoLithography”) format. Another way to obtain the 3D models in STL format is searching projects in open repositories such as “thingiverse.com” and “grabcad.com”, usually fed by users.

Next step is to generate a set of instructions that controls the FDM printer, generally made by softwares called “slicers.” They transform the STL 3D model into a discreet stack of horizontal planes (Fig. 6.1b), which has an associated set of Cartesian coordinates indicating the position and the amount of thermoplastic to be deposited, called GCODE. The GCODE also has the information about the 3D printer configuration, such as speed, temperature, and printer dimensions [1]. Several free softwares such as Slic3r, KISSlicer, and Cura generate the GCODE.

Finally, it is time to print the prototype and test it. A fundamental step of the prototyping concept is feedback; it is important that the user looks back into the first step, “re-think” the model, and proceeds to subsequent steps again.

## 6.2.2 FDM Printers

Different types of FDM 3D printers, either commercial or open-source projects, follow the same printing principles. Likewise a pen drawing and dropping ink on a paper, an extruder is guided on a horizontal plane following a particular coordinate system depositing layers of melted thermoplastics. The extrusion is done by a stepper motor that pushes the filament into the heated nozzle, depositing it on planes sequentially stacked to create the object in a layer-by-layer process. Usually, the first layer is deposited on a heated bed to simplify its adhesion to the bed and to maintain a fairly smooth temperature gradient along the printed object avoiding warping and delamination effects.

Traditional printers such as Prusa Mendel, Prusa i3, MakerBot, and Ultimaker use Cartesian coordinates to define the movement directions of the printing bed and hot nozzle. Usually, the hot bed moves linearly in one direction (Y-axis) and the extruder is moved in other linear direction perpendicular to the bed (X-axis), creating a XY printing plane. The vertical movement is done either moving the extruder upward or the hot bed downward in order to start the next layer. It is interesting to notice that there are other Cartesian projects using other sets of linear and perpendicular coordinate systems, but they are still Cartesian printers. For example, our research group designed and assembled a homemade FDM printer that uses a positioning technique known as CoreXY to move the heated nozzles of the printer [9]. This technique consists of two belt and pulley systems that move the nozzle on two independent and perpendicular directions. By combining these two movements, it is possible to attain any position in the deposition plane [10].

In polar printers, the printing bed moves linearly in the radial direction ( $r$ -axis) and rotates along the  $\theta$ -axis direction. The deposited layers can be stacked either moving the extruder upward or the printing bed downward [11]. There are also printers that define the printing movements without a set of perpendicular coordinates. Two interesting examples are the Delta and the SCARA printers that maintain the printing bed static, moving only the extruder head. The Delta printer consists of three suspended arms that move up and down independently on rails, allowing the nozzle positioning in any location [12]. Finally, the Selective Compliance Assembly Robotic Arm (SCARA) printers use a robotic arm system to move the extruder along a printing plane [11].

It is important to stress that each printer setup has its own pros and cons. For example, traditional Cartesian printers have good structural stability, diminishing errors when the print head moves within the 3D space to give a fine surface finish. They are also well-established setups, so it is easy to find out technical assistance; however, they usually have bigger structural parts, so they are less portable, and a relative lower movement speed, increasing the printing time. On the other hand, polar printers have small structural parts, allowing to print a bigger built volume within a smaller space. The main drawback in polar printers is the difficulty to integrate a heater to the printing bed due to its rotational movements.

## 6.3 Filaments and Composites

There are numerous commercially available thermoplastic filaments having distinct properties, such as hardness, toughness, softness, water-soluble, biodegradable, and/or biocompatible. Moreover, there is a current growing interest in the development of composite filaments to add new functionalities such as electrical conductivity in commercial polymers. In this section, we will list the main properties of the commercially available raw thermoplastic filaments and their composites.

### 6.3.1 Raw Filaments

One of the most used filaments is polylactic acid (PLA), which consists of linear aliphatic polyester chains synthesized from renewable resources such as corn starch, sugar cane, and potatoes [13], being a sustainable polymer, widely exploited as an alternative to petroleum-based materials. PLA is biodegradable and biocompatible, so it can resist low-temperature sterilization processes, an essential requirement for bio-implantable devices. Moreover, it can be used in all commercial FDM 3D printers as it has low glass transition temperature ( $60\text{ }^{\circ}\text{C}$ ), melting point at  $153\text{ }^{\circ}\text{C}$ , and extrusion temperatures ranging from  $175$  to  $195\text{ }^{\circ}\text{C}$ . PLA also has a low thermal expansion coefficient ( $70 \times 10^{-6}\text{ }^{\circ}\text{C}^{-1}$ ), with no need of a hot bed as it has negligible warping of printed models [14]. Despite being soluble in most organic solvents, PLA

is chemically resistant in acidic media, allowing reversible and permanent surface functionalization [15–18].

Likewise PLA, acrylonitrile butadiene styrene (ABS) is also widely used filament for FDM 3D printing. Moreover, ABS is the most used thermoplastic in commercial products, such as Lego™ building blocks. It has glass transition temperature around 112 °C and extrusion temperatures ranging from 220 to 240 °C [19]. Additionally, ABS parts combine toughness and flexibility, exhibiting chemical, heat, and moisture resistances [20, 21]. However, ABS has a thermal expansion coefficient of  $100 \times 10^{-6} \text{ }^\circ\text{C}^{-1}$ , which could lead to warping and delamination of printed parts. So it is essential to maintain a low-temperature gradient along the printed model by using a hot bed at high temperature (110 °C) and a good thermal isolation [14]. The bed adhesion is another drawback, but it can be improved by preparing the hot surface with glue, thin layer of acetone, or printing on polyimide (Kapton™). Finally, ABS is not biodegradable neither biocompatible, precluding some applications [15].

Polyethylene terephthalate (PET) is also a petroleum derivative thermoplastic of the polyester family. It is commonly used in fibers for clothing and vessels for liquid and food storage. PET is a fairly hard material, but its transparency makes it attractive for some niche applications [15], and despite its use as printing filament, the most employed material has been glycol modified PET (PETG). PETG has interesting thermal properties for FDM printing, such as glass transition temperature of 75 °C, extrusion temperatures from 230 to 260 °C, and low thermal expansion coefficient ( $59 \times 10^{-6} \text{ }^\circ\text{C}^{-1}$ ) minimizing warping effects [22].

While PLA, ABS, and PETG are user-friendly and largely used filaments, nylon (polyamide) is a trick material to be used in FDM printers. Firstly, it has a high extrusion temperature (250 °C) and high thermal expansion coefficient ( $\sim 10 \times 10^{-5} \text{ }^\circ\text{C}^{-1}$ ) that leads to large warping effects in the printed object. Generally, the printing bed is kept at 70 °C, but it does not hamper layer warping with nylon. Additionally, there is a weak layer adhesion due to the lack of compression during the printing process, leading to a low overall strength of the printed model [15]. Consequently, efforts have been made to develop composite Nylon materials to improve the mechanical and chemical properties of the filaments.

Polyvinyl alcohol (PVA) is a water-soluble polymer that is mostly used as support material for complex geometries. PVA is extruded at temperatures ranging from 190 to 210 °C, and it does not require heated bed to facilitate the adhesion or to avoid warping process. Therefore, the printing with this material can be tricky because PVA has a large water absorption coefficient compared with standard filaments and that implies in a poor adhesion with other materials due its thermal properties [23].

### 6.3.2 Composite Filaments

Recently, there is a great interest in the development of printable polymer composites with added properties. The materials may feature properties different from the raw polymer filaments, such as high mechanical performance and/or enhanced electrical

and thermal conductivity. The fabrication of polymer composites is promoted by the incorporation of fiber, particle, or nanomaterial reinforcements into raw polymer matrices [24, 25].

Particle incorporation is particularly interesting because it enables homogeneous mixture within the polymer matrix, despite the fact that several properties can be tuned by particle addition in the filament. Nikzad et al. and Hwang et al. showed that both storage modulus and thermal conductivity can be improved by adding iron and copper into ABS matrix. Such composites also reduce the thermal expansion coefficient reducing warping effects [26, 27]. Perez and Wicker observed that ABS composites of thermoplastic elastomer particles (TPE) showed a reduced anisotropy of the tensile strength and modulus when compared with results obtained by Ahn et al. for raw ABS filaments [28, 29]. ABS filaments can also be reinforced with BaTiO<sub>3</sub> nanoparticles in order to tune its dielectric permittivity as shown by Isakov et al. [30].

Mechanical, electrical, and thermal properties can also be modified by the incorporation of nanomaterials such as graphene, carbon nanotubes, and metallic and ceramic nanoparticles. For example, TiO<sub>2</sub>, carbon nanofiber, and multi-walled carbon nanotubes showed at least 7.5% increase in the tensile strength of the printed ABS composite parts compared with raw material [28]. The printed objects become more brittle and showed reduced elongation at yield [28]. However, the ABS matrix can be modified with graphene to improve electrical conductivity and thermal stability [31]. Montmorillonite, a nanoclay material, can be added to ABS to tune both tensile and flexural strength and modulus, thermal stability, and to reduce the thermal expansion coefficient [32].

Another way to enhance polymer properties is through fiber reinforcement. For example, glass [33] and carbon [34] fibers have been added into ABS to modify its mechanical properties. Tekinalp et al. showed that printed parts of ABS-based carbon fiber composites presented higher fiber orientation along the printing direction [35]. They argue that it can explain why the printed parts exhibited similar mechanical properties compared to those fabricated by standard compression model techniques, despite the higher porosity obtained by FDM printing. There are also commercial conductive PLA-based graphene filaments designed to allow 3D printing of electrically conductive parts considering different FDM printers. Nonetheless, after printing, the printed parts displayed a higher electrical resistance than the filament [9, 36].

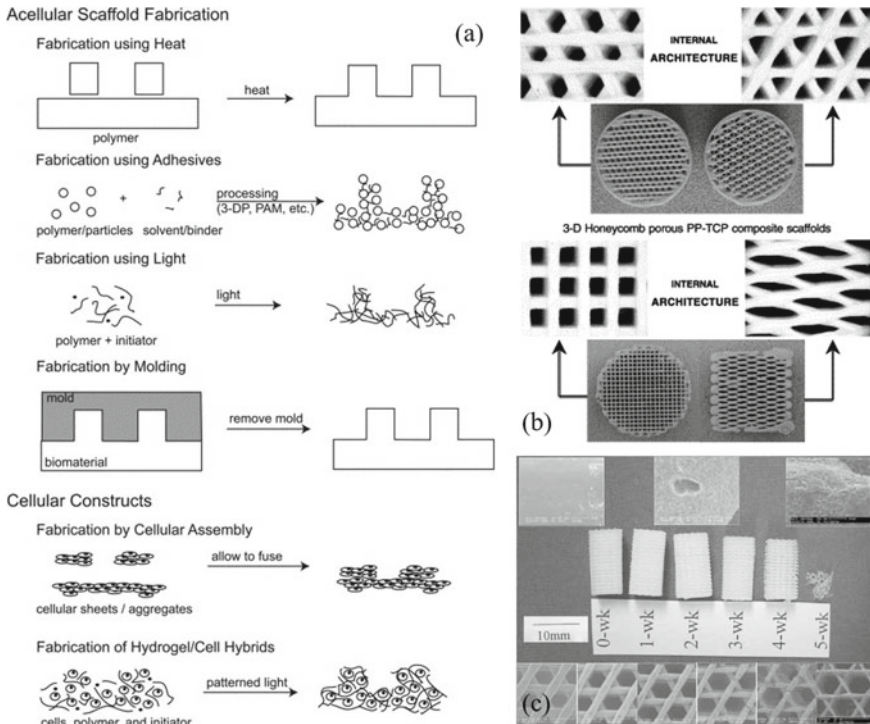
## 6.4 Applications

### 6.4.1 Biomedical

The use of 3D printing in biomedical applications is expected to revolutionize health care, with applications in customized prosthetics, implants, anatomical models [37–39], and drug dosage and delivery [40–42]. Despite significant biomedical advances in 3D printing research, time is required for transformative applications due to safety and regulatory challenges [43, 44]. A usual criticism of FDM printing technology is the difficulty to scale it up industrially. However, its differential lies precisely in the customized production rather than scalability. The biomedical area perfectly exemplifies the need of customization to attend distinct patients.

It is important to stress that the use of 3D printing technologies in biomedical applications differs from bioprinting. Bioprinting is a very promising technique for advancing tissue engineering that uses 3D printing-like techniques to spatially arrange cells within the construct, mimicking the native tissue in its totality and not just in the physical and chemical form [45]. 3D bioprinting systems use AM technologies, such as laser-, inkjet-, or extrusion-based deposition [46, 47]. The last one originates from FDM printing and uses pneumatic, mechanical, or electromagnetic driven systems to deposit the desired biomaterial [48]. The cell-laden material is extruded through a needle and printed as lines forming the 3D structure through a layer-by-layer process [49]. Despite the bioprinting prominence, we will focus here on describing the use of regular FDM technique in biomedical applications.

In the last two decades, the literature has a plethora of FDM studies in bone tissue engineering [50]. Tests usually relies on fabricating scaffolds, which are 3D structures that can mimic the extracellular matrix properties and provide a template for cell attachment and stimulate bone tissue formation (Fig. 6.2a) [51]. The use of FDM has evolved from the manufacture of molds to the fabrication of the scaffold itself from composite materials. Initially, authors used FDM and a thermoplastic wax filament (ICW-06) to fabricate molds to produce ceramic scaffolds [52–54]. In 2001, Hutmacher et al. fabricated scaffolds from poly ( $\epsilon$ -caprolactone) (PCL), which is considered a soft- and hard-tissue-compatible bioresorbable material [55]. They found that PCL scaffolds displayed excellent biocompatibility with human fibroblast and periosteal cell culture systems. In 2002, Too et al. developed 3D non-random porous structures of ABS using FDM to determine their suitability for use in the area of tissue engineering [56]. FDM provided good control and reproducibility of the desired degree of porosity, a crucial parameter to design scaffolds for biomedical applications. In 2003, Kalita et al. fabricated composite scaffolds from polypropylene (PP) polymer and tricalcium phosphate ceramic (Fig. 6.2b) [57]. They showed that these samples were non-toxic, with excellent cell growth during the first two weeks of in vitro testing. In 2007, Lam et al. fabricated composite scaffolds from PCL mixed with  $\beta$ -tricalcium phosphate ( $\beta$ -TCP) and evaluated its degradation rate in alkaline medium (Fig. 6.2c) [58]. Polymer and ceramic composite scaffolds show enhanced



**Fig. 6.2** **a** Methods of 3D tissue fabrication. Reproduced with permission from [50]. Copyright 2004, Elsevier. **b** Scaffolds fabricated from composite filaments via FDM showing the obtained controlled and distinct porosity structures. Reproduced with permission from [57]. Copyright 2003, Elsevier. **c** Microscopic and macroscopic views of NaOH-degraded PCL scaffolds from 0 to 5 weeks. Reproduced with permission from [58]. Copyright 2007, John Wiley & Sons

mechanical properties, biocompatibility, osteoconductivity, and also increased degradation rate [59]. Polyether-ether-ketone (PEEK) is known for its chemical/biological stability and biocompatibility; however, FDM processing conditions impact thermal, mechanical, and dimensional products fabricated with PEEK [60]. Taking these issues into account, Vaezi et al. proposed an extrusion-based additive manufacturing technique integrated with compression molding processes in order to fabricate PEEK/hydroxyapatite composite scaffolds [61]. Recent literature about 3D-printed scaffolds have shown remarkable results using SLA printing due to its high resolution; however, the reduced number of available biodegradable/biocompatible resins hamper some applications [62].

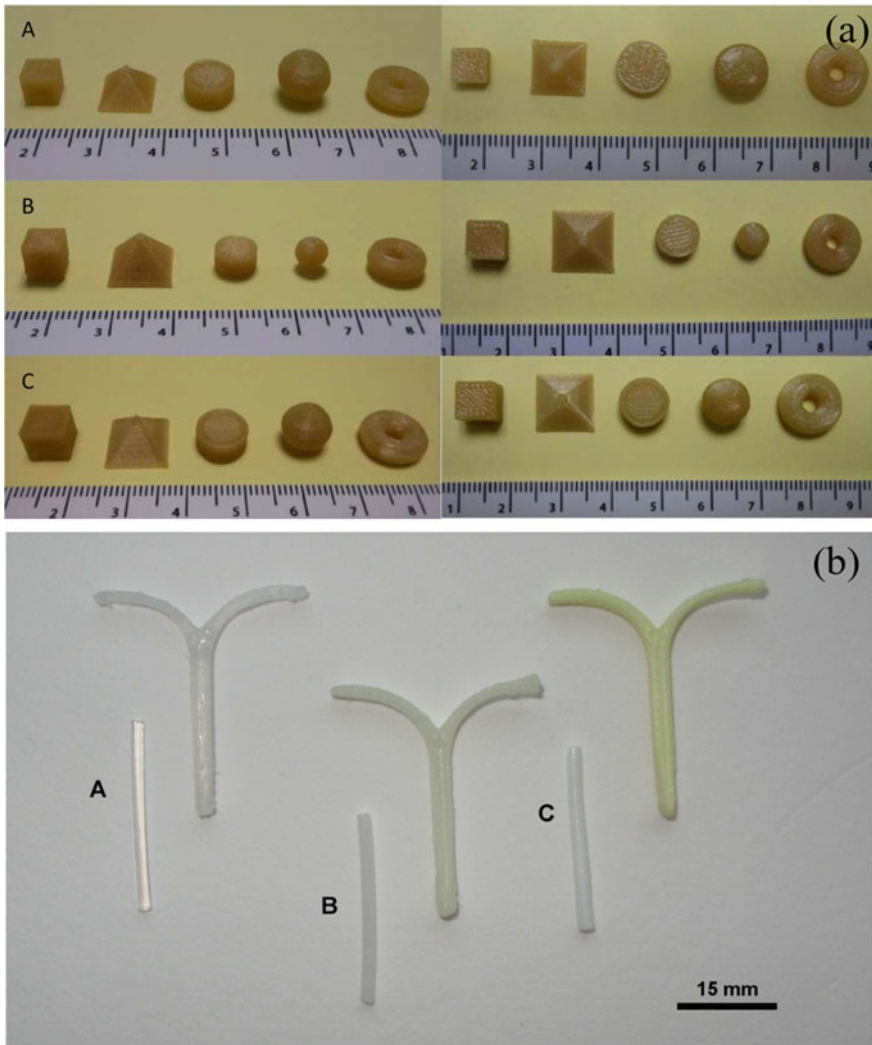
In the past few years, FDM printing has received a lot of attention in pharmaceutical research regarding drug dosage and delivery. Most of the recent papers in the literature use FDM raw thermoplastics mixed with drugs, and the performance is evaluated after extrusion with distinct shapes and sizes. In 2015, Water et al. demonstrated the FDM potential producing a PLA-based drug delivery system

for controlled release products [63]. PLA-based nitrofurantoin (NF) filament was successfully obtained and extruded with up to 30% drug load in two cases, with the addition of 5% of hydroxyapatite (HA) and without it, and samples printed in disc geometries. NF release was dependent on the drug loading as a higher level of released drug was observed from discs having higher drug loads. In the same year, Weisman et al. loaded PLA with gentamicin sulfate and also with methotrexate, creating a new class of bioactive 3D printing filaments [64]. It was found that these compounds retained their effective antimicrobial and cytostatic properties throughout the manufacturing process, despite the heat required for FDM printing. Antibacterial effects and a reduction in proliferation of osteosarcoma cells were observed with all constructs, attesting both technical and clinical viability of these PLA-based composites.

There is also a demand for versatile and adjustable methods for the fabrication of oral tablets, with FDM techniques adapted to engineer and control the dosage of 3D-printed tablets. Skowyra et al. produced tablets for drug delivery from PVA-based filaments loaded with prednisolone, with *in vitro* drug release extended up to 24 h from the printed tablets [65]. Goyanes et al. manufactured tablet of distinct geometries from PVA loaded with paracetamol. Distinct tablet geometries were successfully printed, such as cube, pyramid, cylinder, sphere, and torus (Fig. 6.3a), some of them challenging to manufacture by powder compaction. They showed that the drug release profile depends only on the tablet surface to volume ratio instead of its surface area, indicating the influence of the geometrical shape on the drug release profile [66]. Goyanes et al. also loaded PVA with 4-aminosalicylic acid (4-ASA) and 5-aminosalicylic acid (5-ASA), drugs commonly used in the treatment of inflammatory bowel disease. They argued that the printing temperature plays a fundamental role on the drug degradation and showed that the active 4-ASA (50%) was significantly degraded after being printed, while 5-ASA samples were feasible [67]. Genina et al. showed that certain grades of ethylene-vinyl acetate (EVA) copolymers are suitable to produce 3D-printed drug-loaded implantable prototypes, such as custom-made intrauterine systems and subcutaneous rods loaded with indomethacin drug (Fig. 6.3b) [68].

Most of the literature in biomedical applications reports the use of FDM in the fabrication of scaffolds and drug delivery studies. To illustrate, in 2008, Tek et al. reported FDM as a rapid prototyping technological tool to create devices frequently required in neuroscience research [69]. A skull-based housing platform for stroke electrophysiology studies, a cranial window, and two imaging compatible perfusion chambers were fabricated from ABS filaments. In 2010, Espalin et al. demonstrated that customized polymethylmethacrylate (PMMA) structures with varying porosities can be fabricated by FDM for craniofacial reconstruction and orthopedic spacers (Fig. 6.4a) [70]. By using PMMA (biocompatible polymer) together with FDM, medical implants can be directly printed from medical imaging data, thus improving the current state of art use in medicine. In 2014, Sandler et al. demonstrated the incorporation of antimicrobial NF in PLA and subsequent FDM printing of disc structures, resulting in an inhibition of biofilm colonization [71]. The approach taken is very promising and can pave the way the manufacture of new functional medical devices





**Fig. 6.3** **a** 3D-printed tablets of distinct geometries fabricated from composite filament (PVA matrix and paracetamol) by FDM. Reproduced with permission from [66]. Copyright 2015, Elsevier. **b** Filaments and 3D-printed intrauterine prototypes of EVA containing distinct amount of indomethacin. Reproduced with permission from [68]. Copyright 2016, Elsevier

in the future. In 2017, Mohammed et al. investigated the design methodology for the creation of a whole mandible implant based on the patient's medical imaging data [72]. The model was fabricated in ABS for preliminary evaluation of the structural integrity and dimensional accuracy of the jaw, before the final metal fabrication process (Fig. 6.4b).





**Fig. 6.4** **a** Skull model in ABS and PMMA placed in the cranial defect. Reproduced with permission from [70]. Copyright 2010, Emerald Publishing Limited. **b** Images of the post-processed mandibular implant and the representative FDM model in ABS of the skull/maxilla model with the final implant. Reproduced with permission from [72]. Copyright 2017, Knowledge E

### 6.4.2 *Microfluidics*

Microfluidic is the technology that controls and manipulates small amounts of liquid and gas samples for miniaturized analytical tools in both chemical and biochemical systems, biomedical devices, and systems for fundamental research [73, 74]. Duffy et al. used polydimethylsiloxane (PDMS), an optically transparent, gas- and vapor-permeable elastomer, for the fabrication of complex microfluidic devices [75]. It helped to promote soft lithography, which has then become the most widely adopted method to produce microfluidic devices. Despite all PDMS advantages in microfluidic applications, there are some limitations to implement the material in biomedical research such as its vapor permeability that hampers cell microenvironment studies [76–78]. When compared to soft lithography, 3D printing extends the use of materials beyond PDMS, allowing new possibilities for biomedical research. In addition, it avoids the use of clean rooms, the need to manufacture masks to prepare molds and the use of photosensitive materials, enabling low cost and faster prototyping.

The most exploited 3D printing technique for microfluidics is SLA due to higher channel resolution (50–100  $\mu\text{m}$ ) and transparency of the final device when

compared with other techniques. However, SLA is restricted to photocurable polymers, hindering biomedical applications and printing with composite materials [79, 80]. Within this context, FDM offers loads of polymers and composites for microfluidic biomedical applications. Despite the lower channel resolution, usually hundreds of microns, FDM stills more versatile than other AM techniques, enabling the fabrication of sacrificial molds for PDMS casting, development of microfluidic tools, and fabrication/integration of the final microfluidic device [3, 81].

Gul et al. used a commercial composite PLA filament filled with copper to print sacrificial microchannels molds for PDMS casting, using a 3D printing pen [82]. This technique gives more flexibility to draw simple geometries, but it has poor reproducibility for the fabrication of complex channels. To remove the mold, they used organic acid solution to produce microchannels of 200  $\mu\text{m}$  in diameter. Goh and Hashimoto used water-soluble PVA filament to fabricate microchannels molds and extended the casting materials beyond the PDMS realms, being able to develop microchannels made of hard polymers (rigid polyurethane, epoxy, and NOA 81), soft polymers (flexible polyurethane and PDMS), and hydrogels (TG gelatin PEGDA) [83].

Even though the mold printing extinguishes the need of soft lithography, the complete fabrication of a microfluidic device is interesting because it allows the development in a single-step process, reducing the time required for prototyping. To illustrate, Kitson et al. fabricated within a few hours microreactors for chemical synthesis [84]. They used PP filament and printed different geometries to synthesize organic and inorganic compounds as well as gold nanoparticles using 60–270  $\mu\text{L}$  of reagents. They also exploited 3D geometries of microchannels within the reactors, which is very difficult to achieve using traditional microfabrication techniques that usually confines the flow to two dimensions.

Banna et al. 3D-printed an integrated water quality sensing system using ABS filament and were able to monitor the water pH, conductivity, and temperature [85]. This system was able to operate in flow rates equivalent to the water distribution system without leakage or sensing failure, showing a promising on-site application. The 3D printing technology also allowed the design of a modular interface to facilitate the replacement of sensing units, which were integrated within the printed structures during the printing process.

Bauer and Kulinsky used ABS to fabricate and tested a modular device fully automated colorimetric enzyme-linked immunoassay (ELISA) designed to detect malaria [86]. They integrated arrays of disposable 3D-printed microchannels to an automated system that controls bioassays steps. This lab-on-a-chip device can be used for rapid on-site qualitative diagnostics with good response, suitable for low-resource settings.

In 2014, Krejcova et al. reported a new 3D microfluidic chip fabricated with PLA and equipped with electrodes for the detection of influenza hemagglutinin [87]. They showed that the electrochemical signal of this system has a great potential for rapid, sensitive, and specific detection of influenza virus. Authors emphasize that the microfluidic system can be used also for detection of other specific substances that are important for diagnosis and control of infectious diseases.

In our research group, we exploited the integration of several materials within the microchannel during the printing process. We were able to insert macro electrodes for electrochemical analysis, papers for self-driven flows, membranes, and thin glass sheets for biological applications. As a proof of concept, coated interdigitated electrodes (IDEs) were integrated to develop a 3D-printed microfluidic electronic tongue (Fig. 6.5) that was able to distinguish basic tastants [88]. In the same context, Yuen integrated several membranes within the microchannels to control the flow through three-dimensional channel geometries [89].

## 6.5 Summary

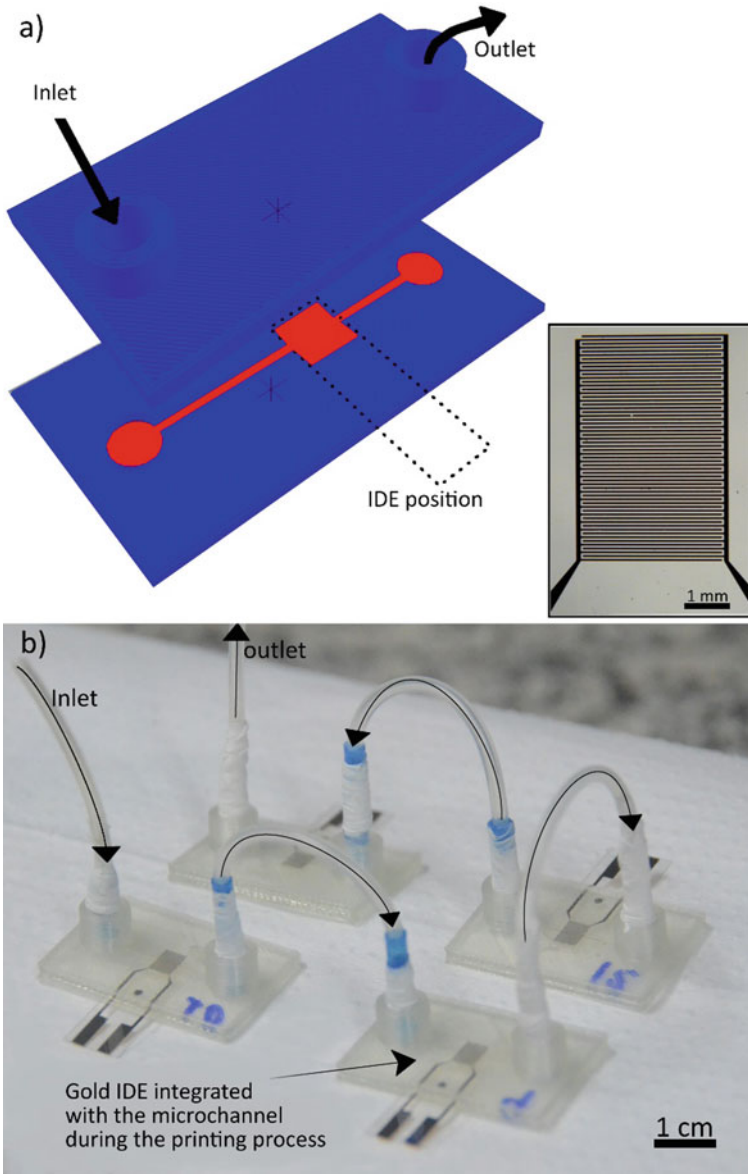
3D printing has been shown to be a fundamental tool in science, education, and biomedical applications, with FDM systems being the most flexible and accessible 3D printing benchtop technique for daily and on-demand use. Among the four main categories of FDM (Cartesian, Delta, polar, and SCARA), Cartesian printers are the most used ones once its technology is better established compared to the others. They also present a good structural stability that plays a crucial role in the final construct.

FDM has a great number of commercial thermoplastic filaments, either raw or composite, which are key factor to vast number of application. In particular, their use in pharmaceutical applications is remarkable. According to the literature, in the past few years, there is an increased use of FDM printing in the fabrication of distinct drug delivery systems. Besides the possibility of personalized controlled dosage, it is also a flexible methodology in the shape and size of drug tablets presenting distinct releases.

Composite filaments have also been applied to 3D print scaffolds for biomedical application. FDM technique allows the use of composites based on biocompatible materials, such as PLA or PCL matrices that may be approved to be used in biomedical devices. Recent literature about 3D-printed scaffolds have shown amazing results using SLA technique due to its high-resolution printed parts; however, there is a limited number of biodegradable/biocompatible resins; therefore, FDM can contribute to overcome this matter.

Despite better resolution reached in laser-based techniques such as SLA, FDM printing is finding its niche in the microfluidic and sensor areas. The open FDM hardware allows great control over the printing process, and the possibility of easily embedding extra elements such as electrodes or membranes into microfluidic devices by simply pausing the printing process greatly widens the range of potential applications. Moreover, the use of composite materials or co-extrusion to integrate devices in one step of fabrication is another great characteristic of FDM systems.

In summary, applications using FDM in distinct areas were described herein, showing that despite some limitations intrinsic to the technique, there are many advantages and possibilities to be explored yet.



**Fig. 6.5** a) GCODE visualization of a microchannel, and the chamber where gold IDEs (inset) were manually inserted at the fourth layer during the printing process. b) Printed e-tongues system used to distinguish the basic tastants. Reproduced with permission from [88]

**Acknowledgements** Authors are grateful for the financial support by the Brazilian funding agencies FAPESP (Grant Nos. 2015/14836-9 and 2017/19862-3), CAPES, and CNPq.

## References

1. Canessa E, Fonda C, Zennaro M (2013) Low-cost 3D printing for science, education & sustainable development, 1st ed. In: ICTP—the abdu Salam international centre for theoretical physics
2. 3D Printing Industry (2017) The Free Beginner’s Guide. <https://goo.gl/IvwkfZ>. Accessed 16 Feb 2017
3. Chen C, Erkal JL, Gross BC et al (2014) Evaluation of 3D printing and its potential impact on biotechnology and the chemical sciences. *Anal Chem* 86:3240–3253
4. Deckard CR, Beaman JJ (1990) Selective laser sintering with assisted powder handling
5. Lindstrom A (2012) Selective laser sintering, birth of an industry. <https://goo.gl/zpY9X6>. Accessed 16 Feb 2017
6. Singh S, Singh M, Prakash C, et al (2019) Optimization and reliability analysis to improve surface quality and mechanical characteristics of heat-treated fused filament fabricated parts. *Int J Adv Manuf Technol* 1–16
7. Singh S, Singh N, Gupta M et al (2019) Mechanical feasibility of ABS/HIPS-based multi-material structures primed by low-cost polymer printer. *Rapid Prototyp J* 25:152–161
8. Burns M (1993) Automated Fabrication. Improving Productivity in Manufacturing, PTR Prentice Hall
9. Gaál G, da Silva TA, Gaál V et al (2018) 3D printed e-Tongue. *Front Chem* 6:1–8
10. Sollmann K, Jouaneh M, Lavender D (2010) Dynamic modeling of a two axes, parallel, H-frame type XY-positioning system. *IEEE/ASME Trans Mechatronics* 15:1–12
11. Yusuf B (2018) 3D printers explained: delta, cartesian, polar, scara. In: All 3DP. <https://all3dp.com/known-your-fdm-3d-printers-cartesian-delta-polar-and-scara>. Accessed 31 Aug 2018
12. Jorgenson L (2017) How to choose between cartesian and delta 3D printers. In: Fargo 3D Print. [www.fargo3dprinting.com/choose-cartesian-delta-3d-printers](http://www.fargo3dprinting.com/choose-cartesian-delta-3d-printers). Accessed 31 Aug 2018
13. Garlotta D (2002) A literature review of poly (lactic acid). *J Polymers Environ* 9
14. Spoerk M, Gonzalez-Gutierrez J, Sapkota J et al (2018) Effect of the printing bed temperature on the adhesion of parts produced by fused filament fabrication. *Plast, Rubber Compos* 47:17–24
15. Squires AD, Lewis RA (2018) Feasibility and characterization of common and exotic filaments for use in 3D printed terahertz devices. *J Infrared Millimeter Terahertz Waves* 39:614–635
16. Rankin TM, Giovinco NA, Cucher DJ et al (2014) Science direct three-dimensional printing surgical instruments: are we there yet? *J Surg Res* 189:193–197
17. Patrício T, Domingos M, Gloria A et al (2013) Fabrication and characterisation of PCL and PCL/PLA scaffolds for tissue engineering. *Procedia CIRP* 5:110–114
18. Heiny M, Wurth JJ, Shastri VP (2014) Chapter 9—progress in functionalized biodegradable polyesters. In: Kumbar SG, Laurencin CT, Deng M (eds) *Natural and Synthetic Biomedical Polymers*. Elsevier, Oxford, pp 167–180
19. Torrado AR, Shemelya CM, English JD et al (2015) Characterizing the effect of additives to ABS on the mechanical property anisotropy of specimens fabricated by material extrusion 3D printing. *Addit Manuf* 6:16–29
20. Ferro CG, Brischetto S, Torre R, Maggiore P (2016) Characterization of ABS specimens produced via the 3D printing technology for drone structural. *Curved Layer Struct* 3:172–188
21. Dev Singh D, Reddy AR (2018) Characterization of additive manufactured ABS and natural ABS specimens. *Int J Mech Prod Eng Res Dev* 8:717–724
22. Trhlíková L, Zmeskal O, Psencik P, Florian P (2016) Study of the thermal properties of filaments for 3D printing. *AIP Conf Proc* 1752:040027–1–040027–6

23. Goyanes A, Buanz ABM, Basit AW, Gaisford S (2014) Fused-filament 3D printing (3DP) for fabrication of tablets. *Int J Pharm* 476:88–92
24. Wang X, Jiang M, Zhou Z et al (2017) 3D printing of polymer matrix composites: A review and prospective. *Compos Part B Eng* 110:442–458
25. Guo N, Leu MC (2013) Additive manufacturing: technology, applications and research needs. *Front Mech Eng* 8:215–243
26. Nikzad M, Masood SH, Sbarski I (2011) Thermo-mechanical properties of a highly filled polymeric composites for fused deposition modeling. *Mater Des* 32:3448–3456
27. Hwang S, Reyes EI, Moon KS et al (2015) Thermo-mechanical characterization of metal/polymer composite filaments and printing parameter study for fused deposition modeling in the 3D printing process. *J Electron Mater* 44:771–777
28. Torrado Perez AR, Roberson DA, Wicker RB (2014) Fracture surface analysis of 3D-printed tensile specimens of novel ABS-based materials. *J Fail Anal Prev* 14:343–353
29. Ahn S-H, Montero M, Odell D et al (2002) Anisotropic material properties of fused deposition modeling ABS. *Rapid Prototyp J* 8:248–257
30. Isakov DV, Lei Q, Castles F et al (2016) 3D printed anisotropic dielectric composite with meta-material features. *Mater Des* 93:423–430
31. Wei X, Li D, Jiang W et al (2015) 3D printable graphene composite. *Nat Publ Gr* 5:1–7
32. Weng Z, Wang J, Senthil T, Wu L (2016) Mechanical and thermal properties of ABS/montmorillonite nanocomposites for fused deposition modeling 3D printing. *Mater Des* 102:276–283
33. Zhong W, Li F, Zhang Z et al (2001) Short fiber reinforced composites for fused deposition modeling. *Mater Sci Eng A* 301:125–130
34. Shofner ML, Lozano K, Rodríguez-Macías FJ, Barrera EV (2003) Nanofiber-reinforced polymers prepared by fused deposition modeling. *J Appl Polym Sci* 89:3081–3090
35. Tekinalp HL, Kunc V, Velez-Garcia GM et al (2014) Highly oriented carbon fiber-polymer composites via additive manufacturing. *Compos Sci Technol* 105:144–150
36. Paula KT, Gaál G, Almeida GFB et al (2018) Femtosecond laser micromachining of polylactic acid/graphene composites for designing interdigitated microelectrodes for sensor applications. *Opt Laser Technol* 101:74–79
37. Rengier F, Mehndiratta A, Von Tengg-Kobligk H et al (2010) 3D printing based on imaging data: review of medical applications. *Int J Comput Assist Radiol Surg* 5:335–341
38. Chae MP, Rozen WM, McMenamin PG et al (2015) Emerging applications of bedside 3D printing in plastic surgery. *Front Surg* 2:1–14
39. Singh H, Singh S, Prakash C (2019) Current Trends in biomaterials and bio-manufacturing. In: *Biomanufacturing*
40. Prasad LK, Smyth H (2016) 3D Printing technologies for drug delivery: a review. *Drug Dev Ind Pharm* 42:1019–1031
41. Alhnan MA, Okwuosa TC, Sadia M et al (2016) Emergence of 3D printed dosage forms: opportunities and challenges. *Pharm Res* 33:1817–1832
42. Norman J, Madurawe RD, Moore CMV et al (2017) A new chapter in pharmaceutical manufacturing: 3D-printed drug products. *Adv Drug Deliv Rev* 108:39–50
43. Ramot Y, Haim-Zada M, Domb AJ, Nyska A (2016) Biocompatibility and safety of PLA and its copolymers. *Adv Drug Deliv Rev* 107:153–162
44. Ventola CL (2014) Medical applications for 3D printing: current and projected uses. *P T* 39:704–711
45. Singh D, Thomas D (2018) The American journal of surgery advances in medical polymer technology towards the panacea of complex 3D tissue and organ manufacture. *Am J Surg* 6:1–2
46. Ozbolat IT, Yu Y (2013) Bioprinting toward organ fabrication: challenges and future trends. *IEEE Trans Biomed Eng* 60:691–699
47. Poomathi N, Singh S, Prakash C et al (2019) Bioprinting in ophthalmology: current advances and future pathways. *Rapid Prototyp J* 25:496–514

48. Cui H, Nowicki M, Fisher JP, Zhang LG (2017) 3D bioprinting for organ regeneration. *Adv Healthc Mater* 6:1601118
49. Blaeser A, Duarte Campos DF, Fischer H (2017) 3D bioprinting of cell-laden hydrogels for advanced tissue engineering. *Curr Opin Biomed Eng* 2:58–66
50. Liu Tsang V, Bhatia SN (2004) Three-dimensional tissue fabrication. *Adv Drug Deliv Rev* 56:1635–1647
51. Bose S, Vahabzadeh S, Bandyopadhyay A (2013) Bone tissue engineering using 3D printing. *Mater Today* 16:496–504
52. Bose S, Darsell J, Hosick H et al (2002) Processing and characterization of porous alumina scaffolds. *J Mater Sci Mater Med* 13:23–28
53. Bose S, Darsell J, Kintner M et al (2003) Pore size and pore volume effects on alumina and TCP ceramic scaffolds. *Mater Sci Eng C* 23:479–486
54. Darsell J, Bose S, Hosick HL, Bandyopadhyay A (2003) From CT scan to ceramic bone graft. *J Am Ceram Soc* 86:1076–1080
55. Hutmacher DW, Schantz T, Zein I et al (2001) Mechanical properties and cell cultural response of polycaprolactone scaffolds designed and fabricated via fused deposition modeling. *J Biomed Mater Res* 55:203–216
56. Too MH, Leong KF, Chua CK et al (2002) Investigation of 3D non-random porous structures by fused deposition modelling. *Int J Adv Manuf Technol* 19:217–223
57. Kalita SJ, Bose S, Hosick HL, Bandyopadhyay A (2003) Development of controlled porosity polymer-ceramic composite scaffolds via fused deposition modeling. *Mater Sci Eng C* 23:611–620
58. Lam CX, Teoh SH, Hutmacher DW (2007) Comparison of the degradation of polycaprolactone and polycaprolactone- ( $\beta$ -tricalcium phosphate) scaffolds in alkaline medium. *Polym Int* 56:718–728
59. Lam CXF, Savalani MM, Teoh SH, Hutmacher DW (2008) Dynamics of in vitro polymer degradation of polycaprolactone-based scaffolds: Accelerated versus simulated physiological conditions. *Biomed Mater* 3:034108
60. Singh S, Prakash C, Ramakrishna S (2019) 3D printing of polyether-ether-ketone for biomedical applications. *Eur Polym J* 114:234–248
61. Vaezi M, Black C, Gibbs DMR et al (2016) Characterization of New PEEK/HA composites with 3D HA network fabricated by extrusion freeforming. *Molecules* 21:1–21
62. Chia HN, Wu BM (2015) Recent advances in 3D printing of biomaterials. *J Biol Eng* 9:1–14
63. Water JJ, Bohr A, Boetker J, et al (2015) Three-dimensional printing of drug-eluting implants: Preparation of an antimicrobial polylactide feedstock material. *J Pharm Sci* 104:1099–1107
64. Weisman JA, Nicholson JC, Tappa K et al (2015) Antibiotic and chemotherapeutic enhanced three-dimensional printer filaments and constructs for biomedical applications. *Int J Nanomed* 10:357–370
65. Skowrya J, Pietrzak K, Alhnan MA (2015) Fabrication of extended-release patient-tailored prednisolone tablets via fused deposition modelling (FDM) 3D printing. *Eur J Pharm Sci* 68:11–17
66. Goyanes A, Robles Martinez P, Buanz A et al (2015) Effect of geometry on drug release from 3D printed tablets. *Int J Pharm* 494:657–663
67. Goyanes A, Buanz ABM, Hatton GB et al (2015) 3D printing of modified-release aminosalicylate (4-ASA and 5-ASA) tablets. *Eur J Pharm Biopharm* 89:157–162
68. Genina N, Holländer J, Jukarainen H et al (2016) Ethylene vinyl acetate (EVA) as a new drug carrier for 3D printed medical drug delivery devices. *Eur J Pharm Sci* 90:53–63
69. Tek P, Chiganos TC, Mohammed JS et al (2008) Rapid prototyping for neuroscience and neural engineering. *J Neurosci Methods* 172:263–269
70. Bourell D, Espalin D, Arcaute K et al (2010) Fused deposition modeling of patient-specific polymethylmethacrylate implants. *Rapid Prototyp J* 16:164–173
71. Sandler N, Salmela I, Fallarero A et al (2014) Towards fabrication of 3D printed medical devices to prevent biofilm formation. *Int J Pharm* 459:62–64

72. Mohammed MI, P. Fitzpatrick A, Gibson I (2017) Customised design of a patient specific 3D printed whole mandible implant. *Knowl Eng* 104
73. McDonald JC, Duffy DC, Anderson JR et al (2000) Fabrication of microfluidic systems in poly (dimethylsiloxane). *Electrophoresis* 21:27–40
74. Whitesides GM (2006) The origins and the future of microfluidics. *Nature* 442:368–373
75. Duffy DC, McDonald JC, Schueller OJA, Whitesides GM (1998) Rapid prototyping of microfluidic systems in poly (dimethylsiloxane). *Anal Chem* 70:4974–4984
76. Sackmann EK, Fulton AL, Beebe DJ (2014) The present and future role of microfluidics in biomedical research. *Nature* 507:181–189
77. Meng C, Ho B, Ng SH et al (2015) 3D printed microfluidics for biological applications. *Lab Chip* 15:3627–3637
78. Waheed S, Cabot JM, Macdonald NP et al (2016) 3D printed microfluidic devices: enablers and barriers. *Lab Chip* 16:1993–2013
79. Hampson SM, Rowe W, Christie SDR, Platt M (2018) 3D printed microfluidic device with integrated optical sensing for particle analysis. *Sens Actuators B Chem* 256:1030–1037
80. Zhu F, Skommer J, Friedrich T, et al (2015) 3D printed polymers toxicity profiling—a caution for biodevice applications. *Proc SPIE Int Soc Opt Eng* 96680Z
81. Boparai KS, Singh R, Singh H (2016) Development of rapid tooling using fused deposition modeling: a review. *Rapid Prototyp J* 22:281–299
82. Gul JZ, Na J, Choi KH (2017) 3D arbitrary channel fabrication for lab on a chip applications using chemical decomposition. *Int J Environ Agric Biotechnol* 2:2340–2347
83. Goh WH, Hashimoto M (2018) Fabrication of 3D microfluidic channels and in-channel features using 3D printed, water-soluble sacrificial mold. *Macromol Mater Eng* 303:1–9
84. Kitson PJ, Rosnes MH, Sans V et al (2012) Configurable 3D-Printed millifluidic and microfluidic “lab on a chip” reactionware devices. *Lab Chip* 12:3267–3271
85. Banna M, Bera K, Sochol R et al (2017) 3D printing-based integrated water quality sensing system. *Sensors* 17:1336
86. Bauer M, Kulinsky L (2018) Fabrication of a lab-on-chip device using material extrusion (3D printing) and demonstration via malaria-Ab ELISA. *Micromachines* 9
87. Krejcová L, Nejdil L, Rodrigo MAM et al (2014) 3D printed chip for electrochemical detection of influenza virus labeled with CdS quantum dots. *Biosens Bioelectron* 54:421–427
88. Gaal G, Mendes M, de Almeida TP et al (2017) Simplified fabrication of integrated microfluidic devices using fused deposition modeling 3D printing. *Sens Actuators B Chem* 242:35–40
89. Yuen PK (2016) Embedding objects during 3D printing to add new functionalities. *Biomicrofluidics* 10:044104

**Gabriel Gaál** is currently a Ph.D. student at the Institute of Physics “Gleb Wataghin” at University of Campinas (Unicamp, Brazil). He graduated in Physics (2015) and obtained his MSc. degree in Physics (2017) from the University of Campinas (Unicamp, Brazil). He has experience in application of 3D printing in microfluidics and electronic tongue sensors.

**Vladimir Gaál** is currently a M.Sc. student at the School of Mechanical Engineering at University of Campinas (Unicamp, Brazil) focusing on mechanical characterization of 3D printed objects. He is also researcher assistant of research team of Professor Varlei Rodrigues at the University of Campinas. He graduated in Physics (2017) at Unicamp, Brazil, and has great expertise in assembling and maintenance of 3D printers.

**Dr. Maria Luisa Braunger** is currently a postdoctoral fellow at the Institute of Physics “Gleb Wataghin” at the University of Campinas (Unicamp, Brazil). She also worked as a visiting scholar at the University of Pennsylvania (UPenn, USA). She graduated in Physics (2008) and obtained a MSc. degree in Applied Physics (2011) from São Paulo State University (UNESP), Campus Rio



Claro. She has received double-degree Ph.D. in Materials Science and Technology from UNESP, Campus Presidente Prudente and in Polymer Chemistry from Université de Pau et des Pays de l'Adour (UPPA, France).

**Prof. Dr. Antonio Riul Jr** has M.Sc. in physics from the University of São Paulo (1995), Ph.D. in Materials Science and Engineering from the University of São Paulo (1998) and postdoctoral studies at the University of Wales (1998–2000), Embrapa/CNPq (2000–2002) and University of Texas at Dallas (2018–2019). He has experience in Physics and Materials Science, focusing on ultrathin films, acting on ultrathin films (Langmuir-Blodgett and LbL), conducting polymers and reduced graphene oxides, “e-tongue” and microfluidic sensors. Currently, he is also working with multifunctional coatings formed by self-healing and conductive nanocomposites.

**Prof. Dr. Varlei Rodrigues** is currently Professor at the Institute of Physics “Gleb Wataghin”, UNICAMP. He has worked on Structural and Electrical Conductance of Metal Atomic Size Nanowires in his MSc. and Ph.D at the Institute of Physics “Gleb Wataghin”, under the supervision of Prof. Dr. Daniel Ugarte. He also have a two years post-doc experience at Ecole Polytechnique Fédérale de Lausanne, EPFL, Switzerland, under the supervision of Prof. Dr. Christian Felix and a one year post-doc at Laboratório Nacional de Luz Síncrotron, LNLS, Brazil. He has experience with scientific instrumentation, metal nanowires fabrication and characterization, electron microscopy, electrical transport characterization, nanoparticle physics, cluster production and 3D printing. He has authored 40 papers, with 1576 total citations, h-factor 16 and 3 chapters. He has concluded the supervision of one PhD thesis and three MSc dissertations.

# Chapter 7

## Integration of FDM and Indirect Rapid Tooling Technique for Fabrication of Low-Cost Hip Implant Replicas for Batch Production: A Case Study



Jaspreet Singh, Rupinder Singh, and Harwinder Singh

### 7.1 Introduction

Last two to three decades witnessed huge investments by the manufacturing industries for the improvement of their production technologies in order to develop the new products [1]. In today's scenario, requirement of shorter lead time and low cost for the fabrication of prototypes and customized and tailor-made products in various industries such as biomedical, automotive, aerospace, etc., comes out to be a major challenge in order to achieve the competitive benefits. With conventional manufacturing techniques, the production of such products becomes costly and time-consuming because of the fabrication of the necessary hard tooling [2]. This requires the transformation of manufacturing sector from traditional to modern techniques for the economic growth of the country. Further, development of new product leads to significant trade-offs between lead time, cost and performance of product [3]. Therefore, different approaches for manufacturing must be adopted to accommodate the market demands.

Additive manufacturing (AM) processes have the potential to overcome the challenges of the modern industry [4]. AM processes have found wide applications in industries such as electronics, automotive, aerospace, biomedical, and ophthalmology [5–7]. The polymer-based multi-material structures fabricated by fused filament fabrication (FFF) technique exhibit variety of applications in aerospace and

---

J. Singh (✉)

School of Mechanical Engineering, Lovely Professional University, Phagwara 144411, India  
e-mail: [erjassi03@yahoo.in](mailto:erjassi03@yahoo.in)

R. Singh

Department of Mechanical Engineering, National Institute of Technical Teachers Training and Research, Chandigarh 160019, India

H. Singh

Department of Mechanical Engineering, GNDEC, Ludhiana 141006, India

© Springer Nature Singapore Pte Ltd. 2020

S. Singh et al. (eds.), *3D Printing in Biomedical Engineering*,

Materials Horizons: From Nature to Nanomaterials,

[https://doi.org/10.1007/978-981-15-5424-7\\_7](https://doi.org/10.1007/978-981-15-5424-7_7)

other manufacturing industries [8]. However, the AM processes cannot replace the traditional manufacturing processes but can enhance the efficiency by fabricating complex parts with high dimensional accuracy [9]. RP involves fabrication of 3D models from the CAD file created by using different software. The information stored in the CAD file is split into slices, and then, the layers are printed one over the other with the aid of the computer [10]. Fused deposition modelling (FDM) being the most economical AM technique has been commonly utilized for the manufacturing of various kinds of industrial parts.

FDM process involves heating of model material like wax, polycarbonate or acrylonitrile butadiene styrene (ABS) by the heaters as it passes through the extrusion head [11]. 3D physical model has been built gradually as the head start depositing the material layer by layer one over the other [12, 13]. Most of the FDM machines use different grades of ABS as build material, whereas some uses wax also. FDM possesses several advantages such as simplicity, flexibility and low operating and maintenance cost as well as ability to fabricate intricate geometries quite easily [14]. Moreover, the replicas prepared through FDM technique have been already employed in silicon moulding (SM) and rapid casting applications [15, 16].

Irrespective of several advantages, the FDM fabricated parts exhibit poor surface characteristics due to layer-by-layer manufacturing (staircase effect) [17, 18]. Researchers employed continuous efforts to improve the surface characteristics of FDM fabricated components such as process parameter optimization, utilizing optimum build orientations, advanced mechanical methods including vapour smoothing, barrel finishing, etc. [19–30]. Dimensional variability caused due to post-processing of FDM parts restricted its applications in precision casting processes [31]. Further, in an attempt of improving the overall performance of FDM fabricated parts, heat treatment involving annealing at different temperature (105, 115 and 125 °C) along with different time duration (20, 25 and 30 min) had been performed and the results indicated improvement in physical, mechanical and quality characteristics of FDM parts [32].

Apart from poor surface finish and dimensional deviation, RP techniques are preferred only for low volume runs due to high process cost and limited material selection [33, 34]. Also, the processability of high-performance materials such as polyether-ether-ketone (PEEK) using three-dimensional (3D) printing technologies exhibits a critical barrier [35]. Rapid tooling (RT) provides solution to the above challenge by utilizing the RP and then applying it to the manufacturing of various tools [36, 37]. Direct tooling and indirect tooling are the two variants of RT. In direct RT, the mould is prepared by adopting any one of the AM techniques and then utilizing those moulds for producing prototypes of different materials [38]. In indirect RT, multiple prototypes were prepared from the mould manufactured from an AM master pattern. Some of the most commonly utilized indirect RT processes includes epoxy resin tooling, spray metal tooling and room temperature vulcanized silicon rubber moulding.

Cheah explained an indirect method for the wax patterns production using SM in order to lower the cost incurred with low quantity production during the IC process [39]. The various direct (SLA, LOM, SLS, FDM, etc.) and indirect routes utilizing

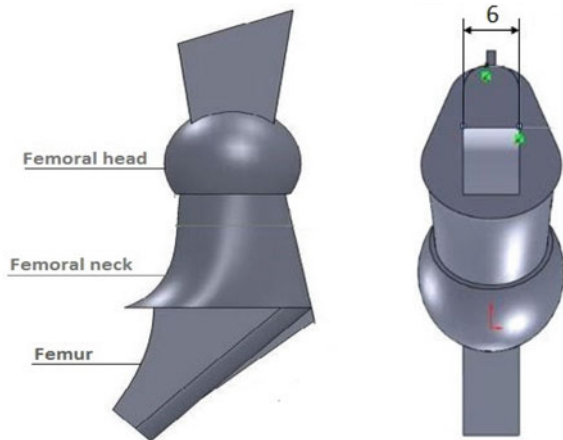
RP processes for rapid production of tooling have been highlighted by the researchers [38]. Rahmati et al. made investigations on the accuracy of wax patterns (H-shaped) fabricated by polyurethane (PU) mould and RTV silicone mould and concluded that good surface finish has been obtained on wax patterns produced by silicone mould, whereas the patterns fabricated by PU mould shows better accuracy [40]. Thian et al. utilized vacuum casting process to fabricate micro-moulds and micro-gears using silicon rubber mould and concluded that the deviation between the master pattern and fabricated prototypes was too small and the proposed process is highly capable to produce dimensionally accurate parts [41]. Singh et al. fabricated plastic components using SM process and reported that the IT grades of the components were consistent and within the allowable range as per ISO standard DIN16901 and UNI EN 20286-I (1995) [42].

The literature review reveals that poor surface characteristics and dimensional deviation are the inherent features of FDM and cannot be eliminated completely. The pre-processing surface finishing techniques for FDM fabricated replicas stressed on optimization studies and cannot improve the surface finish beyond the specific limit. The post-processing finishing techniques are highly effective but the mechanical abrasive action of media distorts the part geometry and affects the dimensional stability especially around the sharp edges and corners. The chemical vapour smoothing technique has been established recently, and the preliminary studies performed by some of the researchers indicated good surface quality and dimensional stability of parts after vapour exposure. But, the surface characteristics of complex FDM parts such as biomedical hip implant undergone vapour smoothing are yet to be ascertained. Further, RP techniques are utilized preferably only for small quantity (5–10 pieces) production due to limitations of material availability and high cost. Silicon moulding (SM) is found to be an established indirect RT technique, and researchers have successfully fabricated wax patterns by this technique to reduce the cost of RP. But still SM process needs to be explored more in order manufacture polyurethanes (PU) replicas for various industrial applications. This research work focuses on combining the route of FDM-CVS-SM with an aim to fabricate low-cost hip implant replicas for batch production.

## 7.2 Methodology and Experimentation

This research work includes two phases. In the first phase, after selecting the benchmark component, FDM technique has been utilized to prepare the ABS replicas, followed by the smoothing process to improve their surface quality and to reduce the staircase effect. The replicas fabricated at best parameter settings based on the results of Taguchi's L18 orthogonal array with regard to dimensional accuracy, shore hardness and surface quality have been selected as a master pattern for the second phase. The second phase constitutes an indirect rapid tooling technique named as silicon moulding (SM) with an aim to create multiple replicas to reduce the cost of AM for small production runs.

**Fig. 7.1** Different views of benchmark component



Hip joint (refer Fig. 7.1) has been selected as a functional prototype in this research. The hip geometry has complex features and sloping profiles which would help the precise evaluation of efficacy of vapour smoothing process. The STL file which acts as an input to FDM machine has been prepared using ‘SolidWorks’ software. The joint consists of a ball-and-socket joint. It basically consists of three parts, i.e. stem, neck and head. The head of hip joint must have excellent surface finish for proper movement while walking.

In the first phase, the hip replicas were fabricated by ‘uPrint SE’ FDM setup of Stratasys, USA. FDM printer converts the three-dimensional STL file into slices. The printer then prints these slices one after another until the entire 3D model is fabricated. After fabrication, the replicas were subjected to hot chemical vapours to enhance the surface quality. The chemical vapour smoothing (CVS) apparatus supplied by Stratasys was utilized for the smoothing purpose. It consists of parallel cooling and smoothing chamber equipped with refrigerator and heaters, respectively. The cooling and drying of the parts are accomplished by the cooling chamber (0 °C), whereas the heating chamber is maintained at 65 °C by the heater present in it. The process initiates once the volatile smoothing fluid enters into the smoothing chamber from the reservoir tank. Once hot, the fumes rise up in the chamber and react with the outer surface of the replicas and thus enhance the surface texture. The smoothing fluid used in this work is acetone because of its high diffusion rate and low toxicity.

The intensive literature survey and pilot experiments have been performed to scrutinize the input parameters having significant effect on various characteristics of fabricated components. Orientation of the parts in the build chamber and layer thickness were observed to be the factors influencing the characteristics of FDM replicas significantly. As the layer thickness decreases, the surface finish improves but the manufacturing time increases as nozzle has to deposit more layers per unit volume. Thus, there is a trade-off between manufacturing time and surface roughness which motivated to use the intermediate value of layer thickness. Layer thickness does not influence the surface roughness much after chemical treatment [43]. So,

value of 0.254 mm as layer thickness was finalized to fabricate all the replicas for the present work. Further, only two levels of orientation ( $0^\circ$  and  $90^\circ$ ) have been selected for the final experimentation as  $45^\circ$  of orientation angle requires much higher support material and build time as compared to other two levels. Although part density does not affect the surface finish, parts fabricated at different densities may lead to variable manufacturing time, material usage, mechanical properties and weight. Three levels of density (solid, high and low) have been taken as input parameters in this research work.

Further, it has been observed that few researchers studied the effect of different CVS parameters on the surface quality of FDM fabricated ABS replicas. However, the studies related to acetone dipping and acetone vapour exposure indicate that the number of cycle and cycle immersion time were the main contributing factors affecting the surface characteristics [24, 43, 44]. The methodology recommended by the manufacturer of vapour smoothing station includes pre-cooling the parts initially for 15–20 min, followed by vapour exposure in smoothing chamber for 5–25 s and finally post-cooling the parts for 15–20 min in cooling chamber completes the one cycle. Also, it has been reported to repeat the cycle three to five times in order to obtain best results. The replicas are required to be hanged with a cotton string attached to a rod in smoothing chamber and immediately hanged in cooling chamber after specific duration of exposure. In the present work, number of cycles of vapour exposure and cycle time were the two selected CVS process parameters. The selected levels of different parameters for FDM and CVS process have been shown in Table 7.1.

The process diagram (P-diagram) of combined FDM-CVS process is shown in Fig. 7.2. The diagram highlights the input factors, output factors and noise factors of the process, while there are no signal factors as FDM-CVS is not a dynamic process. The first step is to identify the input factors and outputs parameters. The present research work includes input parameters as orientation angle, part density, number of cycles and cycle time. There are some factors which are beyond the control such as environmental conditions which may affect the cooling and heating rate of FDM replicas. These are categorized under noise factors which cannot be controlled but their effect must be minimized using different technique. The experiments were conducted in randomized order to eliminate errors due to changes in ambient conditions, while measurements were replicated and repeated at least three times using standard procedures [45]. In this study, factor (A) 1 degree of freedom whereas factors (B, C, D) each have two degrees of freedom. Thus, the total number of degrees of freedom for the selected four parameters is 7. Therefore, the most suitable orthogonal array with a blend of two-level and three-level factors was distinguished as

**Table 7.1** Parameters and their levels

Process	Parameters	Symbol	Levels		
			1	2	3
FDM	Orientation	A	$0^\circ$	$90^\circ$	–
	Part density	B	High	Low	Solid
CVS	No. of cycles	C	3	4	5
	Cycle time (s)	D	4	6	8

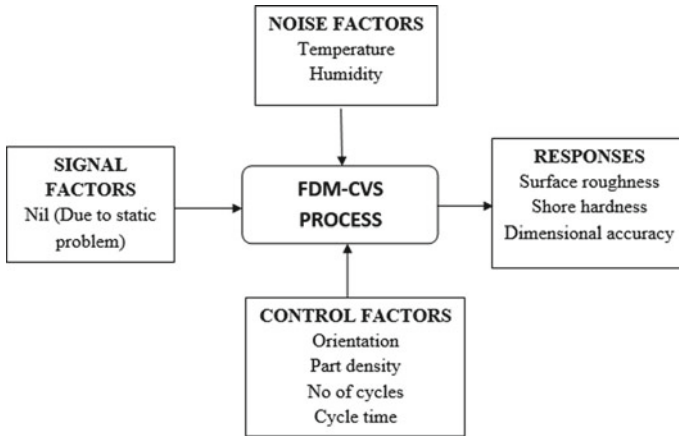


Fig. 7.2 P-diagram of combined FDM-CVS process

L18 ( $2^1 \times 3^7$ ) with 17 degrees of freedom. Table 7.2 shows the assigned factors and their levels to four columns of L18 OA.

Table 7.2 Control log for experimentation

Run order	Orientation (°)	Part density	No. of cycles	Cycle time (s)
1	90	Low	4	6
2	90	High	5	8
3	0	Solid	5	6
4	90	High	3	4
5	0	Low	4	4
6	0	Low	3	8
7	0	High	3	6
8	0	Solid	4	4
9	0	Low	5	6
10	90	Solid	3	6
11	90	Solid	4	8
12	0	Solid	3	8
13	90	Solid	5	4
14	90	Low	5	8
15	90	High	4	6
16	90	Low	3	4
17	0	High	4	8
18	0	High	5	4

## 7.3 Results and Discussion

The results of each phase have been discussed in the following sections.

### 7.3.1 Phase I (FDM-CVS Process)

As regard to the first phase, experiments were performed according to the selected DOE for so as to analyse the impact of change in input process variables on the surface quality, dimensional accuracy and hardness of fabricated replicas. The experiments were performed in random order to minimize the error. The impact of CVS process on the surface quality has been evaluated by measuring the average surface roughness ( $R_a$ ). The three reading of  $R_a$  at femur (refer Fig. 7.1) had been recorded for each replica before and after vapour smoothing. The Digital Durometer (supplied by Samruddhi Industries) has been employed for measurement of shore D hardness ( $H_d$ ) of ABS replicas fabricated by FDM as per ASTM D 2240 standard. The indentation hardness of soft materials thermoplastic elastomers, polymers, vulcanized rubber, elastomeric and cellulose materials is measured by Durometer on various scales such as A, B, C, D, O, OO and M. The hardness tester has least count  $0.5 H_d$  and ranges from 0 to 100. The three readings were taken for each replica before and after vapour smoothing, and average was taken as final reading. Dimensional variations in ABS replicas before and after vapour smoothing have been measured by coordinate measuring machine (CMM) adopting ISO 10360-2 (2009) standards. In the present work, one critical dimension on hip implant (as shown in Fig. 7.1) has been identified and measured by CMM before and after the smoothing operation with an aim to estimate the dimensional accuracy in terms of dimensional deviation ' $\Delta d$ ' [46].

The observations of surface roughness in terms of ' $R_a$ ' value, shore hardness and the value of dimensions have been shown in Table 7.3. The observations indicated that the replicas exhibit better surface finish at  $90^\circ$  orientation with solid interior. Also, the surface finish of fabricated replicas has been improved dramatically after the smoothing process. Figure 7.3a, b represents the effect of smoothing operation on the fabricated hip replica. It has been observed that smoothing operation almost eliminates the effect of layered fabrication of FDM process called stair step effect.

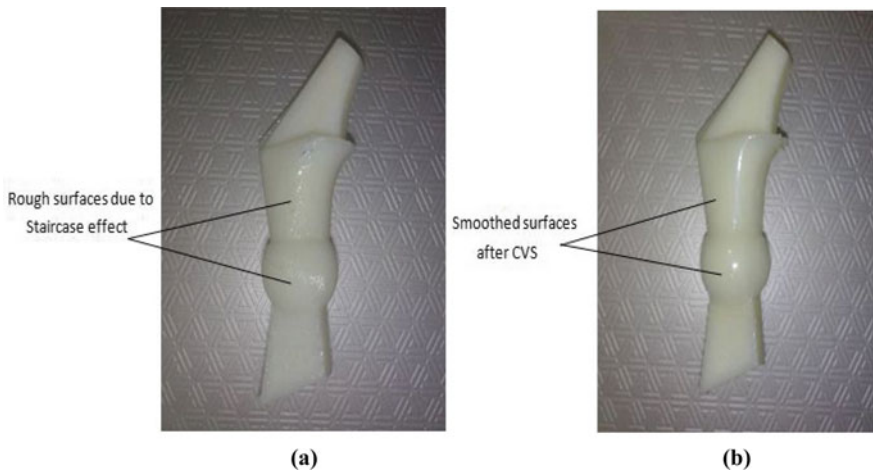
The scanning electron microscope (SEM) images taken for the same fabricated replica have been shown in Figs. 7.4 and 7.5, respectively. SEM images show dramatic improvement in surface quality of the replica after the smoothing operation. It was due to reflow of the material from peaks to valleys forced by the hot vapours of the acetone which ultimately results in smoothed surface finish. Also, the ' $R_a$ ' value of all the fabricated replicas after the smoothing operation becomes almost same. The percentage improvement in surface finish after the CVS process for all the replicas has been calculated and shown in Table 7.4.

The observations of Table 7.3 indicated that shore hardness of all the replicas increases slightly after the smoothing operation. The microscopic images taken by

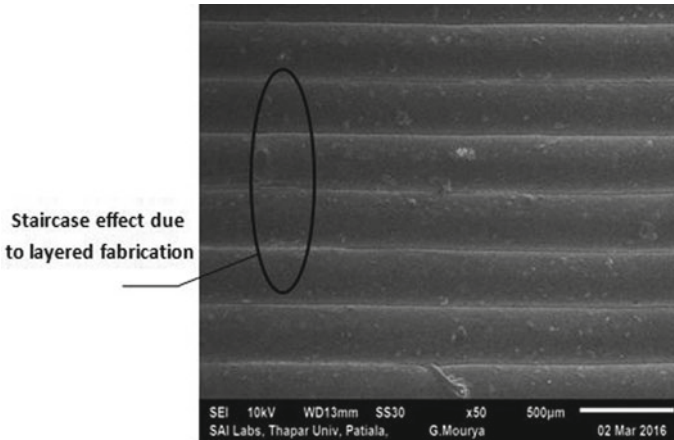


**Table 7.3** Observations of responses before and after CVS

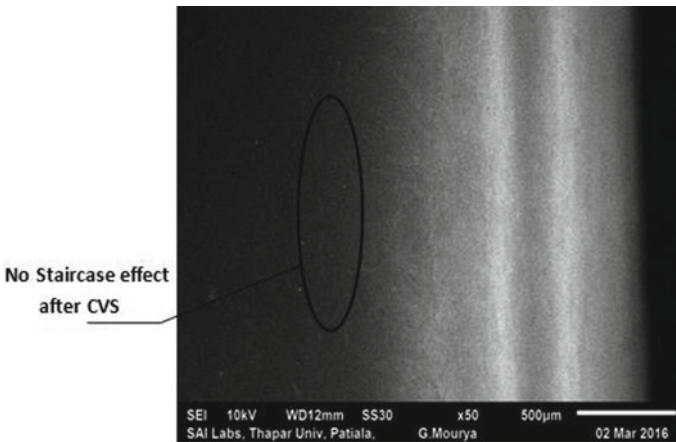
Run order	Observations after FDM			Observations after CVS		
	$R_a$ ( $\mu\text{m}$ )	SH ( $H_d$ )	Dimension (mm)	$R_a$ ( $\mu\text{m}$ )	SH ( $H_d$ )	Dimension (mm)
1	7.368	66	6.038	0.310	70.5	6.024
2	5.751	71	6.019	0.192	75.5	6.007
3	8.472	74.5	6.041	0.301	78	6.017
4	5.495	69.5	6.024	0.249	72.5	6.015
5	8.219	64.5	6.02	0.376	68	6.012
6	8.311	64	6.019	0.386	67	6.013
7	8.658	69.5	6.023	0.325	72	6.012
8	8.586	74	6.031	0.361	76.5	6.019
9	8.32	64	6.012	0.347	69.5	6.01
10	5.006	74.5	6.043	0.194	77.5	6.029
11	5.225	75.5	6.041	0.168	79.5	6.024
12	8.436	73.5	6.036	0.34	75	6.019
13	5.106	75.5	6.043	0.187	79	6.024
14	7.942	66	6.038	0.276	72	6.019
15	5.212	71	6.022	0.204	74.5	6.013
16	7.59	65	6.036	0.355	68	6.026
17	8.547	69.5	6.014	0.286	73.5	6.005
18	8.742	70	6.017	0.335	74	6.008



**Fig. 7.3** Specimen **a** before and **b** after the smoothing operation



**Fig. 7.4** SEM image before the smoothing operation



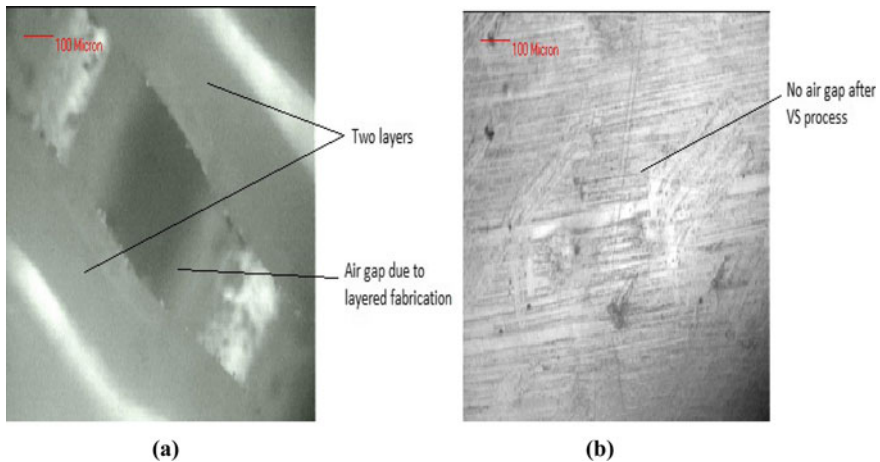
**Fig. 7.5** SEM image after the smoothing operation

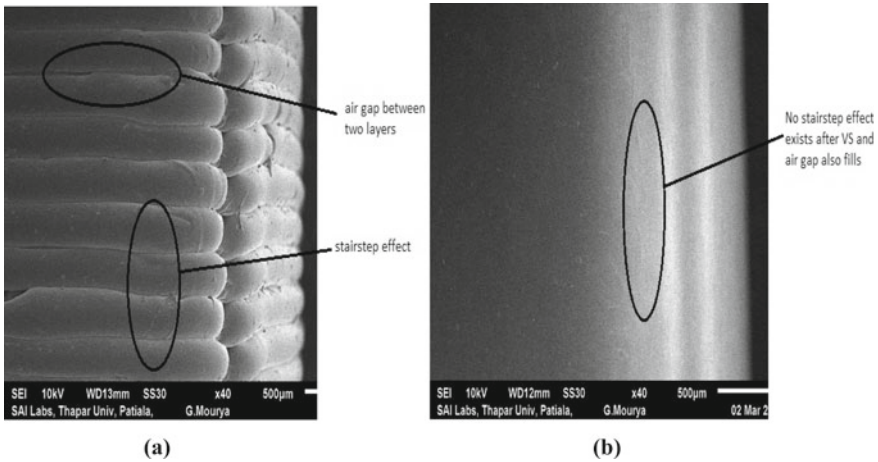
metallurgical microscope at magnification of  $100\times$  before and after smoothing operation for one of the ABS replicas have been shown in Fig. 7.6. Figure 7.6a clearly shows existence of air gap between the two layers during the fabrication process of the replica by the FDM technique. After the smoothing operation, the air gap almost filled by the flow of material which ultimately reduces the stair-step effect and thus improves the shore hardness (refer Fig. 7.6b). From the SEM images (refer Fig. 7.7), the same phenomenon has been noticed.

Positive deviation from the drawing dimension has been observed (refer Table 7.3) for the selected dimension (6 mm) after the FDM process. Also, it has been observed that the CVS process reduces the dimension slightly (refer Table 7.3). This was due to the reflow of material that takes place during the CVS process. Absolute deviation

**Table 7.4** Final responses along with signal-to-noise ratio

Run order	Final responses after CVS process			S/N Ratio (dB) for each response after CVS		
	Percentage improvement in $R_a$	SH ( $H_d$ )	' $\Delta d$ ' (mm)	Percentage improvement in $R_a$	SH	' $\Delta d$ '
1	95.8	70.5	0.024	39.63	36.96	32.40
2	96.7	75.5	0.007	39.71	37.55	43.10
3	96.4	78	0.017	39.68	37.84	35.39
4	95.5	72.5	0.015	39.60	37.20	36.48
5	95.4	68	0.012	39.59	36.65	38.42
6	95.4	67	0.013	39.59	36.52	37.72
7	96.2	72	0.012	39.66	37.15	38.42
8	95.8	76.5	0.019	39.63	37.68	34.42
9	95.8	69.5	0.01	39.63	36.84	40.00
10	96.1	77.5	0.029	39.65	37.78	30.75
11	96.8	79.5	0.024	39.72	38.00	32.40
12	96.0	75	0.019	39.65	37.50	34.42
13	96.3	79	0.024	39.67	37.95	32.40
14	96.5	72	0.019	39.69	37.15	34.42
15	96.1	74.5	0.013	39.65	37.44	37.72
16	95.3	68	0.026	39.58	36.65	31.70
17	96.7	73.5	0.005	39.71	37.33	46.02
18	96.2	74	0.008	39.66	37.38	41.94

**Fig. 7.6** Microscope image **a** before and **b** after the CVS process



**Fig. 7.7** SEM image **a** before and **b** after the CVS process

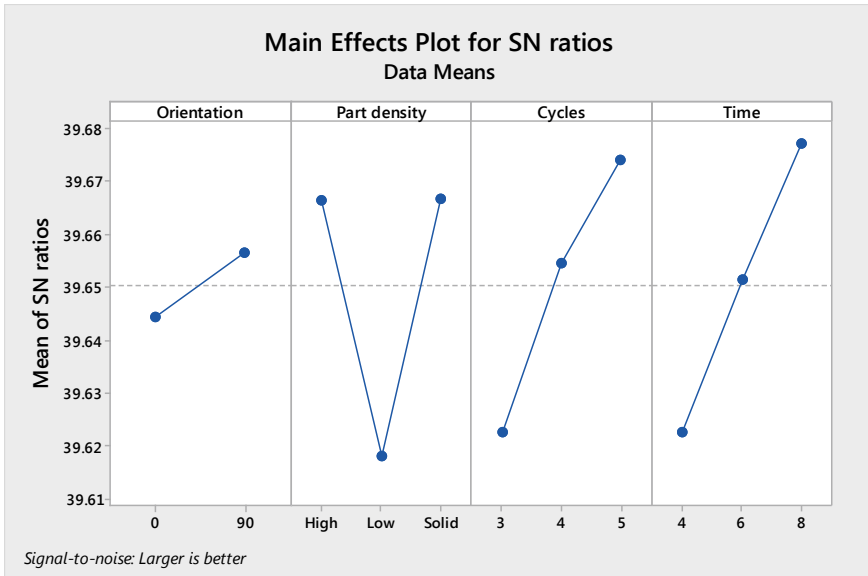
between the final dimension and the drawing dimension has been measured and shown in Table 7.4. Since the main aim is to achieve maximum improvement in surface finish and shore hardness along with minimum ‘ $\Delta d$ ’, so S/N ratios has been calculated (refer Table 7.4) on the basis of ‘larger is better’ approach for the ‘ $R_a$ ’ value and ‘SH’ using Eq. (1), whereas the same has been calculated based on ‘smaller is better’ approach for the ‘ $\Delta d$ ’ using Eq. (2). The effect of input parameters on the mean S/N ratio plots for different responses have been shown in Figs. 7.8, 7.9 and 7.10.

$$S/N = -10 \text{Log} \left[ \frac{1}{r} \sum_{i=1}^r \frac{1}{Y_i^2} \right] \tag{1}$$

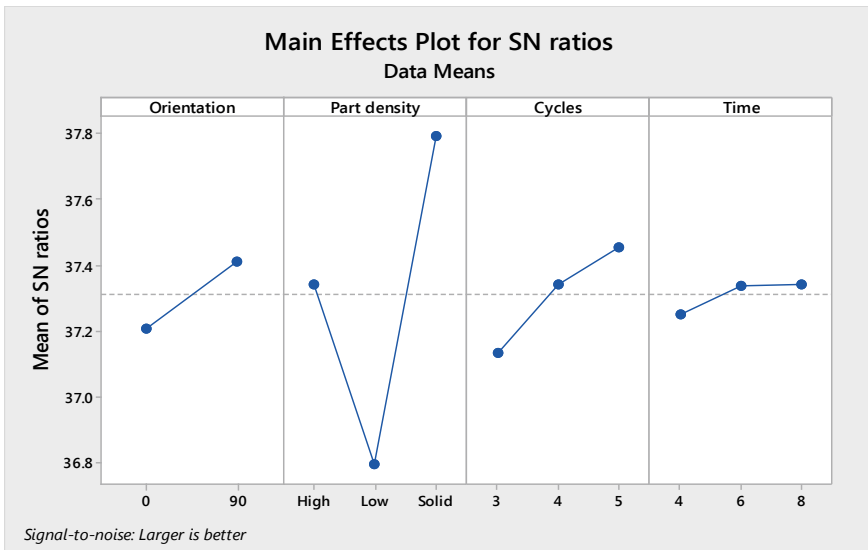
$$S/N = -10 \log \left[ \frac{1}{r} \sum_{i=1}^r Y_i^2 \right] \tag{2}$$

- $Y_i$  Observed value of the response characteristic
- $r$  Number of repetitions.

Figure 7.8 indicates that the maximum improvement in ‘ $R_a$ ’ value after the smoothing operation has been observed for replicas prepared at  $90^\circ$  of orientation angle with solid interiors. It was due to the fact that replicas with solid interior have negligible gap between the consecutive layers which resulted in uniform flow of ABS material during the smoothing operation and thus more improvement obtained in surface finish. Further, more and more improvement has been observed as the number of cycles of exposure increases due to repeated reflow of the material from peaks to valleys. With increase in cycle time from 4 to 8 s, the improvement in ‘ $R_a$ ’ value increases rapidly. The reason behind this was that more time of CVS exposure



**Fig. 7.8** Mean S/N ratio plot for improvement in surface roughness



**Fig. 7.9** Mean S/N ratio plot for shore hardness

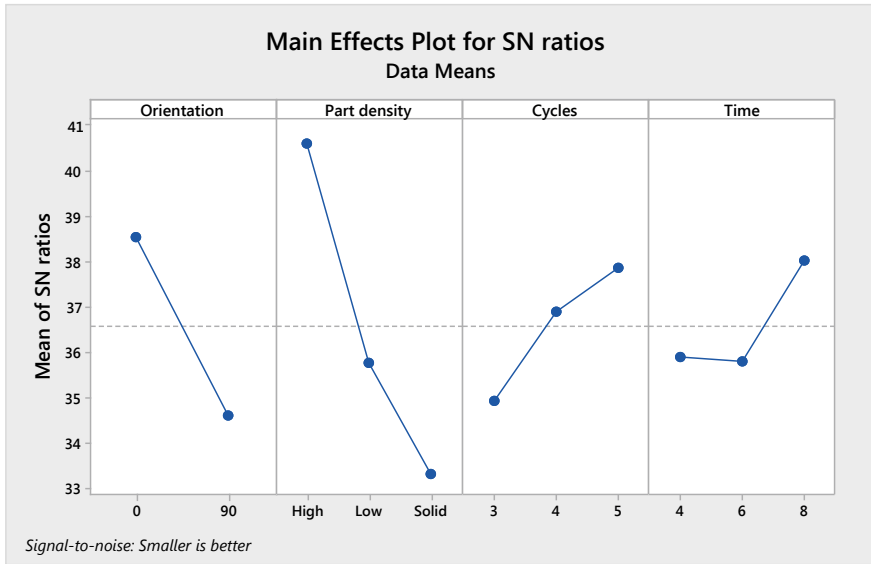


Fig. 7.10 Mean S/N ratio plot for dimensional deviation

during each cycle results in proper melting and provides extra time for flow of ABS material which drastically improves the ‘ $R_a$ ’ value. Figure 7.8 indicates that with regard to maximum improvement in ‘ $R_a$ ’ value,  $A_2$ ,  $B_3$ ,  $C_3$  and  $D_3$  are the optimum parameter levels as they yields the maximum value of S/N ratio.

The part interior style (part density) majorly affects the shore hardness and as the part density increases, the hardness value improves. It was quite obvious that the gap between the adjacent layers reduces as the part density changes from low to solid which ultimately increases the hardness value. Smoothing operation has significant effect on the shore hardness of fabricated replicas. The hardness value increases as the number of cycles of CVS process increases. It was mainly because of again and again reflow of the material which ultimately fills the air gap formed during layered manufacturing. Also, the increase in cycle time of CVS process improves the hardness value slightly but its effect was very little. Figure 7.9 indicates that the optimum parameters with regard to shore hardness were  $A_2$ ,  $B_3$ ,  $C_3$  and  $D_3$ .

Table 7.3 indicates FDM process yields slightly oversized replicas. However, after smoothing process, the selected dimension decreases due to material reflow, and thus, the smoothing becomes beneficial as it reduces the overall deviation. Figure 17.0 indicates that  $0^\circ$  orientation with high part density results in minimum deviation as compared to other parametric settings. As the number of cycles increases, more and more flow of the material occurs during each cycle which ultimately reduces the overall deviation. But this may affect adversely on the other very small dimensions of the replicas. Further, with increase in cycle time from 4 to 8 s, the overall deviation decreases as ABS material gets more time to flow from peaks to valleys. Figure 7.10

**Table 7.5** Input and output parameter constraints

Parameter	Goal	Lower range	Upper range
Orientation	Within region	0°	90°
Part density	Within region	High	Solid
No. of cycles	Within region	3	5
Cycle time	Within region	4	8
S/N ratio ( $R_a$ )	Maximize	39.58	39.71
S/N ratio (SH)	Maximize	36.52	38.00
S/N ratio ( $\Delta d$ )	Maximize	30.75	46.02

indicates that the optimum parameters with regard to dimensional deviation were  $A_1$ ,  $B_1$ ,  $C_3$  and  $D_3$ .

### 7.3.1.1 Combined Optimization

Based on the results, it has been noticed that the optimum levels of parameters for all the responses were different. So, combined optimized levels of the selected parameters have been obtained using Minitab 17 software when all the responses were considered simultaneously. Equal weight and importance have been assigned to each input and output parameters. The constraints set and the suggested parametric levels have been shown in Tables 7.5 and 7.6, respectively. The actual value of responses has been calculated on the basis of S/N ratio by utilizing Eqs. (1) and (2) and shown in Table 7.6.

Further, validity and repeatability of results have been checked by performing four confirmatory experiments at suggested parametric settings as given in Table 7.6. The observed values regarding the dimensional deviation, shore hardness and improvement in surface finish (refer Table 7.7) indicate close and consistent results which ensure the repeatability of the combined process.

**Table 7.6** Suggested parametric levels

Parameter	Suggested value	Actual value
Orientation	0°	0°
Part density	High	High
No of cycles	5	5
Cycle time	8	8
S/N ratio ( $R_a$ )	39.71	96.71%
S/N ratio (SH)	37.41	74.21 $H_d$
S/N ratio ( $\Delta d$ )	45.34	0.005 mm
Desirability	0.818	0.818

**Table 7.7** Results of confirmatory experiments

Exp No.	Linear dimension (mm)	$\Delta d$ (mm)	SH ( $H_d$ )	Percentage improvement in $R_a$
1	6.007	0.007	75.5	96.2
2	6.006	0.006	74	96.4
3	6.007	0.007	75	96.7
4	6.004	0.004	74	96.3

### 7.3.2 Phase II (SM Process)

In this research work, the master pattern required for fabricating the silicon mould is obtained from the results of first phase (FDM-CVS). The replica fabricated at best parameter settings in first phase (FDM-CVS) on the basis of Taguchi's L18 orthogonal array results with regard to surface finish, dimensional accuracy and shore hardness has been selected as a master pattern for the second phase. Four replicas have been fabricated at best parameter settings to create multiple cavity silicon mould. The steps involved in silicon mould preparation have been shown in Fig. 7.11.

Initially after attaching the gating system parts (sprue, riser, runner, etc.) to the fabricated master patterns, a coloured tape was pasted on the edges of the patterns so as to form the parting line. Further, in order to prevent the sticking of pouring resins with the surface of the patterns, a release agent was sprayed on the surface of master patterns, and then, they were put in a frame. In the next step, mixture of silicon rubber (VTV-750) and catalyst (CAT 740) that acts as hardener in the ratio of 10:1 were prepared and degassed by vacuum casting machine for 15 min in order to remove the air was poured into the frame. The mould was left for curing for about 16–18 h. After curing, the frame was opened and silicon mould was removed from it. The mould was ready for cutting and was cut with the surgical blade from the parting surface referring the coloured tape for the removal of the master patterns. The release agent was again applied to the cavities, and the mould was re-assembled. After this, the mould was ready for vacuum casting (VC) of different polyurethane (PU) materials. In this research work, multiple replicas were prepared by using Renishaw 6130 and Axson PX223 PU resins. The replicas prepared by this process are shown in Fig. 7.12. Surface texture and dimensional accuracy measured on multiple fabricated replicas were almost equivalent to those fabricated by traditional moulding techniques. So, the replicas fabricated by this route can be employed as plastic-based sacrificial patterns in investment casting applications for batch production and various end-user applications.



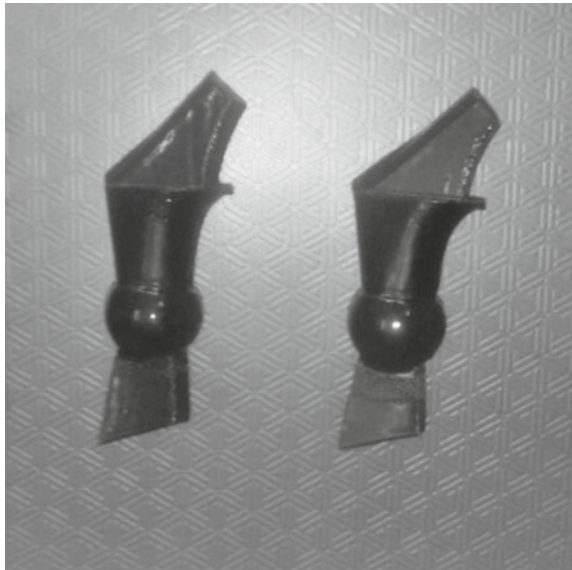


**Fig. 7.11** Steps of preparing the silicon mould

### 7.3.3 Cost Comparison

The cost incurred for making the replicas during FDM process and SM process has been compared for twenty-five runs of silicon mould. Higher the mould life, lesser will be the mould cost per run. Based on the calculations (refer Table 7.8), 69.3% of saving in cost has been achieved for fabricating the multiple replicas by employing SM process as compared to FDM process. This ensures the capability of SM process to produce cost-effective acceptable replicas for batch production applications.

**Fig. 7.12** Fabricated prototypes of PU material



**Table 7.8** Cost comparison for replicas fabricated by FDM and SM process

S. No.	Process	Description	Cost (USD)
1	FDM	Average cost of making each selected replica	\$7
2	SM	Cost of making multi-cavity (four) silicon mould	\$72
		Average mould cost for 25 runs	$72/25 = \$2.9$ per run
		Cost of fabricating four PU replicas	\$5.75
		Cost of making each replica including mould cost	$(5.75 + 2.9)/4 = \$2.15$
		Percentage saving in cost per replica	$[(7 - 2.15)/7] \times 100 = 69.3\%$

### 7.4 Conclusions

- The present book chapter demonstrates the procedure for fabrication of low-cost hip implant replicas for batch production by combining the FDM, CVS and SM process.
- The surface quality and shore hardness of fabricated replicas enhanced significantly after the CVS process due to reduction of stair step effect and filling of air gap by reflow of the material.
- FDM process yields slightly oversized dimensions. However, the material reflow caused during the smoothing process reduces the selected dimension and thus decreases the overall deviation.

- 0° orientation, high part density, five number of cycles and eight seconds of cycle time were the optimum levels of the selected parameters for combined optimization.
- Multiple PU replicas were fabricated successfully by SM process to reduce the overall cost of each replica.
- Percentage saving in cost of 69.3% for fabricating multiple replicas by SM process ensures the capability of the process to produce cost-effective replicas for batch production applications.

## References

1. Folkestad JE, Johnston RL (2001) Resolving the conflict between design and manufacturing: integrated rapid prototyping and rapid tooling (IRPRT). *J Ind Technol* 17(4):1–7
2. Charvat O (2006) Možnosti aplikace metod RP's použitím technologie vytavitelneho modelu. Dissertation, Faculty of Mechanical Engineering, Department of Foundry Engineering, Brno University of Technology
3. Bernard A, Fischer A (2002) New trends in rapid product development. *CIRP Ann Manuf Technol* 51(2):635–652
4. Wohlers T (2012) Wohlers report 2012: executive summary. Wohlers Associates, Fort Collins, CO
5. Anasane S, Pandey A, Rathi KK, Panda N, Ravi B (2007) Total knee prosthesis: design, manufacture, and testing. In: Proceedings of team tech 2007 Faro, 4–6 October, 2007, Indian Institute of Science, Bangalore, India, pp 1–7
6. Budzik G (2010) Geometric accuracy of aircraft engine blade models constructed by means of the generative rapid prototyping methods FDM and SLA. *Adv Manuf Sci Technol* 34(1):33–43
7. Poomathi N, Singh S, Prakash C, Patil RV, Perumal PT, Barathi VA, Balasubramanian KK, Ramakrishna S, Maheshwari NU (2018) Bioprinting in ophthalmology: current advances and future pathways. *Rapid Prototyping J*. <https://doi.org/10.1108/RPJ-06-2018-0144>
8. Singh S, Singh N, Gupta M, Prakash C, Singh R (2018) Mechanical feasibility of ABS/HIPS-based multi-material structures primed by low-cost polymer printer. *Rapid Prototyping J*. <https://doi.org/10.1108/RPJ-01-2018-0028>
9. Nourghassemi B (2011) Surface roughness estimation for FDM systems. M.E thesis, Ryerson University, Toronto
10. Wohlers TT (2006) Wohlers report 2006: RP, RT, RM state of the industry, annual worldwide progress report. Wohlers Associates Inc., Fort Collins, CO
11. Chhabra M, Singh R (2011) Rapid casting solutions: a review. *Rapid Prototyping J* 17(5):328–350
12. Noorani R (2005) *Rapid prototyping—principles and application*. Wiley, New Jersey
13. Upcraft S, Fletcher R (2003) The rapid prototyping technologies. *Assembly Autom* 23(4):318–330
14. Ahmad M, Hayat N, Shah FH (2015) Rapid development of complex shaped customized products. *J Braz Soc Mech Sci Eng* 37(1):263–274
15. Singh J, Singh R, Singh H, Verma AK (2018) Investigations for mechanical properties and biocompatibility of SS-316L implant prepared as rapid investment casting for batch production. *Sadhana Acad Proc Eng Sci* 43(5):1–10
16. Singh J, Singh R, Singh H (2017) Experimental investigations for dimensional accuracy and surface finish of polyurethane prototypes fabricated by indirect rapid tooling: a case study. *Prog Addi Manuf* 2(1):85–97
17. Rao AS, Dharap MA, Venkatesh JVL (2014) Development of rapid tooling for investment casting using fused deposition modeling process. *Adv Mater Res* 970:155–165

18. Hanus A, Špirutová N, Beňo J (2011) Surface quality of foundry pattern manufactured by FDM method. *Rapid Prototyping Arch Foundry Eng* 11(1):15–20
19. Vasudevarao B, Natarajan DP, Henderson M (2000) Sensitivity of RP surface finish to process parameter variation. In: *Proceedings of 11th solid freeform fabrication symposium*, August 8–10, Austin, USA, pp 252–258
20. Sreedhar P, Manikandan CM, Jothi G (2012) Experimental investigation of surface roughness for fused deposition modeled part with different angular orientation. *Int J Adv Des Manuf Technol* 5(3):21–28
21. Pandey PM, Reddy NV, Dhande SG (2003) Improvement of surface finish by staircase machining in fused deposition modeling. *J Mater Process Technol* 132(1):323–331
22. Boschetto A, Bottini L (2014) Roughness prediction in coupled operations of fused deposition modelling and barrel finishing. *J Mater Process Technol* 219:181–192
23. Fischer M, Schoppner V (2014) Finishing of ABS-M30 parts manufactured with fused deposition modeling with focus on dimensional accuracy. In: *Proceedings of 25th solid freeform fabrication symposium*, Austin, 4–6 Aug 2014, pp 923–934
24. Galantucci LM, Lavecchia F, Percoco G (2010) Experimental study aiming to enhance the surface finish of fused deposition modeled parts. *CIRP Ann Manuf Technol* 58(1):189–192
25. Singh J, Singh R, Singh H (2017) Investigations for improving the surface finish of FDM based ABS replicas by chemical vapor smoothing process: a case study. *Assembly Autom* 37(1):13–21
26. Singh J, Singh R, Singh H (2016) Repeatability of linear and radial dimension of ABS replicas fabricated by fused deposition modelling and chemical vapor smoothing process: a case study. *Measurement* 94:5–11
27. Chohan JS, Singh R, Boparai KS, Penna R, Fraternali F (2017) Dimensional accuracy analysis of coupled fused deposition modeling and vapour smoothing operations for biomedical applications. *Compos B* 117:138–149
28. Singh J, Singh R, Singh H (2017) Experimental investigation for shore hardness of ABS replicas fabricated by fused deposition modelling and vapor smoothing process. *Int J Adv Mechatron Rob* 9(1):29–34
29. Kalyan K, Singh J, Phull GS, Soni S, Singh H, Kaur G (2018) Integration of FDM and vapor smoothing process: analyzing properties of fabricated ABS replicas. *Mater Today Proc* 5(14):27902–27911
30. Mohamed OA, Masood SH, Bhowmik JL (2015) Optimization of fused deposition modeling process parameters: a review of current research and future prospects. *Adv Manuf* 3(1):42–53
31. Pattnaik S, Jha PK, Karunakar DB (2014) A review of rapid prototyping integrated investment casting processes. *Proc Inst Mech Eng Part L J Mater Des Appl* 228(4):249–277
32. Singh S, Singh M, Prakash C, Gupta MK, Mia M, Singh R (2019) Optimization and reliability analysis to improve surface quality and mechanical characteristics of heat-treated fused filament fabricated parts. *Int J Adv Manuf Technol* 102:1521–1536
33. Boparai K, Singh R, Singh H (2016) Development of rapid tooling using fused deposition modeling: a review. *Rapid Prototyping J* 22(2):281–299
34. Singh J, Singh R, Singh H (2018) Surface roughness prediction using Buckingham's Pi-theorem for SS-316L hip implant prepared as rapid investment casting. *Mater Today Proc* 5(9):18080–18088
35. Singh S, Prakash C, Ramakrishna S (2019) 3D printing of polyether-ether-ketone for biomedical applications. *Eur Polym J*. <https://doi.org/10.1016/j.eurpolymj.2019.02.035>
36. Rosochowski A, Matuszak A (2000) Rapid tooling: the state of the art. *J Mater Process Technol* 106:191–198
37. Kruth PJ (1991) Material increases manufacturing by rapid prototyping techniques. *CIRP Ann Manuf Technol* 40(2):603–614
38. Pal DK, Ravi B (2007) Rapid tooling route selection and evaluation for sand and investment casting. *Virtual Phys Prototyping J* 4:197–207
39. Cheah CM, Chua CK, Lee CW, Feng C, Tonog K (2005) Rapid prototyping and tooling techniques: a review of applications for rapid investment casting. *Int J Adv Manuf Technol* 25:308–320

40. Rahmati S, Akbari J, Barati E (2007) Dimensional accuracy analysis of wax patterns created by RTV silicon rubber molding using Taguchi approach. *Rapid Prototyping J* 13(2):115–122
41. Thian SCH, Tang Y, Tan WK, Fuh JYH, Wong YS, Loh HT, Lu L (2008) The manufacture of micromould and microparts by vacuum casting. *Int J Adv Manuf Technol* 38:944–948
42. Sharma V, Singh R (2011) Investigations for modeling the silicon moulding process for plastic components. *Int J Mater Sci Eng* 2(1–2)
43. Galantucci LM, Lavecchia F, Percoco G (2010) Quantitative analysis of a chemical treatment to reduce roughness of parts fabricated using fused deposition modeling. *CIRP Ann Manuf Technol* 59(1):247–250
44. Garg A, Bhattacharya A, Batish A (2016) On surface finish and dimensional accuracy of FDM parts after cold vapor treatment. *Mater Manuf Processes* 31(4):522–529
45. Montgomery DC (2008) *Design and analysis of experiments*. Wiley, New Jersey
46. Singh J, Singh R, Singh H (2017) Dimensional accuracy and surface finish of biomedical implant fabricated as rapid investment casting for small to medium quantity production. *J Manuf Process* 25(1):201–211

**Dr. Jaspreet Singh** is associate professor in the School of Mechanical Engineering, Lovely Professional University, Jalandhar, India. He has received Ph.D. in Mechanical Engineering from Guru Nanak Dev Engineering College, Ludhiana, India. His area of research is additive manufacturing, rapid investment casting and application of 3D printing for non-structural engineering applications. He has contributed extensively in additive manufacturing literature with publications appearing in *Journal of Manufacturing Processes*, *Measurement*, *Assembly Automation* and *Materials Today: Proceedings*.

**Prof. Rupinder Singh** is Professor in the Department of Production Engineering, Guru Nanak Dev Engineering College, Ludhiana, India. He has received Ph.D. in Mechanical Engineering from Thapar Institute of Engineering and Technology, Patiala, India. His area of research is non-traditional machining, additive manufacturing and development of porous biomaterials using 3D printing and rapid prototyping techniques. He has more than 18 years of teaching and research experience. He has contributed extensively to the world in additive manufacturing literature with publications appearing in *Journal of Manufacturing Processes*, *Composite Part B*, *Rapid Prototyping Journal*, *Journal of Mechanical Science and Technology*, *Measurement*, *International Journal of Advance Manufacturing Technology*, and *Journal of Cleaner Production*. He authored 17 books and ~3 chapters. He has received more than 3 crores research grants from various funding agencies such as DST-SERB, AICTE, CSIR, DAE, IE. He is working with Prof. Seeram Ramakrishna, NUS Nanoscience and Nanotechnology Initiative and Prof. Fernando Fraternali, Full Professor of Structural Mechanics, Department of Civil Engineering, University of Salerno.

**Prof. Harwinder Singh** is professor in Department of Mechanical Engineering, Guru Nanak Dev Engineering College, Ludhiana, India. He has received Ph.D. in Mechanical Engineering from Punjabi University, Patiala, India. His area of research is additive manufacturing, rapid tooling and industrial engineering. He has more than 18 years of teaching and research experience. He has contributed extensively to the world in additive manufacturing and industrial engineering literature with publications appearing in *Journal of Manufacturing Processes*, *Rapid Prototyping Journal*, *Measurement*, *International Journal of Advance Manufacturing Technology*.

# Chapter 8

## Biomaterials and Fabrication Methods of Scaffolds for Tissue Engineering Applications



Atul Babbar, Vivek Jain, Dheeraj Gupta, Sunpreet Singh, Chander Prakash, and Catalin Pruncu

### 8.1 Biomaterials

The definition of biomaterials by American Institute of health is as “any material or combination of material, it may synthetic or natural in nature, which can use for any time period in human body, which can replace the tissue or function of the body to enhance the quality of life of any person” [1]. In the history of artificial implants, the first material which was used to replace the cranial defects was gold by Egyptians and Romans. During the period of the 1900s, the placenta was used as a biomaterial [2]. The polymethyl methacrylate (PMMA) was the first polymer which was accepted.

There are basically three categories of the biomaterials based on tissue reactions [3].

**Bio Tolerant Materials:** These materials can separate from bone tissue by a layer of fibrous tissue.

**Bioactive Materials:** Such material has the property of constructing chemical bonds with other bone tissue. The collagen phase of the adjacent bone is deposited on the implant surface.

---

A. Babbar (✉) · V. Jain · D. Gupta  
Department of Mechanical Engineering, Thapar Institute of Engineering and Technology, Patiala  
147004, India  
e-mail: [atulbabbar123@gmail.com](mailto:atulbabbar123@gmail.com)

S. Singh · C. Prakash  
Department of Mechanical Engineering, Lovely Professional University, Phagwara, India

S. Singh  
Department of Mechanical Engineering, National University of Singapore, Singapore, Singapore

C. Pruncu  
Department of Mechanical Engineering, Imperial College of London, London, UK

**Bioinert Materials:** Under this category, it is possible to have direct contact with the adjacent bone tissue. No chemical reactions will occur between the implant material and bone tissues.

The adaptation of the biomaterial depends upon the type of material used, load applied and most importantly the age of the patient [4]. The surface of the material can be enhanced by adding appetite sequences to provide a 3D structure to support the matrix formation [5]. The new technologies are being continuously developed to support new specifications and applications. Orthopaedic, cardiovascular and drug delivery materials comprise the largest market of the implant materials and alone dental implant market costs around 1 U\$ billion.

### 8.1.1 Types of Biomaterials

A biomaterial or implants are defined as any material that is used to exchange or reconstruction function to body tissue and permanent in contact with body fluids. The implant materials should be biocompatible and should not elicit an ineffective response from the body. It should be non-toxic [6]. The biomaterial should have higher mechanical properties to serve as a replacement of human body tissues. A biomaterial should be easily machined into different shapes and structure at low cost. Generally, implant materials can be divided into the following categories [7–10].

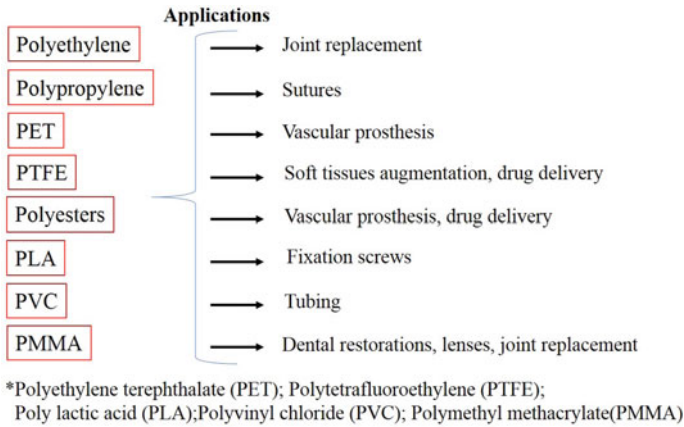
- Metals
- Polymers
- Ceramics and composites.

#### Metals

In the previous decades, most of the common orthopaedic surgeries have been performed for the implantation of metal implants. Applications of the metallic implants are in wire, screw and total joint replacement such as hips joint, knees joint, shoulders, ankles, etc., as shown in Table 8.1. There are some basic metals

**Table 8.1** Applications of different metals [19]

S. No.	Metal	Principle applications
1	316L stainless steel	Fracture fixations, surgical instruments
2	Pure titanium and its alloys	Bone replacements, fixations, dental implants
3	Nickel and titanium alloys	Bone plates, stunts and orthopaedic wires
4	Magnesium	Bio gradable plates and screw
5	Gold alloys	Dental restorations
6.	Silver products	Antibacterial agents



**Fig. 8.1** Applications of different polymers [20, 22, 23]

which have been used in the metallic implants such as stainless steels, pure titanium and its alloy, gold alloys, silver products, platinum and nickel-titanium alloys [11–18].

### Polymers

There are various types of polymers which have been used in the biomedical field. The application range of such polymers varies from facial treatments to liver and heart valves and from dentistry to total knee and hip joints [20, 21]. Figure 8.1 illustrates the applications of different type of polymers.

### Glass and Ceramics

Some glasses and ceramics are mostly used in orthopaedic surgeries due to their good biocompatibility and mechanical properties. These materials are very hard and can resist high load capacity inside the human body [24, 25]. In the advance era, the fabrication and machining of these materials are cost-effective and easily available [11]. Applications of ceramics and glasses in the human body vary according to the position of implants [26]. Table 8.2 shows the applications of the biomaterial ceramics and glass materials.

## 8.2 Polymer Scaffold in Tissue Engineering

There are various conventional and non-conventional techniques to fabricate the porous material or polymer scaffold for tissue engineering. The aim of the bone tissue engineering is to enhance the role of traditional bone repair methods by using biodegradable polymer scaffold to increase the mechanism of the human body to repair the bone fracture [31]. The polymer scaffold should be designed to match the mechanical and structural properties of the target tissue. The polymer scaffold with similar



**Table 8.2** Applications of different type of glass and ceramics [27–30]

S. No.	Glass and ceramics	Principle applications
1	Alumina	Joint replacements and dental implants
2	Zirconia	Joint replacement
3	Calcium phosphate	Bone repair and surface coating
4	Bioactive glass	Bone replacements
5	Porcelain	Dental restorations
6	Carbons	Heart valves and dental implants

properties to native bone has many advantages. Porosity, the structure of pores, interconnectivity of pores and mechanical characterisation of the scaffold affect the effectiveness of polymer scaffolds [32]. It has been found that the interconnectivity and porosity throughout the scaffold required to promote the cell culture, loading and migration of cells, tissue growth and flow of body fluid [33]. The traditional fabrication techniques have the drawback of poor permeability and interconnectivity between the porous. The development of non-conventional methods to fabricate scaffold leads to control of pore morphology.

### **8.2.1 Traditional Tissue Repair Methods**

Tissue repair is an ultimate method of surgery since ancient time and can be classified into two foams: (1) tissue grafting and organ transplantation and (2) alloplastic and synthetic material replacement. When the bone tissue is unable to resist the load of the body, the damaged tissue is replaced with the artificial material used to fill the bone injury. Moreover, the damaged bone tissue cannot be taken from the other part of the body or from other human beings since it can cause transmission infection.

### **8.2.2 Tissue Engineering**

Tissue engineering introduced in the year 1990 to address the drawbacks of tissue grafting and alloplastic tissue repair techniques [34]. This technique is used to transplant the cells, genes and proteins through the porous structure known as a scaffold. Tissue engineering aims for regenerating a load-bearing tissue, and hence, scaffold should resist the mechanical function to aid biological delivery [35, 36]. The fabrication of porous scaffold can help in understanding the role of the scaffold structural parameters on mechanical characteristics and efficiency [37–39]. The techniques used to fabricate the scaffold have a major role in the morphology of the scaffold.

**Table 8.3** Different casting techniques with unique factors and applications [40–44]

S. No.	Method	Polymers	Unique factors	Applications
1	Solvent casting	PLLA, PLGA	Porous scaffold control	Bone engineering
2	Ice particle leaching	PLLA, PLGA	Pore structure control	Tissue engineering
3	Gas foaming	PLLA, PDLLA	Porosity control	Drug delivery
4	Solvent evaporation	PLGA, PLAGA	High density cell culture	Bone repair

There are number of methods to fabricate the scaffold; each one has its advantages and disadvantages. The medical applications of the different polymers in tissue engineering have been shown in Table 8.3.

## 8.3 Traditional Scaffold Casting Methods

### 8.3.1 Solvent Casting

Solvent casting is a method that involves dispersing mineral or organic particles in a polymer solution [45]. Casting or freeze-drying is then performed as a dispersion process in order to produce porous scaffold [39]. This basic method has been used to fabricate scaffolds using various polymers but while the approach is relatively simple, there are disadvantages such as the use of toxic solvents and residual solvent that remains in the scaffold and it may harmful for human body [46].

### 8.3.2 Gas Foaming

Gas foaming is a method used under high pressure. In this process, a polymer solid disc is formed with the help of compression moulding machine under high temperature and pressure [47–49]. Subsequently, polymer disc is placed in the high-pressure CO<sub>2</sub> chamber for some days. This time period is provided for creating the pores for tissue growth due to the infiltration of the gas. This technique is sufficient for a high degree of porosity in the final scaffold without affecting the bioactivity and the pore size in the range of 100  $\mu$ .

### 8.3.3 Melt Processing

This method has been introduced to use more than one polymer, mixed together and exposed to the temperature above the melting point of the two polymers [50]. In this method, both polymers are continuous in the structure and allow for the interconnected pores network. The process of melting of polymer involves the use of NaCl, polymer and an extruder. Extruder provides the homogenous and well-blended mixture. The salt particles present in the mixture can also break down during mixing and result in the small pore size. Polymer network produced in this way is usually too small for most tissue engineering applications [51].

## 8.4 Fabrication of Scaffolds with Additive Manufacturing

The process “additive manufacturing (AM)” adds material in layer formation or pattern to fabricate the required shape and size instead of material removing [52]. The flow chart of the additive manufacturing procedure is shown in Fig. 8.2. AM is used in several areas such as prototyping, aerospace, military, buildings and cars 3D printing, home applications and biomedical engineering. This 3D printing technique uses software which slices the 3D model into various layers. Each layer performed on the build platform by the printer; once the first layer is completed, the platform goes downwards according to layer thickness or equal to layer thickness; and another layer is fabricated over the previous layer. 3D printing technique significantly decreases the waste because in 3D printing, the material is placed only in the required location; the rest will be left as empty space [53–55].

From last few years, scientist and engineers have performed rigorous research to use 3D printing technology to fabricate artificial body parts and organs. This technique helps to create artificial implants for the patient’s body the same as the fabrication of plastic and metal parts. Another application of 3D printing in the biomedical field is creating body parts out of metal or other material to replace the damaged and lost limbs. With the help of the advancement of 3D printing, now the doctor firstly scans the patient’s body and bone structure. The design engineers help to recreate the artificial part in the laboratory which helps to meet the exact requirements of the patient.

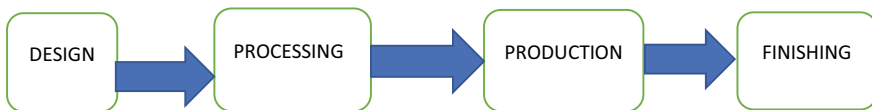


Fig. 8.2 Flow diagram of the additive manufacturing

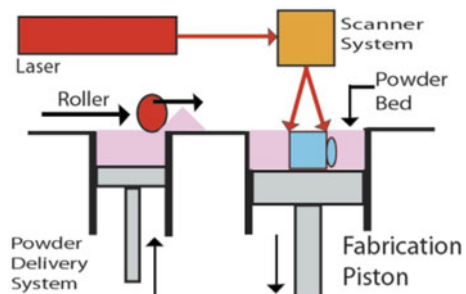
### 8.4.1 Stereolithography

Stereolithography is a process in which an ultraviolet laser is used to fabricate parts layer by layer. The resin is placed on the machine bed and laser beam strike on it and melt it. For each layer, the laser strikes on the surface of the resin. The high-voltage laser light cures and solidifies the pattern as per design traced on the resin and helps to join with the lower layer [56, 57]. Once the pattern is traced, the elevator platform descends by a distance equal to the layer thickness of a single layer which generally varies in the range of 0.05–0.15 mm. Once the single layer is completed, the resin blade moves over the section of the part to fill fresh material and process is repeated until the final output created. Once the required part is created, it is immersed in a chemical bath to remove the support material and excessive resin and subsequently cured in an oven for some time [58].

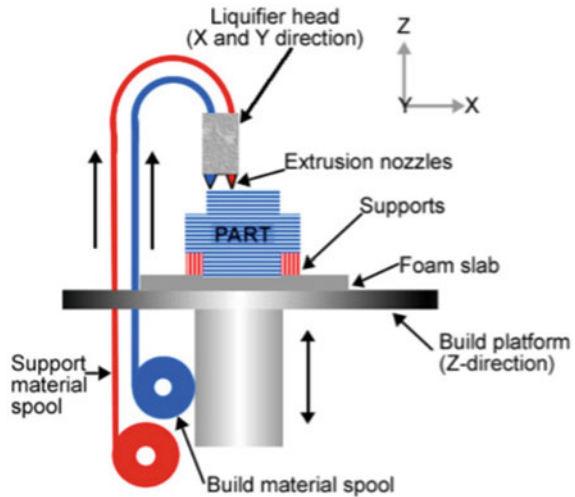
### 8.4.2 Selective Laser Sintering

The selective laser sintering technique is another kind of 3D printing technology. The form of input material is the major difference between stereolithographic and selective laser sintering. The small powder form particles are used as input material. The highly powered carbon dioxide laser is used to perform the manufacturing operation. The highly powered laser scanned the cross section and melts the material. The movement in *X*-axis and *Y*-axis is controlled by the laser head, and the movement in *Z*-axis is controlled by the machine bed (refer to Fig. 8.3). The density of the final part is based upon the peak power of laser instead of laser time. The powder used in the chamber is preheated so that it can help to raise the temperature in less time. This technique can be used for various materials such as polymer, nylon, metals and alloys [59, 60].

**Fig. 8.3** Selective laser sintering process [61]



**Fig. 8.4** Fused deposition modelling machine (under CC Licences) [62]



### 8.4.3 Fused Deposition Modelling

The fused deposition modelling is widely used in production application of each sector. It is generally based on the additive principle of manufacturing. The input material is basically used in the form of a plastic filament or metal wire. The extrusion nozzle converts the material from solid form to liquid as evidently in Fig. 8.4. The raw material extrudes from the nozzle in the form of thin filament and deposit and solidifies over the printer's platform. Subsequently, another layer extrudes out from the nozzle and diffuses with the previous layer, and hence, material takes its final shape with layer-by-layer addition of the material. All operations of the FDM machine are numerically controlled. The process parameters are decided manually in the software package. The X-axis and Y-axis movements are controlled by extrusion nozzle, and Z directions are controlled by machine bed. The movements are controlled by Stepper motors or servo motors.

## 8.5 Process Parameters for Additive Manufacturing

The process parameters play a vital role in the properties of the fabricated sample in 3D printing. It has been observed that the different process parameter has a significant effect on the behaviour of the final specimen. Some parameters play a major role, while other parameters play a minor role in the characterisation of 3D-printed samples, which have been discussed below.

### Infill Percentage

The infill percentage of workpiece plays a major role in mechanical characterisation. In 3D printing, the term “infill” means the structure inside the object that required to print. Figure 8.5 shows the different infill percentage of 3D specimens. The workpiece with 100% infilling shows dense structure [63, 64]. The infill percentage of the design is provided in the software. Print weight, build time, usage material in fabrication and strength of part are another influencing parameters. The sample with 100% in filling has great mechanical strength and other properties instead of 5, 10 and 20%.

### Infill Pattern

The infill pattern is the way of filling the inside portion of the workpiece. The mechanical properties of any workpiece directly depend upon the infill pattern. When using any infill pattern, it will decide the mechanical characterisation of that particular workpiece [53, 66, 67]. Nowadays, various types of infill patterns options are available in 3D printers as shown in Fig. 8.6; each has some advantages and limitations between the strength of the material, build time or print time and required material for fabrication.

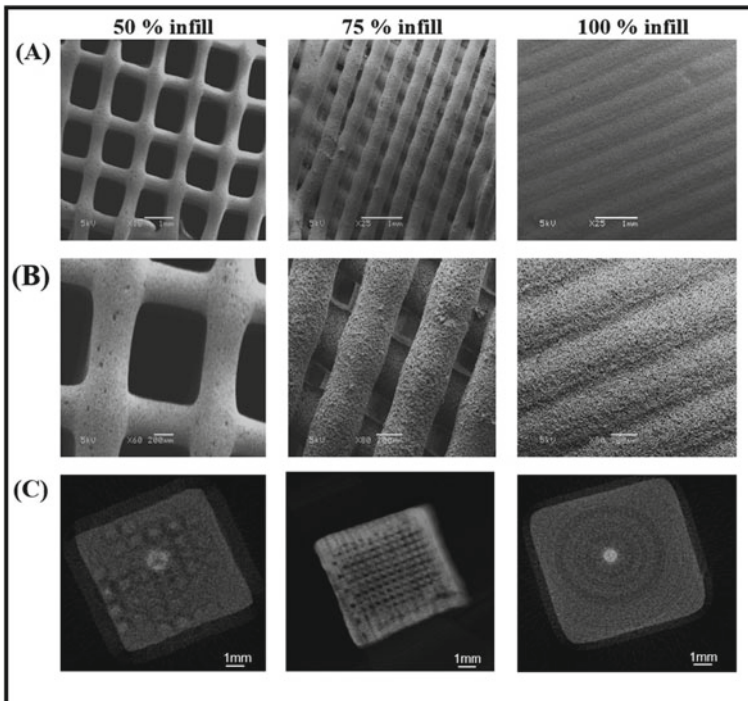
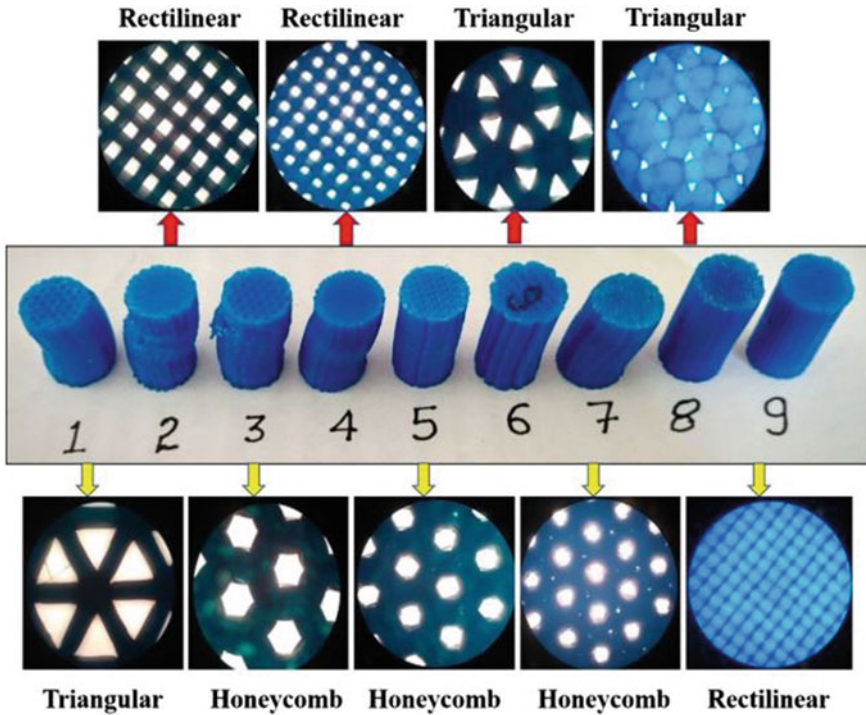


Fig. 8.5 Different infill percentage [65]



**Fig. 8.6** Different infill patterns [32]

The simplified 3D software provides six different types of patterns with some of the most popular. The designer can select any one of the infill patterns and fabricate the workpiece. Followings are the most common uses infill patterns are as follows:

- 1 Rectilinear
- 2 Grid
- 3 Triangular
- 4 Wiggle
- 5 Fast honeycomb
- 6 Full honeycomb.

### Layer Thickness

The layer thickness in 3D printing can describe as the height of the individual successive layer. The 3D printing works on the principle of layer formation, extruder moves on the bed of the machine and fabricates a single layer as per the design of the sample. The thickness of the single layer is controlled by the servo motor speed, which is connected with a printing machine and controlled according to the design of the workpiece. When the single layer is fabricated, the extruder repeats the same process until

final completion of the job. The build time and surface roughness directly depends upon the layer thickness [68].

### **Layer Width**

As the name suggests, layer width in 3D printing represents the measure of the width of a single layer. The width of the single layer can be decided in the software. The layer height or layer thickness and layer width are co-relative to each other. During fabrication of parts, layer width and layer thickness are controlled by the servo motor as per directions are given in the software file.

### **Printing Speed**

The printing speed generally can be classified into three stages such as high speed, medium speed and low speed. The low speed is around 40–50 mm/s, and high build time, medium infill speed is generally from 80 to 100 mm/s. The third and last stage is high infill speed up to 150 mm/s. It has been reported that the build time increases with decrease in the infill speed. A small part with low quality can print in less than 10 min. However, more time would be required for large size parts and high-quality standards.

### **Build Orientation**

Build orientation plays an important role in the properties of the building part. Fabrication of the parts with different directions of the orientations may result in the significant change in the print quality. For example, if a designer fabricates the two cylinders with a different orientation, the dimensions of the cylinders are 10 mm outside diameter and 6 mm inside diameter with 20 mm height. The printing of the first part with its centre axis vertical, and the printer would construct a series of concentric circle layered on the top of other. The result will be a smooth outer surface. On the other side, the second part printed with its centre axis horizontally, the part print as the series of rectangles layered on the top of last one. The surface of the cylinder which touches the platform will be flat. There will be a difference between the characterisation of both parts.

### **Raster Angle**

Raster angle is the direction of layer fabrication with respect to the platform axis. It gives a significant result on the characterisation of the part with different raster angle. It varies from 0° to 90°.

### **Temperature**

The temperature is the main parameter in 3D printing because melting temperature, glass transition temperature and bed temperature are different for different materials. For example, the glass melting temperature of polylactic acid is near to 180 °C and glass transition temperature near about 60 °C. On the other hand, the glass transition temperature of ABS near to 105 °C.



## 8.6 Properties of PLA Polymer

PLA is a biocompatible polymer which has excellent biocompatibility due to which polymer is mainly suited for biomedical applications. The polymer scaffold can float into the water because of its low densities. The strength of the PLA polymer is lower than the metallic implants and decreases with the decreasing density of the material. There is no side effect of PLA polymer in the human body. The process parameters chosen for the fabrication of scaffolds have a significant effect on its properties.

### Mechanical Properties

When polymer scaffolds are compared to dense polymer structure, the scaffold behaves differently in testing due to their internal structure. Conventional testing techniques such as compression test and tensile test are used to measure the tensile and compressive strength of the scaffolds. The polymer scaffold behaves differently with different process parameters and the internal structure of the scaffold. Followings are the different mechanical properties of the dense PLA polymer (Table 8.4).

### Thermal Properties

Poly(lactic acid) is a biodegradable and bioactive polymer which is produced from the renewable energy sources such as cassava roots, chips or stretch and sugarcane. In 2010, poly(lactic acid) had the second biggest consumption volume of any bioplastic in the world. Followings are some thermal properties of the PLA polymer (Table 8.5).

### Biocompatibility

Biocompatibility is a degree to which implant materials result in tissue engineering. There are several biomedical materials available such as stainless steel, titanium and

**Table 8.4** Mechanical properties of PLA [69–71]

S. No.	Properties	Range
1	Tensile strength	50–60 MPa
2	Elongation at break	6%
3	Young's modulus	3.5 GPa
4	Flexural strength	80 MPa
5	Shear module	2.4 GPa
6	Flexural module	4.0 GPa
7	Density	1.25 g/cm <sup>2</sup>

**Table 8.5** Thermal properties of PLA [70, 72, 73]

S. No.	Properties	Range
1	Glass transition temperature	60–65 °C
2	Melting temperature	173–178 °C
3	Crystallinity temperature	37 °C
4	Heat resistance temperature	110 °C

**Table 8.6** Mechanical properties of different bones [74–77]

S. No.	Bones	Compressive strength (MPa)	Tensile strength (MPa)	Young's modulus (GPa)
1	Cancellous bone	4–12	N/A	0.02–0.5
2	Cortical bone	130–180	60–120	3–30
3	Cartilage	N/A	3.7–10.5	0.7–15.3 (MPa)
4	Ligament	N/A	13–46	0.065–0.541
5	Tendon	N/A	24–112	0.143–2.31

its alloys. If material has less negative tissue reactions occurs, it means the material has a more biocompatible nature. For example, gold is the most biocompatible metal compared to others but it is too soft, ductile and costlier. The biocompatibility of any metal or material depends upon the weight relative to its mechanical properties. In the case of metals, the corrosion resistance test is the main way to check the biocompatibility of any metal, because the corrosion rate of any metal can decide the response of reaction. Implant material should have corrosion resistant nature. Adjacent tissues may discolour and can be allergic in the patient's body due to the release of elements.

### Mechanical Properties of Human Body Tissues

The human body has different kind of bones relative to their properties. Some bones have great mechanical strength, and some others have very low. The following table shows the different properties of the different bones (Table 8.6).

## 8.7 Applications of Polymer Scaffolds in Biomedical

Polymer scaffold is widely used in biomedical engineering. In previous decades, it was only used in the form of medical devices. The foremost requirement of the biomedical implants is the choice of the material as per adequacy of the human body. A material which is used for implant manufacturing should have some properties in order to have long life usage inside the body without any side effects. Some polymeric material is widely used for medical purpose in these days such as tissue engineering, artificial organ and implants, bone repair screws and dentistry. Following are the main applications of the polymer related biomaterials.

### Tissues Scaffolding

Biomaterials play a vital role in tissues scaffolding, working as a three-dimensional support structure for the regeneration of cells as shown in Fig. 8.7. Polymers are the most popular biomaterial in tissue growing due to their mechanical similarity with the bone structure. Most polymers can break into natural products. Biomaterials should have similar chemical properties as required in the tissues engineering [78].

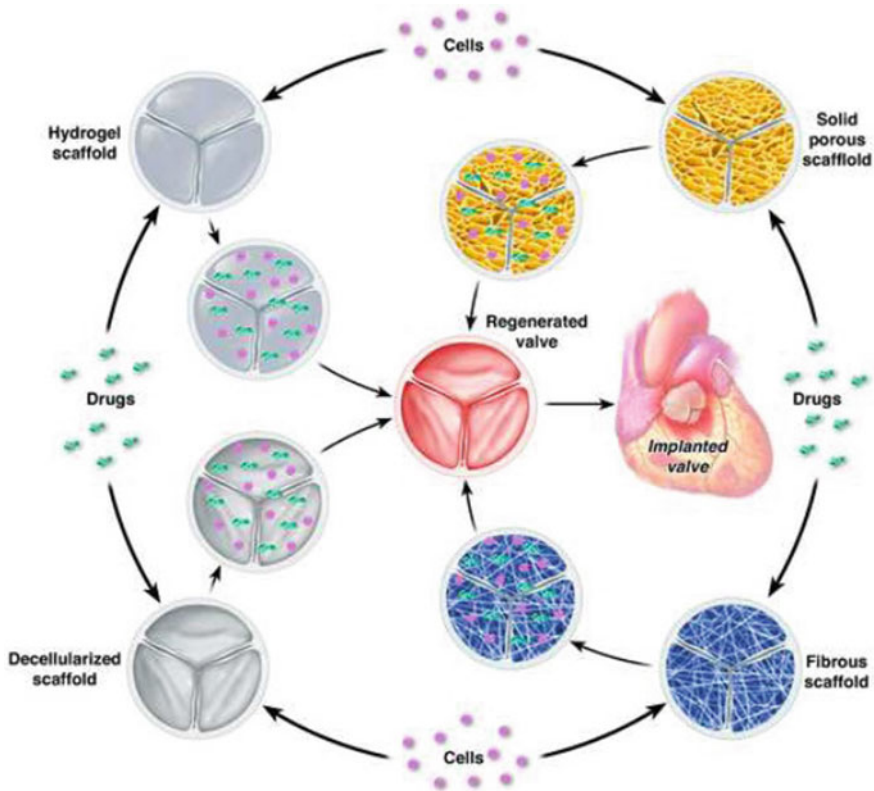


Fig. 8.7 Regeneration of tissue engineering [79]

### Implantation of Medical Devices

In drug delivery control systems, stents are coated with a layer of biodegradable and bioresorbable materials [80]. The biodegradable polymer is also candidate material for biodegradable stents due to their suitable properties to control drug release and good mechanical characteristics to prevent stents from deforming or fracturing [81]. The major advantage of the usage of degradable implants is no need for surgery to remove the implants after recovery. Nowadays, most of the bone fixation screws, pins and plates are fabricating from degradable materials.

### Joint Prostheses

Joints are necessary inside the body parts for the movement. The hip joint, knee joint and elbow are some examples of body joints. From the last few decades, the artificial hip joint and knee joint replacement is most commonly applied in human beings. The acetabular part and femoral part fixed with each other. The shaft of the femoral stem is specially tapered.

### **Dentistry**

A vast variety of materials like polymer and metals are used in the dentistry like cavity filling, fluting, crown and bridge, prosthetic, orthodontic and periodontal treatment of teeth. The choice of dentistry material is the pivot on its properties such as mechanical and biomedical properties of tooth structure.

### **Bone Repair**

Bone is a structural compound consists of collagen fibres with hydroxyapatite crystals [82]. Bone also provides space for some other constituents such as bone cells and blood vessels. Bone fractures behave in contrasting kind of ways, and it can be classified into two types: internal fixation and external fixation. The external fixations are used when no need for surgery or can say that without any opening. On the other side, internal fixation required surgery for recovery of the fracture [83].

### **Drug Delivery System**

The biodegradable polymers are useful for drug delivery. There are some drawbacks of the oldest methods of drug delivery like injections or tablets. The most prominent way to drug delivery is that the drug is held in a polymer membrane or matrix and diffuses out into the implantation of the tissue. In some cases, the dissolution of the polymer contributes to the release mechanism. In these days, biodegradable polymers such as PLA are widely used for drug delivery system [32].

## **8.8 Conclusion**

Tissue engineering (TE) plays a significant role in the biomedical applications. The scaffolds have a great importance in the TE applications. These biological substitutes not only improve but also restore the basic tissue function by providing a healthy environment. Further, scaffolds assist in tissue's growth, cell attachment, proliferation and migration during in vivo and in vitro implantation. Additive manufacturing-based scaffold fabrication technique has showed its potential for manufacturing the scaffolds. However, design parameters are critical during the selection of the specific technique and this decision is made on the basis of cost, simplicity, biocompatibility and architecture characteristics (framework and porosity). The selection of the suitable biomaterial is another critically important parameter for the fabrication of the scaffolds. The materials processed with the FDM technique are limited owing to the lack of suitable thermal and viscoelastic properties. The parameters such as printing speed, infill pattern, infill percentage, build orientation, layer thickness and raster angle can be either software or user controlled. Development of the new design and hybrid biomaterial use has extended the applicability of the existing techniques with the addition of stem cells in the various tissue engineering applications.

## References

1. Bronzino JD (1999) Biomedical engineering handbook. CRC press
2. Leali PT, Merolli A (2009) Fundamentals of biomaterials. In: Merolli A, Joyce TJ (eds) Biomaterials in hand surgery. Springer, Milano. [https://link.springer.com/chapter/10.1007/978-88-470-1195-3\\_1](https://link.springer.com/chapter/10.1007/978-88-470-1195-3_1)
3. Laurencin C, Khan Y (eds) (2013) Regenerative engineering. CRC Press, Boca Raton. <https://doi.org/10.1201/b14925>
4. Klinkmann H, Wolf H, Schmitt E (2015) Definition of biocompatibility
5. Burg KJL, Porter S, Kellam JF (2000) Biomaterial developments for bone tissue engineering. Biomaterials. [https://doi.org/10.1016/S0142-9612\(00\)00102-2](https://doi.org/10.1016/S0142-9612(00)00102-2)
6. Karageorgiou V, Kaplan D (2005) Porosity of 3D biomaterial scaffolds and osteogenesis. Biomaterials
7. Chen Q, Thouas GA (2015) Metallic implant biomaterials. Mater Sci Eng R Rep 87:1–57
8. Saini M (2015) Implant biomaterials: a comprehensive review. World J Clin Cases. <https://doi.org/10.12998/wjcc.v3.i1.52>
9. von der Mark K, Park J (2013) Engineering biocompatible implant surfaces. Prog Mater Sci 58:327–381. <https://doi.org/10.1016/j.pmatsci.2012.09.002>
10. Puleo DA, Nanci A (1999) Understanding and controlling the bone-implant interface. Biomaterials 20:2311–2321
11. Publications S (2017) Parametric study of magnetic abrasive finishing of UNS C26000 flat brass plate. 9:83–89
12. Babbar A, Singh P, Farwaha HS (2017) Regression model and optimization of magnetic abrasive finishing of flat brass plate. Indian J Sci Technol 10:1–7. <https://doi.org/10.17485/ijst/2017/v10i31/i113860>
13. Sharma A, Babbar A, Jain V, Gupta D (2018) Enhancement of surface roughness for brittle material during rotary ultrasonic machining. In: Chang G (ed) MATEC Web of conferences. p 01006
14. Babbar A, Sharma A, Jain V, Jain AK (2019) Rotary ultrasonic milling of C/SiC composites fabricated using chemical vapor infiltration and needling technique. Mater Res Expr 6:085607. <https://doi.org/10.1088/2053-1591/ab1bf7>
15. Witte F, Eliezer A (2012) Biodegradable metals. Degradation of implant materials. Springer New York, New York, NY, pp 93–109
16. Prasad K, Bazaka O, Chua M et al (2017) Metallic biomaterials: current challenges and opportunities. Materials (Basel) 10:884. <https://doi.org/10.3390/ma10080884>
17. Kumar M, Babbar A, Sharma A, Shahi AS (2019) Effect of post weld thermal aging (PWTA) sensitization on micro-hardness and corrosion behavior of AISI 304 weld joints. J Phys: Conf Ser 1240:012078. <https://doi.org/10.1088/1742-6596/1240/1/012078>
18. Babbar A, Kumar A, Jain V, Gupta D (2019) Enhancement of activated tungsten inert gas (A-TIG) welding using multi-component TiO<sub>2</sub>-SiO<sub>2</sub>-Al<sub>2</sub>O<sub>3</sub> hybrid flux. Measurement 148:106912. <https://doi.org/10.1016/j.measurement.2019.106912>
19. Davis JR (2003) Handbook of materials for medical devices. ASM Int 205–216. <https://doi.org/10.1361/hmmd2003p001>
20. Shoichet MS (2010) Polymer scaffolds for biomaterials applications. Macromolecules. <https://doi.org/10.1021/ma901530r>
21. Balint R, Cassidy NJ, Cartmell SH (2014) Conductive polymers: towards a smart biomaterial for tissue engineering. Acta Biomater 10:2341–2353. <https://doi.org/10.1016/j.actbio.2014.02.015>
22. Cheung H-Y, Lau K-T, Lu T-P, Hui D (2007) A critical review on polymer-based bio-engineered materials for scaffold development. Compos Part B Eng 38:291–300. <https://doi.org/10.1016/j.compositesb.2006.06.014>
23. Cheung HY, Lau KT, Lu TP, Hui D (2007) A critical review on polymer-based bio-engineered materials for scaffold development. Compos Part B Eng. <https://doi.org/10.1016/j.compositesb.2006.06.014>

24. U MT (2011) Bioactive materials and tissue engineering. In: Bioactive materials in medicine. Elsevier, Amsterdam, pp 70–93
25. TU M (2011) Bioactive materials and tissue engineering. In: Bioactive materials in medicine: design and applications
26. Daculsi G, Baroth S, Sensebé L et al (2011) Association of cells and biomaterials for bone reconstruction. IRBM. <https://doi.org/10.1016/j.irbm.2011.01.031>
27. Kokubo T (2008) Bioceramics and their clinical applications. Woodhead Publishing Limited
28. Simchi A, Tamjid E, Pishbin F, Boccaccini AR (2011) Recent progress in inorganic and composite coatings with bactericidal capability for orthopaedic applications. *Nanomed Nanotechnol Biol Med*
29. Cormack AN, Tilocca A (2012) Structure and biological activity of glasses and ceramics. *Philos Trans R Soc A Math Phys Eng, Sci*
30. Cormack AN, Tilocca A (2012) Structure and biological activity of glasses and ceramics. *Philos Trans R Soc A Math Phys Eng Sci* 370:1271–1280. <https://doi.org/10.1098/rsta.2011.0371>
31. Singh S, Prakash C, Ramakrishna S (2019) 3D printing of polyether-ether-ketone for biomedical applications. *Eur Polym J* 114:234–248. <https://doi.org/10.1016/j.eurpolymj.2019.02.035>
32. Singh D, Babbar A, Jain V et al (2019) Synthesis, characterization, and bioactivity investigation of biomimetic biodegradable PLA scaffold fabricated by fused filament fabrication process. *J Braz Soc Mech Sci Eng* 41:121. <https://doi.org/10.1007/s40430-019-1625-y>
33. Baker BM, Gee AO, Metter RB et al (2008) The potential to improve cell infiltration in composite fiber-aligned electrospun scaffolds by the selective removal of sacrificial fibers. *Biomaterials*. <https://doi.org/10.1016/j.biomaterials.2008.01.032>
34. Yang H, Sun M, Zhou P et al (2011) Silk fibroins modify the atmospheric low temperature plasma-treated poly (3-hydroxybutyrate-co-3-hydroxyhexanoate) film for the application of cardiovascular tissue engineering. *J Biomed Sci Eng*. <https://doi.org/10.4236/jbise.2010.312149>
35. O'Brien FJ (2011) Biomaterials & scaffolds for tissue engineering. *Mater, Today*
36. Misra A (2017) Biotechnology: recent trends and emerging dimensions. CRC Press
37. Patel H, Bonde M, Srinivasan G (2011) Biodegradable polymer scaffold for tissue engineering. *Trends Biomater Artif Organs*
38. Wu S, Liu X, Yeung KWK et al (2014) Biomimetic porous scaffolds for bone tissue engineering. *Mater Sci Eng R Rep*
39. Hutmacher DW (2006) Scaffolds in tissue engineering bone and cartilage. In: *The Biomaterials: Silver Jubilee Compendium*
40. Deville S, Saiz E, Tomsia AP (2006) Freeze casting of hydroxyapatite scaffolds for bone tissue engineering. *Biomaterials* 27:5480–5489. <https://doi.org/10.1016/j.biomaterials.2006.06.028>
41. Makris EA, Gomoll AH, Malizos KN, et al (2015) Repair and tissue engineering techniques for articular cartilage. *Nat Rev Rheumatol*
42. Burg KJ, Porter S, Kellam JF (2000) Biomaterial developments for bone tissue engineering. *Biomaterials* 21:2347–2359. [https://doi.org/10.1016/S0142-9612\(00\)00102-2](https://doi.org/10.1016/S0142-9612(00)00102-2)
43. Bose S, Vahabzadeh S, Bandyopadhyay A (2013) Bone tissue engineering using 3D printing. *Mater, Today*
44. Vasita R, Katti DS (2006) Nanofibers and their applications in tissue engineering. *Int J Nanomedicine* 1:15–30. <https://doi.org/10.1155/2011/290602>
45. Jeon NJ, Noh JH, Kim YC et al (2014) Solvent engineering for high-performance inorganic–organic hybrid perovskite solar cells. *Nat Mater* 13:897–903. <https://doi.org/10.1038/nmat4014>
46. An J, Teoh JEM, Suntornd R, Chua CK (2015) Design and 3D printing of scaffolds and tissues. *Engineering*. <https://doi.org/10.15302/j-eng-2015061>
47. Murphy WL, Dennis RG, Kileny JL, Mooney DJ (2002) Salt fusion: an approach to improve pore interconnectivity within tissue engineering scaffolds. *Tissue Eng*. <https://doi.org/10.1089/107632702753503045>
48. Colosi C, Costantini M, Barbetta A et al (2013) Morphological comparison of PVA scaffolds obtained by gas foaming and microfluidic foaming techniques. *Langmuir* 29:82–91. <https://doi.org/10.1021/la303788z>

49. Kim T, Yoon J, Lee D, Park T (2006) Gas foamed open porous biodegradable polymeric microspheres. *Biomaterials* 27:152–159. <https://doi.org/10.1016/j.biomaterials.2005.05.081>
50. Castro-Aguirre E, Iniguez-Franco F, Samsudin H, Fang X, Auras R (2016) Poly(lactic acid)—mass production, processing, industrial applications, and end of life. *Adv Drug Deliv Rev* 107:333–366
51. Liu X, Ma PX (2004) Polymeric scaffolds for bone tissue engineering. *Ann Biomed Eng* 32:477–486
52. Józwick J, Ostrowski D, Milczarczyk R, Krolczyk GM (2018) Analysis of relation between the 3D printer laser beam power and the surface morphology properties in Ti–6Al–4 V titanium alloy parts. *J Braz Soc Mech Sci Eng* 40. <https://doi.org/10.1007/s40430-018-1144-2>
53. Wong KV, Hernandez A (2012) A review of additive manufacturing. *ISRN Mech Eng* 2012:1–10. <https://doi.org/10.5402/2012/208760>
54. Bhadeshia HKDH (2016) Additive manufacturing. *Mater Sci Technol* 32:615–616. <https://doi.org/10.1080/02670836.2016.1197523>
55. FUJIKAWA T (2014) Additive manufacturing technology. *J Japan Soc Powder Powder Metall* 61:216. <https://doi.org/10.2497/jjpspm.61.216>
56. Bartolo PJ (2013) Summary for policymakers. In: Intergovernmental Panel on Climate Change (ed) *Climate change 2013—the physical science basis*. Cambridge University Press, Cambridge, pp 1–30
57. Bartolo PJ, Mitchell G (2003) Stereo-thermal-lithography: a new principle for rapid prototyping. *Rapid Prototyp J* 9:150–156. <https://doi.org/10.1108/13552540310477454>
58. Taufik M, Jain PK (2014) Role of build orientation in layered manufacturing: a review. *Int J Manuf Technol Manag*. <https://doi.org/10.1504/ijmtm.2013.058637>
59. Kruth JP, Wang X, Laoui T, Froyen L (2003) Lasers and materials in selective laser sintering. *Assem Autom* 23:357–371. <https://doi.org/10.1108/01445150310698652>
60. Kruth J, Mercelis P, Van Vaerenbergh J et al (2005) Binding mechanisms in selective laser sintering and selective laser melting. *Rapid Prototyp J* 11:26–36. <https://doi.org/10.1108/13552540510573365>
61. Sohrabpoor H, Negi S, Shaiesteh H et al (2018) Optimizing selective laser sintering process by grey relational analysis and soft computing techniques. *Optik (Stuttg)*. <https://doi.org/10.1016/j.ijleo.2018.08.040>
62. Satyanarayana B, Prakash KJ (2015) Component replication using 3D printing technology. *Procedia Mater Sci* 10:263–269. <https://doi.org/10.1016/j.mspro.2015.06.049>
63. Decuir F, Phelan K, Hollins BC (2016) Mechanical strength of 3-D printed filaments. In: 2016 32nd Southern biomedical engineering conference (SBEC). IEEE, pp 47–48
64. Alafaghani A, Qattawi A (2018) Investigating the effect of fused deposition modeling processing parameters using Taguchi design of experiment method. *J Manuf Process* 36:164–174. <https://doi.org/10.1016/j.jmapro.2018.09.025>
65. Roopavath UK, Malferrari S, Van Haver A et al (2019) Optimization of extrusion based ceramic 3D printing process for complex bony designs. *Mater Des* 162:263–270. <https://doi.org/10.1016/j.matdes.2018.11.054>
66. Vaezi M, Seitz H, Yang S (2013) A review on 3D micro-additive manufacturing technologies. *Int J Adv Manuf Technol* 67:1721–1754. <https://doi.org/10.1007/s00170-012-4605-2>
67. Vaezi M, Seitz H, Yang S (2013) A review on 3D micro-additive manufacturing technologies. *Int J Adv Manuf Technol* 67(5–8):1721–1754
68. Wu W, Geng P, Li G et al (2015) Influence of layer thickness and raster angle on the mechanical properties of 3D-printed PEEK and a comparative mechanical study between PEEK and ABS. *Mater (Basel)*. <https://doi.org/10.3390/ma8095271>
69. Farah S, Anderson DG, Langer R (2016) Physical and mechanical properties of PLA, and their functions in widespread applications—a comprehensive review. *Adv Drug Deliv Rev* 107:367–392. <https://doi.org/10.1016/j.addr.2016.06.012>
70. Farah S, Anderson DG, Langer R (2016) Physical and mechanical properties of PLA, and their functions in widespread applications—a comprehensive review. *Adv Drug Deliv Rev* 107:367–392



71. Kamthai S, Magaraphan R (2015) Thermal and mechanical properties of polylactic acid (PLA) and bagasse carboxymethyl cellulose (CMC B) composite by adding isosorbide diesters. In: AIP conference proceedings, vol 1664(1). AIP Publishing LLC, p 060006
72. Hamad K, Kaseem M, Yang HW et al (2015) Properties and medical applications of polylactic acid: a review. *Express Polym Lett* 9:435–455. <https://doi.org/10.3144/expresspolymlett.2015.42>
73. Hamad K, Kaseem M, Yang HW et al (2015) Properties and medical applications of polylactic acid: a review. *Express Polym Lett*. <https://doi.org/10.3144/expresspolymlett.2015.42>
74. Babbar A, Jain V, Gupta D (2019) Neurosurgical bone grinding. *Bio manufacturing*. Springer International Publishing, Cham, pp 137–155
75. Singh G, Jain V, Gupta D, Ghai A (2016) Optimization of process parameters for drilled hole quality characteristics during cortical bone drilling using Taguchi method. *J Mech Behav Biomed Mater* 62:355–365. <https://doi.org/10.1016/j.jmbbm.2016.05.015>
76. Singh G, Jain V, Gupta D, Sharma A (2018) Parametric effect of vibrational drilling on osteonecrosis and comparative histopathology study with conventional drilling of cortical bone. *Proc Inst Mech Eng Part H J Eng Med* 232:975–986. <https://doi.org/10.1177/0954411918794983>
77. Singh G, Jain V, Gupta D (2017) Multi-objective performance investigation of orthopaedic bone drilling using Taguchi membership function. *Proc Inst Mech Eng Part H J Eng Med* 231:1133–1139. <https://doi.org/10.1177/0954411917735129>
78. Banoriya D, Purohit R, Dwivedi RK (2017) Advanced application of polymer based biomaterials. In: *Materials today: proceedings* 4(2):3534–3541
79. Jana S, Tefft BJ, Spoon DB, Simari RD (2014) Scaffolds for tissue engineering of cardiac valves. *Acta Biomater* 10:2877–2893. <https://doi.org/10.1016/j.actbio.2014.03.014>
80. Martin DM, Boyle FJ (2011) Drug-eluting stents for coronary artery disease: A review. *Med Eng, Phys*
81. Moore SS, O’Sullivan KJ, Verdecchia F (2016) Shrinking the supply chain for implantable coronary stent devices. *Ann Biomed Eng*. <https://doi.org/10.1007/s10439-015-1471-8>
82. Enderle JD, Bronzino JD (2012) *Introduction to biomedical engineering*. Academic press
83. Ong K, Yun M, White J (2015) New biomaterials for orthopedic implants. *Orthop Res Rev*. <https://doi.org/10.2147/orr.s63437>

**Mr. Atul Babbar**, Ph.D. Research Scholar, Mechanical Engineering Department, Thapar Institute of Engineering and Technology, Patiala, India. He has been working on osteonecrosis and neurosurgical bone grinding operations for the treatment of benign and cancerous brain tumors. His core research area is biomedical machining and working on novel ways of bone machining for preventing deleterious consequences due to thermogenesis.

**Dr. Vivek Jain** is currently Associate Professor in the Department of Mechanical Engineering at the Thapar Institute of Engineering and Technology, Patiala, India. He has 14 years of teaching and industrial experience. He obtained his Bachelor’s Degree in Mechanical Engineering from Rajiv Gandhi College of Engineering, Research and Technology, Chandrapur-442 403 (Maharashtra), formally (Chandrapur Engineering College, Chandrapur) India, and Master’s from Guru Nanak Dev Engineering College, Ludhiana, Punjab. He completed his Doctoral Degrees from the Indian Institute of Technology Roorkee, India. He has guided two doctoral thesis and 22 M.Tech dissertations and is currently supervising four doctoral theses and 03 more M.Tech dissertations. He has published more than 40 articles in journals and conferences. He is a reviewer for various international/national journals. He has filed three Indian patent. He has completed two internally funded research projects. Currently, he is Co-Principal Investigator for one SERB-DST funded project.



**Dr. Dheeraj Gupta** is currently Associate Professor in the Department of Mechanical Engineering at the Thapar Institute of Engineering and Technology, Patiala, India. He has 10 years of teaching and research experience. He obtained his Bachelor's Degree in Mechanical Engineering from Shri Govindram Seksaria Institute of Technology and Science, Indore, India, and Master's and Doctoral Degrees from the Indian Institute of Technology Roorkee, India. He has guided 02 Ph.D. and 17 M.Tech dissertations and is currently supervising four doctoral theses and three more M.Tech dissertation. He has published more than 70 articles in journals and conferences. He is a reviewer to various international journals. He has filed two Indian patent. He has completed two internally funded research projects. Currently, he is Principal Investigator for one SERB-DST funded project.

**Dr. Sunpreet Singh** is post-doc fellow in the School of Mechanical Engineering, National Univeristy of Singapore, Singapore. He has received Ph.D in Mechanical Engineering from Guru Nanak Dev Engineering College, Ludhiana, India. His area of research is additive manufacturing and application of 3D printing for development of new biomaterials for clinical applications. He has contributed extensively in additive manufacturing literature with publications appearing in Journal of Manufacturing Processes, Composite Part B, Rapid Prototyping Journal, Journal of Mechanical Science and Technology, Measurement, International Journal of Advance Manufacturing Technology, and Journal of Cleaner Production. He authored 10 chapters and monographs. He is working with joint collaboration with Prof. Seeram Ramakrishna, NUS Nanoscience and Nanotechnology Initiative and Prof. Rupinder Singh, Manufacturing Research Lab, GNDEC, Ludhiana.

**Dr. Chander Prakash** is Associate Professor in the School of Mechanical Engineering, Lovely Professional University, Jalandhar, India. He has received Ph.D in Mechanical Engineering from Panjab University, Chandigarh, India. His area of research is biomaterials, rapid prototyping and 3-D printing, advanced manufacturing, modeling, simulation, and optimization. He has more than 11 years of teaching experience and 6 years research experience. He has contributed extensively to the world in the titanium- and magnesium-based implant literature with publications appearing in Surface and Coating Technology, Materials and Manufacturing Processes, Journal of Materials Engineering and Performance, Journal of Mechanical Science and Technology, Nanoscience and Nanotechnology Letters, Proceedings of the Institution of Mechanical Engineers, Part B: Journal of Engineering Manufacture. He authored 50 research papers and 10 chapters. He is also Editor of three books: "Current Trends in Bio-manufacturing", Springer Series in Advanced Manufacturing, Springer International Publishing AG, Gewerbestrasse 11, 6330 Cham, Switzerland., Dec. 2018; "3D Printing in Biomedical Engineering", Book series Materials Horizons: From Nature to Nanomaterials, Springer International Publishing AG, Gewerbestrasse 11, 6330 Cham, Switzerland., August 2019, and "Biomaterials in Orthopaedics and Bone Regeneration—Design and Synthesis", Book series Materials Horizons: From Nature to Nanomaterials, Springer International Publishing AG, Gewerbestrasse 11, 6330 Cham, Switzerland., March 2019. He is also Guest Editor of three journals: Guest Editor of Special Issue of "Functional Materials and Advanced Manufacturing", Facta Universitatis, Series: Mechanical Engineering (Scopus Index), Materials Science Forum (Scopus Index), and Special Issue on "Metrology in Materials and Advanced Manufacturing", Measurement and Control (SCI indexed).

**Dr. Catalin Pruncu** is a Research Fellow with a keen interest in design mechanics, solid mechanics, fracture mechanics, tribology, microstructure characterization and finite element modelling (FEM). Dr. Catalin has good experience in virtual engineering and experimental testing methodology from fundamental to applied research. Dr. Pruncu really enjoys working in successful partnerships with different colleagues, especially where he performs research across disciplines, having the possibility to share ideas and learn from each other.

# Chapter 9

## Rapid Prototyping Methods in Manufacturing of Biomedical Implants: A Review



Ajith Gopinath, Tobias Waclawczyk, Raman Bedi, Avinash Babu,  
Shijo Thomas, and Praise Tom

### Nomenclature

FDM	Fused deposition modeling
CT	Computerized tomography
MRI	Magnetic resonance imaging
SLA	Stereolithography
SLM	Selective laser melting
SLS	Selective laser sintering
DLP	Digital light processing
CAD	Computer-aided design
UV	Ultra violet
FEA	Finite element analysis
RP	Rapid prototyping
PP	Polypropylene
2D	Two dimensional
3D	Three dimensional
AM	Additive manufacturing.

---

A. Gopinath (✉) · R. Bedi · A. Babu · S. Thomas · P. Tom  
Christ Deemed to be University, Bengaluru 560029, India  
e-mail: [ajith.gopinath@christuniversity.in](mailto:ajith.gopinath@christuniversity.in)

T. Waclawczyk  
University of Augsburg, Augsburg 86159, Germany

© Springer Nature Singapore Pte Ltd. 2020  
S. Singh et al. (eds.), *3D Printing in Biomedical Engineering*,  
Materials Horizons: From Nature to Nanomaterials,  
[https://doi.org/10.1007/978-981-15-5424-7\\_9](https://doi.org/10.1007/978-981-15-5424-7_9)

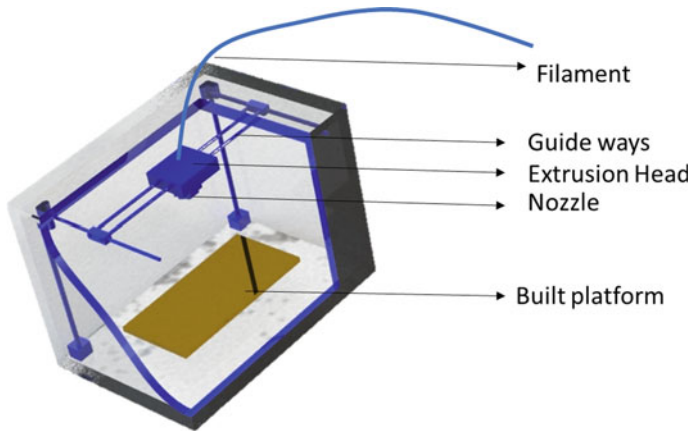
## 9.1 Introduction

Biomedical implants are a constantly improving market. The biomedical implants, due to its specificity to each patient and the high degree of accuracy required, must be of extremely high quality. Constant researches have been happening in this field for the manufacturing and development of the bio-implants. The methods of manufacturing have evolved over centuries, and additive manufacturing is one of the most advanced and sophisticated methods by which the bio-implants can be manufactured without compromising on the quality and the properties. Additive manufacturing can be deployed to manufacture the various functional parts in a much faster way. Additive manufacturing through intensive research over two decades has found its application in energy, aerospace, biomedical, automotive, and other fields. The addition of material layer by layer finds answer for much complex geometries which could not be achieved with the conventional processes [1]. The dimensional accuracy obtained is much higher when compared to the traditional methods of manufacturing. The technique can be subdivided into different categories based on the state of precursor material or raw material such as liquid-based, powder-based, and solid-based. Stereolithography, selective laser sintering, and 3D printing are some of the widely used manufacturing techniques [2].

Fused deposition modeling is one of the additive manufacturing techniques in which the input material is solid. The machine consists of an extrusion head which heats up the solid wire fed into it and thereby depositing it one over the other in layers to complete a 3D model. The guide ways facilitate the movement of the extrusion head in  $X$ ,  $Y$ , and  $Z$  axes [3]. Additive manufacturing finds its application in biomedical field because of the accurate manufacturability of specific parts. The rapid prototyping techniques have been used during the last two decades to manufacture biocompatible scaffolds and custom-made medical implants, using polymer-derived composites, ceramics, and other biocompatible materials (Fig. 9.1).

Recent advancement in the biomedical application has shown the manufacture of biodegradable composites as the implant material used in tissue engineering. Some of the advantages of rapid prototyping over the conventional methods of manufacture are the dimensional accuracy and reproducibility along with the freedom in custom shaping and sizing which can be used for the manufacture of tuned pores of numerous scales and forms [4].

Ceramics have also been an area of constant research since its inception centuries ago. The traditional and engineering ceramics are manufactured in numerous ways; however, these techniques are laborious and expensive in nature. In many of the researches, high-density alumina were used as the material for manufacturing the bio-implants for the joints because of various properties such as bio-inertness, abrasion resistance, strength, and chemical inertness, whereas bio-implants for spinal fusion was manufactured with bioglass/glass ceramic because of its superior mechanical properties, good biocompatibility, and nontoxicity. Additive manufacturing process has proven to be very flexible since more than one processes can be combined for the fabrication of finished components with a variety of materials such as zirconia



**Fig. 9.1** Schematic representation of rapid prototyping apparatus, fused deposition modeling machine (FDM)

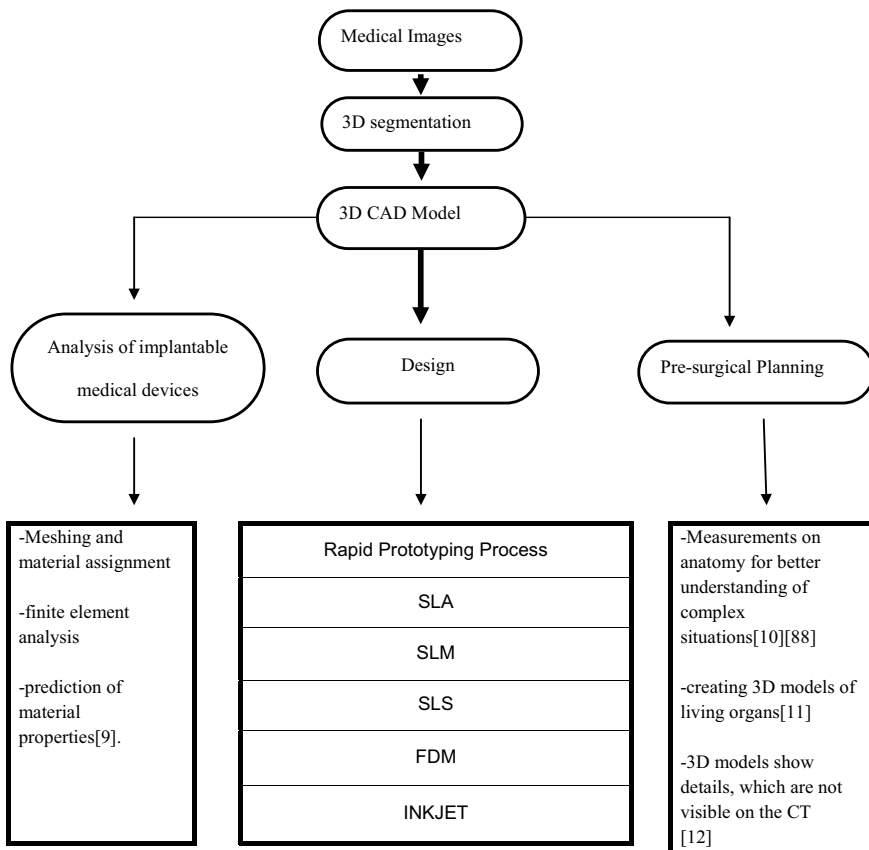
and alumina [5]. Additive manufactured bones have to be rough in order to facilitate better attachment with the tissues [1]. Fracture rate was found to reduce when zirconia was added to aluminum, thus making monolithic ceramic prosthesis more reliable. Reduction in wear rate was also observed for the ceramic composite hip implants when compared to others [6]. Many methodologies were assessed by the authors for the fabrication of the monolithic ceramic components with multiscale porosity and varied morphology for different industrial applications [7].

Particulate setting instead of being suspended in liquid resin, pore generation during bubble formation, and longer curing time are the major problems while fabricating monolithic ceramic materials. Some of the problems can be get rid of by optoform process in which a paste is used instead of photopolymer liquid [8]. Polysiloxane due to its bio-inertness and nontoxic nature have been a preferred material in many biomedical and cosmetic applications [9]. Additive manufacturing provides more flexibility in manufacturing and finds numerous applications such as the manufacturing of prosthesis and complex automobile components. The manufacturing of prostheses requires high technical expertise and dimensional accuracy. The fabrication of the prostheses with conventional casting method is time-consuming and is a tedious process which is eliminated by the advent of additive manufacturing.

## 9.2 Methodology of 3D Printing for Bio-Implant Manufacturing

Biomedical field has seen vast improvements in the area of implant manufacturing after the advent of rapid prototyping into the sector. The materials used for the process are also varied in scope of improving the properties of the implant. The

patient-specific implants can be manufactured with the help of rapid prototyping as explained in Fig. 9.2. The CT scan/MRI imaging provides the 3D model of the bio-implant required which is then converted to the STL format with interface software. Analysis of the 3D cad model can be done to simulate the working of the organ. However, before the actual printing of the material, a presurgical planning is done to understand the anatomy of the material in times of complex situations. Even it can be used to create 3D models of living organs which show details invisible in CT scan [10–12]. Dimensional deviation and surface roughness are two conflicting results when the number of layers is considered as the deciding parameter [13]. The rapid prototyping is even used for the treatment of traumatic injuries and cancerous injuries in bones [14].



**Fig. 9.2** Flowchart of the process of bio-implant manufacturing by rapid prototyping

### 9.3 Material and Process Parameters for Different Rapid Prototyping Methods

#### 9.3.1 Stereolithography

Stereolithography is a liquid-based additive manufacturing technique in which the resin is cured with a UV light source to form the required shape as per the CAD model. UV curable resin is deployed in VAT tray for this process, and UV light is made to fall on the thin layer of resin over the loaded tray. The layer cures, and then, the platform is displaced vertically by a very small distance, in micrometers, so that another layer of liquid comes above the cured layer of resin, which is then cured by the UV light. This process continues until a perfect solid shape is obtained. A KUDO stereolithography machines is shown in Fig. 9.3.

The dimensional accuracy of the solid is attributed to the layer thickness of the solid manufactured. Similar operations are performed in the other techniques, but instead the UV light laser is used in selective laser sintering, whereas in 3D printing, binder is used to bind the powder together which is then postsintered to obtain the final component [1].

The scientists have reported the fabrication of carbon fiber tows of 10 mm where the liquid precursor was injected to one end of the tow which was then dried and pyrolyzed under infrared radiation furnace made with 650 W, JCD-G5.3 halogen. Specimen was then cooled and returned to injector for next cycle. Next specimens were made with 8, 16, 40, and 80 cycles of infiltration. In order to avoid crack formation, specific care was taken. The layers have to be very thin to facilitate flash pyrolysis. Flash pyrolysis is an advanced method in which each layer is exposed to infrared radiation for a few seconds which avoids the need of sintering the green mould [15]. Computed tomographic (CT) data can be converted into a format that can be used by any 3D printer. Hydroxyapatite cannot be cured by the laser only



Fig. 9.3 Stereolithography KUDO 3D printing machine

the resin, which functioned as a binder. But the 3D modeling software gives the opportunity of using crosshatch patterns to regulate the porosity inside the implant. The resin was burnt out afterwards and the result was the hydroxyapatite prosthesis [16].

A hybrid steriolithography/3D printing process was deployed to fabricate 3D structures with electronic circuits embedded in it. The process consisted of multiple starts and stops and multiple intermediate processes. The uncured resin was removed, and electronic circuits were embedded into it, and further processes were done to manufacture the complete part [17]. The demonstration of the practical applicability of the silicone-alginate composite as an implant material was shown by manufacturing an electrode. The implantable silicone electrode or myoplant electrode from Lewis et al. was used as a model, with which myogenic signals can be detected. This electrode consists of two silicone layers glued together. The implant consisted out of two composite layers between which two electrode contacts were embedded. The structure and geometry of the implant were based on an implantable silicone electrode. Myoplant electrodes have already been successfully used to derive myogenic signals. Indirect rapid prototyping method was used in this case to manufacture the mould for making the myoplant electrodes [18].

One of the researchers has carried out the morphological characterization of the transitional structure between bone and cartilage, and the data were used to fabricate beta tricalcium phosphate scaffold using steriolithography and gel casting. The scaffold fabricated had 700–900  $\mu\text{m}$  pore size, 50–65% porosity, and 12 MPa compressive strength [19].

Stereolithography enables to construct plastic models with the exact valvular design of human aortic and pulmonary homografts. These stereolithographic models were then used as physiologic patterns to generate scaffolds for the tissue engineering of heart valves [20] (Table 9.1).

Steriolithography is one of the most commonly available types of rapid prototyping. It is comparatively less costly to other rapid manufacturing techniques. However, the need of postprocessing is inevitable in this kind of manufacturing. The method is suited for the manufacture of ceramics. This can be achieved by using alumina/zirconia as fillers in the photosensitive resin and photoinitiators. Once the monomers start the polymerization and the final shape is achieved, the part is subjected to sintering or postprocessing during which the final part of the ceramic material is obtained devoid of the photopolymers [21–23].

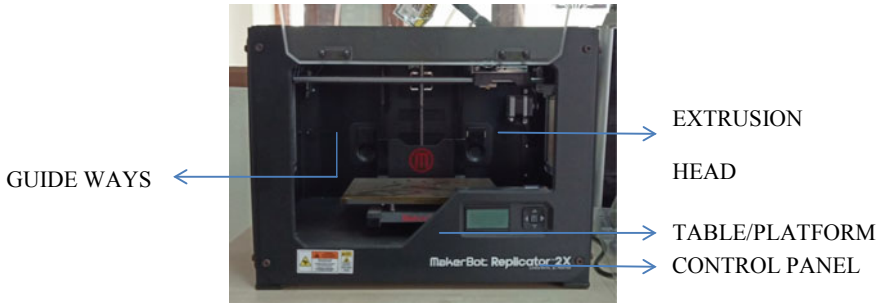
## 9.4 Fused Deposition Modeling

Fused deposition modeling [FDM] is one of the rapid prototyping processes where solid starting material is also used along with the liquid precursor (Fig. 9.4). In this technique, a nozzle is the main component, which is attached on a movable head. Through this nozzle, the material is fed on to the tray. The material as filament is fed into the head, which is heated up to a desired temperature. The temperature right

**Table 9.1** Process parameters and material specifications chosen for different applications in stereolithography

Application/implant	Process parameters	Material used	Material properties	References
Orbital floor prosthesis	Section thickness, thickness, threshold value, imaging plane, and reconstruction algorithm (3)	Hydroxyapatite	Biocompatible and osteoconductive, slow to biodegrade	[16]
Osteochondral beta-tricalcium phosphate/collagen scaffold	Laser power, scan speed, laser spot size	$\beta$ -TCP-collagen	Biocompatibility, mechanical strength	[19]
Polymer/alumina composite components	Orientation, size of access holes to relieve the viscous resin stuck inside the structure	$\alpha$ -Alumina—Filler, (polyethylene glycol 400 diacrylate, SR344 Cray Valley)—photosensitive resin, (2-2dimethoxy-2-phenylacetophenone, Fluka)—Photo Initiator	Mechanical strength, shrinkage factor	[21–23]





**Fig. 9.4** Second-generation maker bot, fused deposition modeling machine

above the melting point melts the material and enables the layer-by-layer deposition to culminate the final 3D component. Multi nozzles are also used in current researches to deposit different materials. This enables that, e.g., solids, like scaffolds can be manufactured along with complex cell constructs with different properties and characteristics [6, 12]. Considering the specific energy that is used for incompressible melting has FDM printing differences compared to other additive manufacturing techniques. As a result of which the following equation is essential for the whole process:

$$\rho c_p \left( \frac{dT}{dt} + ((\vec{v}) \cdot \nabla) T \right) = -\nabla \cdot \vec{q} - (\vec{\tau} \cdot \nabla \vec{v}) + \phi$$

$\rho$  = density,  $p$  = applied pressure,  $T$  = temperature,  $\tau$  = surface force,  $v$  = velocity,  $\phi$  = internal energy,  $q$  = energy per unit time and volume [24].

Fused deposition modeling even after being one of the most widely used rapid prototyping methods is used rarely for the manufacture of biomedical implants. This is due to the fact that plastic materials that are compatible with the machine are often not biocompatible. The plastic materials have reactions with the living tissues which can cause problems in the longer run. Hence, this method is usually adapted to manufacture patterns and molds for manufacturing the original part. However, with the usage of suitable materials, bio-implants have also been manufactured. The lower costs of manufacturing and the comparatively simpler process are some of the advantages of this type of rapid prototyping (Table 9.2).

### 9.4.1 Selective Laser Melting

Additive manufacturing finds wide application in the field of biomedical as the recent advancements in the technology facilitates it to manufacture bioscaffolds for tissue

**Table 9.2** Process parameters and material specifications chosen for different applications of fused deposition modeling

Application	Process parameters	Material used	References
Cranial implants, femur bone	Size of granules, nozzle design, inlet and exit temperature of material, speed of deposition, layer orientation, tip wipe frequency, and porosity	PMMA (polymethyl methacrylate)	[87]
Hip joint pattern		acrylonitrile butadiene styrene	[88]
Composite scaffolds		PP-TCP composite	[3, 89]

engineering, artificial organs, orthopedic implants, etc. Ti6Al4V with tailored properties to mimic that of a bone has been manufactured as well as replacement for hip was manufactured with Ti material [25–27]. SLM has been used to manufacture ceramic materials as well as the implant parts with biocompatible alloys of metals. The use of rapid prototyping provides the versatility in the processes such that the difficult internal architectures are managed and the reproducibility of the work is very high. The process can be used both as a direct method of manufacture and as an indirect method by manufacturing the molds for manufacturing the implant [10, 28–30].

The CAD model of the part to be manufactured has to be fed into the machine in STL format. 3D printing and selective laser melting are powder-based additive manufacturing processes and in 3D printing very thin layer of powder is deposited on top of the tray and binder is added on top of it. Here, binder plays a very vital role to solidify the material and the process will be continued till a complete solid structure is obtained [31].

Flexible geometry and a shorter processing time are the major advantages of 3D printing over other conventional manufacturing methods. However, the challenges in this process will be the higher melting point of the ceramics, which is one of the frequently used biomaterial, when compared to that of the metals and polymers, and the development of cracks during solidification [6] (Table 9.3).

### 9.4.2 Inkjet Printing

The inkjet printing technique is based on 2D printing layer by layer. A suspension which contains the finest particles is printed in the drop form. The main challenge of the ink development is to reduce the particle size to enable a resolution in the range of 16–50 μm. By shifting the print heads in the z-axis, layers are created by repeated printing of drops. A postprocessing procedure is required to obtain properties similar to those of the pressed material [32, 33]. Common procedures are sintering, cooling (e.g., by crystallization), or chemical changes (e.g., crosslinked network of polymers through UV—curing) [34].

**Table 9.3** Process parameters and material specifications chosen for different applications for selective laser melting

Application/implant	Process parameters	Material used	Material properties	References
High strength oxide ceramics	Preheating temperature of 1600 °C, particle shape (spherical shape), scanning speed: 200 mm/s. Laser beam diameter: 200 mm. Layer thickness: 50 mm	ZrO <sub>2</sub> /Al <sub>2</sub> O <sub>3</sub> powder	Good flexural properties	[31, 66]
Dental implants	Pore size, strut thickness, dense core of different diameters	Ti6Al4V	Good biocompatibility, high corrosion resistance, and high strength-to-weight ratio	[67]
Metal components	Surface structure of metallic powder, porosity of powder bed, vaporization, and heat loss	Ti and Ti alloys, Ni-based superalloys	Laser absorptivity	[90]
Titanium gyroid scaffolds	Particle shape and size	Pure titanium (CP-Ti) and Ti-6Al-4V (Ti64)	Biocompatibility, specific strength, corrosion resistance	[91]

Inkjet printing has frequently been used in the field of bioengineering, especially in bioprinting with excellent outcomes of DNA chips [35], protein arrays [36] and cell patterns [36] or direct printing of enzymes [37]. However, not much researches have been conducted on the fabrication of biomedical implants [38].

Liravi F et al. was the first research group who introduced a direct additive manufacturing of polysiloxane through inkjet printing. Polysiloxane due to its bio-inertness and nontoxic nature has been a preferred material in many biomedical and cosmetic applications. Before the first research group began, the unique properties of the material have only been used to manufacture casting moulds, which are an ineffective and knowledge-based process. With the use of additive manufacturing techniques, the whole process got optimized and reduced the production time radically. The

**Table 9.4** Process parameters and material specifications chosen for different applications for inkjet printing

Application/implant	Process parameters	Material used	Material properties	References
3D-printed cardiac model, aortic arch reconstruction	Layer thickness	Rigid plastic material	Mechanical strength and plasticity	[39, 74]
Viable mammalian cells	Nozzle temperature, volume of print droplet	Chinese Hamster Ovary (CHO-B2) cells, primary embryonic motoneurons	Cell generation capability	[92]
Protein microdeposition	Droplet diameter	Horseradish peroxidase	Immunologic and hybridization reactions capability	[75, 37]

research group optimized the process parameters by employing design of experiments required for the fabrication of the prostheses. The process parameters which were considered and optimized for the fabrication of the prostheses were pressure ( $P$ ), printing velocity ( $V$ ), and working distance (WD) (distance between substrate and nozzle tip) [9] (Table 9.4).

The applications of 3D inkjet printing are not just limited to the printing of the implants but it also has helped in simulation training of heart, where the doctors printed a 3D model for presurgical planning and understood the intricate patient-specific features and could complete the surgery with better precision [39].

### 9.4.3 Selective Laser Sintering

Selective laser sintering is a type of additive manufacturing process in which the powder is sprayed as a thin layer which is then solidified by a laser which is selectively used to bind the material together at the desired places. After each layer is deposited, the tray is moved by some nanometers down and another layer of powder is deposited on top of the already fused solid, which is then again melted and binded together by the laser. One of the advantages of the selective laser sintering is that it does not require support structure unlike the other processes like FDM. The raw material itself will act as the supporting material [40–45] (Table 9.5).

Most of the scientists have used selective laser sintering for printing bioscaffolds. This is an integral part of tissue engineering. Tissue engineering works by the principle of coaxing different cell types into synthesizing new tissue. For this, they are seeded onto a desirable 3D hydrogel scaffold under specific favorable environment conditions. Thus, they can even be grown into fully functional organs [46]. The 3D model can be even subjected to FEA analysis to predict the failure. Material can

**Table 9.5** Process parameters and material specifications chosen for different applications for selective laser sintering

Application/implant	Process parameters	Material used	Material properties	References
Biopolymer scaffolds	Laser power, scan spacing, laser energy density, scanning speed	Poly(3-hydroxybutyrate-co-3-hydroxyvalerate), titanium powder and silica sol, polyamide PA-2200	Favorable surface chemistry for cell attachment and proliferation, biocompatibility, bioactivity, biodegradability	[70–73]

be assigned to the model and meshing can be done thereby predicting the material properties [9].

There are many other scientists who have made modifications on the existing 3D printing machines to obtain the desired results. Sahmani et al. [47] tested open porous nanoclay biocomposite scaffolds fabricated using space holder technique for bone implants. Because of less mechanical and chemical stability, these scaffolds cannot be used for load bearing applications, and Liu et al. [48] fabricated a scaffold based on polysaccharides for the same application. Akash et al. [49] found that the tensile and flexural strength of a hybrid composite made with silk fiber reinforcement matches to that of femur bone and hence is a suitable implant material, and Chan et al. [50] studied various properties of composites reinforced with glass fibers. Hu et al. [51] studied the mechanical properties and microstructure of composites developed based on the structure of skin of a fish and observed that addition of Ti increased the toughness of the composite. Ramesha [52] reviewed plant fiber based biocomposites and found that the mechanical properties were enhanced when fibers were treated with different alkaline solutions. Sahmani et al. [53] studied the vibrational effect on the nanocomposite implant subjected to axial compression in prebuckling and postbuckling regions, whereas Yang et al. [54] developed bio-implants that can be used for theranostics for cancer patients.

The applications of rapid prototyping are not just limited to printing implants and parts but also to health monitoring devices. Sharma et al. [55] used RP method to produce health monitoring devices which may be inserted inside the human body and hence can be used for patients with chronic diseases so that the process of recovery can be closely monitored. Wang et al. [56] attempted to convert 2D biomedical images to 3D using rapid prototyping technique. Shreepad et al. [57] studied the structural and mechanical properties of the scaffolds produced using RP technique and observed that the properties nearly match to those of human bones and teeth. Whitley et al. [58] presented a clinical report based on the dental implants fabricated in the laboratory using stereolithographic printing, and Robinson et al. [59] analyzed the potential of additive manufacturing technique for application in different fields.

More researches have happened, and many authors have compared, analyzed, and modified rapid prototyping based on applications and methods. One of the additive manufacturing processes which is called as rapid freeze casting is used to make solids of ice by the principle of layer by layer manufacturing, where water droplets are deposited over the already solidified layers of solid [13–16]. Researchers have done considerable amount of work in developing the method to fabricate ceramic and metal components with suspended particles of ceramics and metals in the photo-curable resin [8, 22, 23, 60, 61].

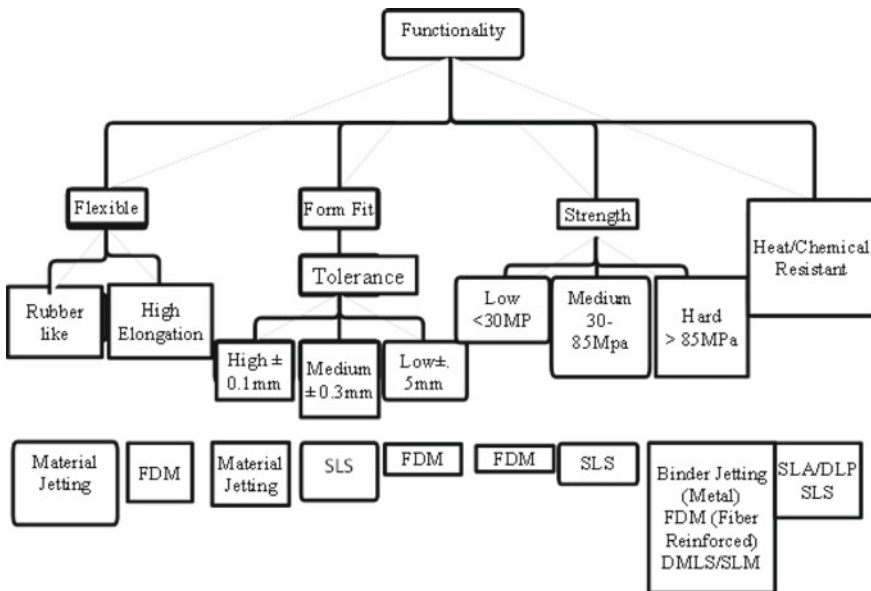
Banoriya et al. [62] reviewed the use of rapid prototyping method [62] in various fields and gave insight of how it can be used for making scaffolds in biomedical applications, whereas Kochan et al. [63] highlighted the problems faced relating to rapid prototyping technique (machine design, rapid tooling, product development, etc.). Lal et al. [64] reviewed the biocomposites fabricated using 3D printing technique via rapid prototyping for orthopedic trauma surgery.

### 9.5 Discussion

Figure 9.5 classifies the rapid prototyping methods on the basis of the functionality. Biomedical implants on the basis of their rigidity have been classified into flexible, form fit, strength, heat/chemical resistant. This chart has been prepared to categorize the methods that can be used for the specific needs.

Flexible implants are often manufactured with material jetting and fused deposition modeling. Material jetting can also be used to manufacture materials with higher tolerance values. The material which requires lower tolerance is manufactured with FDM. Based on the strength factor, harder materials are manufactured with binder jetting and ones with lower strength are contrived with FDM [9]. SLA/SLS is used to produce heat and chemical resistant parts. Considering the functionality of the product on the specific application the researcher has to choose his 3D printing technology based on these parameters. Bio-implants in the body are having different functions. For instance, a knee cap has to be strong as well as slightly flexible. So based on the functionality of the implant a suitable 3D printing technology, fused deposition modeling or selective laser sintering can be the preferred method adopted for this application.

High strength implants can be manufactured by fused deposition modeling, selective laser sintering/melting, and inkjet printing. DMLS or direct metal laser melting is also a kind of selective laser melting where metal components are printed. This is one of the latest technologies used and is considered to be the future of 3D printing.



**Fig. 9.5** Classification of rapid prototyping methods based on functionality of the bio-implants manufactured

Table 9.6 compiles and compares different rapid prototyping methods based on its application, materials used in each process, the resolution of the printing, the cost incurred for the process, and advantages and disadvantages for the process. Selective laser sintering is mostly used to manufacture bioscaffolds and dental implants. The cost of the process is higher when compared to the other processes because of the involvement of laser and the postprocessing of the product. One of the main advantages of this process is that a wide range of materials can be used for this process. However, the powdery surface texture is a demerit of the process [44, 29, 65].

Selective laser melting is also comparatively costlier process since a high intensity laser is required which melts and fuses the powders together. Metal powders and ceramic powders are the starting material in this process, and 20–100  $\mu\text{m}$  thickness is possible with this process. High strength oxide ceramics, metal components, and scaffolds are usually manufactured with this process. Higher cost and postprocessing are the demerits of this process, whereas the higher strength and the higher complexity of the components manufactured are an added advantage [31, 66, 67].

Steriolithography is comparatively a less expensive process to manufacture products with good surface finish and accuracy. The lesser cost and the comparative ease of the process make it a desirable candidate for many researchers. Myoplast electrodes, orbital floor prosthesis, hemi knee joint mould, cranio-plastic implant, and surgical drilling templates are some of the biomedical applications where steriolithography is used for. The SLA printing has a resolution of 5–50  $\mu\text{m}$  [55, 58, 68, 69]. The scattering of the light and the curing time of each layer is one of the main challenges in this kind of printing.

Fused deposition modeling uses solid material as the raw material for printing. The materials used for the process are acrylonitrile butadiene styrene or PLA material. This limits its flexibility in the biomedical field. However, the lesser cost of the process and the simplicity of the machine have resulted in wide acceptance of the machine among the research field. Mostly, FDM is used to manufacture plastic components and is mostly suited for automotive and general engineering applications. In biomedical field, FDM is used to manufacture bioscaffolds mostly which allows the tissue growth. One of the main advantages for this process is the lower cost and the higher mechanical strength of the parts produced, whereas the high temperature required to melt the solid wires is one of the challenges in this type of prototyping [70–73].

Inkjet printing is one the most advanced forms of 3D printing which is the most versatile prototyping method when compared to the other methods. This type of printing can use a variety of starting materials such as polysiloxanes, wax, cells, and enzymes. This versatility is the biggest advantage of inkjet printing.

In Table 9.6, '\$' symbol indicates comparative cost, with \$ being least and \$\$\$\$ being the maximum. Products with different porosity and plasticity can be printed with this type of manufacturing method. This method has the following advantages like the highest accuracy, surface finish, and the least time for manufacturing. However, the cost of the machine, installation, and maintenance is very high. The layer thickness can be from 16 to 50  $\mu\text{m}$  [9, 37, 39, 74, 75].



**Table 9.6** Comparison of rapid prototyping methods on the basis of materials used, resolution, cost, advantages, and disadvantages

RP technology	Bio-application	Materials	Resolution ( $\mu\text{m}$ )	Approximate cost	Advantages	Disadvantages	References
SLS	Bespoke dental implants, bone scaffold (hip joint, knee)	CoCr, bioactive glass	50–100	\$\$\$	Broad range of materials available, good mechanical properties	Powdery surface	[29, 44, 65]
SLA	Myoplast electrodes, orbital floor prosthesis, hemi knee joint mould, cranio-plastic implant, surgical drilling templates	Hydroxy-apatite (HA) SL Y-C 9300 “Stereocoll” silicone-alginate composite	0.5–50	\$\$	High accuracy, smooth surface	Limited use for mechanical parts	[55, 58, 68, 69]
FDM	Hip joint, composite scaffolds	Thermoplastic filament, SS316L, acrylonitrile butadiene styrene, PP-TCP	250–700	\$	High mechanical strength, low cost	High temperature during printing required	[13, 93]
SLM	High strength oxide ceramics, dental implants, metal component, titanium gyroid scaffolds	Metal powders, ceramic powders	20–100	\$\$\$\$	Highest mechanical strength, variety of complex forms possible	Highest price, postprocessing required	[31, 66, 67]
Inkjet	Wax template, prosthesis	Polysiloxane	16–50	\$\$\$	Best surface finish, fast printing time, most accurate 3D printing method	Limited use for mechanical parts, very brittle, expensive ink magazine	[9, 37, 39, 74, 75]

A lot of research has been carried out in the field of biomedical to manufacture biomedical implants and scaffolds by additive manufacturing [76–86]. The challenge in the process is that each patient needs vary from each other and that every single design has to be unique. The printing of biomedical implants or tissues is still an important research field around the world. Especially the manufacturing of surfaces is in actual cases a complex problem. Dental prostheses and dental bridges, shoulders, knees, hips, and spinal cord implants have different specific surface properties but are manufactured by additive manufacturing and have also been certified in the market [66]. Hence, the selection of the type of additive manufacturing process is the most important step in the manufacturing of the process. The selection should be based on the above-mentioned criteria and the kind of biomedical application it has to be used for.

## 9.6 Summary

Additive manufacturing is the most widely accepted method for bio-implant manufacturing in the current market. Various researches in the area of biomedical implant manufacturing by rapid prototyping were studied, compared, and analyzed. This research has classified the rapid prototyping methods on the basis of specific parameters such as functionality, cost, material used, the maximum resolution of the parts printed, advantages, disadvantages, and the process parameters used in each process. The relevance of rapid prototyping method in biomedical implant manufacturing over other conventional methods like casting and machining is prominent because of its flexibility and the ease of printing complex shapes. The advantages and disadvantages of various rapid prototyping methods were studied and recorded. An empirical table was prepared which can be used to identify the most suitable rapid prototyping method, for the bio-implant manufacturing, based on the parameters considered. SLS, SLM, SLA, FDM, and INKET are chosen the chosen methods of the current study. The process parameters and materials used for each method were collected from different literatures and compiled. In prototyping method with solid as the starting material, which is FDM, the process parameters that were considered are size of granules, nozzle design, inlet and exit temperature of material, speed of deposition, layer orientation, tip wipe frequency, and porosity. Usage of FDM in the field of biomedical implant manufacturing is limited because of limitations in the usage of the starting material which are mostly plastic. Stereolithography has an advantage over FDM in terms of the biomedical implant manufacturing due to the wide variety of materials that can be used for this process. Ceramic manufacturing is also possible with SLA with the proper mixture of ceramic powder, photoinitiators, and monomers. The postprocessing treatment removes the other material, and finally, it is left with the ceramic component. The smooth surfaces that can be manufactured from SLA is one of the specialities of this process. SLS and SLM use similar methodology of printing where the powders are fused together with laser or by melting them together. This method has an advantage since a variety of materials can be used for

this process. However, the increased cost of the machines is a disadvantage of these processes. Inkjet printing with its highly versatile printing method is one of the most widely used rapid prototyping methods for biomedical applications. This method could utilize more starting materials, and the droplet deposition technique allows it to manufacture complex shapes without much difficulty. However, the increased cost of the machine is one of the disadvantages of this highly flexible process.

## References

1. Guo N, Leu MC (2013) Additive manufacturing: technology, applications and research needs. *Front Mech Eng*
2. Kumar S, Kruth J (2010) Composites by rapid prototyping technology. *Mater Des* 31(2):850–856
3. Bellini A, Shor L, Guceri SI (2005) New developments in fused deposition modeling of ceramics. *Rapid Prototyp J* 11(4):214–220
4. Taboas JM, Maddox RD, Krebsbach PH, Hollister SJ (2003) Indirect solid free form fabrication of local and global porous, biomimetic and composite 3D polymer-ceramic scaffolds. *Biomaterials* 24:181–194
5. Tripathy S, Bhattacharya D (2013) Journal of asian ceramic societies rapid synthesis and characterization of mesoporous nanocrystalline  $MgAl_2O_4$  via flash pyrolysis route. *Integr Med Res* 1(4):328–332
6. Eckel ZC, Zhou C, Martin JH, Jacobsen AJ, Carter WB, Schaedler TA (2015) Additive manufacturing of polymer-derived ceramics, vol 58, pp 1–10
7. Yeon S, Reddington P, Gogotsi Y, Vakifahmetoglu C, Colombo P, Fischer JE (2009) Carbide-derived-carbons with hierarchical porosity from a preceramic polymer. *Carbon N Y* 48(1):201–210
8. Brady GA, Halloran JW (1997) Stereolithography of ceramic suspension. *Rapid Prototyp J* 3(2):61–65
9. Liravi F, Darleux R, Toyserkani E, Normale S, De Rennes K (2015) Nozzle dispensing additive manufacturing of polysiloxane : dimensional control. *Int J Rapid Manuf* 5(1):20–43
10. Peltola SM, Melchels FPW, Grijpma DW, Kellomäki M (2008) A review of rapid prototyping techniques for tissue engineering purposes. *Ann Med* 40(4):268–280
11. Rengier F et al (2010) 3D printing based on imaging data: Review of medical applications. *Int J Comput Assist Radiol Surg* 5(4):335–341
12. Webb PA (2000) A review of rapid prototyping (RP) techniques in the medical and biomedical sector. *J Med Eng Technol* 24(4):149–153
13. Singh J, Singh R, Singh H, Verma AK (2018) Investigations for mechanical properties and biocompatibility of SS-316L implant prepared as rapid investment casting for batch production. *Sādhana* 43(5):1–10
14. Frank MC, Hunt CV, Anderson DD, Mckinley TO, Brown TD (2008) Rapid manufacturing in biomedical materials : using subtractive rapid prototyping for bone replacement
15. Zoli L, Sciti D, Liew L, Terauds K, Azarnoush S, Raj R (2016) Additive manufacturing of ceramics enabled by flash pyrolysis of polymer precursors with nanoscale layers. *J Am Ceram Soc* 99:57–63. <https://doi.org/10.1111/jace.13946>
16. Levy RA, Chu TMG, Halloran JW, Feinberg SE, Hollister S (1997) CT-generated porous hydroxyapatite orbital floor prosthesis as a prototype bioimplant. *Am J Neuroradiol* 18(8):1522–1525
17. Lopes AJ, Macdonald E, Wicker RB (2012) Integrating stereolithography and direct print technologies for 3D structural electronics fabrication. *Rapid Prototyp J* 18(2):129–143

18. Medizin BT, Fakult M, Medizin T (2016) Development of an implant and biomaterials based on polydimethylsiloxane and alginate
19. Bian W (2014) Fabrication of a bio-inspired beta-tricalcium phosphate/collagen scaffold based on ceramic stereolithography and gel casting for osteochondral tissue engineering
20. Sodian R et al (2002) Application of stereolithography for scaffold fabrication for tissue engineered heart valves. *ASAIO J* 48(1):12–16
21. Arnaud Bertsch, SJ, PRS (2004). Microfabrication of ceramic components by microstereolithography. *J Micromech Microeng* 14:197–203. <https://doi.org/10.1088/0960-1317/14/2/005>
22. Doreau BF, Chaput C, Chartier T (2000) Stereolithography for manufacturing ceramic parts. *Adv Eng Mater* 2(8):493–496
23. Chartier T, Chaput C, Doreau F, Loiseau M (2002) Stereolithography of structural complex ceramic parts. *7:3141–3147*
24. Lee J, An J, Chua CK (2017) Fundamentals and applications of 3D printing for novel materials. *Appl Mater Today* 7:120–133
25. Chang R, Emami K, Wu H, Sun W (2010) Biofabrication of a three-dimensional liver microorgan as an in vitro drug metabolism model. *Biofabrication* 2(4)
26. Heinel P, Rottmair A, Körner C, Singer RF (2007) Cellular titanium by selective electron beam melting. *Adv Eng Mater* 9(5):360–364
27. Heinel P, Müller L, Körner C, Singer RF, Müller FA (2008) Cellular Ti–6Al–4V structures with interconnected macro porosity for bone implants fabricated by selective electron beam melting. *Acta Biomater* 4(5):1536–1544
28. Cooke MN, Fisher JP, Dean D, Rimnac C, Mikos AG (2003) Use of stereolithography to manufacture critical-sized 3D biodegradable scaffolds for bone ingrowth. *J Biomed Mater Res Part B Appl Biomater* 64(2):65–69
29. Velez M, Kolan KCR, Leu MC, Hilmas GE, Brown RF (2011) Selective laser sintering fabrication of 13–93 bioactive glass bone scaffolds. *Ceram Trans* 228:185–193
30. Sachlos E, Czernuszka JT, Gogolewski S, Dalby M (2003) Making tissue engineering scaffolds work. Review on the application of solid freeform fabrication technology to the production of tissue engineering scaffolds. *Eur Cells Mater* 5:29–40
31. Wilkes J et al (2013) Additive manufacturing of  $ZrO_2$ – $Al_2O_3$  ceramic components by selective laser melting
32. Singh BM, Haverinen HM, Dhagat P, Jabbour GE (2010) Inkjet printing—process and its applications. *90014:673–685*
33. Kollenberg W, Nikolay D (2018) Additive fertigung keramischer bauteile. *Keram Z* 70(1–2):22–25
34. Hon KKB, Li L, Hutchings IM (2008) Direct writing technology—advances and developments. *CIRP Ann Manuf Technol* 57:601–620
35. Okamoto T, Suzuki T, Yamamoto N (2000) Microarray fabrication with covalent attachment of DNA using bubble jet technology. *Nat Biotechnol* 18(4):438–441
36. Roth EA, Xu T, Das M, Gregory C, Hickman JJ, Boland T (2004) Inkjet printing for high-throughput cell patterning. *Biomaterials* 25:3707–3715
37. Derby B (2008) Bioprinting : inkjet printing proteins and hybrid cell-containing materials and structures. *J Mater Chem* 18(47):5717–5721
38. Online VA, Chiolerio A, Roppolo I, Sangermano M (2013) Radical diffusion engineering : tailored nanocomposite materials for piezoresistive inkjet printed strain. *RSC Adv* 3(10):3446–3452
39. Olivieri LJ et al (2016) “Just-in-time” simulation training using 3-D printed cardiac models after congenital cardiac surgery. *World J Pediatr Congenital Heart Surg* 7(2):164–168
40. Pham DT, Dimov S, Lacan F (1999) Selective laser sintering: applications and technological capabilities. *J Eng Technol Capab* 213:435–449
41. Das S, Wohlert M, Beaman JJ, Bourell DL (1998) Producing metal parts with selective laser sintering/hot isostatic pressing. *JOM* 50(12):17–20
42. Kumar S, Kruth J (2009) Composites by rapid prototyping technology. *Mater Des* 1–23

43. Kruth JP, Levy G, Klocke F, Childs THC (2007) Consolidation phenomena in laser and powder-bed based layered manufacturing. *CIRP Ann Manuf Technol* 56(2):730–759
44. Kruth PMJ-P, Vandenbroucke B, Van Vaerenbergh J (2005) Benchmarking of different SIs/Slm processes as rapid manufacturing techniques
45. Kumar S (2003) Selective laser sintering: a qualitative and objective approach. *JOM* 55(10):43–47
46. Mannoor MS et al (2013) 3D printed bionic ears. *Nano Lett* 13(6):2634–2639
47. Sahmani S, Shahali M, Khandan A, Saber-samandari S, Aghdam MM (2018) Applied clay science analytical and experimental analyses for mechanical and biological characteristics of novel nanoclay bio-nanocomposite scaffolds fabricated via space holder technique. *Appl Clay Sci* 165(August):112–123
48. Liu H, Cao Z (2017) Highlights Carbohydr. Polym
49. Akash S, Avinash S, Ramachandra M (2018) A study on mechanical properties of silk fiber reinforced epoxy resin bio-composite with SiC as filler addition. *Mater Today Proc* 5(1):3219–3228
50. Chan YH, Lew WZ, Lu E, Loretz T, Lu L, Lin CT, Feng SW (2017) An evaluation of the biocompatibility and osseointegration of novel glass fiber reinforced composite implants: in vitro and in vivo studies *Den Mater* 34(3):470–485. <https://doi.org/10.1016/j.dental.2017.12.001>
51. Hu X, Sun Z, Zhang C, Wang X, Wu K (2018) Microstructure and mechanical properties of bio-inspired Cf/Ti/Mg laminated composites. *J Magnes Alloy* 6(2):164–170
52. Ramesh M, Palanikumar K, Reddy KH (2017) Plant fibre based bio-composites: sustainable and renewable green materials. *Renew Sustain Energy Rev* 79(May):558–584
53. Sahmani S, Khandan A, Aghdam MM (2018) Author's accepted manuscript. *Ceram Int*
54. Yang B, Lin H, Dai C, Chen Y, Shi J (2018) 'Stepwise Extraction' strategy-based injectable bioresponsive composite implant for cancer theranostics. *Biomaterials* 166:38–51
55. Sharma S, Saeed A, Johnson C, Gadegaard N, Cass AE (2017) Rapid, low cost prototyping of transdermal devices for personal healthcare monitoring. *Sens Bio Sens Res* 13:104–108
56. Wang CS, Wang WHA, Lin MC (2010) STL rapid prototyping bio-CAD model for CT medical image segmentation. *Comput Ind* 61(3):187–197
57. Shreepad S, Ravi W (2015) New revolutionary ideas of material processing—a path to biomaterial fabrication by rapid prototyping. *Procedia Soc Behav Sci* 195:2761–2768
58. Whitley D, Eidson RS, Rudek I, Bencharit S (2017) In-office fabrication of dental implant surgical guides using desktop stereolithographic printing and implant treatment planning software: a clinical report. *J Prosthet Dent* 118(3):256–263
59. Robinson DKR, Lagnau A, Boon WPC (2018) Innovation pathways in additive manufacturing: methods for tracing emerging and branching paths from rapid prototyping to alternative applications. *Technol Forecast Soc Change* 0–1
60. Monneret S, Loubère V, Corbel S (1999) Microstereolithography using a dynamic mask generator and a non-coherent visible light source, vol 3680, pp 553–561
61. Sun C, Fang N, Wu DM, Zhang X (2005) Projection micro-stereolithography using digital micro-mirror dynamic mask. *Sens Actuators A: Phys* 121:113–120
62. Banoriya D, Purohit R, Dwivedi RK (2015) Modern trends in rapid prototyping for biomedical applications. *Mater Today Proc* 2(4–5):3409–3418
63. Kochan D, Kai CC, Zhaohui D (1999) Rapid prototyping issues in the 21st century. *Comput Ind* 39(1):3–10
64. Lal H, Patralekh MK (2018) 3D printing and its applications in orthopaedic trauma: a technological marvel. *J Clin Orthop Trauma* 9(3):260–268
65. Meng C, Ho B, Ng SH, Yoon Y (2015) A review on 3D printed bioimplants. *Int J Precis Eng Manuf* 16(5):1035–1046
66. Konrad W (2010) Net shaped high performance oxide ceramic parts by selective laser melting. *Phys Procedia* 5:587–594
67. Wally ZJ et al (2018) Selective laser melting processed Ti6Al4V lattices with graded porosities for dental applications. *J Mech Behav Biomed Mater*

68. He J, Li D, Lu B, Wang Z, Zhang T (2006) Custom fabrication of composite tibial hemi-knee joint combining CAD/CAE/CAM techniques. *Proc Inst Mech Eng Part H J Eng Med* 220(8):823–830
69. Haddadin KJ, Soutar DS, Webster MH, Robertson AG, Oliver RJ, MacDonald DG (2000) Custom cranioplasty using stereolithography and acrylic. *Br J Plast Surg* 53:200–204
70. Diermann SH, Lu M, Zhao Y, Vandi L, Dargusch M (2018) Synthesis, microstructure, and mechanical behaviour of a unique porous PHBV scaffold manufactured using selective laser sintering. *J Mech Behav Biomed Mater* 84(April):151–160
71. Gayer C et al (2018) Influence of the material properties of a poly (D, L-lactide)/ $\beta$ -tricalcium phosphate composite on the processability by selective laser sintering. *J Mech Behav Biomed Mater*
72. Liu F, Lee R, Lin W, Liao Y (2013) Selective laser sintering of bio-metal scaffold. *Procedia Soc Behav Sci* 5:83–87
73. Singh JP, Pandey PM (2013) fitment study of porous polyamide scaffolds fabricated from selective laser sintering. *Procedia Eng* 59:59–71
74. Chen SA, Ong CS, Malguria N, Vricella LA, Garcia JR, Hibino N (2018) Digital design and 3D printing of aortic arch reconstruction in HLHS for surgical simulation and training. *World J Pediatr Congenital Heart Surg* 9(4):454–458
75. Microdeposition P, Printer J (2000) Short technical reports, vol 496, pp 492–496
76. Singh S, Prakash C, Gupta MK (2020) On friction-stir welding of 3D printed thermoplastics. In: *Materials forming, machining and post processing*, pp 75–91. Springer, Cham
77. Singh S, Prakash C, Wang H, Yu XF, Ramakrishna S (2019) Plasma treatment of polyether-ether-ketone: a means of obtaining desirable biomedical characteristics. *Eur Polym J*
78. Singh S, Prakash C, Antil P, Singh R, Królczyk G, Pruncu CI (2019) Dimensionless analysis for investigating the quality characteristics of aluminium matrix composites prepared through fused deposition modelling assisted investment casting. *Materials* 12(12):1907
79. Prakash C, Singh S, Singh R, Ramakrishna S, Pabla BS, Puri S, Uddin MS (eds) (2019) *Biomanufacturing*
80. Singh H, Singh S, Prakash C (2019) Current trends in biomaterials and bio-manufacturing. In: *Biomanufacturing*, pp 1–34. Springer, Cham
81. Singh S, Prakash C, Ramakrishna S (2019) 3D printing of polyether-ether-ketone for biomedical applications. *Eur Polym J*
82. Malik A, Pradhan S, Mann GS, Prakash C, Singh S (2019) Subtractive versus hybrid manufacturing
83. Singh S, Prakash C, Singh M, Mann GS, Gupta MK, Singh R, Ramakrishna S (2019) Poly-lactic-acid: potential material for bio-printing applications. In: *Biomanufacturing*, pp 69–87. Springer, Cham
84. Poomathi N, Singh S, Prakash C, Patil RV, Perumal PT, Barathi VA, Balasubramanian KK, Ramakrishna S, Maheshwari NU (2019) Bioprinting in ophthalmology: current advances and future pathways. *Rapid Prototyp J*
85. Singh S, Singh N, Gupta M, Prakash C, Singh R (2019) Mechanical feasibility of ABS/HIPS-based multi-material structures primed by low-cost polymer printer. *Rapid Prototyp J*
86. Singh S, Singh M, Prakash C, Gupta MK, Mia M, Singh R (2019) Optimization and reliability analysis to improve surface quality and mechanical characteristics of heat-treated fused filament fabricated parts. *Int J Adv Manuf Technol* 102(5–8):1521–1536
87. Espalin D et al (2010) Fused deposition modeling of patient-specific polymethylmethacrylate implants
88. Singh R, Singh S, Kapoor P Development of biomedical implant (hip joint) by combining fused deposition modelling and investment casting
89. Jafari MA, Han W, Mohammadi F, Safari A, Danforth SC, Langrana N (2000) A novel system for fused deposition of advanced multiple ceramics. 6(3):161–174
90. Zhang ZH, Wang YP, Liu G, Li YL, Shen J, Yan M (2018) Selective laser melting of typical metallic materials: an effective process prediction model developed by energy absorption and consumption analysis

91. Arash Ataee CW, Li Y, Brandt M (2018) Ultrahigh-strength titanium gyroid scaffolds manufactured by selective laser melting (SLM) for bone implant applications. *Acta Mater*
92. Xu T, Jin J, Gregory C, Hickman JJ, Boland T (2005) Inkjet printing of viable mammalian cells. *Biomaterials* 26:93–99
93. Kalita SJ, Bose S, Hosick HL, Bandyopadhyay A (2003) Development of controlled porosity polymer-ceramic composite scaffolds via fused deposition modeling. *Mater Sci Eng C* 23(5):611–620

**Mr. Ajith Gopinath** is Assistant Professor in the Department of Mechanical Engineering, Faculty of Engineering, CHRIST (Deemed to be University), Bengaluru, India. He has done his masters from VIT University, Chennai, Tamil Nadu, India, with over 6 years of teaching experience. His area of research is additive manufacturing, fibre-reinforced composites, metallurgy and design, with over five research publications in reputed journals.

**Mr. Tobias Waclawczyk** B.Sc., University of Augsburg. His area of research is focused on material science and lightweight constructions for aerospace applications. Tobias was fascinated by additive manufacturing and completely focused his attention on this technology. After completing his research on additive manufacturing in the medical sector at the Christ University in Bangalore, India, he moved on to Volkswagen AG, Germany, where he undertook research on the potential of additive manufacturing in the future of the automotive sector.

**Mr. Raman Bedi** is an alumnus of Department of Mechanical and Automobile Engineering, CHRIST (Deemed to be University). He was a Gold Medalist and also received an award for the Best Outgoing Student of his batch. Being an enthusiast learner, he had a keen interest in the field of research, having three publications in the field of thermal engineering and one in the field of manufacturing engineering.

**Mr. Avinash Babu** is Assistant Professor in Mechanical Engineering, CHRIST (Deemed to be University), Kengeri, Bangalore, India. He completed Master's Degree in Machine Design, from Karunya University, Coimbatore, India. He has 5 years of teaching and research experience. His area of research is metallic foams, rapid prototyping, and functionally graded materials and product design. He is currently pursuing Ph.D. in functional graded material.

**Dr. Shijo Thomas** is Assistant Professor in the Department of Mechanical Engineering, CHRIST Deemed to be University, Bangalore, India. He has received Bachelor of Engineering in Mechanical Engineering and Masters of Engineering in Manufacturing Engineering from Anna University, Chennai, India; Masters in Business Administration in Technology Management from Bharathiar University, Coimbatore, India; and Ph.D. in Mechanical Engineering from Vellore Institute of Technology, Vellore, India. He has an experience of 6 years in teaching and research. His research interest includes sintering technology, metal matrix nanocomposites, physical and mechanical metallurgy and manufacturing of composites. He has contributed extensively in the field of multi-walled carbon nanotubes (MWCNT)-reinforced aluminum nanocomposites. He is working with joint collaboration with other universities around the world.

**Mr. Praise Tom** is an Assistant Professor at CHRIST (Deemed to be) University, Bangalore, India. He has done his graduation in Mechanical Engineering under Kannur University, Kerala, India, and post-graduation in CAD/CAM at Vellore Institute of Technology, Chennai, Tamil Nadu, India. He has enormous teaching experience in the field of materials, finite element methods and theory of machines. His area of research is nanocomposites, multibody dynamics and vibration control.

# Chapter 10

## PLA-HAp-CS-Based Biocompatible Scaffolds Prepared Through Micro-Additive Manufacturing: A Review and Future Applications



Nishant Ranjan, Rupinder Singh, I. P. S. Ahuja, Mustafizur Rahman, and Seeram Ramakrishna

### Abbreviations Used

### Nomenclatures

PCL	Polycaprolactone
H	Hydroxyapatite
P	Poly(lactic acid)
PEG	Poly (ethylene glycol)
PHMGCL	Phenylmagnesium chloride
TCP	Tricalcium phosphate
PP	Polypropylene
Al <sub>2</sub> O <sub>3</sub>	Alumina
CaP	Calcium phosphate
PLLA	Poly(L-lactic acid)
DEF	Diethyl fumarate
PU	Polyurethane

---

N. Ranjan · R. Singh (✉)

Department of Production Engineering, Guru Nanak Dev Engineering College, Ludhiana 141006, India

e-mail: [rupindersingh78@yahoo.com](mailto:rupindersingh78@yahoo.com)

N. Ranjan · I. P. S. Ahuja

Department of Mechanical Engineering, Punjabi University, Patiala, India

M. Rahman

Department of Mechanical Engineering, Universiti Malaysia Pahang, Pekan, Malaysia

S. Ramakrishna

Department of Mechanical Engineering, National University of Singapore, Sovereign, Singapore

© Springer Nature Singapore Pte Ltd. 2020

S. Singh et al. (eds.), *3D Printing in Biomedical Engineering*,

Materials Horizons: From Nature to Nanomaterials,

[https://doi.org/10.1007/978-981-15-5424-7\\_10](https://doi.org/10.1007/978-981-15-5424-7_10)



PS	Polysulfone
PET	Polyethylene terephthalate
PA	Polyacetal
PMMA	Polymethylmethacrylate
PTFE	Polytetrafluoroethylene
PEEK	Polyetheretherketone
SR	Silicone rubber
PE	Polyethylene
3DP	3D printing
FSF	Feedstock filament
MFI	Melt flow index
T <sub>g</sub>	Glass transition temperature
MT	Melting temperature
FFF	Fused filament fabrication

## 10.1 Introduction

The rigid tissues (bones) comprise two structures (cancellous and cortical). The inward piece of bone (cancellous) is lighter than outer part having 45–88% of volumetric porosity. Cortical bone (external layer of bone) is thick and heavy in comparison with inner part of the bone having  $\leq 10\%$  of volumetric porosity. These two kinds of bone experience dynamic renovating development, separation, and resorption that are controlled by means of associations among osteocyte, osteoblast, and osteoclast cells [1]. Bone has self-mending capacities [2], but to recuperate much of the time, outer intercession is expected to reestablish typical tasks [3, 4]. Nowadays, various treatment choices for bone/scaffold repair (like autograft, allograft, bone tissue building) are common practices [5, 6]. Effective utilization of bone tissue building can maintain a strategic distance from difficulties identified with other treatments. Aside from material issues, an unmistakable comprehension of science including cells, extracellular matrix, and development factors are concerns in bone tissue structurally and biochemically support of surrounding cells [7]. Scaffolds are necessary piece of bone tissue regeneration/fabrication platform. These platforms are 3-D biocompatible structures which can improve and increase cellular matrix properties (like cell action and protein creation through biochemical and mechanical cooperations) and give a layout to cell connection and animate bone tissue arrangement in vivo study [3, 5–7].

In the beginning period, bone in-growth occurs at outskirts of platforms with negative slope in mineralization [4, 5]. Open and interconnected pores enable supplements and particles to encourage cell in-growth, just as waste material evacuation [4, 6, 8]. Since higher porosity (volumetric) builds surface zone per unit volume, the biodegradation energy of frameworks can be affected by shifting pore parameters. Biodegradation through a cell intervened process or substance disintegration is both

imperative to fix and framework supplanting with new bone with no remainder [8]. A base pore in the range of 95 and 145  $\mu\text{m}$  is required for fast and healthy bone tissue regeneration/development [4, 9] notwithstanding improved bone arrangement and vascularization are accounted for platforms with pore measure bigger than 295  $\mu\text{m}$  [9–11]. Pore estimate likewise assumes an imperative job in matrix generation and association [12]. Pore volume additionally controls the porousness of supplements to the platform and their mechanical properties. Porousness in PCL expanded with higher pore volume and brought about better bone recovery, vein penetration, and compressive quality in vivo, when other pore parameters were kept the equivalent [13]. Aside from natural execution, the underlying mechanical properties and quality debasement rate should coordinate that of the host tissue for ideal bone mending [14]. The energy of permeable platforms is profoundly influenced by pore size and geometry [15–19]. Permeable bone frameworks can be made by an assortment of techniques. Concoction/gas frothing [20], dissolvable throwing, molecule/salt filtering [12, 21, 22], and thermally actuated stage separation [23, 24] are portion of those that have been utilized broadly. Be that as it may, pore size, shape, and its interconnectivity cannot be completely controlled in these methodologies. In addition, platforms with custom fitted porosity for explicit imperfections are hard to produce with the vast majority of these methodologies [21–24]. Such frameworks can be structured and created utilizing added substance producing by MAM approaches. The diverse MAM approach (like 3D printing) and strong freestyle manufacture (SFF) permit complex shapes creation specifically from a CAD data [1, 25–28]. In MAM approaches, 3D frameworks are made L–B–L [1, 29–31]. These AM strategies can be delegated—(a) expulsion (disfigurement+hardening), (b) polymerization, (c) laser-helped sintering, and (d) coordinate composition-based procedures. Bone/teeth fix or recovery is a typical and entangled clinical issue in orthopedic/dental medical procedure. Table 10.1 condenses a portion of the MAM systems toward bone tissue engineering applications including their points of interest and drawback.

For bone/tissue building; 3DP is useful for just in time manufacturing with controlled porosity using a CAD data [66–70]. Before the final printing, some controlled parameters (like powder squeezing thickness, latch drop volume, folio immersion, powder wettability, etc.) need to be ascertained for final part [69–76].

## 10.2 Scaffold 3D Printing

Major considerations for scaffold are biocompatibility/biodegradability, pore interconnectivity, pore sizes, uniform porosity, and thermo-mechanical properties. It would likewise be advantageous if framework materials could act as substrates for connection, expansion, and separation of cells. Besides, as cells multiply and separate, the platform must have the capacity to withstand the powers being connected by the cells. The mechanical and tensile strength of the platform must be stable in order to withstand everyday action and typical body developments [77]. The commercial materials, for example, alginate, C, collagen, fibronectin, and hyaluronic corrosive,

have leeway over manufactured materials as they give more inherently organic capacities. Utilizing normally inferred materials, which regularly establish or possess the ECM, results in a superior copying of certifiable ECM, and this in this way upgrades cell connection and controls cell expansion more productively than engineered polymers [78]. The utilization of engineered polymers, for example, PCL and poly(lactic-co-glycolic acid) (PLGA) for framework, has yielded higher mechanical as well as

**Table 10.1** MAM for bone scaffolds/implants

Process specifications		Materials	Merits (+)/demerits (-)	Citations
Inkjet writing/3D plotting	<ul style="list-style-type: none"> <li>→ Viscous extrusion-based material based on computer-aided design data</li> <li>→ Strand deposition at fixed rate and pressure</li> </ul>	<ul style="list-style-type: none"> <li>→ PCL</li> <li>→ H</li> <li>→ Bioactive glasses</li> </ul>	<ul style="list-style-type: none"> <li>+</li> <li>→ Mild condition allows drug and biomolecules plotting</li> <li>-:</li> <li>→ Heating restricts the biomolecule incorporation for some materials</li> </ul>	[32–38]
FFF	<ul style="list-style-type: none"> <li>→ Strands of heated polymer/ceramics and composition of polymers with ceramics extrusion through heated nozzle</li> </ul>	<ul style="list-style-type: none"> <li>→ PCL/TCP/PP</li> <li>→ Al<sub>2</sub>O<sub>3</sub></li> </ul>	<ul style="list-style-type: none"> <li>+</li> <li>→ Platform/support is not required</li> </ul>	[26, 29, 39–45]
Robo-casting	<ul style="list-style-type: none"> <li>→ Direct writing of liquid using a nozzle</li> </ul>	<ul style="list-style-type: none"> <li>→ H/P</li> <li>→ H/PCL</li> </ul>	<ul style="list-style-type: none"> <li>+</li> <li>→ Independent nozzle movement in 3D</li> <li>→ Precise thickness controlled</li> <li>→ No need of support required</li> </ul>	[46]
SLS	<ul style="list-style-type: none"> <li>→ In this process, powder bed is to be prepared</li> <li>→ In this process, powder is added layer by layer</li> <li>→ Sintering each layer using laser source as per CAD data</li> </ul>	<ul style="list-style-type: none"> <li>→ PCL/H</li> <li>→ H is mixed with PDLLA</li> <li>→ PDLLA</li> <li>→ PHBV</li> <li>→ Nano H</li> </ul>	<ul style="list-style-type: none"> <li>+</li> <li>→ No support required</li> <li>→ No post-processing</li> <li>-:</li> <li>→ Resolution control as per diameter of laser beam</li> </ul>	[47–52]
Laser-assisted Bio-printing (LAB)	<ul style="list-style-type: none"> <li>→ Desired material must be coated on ribbon</li> <li>→ Laser pulse energy techniques are to use for deposition controlling.</li> </ul>	<ul style="list-style-type: none"> <li>→ H/H mixed with osteoblast cell</li> <li>→ Zirconium</li> <li>→ Human umbilical vein endothelial cell</li> </ul>	<ul style="list-style-type: none"> <li>+</li> <li>→ Control and perfect condition for working in biomedical application</li> <li>→ It is best suitable for cell, in organic and organic</li> <li>→ Best controlled process</li> <li>-:</li> <li>→ Equally distributed ribbons needed</li> </ul>	[53–56]

(continued)

**Table 10.1** (continued)

Process specifications		Materials	Merits (+)/demerits (-)	Citations
SLA	<p>→ In this process, at focal point, polymeric materials are solidifying, and non-exposed polymeric materials remain unchanged and present in liquid form.</p> <p>→ In this process, platform is moving in downward direction and layer by layer fabricated</p>	<p>→ PPF mixed with DEF</p> <p>→ PPF mixed with composition of DEF and H</p> <p>→ PDLLA is mixed with H</p>	<p>+:</p> <p>→ By the help of this process, very difficult and internal feature is easily obtained</p> <p>-:</p> <p>→ This process/techniques are mostly applicable for photopolymers</p>	[57–65]

Note PCL Polycaprolactone, TCP Trichloropropane, PP Polypropylene, PPF poly(propylene fumarate), DEF Diethyl fumarate, PDLLA Poly-D, L-lactic acid, PHBV Poly(3-hydroxybutyrate-co-3-hydroxyvalerate)

tensile qualities with higher processability and controllable debasement rates [78, 79]. Be that as it may, these manufactured polymer frameworks have moderately low organic movement, regarding advancing tissue recovery. Notwithstanding being less naturally dynamic, the inherent hydrophobicity of engineered polymers, for example, polyesters, for the most part results in poor cell grip [80], which results in imperfect multiplication and separation, at last prompting substandard tissue arrangement [78]. For 3DP frameworks using grain size and grain measure, disseminations must be considered to create permeable scaffolds [81], as these components affect miniaturized scale porosity which has been believed to impact cell appropriation, connection, expansion, and separation [82, 83]. To accomplish bio-mimicry, platforms should be organically dynamic, have high mechanical qualities, be anything but difficult to process, and have controllable corruption rates. To make these intricate frameworks, mixture frameworks involving both manufactured and regular polymers have been utilized and are probably going to be utilized later on [84–86]. To be a feasible alternative for tissue recovery, it is essential to remember that the materials utilized for 3DP of frameworks for tissue designing ought to be printable with a high level of reproducibility. Such materials ought to likewise be financially savvy and pliable to frame the ideal morphology of the structure platform.

### 10.2.1 3DP of Metals as Scaffold

Metals for use in 3DP of scaffolds include Fe, Co, Cr, treated steel, and Ti compound [86–89]. These are appealing materials for use in the 3DP because of better mechanical properties, which appear like bone [90, 91]. Besides showing high mechanical sound qualities, metals are promising materials for in vivo studies [92, 93]. Further work may be performed to build up the practicality of utilizing certain metal materials as parts of 3DP frameworks notwithstanding having been effectively

utilized in 2D platforms. The present confinements include: (1) the 3DP innovation accessible, accordingly restricting the sort of metals that can be utilized and (2) the poisonous quality of metal particles caused by metal erosion and corruption inside the body. This consumption produces metal particles that might be harmful to the body at high fixations, and with the absence of a leeway pathway, a framework intended to catch the metal particles or keep away from fundamental lethality is essential notwithstanding platform manufacture [82, 94]. Another parameter that prevents the utilization of metals is long corruption times, which results in practical tissue conforming to the framework instead of eventually supplanting the platform. Nevertheless, the utilization of moment or follow measures of metals to expand the mechanical quality of current platforms has demonstrated some guarantee [95–97]. Nevertheless, biodegradable metals have developed as conspicuous possibility for 3DP of frameworks [98]. Printing of 3D platforms utilizing biodegradable metals for bone recovery indicates guarantee and ought to be additionally inquired about utilizing an assortment of metal materials to expand the accessibility of materials for 3DP. Despite the fact that these materials and frameworks might be intended for bone substitution, they may have numerous different applications for different tissues since nonmetallic platforms are less hearty and can crumple under the contractile power connected by cells amid cell connection and expansion [69]. As the accessibility of biodegradable metals consistently builds, the requirement for, and complexities expedited by, changeless prosthetics and metal new parts can be decreased, subsequently enabling patients to recover their very own bone in a definitive nonattendance of non-physiological materials. The research on metals as biomaterials for 3DP platforms is essential because of the conventional thought of non-biodegradability and restricted processability [87, 99]. Nevertheless, the execution of biodegradable metal plans to counter this idea and increment the common sense of utilizing metals in 3DP of increasingly creative and successful frameworks. Biodegradable metals are an undiscovered hotspot for 3DP of platforms for tissue designing, as they could give extra mechanical solidarity to the current frameworks to withstand most compressive and elastic powers.

### **10.2.2 Ceramics**

Ceramics contain both components (metallic and nonmetallic) and have been utilized as materials for 3DP inserts/platforms because of their high mechanical and tensile quality and biocompatibility [3]. Pottery is fit for inserts/platform manufacture for bone recovery essentially because of their apatite-mineralization capacity [100]. The ‘H’ itself a clay is usually found in human teeth and bones [101], along these lines making the utilization of ‘H’, or comparative earthenware production, alluring materials for making platforms with solid mechanical properties like that of common bone. The ‘H’ has gathered much consideration in the field of regenerative drug and, overall, is a regularly utilized material for 3DP frameworks. In one investigation, a quick prototyping system was utilized to make 3DP platforms from ‘H’ with complex

inner structures with inclines of  $45^\circ$  to take into account cell multiplication within the structure [102]. The interconnecting channels with pore sizes of  $500\ \mu\text{m}$  in the structured platforms showed the capacity to encourage mouse MC3T3E1 cell expansion, representing the capability of H-frameworks to recover bone. Another examination utilized PC helped 3D imprinting in a fast prototyping system to manufacture H and tricalcium phosphate (TCP) frameworks. The platforms were made utilizing H and tricalcium phosphate in an L-B-L process pursued by sintering [69]. These scaffolds were seeded with human osteoblasts that were segregated from human iliac peak cancellous bone and demonstrated high biocompatibility and low toxicity. The outcomes give additional proof that H-materials show biocompatibility and the capacity to aid cell development and suitability. Even more as of late, the ceramics,  $\text{CaSiO}_3$ , was utilized to make platforms with higher bone mending limit than that of tricalcium phosphate frameworks [100]. Another clay material normally utilized for 3DP bone platforms is calcium phosphate [75, 103, 104], which, when joined with different ceramics, for example, 'H' [75] and TCP [104], yields frameworks with pore sizes of  $300\ \mu\text{m}$  that are sufficiently substantial to permit supplement exchange for cells. These platforms/inserts were likewise manufactured with greater than 97.5% exactness contrasted with the PC-helped configuration, considering future frameworks to be ideal for cell connection and multiplication [75]. Different examinations have likewise demonstrated the printability of calcium phosphate with other mixed mixes, for example, calcium sulfate, to make a powder composite with a water-based folio [103]. Utilizing a mix of ceramic materials for 3DP of platforms ought to be additionally researched to make a material with high accuracy configuration, having sufficient compressive quality, and the capacity to advance cell multiplication and separation that can be relevant to both non-stack-bearing and load-bearing orthopedic applications.

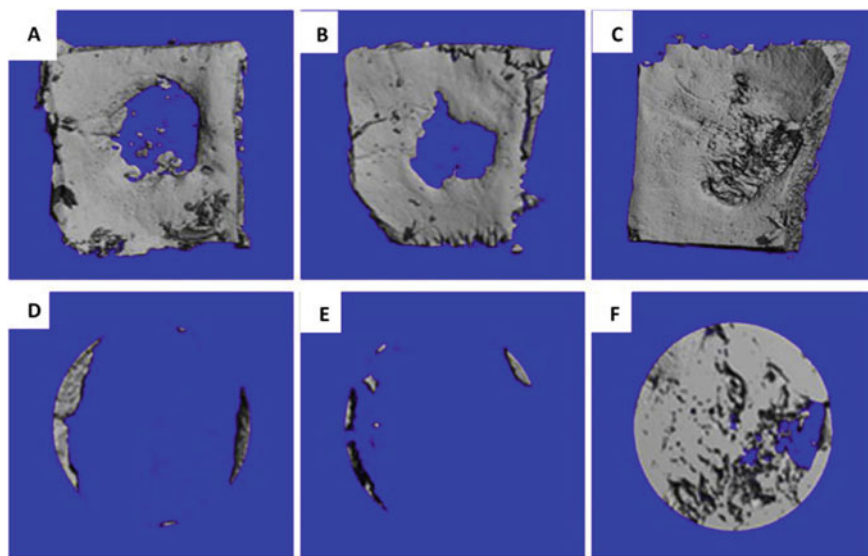
### 10.2.3 *Polymers*

Polymers speak to a noteworthy classification of materials with potential for use in the 3DP of platforms for tissue designing [105]. Hydrogels are appealing biomaterials for tissue designing since they have movable mechanical and tensile properties which are biocompatible and can be hydrated while staying insoluble and keeping up their 3D structure. Furthermore, the hydrating properties of hydrogels enable them to imitate those of organic tissue [106, 107]. Both PCL and poly(DL-lactide-coglycolide) (P-D-L-GA) scaffolds/inserts have been made utilizing MAM. The utilization of these platforms in the deformities of rabbit tibias exhibited their security just as their ability to advance the age of bone tissue [108]. Preference of utilizing engineered polymer materials, for example, PLGA and PCL, is that the FDA for clinical use [109] has endorsed both these manufactured polymers. Another favorable position of utilizing PCL polymers and PLGA copolymers is the low harmfulness of their debasement items, which sustains into metabolic pathways. A burden of

utilizing PLGA is that it can cause provocative reactions when there is a development of acidic oligomers [110]. Aggravation assumes a key job in tissue recovery [111]; however, it is critical to control or restrain this reaction, as abnormal amounts of irritation can prompt fibrosis bringing about poor tissue work, or even dismissal of the embedded platform. In this manner, it is critical to comprehend the fiery impact of the specific biomaterial(s) utilized and the framework structure used to produce the ideal tissue. The provocative reaction, mostly mounted by the inborn invulnerable framework, advances the enrollment of cells (principally neutrophils and monocytes) to the territory of tissue harm to help with tissue fix and recovery [112]. In one investigation, 3D printed 'P' and 'C' platforms were contrasted for their capacity with incite aggravation and subsequently effect on tissue recovery [113]. Through the examination of macrophage morphology and human monocyte cytokine profiles, it was presumed that the provocative properties of the platforms/inserts were controlled by both framework geometry and structure. Another intriguing normal for these polymers is their rate of biodegradation, which is frequently too quick when PLGA is utilized and too moderate when PCL is utilized. In a polymer debasement test performed utilizing frameworks, it was appeared with practically identical convergences of PCL and PLGA, PLGA corrupted by 18% at 14 days and 56% by 28 days contrasted with PCL whose debasement was 33% at 21 days, and 39% at 28 days [114, 115]. Long haul mending might be vital in open bone breaks [116, 117]. PCL is potentially an ideal decision for open cracks because of its slower corruption rate. A more extended recuperating period is frequently required in open cracks in light of the fact that the bone has infiltrated the skin which can in many cases lead to diseases that expansion the ideal opportunity for mending. The moderate corruption rate of PCL enables the platform to offer help for developing cells for a more extended time-frame empowering increasingly thick tissue to shape [108]. For shut cracks (broken bone that has not infiltrated the skin), PLGA could be a potential possibility for bone recovery. PCL-based copolymers, for example, PCL-PLGA-PLGA [118] and PCL-PEG-PCL [119], have been combined to control the debasement of PCL for controlled medication discharge applications. Nevertheless, these copolymers can possibly be utilized for tissue designing applications too. Other manufactured polymers utilized for framework incorporate PGA, PPF, and PHB. Normal polymers, for example, proteins and polysaccharides, have additionally been utilized for platform manufacture, and among these polymers, the most well-known contender for tissue designing has been collagen type 1 [120]. Collagen platforms stacked with cationic PEI-pDNA edifices were used by some researchers in bone recovery for rodents (Fig. 10.1) [121].

### 10.3 Mechanical Properties of Tissues and Materials

Normally, tissues are gathered into hard and delicate tissue. As a rule, the hard tissues are stiffer (versatile modulus) and more grounded (rigidity) than delicate tissues (Table 10.2). Considering the basic or mechanical similarity with tissues, metals, or



**Fig. 10.1** In vivo bone formation in rat calvarial defects implanted with collagen scaffolds [121]

**Table 10.2** Tensile strength of hard/soft tissues [60, 61]

Hard tissues with respective tensile strength	Dentine	39.3 MPa
	Cancellous bone	7.4 MPa
	Enamel	10 MPa
	CB (TD)	52 MPa
	CB (LD)	133 MPa
Soft tissue with respective tensile strength	AT (LD)	0.1 MPa
	Skin	39.3 MPa
	Ligament	7.4 MPa
	Articular cartilage	133 MPa
	Fibrocartilage	52 MPa
	Tendon	10 MPa
	AT (TD)	1.1 MPa
	Intraocular lens	2.3 MPa

pottery is picked for hard tissue applications (Tables 10.2 and 10.3) and polymers for the delicate tissue applications (Tables 10.2 and 10.4). One of the serious issues in orthopedic medical procedure is firmness between the bone and metallic inserts, which needs to be addressed [122, 123].

The advancement in polymer-based composite biomaterials including non-appearance of erosion and weakness disappointment of metal compounds and arrival



**Table 10.3** Mechanical properties of ceramic and metallic biomaterials [60, 61]

Material	Strength in tensile (MPa)
<i>Metal alloys</i>	
Amalgam	58
S.S.	578
Ti-alloy	965
Co-Cr alloy	1076
<i>Ceramics</i>	
Hydroxyapatite	50
Alumina	295
Bioglass	42
Zirconia	808

**Table 10.4** Mechanical properties of thermoplastic biomaterials [60–65]

Thermoplastics	Strength (MPa)
PS	75
PU	35
PET	61
PA	67
PMMA	59
PTFE	27.5
PEEK	139
SR	7.6
PLA	72
PE	35

of metal particles (e.g., Ni or Cr which may cause slackening of the inserts, tolerant distress, and unfavorably susceptible skin response) has motivated the use of these materials in commercial biomedical applications. Composite materials have favorable results over metal amalgams in adjusting the previously mentioned inadequacies [124–126].

## 10.4 Case Study

A case study has been reported on P–H–C-based functional prototype prepared by MAM. The P–H–C feedstock filament was prepared on DSE. Multifactor optimization was performed in two stages (a) FSF preparation on DSE and (b) FFF based

upon tensile and flexural samples [127]. Initially, different proportions of P–H–C were selected (Table 10.5).

Based upon Tables 10.5 and 10.6 shows MFI and flow continuity data for FFF.

As observed from Table 10.6, composition/proportion 1 is without reinforcement of H and C in P. This was used for comparison purpose only. So, finally four samples 2, 3, 5, and 6 were used for further investigations of dimensional accuracy and peak strength (Table 10.7).

As observed from Table 10.7, all four FSF diameters are acceptable; however, two proportions. 91–8–1 and 90–8–2% were selected for peak strength view point. To counter-verify the suitability of FSF, thermal stability analysis of four selected proportions was carried out on DSC (Fig. 10.2). Table 10.8 shows result of thermal analysis for P–H–C.

As observed from Table 10.8, T<sub>g</sub> and MT have no significant variations, so all filament compositions are acceptable. But, in the case of crystallinity (%), the composition 80–8–12 is considered better. Finally, based upon Tables 10.7 and 10.8, P–H–C composition as 91–8–1 is recommended for FFF by giving more focus to mechanical properties. Figure 10.3 shows scanning electron microscopy (SEM) image of

**Table 10.5** Material proportion of P–H–C [127]

S. No.	Material composition(P–H–C) (by weight%)
1	100–0–0
2	84–4–12
3	80–8–12
4	76–12–12
5	91–8–1
6	90–8–2
7	89–8–3
8	88–8–4

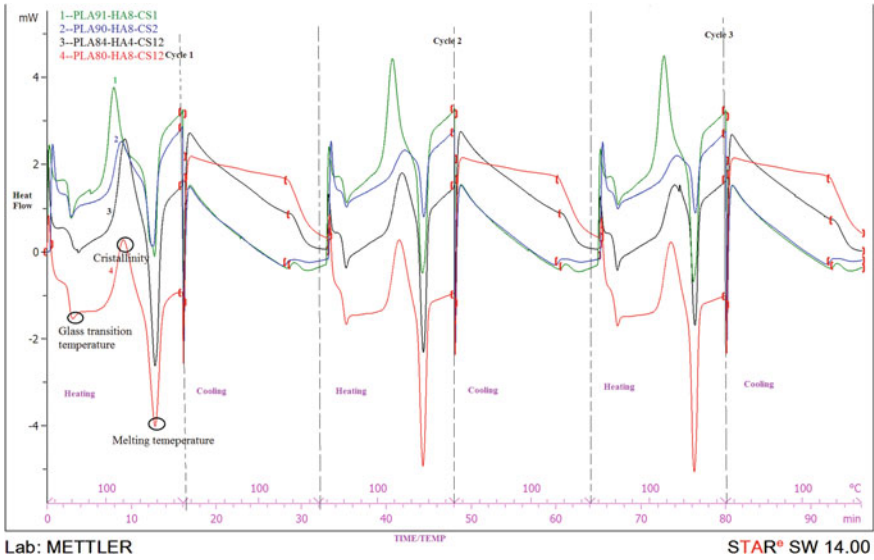
**Table 10.6** P–H–C MFI and flowability [127]

S. No.	P–H–C (by weight%)	MFI (g/10 min)	Flow continuity	Remarks
1	100–0–0	13.52	Yes	AD
2	84–4–12	10.512	Yes	AD
3	80–8–12	9.015	Yes	AD
4	76–12–12	3.125	No	NAD
5	91–8–1	12.352	Yes	AD
6	90–8–2	11.575	Yes	AD
7	89–8–3	7.474	No	NAD
8	88–8–4	4.465	No	NAD

Note AD Adequate, NAD Not Adequate

**Table 10.7** Observations for dimensional accuracy and peak strength [127]

S. No.	Proportion P-H-C	Output properties	
		Average outside diameter (mm)	Peak strength (MPa)
1	84-4-12	1.85	2.10
2	80-8-12	1.78	2.43
3	91-8-1	1.86	3.27
4	90-8-2	1.87	3.23

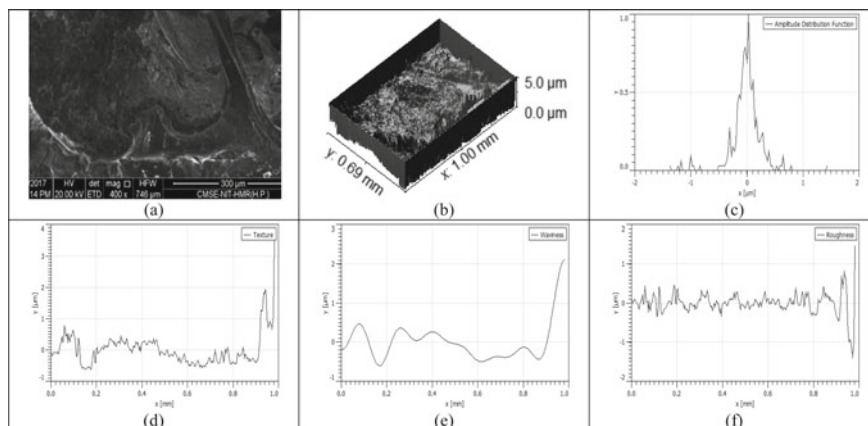


**Fig. 10.2** Thermal analysis of four proportions of P-H-C

**Table 10.8** Thermal properties of P-H-C composites [127]

Compositions	T <sub>g</sub> (°C)	Crystallization (%)	MT (°C)
91-8-1	56.50	3.13	153.17
90-8-2	57.19	10.505	159.875
84-4-12	56.90	7.37	152.46
80-8-12	57.37	1.20	153.95

P-H-C composition 91-8-1 (a), 3D rendered image using image processing software (b), amplitude distribution function (c), surface texture (d), surface waviness (e), and surface roughness (Ra) profile (f) at cutoff length of 0.04 mm. Further based upon Fig. 10.3a, Table 10.9 shows statistical analysis of surface features, which are acceptable as per commercial requirements. The observations are in-line with other investigators [128-134].



**Fig. 10.3** SEM image of P-H-C composition 91-8-1 (a), 3D rendered image using image processing software (b), amplitude distribution function (c), surface texture (d), surface waviness (e), and Ra profile (f)

**Table 10.9** Statistical analysis of surface features

Roughness average ( $R_a$ )	170.1 nm
Root mean square (RMS) roughness ( $R_q$ )	274.3 nm
Maximum height (MH) of roughness ( $R_t$ )	2.83 μm
Maximum roughness valley depth ( $R_v$ )	1.37 μm
Skewness ( $R_{sk}$ )	-1.024
Kurtosis ( $R_{ku}$ )	10.92
Waviness average ( $W_a$ )	338.4 nm

## 10.5 Conclusion and Future Scope

In this review, P-H-C composite feedstock filament has been explored for MAM. Some of the important observations are:

P-H-C is suitable composite material for biomedical applications. In order to prepare FSF with different proportions of P-H-C, experimental study was conducted, and based upon mechanical, continuous flowability, thermal stability, MFI, and dimensional analysis, P-H-C as 91-8-1 (by weight) proportion was recommended in the reported case study.

Series of experimental observations needs to be made to ascertain thermal, rheological, and mechanical properties for best proportion of reinforcement in PLA matrix for preparation of scaffolds/functional prototypes via FFF in biomedical applications. Further for in vivo and in vitro, analysis needs to be conducted for ascertaining the biocompatibility issues.

**Acknowledgements** Financial support by SERB (IMRC/AISTDF/R&D/P-10/2017) was received for this work.

## References

1. Bose S, Vahabzadeh S, Bandyopadhyay A (2013) Bone tissue engineering using 3D printing. *Mater Today* 16(12):496–504
2. Mouriño V, Boccaccini AR (2009) Bone tissue engineering therapeutics: controlled drug delivery in three-dimensional scaffolds. *J Roy Soc Interface* <https://doi.org/10.1098/rsif.2009.0379>
3. Seitz H, Rieder W, Irsen S, Leukers B, Tille C (2005) Three-dimensional printing of porous ceramic scaffolds for bone tissue engineering. *J Biomed Mater Res B Appl Biomater* 74(2):782–788
4. Jones AC, Arns CH, Sheppard AP, Hutmacher DW, Milthorpe BK, Knackstedt MA (2007) Assessment of bone ingrowth into porous biomaterials using MICRO-CT. *Biomaterials* 28(15):2491–2504
5. Rezwan K, Chen QZ, Blaker JJ, Boccaccini AR (2006) Biodegradable and bioactive porous polymer/inorganic composite scaffolds for bone tissue engineering. *Biomaterials* 27(18):3413–3431
6. Müller B, Deyhle H, Fierz FC, Irsen SH, Yoon JY, Mushkolaj S, Boss O, Vorndran E, Gburek U, Degistirici Ö, Thie M. (2009) Bio-mimetic hollow scaffolds for long bone replacement. In: *Biomimetics and bioinspiration*, vol 7401, p 74010D. International Society for Optics and Photonics
7. Salgado AJ, Coutinho OP, Reis RL (2004) Bone tissue engineering: state of the art and future trends. *Macromol Biosci* 4(8):743–765
8. Habibovic P, Gburek U, Doillon CJ, Bassett DC, van Blitterswijk CA, Barralet JE (2008) Osteoconduction and osteoinduction of low-temperature 3D printed bioceramic implants. *Biomaterials* 29(7):944–953
9. Karageorgiou V, Kaplan D (2005) Porosity of 3D biomaterial scaffolds and osteogenesis. *Biomaterials* 26(27):5474–5491
10. Xue W, Krishna BV, Bandyopadhyay A, Bose S (2007) Processing and biocompatibility evaluation of laser processed porous titanium. *Acta Biomater* 3(6):1007–1018
11. Otsuki B, Takemoto M, Fujibayashi S, Neo M, Kokubo T, Nakamura T (2006) Pore throat size and connectivity determine bone and tissue ingrowth into porous implants: three-dimensional micro-CT based structural analyses of porous bioactive titanium implants. *Biomaterials* 27(35):5892–5900
12. Stoppato M, Carletti E, Sidarovich V, Quattrone A, Unger RE, Kirkpatrick CJ, Migliaresi C, Motta A (2013) Influence of scaffold pore size on collagen I development: a new in vitro evaluation perspective. *J Bioact Compat Polym* 28(1):16–32
13. Mitsak AG, Kempainen JM, Harris MT, Hollister SJ (2011) Effect of polycaprolactone scaffold permeability on bone regeneration in vivo. *Tissue Eng Part A* 17(13–14):1831–1839
14. Bandyopadhyay A, Bernard S, Xue W, Bose S (2006) Calcium phosphate-based resorbable ceramics: influence of MgO, ZnO, and SiO<sub>2</sub> dopants. *J Am Ceram Soc* 89(9):2675–2688
15. Banerjee SS, Tarafder S, Davies NM, Bandyopadhyay A, Bose S (2010) Understanding the influence of MgO and SrO binary doping on the mechanical and biological properties of  $\beta$ -TCP ceramics. *Acta Biomater* 6(10):4167–4174
16. Bose S, Tarafder S, Banerjee SS, Davies NM, Bandyopadhyay A (2011) Understanding in vivo response and mechanical property variation in MgO, SrO and SiO<sub>2</sub> doped  $\beta$ -TCP. *Bone* 48(6):1282–1290

17. Das K, Bose S, Bandyopadhyay A (2007) Surface modifications and cell–materials interactions with anodized Ti. *Acta biomat* 3(4):573–585
18. Bodhak S, Bose S, Bandyopadhyay A (2009) Role of surface charge and wettability on early stage mineralization and bone cell–materials interactions of polarized hydroxyapatite. *Acta Biomat* 5(6):2178–2188
19. Tarafder S, Banerjee S, Bandyopadhyay A, Bose S (2010) Electrically polarized biphasic calcium phosphates: adsorption and release of bovine serum albumin. *Langmuir* 26(22):16625–16629
20. Kucharska M, Butruk B, Walenko K, Brynk T, Ciach T (2012) Fabrication of in-situ foamed chitosan/ $\beta$ -TCP scaffolds for bone tissue engineering application. *Mater Lett* 15(85):124–127
21. Cao H, Kuboyama N (2010) A biodegradable porous composite scaffold of PGA/ $\beta$ -TCP for bone tissue engineering. *Bone* 46(2):386–395
22. Sultana N, Wang M (2008) Fabrication of HA/PHBV composite scaffolds through the emulsion freezing/freeze-drying process and characterization of the scaffolds. *J Mater Sci Mater Med* 19(7):2555
23. Hutmacher DW (2006) Scaffolds in tissue engineering bone and cartilage. In: *The Biomaterials: Silver Jubilee Compendium*, pp 175–189
24. Yoshikawa H, Tamai N, Murase T, Myoui A (2009) Interconnected porous hydroxyapatite ceramics for bone tissue engineering. *J Roy Soc Interface* <https://doi.org/10.1098/rsif.2008.0425>
25. Bose S, Suguira S, Bandyopadhyay A (1999) Processing of controlled porosity ceramic structures via fused deposition. *Scr Mater* 41(9):1009–1014
26. Bose S, Darsell J, Kintner M, Hosick H, Bandyopadhyay A (2003) Pore size and pore volume effects on alumina and TCP ceramic scaffolds. *Mater Sci Eng C* 23(4):479–486
27. Mueller B (2012) Additive manufacturing technologies—rapid prototyping to direct digital manufacturing. *Assem Autom* 32(2)
28. Hull CW (1986) inventor; UVP Inc, assignee. Apparatus for production of three-dimensional objects by stereolithography. United States patent US 4, 575, 330
29. Bose S, Darsell J, Hosick HL, Yang L, Sarkar DK, Bandyopadhyay A (2002) Processing and characterization of porous alumina scaffolds. *J Mater Sci Mater Med* 13(1):23–28
30. Pighinelli L, Kucharska M (2013) Chitosan–hydroxyapatite composites. *Carbohydr Polym* 93(1):256–262
31. Xianmiao C, Yubao L, Yi Z, Li Z, Jidong L, Huanan W (2009) Properties and in vitro biological evaluation of nano-hydroxyapatite/chitosan membranes for bone guided regeneration. *Mater Sci Eng C* 29(1):29–35
32. Luo Y, Wu C, Lode A, Gelinsky M (2012) Hierarchical mesoporous bioactive glass/alginate composite scaffolds fabricated by three-dimensional plotting for bone tissue engineering. *Biofabrication* 5(1):015005
33. Sobral JM, Caridade SG, Sousa RA, Mano JF, Reis RL (2011) Three-dimensional plotted scaffolds with controlled pore size gradients: effect of scaffold geometry on mechanical performance and cell seeding efficiency. *Acta Biomat* 7(3):1009–1018
34. Detsch R, Uhl F, Deisinger U, Ziegler G (2008) 3D-Cultivation of bone marrow stromal cells on hydroxyapatite scaffolds fabricated by dispense-plotting and negative mould technique. *J Mater Sci Mater Med* 19(4):1491–1496
35. Wu C, Luo Y, Cuniberti G, Xiao Y, Gelinsky M (2011) Three-dimensional printing of hierarchical and tough mesoporous bioactive glass scaffolds with a controllable pore architecture, excellent mechanical strength and mineralization ability. *Acta Biomat* 7(6):2644–2650
36. Serra T, Planell JA, Navarro M (2013) High-resolution PLA-based composite scaffolds via 3-D printing technology. *Acta Biomat* 9(3):5521–5530
37. Seyednejad H, Gawlitta D, Kuiper RV, de Bruin A, van Nostrum CF, Vermonden T, Dhert WJ, Hennink WE (2012) In vivo biocompatibility and biodegradation of 3D-printed porous scaffolds based on a hydroxyl-functionalized poly ( $\epsilon$ -caprolactone). *Biomaterials* 33(17):4309–4318

38. Fu Q, Saiz E, Tomsia AP (2011) Direct ink writing of highly porous and strong glass scaffolds for load-bearing bone defects repair and regeneration. *Acta Biomater* 7(10):3547–3554
39. Darsell J, Bose S, Hosick HL, Bandyopadhyay A (2003) From CT scan to ceramic bone graft. *J Am Ceram Soc* 86(7):1076–1080
40. Kalita SJ, Bose S, Hosick HL, Bandyopadhyay A (2003) Development of controlled porosity polymer-ceramic composite scaffolds via fused deposition modeling. *Mater Sci Eng C* 23(5):611–620
41. Tsang VL, Bhatia SN (2004) Three-dimensional tissue fabrication. *Adv Drug Deliv Rev* 56(11):1635–1647
42. Lam CX, Savalani MM, Teoh SH, Huttmacher DW (2008) Dynamics of in vitro polymer degradation of polycaprolactone-based scaffolds: accelerated versus simulated physiological conditions. *Biomed Mater* 3(3):034108
43. Lam CX, Teoh SH, Huttmacher DW (2007) Comparison of the degradation of polycaprolactone and polycaprolactone-( $\beta$ -tricalcium phosphate) scaffolds in alkaline medium. *Polym Int* 56(6):718–728
44. Schantz JT, Huttmacher DW, Lam CX, Brinkmann M, Wong KM, Lim TC, Chou N, Guldberg RE, Teoh SH (2003) Repair of calvarial defects with customised tissue-engineered bone grafts II. Evaluation of cellular efficiency and efficacy in vivo. *Tissue Eng* 9(4, Supplement 1):127–39
45. Lam CX, Huttmacher DW, Schantz JT, Woodruff MA, Teoh SH (2009) Evaluation of polycaprolactone scaffold degradation for 6 months in vitro and in vivo. *J Biomed Mater Res Part A* 90(3):906–919
46. Russias J, Saiz E, Deville S, Gryn K, Liu G, Nalla RK, Tomsia AP (2007) Fabrication and in vitro characterization of three-dimensional organic/inorganic scaffolds by robocasting. *J Biomed Mater Res Part A* 83(2):434–445
47. Williams JM, Adewunmi A, Schek RM, Flanagan CL, Krebsbach PH, Feinberg SE, Hollister SJ, Das S (2005) Bone tissue engineering using polycaprolactone scaffolds fabricated via selective laser sintering. *Biomaterials* 26(23):4817–4827
48. Shuai C, Gao C, Nie Y, Hu H, Zhou Y, Peng S (2011) Structure and properties of nano-hydroxyapatite scaffolds for bone tissue engineering with a selective laser sintering system. *Nanotechnology* 22(28):285703
49. Duan B, Wang M, Zhou WY, Cheung WL, Li ZY, Lu WW (2010) Three-dimensional nanocomposite scaffolds fabricated via selective laser sintering for bone tissue engineering. *Acta Biomater* 6(12):4495–4505
50. Lee SH, Zhou WY, Wang M, Cheung WL, Ip WY (2009) Selective laser sintering of poly (l-lactide) porous scaffolds for bone tissue engineering. *J Biomimet Biomater Tissue Eng* 1:81–89
51. Liulan L, Hanqing L, Qingxi H, Limin L, Minglun F (2006). Research of the method of reconstructing the repair bionic scaffold based on tissue engineering, pp 1275–1279
52. Pereira TF, Silva MA, Oliveira MF, Maia IA, Silva JV, Costa MF, Thiré RM (2012) Effect of process parameters on the properties of selective laser sintered Poly (3-hydroxybutyrate) scaffolds for bone tissue engineering: This paper analyzes how laser scan spacing and powder layer thickness affect the morphology and mechanical properties of SLS-made scaffolds by using a volume energy density function. *Virtual Phys Prototyp* 7(4):275–285
53. Catros S, Fricain JC, Guillotin B, Pippenger B, Bareille R, Remy M, Lebraud E, Desbat B, Amédée J, Guillemot F (2011) Laser-assisted bioprinting for creating on-demand patterns of human osteoprogenitor cells and nano-hydroxyapatite. *Biofabrication* 3(2):025001
54. Doraiswamy A, Narayan RJ, Harris ML, Qadri SB, Modi R, Chrisey DB (2007) Laser micro-fabrication of hydroxyapatite-osteoblast-like cell composites. *J Biomed Mater Res Part A* 80(3):635–643
55. Harris ML, Doraiswamy A, Narayan RJ, Patz TM, Chrisey DB (2008) Recent progress in CAD/CAM laser direct-writing of biomaterials. *Mater Sci Eng C* 28(3):359–365
56. Guillotin B, Souquet A, Catros S, Duocastella M, Pippenger B, Bellance S, Bareille R, Rémy M, Bordenave L, Amédée J, Guillemot F (2010) Laser assisted bioprinting of engineered tissue with high cell density and microscale organization. *Biomaterials* 31(28):7250–7256

57. Lan PX, Lee JW, Seol YJ, Cho DW (2009) Development of 3D PPF/DEF scaffolds using micro-stereolithography and surface modification. *J Mater Sci Mater Med* 20(1):271–279
58. Lee JW, Ahn G, Kim DS, Cho DW (2009) Development of nano-and microscale composite 3D scaffolds using PPF/DEF-HA and micro-stereolithography. *Microelectron Eng* 86(4):1465–1467
59. Ronca A, Ambrosio L, Grijpma DW (2013) Preparation of designed poly (D, L-lactide)/nanosized hydroxyapatite composite structures by stereolithography. *Acta Biomater* 9(4):5989–5996
60. Ramakrishna S, Mayer J, Wintermantel E, Leong KW (2001) Biomedical applications of polymer-composite materials: a review. *Compos Sci Technol* 61(9):1189–1224
61. Black J, Hastings G (1998) *Hand book of biomaterial properties*, pp 2–5. Chapman & Hall, Springer, Boston, MA
62. Singh R, Kumar R, Ranjan N, Penna R, Fraternali F (2018) On the recyclability of polyamide for sustainable composite structures in civil engineering. *Compos Struct* 184:704–713
63. Singh R, Ranjan N (2017) Experimental investigations for preparation of biocompatible feed-stock filament of fused deposition modeling (FDM) using twin screw extrusion process. *J Thermoplast Compos Mater*. <https://doi.org/10.1177/0892705717738297>
64. Singh R, Sharma R, Ranjan N (2017) Four-dimensional printing for clinical dentistry. Reference module in materials science and materials engineering, pp. 1–28. Elsevier, Oxford
65. Singh R, Kumar R, Ranjan N (2018) Sustainability of recycled ABS and PA6 by banana fiber reinforcement: thermal, mechanical and morphological properties. *J Inst Eng (India): Ser C*. 1–10. <https://doi.org/10.1007/s40032-017-0435-1>
66. Sachs EM, Haggerty JS, Cima MJ, Williams PA (1993) Inventors; Massachusetts institute of technology, assignee. Three-dimensional printing techniques. United States patent US 5,204,055
67. Sachs E, Cima M, Cornie J (1990) Three-dimensional printing: rapid tooling and prototypes directly from a CAD model. *CIRP Ann Manuf Technol* 39(1):201–204
68. Tarafder S, Balla VK, Davies NM, Bandyopadhyay A, Bose S (2013) Microwave-sintered 3D printed tricalcium phosphate scaffolds for bone tissue engineering. *J Tissue Eng Regen Med* 7(8):631–641
69. Warnke PH, Seitz H, Warnke F, Becker ST, Sivananthan S, Sherry E, Liu Q, Wiltfang J, Douglas T (2010) Ceramic scaffolds produced by computer-assisted 3D printing and sintering: Characterization and biocompatibility investigations. *J Biomed Mater Res B Appl Biomater* 93(1):212–217
70. Vorndran E, Klarner M, Klammert U, Grover LM, Patel S, Barralet JE, Gbureck U (2008) 3D powder printing of  $\beta$ -tricalcium phosphate ceramics using different strategies. *Adv Eng Mater* 10(12)
71. Leukers B, Gülkan H, Irsen SH, Milz S, Tille C, Seitz H, Schieker M (2005) Biocompatibility of ceramic scaffolds for bone replacement made by 3D printing. *Materialwiss Werkstofftech* 36(12):781–787
72. Uhland SA, Holman RK, Morissette S, Cima MJ, Sachs EM (2001) Strength of green ceramics with low binder content. *J Am Ceram Soc* 84(12):2809–2818
73. Amirkhani S, Bagheri R, Yazdi AZ (2012) Effect of pore geometry and loading direction on deformation mechanism of rapid prototyped scaffolds. *Acta Mater* 60(6–7):2778–2789
74. Khalyfa A, Vogt S, Weisser J, Grimm G, Rechtenbach A, Meyer W, Schnabelrauch M (2007) Development of a new calcium phosphate powder-binder system for the 3D printing of patient specific implants. *J Mater Sci Mater Med* 18(5):909–916
75. Detsch R, Schaefer S, Deisinger U, Ziegler G, Seitz H, Leukers B (2011) In vitro-osteoclastic activity studies on surfaces of 3D printed calcium phosphate scaffolds. *J Biomater Appl* 26(3):359–380
76. Arsiwala A, Desai P, Patravale V (2014) Recent advances in micro/nanoscale biomedical implants. *J Control Release* 10(189):25–45
77. Dhandayuthapani B, Yoshida Y, Maekawa T, Kumar DS (2011) Polymeric scaffolds in tissue engineering application: a review. *Int J Polym Sci*



78. Kang R, Le DQ, Li H, Lysdahl H, Chen M, Besenbacher F, Bünger C (2013) Engineered three-dimensional nanofibrous multi-lamellar structure for annulus fibrosus repair. *J Mater Chem B* 1(40):5462–5468
79. Peter SJ, Miller MJ, Yasko AW, Yaszemski MJ, Mikos AG (1998) Polymer concepts in tissue engineering. *J Biomed Mater Res Part A* 43(4):422–427
80. Zhu Y, Gao C, Liu Y, Shen J (2004) Endothelial cell functions in vitro cultured on poly (L-lactic acid) membranes modified with different methods. *J Biomed Mater Res Part A* 69(3):436–443
81. Spath S, Seitz H (2014) Influence of grain size and grain-size distribution on workability of granules with 3D printing. *Int J Adv Manuf Technol* 70(1–4):135–144
82. Do AV, Khorsand B, Geary SM, Salem AK (2015) 3D printing of scaffolds for tissue regeneration applications. *Adv Healthcare Mater* 4(12):1742–1762
83. Walker KJ, Madhally SV (2015) Anisotropic temperature sensitive chitosan-based injectable hydrogels mimicking cartilage matrix. *J Biomed Mater Res B Appl Biomater* 103(6):1149–1160
84. Kim YB, Kim GH (2015) PCL/alginate composite scaffolds for hard tissue engineering: fabrication, characterization, and cellular activities. *ACS Comb Sci* 17(2):87–99
85. Shim JH, Kim JY, Park M, Park JS, Cho DW (2011) Development of a hybrid scaffold with synthetic biomaterials and hydrogel using solid freeform fabrication technology. *Biofabrication* 3(3):034102
86. Lee JS, Hong JM, Jung JW, Shim JH, Oh JH, Cho DW (2014) 3D printing of composite tissue with complex shape applied to ear regeneration. *Biofabrication* 6(2):024103
87. Gu BK, Choi DJ, Park SJ, Kim MS, Kang CM, Kim CH (2016) 3-dimensional bioprinting for tissue engineering applications. *Biomater Res* 20(1):12
88. Wen J, Xu Y, Li H, Lu A, Sun S (2015) Recent applications of carbon nanomaterials in fluorescence biosensing and bioimaging. *Chem Commun* 51(57):11346–11358
89. Saito E, Kang H, Taboas JM, Diggs A, Flanagan CL, Hollister SJ (2010) Experimental and computational characterization of designed and fabricated 50: 50 PLGA porous scaffolds for human trabecular bone applications. *J Mater Sci Mater Med* 21(8):2371–2383
90. Jorge-Mora A, Imaz N, Frutos N, Alonso A, Santiago CG, Gómez-Vaamonde R, Pino-Minguez J, Bartolomé J, O’connor G, Nieto D (2017) In vitro evaluation of laser-induced periodic surface structures on new zirconia/tantalum biocermet for hard-tissue replacement. *Laser Ablation From Fundam Appl*
91. Hong D, Chou DT, Velikokhatnyi OI, Roy A, Lee B, Swink I, Issaev I, Kuhn HA, Kumta PN (2016) Binder-jetting 3D printing and alloy development of new biodegradable Fe-Mn-Ca/Mg alloys. *Acta Biomater* 30(45):375–386
92. Hansen DC (2008) Metal corrosion in the human body: the ultimate bio-corrosion scenario. *Electrochem Soc Interface* 17(2):31
93. Wataha JC, Hobbs DT, Wong JJ, Dogan S, Zhang H, Chung KH, Elvington MC (2010) Titanates deliver metal ions to human monocytes. *J Mater Sci Mater Med* 21(4):1289–1295
94. Jayakumar R, Ramachandran R, Divyarani VV, Chennazhi KP, Tamura H, Nair SV (2011) *Int J Biol Macromol* 48:336
95. Roy M, Balla VK, Bandyopadhyay A, Bose S (2012) MgO-doped tantalum coating on Ti: microstructural study and biocompatibility evaluation. *ACS Appl Mater Interface* 4(2):577–580
96. Lewallen EA, Riester SM, Bonin CA, Kremers HM, Dudakovic A, Kakar S, Cohen RC, Westendorf JJ, Lewallen DG, Van Wijnen AJ (2014) Biological strategies for improved osseointegration and osteoinduction of porous metal orthopedic implants. *Tissue Eng Part B: Rev* 21(2):218–230
97. Gu XN, Li SS, Li XM, Fan YB (2014) Magnesium based degradable biomaterials: A review. *Front Mater Sci* 8(3):200–218
98. Chen G, Ushida T, Tateishi T (2002) Scaffold design for tissue engineering. *Macromol Biosci* 2(2):67–77

99. Zhuang H, Han Y, Feng A (2008) Preparation, mechanical properties and in vitro biodegradation of porous magnesium scaffolds. *Mater Sci Eng C* 28(8):1462–1466
100. Wu C, Fan W, Zhou Y, Luo Y, Gelinsky M, Chang J, Xiao Y (2012) 3D-printing of highly uniform CaSiO<sub>3</sub> ceramic scaffolds: preparation, characterization and in vivo osteogenesis. *J Mater Chem* 22(24):12288–12295
101. Moreno EC, Kresak M, Zahradnik RT (1974) Fluoridated hydroxyapatite solubility and caries formation. *Nature* 247(5435):64
102. Leukers B, Güllkan H, Irsen SH, Milz S, Tille C, Schieker M, Seitz H (2005) Hydroxyapatite scaffolds for bone tissue engineering made by 3D printing. *J Mater Sci Mater Med* 16(12):1121–1124
103. Zhou Z, Buchanan F, Mitchell C, Dunne N (2014) Printability of calcium phosphate: calcium sulfate powders for the application of tissue engineered bone scaffolds using the 3D printing technique. *Mater Sci Eng C* 1(38):1
104. Castilho M, Moseke C, Ewald A, Gbureck U, Groll J, Pires I, Teßmar J, Vorndran E (2014) Direct 3D powder printing of biphasic calcium phosphate scaffolds for substitution of complex bone defects. *Biofabrication* 6(1):015006
105. Gevaert E, Dolle L, Billiet T, Dubruel P, van Grunsven L, van Apeldoorn A, Cornelissen R (2014) High throughput micro-well generation of hepatocyte micro-aggregates for tissue engineering. *PLoS ONE* 9(8):e105171
106. Shapiro JM, Oyen ML (2013) Hydrogel composite materials for tissue engineering scaffolds. *JOM* 65(4):505–516
107. Zhu J, Marchant RE (2011) Design properties of hydrogel tissue-engineering scaffolds. *Expert Rev Med Devices* 8(5):607–626
108. Park SH, Park DS, Shin JW, Kang YG, Kim HK, Yoon TR, Shin JW (2012) Scaffolds for bone tissue engineering fabricated from two different materials by the rapid prototyping technique: PCL versus PLGA. *J Mater Sci Mater Med* 23(11):2671–2678
109. Griffith LG (2000) Polymeric biomaterials. *Acta Mater* 48(1):263–277
110. Intra J, Glasgow JM, Mai HQ, Salem AK (2008) Pulsatile release of biomolecules from polydimethylsiloxane (PDMS) chips with hydrolytically degradable seals. *J Control Release* 127(3):280–287
111. Mountziaris PM, Spicer PP, Kasper FK, Mikos AG (2011) Harnessing and modulating inflammation in strategies for bone regeneration. *Tissue Eng Part B: Rev* 17(6):393–402
112. Rajan V, Murray RZ (2008) The duplicitous nature of inflammation in wound repair wound practice & research. *J Aust Wound Manage Assoc* 16(3):122
113. Almeida CR, Serra T, Oliveira MI, Planell JA, Barbosa MA, Navarro M (2014) Impact of 3-D printed PLA-and chitosan-based scaffolds on human monocyte/macrophage responses: unraveling the effect of 3-D structures on inflammation. *Acta Biomater* 10(2):613–622
114. Sung HJ, Meredith C, Johnson C, Galis ZS (2004) The effect of scaffold degradation rate on three-dimensional cell growth and angiogenesis. *Biomaterials* 25(26):5735–42
115. Moshiri A, Oryan A (2013) Role of platelet rich plasma in soft and hard connective tissue healing: an evidence based review from basic to clinical application. *Hard Tissue* 2(1):6
116. Aydin A, Memisoglu K, Cengiz A, Atmaca H, Muezzinoglu B, Muezzinoglu US (2012) *J Orthop Sci: Official J Jpn Orthop Assoc* 17:796
117. Choi SH, Park TG (2002) Synthesis and characterization of elastic PLGA/PCL/PLGA triblock copolymers. *J Biomater Sci Polym Ed* 13(10):1163–1173
118. Gong CY, Shi S, Dong PW, Yang B, Qi XR, Guo G, Gu YC, Zhao X, Wei YQ, Qian ZY (2009) Biodegradable in situ gel-forming controlled drug delivery system based on thermosensitive PCL-PEG-PCL hydrogel: Part I—synthesis, characterization, and acute toxicity evaluation. *J Pharm Sci* 98(12):4684–4694
119. Inzana JA, Trombetta RP, Schwarz EM, Kates SL, Awad HA (2015) 3D printed bioceramics for dual antibiotic delivery to treat implant-associated bone infection. *Eur cells Mater* 30:232
120. Elangovan S, D’Mello SR, Hong L, Ross RD, Allamargot C, Dawson DV, Stanford CM, Johnson GK, Sumner DR, Salem AK (2014) The enhancement of bone regeneration by gene activated matrix encoding for platelet derived growth factor. *Biomaterials* 35(2):737–747

121. Lam CX, Mo XM, Teoh SH, Hutmacher DW (2002) Scaffold development using 3D printing with a starch-based polymer. *Mater Sci Eng C* 20(1–2):49–56
122. Harris B (1980) The mechanical behaviour of composite materials. In: *Symposia of the society for experimental biology*, vol 34, pp 37
123. Krause WR, Park SH, Straup RA (1989) Mechanical properties of BIS-GMA resin short glass fiber composites. *J Biomed Mater Res Part A* 23(10):1195–1211
124. Hastings GW (1986) Carbon and plastic materials for orthopaedic implants. *Materials sciences and implant orthopedic surgery*, pp 263–284. Springer, Dordrecht
125. Tayton K, Bradley J (1983) How stiff should semi-rigid fixation of the human tibia be? A clue to the answer. *J Bone Joint Surg* 65(3):312–5
126. Tayton KJJ (1983) The use of carbon fibre in human implants: the state of the art. *J Med Eng Technol* 7(6):271–272
127. Singh R, Kumar R, Mascolo I, Modano M (2018) On the applicability of composite PA6-TiO<sub>2</sub> filaments for the rapid prototyping of innovative materials and structures. *Compos Part B Eng* 143:132–140. <https://doi.org/10.1016/J.COMPOSITESB.2018.01.032>
128. Kumar R, Singh R, Hui D et al (2018) Graphene as biomedical sensing element: State of art review and potential engineering applications. *Compos Part B Eng* 134. <https://doi.org/10.1016/j.compositesb.2017.09.049>
129. Singh R, Kumar R, Feo L, Fraternali F (2016) Friction welding of dissimilar plastic/polymer materials with metal powder reinforcement for engineering applications. *Compos Part B Eng* 101. <https://doi.org/10.1016/j.compositesb.2016.06.082>
130. Kumar R, Singh R, Ahuja IPS et al (2018) Weldability of thermoplastic materials for friction stir welding—a state of art review and future applications. *Compos Part B Eng* 137. <https://doi.org/10.1016/j.compositesb.2017.10.039>
131. Kumar R, Singh R, Ahuja IPS et al (2018) Friction welding for the manufacturing of PA6 and ABS structures reinforced with Fe particles. *Compos Part B Eng* 132:244–257. <https://doi.org/10.1016/j.compositesb.2017.08.018>
132. Kumar R, Singh R, Ahuja IPS (2018) Investigations of mechanical, thermal and morphological properties of FDM fabricated parts for friction welding applications. *Meas J Int Meas Confed* 120. <https://doi.org/10.1016/j.measurement.2018.02.006>
133. Kumar R, Singh R (2018) Prospect of graphene for use as sensors in miniaturized and biomedical sensing devices. *Ref Modul Mater Sci Mater Eng* 1–13. <https://doi.org/10.1016/b978-0-12-803581-8.10334-0>
134. Singh R, Kumar R, Kumar S (2017) Polymer waste as fused deposition modeling feed stock filament for industrial applications. *Ref Modul Mater Sci Mater Eng* 1–12. <https://doi.org/10.1016/b978-0-12-803581-8.04153-9>

**Mr. Nishant Ranjan** is a PhD research scholar at Punjabi University, Patiala, and is working in the area of additive manufacturing and feedstock developments. He has authored more than five research paper.

**Prof. Rupinder Singh** is Professor in the Department of Production Engineering, Guru Nanak Dev Engineering College, Ludhiana, India. He has received Ph.D. in Mechanical Engineering from Thapar Institute of Engineering and Technology, Patiala, India. His area of research is non-traditional machining, additive manufacturing and development of porous biomaterials using 3D printing and rapid prototyping techniques. He has more than 18 years of teaching and research experience. He has contributed extensively to the world in additive manufacturing literature with publications appearing in *Journal of Manufacturing Processes*, *Composite Part B*, *Rapid Prototyping Journal*, *Journal of Mechanical Science and Technology*, *Measurement*, *International Journal of Advance Manufacturing Technology*, and *Journal of Cleaner Production*. He authored 17 books and ~3 chapters. He has received more than 3 crores research grants from various

funding agencies such as DST-SERB, AICTE, CSIR, DAE, IE. He is working with Prof. Seeram Ramakrishna, NUS Nanoscience and Nanotechnology Initiative and Prof. Fernando Fraternali, Full Professor of Structural Mechanics, Department of Civil Engineering, University of Salerno.

**Dr. I. P. S. Ahuja** is working as Professor in Mechanical Engineering Department of Punjabi University, Patiala. His research areas are optimization, machining, industrial engineering, and manufacturing. He has authored more than 150 research papers. He served as reviewer of various journals. He guided more than 10 Ph.D. thesis and 20 M.Tech. thesis.

**Professor Dr. MD. Mustafizur Rahman** is a Consultant, a Researcher currently working with the Faculty of Mechanical Engineering, University Malaysia Pahang, Malaysia, since April 2007. Dr. Rahman also served as a Director in the Automotive Engineering Centre, UMP. He received his Ph.D. degree from the Department of Mechanical and Materials Engineering, Universiti Kebangsaan Malaysia, Malaysia. His prior work experience includes Lecturer in the Department of Mechanical Engineering, Khulna University of Engineering and Technology, Khulna, Bangladesh, and as an Assistant Professor in the Department of Industrial and Production Engineering, Shahjalal University of Science and Technology, Bangladesh. He served as a head of the department in the same department. The research work of Dr. Rahman is focused on internal-combustion engine and alternative fuels, fatigue fracture as well as optimization, finite-element analysis, artificial intelligence, advanced machining techniques. He has managed to publish more than 200 papers in international scholarly journals and conferences. He is also the editorial member of several scientific journals. He has been the technical reviewer for over 25 scientific journals as well as the member of the technical board for conferences. He is the Fellow of Association of Computer, Electronics and Electrical Engineers (ACEEE) and Indian Society of Mechanical Engineers (ISME). He has been supervised 11 Ph.D. and 10 M.Sc. Eng. Candidates and more than 35 undergraduate dissertations.

**Prof. Seeram Ramakrishna** is Co-Director, NUS Nanoscience and Nanotechnology Initiative (NUSNNI). He has received his Ph.D. from the University of Cambridge. He is a global leader in electrospinning and nanostructured materials. Since 2001, Seeram's team has contributed significantly to the scientific knowledge in basic research, advances in the process and the applications of nanofibers. Professor Seeram Ramakrishna's research resulted in ~1000 peer-reviewed articles with ~70,000 citations and ~120 H-index. He authored 5 books and ~25 chapters. He has been recognized as a Highly Cited Researcher in Materials Science ([www.highlycited.com](http://www.highlycited.com)) for the past four years. Thomson Reuters listed him among the Most Influential Scientific Minds in the World. NUS Vice-President (research strategy); Dean of Faculty of Engineering; Founding Director of NUSNNI, and Bioengineering; Founding Chair of Global Engineering Deans Council; Vice-President of International Federation of Engineering Education Societies; Board member of Asia Society for Innovation and Policy. EC/FP7 report lists him among the top four researchers of Singapore. He is recognized as world's number one in nanofiber technologies. He also generated intellectual property in the form of 20 patents and licensed technologies to industry and start-ups. He mentors Singapore-based start-ups, namely (a) BioMers International, (b) Insight BioVentures, (c) ceEntek, (d) Hyperion Core and (e) Everest Capital. Moreover, he works with companies such as HP, Schlumberger, BASF, Interplex, GE, Mann Hummel, Kaneka, Mitsubishi, Toray, Unitex, GSK, AMT, etc., for value capture in Singapore.

# Chapter 11

## Dental Crowns by FDM Assisted Vapour Smoothing and Silicon Moulding



R. Singh, Rupinder Singh, and J. S. Dureja

### 11.1 Introduction

Nowadays, the reduction in product cost and cycle time by using additive manufacturing (AM) techniques is well-established fact [1–4]. The AM uses CAD data to print prototypes (both functional/non functional) that can be used at once as finished products [5–8]. Due to the advancement in AM, it has become a reality to get the customized implants as required [9, 10]. These can be produced timely at low cost because of the versatile nature of the 3D printing. Fused deposition modelling (FDM) is low-cost commercial AM process [11–13]. The material (filament) used for FDM is strong in itself but the bonds between the forming layer are much weaker [14, 15]. Due to this, the parts printed during the material extrusion process have poor surface finish and with a defect of stair-stepping [16, 17]. FDM uses the thermoplastic materials to feed into the hot nozzle where it transforms into the semi liquid state [18–20].

The main problems come when the printed parts are used as patterns for casting applications [21, 22]. So, there surface needs post-finishing which can be achieved by a technique called CVS. In CVS technique, the thermoplastic materials are exposed to chemical vapours (e.g. acetone in case of ABS). The acetone vapours improve the

---

R. Singh (✉)  
Punjabi University Patiala, Patiala, India  
e-mail: [ranvirsingh760@gmail.com](mailto:ranvirsingh760@gmail.com)

GNA University, Phagwara, Punjab, India

R. Singh  
Production Engineering Department, Guru Nanak Dev Engineering College, Ludhiana 141006,  
India  
e-mail: [rupindersingh78@yahoo.com](mailto:rupindersingh78@yahoo.com)

J. S. Dureja  
Mechanical Engineering Department, Punjabi University Patiala, Patiala, India

$R_a$  of the parts by breaking the secondary bonds between the layers of the ABS and ultimately softening the outer surface [18]. The CVS as post-processing technique has the potential to reduce the staircase effect [18, 23–25].

Currently, AM technologies are not recommended for medium to large scale production [26–28] and for developing rapid tooling (RT) [29–31] mainly because of high input cost, material-related issues, etc. SM is an established prototyping technique (for batch production) to produce patterns [32] which can be used to overcome limitations of commercial AM processes. In SM process, a master pattern is first manufactured. After that, liquid silicone and hardener in suitable proportion are put in mould box around the pattern. The mould is then left for 12–18 h for healing [33, 34]. The material is then cut usually from the centre and the master is detached. The cavity created is fitted with the runner and the gating system. The mould is then reassembled and suitable materials like wax, PU, etc. are poured as per requirement [35]. Some researchers have highlighted an indirect approach to the production of wax patterns using SM to reduce the costs of batch production during IC process [2]. The numbers of direct and indirect routes (AM assisted with SM) for the rapid manufacture of IC have been widely reported. [29]. Kai et al. outlined that AM approach is the better option from design flexibility view point [30].

Singh and Singh developed macro-model for printing of plastic components via SM in terms of  $\Delta d$  and concluded that the tolerance grades for the prepared components are as per UNI EN 20286-I (1995) standard [32]. Few researchers outlined the  $\Delta d$  of wax patterns printed by room temperature vulcanization (RTV) and SM [33]. Also, researchers have recommended that the  $\Delta d$  of customary IC processes can be enhanced by replacing usual wax-based patterns with contemporary thermoplastic patterns [32–35].

The reported literature on AM, FDM, CVS and SM reveals that lot of work has been done to improve master patterns by independently optimizing the input parameters of the FDM and SM processes, but till now, very little has been reported on comparison of  $R_a$ ,  $\Delta d$  and SH of the dental crowns prepared by FDM assisted with CVS and SM process. In this case study, the functional prototypes as dental crowns have been prepared independently in two stages. In the first stage, effect of CVS, part density and orientation in FDM (with ABS thermoplastic) as digital manufacturing tool on output parameters ( $R_a$ ,  $\Delta d$  and SH of dental crowns as functional prototype from assembly view point) have been investigated. In second stage, SM process has been used for making replicas of dental crowns (prepared in first stage). The process parameters selected for SM are: de-moulding time, hardener proportion in weight percentage and curing temperature. Further, ANOVA has been employed to find out the significance of process parameter from multifactor optimization point of view.

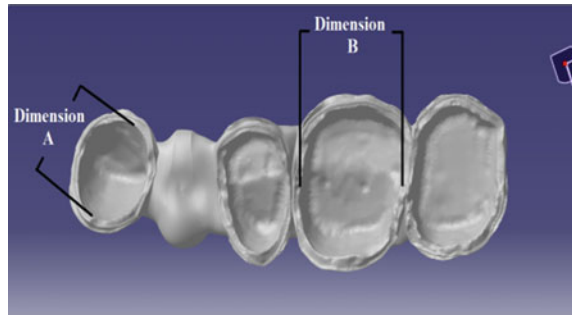
## 11.2 Methodology

### 11.2.1 Stage 1

In this stage, dental crown (see Fig. 11.1) has been selected for case study. This work was divided into two phases. Samples of ABS material were manufactured in the first phase (preprocessing phase) on commercial FDM setup “Make: uPrint-SE, Stratasys USA” by varying the “orientation” and “part density” as input variables. The prototypes were subjected to the CVS in second stage (post-processing phase). The CVS process has been carried out with acetone on “Stratasys, USA finishing touch smoothing station.”

The exposure time of the prototypes to chemical vapors is one of the parameters chosen in the second phase. The selected levels for two phases of experimentation are shown in Table 11.1. The hardness and dimensional precision of the specimens have been measured before and after the CVS process. Two dimensions “A” and “B” (see Fig. 11.1) have been selected judiciously for dimensional accuracy. The dimensions A and B have been measured before and after the CVS process, but no variation in average deviation of both dimensions were observed (see Table 11.2). The  $R_a$  value of the specimens was measured before and after the CVS by “Mitutoyo SJ-210

**Fig. 11.1** Benchmark (dental crown)



**Table 11.1** Two-phase factors and their levels (stage 1)

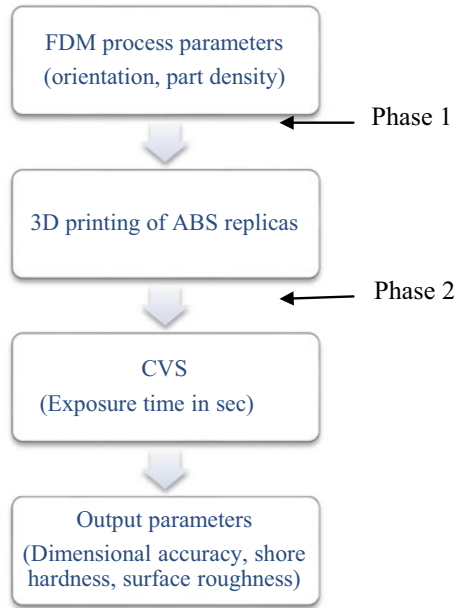
Phase 1					Phase 2				
Factor	Symbol	Levels			Factor	Symbol	Levels		
Angle of orientation	A	1	2	3	Exposure time in s (CVS)	C	1	2	3
		0°	30°	45°			10	20	30
Density	B	Low	Medium	High					

*Note* Low, medium and high density refers to part density as 25, 50 and 75%. This actually refers to the closeness of consecutive layers while printing

**Table 11.2** Dimensions before and after CVS (stage 1)

Dimension	Nominal dimension (mm) before CVS	Nominal dimension (mm) after CVS	Average deviation ( $\Delta d$ )
A	13.93	14.04	0.11
B	20.54	20.65	0.11

**Fig. 11.2** Flow chart for stage 1



roughness tester.” For better understanding, flowchart of whole process is shown in Fig. 11.2.

**11.2.1.1 Analysis for Stage 1**

Based upon Table 11.1, Taguchi L9 orthogonal array (O.A) was used in both phases 1 and 2 for dimensional accuracy (Table 11.3), shore hardness (Table 11.4) and surface roughness (Table 11.5). Further based upon Table 11.3, Fig. 11.3 shows S/N ratio plot for  $\Delta d$ . As observed from Fig. 11.3, parts printed at 45° orientations with low density, 30 s exposure time are the best settings for controlling  $\Delta d$ . Based upon Table 11.4, Fig. 11.4 shows the S/N ratio plot for SH. As observed from Fig. 11.4, the parts printed at 30° orientations with low density, 20 s exposure time are the best settings. Further based upon Table 11.5, Fig. 11.5 shows S/N ratio plot for  $R_a$ .



**Table 11.3** S/N ratio for  $\Delta d$  (phases 1 and 2)

S. No.	Angle of orientation	Part density	Output from phase 1 (dimension A) mm	Output from phase 1 (dimension B) mm	Exposure time (s) CVS (s)	Output from phase 2 ( $\Delta d$ )	S/N ratio (dB)
1	0°	Low	20.77	13.95	10	0.12	18.41
2	0°	Medium	20.83	13.98	20	0.16	15.91
3	0°	High	20.64	13.92	30	0.18	14.89
4	30°	Low	20.63	13.89	20	0.19	14.42
5	30°	Medium	20.63	13.86	30	0.21	13.55
6	30°	High	20.56	13.82	10	0.26	11.7
7	45°	Low	20.65	14.01	30	0.08	21.93
8	45°	Medium	20.54	13.93	10	0.11	19.17
9	45°	High	20.61	13.97	20	0.15	16.47

*Note* For S/N ratio calculation output at phase 2 has been considered for minimum the better type case

**Table 11.4** S/N ratio for shore hardness from phases 1 and 2

S. No.	Angle of orientation	Part density	Output from stage 1 (SH)	Exposure time (s) CVS (s)	Output from stage 2 (SH)	S/N ratio (dB)
1	0°	Low	77	10	72	37.14
2	0°	Medium	75	20	69	36.77
3	0°	High	76	30	67	36.52
4	30°	Low	82	20	79	37.95
5	30°	Medium	78	30	73	37.26
6	30°	High	81	10	77	37.72
7	45°	Low	79	30	74	37.38
8	45°	Medium	80	10	73	37.26
9	45°	High	83	20	75	37.50

*Note* For S/N ratio calculation output at phase 2 has been considered for maximum the better type case

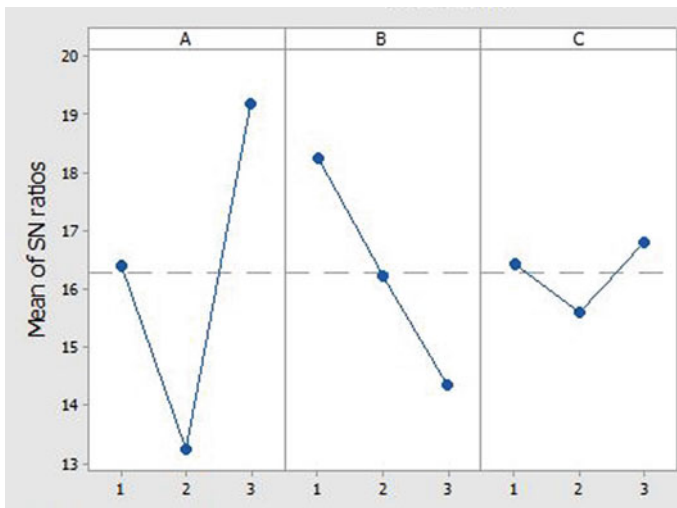
As observed from Fig. 11.5, parts printed at 45° orientations, at high density, 30 s exposure time are the best settings.

Based on Table 11.3 and Fig. 11.3, variance analysis (ANOVA) was carried out (see Table 11.6). As observed from Table 11.6, parameters “A” and “B” are significantly affecting the  $\Delta d$  of ABS parts as *p* values for these are less than 0.05 at 95% confidence level. Further, the percentage contribution of these parameters is 67.86% and 28.98%, respectively. Similarly, based upon Table 11.4 and Fig. 11.4, Table 11.7 shows that all three input parameters are significantly affecting the SH of ABS parts as *p* values for these are less than 0.05. Further, the percentage contribution of these

**Table 11.5** S/N ratio for surface roughness from phases 1 and 2

S. No.	Angle of orientation	Part density	Output from stage 1 ( $R_{a1}$ ) ( $\mu\text{m}$ )	Exposure time (s) CVS (s)	Output from stage 2 ( $R_{a1}$ ) ( $\mu\text{m}$ )	S/N ratio (dB)
1	0°	Low	7.997	10	0.508	5.88
2	0°	Medium	8.317	20	0.746	2.54
3	0°	High	8.86	30	0.329	9.65
4	30°	Low	8.963	20	0.722	2.82
5	30°	Medium	8.34	30	0.565	4.95
6	30°	High	8.478	10	0.383	8.33
7	45°	Low	7.78	30	0.236	12.54
8	45°	Medium	6.992	10	0.231	12.72
9	45°	High	7.192	20	0.213	13.43

Note For S/N ratio calculation Output at phase 2 has been considered for minimum the better type case



**Fig. 11.3** Main effect plots for mean S/N ratio ( $\Delta d$ )

parameters is 70.35%, 15.01% and 14.72, respectively. Based upon Table 11.5 and Fig. 11.5, Table 11.8 shows ANOVA of S/N ratio for  $R_a$ . It was observed that all three parameters significantly affect the  $R_a$  of ABS parts as p values for these are less than 0.05. Further, the percentage contribution of these parameters is 71.69%, 17.54% and 10.38%, respectively.

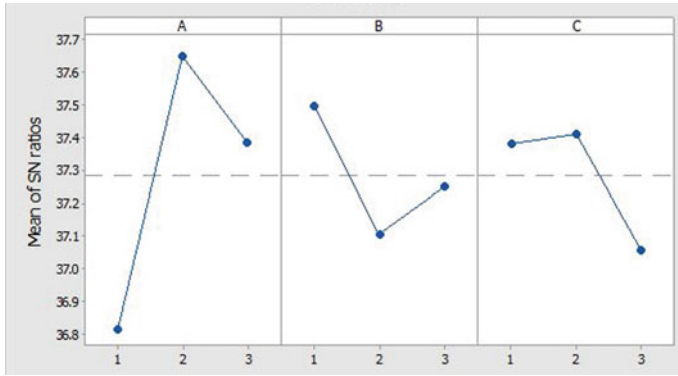


Fig. 11.4 Main effect plots for mean S/N ratio (SH)

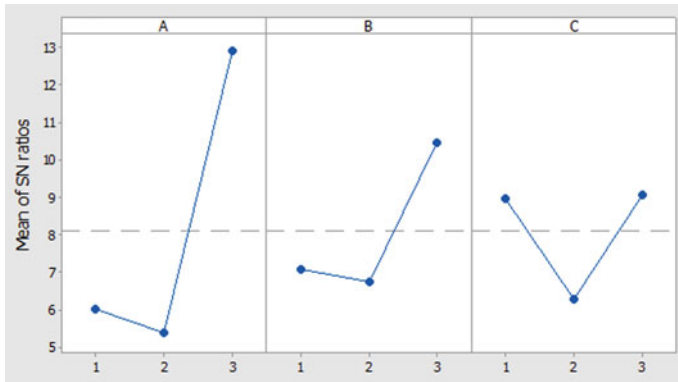


Fig. 11.5 Main effect plots for mean S/N ratio (Ra)

Table 11.6 ANOVA of S/N ratio for  $\Delta d$

Parameter	DoF	SS	P	Percentage contribution (%)
A	2	53.52	0.005*	67.86
B	2	22.85	0.011*	28.98
C	2	2.225	0.105	2.82
Error	2	0.262		0.33
Total	8	78.86		100

DoF degree of freedom, SS sum of square, P probability, \* significant parameters

### 11.2.1.2 Optimization and Confirmation Experiments for Stage 1

For stage 1, it was observed that significant factors and their percentage contribution for the three responses were different (see Figs. 11.3, 11.4 and 11.5; Tables 11.6, 11.7,

**Table 11.7** ANOVA of S/N ratios for SH

Parameter	DoF	SS	P	Percentage contribution (%)
A	2	1.090	0.005	70.35
B	2	0.234	0.025	15.01
C	2	0.229	0.025	14.72
Error	2	0.005		0.38
Total	8	1.561		100

**Table 11.8** ANOVA of S/N ratio for  $R_a$

Parameter	DoF	SS	P	Percentage contribution
A	2	104.39	0.005	71.69
B	2	25.529	0.021	17.54
C	2	15.113	0.034	10.38
Error	2	0.534		0.36
Total	8	145.48		100

11.8). The best parameters for the three answers are different. Therefore, instead of arbitrarily optimizing the single response, overall process optimization was used. Table 11.9 shows the constraints set and the optimal values in Minitab software.

Starting in stage 1, the calculated  $\Delta d$ ,  $R_a$  and SH corresponding to S/N ratio of 21.33, 12.76 and 37.69 are 0.079 mm, 0.198  $\mu\text{m}$  and 78 SH, respectively. In order to check the validity of the results suggested by the software, two confirmation tests with optimum parameter values in Table 11.9 were carried out. The  $\Delta d$ ,  $R_a$  and SH for the two confirmation tests were found to be (0.074, 0.080 mm), (0.182, 0.192  $\mu\text{m}$ ) and (79 SH, 77 SH), respectively.

**Table 11.9** Optimum values and constraints with desirability

Parameter	Set goal	Lower limit	Higher limit	Weight	Importance
Angle of orientation	Region constraint	0	45°	1	1
Part density	Region constraint	Low	High	1	1
Exposure time	Region constraint	10 s	30 s	1	1
S/N ratio (SH)	Maximum	36	37	1	1
S/N ratio ( $\Delta d$ )	Maximum	11	21	1	1
S/N ratio ( $R_a$ )	Maximum	2	13	1	1

Optimum values (stage 1)

Angle of orientation	Density	Exposure time	S/N ratio ( $\Delta d$ )	S/N ratio (SH)	S/N ratio ( $R_a$ )	Desirability
45°	Low	10 s	21.33	37.69	12.76	0.924

## 11.2.2 Stage 2

In stage 2, based upon input parametric settings in Table 11.9, one ABS master pattern has been prepared and CVS cycle has been performed. Again as per Fig. 11.1, dimension A for silicon moulding process has been selected for further evaluation. The silicone rubber mixture consisting of “VTV-750” silicone rubber and “CAT 740” catalyst as hardener in a ratio of 10:1 has been prepared. Figure 11.6a–h shows the different steps involved in SM. After making the mould, it is ready for vacuum casting (VC). The  $\Delta d$  and  $R_a$  values of the mould cavity have been checked before the pouring of PP resins and found to be within the acceptable range. For this case study PP resins “Renishaw 8040” was used. The PP consists of two resins: (A) polymeric polyol with hydroxyl group as hardener; (B) di-isocyanate compound as softener. Table 11.10 shows the various properties of Renishaw 8040 (commercially used PP resin). The replicas prepared by VC are shown in Fig. 11.7.

Table 11.11 shows the parameters of the input and their levels for stage 2.

### 11.2.2.1 Analysis for Stage 2

In stage 2, shrinkage was observed in all experiments (see Table 11.12). The maximum average deviation percentage is 1.11%. The value of  $R_a$  was observed for the selected material in the range from 0.4 to 0.9  $\mu\text{m}$ . Since the aim is to achieve minimum  $\Delta d$  and  $R_a$ , so S/N ratio based on “lower is better” has been calculated. For SH to be maximum, S/N ratio based on “larger is better” was selected.

ANOVA was performed on calculated S/N ratios for the analysis of results (Tables 11.13, 11.14 and 11.15). The  $P$ -value below 0.05 (Tables 11.13, 11.14 and 11.15) shows significant model terms.

Based upon Tables 11.12, 11.13, 11.14 11.15, Figs. 11.8, 11.9 and 11.10 show S/N ratio plots for  $\Delta d$ ,  $R_a$  and SH. As observed from Fig. 11.8, minimum  $\Delta d$  was observed when curing temperature is 60 °C and it increases with increase in curing temperature. This may be due to the fact that by increasing the temperature, it shrinks the material more and which causes more deviation. So, it has been observed that optimum parameter setting that minimizes the  $\Delta d$  is  $A_3$ ,  $B_1$  and  $C_1$  (see Fig. 11.8). It has been observed that hardener percentage and curing temperature have very little effect as their percentage contribution is very less as seen from the ANOVA Table 11.14. De-moulding time (min) affects the  $R_a$  significantly as seen from its high  $F$ -value in the ANOVA Table 11.14. The  $R_a$  increases with increase in de-moulding time (min) and minimum  $R_a$  is observed when de-moulding time is 90 min. So, it has been observed that optimum parameter setting that minimizes the  $R_a$  is  $A_1$ ,  $B_1$  and  $C_1$  (see Fig. 11.9).

As observed from Table 11.15 and Fig. 11.10, curing temperature affects the SH significantly. It has been observed that best parameter settings that maximize the SH is  $A_3$ ,  $B_2$  and  $C_3$ .



(a) Gate attached to FDM pattern



(b) Assembly put in a frame



(c) Mixing rubber, hardener and pouring into the frame



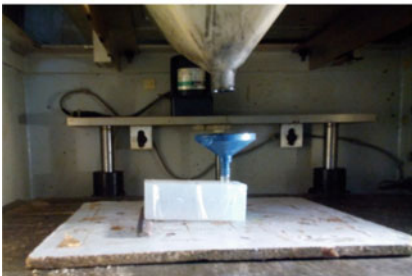
(d) Cured mould



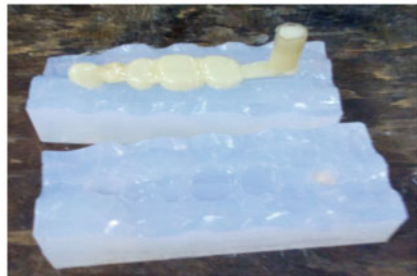
(e) Cut the mould for removing the pattern



(f) Mould ready for casting



(g) Pour the material into mould



(h) After pouring final component is ready

**Fig. 11.6** Steps involved in SM process

**Table 11.10** Properties of Resin 8040

Material	A	B	Mixture
	Polyol	Isocyanate	–
Density @ 25 °C (g/cm <sup>3</sup> )	0.99	1.14	1.08
Viscosity @ 25 °C (cPs)	1200	140	420
Pot life @ 25 °C	–	–	5 min
De-mould time at 65 °C	–	–	50–80 min

**Fig. 11.7** Fabricated replicas of PP materials



**Table 11.11** Input parameters and their levels (stage 2)

Parameters	Symbol	Levels		
		Level 1	Level 2	Level 3
Hardener %	A	100:90	110:90	120:90
De-moulding time (min)	B	90 min	105 min	120 min
Curing temperature (°C)	C	60 °C	70 °C	80 °C

**11.2.2.2 Optimization and Confirmation Experiments for Stage 2**

From Tables 11.13, 11.14 and 11.15, it has been observed that significant factors and their percentage contribution for the three responses are different for stage 2. Table 11.16 shows the set constraints and the optimal values for multifactor optimization.

From stage 2, the calculated  $\Delta d$ ,  $R_a$  and SH corresponding to S/N ratio of 14.91, 4.84 and 38.04 are 0.096 mm, 0.295  $\mu\text{m}$  and 83 SH, respectively. In order to verify the validity of the results suggested by the software, two confirmation tests with optimum parameter values were carried out. The  $\Delta d$ ,  $R_a$  and SH for the two confirmation tests were found to be (0.091, 0.097 mm), (0.325, 0.342  $\mu\text{m}$ ) and (84 SH, 85 SH),

**Table 11.12** S/N ratio for the three responses (stage 2)

S. No.	Hardener ratio (%)	De-moulding time (min)	Curing temp (°C)	$\Delta d$ (mm)	$R_d$ ( $\mu\text{m}$ )	SH	S/N ratio for $\Delta d$	S/N ratio for $R_d$	S/N ratio for SH
1	100:90	90	60	0.17	0.492	72	15.39	6.160	37.14
2	100:90	105	70	0.27	0.602	82	11.37	4.408	38.27
3	100:90	120	80	0.19	0.769	79	14.42	2.281	37.95
4	110:90	90	70	0.25	0.741	74	12.04	2.603	37.38
5	110:90	105	80	0.20	0.698	80	13.97	3.122	38.06
6	110:90	120	60	0.18	0.873	67	14.89	1.179	36.52
7	120:90	90	80	0.16	0.716	81	15.91	2.901	38.16
8	120:90	105	60	0.17	0.632	79	15.39	3.985	37.95
9	120:90	120	70	0.23	0.914	77	12.76	0.781	37.72



**Table 11.13** ANOVA table for  $\Delta d$

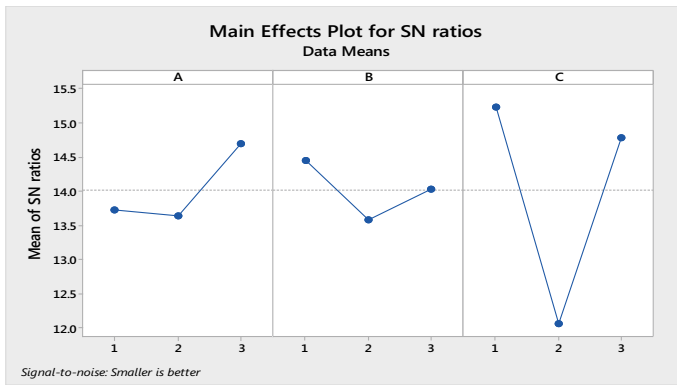
Parameter	DoF	SS	<i>P</i>	Percentage contribution
A	2	2.0421	0.010	9.82%
B	2	1.1328	0.018	5.44%
C	2	17.5926	0.001	84.62%
Error	2	0.0208		0.10%
Total	8	20.7884		100

**Table 11.14** ANOVA table for  $R_a$

Parameter	DoF	SS	<i>P</i>	Percentage contribution
A	2	6.9736	0.061	31.90%
B	2	12.0057	0.036	54.93%
C	2	2.4298	0.156	11.11%
Error	2	0.4502		2.05%
Total	8	21.8593		100

**Table 11.15** ANOVA table for SH

Parameter	DoF	SS	<i>P</i>	Percentage contribution
A	2	0.63980	0.038	24.55%
B	2	0.79207	0.031	30.40%
C	2	1.14813	0.022	44.06%
Error	2	0.02536		0.97%
Total	8	2.60537		100



**Fig. 11.8** Main effect plots of S/N ratios for  $\Delta d$

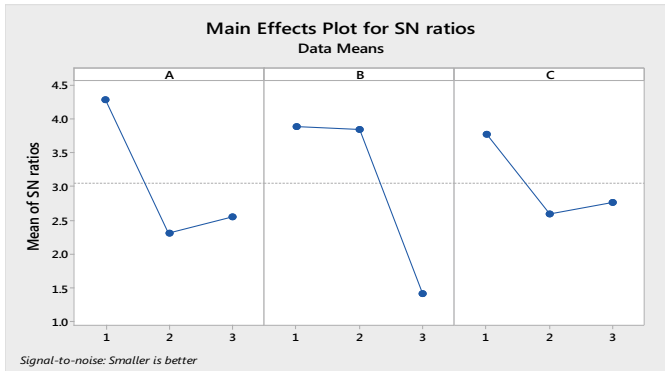


Fig. 11.9 Main effect plots of S/N ratios for  $R_a$

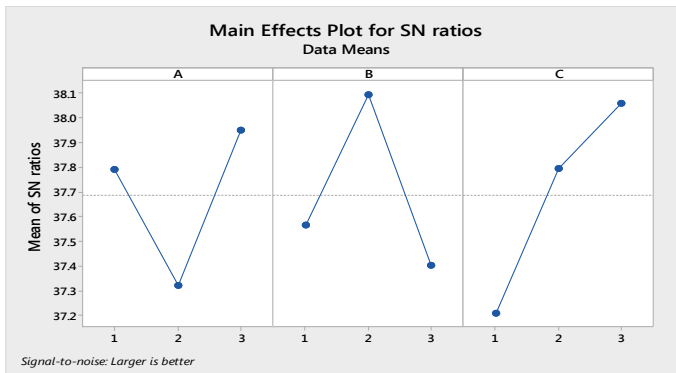


Fig. 11.10 Main effect plot of S/N ratios for SH

respectively. The surface roughness profile ( $R_a$ ) of the two samples manufactured in optimal parameters is shown in Fig. 11.11.

### 11.3 Results and Discussion

After completion of stage 2, the tolerance (IT) grades of the fabricated components with SM were deduced (see Table 11.17).

Initially, the measured dimensions have been used to evaluate the tolerance unit “ $n$ ” that drives from the fundamental tolerance “ $I$ ”, as per UNI EN 20286-I (1995). The “ $i$ ” and “ $n$ ” were calculated by using Eqs. 1 and 2:

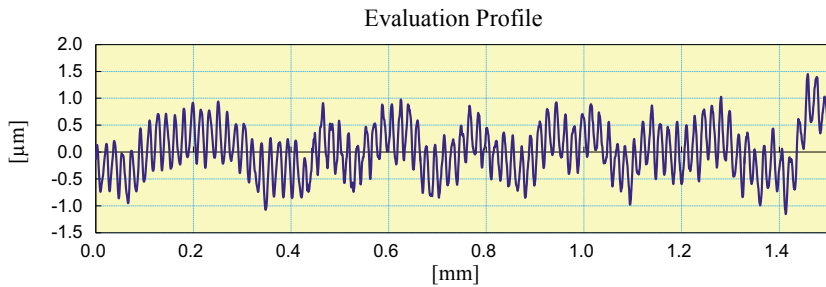
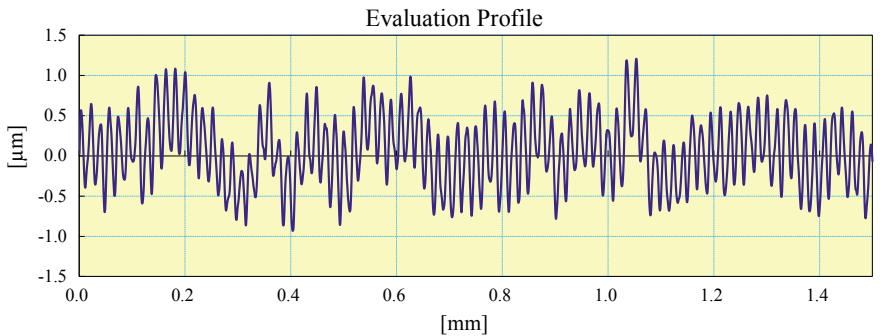
$$i = 0.45\sqrt[3]{D} + 0.001D \tag{1}$$

**Table 11.16** Suggested constraints and optimum values (stage 2)

Parameter	Set goal	Lower limit	Higher limit	Weight	Importance
Hardener %	Region constraint	100:90	120:90	1	1
De-moulding time (min)	Region constraint	90 min	120 min	1	1
Curing temperature (°C)	Region constraint	60 °C	80 °C	1	1
S/N ratio ( $\Delta d$ )	Maximum	11.3727	15.9176	1	1
S/N ratio ( $R_a$ )	Maximum	0.7811	6.1607	1	1
S/N ratio (SH)	Maximum	36.5215	38.2763	1	1

*Optimum values (stage 2)*

Hardener %	De-moulding time (min)	Curing temperature (°C)	S/N ratio ( $\Delta d$ )	S/N ratio ( $R_a$ )	S/N ratio (SH)	Desirability
100:90	90 min	80 °C	14.9139	4.8463	38.0434	0.79930



**Fig. 11.11** Evaluation profile for  $R_a$

**Table 11.17** IT grade calculations

Exp. No.	Nominal dimension (mm)	Tolerance value “n”	IT grade
1	13.87	157.0	IT12
2	13.77	249.3	IT13
3	13.85	175.4	IT12
4	13.79	230.9	IT13
5	13.84	184.7	IT12
6	13.86	166.2	IT12
7	13.88	147.7	IT12
8	13.87	157.0	IT12
9	13.81	212.4	IT13

$$n = 1000 \left( \frac{|D_N - D_M|}{i} \right) \tag{2}$$

Here: “*D*” is the geometric mean of range of nominal size, *D<sub>N</sub>* is the nominal dimension, *D<sub>M</sub>* is the measured dimension. The dimension *B* (14.04 mm) of the master manufactured by combined processes of FDM and CVS (Table 11.2) was taken as nominal dimensions in this work. The standard basic measuring step is 10–18 mm. In experiment 1, the value of “*n*” for the selected dimension is calculated as follow:

$$D = (10 \times 18)^{1/2} = 13.416 \text{ mm}$$

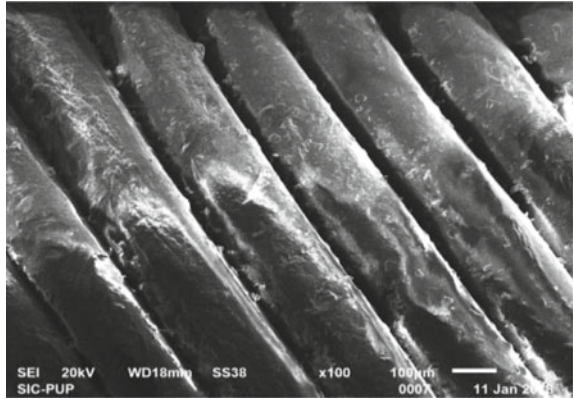
$$i = 0.45(13.416)^{1/3} + 0.001(13.416) = 1.0827 \text{ }\mu\text{m}$$

$$n = 1000(14.04 - 13.87)/1.0827 = 157.01$$

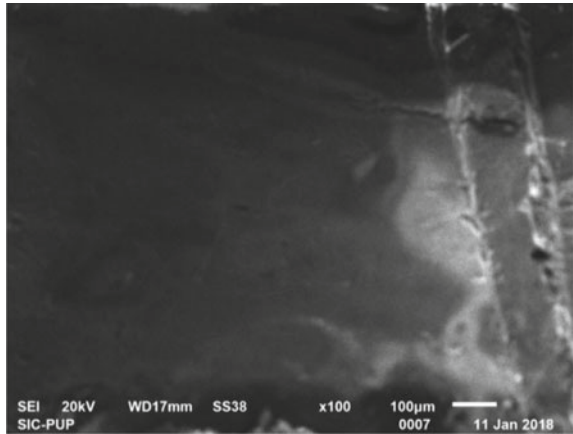
It was observed that the measured dimensions were lower than the nominal dimensions in all experiments. It was due to the shrinkage that occurs when the replicas are solidified, as the plastic changes state from liquid to solid. This can be compensated by giving the master pattern a shrinkage allowance. Figures 11.12 and 11.13 show SEM of FDM printed and CVS samples, respectively. Figure 11.14 shows SEM image of SM samples fabricated at optimum parameter settings. The SEM-based photomicrographs of the samples show that exposing FDM prototypes to CVS causes re-flow of the ABS material and resulted into the formation of fine layer of ABS on the surface of the prototypes and thus improve Ra.

Figure 11.12 clearly shows the stair case effect of FDM printed samples, which have been removed by CVS (Fig. 11.13). As observed from Fig. 11.14, no stair case effect has been observed at SM stage; hence, excellent reproducibility of replicas is expected.

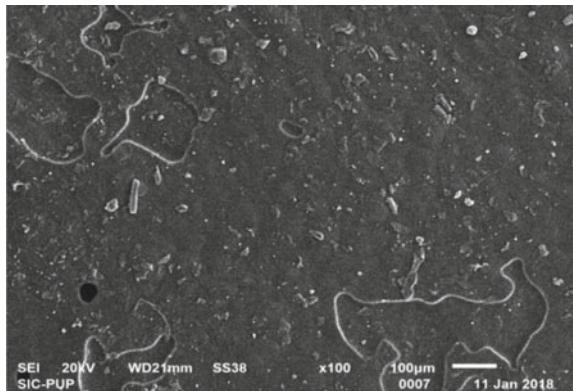
**Fig. 11.12** SEM image of FDM fabricated component



**Fig. 11.13** SEM image of after CVS process



**Fig. 11.14** SEM image of sample after SM



## 11.4 Conclusions

Following are the conclusions made from the present study:

- In stage 1, it has been found that the combined optimized setting (predicted from S/N ratio): 45° orientation, low part density and 10 s exposure time.
- After SM process, shrinkage was reported (for selected dimensions) in stage 2. The PP material shows good  $R_a$  after SM.
- The best parametric settings for all the responses (for 8040 PP material) are: 100:90 hardener percentage, de-moulding time 90 min, curing temperature of 80 °C.
- IT grades for the dimensions of replicas are acceptable as per ISO UNI EN 20286-I (1995) and DIN 16901. So, the prototypes can be used as end products or master for IC.

## References

1. Pandey A, Singh G, Singh S, Jha K, Prakash C (2020) 3D printed biodegradable functional temperature-stimuli shape memory polymer for customized scaffolds. *J Mech Behav Biomed Mater*, 103781
2. Cheah CM, Chua CK, Lee CW, Feng C, Totong K (2005) Rapid prototyping and tooling techniques: a review of applications for rapid investment casting. *Int J Adv Manuf Technol* 25(3–4):308–320
3. Sood AK, Ohdar RK, Mahapatra SS (2010) Parametric appraisal of fused deposition modelling process using the gray Taguchi method. *Proc Inst Mech Eng Part B J Eng Manuf* 44:135–145
4. Chhabra M, Singh R (2011) Rapid casting solutions: a review. *Rapid Prototyping J* 17(4)
5. Anitha R, Arunach AS, Radhakrishnan P (2001) Critical parameters influencing the quality of prototypes in fused deposition modelling. *J Mater Process Technol* 118:385–388
6. Armillotta A (2013) Assessment of surface quality on textured FDM prototypes. *Rapid Prototyping J* 12:35–41
7. Kumar R, Singh R, Hui D, Feo L, Fraternali F (2018) Graphene as biomedical sensing element: state of art review and potential engineering applications. *Compos B Eng* 134:193–206
8. Bassoli E, Gatto A, Luliano L, Violente MG (2007) 3D printing technique applied to rapid casting. *Rapid Prototyping J* 13:148–155
9. Ma S, Gibson I, Balaji G, Hu QJ (2007) Development of epoxy matrix composites for rapid tooling applications. *J Mater Process Technol* 192(193):75–82
10. Chen L, He Y, Yang Y, Niu S, Ren H (2016) The research status and development trend of additive manufacturing technology. *Int J Adv Manuf Technol*. <https://doi.org/10.1007/s00170-016-9335-4>
11. Singh S, Singh G, Prakash C, Ramakrishna S (2020) Current status and future directions of fused filament fabrication. *J Manuf Process* 55: 288–306
12. Rodriguez JF, Thomas JP, Reynaud JE (2001) Experimental investigations Mechanical behaviour of acrylonitrile butadiene styrene (ABS) fused deposition materials. *Rapid Prototyping J* 7(3):148–158
13. Bhargav A, Sanjairaj V, Rosa V, Feng LW, Fuh YH (2017) Applications of additive manufacturing in dentistry: a review. <https://doi.org/10.1002/jbm.b.33961>
14. Boschetto A, Giordano V, Veniali F (2013) Surface roughness prediction in fused deposition modelling. *Int J Adv Manuf Technol* 67:2727–2742

15. Boparai K, Singh R, Singh H (2016) Development of rapid tooling using fused deposition modelling: a review. *Rapid Prototyping J* 22(2)
16. Percoco G, Lavecchia F, Galantucci LM (2012) Compression properties of FDM rapid properties treated with a low cost chemical finishing. *J Appl Sci Eng Technol* 4:3838–3842
17. Boschetto A, Giordano V, Veniali F (2016) Modelling micro geometrical profiles in fused deposition process. *Int J Adv Manuf Technol* 61:945–956
18. Chung S, Park S, Lee I, Jeong H, Cho D (2005) Replication techniques for a metal micro-component having real 3D shape by micro casting process. *Microsys Technol* 11:424–428
19. Galantucci LM, Lavecchia F, Percoco G (2009) Experimental study aiming to enhance the surface finish of fused deposition modeled parts. *Ann Manuf Technol* 58:189–192
20. Garg A, Bhattacharya A, Batish A (2015) On surface finish and dimensional accuracy of FDM parts after cold vapour treatment. *Mater Manuf Process* 1–24
21. Gurralla PK, Regalla SP (2014) Part strength evolution with bonding between filaments in fused deposition modelling. *Virtual Phys Prototyping* 141–149
22. Gao H, Kaweesa VD, Moore J, Meisel AN (2016) Investigating the impact of acetone vapor smoothing on the strength and elongation of printed ABS parts. *Miner Metals Mater Soc.* <https://doi.org/10.1007/s11837-016-2214-5>
23. Zinniel RL (2011) Vapour smoothing surface finishing system. U.S. Patent No. 8075300 B2
24. Singh J, Singh R, Singh H (2016) Repeatability of linear and radial dimension of ABS replicas fabricated by fused deposition modelling and chemical vapour smoothing process: a case study. *Measurement* 94:5–11
25. Kuo CC, Liu LC, Teng WF, Chang HY, Chien FM, Liao SJ, Kuo WF, Chen CM (2016) Preparation of starch acrylonitrile-butadiene-styrene copolymers (ABS) biomass alloys and their feasible evaluation for 3D printing applications. *Compos Part B* 86:36–39
26. Singh J, Singh R, Singh H (2017) Investigations for improving the surface finish of FDM based ABS replicas by chemical vapour smoothing process: a case study. *Assembly Autom* 37(1):13–21
27. Dinesh P, Ravi R (2007) Rapid tooling route selection and evaluation for sand and investment casting. *Virtual Phys Prototyping* 2:197–207
28. Kuo CC, Mao CR (2015) Development of a precision surface polishing system for parts fabricated by fused deposition modeling. *Mater Manuf Process.* ISSN: 1042-6914
29. Singh J, Singh R, Boparai KS (2016) Parametric optimization of fused deposition modelling and vapour smoothing processes for surface finishing of biomedical implant replicas. *Measurement* 94:602–613
30. Kai CC, Howe CT, Hoe EK (1998) Integrating rapid prototyping and tooling with vacuum casting for connector. *Int J Adv Manuf Technol* 14:617–623
31. Thian SCH, Tang Y, Tan WK, Fuh JYH, Wong YS, Loh HT, Lu L (2008) The manufacture of micro mould and micro parts by vacuum casting. *Int J Adv Manuf Technol* 38:944–948
32. Singh R, Singh B (2010) Process capability of rapid manufacturing for plastic components. LAP Lambert Academics Publication Germany. ISBN 978-3-8433-8735-4:76
33. Rahmati S, Akbari J, Barati E (2007) Dimensional accuracy analysis of wax patterns created by RTV silicon rubber molding using Taguchi approach. *Rapid Prototyping J* 13(2):115–122
34. Tang Y, Tan, Fuh WK, Loh JYH, Wong HT, Thian YS, Lu SCH (2007) Micro mould fabrication for micro-gear via vacuum casting. *J Mater Process Technol* 192–193:334–339
35. Sharma V, Singh R (2011) Investigations for modelling the silicon moulding process for plastic components. *Int J Mater Sci Eng* 2(1–2)

**Mr. Ranvir Singh** Ph.D. Research Scholar, Mechanical Engineering Department, Punjabi University, Patiala, India. He is working as Assistant Professor at GNA University, Phagwara, India. His area of research is additive manufacturing, investment casting and metal matrix composites.

**Prof. Rupinder Singh** is Professor in the Department of Production Engineering, Guru Nanak Dev Engineering College, Ludhiana, India. He has received Ph.D. in Mechanical Engineering from Thapar Institute of Engineering and Technology, Patiala, India. His area of research is non-traditional machining, additive manufacturing and development of porous biomaterials using 3D printing and rapid prototyping techniques. He has more than 18 years of teaching and research experience. He has contributed extensively to the world in additive manufacturing literature with publications appearing in Journal of Manufacturing Processes, Composite Part B, Rapid Prototyping Journal, Journal of Mechanical Science and Technology, Measurement, International Journal of Advance Manufacturing Technology, and Journal of Cleaner Production. He authored 17 books and ~3 chapters. He has received more than 3 crores research grants from various funding agencies such as DST-SERB, AICTE, CSIR, DAE, IE. He is working with Prof. Seeram Ramakrishna, NUS Nanoscience and Nanotechnology Initiative and Prof. Fernando Fraternali, Full Professor of Structural Mechanics, Department of Civil Engineering, University of Salerno.

**Prof. Jasminder Singh Dureja** is working as Professor in the Department of Mechanical Engineering, Punjabi University, Patiala, India. He obtained his doctoral degree in Mechanical Engineering, Punjabi University, Patiala, India. He is a life member of ISTE. His areas of interest are hard tuning, tool wear, condition-based maintenance and monitoring apart from statistical modeling and optimization, machining of aerospace alloys under minimum quantity lubrication machining/near dry machining, green manufacturing, etc.



# Chapter 12

## Complex Shapes Prosthetics Process: An Application of Fused Deposition Modeling Technology



Tan Thang Nguyen, Hoang Vu Nguyen, Minh Phung Dang,  
and Thanh-Phong Dao

### 12.1 Introduction

Nowadays, a huge number of existing disabilities devices have been facing a few difficult problems in modeling, analysis, and fabrication, etc. Specifically, in Vietnam, a developing country, many disabled people have missed lower limbs or upper limbs, named prosthetics, by causes of US and Vietnam War. This caused physical disability for human and sociality as well as economic cost for the country. Therefore, there is a need to develop devices, techniques, and knowledge to disabled people in Vietnam, a specific case in this study.

It is well-known that 3-D printing technology has been used for bioengineering and other various fields such as arts, food industry, aerospace, consumer products, medical and manufacturing. In biomedical engineering, 3-D technique permits a high cost-effectiveness and increased mass production.

Until now, designers can use computer-aided design (CAD) and rapid prototyping (RP) in order to facilitate pseudo-prototypes before a real fabrication and manufacturing. Nowadays, the fused deposition modeling (FDM) process is an alternatively effective technique for prosthetics and biomedical engineering. Figure 12.1 illustrates a hot thermoplastic extrusion with high accuracy. In the present work, the FDM process is utilized for creating a virtual model of prosthetics with lower limb.

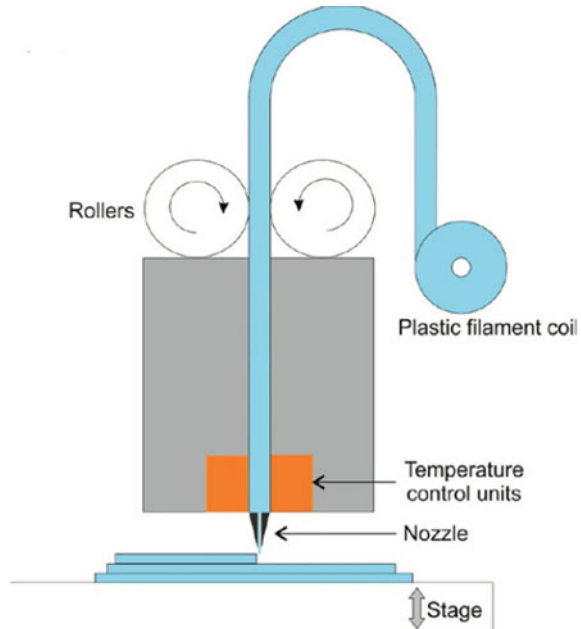
---

T. T. Nguyen · H. V. Nguyen · M. P. Dang  
Ho Chi Minh City Industry and Trade College, Ho Chi Minh City, Vietnam

T.-P. Dao (✉)  
Division of Computational Mechatronics, Institute for Computational Science, Ton Duc Thang  
University, Ho Chi Minh City, Vietnam  
e-mail: [daothanhphong@tdtu.edu.vn](mailto:daothanhphong@tdtu.edu.vn)

Faculty of Electrical & Electronics Engineering, Ton Duc Thang University, Ho Chi Minh City,  
Vietnam

**Fig. 12.1** Schematic diagram of fused deposition modeling [1]



Considering tissue engineering, in the early 1980s, Hull [1] used a .stl file in a CAD file so as to communicate to the 3-D printer. Later, there are a lot of companies such as DTM, Z corporation developed 3-D systems in this period of time [2]. Sean and Anthony [3] used 3-D printing for making skin, bone, vascular grafts, tracheal splints, heart tissue, and cartilaginous structures. Nicholas et al. [4] used this process to prosthetic production.

By using the computer-aided design and manufacturing (CAD/CAM) processes, a variable impedance prosthetic socket for an amputee was developed by David and Hugh [5]. In the past, 3-D printer was utilized so as to make lower limb prosthesis [6]. In addition, helical cooling channel (HCC) has been used during the modification of a prosthetic socket. The HCC process provides benefits through considerations of reducing thermal effect [7]. Regarding the organ models, a 3-D printing FDM based on the computed tomography scan was applied in Ref. [8]. However, FDM organ models are still limited by resolution and printing accuracy compared with instance stereolithography [9] or nasal casts [10]. In addition, many studies used the FDM process for medical engineering [11, 12]. Considering material with low cost and high strength, polymers are proper materials, such as collagen [13], gelatin [14], alginate [15], hyaluronic acid [16], PVA [17], and polyester-urethanes [18], which are commonly used for 3-D printing. Besides, some focused on compliant prosthetic ankle foot by taking advantage of compliant mechanism and flexure hinge [19–22]. Until now, according to Vietnam conditions, there is a lack of study on making 3-D prosthesis by fused deposition modeling process.

The aim of this chapter is to discuss the strength analysis of parts of the prosthesis by applying the fused deposition modeling process in Inventor software where socket is made from 200 mc machine, and calves are made of ABS material.

## 12.2 ISPO Processing

According to the processing had been transferred by International Society for Prosthetics and Orthotics (ISPO), orthopedy doctor will examine and give patient lots of useful pieces of advice for making decisions to select prosthetic parts, after that, orthopedy technician will take the measurement of patient and the socket plaster cast will make by hand. The ISPO' processing is summarized, as illustrated in Fig. 12.2. In order to get the exact measurement, the prosthetists often use experiences and knowledge so as to adjust the pressure with the hands. The goal of this step is to produce a suitable socket. We need to remove the wrap cast carefully when the plaster is already set.

## 12.3 FDM Processing

As illustrated in Fig. 12.3, the first step is consulted by biomechanic doctor. And then, the CAD models of socket, cavet and connecting parts were built. Next, these models were exported as files with \*.slt file. Finally, those files are fabricated by FDM machine.

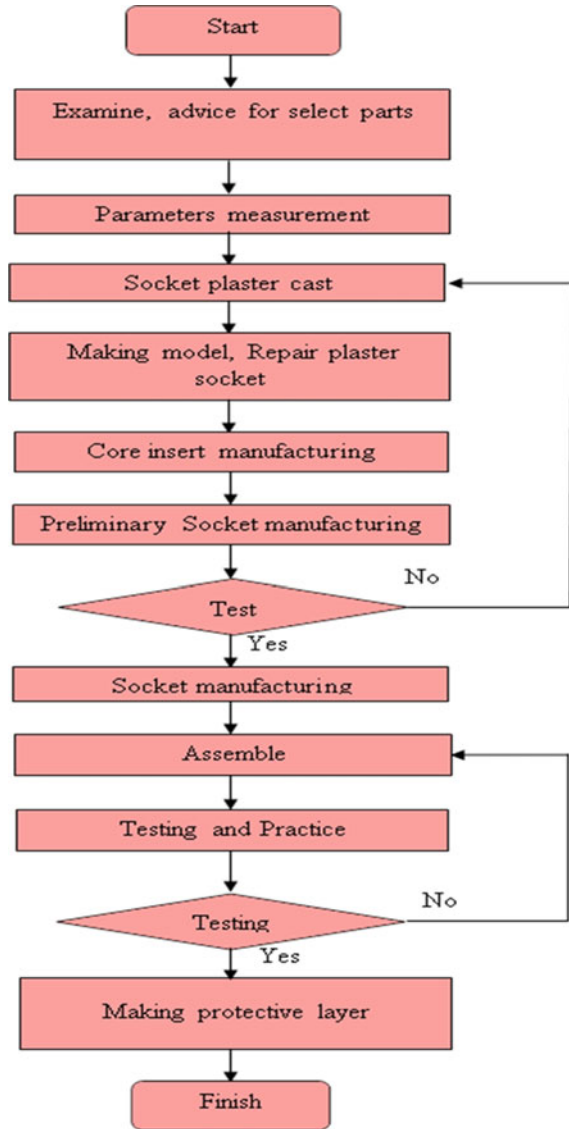
As depicted in Fig. 12.3, the rapid prototyping (RP) based on 3-D modeling in a software can achieve an efficiency and a high performance at a low cost and time. This process can be considered as a virtual technique so as to create a physical model before conducting a real production.

### 12.3.1 *Input Information*

This study has created a 3-D metric set, as shown in Fig. 12.4. The purpose of this study is to overcome the error due to manual measurement through the ISPO measure.

When we acquired the exact parameters, we need to determine the size of the standard ring, as shown in Fig. 12.5. Since the residual limb is the common standard, each individual patient needs to revise the correlation between the points of load-bearing and unbearable on the residual limb, so that the residual limb can hold a dead end without causing discomfort to the patient.

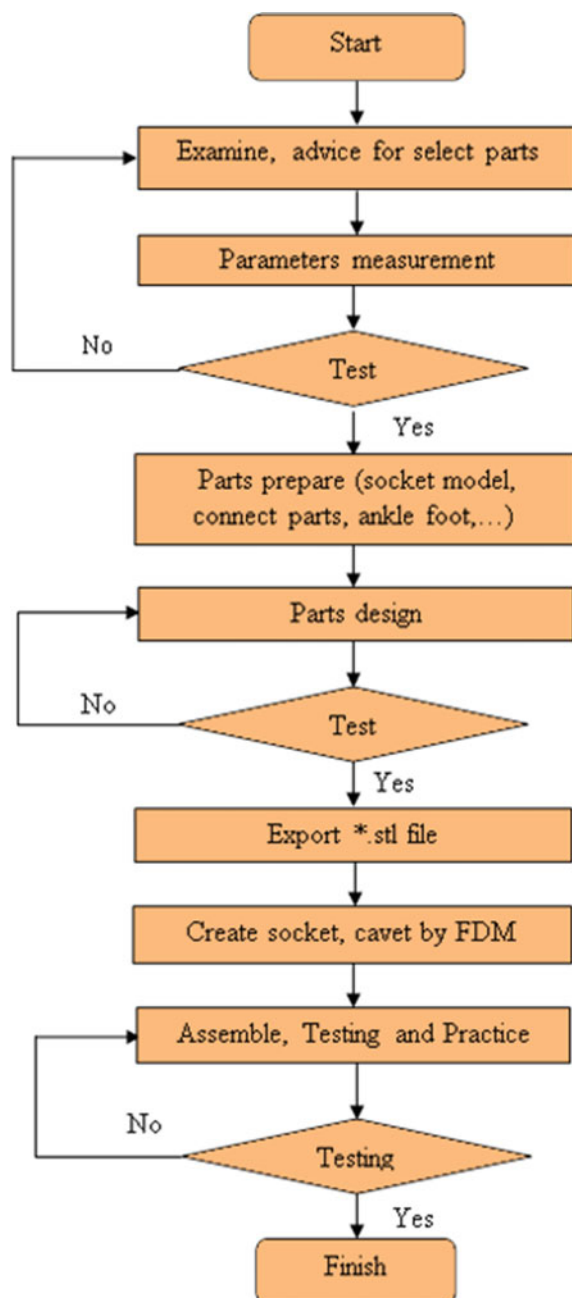
**Fig. 12.2** A schematic diagram of producing prosthetics and orthotics by ISPO

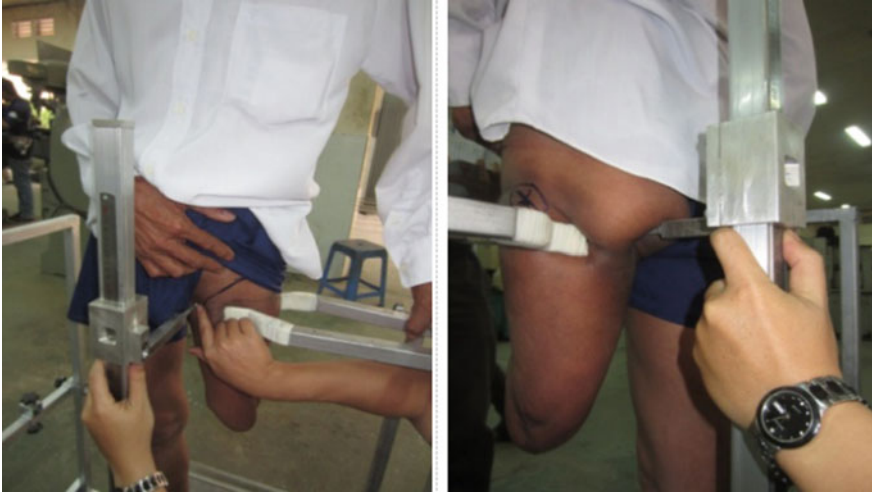


### 12.3.2 Parts Design

After having all the socket specifications and other city sales, the patient’s official socket has been completely designed. Through examination, measurement, and consultation of doctors, data on the size of the residual limb and other parts are determined and designed, as shown in Fig. 12.6.

**Fig. 12.3** Schematic diagram of FDM process





**Fig. 12.4** 3-D metric set



**Fig. 12.5** Standard ring from ISPO

After we get the real measurement of all the data, we proceed to assemble semifinished products and sockets together on the software. The mounting condition is the center of mechanical knee joint rotation on the prosthetic leg which is 2–2.5 cm higher than that of the knee joint.



**Fig. 12.6** All parts design

**Table 12.1** ABS properties

Material	ABS
Gravity	1.06 g/cm <sup>3</sup>
Weight	0.7 kg
Surface area	249,175 mm <sup>2</sup>
Volume	713,442 mm <sup>3</sup>
Mesh	0.1 mm

### 12.3.3 Strength Testing

Based on the criteria of mechanical biochemistry, we must ensure that the inner surface of the socket is suitable for patients, the outer surface of the socket is similar in shape with the healthy leg to achieve aesthetic and safety factor when using is 1.5, then the socket has officially been designed to suit patients with a maximum weight of 113 kg. ABS material was used for fabricate socket and cavet with the properties shown in Table 12.1. First of all, only one small prototype was designed and analyzed by Inventor software because of the low cost. The strength testing results show that the socket has enough strength conditions as shown in Table 12.2. After that, the prototype was made by FDM mc 200 machines.

The experiment was built with model test equipment shown in Fig. 12.7 and the theory of testing shown in Table 12.3.

Piston provides  $F_x$  force to lever arm that installs at the position as shown in Table 12.3. There are three different positions at vertical, tilt, and angle degrees 16, -16 to vertical that deal with real situation. The socket was broken at 157 kg that indicates it suitable to use as shown in Table 12.3.

Finally, the real socket was designed and tested by Inventor software. The testing results in Table 12.4 show that the real socket has enough strength conditions.

### 12.3.4 Manufacturing


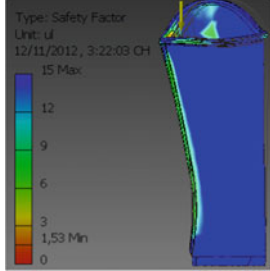

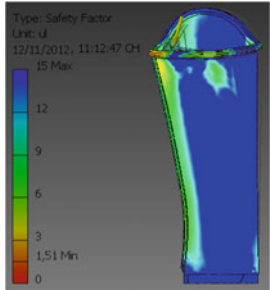

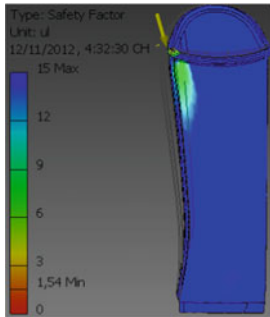
The rapid prototyping process was performed on FDM 200 mc machine at the laboratory of Ho Chi Minh City University of Technical Education. After processing, the semifinished products are assembled and fixed, as shown in Fig. 12.8.

## 12.4 Assemble and Experiment

Parts of prosthetic were assembled by orthopedic technician and experiment by orthopedic doctor. Finally, the prosthetic leg is tested by the patient as shown in Fig. 12.9. The patient feels comfortable and the doctor confirms that the prosthetic leg is full compliance for patients.



**Table 12.2** Strength testing results

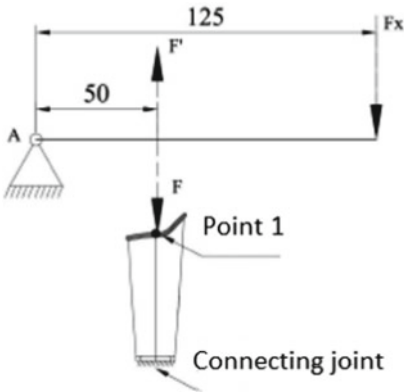
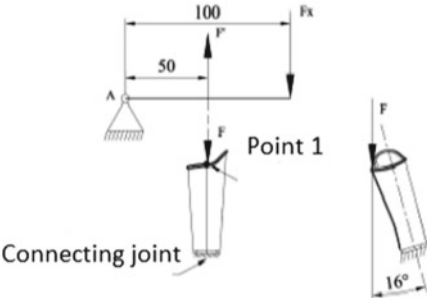
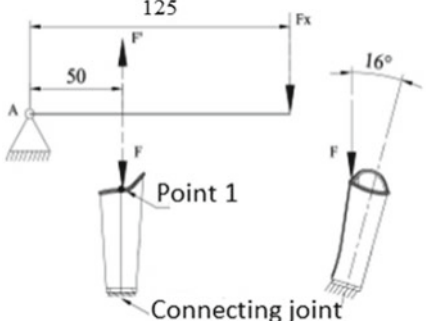
No.	Force diagram	$F$		Results
		$F_{Max}$ $M_{CP}$	$F_{MAX}$	
1		130 kg	200 kg	 Minimum safety factor: 1.53
2		115 kg	170 kg	 Minimum safety factor: 1.54
3		110 kg	165 kg	 Minimum safety factor: 1.54

**Fig. 12.7** Model test

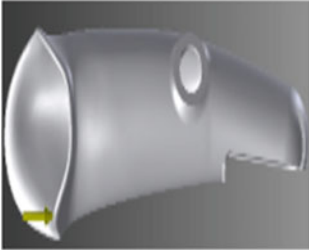
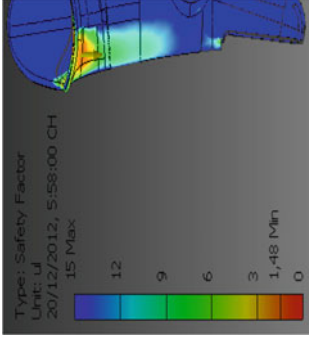
## 12.5 Conclusions and Future Works

This chapter presented an application of fused deposition modeling technology for creating the prosthetics with complex shapes. It could help to produce prototypes quickly at low cost. The socket and cavet were built by FDM 200 mc machine. And then, the prosthetic was assembled and succeeds experiment under the supervision of orthopedic doctor. The purpose of this study was to make a comfortable prosthetic socket that could bear a human weight up to 113 kg. Besides that, the results are expected to generate a highly maneuverable socket specification. The results of this study could be used for another patient easily.

**Table 12.3** Results of model test

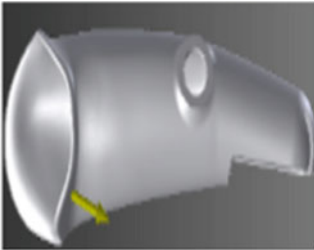
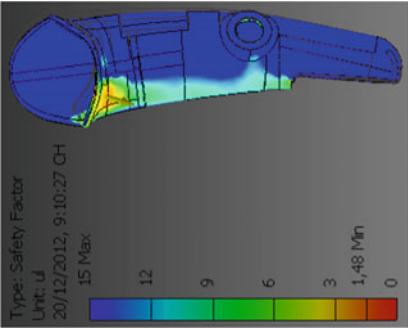
No.	Force diagrams	$P$	$F$	Results
1		8 kg/cm <sup>2</sup>	140 kg	Socket safe
2		9 kg/cm <sup>2</sup>	126 kg	Socket safe
3		9 kg/cm <sup>2</sup>	157 kg	Socket broken

**Table 12.4** Results of socket test

No.	Force diagrams 	$F, M$		$F_{Max}, M_{CP}$
		$F_{Max}$ $M_{CP}$	$F_{Max}$	
1		150 kg	220 kg	$F_{Max}, M_{CP}$ Safety factor  Minimum safety factor: 1,45

(continued)

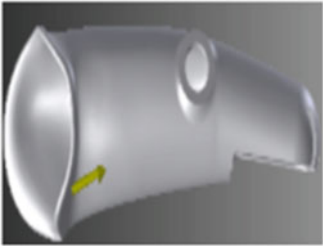
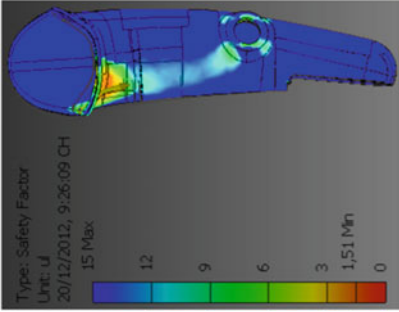
**Table 12.4** (continued)

No.	Force diagrams	$F, M$		$F_{Max}, M_{CP}$	Safety factor
		$F_{Max}$	$M_{CP}$		
2		113 kg		170 kg	

Minimum Safety factor: 1.48

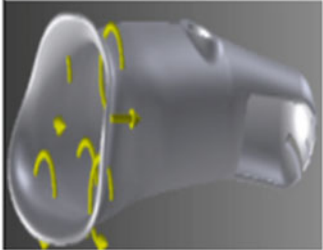
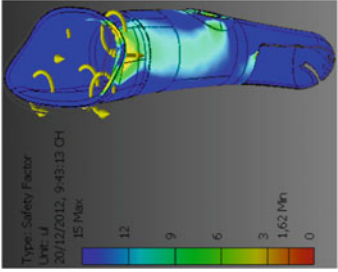
(continued)

**Table 12.4** (continued)

No.	Force diagrams	$F, M$		$F_{Max}, M_{CP}$
		$F_{Max}$ $M_{CP}$	$F_{Max}$	
3		160 kg	240 kg	<p><math>F_{Max}, M_{CP}</math></p> <p>Safety factor</p>  <p>Minimum safety factor: 1.51</p>

(continued)

**Table 12.4** (continued)

No.	Force diagrams	$F, M$		$F_{Max}, M_{CP}$	
		$F_{Max}$ $M_{CP}$	$F_{Max}$	Safety factor	
4		$F = 113 \text{ kg}$ $M = 113,000 \text{ N mm}$	$F = 240 \text{ kg}$ $M = 200,000 \text{ N mm}$		



**Fig. 12.8** Socket fabricate with FDM mc 200 machine



**Fig. 12.9** Patient testing with prosthetic leg

**Acknowledgements** This research is funded by Vietnam National Foundation for Science and Technology Development (NAFOSTED) under grant number 107.01-2019.14.



## References

1. Schubert C, Van Langeveld MC, Donoso LA (2014) Innovations in 3D printing: a 3D overview from optics to organs. *British J Ophthalmol* 98:159–161
2. Gross BC, Erkal JL, Lockwood SY, Chen C, Spence DM (2014) Evaluation of 3D printing and its potential impact on biotechnology and the chemical sciences. ACS Publications
3. Murphy SV, Atala A (2014) 3D bioprinting of tissues and organs. *Nat Biotechnol* 32:773
4. Herbert N, Simpson D, Spence WD, Ion W (2005) A preliminary investigation into the development of 3-D printing of prosthetic sockets. *J Rehabil Res Dev* 42:141
5. Sengeh DM, Herr H (2013) A variable-impedance prosthetic socket for a transtibial amputee designed from magnetic resonance imaging data. *JPO J Prosthet Orthot* 25:129–137
6. Comotti C, Regazzoni D, Rizzi C, Vitali A (2015) Multi-material design and 3D printing method of lower limb prosthetic sockets. In: *Proceedings of the 3rd 2015 workshop on ICTs for improving patients rehabilitation research techniques*, pp 42–45
7. Webber CM, Davis BL (2015) Design of a novel prosthetic socket: assessment of the thermal performance. *J Biomech* 48:1294–1299
8. Berkenfeld K, Bernauer M, McConville JT, Lamprecht A (2018) Investigating cascade impactor performance using a modified 3D printed induction port. *Int J Pharm* 535:402–409
9. Collier GJ, Kim M, Chung Y, Wild JM (2018) 3D phase contrast MRI in models of human airways: validation of computational fluid dynamics simulations of steady inspiratory flow. *J Magn Reson Imaging* 48:1400–1409
10. Warnken ZN, Smyth HD, Davis DA, Weitman S, Kuhn JG, Williams RO III (2018) Personalized medicine in nasal delivery: the use of patient-specific administration parameters to improve nasal drug targeting using 3D-printed nasal replica casts. *Mol Pharm* 15:1392–1402
11. Bloomquist CJ, Mecham MB, Paradzinsky MD, Januszewicz R, Warner SB, Luft JC et al (2018) Controlling release from 3D printed medical devices using CLIP and drug-loaded liquid resins. *J Controlled Release* 278:9–23
12. Tappa K, Jammalamadaka U (2018) Novel biomaterials used in medical 3D printing techniques. *J Funct Biomater* 9:17
13. Rhee S, Puetzer JL, Mason BN, Reinhart-King CA, Bonassar LJ (2016) 3D bioprinting of spatially heterogeneous collagen constructs for cartilage tissue engineering. *ACS Biomater Sci Eng* 2:1800–1805
14. Laronda MM, Rutz AL, Xiao S, Whelan KA, Duncan FE, Roth EW et al (2017) A bioprosthetic ovary created using 3D printed microporous scaffolds restores ovarian function in sterilized mice. *Nat Commun* 8:15261
15. Markstedt K, Mantas A, Tournier I, Ávila HM, Hägg D, Gatenholm P (2015) 3D bioprinting human chondrocytes with nanocellulose-alginate bioink for cartilage tissue engineering applications. *Biomacromolecules* 16:1489–1496
16. Nguyen D, Hägg DA, Forsman A, Ekholm J, Nimkingratana P, Brantsing C et al (2017) Cartilage tissue engineering by the 3D bioprinting of iPS cells in a nanocellulose/alginate bioink. *Sci Rep* 7:658
17. Tan Z, Parisi C, Di Silvio L, Dini D, Forte AE (2017) Cryogenic 3D printing of super soft hydrogels. *Sci Rep* 7:16293
18. Haryńska A, Kucinska-Lipka J, Sulowska A, Gubanska I, Kostrzewa M, Janik H (2019) Medical-grade PCL based polyurethane system for FDM 3D printing—characterization and fabrication. *Materials* 12:887
19. Nguyen TT, Dao T-P, Huang S-C (2017) Biomechanical design of a novel six DOF compliant prosthetic ankle-foot 2.0 for rehabilitation of amputee. In: *ASME 2017 international design engineering technical conferences and computers and information in engineering conference*. American Society of Mechanical Engineers
20. Nguyen TT, Le HG, Dao T-P, Huang S-C (2017) Evaluation of structural behaviour of a novel compliant prosthetic ankle-foot. In: *2017 international conference on mechanical, system and control engineering (ICMSC)*. IEEE, pp 58–62

21. Chau NL, Le HG, Dao T-P, Dang VA (2019) Design and optimization for a new compliant planar spring of upper limb assistive device using hybrid approach of RSM–FEM and MOGA. *Arabian J Sci Eng* 1–16
22. Chau NL, Le HG, Dao T-P, Dang MP, Dang VA (2019) Efficient hybrid method of FEA-based RSM and PSO algorithm for multi-objective optimization design for a compliant rotary joint for upper limb assistive device. *Math Prob Eng* 2019

**Mr. Tan Thang Nguyen** is Lecture in Ho Chi Minh City Industry and Trade College, Ho Chi Minh City, Vietnam. He received his B.S. degree in mechanical engineering from the Ho Chi Minh City University of Technology and Education, Vietnam, in 2008. He received his M.S. degree in mechanical engineering from the National Kaohsiung University of Applied Sciences, Taiwan, ROC, in 2011. He is currently a Ph.D. student at Ho Chi Minh City University of Technology and Education, Ho Chi Minh City, Vietnam. His research interests include compliant mechanism, bio-inspired structure, actuator, rehabilitation, prosthetics, hybrid optimization algorithm, applied soft computing, design optimization.

**Mr. Hoang Vu Nguyen** is Lecture in Faculty of Mechanical Engineering, Ho Chi Minh City Industry and Trade College, Ho Chi Minh City, Vietnam. He received his B.S. and M.S. degree in mechanical engineering from the Ho Chi Minh City University of Technology, Vietnam, in 1984 and 2000, respectively. His research interests include mechanical design.

**Mr. Minh Phung Dang** is Lecture in Faculty of Mechanical Engineering, Ho Chi Minh City Industry and Trade College, Ho Chi Minh City, Vietnam. He received his B.S. and M.S. degree in mechanical engineering from the Ho Chi Minh City University of Technology and Education, Vietnam in 2007 and 2009, respectively. He is currently a Ph.D. student at Ho Chi Minh City University of Technology and Education, Ho Chi Minh City, Vietnam. His research interests include compliant mechanism, ultra-precision positioning system, hybrid optimization algorithm, applied soft computing, design optimization.

**Dr. Thanh-Phong Dao** is Assistant Professor in the Institute for Computational Science, Ton Duc Thang University, Ho Chi Minh City, Vietnam. He received his B.S. degree in mechanical engineering from the Ho Chi Minh City University of Technology and Education, Vietnam, in 2008. He received his M.S. and Ph.D. degree in mechanical engineering from the National Kaohsiung University of Applied Sciences, Taiwan, ROC, in 2011 and 2015, respectively. He is currently a researcher at the Institute for Computational Science, Ton Duc Thang University, Ho Chi Minh City, Vietnam. His research interests include compliant mechanism, bio-inspired structure, actuator, rehabilitation, prosthetics, hybrid optimization algorithm, applied soft computing, optimization, design optimization.

# Chapter 13

## Improvement of Human Gait in Foot Deformities Patients by 3D Printed Ankle–Foot Orthosis



Harish Kumar Banga, Parveen Kalra, R. M. Belokar, and Rajesh Kumar

### 13.1 Introduction

Pre-assembled orthotic gadgets are reasonable and intended to fit a scope of patients. Because of this restricted plans, it would not give redid solace and usefulness. Be that as it may, delivering a custom-fit orthosis is an arduous and tedious manual process achieved just by master orthotist. The technique to make a give can take up a role as much as four long stretches of manufacture time per unit whenever performed by an accomplished expert. To make the orthotics in light of the cast, it will take days. The cast will likewise consume room while putting away and must be kept for a couple of months, and after, that another cast must be made [1–4].

In present-day focused world, makers need to discharge an as good as ever item to the market as quick as conceivable to have the capacity to contend in the worldwide market. The presentation of fast prototyping in the beginning periods of item improvement has extraordinarily decreased the advancement time span and cost engaged with model assembling. Quick prototyping (RP) is the way toward creating a three-dimensional parts or models straightforwardly from CAD illustrations. The uses of fast prototyping are progressing at quick pace. They have moved from making models for parts to a few building applications. Among the advancing RP applications are the making of molds for bite the dust throwing and making of parts to be utilized in the gathering of items. Regarding medicinal utilize, RP is utilized to make models utilizing three-dimensional designs from X-beam gear and these models are utilized to study and plan medical procedure. Techniques are being created to lead remote medical procedure by virtual reality utilizing RP models. Notwithstanding the past application, quick prototyping is additionally being utilized to make body

---

H. K. Banga (✉) · P. Kalra · R. M. Belokar · R. Kumar  
Production and Industrial Engineering Department, Punjab Engineering College (Deemed to Be University), Chandigarh, Punjab 160012, India  
e-mail: [drhkbanga@gmail.com](mailto:drhkbanga@gmail.com)

parts known as orthotics and prosthetics [5]. This investigation work is focused on illustrating lower leg-foot orthoses (AFOs) through making sense of and produces by quick prototyping. An orthosis is described by the International Standards Organization as a remotely associated device used to adjust the fundamental and useful qualities of the neuromuscular and skeletal structure. Lower leg-foot orthoses cannot avoid being orthoses that encompass the lower leg joint and the whole or part of the foot. AFOs are wanted to control development, correct distortion or conceivably compensate for deficiency of the leg [6–10]. With our present advancement, we can quicken the amassing method by using making sense of to assemble 3D CAD data on the patient's foot. Remedial reverse engineering is required to use the reverse engineering advancement to revamp 3D models of the anatomical structures and biomedical things for plan and amassing of therapeutic things. Making sense of is generally portrayed as a methodology of separating an inquiry or existing system, to recognize its fragments and their interrelationships, and investigate how it works remembering the ultimate objective to update or convey a copy without access to the arrangement from which it was at first made.

Through figuring out, we can dissect the 3D examined information and outline the most appropriate orthoses for the patient. The way toward outlining orthoses utilizing figuring out programming would allow changes in the standard plan to meet the correct needs of every patient. Moreover, the utilization of 3D scanner and modernized programming in manufacturing understanding particular orthotic gadgets can possibly convey exceptional solace because of the precise information gave through 3D checking. Quick prototyping is the name given to an expansive gathering of related advances which might be used to make physical inquiries especially from CAD information assets. These systems are stand-out in that they incorporate and protection substances in layers to define items. Such structures are furthermore regarded by using the names included substance advent, three-dimensional printing, and stable unfastened-form advent and layered amassing [11–14]. They provide purposes of enthusiasm for various programs stood out from standard subtractive fabricate structures, as an instance, getting ready or turning:

- i. Objects may be framed with any geometric multifaceted nature or unpredictability without the requirement for make bigger system setup or last get together;
- ii. Objects may be produced the use of various substances, or as composites, or substances may even be fluctuated in a controlled manner at any place in a protest;
- iii. Additive creation frameworks lessen the improvement of complicated articles to a sensible, clean and commonly quick manner. These homes have resulted of their extensive use as a manner to lessen time to marketplace in production. Today's systems are heavily used by engineers to higher understand and speak their product designs in addition to make speedy tooling to fabricate the ones products. Surgeons, architects, artists and people from many other disciplines also robotically use the technology.

### 13.1.1 Background

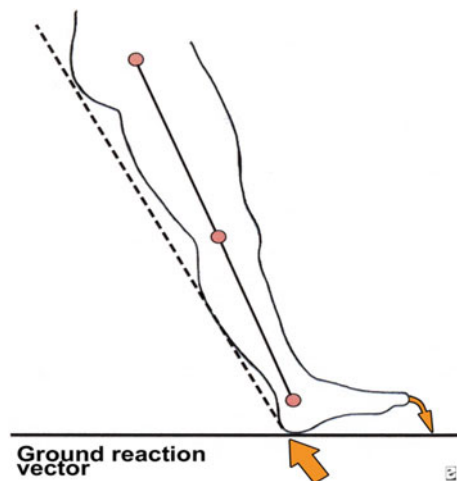
Foot drop is a misleadingly dependable requires a likely snared bother. It tends to be depicted as a basic deficiency of decay leg and toe dorsiflexion. The foot and decrease leg dorsiflexors incorporate the tibialis the front, the extensor hallucis longus (EHL) and the extensor digitorum longus (EDL). These solid tissues engage the body to clean the foot amidst swing stage and control plantar flexion of the foot on back zone strike [15–18]. Weakness in this storing up of muscle tissue brings about an equinovarus distortion. This is some of the time insinuated as steppage walk, in gentle of reality that the patient tends to stroll with a distorted flexion of the hip and knee to save the feet from getting at the ground in the midst of swing level. In the midst of walk, the power of foot bottom spot strike outperforms body weight, and the course of the floor reaction vector goes at the back of the lower leg and acknowledgment (see the photo underneath knee) (Fig. 13.1).

#### 13.1.1.1 Anatomy

Strands from the dorsal pieces of the ventral rami of L4-S1 are found in the peroneal nerve, which is encouraged with the tibial nerve to fuse the sciatic nerve. The sciatic nerve leaves the pelvic pit at the more basic sciatic foramen, essentially unremarkable showed up diversely in connection to the piriformis. It bifurcates to shape the peroneal and tibial nerves either in the distal third of the thigh or at the midhigh level.

The lower leg partitioning shallow and gigantic branches. The shallow branch goes between the two pioneers of the peronei and continues down the lower leg to lie between the peroneal tendon and the sidelong edge of the gastrocnemius [19–23] (Fig. 13.2).

**Fig. 13.1** Forces acting on ankle during walking



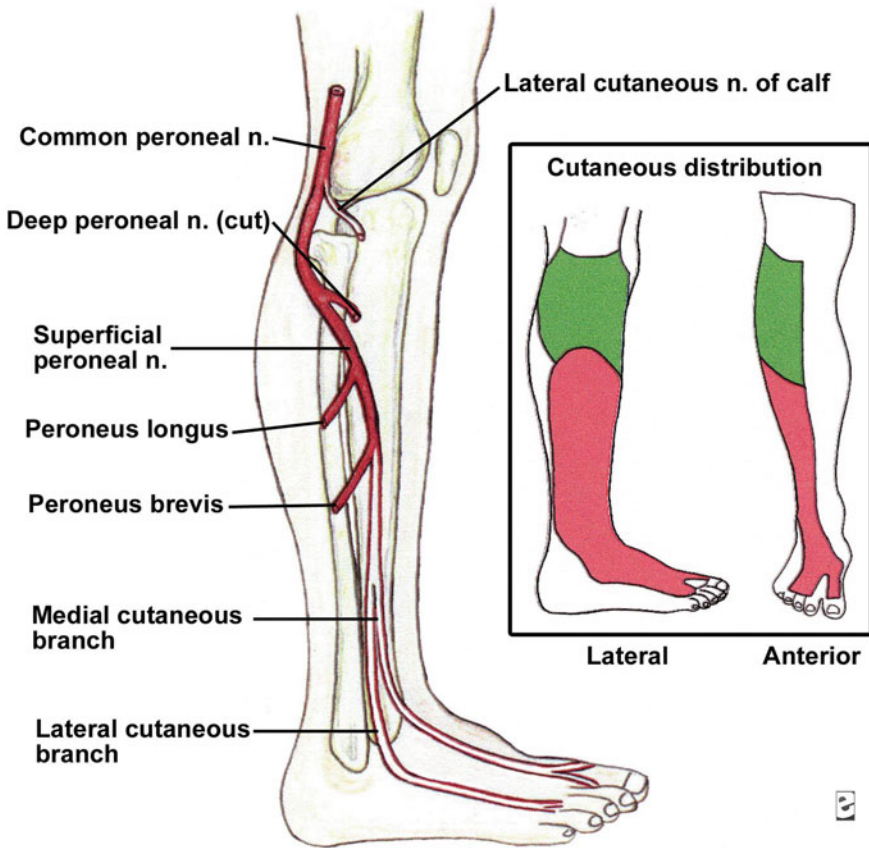


Fig. 13.2 Anatomy of ankle nerve system

### 13.1.1.2 Causes

Foot drop is because of inadequacy or absence of development of the muscle tissue drew in with lifting the front bit of the foot [24]. The concealed purposes behind foot drop are moved and may include:

- i. Nerve hurt.

The most extreme broadly analyzed purpose behind foot drop is strain of a nerve in your leg that controls the muscle tissues related with lifting the foot. This nerve can in like manner be hurt in the midst of hip or knee substitution clinical way, which may reason foot drop. Nerve root hurt ("crushed nerve") in the spine can similarly reason foot drop.

- ii. Muscle or nerve issue.  
Various types of solid dystrophy, an obtained ailment that causes dynamic muscle weakness, may add to foot drop. Diverse disarranges, for example, polio or Charcot-Marie-Tooth issue, in like manner would motive be able to foot drop.
- iii. Cerebrum and spinal string inconvenience. Scatters that influence the spinal string or cerebrum—for instance, amyotrophic parallel sclerosis (ALS), diverse sclerosis or stroke—may purpose foot drop.

### 13.1.1.3 Symptoms

Foot drop makes it difficult to support the front bit of your foot, so it might defer the floor when you walk. To counter this, you can raise your thigh while you walk, around despite the fact that you have been mountaineering stairs (steppage walk), to allow your foot to clear the floor. This unconventional walk may likewise make you smack your foot down onto the floor with each movement you are taking. On occasion, the skin on the absolute best purpose of your foot and feet can likewise encounter numb [25–30].

Foot drop often affects just a single foot. Contingent upon the hidden reason, be that as it can, it is possible for the two feet to be influenced.

### 13.1.1.4 Definition

Foot drop, from time to time called drop foot, is a general term for burden lifting the front piece of the foot. On the off chance that you have foot drop, you may drag the front of your foot on the ground when you walk. Foot drop is not an infection. Or then again potentially, foot drop implies that a covered neurological, solid or anatomical issue [31].

A part of the time foot drop is transient. In different cases, foot drop is endless. In the event that you have foot drop, you may need to wear a prop on your lower leg and foot to hold your foot in a typical position.

### 13.1.1.5 Tests and Diagnosis

Foot drop is usually dismembered amidst a physical test. Your lord should watch you walk and may check a part of your leg muscles for shortcoming. The individual may in addition check for deadness on your shin and on the most critical motivation behind your foot and toes. Sometimes, extra testing is recommended [32–35].

### 13.1.1.6 Imaging Tests

Foot drop is a part of the time realized by an extra of bone in the spinal channel or with the guide of a tumor or irritates pushing at the nerve inside the knee or spine. Imaging tests can help pinpoint these sorts of issues [36].

- I. X-bars. Plain X-shafts make use of a low degree of radiation to acknowledge a delicate tissue mass or a bone harm that would reason your pointers.
- II. Ultrasound. This headway uses sound waves to make photographs of inward systems. It might be associated with check for pimples or tumors that may push at the nerve.
- III. Modernized tomography (CT) filters through. Electronic tomography joins X-shaft photos taken from an expansive extent of edges to framework pass-sectional points of view of structures inside the packaging.
- IV. Attractive resounding imaging (MRI). This research makes use of radio waves and a strong engaging field to make isolated sneak peaks. X-bar is expressly prized in envisioning sensitive tissue disasters that could a nerve.

### 13.1.1.7 Nerve Tests

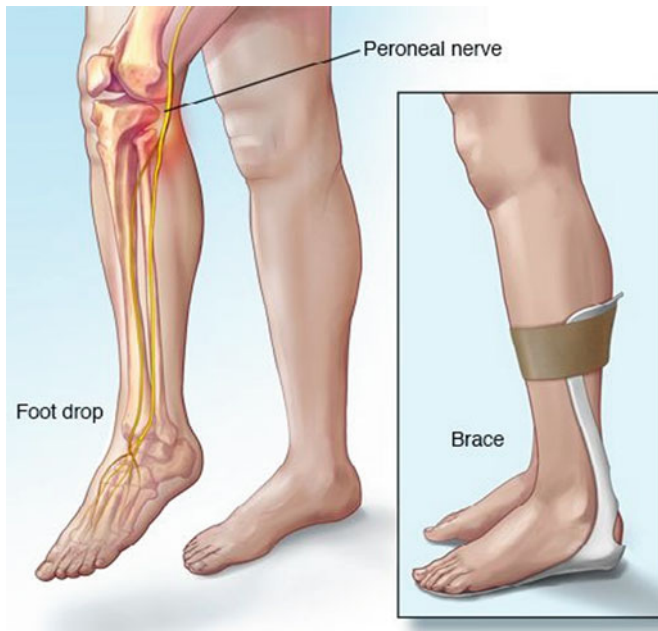
Electromyography (EMG) and nerve conduction considers measure electrical action in the muscles and nerves. These tests can be ungainly; at any rate, they are extremely helpful in picking the region of the harm along the affected nerve [37].

### 13.1.1.8 Treatments and Drugs

Treatment for foot drop relies upon the hidden reason. In the event that the simple motive is successfully dealt with, foot drop may additionally beautify or maybe vanish [23]. On the off threat that the essential cause cannot be treated, foot drop might be lasting. Particular remedy for foot drop may encompass:

- i. Braces or helps. A prop in your decrease leg and foot or guide that fits into your shoe can assist maintain your foot in an average function.
- ii. Physical remedy. Activities that enhance your leg muscle mass and help you hold up the scope of motion for your knee and lower leg may also beautify stroll troubles related with foot drop. Extending practices are especially critical to keep the improvement of solidness within the foot sole vicinity.
- iii. Nerve incitement. In a few instances, empowering the nerve that lifts the foot enhances foot drop.
- iv. Surgery. Contingent on the cause, and in case your foot drop is normally new, nerve clinical process is probably useful. In the occasion that foot drop is lengthy-standing, your expert might also advise scientific system that wires decrease leg or foot bones or a method that exchanges an operating ligament to a change function (Fig. 13.3).





**Fig. 13.3** Use of ankle-foot orthosis for foot drop patients

## 13.2 Ankle-Foot Orthosis

An AFO can be used for foot drop even as cautious fix is not supported or all through cautious or neurologic recovery. The specific explanation behind an AFO is to offer toe dorsiflexion inside the course of the swing territory, normal or flat adequacy at the lower leg for the range of position, and, if urgent, push off affectation at some stage in the past due position divide. An AFO is profitable elegant if the foot can advantage plantigrade limit when the patient is status. Any equinus contracture obstructs its productive use [38].

The best commonly used AFO in foot drop is created of polypropylene and increases into a shoe. If its miles slice to fit front to the malleoli, it gives rigid immobilization. This instrument is used meanwhile as lower leg precariousness or spasticity is astounding, much the same as the case in sufferers with best motor neuron sicknesses or stroke [39].

If the AFO suits back to the malleoli (back leaf spring type), plantar flexion at effect point strike is permitted, and push off returns the foot to free for the swing segment. This gives dorsiflexion help with times of out of shape or slight spastic equinovarus mutilation. A shoe-get orthosis that associates explicitly to the heel counter of the shoe besides may be used. A view through Menotti et al. suggested that front AFOs are related to decay power expenses of by strolling and favored

degrees of saw comfort over back AFOs are and thusly may likewise enable people with foot drop to walk longer divisions while utilizing less genuine undertaking.

### **13.3 Methodology**

#### ***13.3.1 Manufacturing Techniques of AFO***

The process will be used to create orthotic devices is additive manufacturing. Computer-assisted design (CAD) systems have also being used to assist in creating the positive improving consistency and repeatability of this process, but the process remains slow and complex and it requires considerable input from experienced craftsmen. Furthermore, in these traditional processes, the possibilities for innovation or product development are limited. With CAD systems, it will be observed that orthoses rejection ratio has been reduced combined with time reduction up to 50% and cost saving up to 25–50% [26–30] as shown in Fig. 13.4.

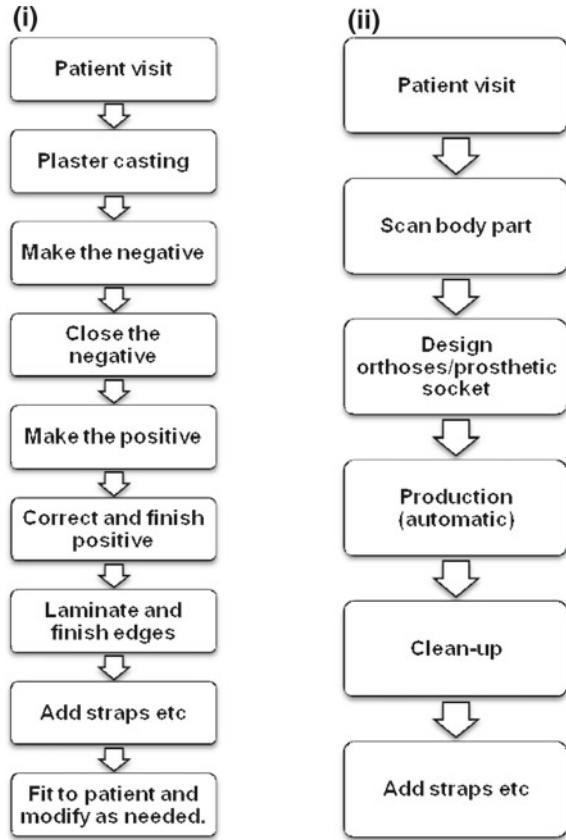
A standard AFO was characterized to best understand the performance characteristics required of a spring ankle–foot orthotic. These characteristics, in combination with the study of human biomechanics, were used to choose optimum material and size. The flowchart shown below details the steps in the prototype development process

Each of the individual work flows shown in Fig. 13.5 above merged to create the final prototype through use of the best process. Upon completion of the final prototype comparative testing was done to show the similarities in performance between the standard AFO and the prototype.

#### ***13.3.2 3D Scanning Techniques of Foot Drop Patients***

During the scanning process as shown in Fig. 13.6, numerous 3D outputs of the question are gained from different bearings and every one of the information is consolidated naturally into a solitary and finish 3D surface model. Normal examining times extend from a couple to 15 min; the moderately long aggregate filtering time is less significant, since the full robotization of the procedure gives the administrator flexibility to perform different undertakings amid the checking procedure. Likewise, no particular specialized know-how in 3D checking is required to play out the procedure. The 3D profiles procured progressively by the laser scanner can be moved into the reference framework characterized by the receptor. The filtering procedure is in this way extremely straightforward and natural: the administrator move, totally unreservedly, the hand-held scanner over the protest, while the obtained 3D profiles are appeared continuously on the screen.

**Fig. 13.4** (i) Traditional process, (ii) Possible AM process



The essential system for all quick prototyping strategies can be compressed as takes after:

- i. A CAD show is built and afterward changed over to STL design. The determination can be set to limit stair venturing.
- ii. The RP machine forms the STL document by making cut layers of the model.
- iii. The first layer of the physical model is made. The model is then brought down by the thickness of next layer, and the procedure is then rehashed until consummation of the model.
- iv. The demonstration and any backings are expelled. The surface of the model is then completed and cleaned.

The phases of 3D scanning as shown in Figs. 13.7 and 13.8 and CAD designing the production of an AFO, with a reasonable quality of image in terms of its resolution, before sending it to a 3D printer. Based on the observed result, the project purpose is feasible but further refinement of the process is necessary at this stage. It was concluded that using a 3D laser scanner can provide a high quality of image of scanning for the AFO making purposes comparing to those that used in previous

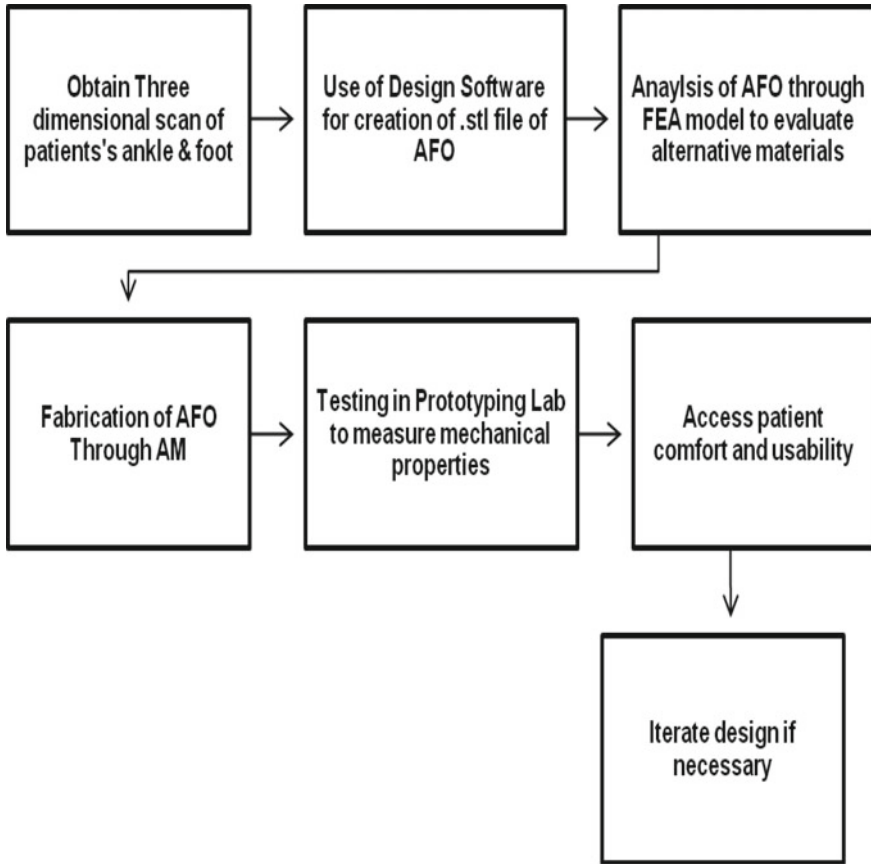


Fig. 13.5 Flow of AFO prototype development

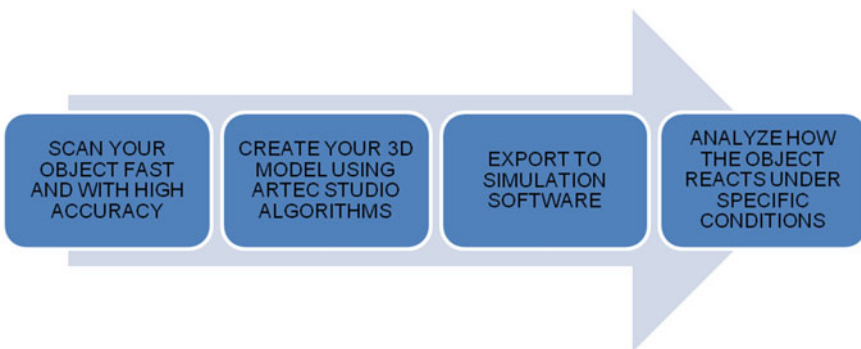
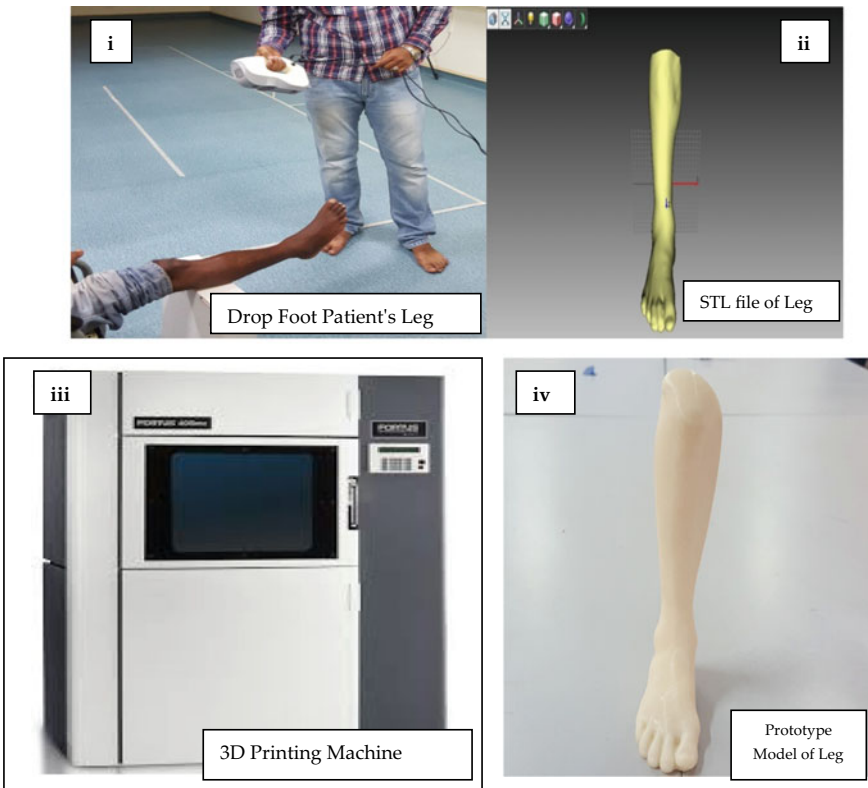
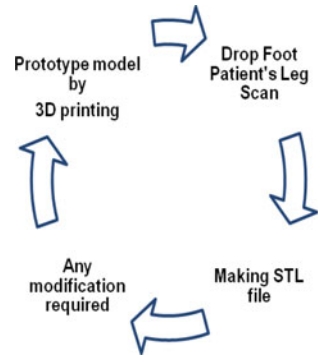


Fig. 13.6 Process for scanning object

**Fig. 13.7** Flow process of scanning and 3D printing of foot drop patients leg



**Fig. 13.8** (i) Scanning of foot drop patients leg, (ii) Making STL of leg, (iii) SLS 3D printing machine, (iv) Prototype model of leg

studies. The CAD tools were suitable to reduce the size of the original, large scan, mesh making and offsetting.

### 13.4 Clinical Gait Analysis of Foot Drop Patients

The term gait refers to the pattern of walk of an individual. Gait analysis consists of the various scientific measurement and analysis linked with locomotion. The gait measurement techniques used in the Gait Laboratory of the Physical and Rehabilitation Medicine Department at PGIMER Chandigarh are broadly classified into four types [40–42].

- i. Camera motion analysis,
  - ii. 16 force plate-based force analysis,
  - iii. Biometrics EMG analysis,
  - iv. Sway analysis.
- i. Three markers on each shank: head of fibula, lateral malleolus, lateral bar (same way for the bar on the tight, see Fig. 13.9);
  - ii. One marker on each foot:

Fifth metatarsal joint and emispherical markers: b1 marker on each heel: (only for standing trial) be careful that the two markers on the fifth metatarsal joint and on the heel have to stay on the same plane (see Figs. 13.10 and 13.11).

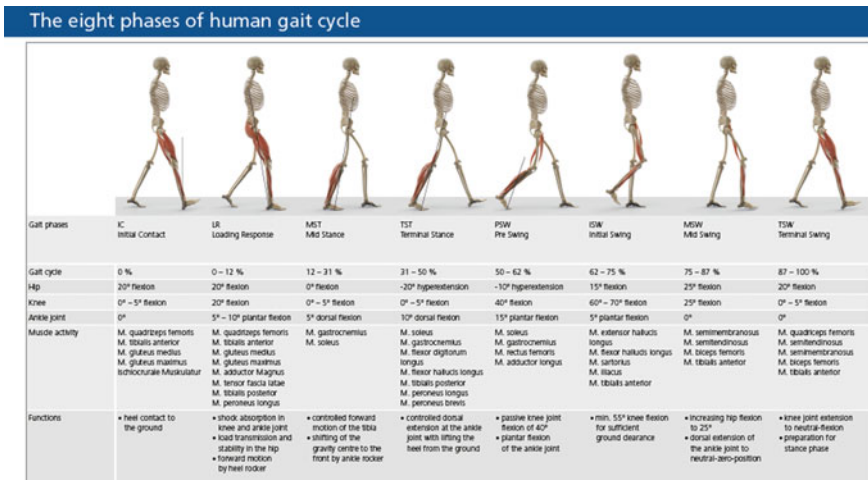


Fig. 13.9 Phases of gait laboratory

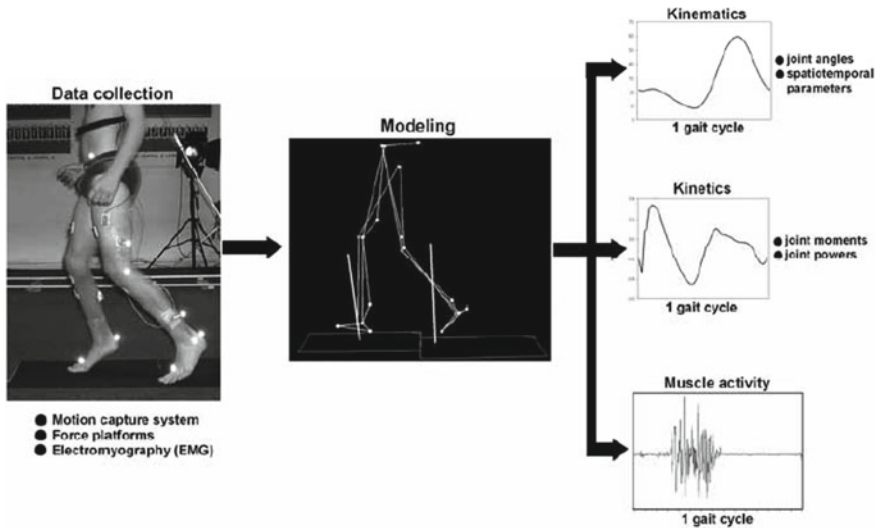


Fig. 13.10 Data collection and analysis process for instrumented gait analysis

### 13.4.1 Gait Analysis of Foot Drop Patients

The trial of foot drop patients in clinical gait laboratory is done as shown in Fig. 13.12. Which will help to check how much improvement of gait cycle with 3D printed ankle-foot orthosis?

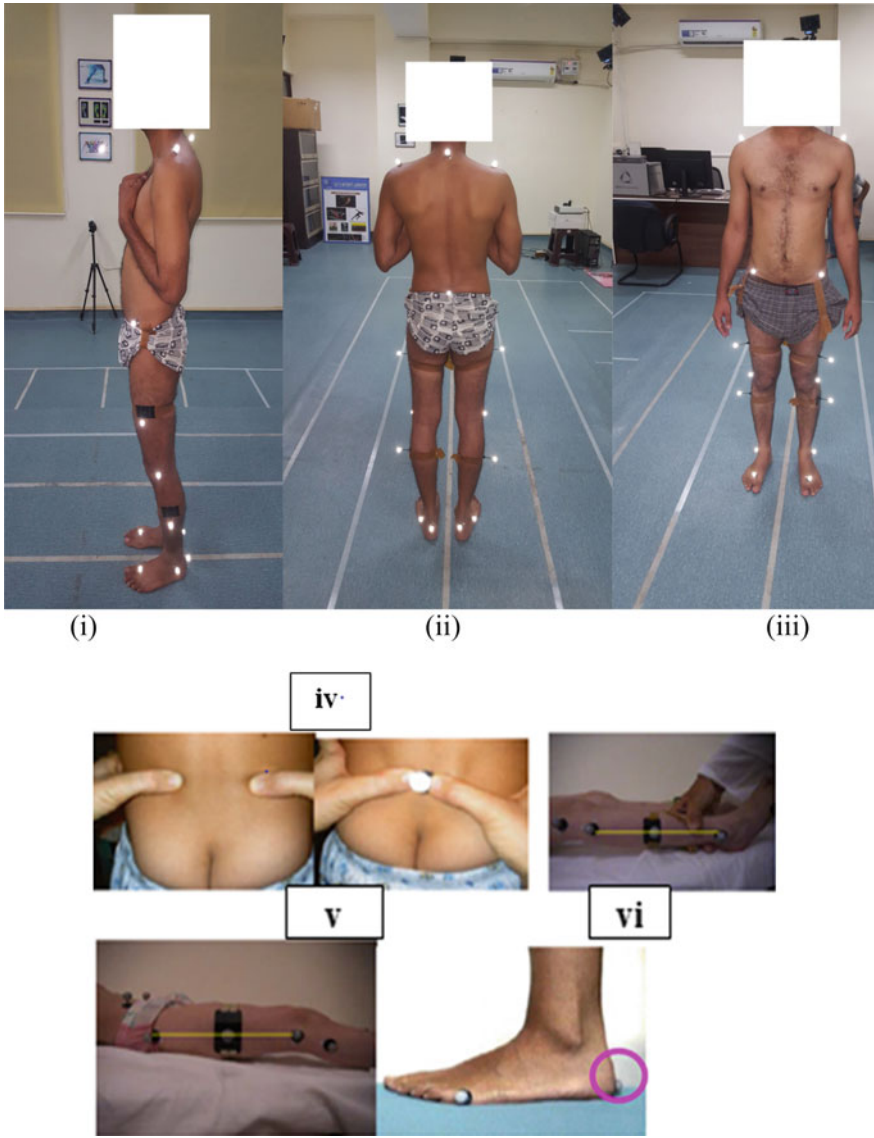
The clinical gait analysis trial with old and customized design 3D printed ankle-foot orthosis is performed as shown in Fig. 13.13 to check ankle joint stability in foot drop patients.

## 13.5 Significant Findings

The different phases of 3D scanning and CAD designing the production of an AFO, with a reasonable quality of the image in terms of its resolution, before sending it to a 3D printer. Based on the observed result, the research purpose is feasible but further refinement of the process is necessary at this stage.

It was concluded that using a 3D laser scanner can provide a high quality of image of scanning for the AFO making purposes comparing to those that used in previous studies. The CAD tools were suitable to reduce the size of the original, large scan, mesh making and offsetting the mesh in order to make 5 mm thickness for the final AFO design.

1. In show off AFO layout patients stands as a great deal as blood course circulate to foot and cannot walk truly are being long past up in competition to inside the



**Fig. 13.11** Subject with the markers positioning on his skin (i) back view, (ii) lateral view, (iii) frontal view (Figures from Motion and Gait Analysis Laboratory at PGIMER, Chandigarh), (iv) the method in order to find the Posterior Iliac crests and (v) the positioning of “sacral” marker, (vi) positioning of the bars





**Fig. 13.12** Gait analysis of foot drop patients

midst of complete deal make use of. Another arrangement of AFO for foot drop patients has been made to conquer this issue and restrained detail displaying and expand exam has in like way been executed.

2. Utilization of 3D human accessible scanner (Artec Eva) to get accurate measurements of foot drop patients.
3. New format of AFO is created with the aid of 3D printing technology (SLS) which is greater time and cost. It examinations the shape and lead of fabric of modern-day usable AFO and 3D published AFO.
4. By making use of 3D printing (SLS) innovation AFO shape some other fabric Nylon-Poly Amide (type of Plastic) has been made.
5. Selective laser sintering (SLS) three-dimensional printing having the principle advantage is that the manufactured fashions are permeable (generally 60% of the



**Fig. 13.13** Gait analysis with old and new ankle-foot orthosis

thickness of normal factors), as an end result weakening their great and ground wrap up.

6. Considering its heartiness and capability to supply complicated entire elements, SLS can deliver massive money and time saving blessings for little run components that would normally require some collecting with popular assembling. It is an ideal marriage of usefulness, high-quality and unpredictability.
7. It continues up the focal point of weight line of motion in nonpartisan position (center of base of help). And furthermore balances out the foot, which as a consequence decreases the danger of harm and improves stride strength and adjust.
8. It can lessen plantar weight by redistribution of plantar weight. It moreover assists to upgrade ordinary probability dispersion of plantar stacking, which is

fundamental importance to decrease carry down furthest point torment amid taking walks.

### 13.6 Scope of Future Works

Future works of the design of Artec Eva Studio 12 Professional will focus on optimization of the computerized design process. Improvement of image processing for the 3D scanned data will be researched so as to simplify current processes. The mechanical structure of compliant finger joint will be further developed, and algorithms of parameter optimization will be developed. The thumb joint will be designed and tested. More materials and embedded sensors could be tested and optimized. Software interface will be developed. In the future, the AFOs with sensor can provide accuracy indicate that when do they need to replace the AFOs. Future works on the development of the AFO test bed will focus on the design of the clamp elements so as to provide quantitative body weight during the gait. Actual human gait cycle data and ankle stiffness could be implemented into the control system so as to verify the functional analysis of the AFO. Further study of the energy return in gait will be analysis in this AFO test bed. Control system will be developed in the real-time machine so as to improve the performance.

**Declaration of Conflicting Interests** No potential conflicts of interest with respect to the research, authorship and publication of this article as declared by author(s).

#### Funding

The author(s) received no financial support for the research, authorship and publication of this article.

### References

1. Abboud RJ (2002) Relevant foot biomechanics. *Curr Orthop* 6:165–179
2. Alexander MA, Xing SY, Bhagia SM (2011) Lower limb orthotics [Online]. *Webmd Llc.* (2011). Available <http://Emedicine.Medscape.com/Article/314838-Overview#Aw2aab6b5>. Accessed 22 Sept 2011
3. American Orthotic and Prosthetic Association Inc. Evidence Note (2008) The use of ankle-foot orthoses in the management of stroke. 5(12):120–128
4. Banga HK, Parveen K, Belokar RM, Kumar R (2014) Rapid prototyping applications in medical sciences. *Int J Emerg Technol Comput Appl Sci (IJETCAS)* 5(8):416–420
5. Banga HK, Belokar RM, Madan R, Dhole S (2017) Three dimensional gait assessments during walking of healthy people and drop foot patients. *Defence Life Sci J* 2(1):14–20
6. Banga HK, Belokar RM, Kalra P, Madan R (2018) Fabrication and stress analysis of ankle foot orthosis with additive manufacturing. *Rapid Prototyping J* 24(1):301–312
7. Banga HK, Belokar RM, Kumar R (2017) A novel approach for ankle foot orthosis developed by three dimensional technologies. In: 3rd International conference on mechanical engineering and automation science (ICMEAS 2017), University of Birmingham, UK, vol 8(10), pp 141–145

8. Boehler W, Marbs A (2002) 3D scanning instruments. In: Proceedings of the CIPA WG 6 international workshop on scanning for cultural heritage recording, Ziti, Thessaloniki, vol 3(12), pp 9–18
9. Brackx B, Van Damme M, Matthys A, Vanderborght B, Lefeber D (2012) Passive ankle–foot prosthesis prototype with extended push-off. *Int J Adv Robotic Syst* 1(10):19–28
10. Bennett BC, Russell SD, Abel MF (2012) The effects of ankle foot orthoses on energy recovery and work during gait in children with cerebral palsy. *Clin Biomech (Bristol, Avon)* 27(3):287–291
11. Bregman DJJ, Rozumalski A, Koops D, De Groot V, Schwartz M, Harlaar J (2009) A new method for evaluating ankle–foot orthosis characteristics. *Gait Posture* 30(6):144–149
12. Brehm M-A, Harlaar J, Schwartz M (2008) Effect of ankle–foot orthoses on walking efficiency and gait in children with cerebral palsy. *J Rehabil Med* 4(9):529–534
13. Bowker P (1993) Biomechanical basis of orthotic management. *Oxford England* 2(10):19–28
14. Chen C-L, Yeung K-T, Wang C-H, Chu H-T, Yeh C-Y (1999) Anterior ankle–foot orthosis effects on postural stability in hemiplegic patients. *Arch Phys Med Rehabil* 8(5):1587–1592
15. Chu TM, Reddy NP, Padovan J (1995) Three-dimensional finite element stress analysis of the polypropylene, ankle–foot orthosis: static analysis. *Med Eng Phys* 17(5):372–379
16. Cook D, Gervasi V, Rizza R, Kamara S, Xue-Cheng L (2010) Additive fabrication of custom pedorthoses for clubfoot correction. *Rapid Prototyping J* 16:189–193
17. Mavroidis C, Ranky RG, Sivak ML, Patriiti BL, Dipisa J (2011) Patient specific ankle–foot orthoses using rapid prototyping. *J Neuroeng Rehabil* 1(5):252–259
18. Crabtree CA, Higginson JS (2009) Modeling neuromuscular effects of ankle foot orthoses (AFO's) in computer simulations of gait. *Gait Posture* 29:65–70
19. De Burgh J (2003) *The human body—an essential guide to how the body works*. Grange Books, Rochester
20. Schrank ES, Stanhope SJ (2011) Dimensional accuracy of ankle–foot orthoses constructed by rapid customization and manufacturing framework. *J Rehabil Res Dev* 48:31–42
21. Edelstein JE, Bruckner J (2002) *Orthotics: a comprehensive clinical approach*. Wiley, Slack, New Jersey
22. Fan GAO, Carlton W, Kapp S (2009) Development of a motorized device for quantitative investigation of AFO's. In: 4th International conference on bioinformatics and biomedical engineering, vol 15(3), pp 112–119
23. <https://www.mayoclinic.org/diseases-conditions/foot-drop/diagnosis-treatment/drc-20372633>
24. Singh H, Singh S, Prakash C (2019) Current trends in biomaterials and bio-manufacturing. In: *Bio manufacturing*. Springer, Singapur
25. Foot Drop Disease Pictures. [www.epainassist.com](http://www.epainassist.com)
26. Anatomy of ankle nerve system. [www.epainassist.com](http://www.epainassist.com)
27. Poomathi N, Singh S, Prakash C, Patil RV, Perumal PT, Barathi VA, Balasubramanian KK, Ramakrishna S, Maheshwari NU (2018) Bioprinting in ophthalmology: current advances and future pathways. *Rapid Prototyping J*
28. Silva P, Silva MT, Martins J (2009) A review of thermoplastic ankle–foot orthoses adjustments/replacements in young cerebral palsy and spina bifida patients. *JPO J Prosthet Orthot* 7:15–22
29. Singh S, Singh M, Prakash C, Gupta MK, Mia M, Singh R (2019) Optimization and reliability analysis to improve surface quality and mechanical characteristics of heat-treated fused filament fabricated parts. *Int J Adv Manuf Technol*: 1–16
30. Singh S, Singh N, Gupta M, Prakash C, Singh R (2019) Mechanical feasibility of ABS/HIPS-based multi-material structures primed by low-cost polymer printer. *Rapid Prototyping J* 25(1):152–161
31. Singh S, Prakash C, Ramakrishna S (2019) 3D printing of polyether-ether-ketone for biomedical applications. *Eur Polym J* (2019)
32. Milusheva SM, Tosheva EY, Toshev YE, Taiar R (2012) Ankle foot orthosis with exchangeable elastic elements series on biomechanics. *23(1):322–330*

33. Milusheva S, Tochev D, Stefanova L, Toshev Y (2011) Virtual models and prototype of individual ankle foot orthosis. In: Isb Xxth congress—Asb 29th annual meeting, 31 July–5 Aug, Cleveland, Ohio
34. South BJ, Fey NP, Bosker G, Neptune RR (2009) Manufacture of energy storage and return prosthetic feet using selective laser sintering. *J Biomech Eng* 132:015001
35. Staats TB, Kriechbaum MP (1989) Computer aided design and computer aided manufacturing of foot orthoses. *JPO J Prosthet Orthot* 1:182–186
36. Sungjae H, Jungyoon K, Jinbock Y, Kisik T, Kihong R, Youngho K (2006) Development of an active ankle foot orthosis for the prevention of foot drop and toe drag. *Biomed Pharm Eng* 1:418–423. International Conference on ICBPE
37. Chu T-M, Reddy NP (1995) Stress distribution in the ankle–foot orthosis used to correct pathological gait. *J Rehabil Res Dev* 32(4):349–360
38. Tortora GJ, Derrickson BH (2008) Principles of anatomy and physiology. Wiley, USA
39. Waters RL, McNeal D, Perry J (1975) Experimental correction of footdrop by electrical stimulation of the peroneal nerve. *J Bone Joint Surg* 8(57):1047–1054
40. Whittle M (2007) Gait analysis: an introduction. Butterworth-Heinemann Elsevier, Philadelphia
41. Winter DA (2009) Biomechanics and motor control of human movement. Wiley, New Jersey
42. Ai YW, Yan H, Jian WZ, Yang W (2014) A new method of digital manufacturing of orthoses. *Comput Model New Technol* 3(18):271–275

**Dr. Harish Kumar Banga** did his B.Tech. (Mechanical Engineering) from Government Engineering College, Bathinda, in 2007 and ME (Production Engineering) from PEC University of Technology, Chandigarh, in 2010 and completed his Ph.D. in the area of additive manufacturing with collaboration with orthopedic department of PGIMER Chandigarh in 2018 from Punjab Engineering College, Chandigarh. Presently, he is Assistant Professor in the Department of Production and Industrial Engineering, Punjab Engineering College, Chandigarh. His areas of research rapid prototyping and 3-D printing, ergonomics, human gait analysis and robotics. He published more than 20 research papers in national and international journals.

**Dr. Parveen Kalra** did his graduation in Mechanical engineering from PEC university of Technology, Chandigarh, in 1987 and post-graduation in Industrial Robotics from Memorial University, Canada, in 1989, and obtained his PhD in Mechanical Engineering from Punjab University, Chandigarh, in 1995. Presently, he is Professor in the Department of Production and Industrial Engineering in Punjab Engineering College, Chandigarh. His area of specialization is human engineering, industrial design, CAD/CAM and robotics. He has published more than 85 research papers in international and national journals. He is a member of ISTE. He carried out design analysis and also carried out detail discussion on results to conclude the manuscript.

**Dr. Rajendra M. Belokar** did his graduation in Production Engineering from Amravati University, Amravati, in 1987. He did post-graduation and Ph.D. from Punjab University, Chandigarh, in 1999 and 2010, respectively. Presently, he is Professor in the Department of Production and Industrial Engineering, Punjab Engineering College, Chandigarh. He published more than 75 research papers in national and international journals. He published one book, and two books are in press. He is Sr. Member SME (USA), M.I.E. C. Eng (I), LM-ISTE, Member-INVEST, and Member APICS (USA).

**Dr. Rajesh Kumar** is working as an Assistant Professor in the Department of Mechanical Engineering, UIET, Panjab University, Chandigarh. He published more than fifty research papers in national and international journals. He did his graduation from Punjab Engineering College, Chandigarh in 1999. He did post-graduation and Ph.D. from PEC University of Technology, Chandigarh, in 2004 and 2012 respectively. His areas of interest are Finite Element Analysis,

Additive Manufacturing, CAD/CAM, and Robotics. He has participated and organized many workshops, seminars, and FDP's and delivered numerous expert lectures.

# Chapter 14

## Influence of Laser Power and Scan Speed During Laser-Assisted Multi-layer Additive Manufacturing Using Finite Element Modeling



Sapam Ningthemba Singh, Yadaiah Nirsanametla, Sohini Chowdhury,  
and M. Muralidhar

### 14.1 Introduction

The conventional manufacturing methodologies have long been the dominant method to produce most of the biomedical products available. These processes are convenient and easier to operate as compared to unconventional machining and manufacturing processes. However, most of the biomedical products require complex shape and high level of user customization. Additive manufacturing (AM) is one of the prominent emerging manufacturing technologies in the era of the Internet of things (IoT), fast computers, Industry 4.0, which can produce objects and parts that conventional processes cannot produce or offer more advantages in doing so. AM is the process of manufacturing objects by joining materials from a 3D design data usually layer upon layer [1]. Rapid prototyping and 3D printing are the common terms often used along with AM having similar meanings. But, technically rapid prototyping by definition is mostly used to produce prototypes, while 3D printing is the collective term applied to manufacturing processes where the product is directly manufactured from a CAD file which is usually an STL file. The conventional manufacturing process, also known as subtractive manufacturing, uses the basic idea of material removal by machining process from the whole workpiece to make the final product. Unlike conventional manufacturing processes, AM employs the reverse idea in which materials are added layer upon layer by reading the 3D model data. With an AM machine, a product can

---

S. N. Singh · Y. Nirsanametla (✉) · S. Chowdhury · M. Muralidhar  
Department of Mechanical Engineering, North Eastern Regional Institute of Science and  
Technology (NERIST), Nirjuli, Arunachal Pradesh 791109, India  
e-mail: [ny@nerist.ac.in](mailto:ny@nerist.ac.in)

S. N. Singh  
Department of Mechanical Engineering, National Institute of Technology Silchar, Silchar, Assam  
788010, India

be manufactured directly from a 3D design data without considering other elements such as the type of machines, cutting tool and fixtures, which is needed in case of conventional manufacturing processes. This leads to efficient material utilization, energy saving and avoiding many other constraints. Hence, creating AM technique is a more desirable manufacturing process in the mainstream of Industry 4.0.

Though it sounds simple in words, the AM process involves complex thermal and microstructural properties alteration during material deposition in layers as well as during interaction between the layers. This may lead to undesirable consequences on the finished product. Despite the freedom in design, it still needs certain optimization. There are several other parameters that influence the overall performance and quality of the finished product manufactured by the AM process. Due to such problems, many researchers have conducted their research, both experimentally and numerically, on various fields related to AM. In recent years, most of the research work is being emphasized on understanding the working principle of AM process, material and heat interaction and its effects on the mechanical attributes, shape and surface roughness of the final product. Intensive research on transient thermal distribution, melt-pool evolution and microstructural characterization of the manufactured parts has been carried out by several researchers. There are three basic stages during an AM process [2]:

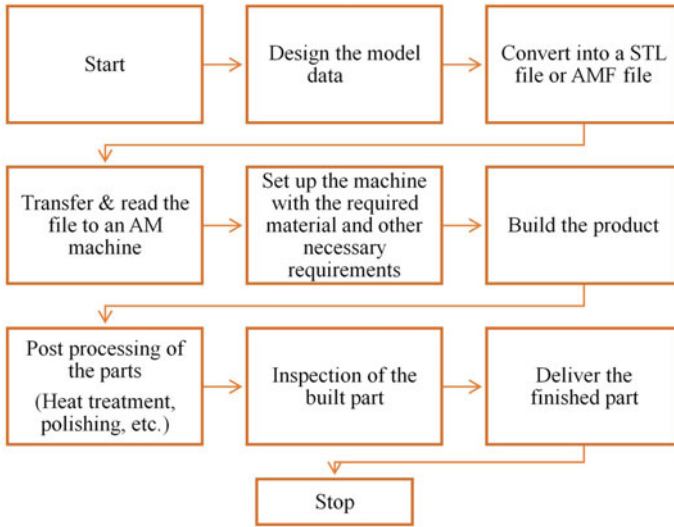
- a. Designing the product model in a CAD software and converting it to a suitable AM file format such that AM machine can understand and execute the commands.
- b. After transferring it to the AM machine, the actual fabrication process is carried out in an AM machine.
- c. In the post-manufacturing operations, heat treatment, surface finishing, etc., are performed. The above-mentioned AM stages can be visualized more effectively from Fig. 14.1.

### ***14.1.1 Types of AM Processes***

There are seven major categories of AM process, out of which three categories utilizes laser as the source of power to join the material. Powder bed fusion, Vat polymerization and directed energy deposition are the laser-based AM methodologies. Sheet lamination, material jetting, binder jetting and material extrusion utilizes either electron-beam-based technology or inkjet technology to adhere the layers. Selective laser melting (SLM), selective laser sintering (SLS) and other types of AM process are derivatives of the above-mentioned types. Some of the major types of laser-based AM processes are discussed as follows:

*Laser beam melting* (LBM): It can manufacture fully dense, geometrically complex models with the ability to attain mechanical and material properties which are comparable with respect to the conventional machining processes [3, 4]. For this reason, LBM is considered as one of the most widely used AM processes. This should not be confused with the *laser beam machining* process. A laser source of solid state, a laser deflection mechanism, a powder feeding mechanism, a base or





**Fig. 14.1** A typical additive manufacturing process

a building platform, and a roller or a scrapper constitute the major elements of a LBM machine. The laser source is adjusted, deflected and concentrated to the area of interest, i.e., the material layer by using the laser deflection mechanism. After the first layer is completed, the built platform is lowered down by the same thickness of the layer and the process is repeated until the product is completely manufactured. A heater can also be used to preheat materials and alloys which are having high liquidus temperature in order to achieve uniform melting of the material (powder). In laser sintering (LS) technique, the powder is heated to the sintering point. In indirect LS, a mixture of powder and a binder operation is used thus improving the overall material built quality and property. A de-binding process is carried out to eliminate the binder material after the laser scanning. Materials used in LBM can be of pure metals such as Al, Ti, Cr, Fe, Cu and compounds like Fe-Cu, Cu-Sn, Fe-Sn, nickel cobalt-based alloys, titanium alloys, stainless steel and tool steel materials.

*Laser metal deposition (LMD):* It is also called as direct metal deposition (DMD), direct laser deposition (DLD), laser cladding, direct energy deposition (DED), laser engineered net shaping (LENS) or laser deposition welding [5, 6]. In this case, the powder is fed by a nozzle. Basic components of LMD are same as LBM except that the roller is replaced by a nozzle to supply the powder which can be supplied axially or laterally using inert gas stream [7, 8]. *Wire feeding* of materials is another type of laser-based AM. This type avoids the preprocessing of materials to make it as powder material. It can be used for larger components but moderate in complexity. Wire-based laser AM has some unique advantages including lower costs, neat and clean working environment, low wastage of material and higher metal deposition rate than other AM methods. In wire deposition process, hot wire deposition or central wire feeding is used [9].

**Table 14.1** Types of major additive manufacturing processes

Laser beam-based AM	Electron beam-based AM	Other AM processes
VAT polymerization Powder bed fusion Direct energy deposition Laser beam melting Stereolithography SLM, SLS, etc.	Electron beam melting Electron beam sintering, etc.	Wire feeding Inkjet-based AM processes Sheet lamination Binder jetting Material extrusion, etc.

*Stereolithography (SLA)*: The AM process of building a part using concentrated laser scanning on a vat of liquid resin photopolymer in a moving platform is known as stereolithography (SLA) [10]. After contact with appropriate low wavelength lasers, each layer is solidified and lowered down by an amount equal to the layer thickness. The laser is applied again, and the same process continues till the manufacturing is complete. It is mainly used in prototypes and non-structural parts. SLA boasts of having the ability to obtain higher dimensional accuracy and smoother surface finish [11]. SLA cannot process metals, and it incurs more cost as compared to other AM methods. It requires more support base and has limited availability of resins [12]. Other types of AM process are given in Table 14.1.

The first step of an AM process is to convert the 3D model CAD design to a file format which the AM machine can understand and execute the commands. AM file format contains data about the surface of the object usually in G code. The AM machine then decodes the information and the machining takes place. There are two main types of AM files: *STL* file or *STereoLithography file* and *Additive manufacturing file format (AMF)*.

STL is a native file format for the AM process. It is also known as Standard Triangle Language or Standard Tessellation Language which gives the surface geometry of a 3D model for the AM machine [12]. As the name suggests, STL uses a combination of multiple triangles to create the surface of the object. A low resolution of triangles means poor surface finish and distortion in shape. Higher resolution allows manufacturing of products with a smooth surface finish.

Another file format for the AM is the additive manufacturing file format (AMF) designed, defined and developed under ISO/ASTM 52915:2016(E) [13]. It is an extensible markup language (XML)-based file format for AM process. Unlike the previous STL format, AMF has the provision to provide and encode data about the color, materials, lattices and constellations which are required during the AM process. It gives the leverage of embedding more information on the file itself without any other extra methods or add-ons. It also helps in designing more complex products such as products having different colors, a mixture of materials, etc. Even though AMF offers more flexibility and above-mentioned advantages, STL format is more widely used due to the fact that STL is the first AM file format. However, this trend is changing as AM machine manufacturers start adopting the new AMF format rather than STL as their main file format.

The previous and current ways of generating the sliced layer of AM in either STL or AMF have some problems and defects which result in irregularities and error in the final shape of the overall model. The sliced layers are produced by cutting the whole model using a rectangular plane parallel to the support base and then by extruding the layer to form a small volume of the layer. This method of slicing arises two main errors or effects commonly known as *staircase effect* and *systematic distortion*. The staircase effect is the result of extruding the slice only by square or rectangular blocks that results in the staircase-like structure as a whole. The staircase effect is directly proportional to the thickness of layers. It is usually solved by polishing operation in the post-processing stage [14]. The systematic distortion is the direct result of the staircase effect. This is due to the cumulative iteration of staircase effects which will result in major distortion of the model as a whole. Bottom-up slicing, top-down slicing and radial geometry extrusion of the 3D model are some measures to reduce this effect. The new methods are concerned with extruding the model as exactly as possible such that errors can be reduced in the post-processing operation [14–18].

### 14.1.2 Process Parameters of the AM Process

The principal process parameters of AM processes are raw material, powder grain size, laser power, laser diameter, scanning pattern, scanning velocity. Additionally, point distance, exposure time, layer thickness, scanning and building direction have major effects on the quality of the parts produced such as surface microstructure, density, fatigue strength, hardness, stiffness and surface roughness [19]. Void formation is basically due to the air gap which has a large influence on the final product's microstructure. By analyzing the influence of major process parameters and controlling them as per requirement, AM process has the ability to obtain a final product which has better quality when compared with the products fabricated by conventional manufacturing processes. A detailed explanation of some of the main process parameters is described below:

*Laser power:* Laser power is the foremost key element in AM process. It is the heat source on which the whole process depends. Higher laser power means high energy input, and it takes less time to melt the material. Low laser power means incomplete melting of the material resulting in poor surface finish, irregularities in grain structures, etc.

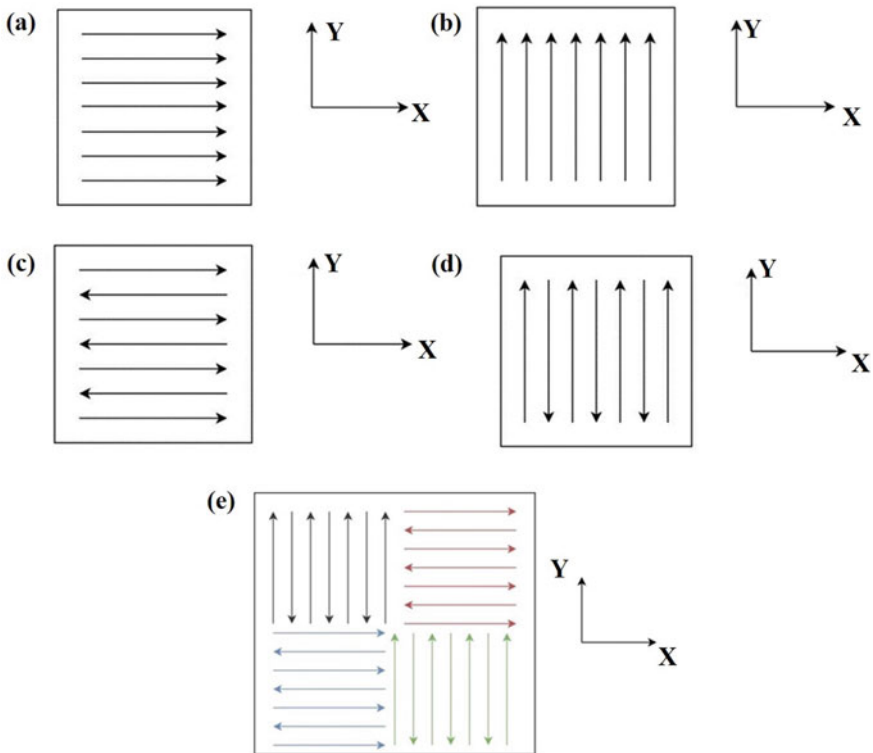
*Laser diameter:* It is the area of laser influence. Large laser diameter means less scanning time and hence faster machining time. However, a large spot diameter limits the resolution accuracy.

*Scanning velocity:* It is the speed in which the material is scanned by the laser. A high scanning velocity leads to incomplete melting of the material while slow scanning velocity refers to over melting of the material.

*Scanning pattern:* Scanning pattern has a significant impact in the final microstructure of the product. The temperature difference between the layers and across the cross-sectional area of the product is different for different scanning patterns. Such a

difference in temperature results in different microstructural patterns due to different heating and cooling patterns. Figure 14.2 represents the different laser scanning patterns such as  $x$ -unidirectional,  $y$ -unidirectional,  $x$ -bi-directional,  $y$ -bi-directional and island pattern. Moreover, research in the area of scanning pattern and its influence on the final mechanical properties and object's structure is needed. The current existing scanning modes are also lacking information about when to use, to which material it suits, which pattern is best for a particular material, etc. Extensive research in this area will help to increase the effective use of AM processes thus avoiding material defect and low-quality final products. In addition, the combined effect of scanning pattern, scanning orientation and time delay between the successive scan also plays a significant role in the final strength of the product.

*Layer thickness:* Thicker layer is directly associated with the power requirement to melt through it. On the contrary, thin layer implies less power requirement to melt the material. However, manufacturing a whole product with thin layers means longer manufacturing time of the product. Even though thicker layers are desirable, there are constraints on maximum power supply in AM machine. Hence, it is inevitable to



**Fig. 14.2** Different laser scanning patterns: **a**  $x$ -unidirectional, **b**  $y$ -unidirectional, **c**  $x$ -bi-directional, **d**  $y$ -bi-directional and **e** island pattern

compromise the manufacturing time due to machine limitations with regard to layer thickness.

*Powder size:* For AM process based on the powder materials, powder size also has an impact on the final quality of the product. Larger powder grain size requires higher energy input, and there are possibilities that grains are left without proper melting. The voids left in between the powder materials are different for different powder sizes which will result in different final mechanical characteristics and microstructures of the product.

All of the above parameters are inter-dependent. For example, high laser power does not mean that the powder materials will always properly melt. If the scanning velocity of the laser is high combined with large powder size, then it will result in a poor material quality. Hence, selection of an optimum process parameters is necessary to have a quality product. All the process parameters and different nature of operations will lead to different porosities in the final product along with unique microstructural characteristics and tensile strength. Inspecting such properties, learning how to overcome the defects and avoiding low porosity of metals, increasing the tensile strength without compromising the manufacturing time and power requirements will increase the efficiency of AM processes. Some additional factors influencing the final product of a part manufactured by AM process are presented in Fig. 14.3.

There are some design and practical limitations of AM method. The difference in final microstructures in between the layers is bound to occur even if it is very minimal due to its nature of the operation and difference in cumulative heat transfer as the number of layer increases. Another limiting factor is the size of the product an

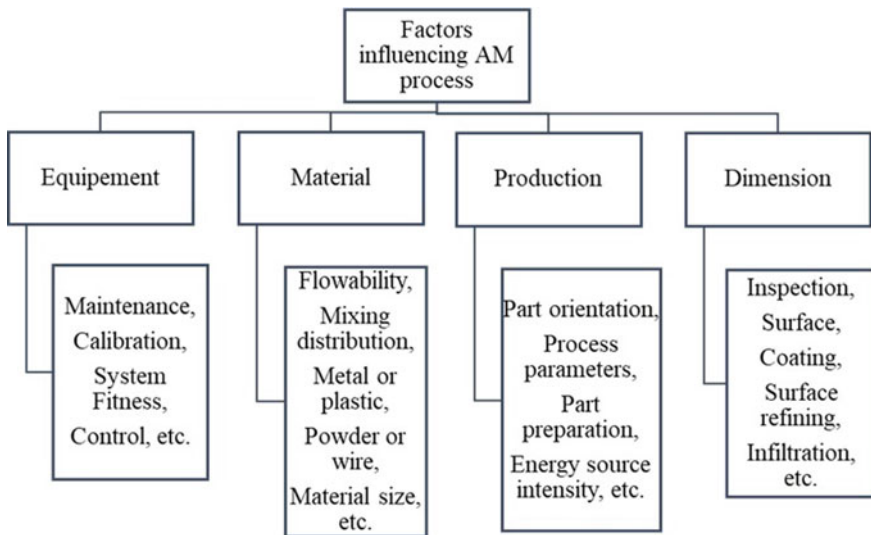


Fig. 14.3 Different types of influencing factors during an AM process

AM machine can offer. Any attempt to change the current system will need a very detailed change in terms of heat transfer and distribution in a product and its influence on the final mechanical properties and microstructural attributes in the final product. Hence, both experimental and numerical analyses are needed for any improvement in the AM machine and to have an economically viable commercial manufacturing method. For a laser-based AM process, controlling melt-pool size and evolution of melt-pool is very important to control and maintain the final mechanical properties, but it is not limited to thermal strain, surface roughness, microstructure and strength. Out of the above-mentioned process parameters, beam power and scanning velocity are the two major elements. Therefore, it is very important to analyze the evolution of melt-pool shape and dimensions under different processing conditions and their effects.

Analyzing each and every process parameter will consume huge amount of computational work, and it will take considerably large duration. Finite element analysis is one of the most popular approaches to compute complex problems and analyze heat flow, stress, failure, etc. In order to understand how finite element modeling provides results with a high level of accuracy, it is very important to study some of the research that has been carried out by previous researchers.

### ***14.1.3 Numerical and Experimental Investigations of the AM Process***

Both numerical and experimental analyses have important significances in order to achieve an efficient fabrication process. Data established from experiments can be used to validate and verify the numerical models and analysis. With the ever-increasing computing power and its technology, the applications of numerical analysis and its effect on engineering fields have been increasing tremendously. Experimental data can also be used to develop new thermal models. The FE models can be analyzed for studying the insights of physics involved during AM process which cannot be comprehended through experiments. This in turn will also provide an aid to optimize certain process parameters based on desired requirements. Hence, adjustment of process parameters is a prime necessity in case any alteration in the product is required. Numerical modeling and optimization techniques are very helpful in these scenarios so that the highest possible efficiency can be delivered without compromising the quality of the product. Every set of data cannot be recorded in an experiment due to practical and technological limits such as measuring temperature using infrared cameras and thermocouples at preferred locations in the sample during fabrication process, inspecting mechanical and microstructural attributes. However, few experimental data can be used to verify the results of the numerical analysis. If the result is within the acceptable limit, the numerical model is determined to be correct and acceptable and it can be used for all experimental trials. On account of modern personal computers and supercomputers, the model data of every simulation step can

be retrieved easily. Thus, numerical modeling and analysis help in predicting limits, simulating certain conditions, calculating costs and duration at a very high accuracy level. This is why both numerical analysis and experimental analysis are important and should work together to compliment to each other.

#### *Numerical investigation of laser-based AM process*

Modeling and analyzing the fabrication of an object by an AM process accurately help in determining the exact nature of heat transmission and stress distributions involved in the particular process. For FEM process defining the model geometry, discretization, boundary conditions, application of loads are very important and key steps to comprehend the AM process. Yuze et al. showed a generic analytical model of a laser additive manufacturing process (LAM) [20]. The moving laser heat source was assumed as Gaussian distribution and Rosenthal's 3D model. Also, the 3D melt-pool geometry considered the Brewster effect. A single-layer laser melting of SS grade 316L powder with AISI 316L as the base material was simulated to analyze the influence of various process elements such as laser intensity, scanning velocity, spot diameter on the melt-pool size, thermo-mechanical properties [21]. The analysis helped in finding the quality of the built part, thermal distribution and distortion. However, analyzing a single-layer deposition does not represent the nature of the fabrication process where multiple layers and multiple tracks are involved. Hence, a more complex analysis consisting of multi-layers will give more accurate results.

Most of the numerical analysis performed in the past did not consider the factors such as the air content, sulfur content on the metals. Gan et al. have examined the effect of surface-active elements during laser additive manufacturing process. Also, the authors have analyzed the mass transport of sulfur in sulfur-containing metal during the process [22]. It was determined that the sulfur distribution is time-dependent, non-uniform and decreases along centerline of the top surface. A numerical simulation of LAM of Inconel 718 components and Ti-641-4V materials was carried out to determine residual stress and distortion distribution [23]. It was observed that Ti-641-4V suffers more residual stress than Inconel 718 material. The residual stress decreases with decreasing layer thickness as more time is exposed to the melt-pool. Further, residual stress was reduced by another 20% when the laser power source was doubled; however, the distortion level was enhanced by 2.5 times. Moreover, in extreme conditions, when stress changes from tensile to compressive state the layers were seem to segregate from each other. The parts fabricated by AM process are susceptible to defects and distortions due to non-uniformity in the material deposition in the layers. The distortion and defects can be minimized by using thermal strain parameters [24]. Lower thermal strain can be obtained if the heat input is maintained at a minimum level where interlayer bonding is possible.

However, low laser power with high scan speed have short exposure to heat and shorter duration for melting of metals, and thus, it has very low weldability [25]. The temperature gradient along the depth increases as the laser intensity increases but reduces with increasing scanning velocity. It is evident that an optimum condition of laser intensity, scanning velocity, laser diameter is needed for an AM process in order to have good weldability and low residual stresses.

Moreover, bio-implants have the problem of stress shielding that causes the implant to prematurely loosen and reduce the lifespan of the implant. Additively manufactured bio-implants have the ability to manufacture customized bio-implants to reduce the stress shielding [26]. A computer model was developed to simulate and estimate the effective elastic modulus of biomaterials with high-volume porosity [27]. Employing multiple lasers to improve manufacturing lead time (MLT) is another concept in the AM. A simulated study of multi-laser powder bed fusion (ML-PBF) on Ti-6Al-4V demonstrated that scanning time is reduced by almost 75% by employing four lasers [28]. The residual stress was reduced by employing island division schemes, but it resulted in non-uniform and anisotropic stress distribution. Hence, to obtain a uniform residual stress distribution, a proper model geometry, defining accurate laser orientation and a synchronized process, is required.

The microstructure of an additively manufactured object depends on chemical composition of the powder dilution, part orientation, melting rate, solidification rate and maximum temperature attained. The melt-pool can be fully melted or semi-melted solid compositions depending on the initial material temperature, laser power input, scanning velocity, layer thickness and temperature distribution across the whole deposited material. The nature of melt-pool governs different microstructure and morphology of the built surface [29–32]. Although most of the AM processes take place in an inert gas environment, there is little effect on the final product. However, the application of inert gases has effects on porosity, grain size and compression strength in final material [33]. The effect of cooling rate was analyzed by Ali et al. [34]. The authors showed that the cooling rate and chemical composition constitute the major factors affecting the microstructure of the final object. It was also found that the cooling rate can be adjusted to obtain specific carbide morphologies in the build clad. A cooling rate of 1500 K/s is required to form dendritic structures of higher percentage in Fe materials. However, very slow solidification rate resulted in floatation of TiC particles for a Fe–Ti–C system [29, 32, 35]. Furthermore, lesser percentage content of TiC beneath the Fe–Ti–C surface resulted in low wear resistance and excellent hardness property [32].

A simulation model with the combination of FEM and stochastic analysis was developed to understand the microstructural evolution of an Nb-bearing in AM process. The model can analyze the growth of dendrite, nucleation, formation of Laves phase particles and segregation of Niobium (Nb) during the solidification process [35]. The extensive study was conducted to understand the resultant microstructure and solidification conditions. Laves phase formation is evolved for a small equally distanced dendrite arm with high cooling rate coupled with low-temperature gradient. Furthermore, Laves particles of larger width are not desirable since, it reduces mechanical strength in an object [36–39]. It was also found that long chain morphology is present for high laser intensity, while discrete Laves phase particles are present for low laser power intensity. Lowering the required minimum input energy level to a required minimum is desirable to prevent the formation of Laves phase particles. Presence of large Laves phase particles causes hot cracking [40, 41].



Zinoviev et al. developed a 2D numerical model to simulate the evolution of grain structure in a LAM process. Using the Goldak heat source and cellular automata method, grain growth was evaluated [42]. A cellular automata model was used to examine morphological changes in SS 316 steel. The proposed model was adopted to test the grain growth [41, 43]. Before incorporating these simulation results directly into practical applications, the model should be calibrated and verified with some experimental data. Hence, it is necessary to analyze the experiment process extensively.

#### *Experimental investigations of laser-based AM process*

With several years of experimental research in laser-based AM processes, improvements in terms of metal deposition rate, energy consumption, a decrease in surface roughness and other parameters have been observed. However, the basic constraints in AM process, i.e., lack of better surface finish, different mechanical properties within the manufactured product and slow manufacturing speed are still prominent. Hence, there is still much research required to perform in order to set the level as par with the conventional machining process. In this subsection, some research and attempts to develop a new and improved laser-based AM processes are discussed along with their advantages and limitations in terms of feasibility and economics.

Most of the experimental works concentrate on method feasibility and the influence of various process parameters on the final product. The effects of laser beam parameters such as the pulse width, laser power, frequency and angle of the laser on the performance of beam and forming of materials during a single or multi-layer process are [44]:

- (a) A compressed plasma arc effect can be observed due to laser power, pulse width, laser angle and frequency.
- (b) The plasma arc decreases with the increase in laser power. With the increase in laser power, energy absorbed is increased and then improves ionization and magnetic effects which results in the decrease of the plasma arc. The same phenomenon of decreasing plasma arc influence can be observed in case of increased pulse width.
- (c) The number of repeating pulses applied in a single time unit is called the pulse repetition frequency (PRF). The plasma arc increases after PRF of 50 Hz. This shows that the plasma arc initially decreases up to a certain frequency and then enhances. This is because the average power density increases and due to continuous iteration of power supply overall temperature increases.
- (d) The deposition width of plasma and hybrid laser is smaller than pure plasma arc. However, a higher height and a better quality of surface is achieved.

Liu et al. conducted an experiment on a Cu matrix in a Fe-Cu-Ni-C alloy. The basic idea is that the property of an alloy can be easily changed by changing the percentage of its constituent elements. The experiment is conducted in such a way that the material components are changed when the alloy is subjected to indirect selective laser sintering [45]. Some of the AM processes use powder materials. These powders can be supplied either by powder movers or nozzles. Powder supplied by nozzles is

assumed to follow Gaussian distribution [46]. Small focal distance and focus radius lead to bigger powder concentration. The maximum concentration can be obtained at a nozzle cone angle of  $60^\circ$ . For some high melting point materials such as W-Ni-Fe, preheating of the material with high scanning energy, a small gap between each scan and low scan speed help to obtain better quality products [47]. SLM of AISI 316L austenitic stainless steel has 99.9% density, 30% more elongation rate when evaluated with SLM of wrought iron [48]. However, the resilience test revealed a lower value than wrought iron while the same hardness magnitude was obtained.

New methods and new materials are being tested for its feasibility by AM processes. Use of metallic cellular materials is an emerging concept in AM industry. Cellular metallic materials are the materials with structures and properties similar to cellular materials like materials having gaseous voids in it is one such example [49]. These materials can be formed by stirring foaming agents, pressure infiltration of a ceramic mold, vapor phase or electrodeposition onto a polymer foam and high-pressure inert gas expansion trapped in pores [50]. Use of metallic cellular materials for AM process was achieved by Williams et al. [50]. The previous approach by Hattiangadi et al. [51] and Chiras et al. [52] resulted in porous parts [53], and the authors were unable to manufacture unsupported parts and free-standing structures [54]. SLM and EBM methods have been successfully used to manufacture fully dense parts. Current and future research should include manufacturing of fully dense cellular materials with mechanical properties that are tantamount to that of conventional processes. Emphasis should be given in improving the ability to use different coating materials and reduction of costs. Overall reduction of cost is possible only when there is mass adoption of AM machines. However, for the AM machines to adopt in industries, it must have efficient and accurate operations in terms of surface finish, flexibility in the control system and flexibility in machinability of different materials. Hence, further research efforts should concentrate on the field of efficient operation, improvement in the material finish and quality. For this to achieve, a better understanding of the melt-pool evolution and nature of temperature change is required.

#### ***14.1.4 Advances of the AM Process in Biomaterials and Biomedical Devices***

It is fair enough to say that the AM is far away to reach the stage to finally deploy and adapt to the mainstream manufacturing industry on a very wide scale. This is because of the limitations and problems mentioned above such as poor surface quality, high-temperature gradient, change in the microstructure and slow manufacturing time. But, it is also safe to say that the technology has developed dramatically to the extent that some of the AM types such as SLM, stereolithography are employed by some major companies either in beta stages or in industrial productions. In this section, the latest technological breakthroughs achieved by the research communities

and their possible effects on the whole industry are discussed. The use of additive manufacturing in biomedical research to a level where tissue engineering can be achieved via additive manufacturing is a promising field. All such advances are the results of years of painstaking research contributed to AM from various sections. Some of the latest advances that are being discussed in this section may not be the best as compared to other manufacturing processes. But, every industry in the past has years of research and development to reach the very best. AM is on its transition from a process of research interest to large-scale industrial implementation.

An important field that garnered attention is the application of AM in biomedical research and industries. Though conventional machining processes are being used to manufacture bio-implants, AM process has certain advantages that it is very much suitable for customized models. This can be further explained that every problem or model of an implant is different for each patient. So, conventional machining processes have to modify the manufacturing systems including supply system, tool accuracy and machine size that is required for each implant requirements. This gives an edge for the AM process over the conventional machining processes in the field of biomedical implants. Other advantages include on-demand manufacturing, remote manufacturing from remote areas and smaller footprints for the manufacturing facility [55].

In early stages, even though AM was used to manufacture bio-implants, it was mainly used for model production, testing but not for a real replacement of an implant [56]. As the technology advances, the AM is being used to create implants, prostheses and drug delivery systems which are becoming a major advancement in the fields of biotechnology, pharmaceuticals, health care, etc. [57]. In tissue engineering technology, bioprinting with the help of additive manufacturing is gaining attraction and paving way to print actual live organs. Jetting, extrusion and laser-based bioprinting AM processes are most commonly used in bioprinting. However, the variation of cell properties and biological functions due to variation in material and layer deposition, cell damaged by laser requires intensive care from the process starting to ending. Also, it leads to major dimensional inaccuracies due to extrusion-based prints. It is now possible to print exact model of patient's eye anatomy which will allow the surgeons [58]. Bio-inert is often associated with bio-implants because bio-implants often fail or lack the ability to interact and associate with the cells as well as tissues causing many problems [59]. Another challenge is that metallic implants are bound to have corrosion even in alloys because of the nature and chemicals present in the human body [60]. For ceramics used in biomedical, the lack of sintering due to low temperature is the main problem. Higher energy input with better penetration ability will help to solve this problem. Biodegradable polymers are most widely used for internal bio-implants due to the ability to adapt to the internal biosystems and to interact with the biomaterial by the body. However, these polymers tend to release acids due to reactions with the living body systems, excessive release of these acids may cause local inflammation, and delay in healing process which are the main drawback in biodegradable material as of now [61]. However, it is expected to have new improved materials in the years to come with the much ongoing research.

Significant improvement can be seen in making drug delivery systems. The main problem was the inability to process the materials used in drug delivery systems [62, 63]. Another problem is the inability to sinter the material after the drugs are loaded [55]. The same problem was associated with bone implants and dental works. Much improvement has been made in making the powder material more homogenous and more uniform in powder material size, laser power concentration and higher-resolution feedback systems. With these improvements, AM has progressed over the last decade to a level where certain parts of biomedical parts can be manufactured with the same or even better quality as conventional manufacturing processes. Calcium phosphates, silicates, alumina, porcelain and zirconia are mainly used in these applications.

Some other applications include skin coating, plates for bone, optical applications and cartilage repair. In these applications, biodegradable polymers such as polyglycolic acid (PGA), polylactic acid (PLA), polydioxanone (PDS), polyethylene glycol/oxide are mainly employed [64–66]. Recent research has paved the way to manufacture materials such as polyether ether ketone (PEEK), polycaprolactone (PCL), functionalized polyurethanes, polypropylene fumarate (PPF) [67–69]. PEEK has applications in orthopedic implants, scaffolds, artificial organs, surgical guides, prostheses, drug vessels, etc. Out of the commonly available and widely used AM processes are fused deposition modeling and selective laser sintering. The major challenges of PEEK for biomedical applications are low integration to bone, high wear rate, inherent printing issues related to AM [70]. The main obstacle in cell adaptation for metallic bio-implants is low wettability due to high surface energy, smooth surfaces and low porosity. The inherent disadvantages of AM process such as high surface roughness, porosity in the melt-pool turn out to be very effective in case of bio-implants. For example, high elastic modulus is not desirable due to stress shielding. But an additively manufactured part with inherent high porosity will reduce the high elastic modulus, and it will also help in better bone and cell growth around the implant [71]. A SLM manufactured sample of SS 316L has a fatigue limits of 108 MPa which is lower than a turned surface which showed 267 MPa [72]. Similarly, for Ti-6Al-4V the fatigue limit was determined as 267 MPa using SLM, while the same material was determined as 500 MPa for a polished surface [73]. The current and future research is directed toward the development of the AM process that has the ability to process multi-materials simultaneously without changing chemically and produce the same quality product multiple times from the same machine. Acrylonitrile butadiene styrene (ABS) and high-impact polystyrene (HIPS) are different materials in terms of impact strength. Multi-material fabrication of these two materials can provide enhanced properties like high impact strength in certain section by maintaining the tensile strength and lightness. A study carried out by Sunpreet et al. showed the possibility of fused fabrication of these two materials with promising results [74]. Tailoring of final mechanical properties requires post-processing of the product like annealing. It was found that annealing of ABS material reduced the porosity and interlayer gap, but brittle fracture be present at cross sections [75]. However, annealing time has negligible effect. With the rise of nanotechnology and nanorobots, the need of AM machines to have the ability to

manufacture very small parts in micro- and nanoscale is of paramount importance so that such AM-based nanoproducts can be manufactured and deployed in real-world scenario.

Significant efforts have been put to improve the resolution of AM machines for biomaterials without affecting its composition and without letting it react while processing the materials. Continuous liquid interface production (CLIP) is the process where oxygen is used as a barrier to avoid photoinitiation process causing polymerization continuously upward [76]. Recent development includes the ability to print liquid metal droplets using 3D inkjet printing which allows the metals to reduce to nanoparticles and print it through piezoelectric dispensing heads [77, 78]. Laser-induced forward transfer (LIFT) is another method that allows reducing the resolution of the machine [79]. The major applications include wearable devices, electrodes for monitoring in the pacemaker and signal transmission in intracochlear devices. Live cell or tissue printing was achieved by Phamduy et al. using laser direct write (LDW) where a cancer cell was printed onto a live rat to study the stages and evolution of cancer and angiogenesis in the rat when the cancer cell is printed in it [80–83]. This is one of the major steps which may eventually lead to a full live organ printing in the future.

An effort to reduce the MLT is to increase the layer thickness. But, the layer thickness cannot be increased more than a certain limit to avoid incomplete melting. The layer thickness should be limited to a range where the current laser capability can process. A FEM analysis of a high layer thickness laser-based AM process is developed in this study to investigate the effect of laser power and scanning velocity on the melt-pool and time-temperature distribution.

## 14.2 Mathematical Background

Selective laser melting offers the ability to process parts by applying a concentrated laser source onto a layer made of powder. By repeated procedure of melting phenomena the whole part is generated. During this process, the layers undergoes repeated phase transformation due to difference in heat applied from the laser source. Transient thermal distribution, uniform and non-uniform grain growth are occurred during the process. Some of the thermal energy is lost either due to convection or radiation. This process can be understood mathematically as discussed further in the following subsections.

### *Governing equations and boundary conditions*

Initially, transient thermal analysis is performed to determine the time–temperature history at each specific points of the deposited material over the layers as well as substrate. The transient heat conduction equation for a three-dimensional heat flux can be represented as [84]

$$k \left( \frac{\partial^2 T}{\partial x^2} + \frac{\partial^2 T}{\partial y^2} + \frac{\partial^2 T}{\partial z^2} \right) + \dot{Q} = \rho c_p \left( \frac{\partial T}{\partial t} + v \frac{\partial T}{\partial y} \right), \quad (14.1)$$

where  $k$  is the thermal conductivity,  $\rho$  is the density of the material,  $C_p$  is the specific heat,  $v$  is the velocity vector,  $T$  is the temperature variable (K),  $\nabla$  is gradient operator,  $k$  is the thermal conductivity,  $\dot{Q}$  is the rate of internal heat generation per unit volume. The initial temperature distribution at time  $t = 0$  is defined as:

$$T(x, y, z)|_{t=0} = T_0, \quad (14.2)$$

where  $T_0$  represents the ambient temperature which is considered 298 K.

The latent heat of conduction within the melt-pool is the main domain where most of thermal transmission takes place besides convection and radiation thermal losses from all the surfaces. The natural boundary condition can be represented mathematically which involves Newton's Law of Cooling and gray-surface body behavior [85–91]:

$$k \frac{\partial T}{\partial n} - q + q_c + q_r = 0, \quad (14.3)$$

where  $q_r$  and  $q_c$  are the heat loss due to radiation and convection and radiation and  $q$  is the input heat flux. Convective and radiation heat loss can be expressed as:

$$q_c = h(T - T_0) \quad (14.4)$$

$$q_r = \sigma \epsilon (T^4 - T_0^4) \quad (14.5)$$

where  $h$  is the coefficient for heat convection,  $\sigma$  is the Stefan–Boltzmann constant,  $\epsilon$  is the melt-pool emissivity,  $T_0$  is the initial temperature and  $T$  is the instantaneous temperature at that given time.

#### *Heat source model*

The Gaussian heat distribution model is the most common model used in the laser additive manufacturing process since; heat distribution follows Gaussian distribution. Gaussian distributed 'disk' heat source model is used to simulate the distribution of laser heat source onto the powder layers from the laser source. It can be represented as [84].

$$q = \frac{3\eta P}{\pi r^2} \exp\left(\frac{-3(x^2 + y^2)}{r^2}\right), \quad (14.6)$$

where  $q$  is heat flux rate,  $\eta$  is the laser absorption coefficient,  $P$  is the laser power,  $r$  is the effective laser beam radius,  $x$  and  $y$  are the respective positions of the laser beam at the given time. For the heat source to move, velocity and time have to give along the axis of movement.

**Table 14.2** Temperature-dependent material properties of Inconel 718 [92, 93]

Temperature (K)	Thermal conductivity (W/m K)	Temperature (K)	Specific heat (J/kg K)
378	14.7	560	480
485	15.7	667	491
579	17.8	767	511
677	18.3	866	537
781	19.7	968	570
881	21.2	1071	612
981	22.9	1173	655
1080	23.7	1271	707
1187	27.7		
1277	30.4		

### 14.3 Finite Element Modeling

The FEM of a laser-based AM process for Inconel 718 is taken. The results include the temperature distribution and melt-pool geometry at different layers under different operating conditions. It also deals with details of the material composition and the temperature-dependent material properties. The influence of process parameters on the melt-pool shape and temperature distribution is also discussed.

#### 14.3.1 Material Properties

An FE-based model is developed based on necessary boundary conditions and material properties such as temperature-dependent material properties, correct mesh size, process parameters. Inconel 718 is considered in this study for analyzing the evolution of melt-pool and transient temperature distribution during SLM process. Two key parameters are considered, i.e., laser power and laser scanning velocity. Specific heat capacity and thermal conductivity are the main temperature-dependent properties that affect the heat transfer during the SLM process along with density and emissivity even though its effect is low. Specific heat, density and thermal conductivity of Inconel 718 materials are presented in Table 14.2. Also, temperature-independent material properties are presented in Table 14.3.

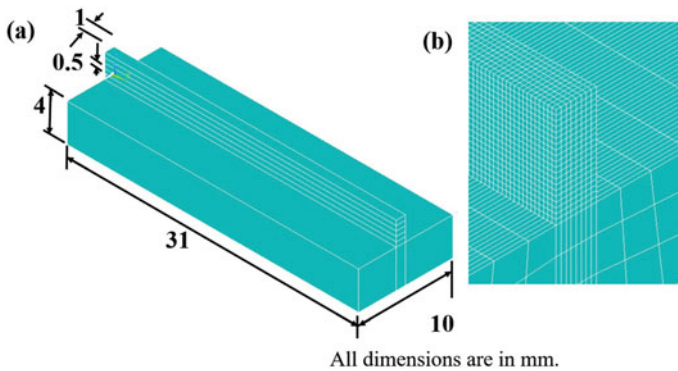
#### 14.3.2 FE Model

An FE-based transient thermal model is developed for transient thermal analysis using the ANSYS parametric design language (APDL). The SOLID70 element is

**Table 14.3** Material properties that taken into consideration for simulation [93]

Property	Value	Unit
Density	8190	kg m <sup>-3</sup>
Ambient temperature	300	K
Thermal conductivity	11.4	W m <sup>-1</sup> K <sup>-1</sup>
Specific heat capacity	435	J kg <sup>-1</sup> K <sup>-1</sup>
Melting point	1609–1700	K
Latent heat	152 × 10 <sup>3</sup>	J/kg <sup>-1</sup>
Coefficient of thermal expansion	1.3 × 10 <sup>-5</sup>	K <sup>-1</sup>

used in the FE thermal analysis. It has eight nodes and a single degree of freedom (temperature) at each node. It is used because the model consists only of straight surfaces. SOLID90 should be used which has 20 nodes and a single DOF at each node if the model has curve boundaries. If the analysis continues for structural analysis, the element should be replaced with SOLID45. Figure 14.4 shows the FE model for Inconel 718. The substrate size is 10 mm × 31 mm × 4 mm with a layer size of 1 mm × 31 mm × 0.5 mm. Figure 14.4b presents the meshed FE model along with a magnified view. The process parameters considered in this study are given in Table 14.4. Element’s death and birth feature is implemented to mimic the adding layers during the manufacturing.



**Fig. 14.4** **a** Schematic of multi-layer model and **b** the FE model

**Table 14.4** Process variables employed for Inconel 718

Data set no.	1	2	3	4	5	6
Speed (mm/s)	150	150	200	200	300	300
Power (W)	200	250	200	250	200	250

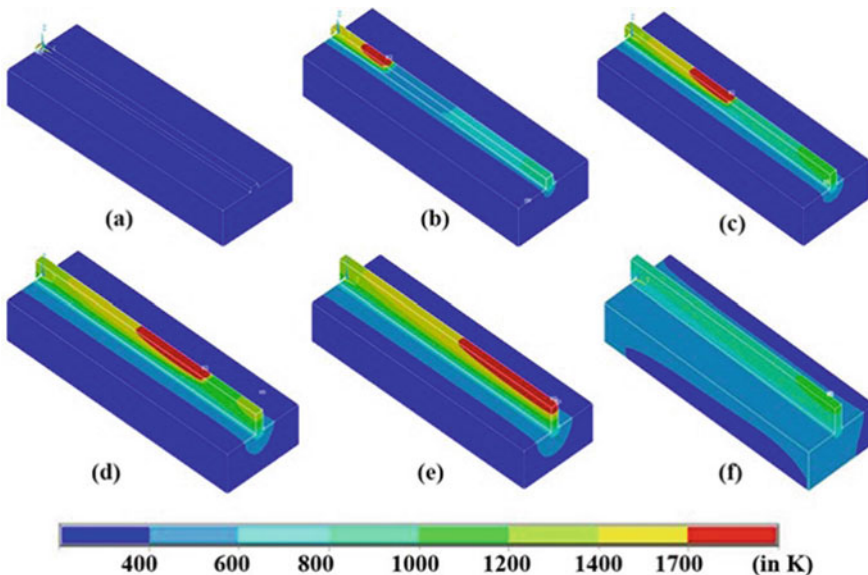


## 14.4 Results and Discussions

This section discusses the response of process parameters in terms of temperature distribution and melt-pool dimensions. The effects of laser power as well as the laser scanning velocity are also discussed in detail. The results show that for the current dimensions and high layer thickness, complete melting and sintering of layers are observed.

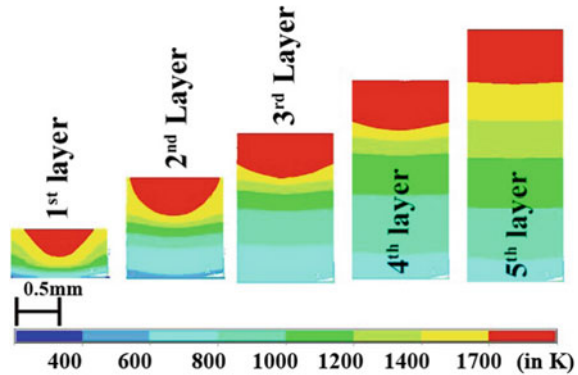
### 14.4.1 Melt-Pool Evolution and Temperature Distribution

When the laser power is applied along the direction of laser scanning, the temperature is highest at the centerpoint of the laser source. As the laser moves along a layer, the size of the melt-pool length increases. Moreover, the length of the melt-pool also increases as the number of layer increases as shown in Fig. 14.5. Figure 14.5 represents the laser movement at different locations when the laser power is 200 W and scanning velocity is  $150 \text{ mm s}^{-1}$ . Figure 14.5a shows the movement of laser power in the first layer, (b) at a distance of 7.75 mm from the origin in the second layer, (c) at the middle of third layer, (d) at a distance of 23.25 mm from the origin in fourth layer, (e) at the end of fifth layer and (f) the cooling process after the laser scanning is over.



**Fig. 14.5** 3D transient view of laser scanning during a laser AM process of 5 layers for  $P = 200 \text{ W}$  and  $v = 150 \text{ mm s}^{-1}$

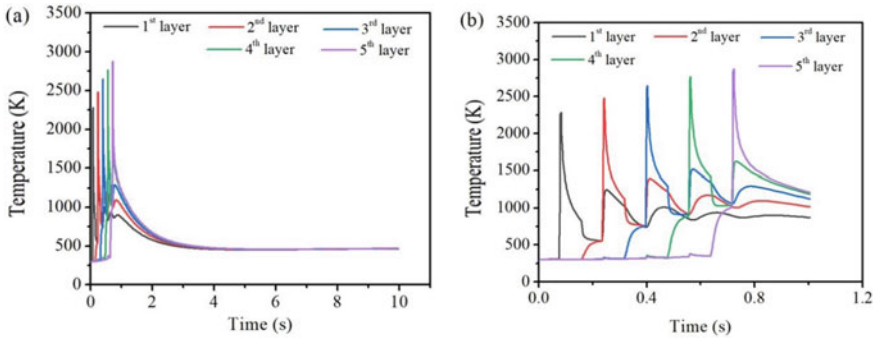
**Fig. 14.6** Cross-sectional view of the evolution of melt-pool of five layers during laser AM when  $P = 200 \text{ W}$  and  $v = 200 \text{ mm s}^{-1}$



The cross-sectional view of the melt-pool at the end of each layer for five layers is shown in Fig. 14.6. Both the width and depth of the melt-pool increase as the number of layers increases. The shape of the melt-pool also changes from a semi-hemispherical to a nearly flat shape as the layer changes from the first layer to fifth layer. As the layer width is only 1 mm, therefore, after deposition of second layer the melt-pool width is determined as 1 mm and is expected to keep increasing even if the layer width is more than 1 mm. The zone in red color represents melted region, while yellow region represents the sintered zone. These two zones represent where the actual manufacturing takes place, while others show the temperature range in different parts of the layers as well as in substrate.

At 200 W laser power and  $200 \text{ mm s}^{-1}$  scanning velocity (Fig. 14.6), the width of the melt-pool increases from  $\sim 0.75 \text{ mm}$  to  $\sim 0.97 \text{ mm}$  for first layer and second layer and then it increases to  $\sim 1 \text{ mm}$  for the third layer, and thereafter, it remains constant with further increase in layers. While the depth of the melt-pool increases, the number of layer increases. The depth of melt-pool is  $\sim 0.33 \text{ mm}$ ,  $\sim 0.39 \text{ mm}$ ,  $\sim 0.49 \text{ mm}$ ,  $\sim 0.53 \text{ mm}$  and  $\sim 0.58 \text{ mm}$  for first, second, third, fourth and fifth layers, respectively. From the fourth layer, the shape of the melt-pool merely changes even though the depth increases at layer width of 1 mm.

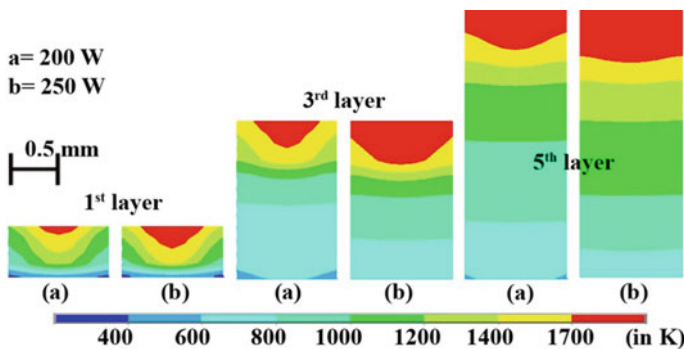
Figure 14.7 represents the time–temperature history of each layer when laser power and scanning velocity is at 200 W and  $200 \text{ mm s}^{-1}$ . The maximum temperature achieved for first, second, third, fourth and fifth layers are 2282 K, 2479 K, 2644 K, 2762 K and 2873 K, respectively. The rapid temperature reduction is due to cooling when the manufacturing process is over. Figure 14.7b shows a magnified view of the time–temperature variation for each layer. It is observed that there are five major temperature peaks for the first layer, four major temperature peaks for the second layer and so on. This is due to the laser power directly applied five times above the point for the first layer, four times for the second layer and so on. The temperature obtained is well beyond the melting point.



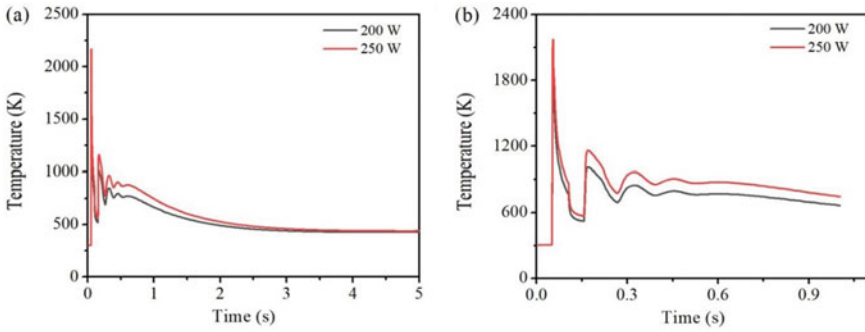
**Fig. 14.7** Time–temperature history **a** when laser power 200 W and scan speed 200 mm s<sup>-1</sup> and **b** zoom view of (a) from 0 to 1.2 s

### 14.4.2 Influence of Laser Beam Power on Melt-Pool and Temperature Distribution

With increasing laser power from 200 to 250 W and at constant scanning velocity of 300 mm s<sup>-1</sup> the temperature, melt-pool width and depth increases. The width of the melt-pool increases from ~0.4 mm for 200 W to ~0.65 mm for 250 W at the end of the first layer. Similarly, from ~0.67 mm for 200 W to ~1 mm for 250 W at the end third layer. However, at the two different laser powers, the melt-pool width is determined as ~1 mm at the end of the fifth layer. The depth of the melt-pool varies from ~0.088 mm for 200 W to ~0.22 mm for 250 W at the end of the first layer, ~0.27 mm for 200 W to ~0.44 mm for 250 W at the end third layer and ~0.41 mm for 200 W to ~0.52 mm for 250 W at the end of fifth layer as shown in Fig. 14.8. Figure 14.9 depicts the maximum temperature attained at the center of the first layer



**Fig. 14.8** Evolution of melt-pool geometry when laser power varies from 200 to 250 W keeping the scanning velocity at 300 mm s<sup>-1</sup>

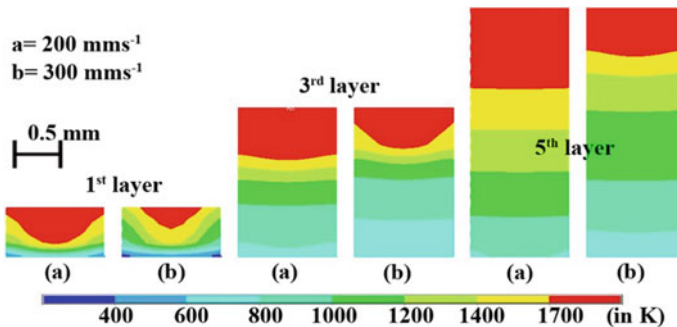


**Fig. 14.9** Time–temperature history at the center of first layer when **a** laser power is 200 and 250 W, and scan speed is  $300 \text{ mm s}^{-1}$  and **b** zoom view of (a) from 0 to 1.2 s

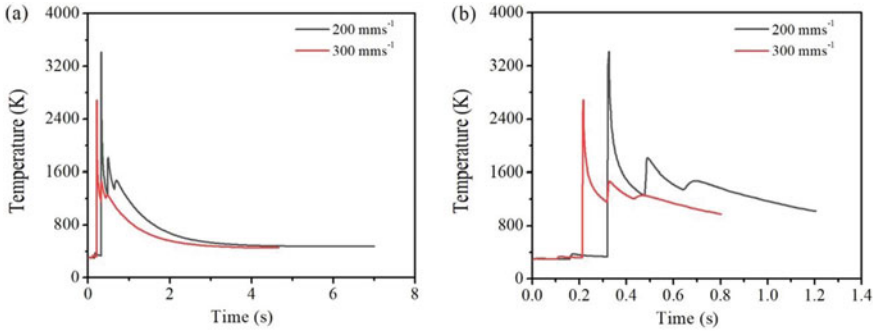
which is 1833 K for 200 W and 2171 K for 250 W at constant scanning velocity of  $300 \text{ mm s}^{-1}$ . This reflects that the temperatures increase with increasing laser power.

### 14.4.3 Influence of Scanning Velocity on Melt-Pool and Temperature Distribution

When the scanning velocity increases at constant laser power, the melt-pool depth and width decrease. It is due to the decreasing temperature as the laser power moves faster. Figure 14.10 represents the evolution of melt-pool shape for first, third and fifth layers for a scanning velocity of 200 and  $300 \text{ mm s}^{-1}$  a constant laser power of 250 W. The melt-pool width for the third layer is more than 1 mm for both the scanning velocities. The melt-pool depth decreases from  $\sim 0.55 \text{ mm}$  for  $200 \text{ mm s}^{-1}$  to  $\sim 0.42 \text{ mm}$  for  $300 \text{ mm s}^{-1}$  in the third layer. Figure 14.11 shows the decreasing



**Fig. 14.10** Evolution of melt-pool for first, third and fifth layers when scanning velocity varies from 200 to  $300 \text{ mm s}^{-1}$  keeping laser power at 250 W



**Fig. 14.11** Temperature variation of the third layer when **a** laser power is 250 W and scanning speed 200 and 300 mm s<sup>-1</sup> and **b** zoomed view of (a) from 0 to 1.2 s

temperature when scanning velocity increases at the start of the third layer. For the third layer, temperature decreases from 3418 K to 2689 K as laser scanning velocity increases from 200 to 300 mm s<sup>-1</sup> as shown in Fig. 14.11.

## 14.5 Conclusions

The fundamental concepts of additive manufacturing technologies along with different classifications and significant process parameters are described in the present chapter. Also, in order to understand quantitatively the influence of laser power and scan speed with respect to time–temperature history and melt-pool development, a FE-based three-dimensional heat transfer process model developed during a five-layer laser-based additive manufacturing. It is observed that the temperature of subsequent layers increases with increasing layer numbers. In the first layer, the substrate played an important part in conducting the heat away from the layers. The results also showed that for low power or high speed, there is no significant effect on the first layer when the laser passes on the fifth layer. For low laser power, incomplete melting of powder materials takes place. However, if the power is high and scanning velocity is low, the layers are properly melted and sintered. It is also found that the dimensions of the melt-pool and temperature enhance with increasing laser power and constant scanning velocity. However, the melt-pool dimensions and temperature decrease when the scanning velocity increases keeping the laser power at constant.

The present proposed model can predict the temperature distribution and evolution of melt-pool under different process parameters for a high layer thickness. It is very helpful in controlling the process parameters. A more realistic model is developed for a multi-layer, multi-track AM process.

**Acknowledgements** This work was supported by TEQIP II grant at the North Eastern Regional Institute of Science and Technology, Itanagar, Arunachal Pradesh, India.

## References

1. International Organization for Standardization (2015) Standard terminology for additive manufacturing—general principles—Part 1: Terminology (52900:2015 (E))
2. Huang SH, Liu P, Mokasdar A, Hou L (2013) Additive manufacturing and its societal impact: a literature review. *Int J Adv Manuf Technol* 67:1191–1203
3. Campanelli SL, Contuzzi N, Angelastro A, Ludovico AD (2010) Capabilities and performances of the selective laser melting process. In: Er MJ (ed) *New trends in technologies: devices, computer, communication and industrial systems*. InTech
4. Mercelis P, Kruth JP (2006) Residual stresses in selective laser sintering and selective laser melting. *Rapid Prototyp J* 12(5):254–265
5. Lawrence J, Alimardani M, Paul CP, Toyserkani E, Khajepour A (2018) Multiphysics modeling of laser solid freeform fabrication techniques. *Advances in laser materials processing*, 2nd edn., pp 665–691 (chapter 22)
6. Kumar S, Sharma V, Singh AK, Chattopadhyaya CS, Hloch S (2013) Determination of layer thickness in direct metal deposition using dimensional analysis. *Int J Adv Manuf Technol* 67:2681–2687
7. Su X, Yang Y, Xiao D, Chen Y (2013) Process ability investigation of non-assembly mechanisms for powder bed fusion process. *Int J Adv Manuf Technol* 64:1193–1200
8. Ocylok S, Alexeev E, Mann S, Weisheit A, Wissenbach K, Kelbassa I (2014) Correlations of melt pool geometry and process parameters during laser metal deposition by coaxial process monitoring. *Phys Procedia* 56:228–238
9. Heralić A, Christiansson AK, Lennartson B (2012) Height control of laser metal-wire deposition based on iterative learning control and 3D scanning. *Opt Lasers Eng* 50:1230–1241
10. Melchels FPW, Feijen J, Grijpma DW, Lopes JA, MacDonald E, Wicker RB (2012) Integrating stereolithography and direct print technologies for 3D structural electronics fabrication. *Rapid Prototyp J* 18:129–143
11. Kumar S, Choudhary AK, Singh AK, Gupta AK (2016) A comparison of additive manufacturing technologies. *Int J Innov Res Sci Technol* 3:147–152
12. Standard Specification for Additive Manufacturing File Format (AMF) Version 1.21, ISO/ASTM 52915:2016(E)
13. Kulkarni P, Dutta D (1996) An accurate slicing procedure for layered manufacturing. *Comput Aided Des* 28:683–697
14. Ahn DD, Kim H, Lee S (2009) Surface roughness prediction using measured data and interpolation in layered manufacturing. *J Mater Process Technol* 209:664–671
15. Chiu YY, Liao YS (2001) A new slicing procedure for rapid prototyping systems. *Int J Adv Manuf Technol* 18:579–585
16. Chen B, Mazumder J (2017) Role of process parameters during additive manufacturing by direct metal deposition of Inconel 718. *Rapid Prototyp J* 23:919–929
17. Cheng B, Chou K (2015) Melt pool evolution study in selective laser melting. In: 26th annual international solid freeform fabrication symposium—an additive manufacturing conference, Austin, TX, USA
18. Kerbrat O, Mognol P, Hascoe J (2011) A new DFM approach to combine machining and additive manufacturing. *Comput Ind* 62:684–692
19. Huang Y, Khamesee MB, Toyserkani E (2016) A comprehensive analytical model for laser powder-fed additive manufacturing. *Addit Manuf* 12:90–99
20. Antony K, Arivazhagan N, Senthilkumaran K (2014) Numerical and experimental investigations on laser melting of stainless steel 316L metal powders. *J Manuf* 16:345–355
21. Gan Z, Yu G, He X, Li S (2017) Surface-active element transport and its effect on liquid metal flow in laser-assisted additive manufacturing. *Int Commun Heat Mass Transfer* 86:206–214
22. Mukherjee T, Zhang W, DebRoy T (2017) An improved prediction of residual stresses and distortion in additive manufacturing. *Comput Mater Sci* 126:360–372
23. Mukherjee T, Manvatkar V, De A, Roy TD (2017) Mitigation of thermal distortion during additive manufacturing. *Scripta Mater* 127:79–83

24. Bauereiss A, Scharowsky T, Körner C (2014) Defect generation and propagation mechanism during additive manufacturing by selective beam melting. *J Mater Process Technol* 214:2522–2528
25. Whiteside E (1989) The effect of stem fit on bone hypertrophy and pain relief in cement less total hip arthroplasty. *Clin Orthop* 247:138–147
26. Hazlehurst K, Wang CJ, Stanford M (2013) Evaluation of the stiffness characteristics of square pore CoCrMo cellular structures manufactured using laser melting technology for potential orthopedic applications. *Mater Des* 51:949–955
27. Compton BG, Post BK, Duty CE, Love L, Kunc V (2017) Thermal analysis of additive manufacturing of large-scale thermoplastic polymer composites. *Addit Manuf* 17:77–86
28. Emamian A, Corbin SF, Khajepour A (2010) Effect of laser cladding process parameters on clad quality and in situ formed microstructure of Fe–TiC composite coatings. *Surf Coat Technol* 7:2007–2015
29. Emamian A, Corbin SF, Khajepour A (2012) The effect of powder composition on the morphology of in situ TiC composite coating deposited by laser-assisted powder deposition (LAPD). *Appl Surf Sci* 261:201–208
30. Emamian A, Alimardani M, Khajepour A (2012) Correlation between temperature distribution and in situ formed microstructure of Fe–TiC deposited on carbon steel using laser cladding. *J Applied surface science* 258:9025–9031
31. Ferrar B, Mullen L, Jones E, Stamp R, Sutcliffe CJ (2012) Gas flow effects on selective laser melting (SLM) manufacturing performance. *J Mater Process Technol* 212:355–364
32. Emamian A, Alimardani M, Khajepour A (2014) Effect of cooling rate and laser process parameters on additive manufactured Fe–Ti–C metal matrix composites microstructure and carbide morphology. *J Manuf Process* 16:511–517
33. Emamian A, Corbin SF, Khajepour A (2011) The influence of combined laser parameters on in situ formed TiC morphology during laser cladding. *Surf Coat Technol* 206:124–131
34. Nie P, Ojo OA, Li Z (2014) Numerical modeling of microstructure evolution during laser additive manufacturing of a nickel-based superalloy. *Acta Mater* 77:85–95
35. Manikandan SGK, Sivakumar D, Rao KP, Kamaraj M (2014) Effect of weld cooling rate on Laves phase formation in Inconel 718 fusion zone. *Mater Prod Technol* 214:358–364
36. Ram GDJ, Reddy AV, Rao KP, Reddy GM (2004) Control of Laves phase in Inconel 718 GTA welds with current pulsing. *Sci Technol Weld Join* 9:390–398
37. Radhakrishna Ch, Rao KP (1997) The formation and control of Laves phase in superalloy 718 welds. *J Mater Sci* 32:1977–1984
38. Bonifaz EA, Richard NL (2009) Modeling cast IN-738 superalloy gas Tungsten arc welds. *Acta Mater* 57:1785–1794
39. Gao Z, Ojo OA (2012) Modeling analysis of hybrid laser-arc welding of single-crystal nickel-base superalloys. *Acta Mater* 60:3153–3167
40. Zhang J, Liou FW, Seufzer W, Newkirk JW, Fan Z, Liu H, Sparks TE (2013) Probabilistic simulation of solidification microstructure evolution during laser-based metal deposition. In: *Proceedings of 2013 annual international solid freeform fabrication symposium—an additive manufacturing conference*, Austin, pp 739–748
41. Zinoviev A, Zinovieva O, Ploshikhin V, Romanova V, Balokhonov R (2016) Evolution of grain structure during laser additive manufacturing. Simulation by a cellular automata method. *Mater Des* 106:321–329
42. Rappaz M, Gandin CA (1993) Probabilistic modelling of microstructure formation in solidification processes. *Acta Metall Mater* 41:345–360
43. Hai Z, Yingping Q, Guilan W, Qiguang Z (2006) The characteristics of arc beam shaping in hybrid plasma and laser deposition manufacturing. *Sci China Ser E: Technol Sci* 49:238–247
44. Liu JH, Shi YS, Chen KH, Huang SH (2007) Research on manufacturing Cu matrix Fe–Cu–Ni–C alloy composite parts by indirect selective laser sintering. *Int J Adv Manuf Technol* 33:693–697
45. Gangxian Z, Dichen L, Anfeng Z, Yiping T (2010) Numerical simulation of powder flow field on coaxial powder nozzle in laser metal direct manufacturing. *Int J Adv Manuf Technol* 49:853–859

46. Zhang DQ, Cai QZ, Liu JH, Zhang L, Li RD (2010) Select laser melting of W-Ni-Fe powders: simulation and experimental study. *Int J Adv Manuf Technol* 51:649–658
47. Tolosa I, Garciandí F, Zubiri F, Zapirai F, Esnaola A (2010) Study of mechanical properties of AISI 316 stainless steel processed by “selective laser melting”, following different manufacturing strategies. *Int J Adv Manuf Technol* 51:639–647
48. Gibson LJ, Ashby MF (1997) *Cellular solids*, 2nd edn. Cambridge University Press, Cambridge, UK
49. Evans AG, Hutchinson JW, Ashby MF (1998) Cellular metals. *Curr Opin Solid State Mater Sci* 3:288–303
50. Williams CB, Cochra KJ, Rosen WD (2011) Additive manufacturing of metallic cellular materials via three-dimensional printing. *Int J Adv Manuf Technol* 53:231–239
51. Hattiangadi A, Bandyopadhyay A (1999) Processing, characterization and modeling of non-random porous ceramic structures. In: *Solid freeform fabrication symposium*, pp 319–326
52. Chiras S, Mumm DR, Evans AG, Wicks N, Hutchinson JW, Dharmasena K, Wadley HNG, Fichter S (2002) The structural performance of near-optimized truss core panels. *Int J Solids Struct* 39:4093–4115
53. Robinson CJ, Zhang C, Ram GDJ, Siggard EJ, Stucker B, Li L (2007) Maximum height to width ratio of freestanding structures built using ultrasonic consolidation. In: *Solid freeform fabrication symposium*, pp 502–516
54. Bose S, Robertson SF, Bandyopadhyay A (2018) A surface modification of biomaterials and biomedical devices using additive manufacturing. *Acta Biomater* 66:6–22
55. Bandyopadhyay A, Bose S (2015) *Additive manufacturing*. CRC Press, Boca Raton
56. Bose S, Ke D, Sahasrabudhe H, Bandyopadhyay A (2018) *Additive manufacturing of biomaterials*. *Prog Mater Sci* 93:45–111
57. Puleo DA, Nanci A (1999) Understanding and controlling the bone-implant interface. *Biomaterials* 20:2311–2321
58. Poomathi N, Singh S, Prakash Ch, Patil RV, Perumal PT, Barathi VA, Balasubramanian KK, Ramakrishna S, Maheshwari NU (2019) Bioprinting in ophthalmology: current advances and future pathways. *Rapid Prototyp J* 25:496–514
59. Aksakal B, Yildirim ÖS, Gul H (2004) Metallurgical failure analysis of various implant materials used in orthopedic applications. *J Fail Anal Prev* 4:17–23
60. Bose S, Bandyopadhyay A (2016) *Materials and devices for bone disorders*. Elsevier, Amsterdam. ISBN: 978-0-12-802792-9
61. Bose S, Sugiura S, Bandyopadhyay A (1999) Processing of controlled porosity ceramic structures via fused deposition process. *Scripta Mater* 41:1009–1014
62. Darsell J, Bose S, Hosick H, Bandyopadhyay A (2003) From CT scans to ceramic bone grafts. *J Am Ceram Soc* 86:1076–1080
63. Stallard CP, Solar P, Biederman H, Dowling DP (2015) Deposition of non-fouling PEO-like coatings using a low temperature atmospheric pressure plasma jet. *Plasma Process Polym* 13:241–252
64. Gloria A, Causa F, Russo T, Battista E, Della Moglie R, Zeppetelli S, De Santis R, Netti PA, Ambrosio L (2012) Three-dimensional poly( $\epsilon$ -caprolactone) bioactive scaffolds with controlled structural and surface properties. *Biomacromolecules* 13:3510–3521
65. Puppi D, Chiellini F, Piras AM, Chiellini E (2010) Polymeric materials for bone and cartilage repair. *Prog Polym* 35:403–440
66. Chiono V, Mozetic P, Boffito M, Sartori S, Giuffredì E (2014) Polyurethane-based scaffolds for myocardial tissue engineering. *Interface Focus* 4:20130045
67. Kurtz SM, Devine JN (2017) PEEK biomaterials in trauma, orthopaedic, and spinal implants. *Biomaterials* 28:4845–4869
68. Tan KH, Chua CK, Leong KF (2003) Scaffold development using selective laser sintering of polyetheretherketone-hydroxyapatite biocomposite blends. *Biomaterials* 24:3115–3123
69. Riemer A, Leuders S, Thöne M, Richard HA, Tröster T, Niendorf T (2014) On the fatigue crack growth behavior in 316L stainless steel manufactured by selective laser melting. *Eng Fract Mech* 12:15–25



70. Singh S, Prakash Ch, Ramakrishna S (2019) 3D printing of polyether-ether-ketone for biomedical applications. *Eur Polym J* 114:234–248
71. Singh H, Singh S, Prakash C (2019) Current trends in biomaterials and bio-manufacturing. In: *Biomufacturing*. Springer, Singapore, pp 1–34
72. Wycisk E, Solbach A, Siddique S, Herzog D, Walther F, Emmelmann C (2014) Effects of defects in laser additive manufactured Ti-6Al-4V on fatigue properties. *Phys Procedia* 56:371–378
73. Tumbleston JR et al (2015) Continuous liquid interface production of 3D objects. *Science* 347:1349–1352
74. Singh S, Singh N, Gupta M, Prakash Ch, Singh R (2019) Mechanical feasibility of ABS/HIPS based multi-material structures primed by low-cost polymer printer. *Rapid Prototyp J* 25:152–161
75. Singh S, Singh M, Prakash C, Gupta MK, Mia M, Singh R (2019) Optimization and reliability analysis to improve surface quality and mechanical characteristics of heat-treated fused filament fabricated parts. *Int J Adv Manuf Technol* 102:1–16
76. Boley JW, White EL, Chiu GT-C, Kramer RK (2014) Stretchable electronics, direct writing of gallium-indium alloy for stretchable electronics. *Adv Funct Mater* 24:3474
77. Materials science (2013) Liquid metal printed in 3D. *Nature* 499:256–257
78. Visser CW, Pohl R, Sun C, Römer G-W, Huis in't Veld B, Lohse D (2015) 3D printing: toward 3D printing of pure metals by laser-induced forward transfer. *Adv Mater* 27:4103–4103
79. Vinson BT, Sklare SC, Chrisey DB (2017) Laser-based cell printing techniques for additive biomufacturing. *Curr Opin Biomed Eng* 2:14–21
80. Sweat RS, Stapor PC, Murfee WL (2012) Relationships between lymphangiogenesis and angiogenesis during inflammation in rat mesentery microvascular networks. *Lymphatic Res Biol* 10:198–207
81. Sweat RS, Sloas DC, Murfee WL (2014) VEGF-C induces lymphangiogenesis and angiogenesis in the rat mesentery culture model. *Microcirculation* 21:532–540
82. Stapor PC, Azimi MS, Ahsan T, Murfee WL (2013) An angiogenesis model for investigating multicellular interactions across intact microvascular networks. *Am J Physiol Heart Circ Physiol* 304:235–245
83. Yadaiah N, Bag S (2014) Development of egg-configuration heat source model in numerical simulation of autogenous fusion welding process. *Int J Therm Sci* 86:125–138
84. Hua T, Jing C, Xin L, Fengying Z, Weidong H (2008) Research on molten pool temperature in the process of laser rapid forming. *J Mater Process Technol* 198:454–462
85. Griffith ML, Keicher DM, Atwood CL, Romero JA, Smugeresky JE, Harwell LD (1995) Free form fabrication of metallic components using laser engineered net shaping (LENSTM). In: *Proceeding of 7th solid freeform fabrication symposium*, pp 125–132
86. Wen S, Shin YC (2010) Modeling of transport phenomena during the coaxial laser direct deposition process. *J Appl Phys* 108
87. Griffith ML, Ensz MT, Puskar JD, Robino CV, Brooks JA, Philliber JA, Smugeresky JE, Hofmeister WH (2000) Understanding the microstructure and properties of components fabricated by laser engineered net shaping (LENS). *MRS proceedings*, vol 625. Cambridge University Press
88. Kelly SM, Kampe SL (2004) Microstructural evolution in laser-deposited multilayer Ti-6Al-4V builds: Part II. Thermal modeling. *Metall Mater Trans A* 35:1869–1879
89. Baufeld B, Van Der Biest O, Gault R, Ridgway K (2011) Manufacturing Ti-6Al-4V components by shaped metal deposition: microstructure and mechanical properties. *IOP Conf Ser: Mater Sci Eng* 26:012001
90. Bontha S, Klingbeil NW, Kobryn PA, Fraser HL (2006) Thermal process maps for predicting solidification microstructure in laser fabrication of thin-wall structures. *J Mater Process Technol* 178:135–142
91. Zhang D, Zhang P, Liu Z, Feng Z, Wang C, Guo Y (2018) Thermofluid field of molten pool and its effects during selective laser melting (SLM) of Inconel 718 alloy. *Addit Manuf* 21:567–578

92. Singh SN, Chowdhury S, Khan Md SM, Manapuram M, Nirsanametla Y (2019) FE based heat transfer analysis of laser additive manufacturing on Ti-6Al-4V alloy. In: 2nd international conference on computational methods in manufacturing (ICCM 2019), IIT Guwahati, Guwahati, India, 8–9 Mar 2019. Paper ID: 025
93. Mills KC (2006) Recommended values of thermophysical properties for selected commercial alloys. Woodhead Publishing Ltd, Cambridge. ISBN 978-1855735699

**Mr. Sapam Ningthemba Singh** is a Ph.D. research scholar at the Department of Mechanical Engineering, National Institute of Technology Silchar, Assam, India. He completed his M.Tech and B.Tech from NERIST. His research interest includes additive manufacturing, additive manufacturing in biomedical applications, finite element method. He is currently working on the performance enhancement of polymer materials to enhance biocompatibility using 3D printing.

**Dr. Nirsanametla Yadaiah** is Assistant Professor in the Department of Mechanical Engineering, North Eastern Regional Institute of Science and Technology (NERIST), Nirjuli, Arunachal Pradesh, India. He has received Ph.D. in Mechanical Engineering from Indian Institute of Technology Guwahati, India. His area of research is Computational Welding Mechanics, Additive Manufacturing, Laser Based Manufacturing Processes and macro-/micro-scale fusion welding processes. He has authored more than 10 journal papers, 1 book, 3 book chapters and many international conferences.

**Ms. Sohini Chowdhury** is a Ph.D. research scholar at the Department of Mechanical Engineering, North Eastern Regional Institute of Science and Technology (NERIST). Her research area include laser based manufacturing processes, additive manufacturing and computational welding mechanics.

**Dr. Manapuram Muralidhar** is a Professor at the Department of Mechanical Engineering, North Eastern Regional Institute of Science and Technology. He received his Ph.D. from Indian Institute of Technology Kharagpur in 2007. He has more than 28 years of teaching experience and 8 years of experience as Deputy/Assistant/Junior Manager at Vizag Steel Plant, Visakhapatnam, Andhra Pradesh, India. His research area is focused on additive manufacturing, Intelligent Manufacturing, Foundry, Forming, Welding, and Production Management. He has conducted many sponsored projects from the funding agencies such as DST, MHRD, MoMSME. He is a member of the professional bodies such as LISTE, LISME, LIW, SMIRE, MAMM, MIMA, MIIF. He was conferred the prestigious award of Rajiv Gandhi Excellence Award by the India International Friendship Society in 2010 for his contribution and achievements. He has guided many Ph.D. students as well as Masters and Graduate students.

# Chapter 15

## Novel and Emerging Materials Used in 3D Printing for Oral Health Care



Anoop Kapoor, Priyanka Chopra, Komal Sehgal, Shaveta Sood, Ashish Jain, and Vishakha Grover

### Abbreviations Used

### Nomenclatures

3DP            3D printing  
AM            Additive manufacturing

---

A. Kapoor

Professor and Head, Sri Sukhmani Dental College and Hospital, Dera Bassi, Punjab, India

e-mail: [dranoop\\_kapoor@rediiff.com](mailto:dranoop_kapoor@rediiff.com)

P. Chopra

Professor, Sri SGT Dental College and Hospital, SGT University, Gurugram, India

e-mail: [drpriyankachopra79@gmail.com](mailto:drpriyankachopra79@gmail.com)

K. Sehgal

Associate Professor, Department of Prosthodontics, Dr. H.S.J. Institute of Dental Sciences, Panjab University, Chandigarh, India

e-mail: [drkomal\\_sehgal@yahoo.co.in](mailto:drkomal_sehgal@yahoo.co.in)

S. Sood

Assistant Professor, Department of Periodontology and Oral Implantology, Dr. H.S.J. Institute of Dental Sciences, Panjab University, Chandigarh, India

e-mail: [drshvetasood@yahoo.com](mailto:drshvetasood@yahoo.com)

A. Jain

Professor and Head, Department of Periodontology and Oral Implantology, Dr. H.S.J. Institute of Dental Sciences, Panjab University, Chandigarh, India

e-mail: [ashish@justice.com](mailto:ashish@justice.com)

V. Grover (✉)

Associate Professor, Department of Periodontology and Oral Implantology, Dr. H.S.J. Institute of Dental Sciences, Panjab University, Chandigarh, India

e-mail: [vishakha\\_grover@rediffmail.com](mailto:vishakha_grover@rediffmail.com)

© Springer Nature Singapore Pte Ltd. 2020

S. Singh et al. (eds.), *3D Printing in Biomedical Engineering*,

Materials Horizons: From Nature to Nanomaterials,

[https://doi.org/10.1007/978-981-15-5424-7\\_15](https://doi.org/10.1007/978-981-15-5424-7_15)

FGM	Functionally graded materials
FDM	Fused deposition modeling
SL	Stereolithography
SLS	Selective laser sintering
PLA	Polylactic acid
PLGA	Polylactic glycolic acid
ABS	Acrylonitrile Butadiene Styrene
HIPS	High-Impact Polystyrene
TPU	Thermoplastic Polyurethane
PET	Polyethylene Terephthalate
PC	Polycarbonate
SFF	Solid Freeform Fabrication
DNA	Deoxyribonucleic acid
PVC	Polyvinyl chloride
HA	Hydroxyapatite
TCP	Tricalcium phosphate
PPF	Polypropylene fumarate
PCL	Polycaprolactone
PEG-DMA	Polyethylene glycol methacrylate
PEG-DA	Polyethylene glycol diacrylate
PEP-DEF	Poly(propylene fumarate) with diethyl fumarate
PVA	Polyvinyl alcohol
PHBV	Poly(3-hydroxybutyric acid-co-3-hydroxy valeric acid)
CHAp	Carbonated hydroxyapatite
BSA	bovine serum albumin
PEEK	Polyether ether ketone
SLM	Selective laser melting
EBM	Electron beam melting
SMA	Shape memory alloys
SMP	Shape memory polymers
NiTi	Nickel-titanium

## 15.1 3D Printing: The Technique and Oral Health

3D printing or additive manufacturing is the most recent revolution witnessed in the field of health care. The technology is basically distinct from the conventional processes of manufacturing, in a way that a desired product (3D structure) can be designed and shaped using a digital model and is formed by ‘layer-by-layer’ deposition of material, which is digitally controlled and operated. 3D printing is also known as additive manufacturing (AM), rapid prototyping, layered manufacturing or solid freeform fabrication [1]. The four most integral components of the process are:

- A digital model of the object,
- Material/s manageable in the minimal forms,
- A deposition system of fabrication materials,
- A digital control system for layer-by-layer apposition.

Medical applications of additive manufacturing include preoperative models, educational anatomic models, splints, templates, external fixators for orthopedics, medical instruments, and biomaterial printing [2, 3]. The upbeat of additive manufacturing technology in this sector largely leans on its ability to create orthotics, prosthetics, and personalized implants, thus limiting much of disability associated with missing body parts. This is all the more relevant for the field of dentistry or oral health care as the essence of dentistry has been talked of as an art and science focused on recreating the morphology, anatomy, and function as close possible to the lost parts of teeth, alveolar bone, and other oral structures. It has largely changed the face of dentistry with its salient features digitization, customization, precision, and time and cost-effectiveness [4].

Certain salient potential advantages [5, 6] of additive manufacturing, which make it a next-gen technologic breakthrough for dentistry, are:

1. The direct conversion of design to product.
2. Greater precision and customization with no additional tooling,
3. Functional designing of intricate biologic tissues,
4. Flexible (hollow or lattice structures) for intraoral use,
5. Minimal material wastage,
6. Less manufacturing time,
7. Cost-effectiveness,
8. Feasibility of chairside construction as well as excellent scalability.

The technique provides an immense opportunity for translation into useful health care products, particularly, dentistry. Commercial success will also depend on adherence and meeting up of some accepted predefined standards regarding properties of existing materials for the similar clinical situations [7] with a cost-effective production process [1].

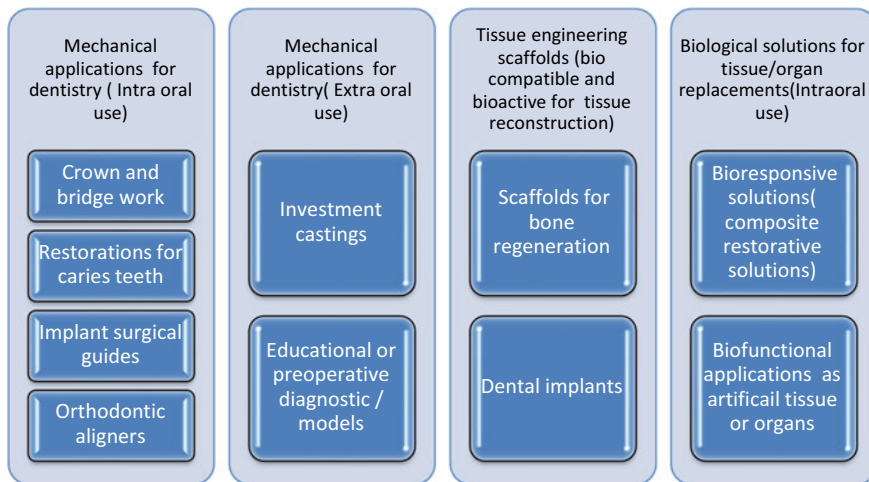
## **15.2 Applications of 3D Printing in Oral Health Care: Material Perspectives**

Dental therapeutic procedures help the patients to achieve optimal health, function, aesthetics, and comfort by restoring the natural oral anatomy and morphology of oral tissues lost/damaged by disease [8]. With the continuous advancements in knowledge and technology, 3D printed appliances have found a broad range of applications in oral health care. Mechanical solutions were the earliest usage in the dental field as many 3D printed inlay/onlay restorations, educational models; surgical templates made up of thermoplastic materials came into being. Thermoplastic materials could

be worked with most of the first generation AM processes, viz. stereolithography. Largely polymer materials were used for these kinds of applications owing to their convenient working parameters and reasonable mechanical and chemical properties. Few high strength, bioinert/biocompatible metals, e.g., titanium and titanium alloys, cobalt-chromium, aluminum alloys, etc., also have been utilized for applications like dental implants, crown and bridge, and dentures prosthesis frameworks. Ceramics is the third category of materials, which have been utilized for some limited applications in oral health care. Keeping the application range in view, even the use of multiple materials in one product, to enhance the clinical performance was attempted and composite materials were developed for 3D printing. With the continuous upsurge in material sciences, some of the materials in combination with the printing technique were harnessed for imparting some biologic functionality in terms of ability to harbor and sustain living/vital cells, nerves and blood vessels, etc., or allow their growth via providing specific microstructure in the printed part. These upgrades led to the use of 3D printed components in tissue engineering by acting as biologic tissue scaffolds. To optimize the biologic applications, it was important to understand the functionality of vital living tissues, for which these customized parts were going to be the replacements. This directed toward the second generation of composites, i.e., functionally graded materials (FGM), which could simulate the functional biologic structural form of the lost/damaged body part by a much gradual and homogenous shift in the properties of combined materials used in a product. Most recently, technologic advances have made it possible to utilize biologic components and inserts, biomimicking scaffold materials to be printed as composite (bioprinting) via integrated printing approaches with newer versions of printing devices.

The field of biomaterial and biomanufacturing is expanding vastly with exponential research in this arena to bring the best usage to the end user, i.e., patient. Rapid advances in the material sciences are trying to keep pace with the novel technologies and equipment used for 3D printing, thus making the novel and diverse applications feasible. How well the 3D printed 'object' serves its intended use in the oral cavity determines its eventual usefulness for clinical application. The durability and functional integration to adjacent oral tissues is vital for the longevity of oral and overall health. Materials used for 3D printing work in integration with the AM process and the focused application. All three factors are significant and complement, coordinate each other to develop a value application. Broadly speaking, there are three major contemporary domains of applications of 3D printing in oral health care from the standpoint of materials (Fig. 15.1). Accordingly, the paper shall provide an update of relevant materials used in 3D printing under three sections:

1. Contemporary materials used for 3D printing,
2. Material updates from tissue engineering perspectives,
3. Emerging materials for novel applications.



**Fig. 15.1** Major domains of 3D printed applications in oral health care from a materials perspective standpoint

### 15.2.1 Contemporary Materials Used in 3D Printing for Oral Health Care

Different AM processes allow for a large range of raw materials to be used for fabrication of structures, due to a diversity of methods used. The majority of the raw materials used for dental and medical purposes may be grouped into binder/powder material combinations include polymers (including resins and thermoplastics), ceramics, and metals. Among these materials, polymers have been most extensively utilized for 3D printing [9–11]. However, different types of materials including metals [12–15], ceramics [16–19], and nowadays, different combinations of these as composites, hybrid, or functionally graded materials (FGM) are being successfully utilized in 3D shapes and structures using AM. A very brief update of the most basic aspects of very commonly used contemporary materials has been provided in this section.

#### 15.2.1.1 Polymers

Mostly, thermoplastic polymers have been utilized within versatile industrial applications. Having a low coefficient of thermal expansion and low glass transition temperature and melting point, the material becomes workable for the intended use. However, strong secondary bonding is necessary for obtaining good final strength as 3D printing procedure is by layer to layer addition. In dental applications also, these materials have been widely used particularly for making models and templates, etc.

### Polylactic Acid (PLA)

Polylactic acid, a biodegradable polymer is most commonly used polymer as an FDM material. Some variants may have opted for intraoral use as the degradation products, e.g., lactic acid can be metabolized by the body. Another advantage of the material is that it needs no ventilation system during the manufacturing process, as no dissemination of any toxic gases or vapors is accompanying. However, PLA has low impact strength and temperature stability, limiting its use as a structural material. The melting temperature of PLA is around 175 °C, but it is workable for flow at a little higher temperature, i.e., 215 °C. The crystalline structure of the material and the presence of methyl (CH<sub>3</sub>) group make it strong, yet a brittle material.

### Acrylonitrile Butadiene Styrene (ABS) Plastic

Acrylonitrile butadiene styrene is another common 3D printing filament material, which is used in dentistry. The material is available in different grades as a different proportion of the three monomers are used for making the final polymer. Though all are known as ABS materials, it provides an abundant variety for customization of the applicability in diverse clinical situations owing to different polymerization processes, chain lengths in structure and crystallization. Issues of toxic gas production during processing need a well-ventilated place for the safe use of this material. The material is amenable to produce smooth surfaces, which have popularized it immensely. The surface disinfection of ABS plastic is done with organic solvents as material properties are not affected by the same. Acetone is a preferred choice for disinfection of ABS plastics. The major disadvantage associated with ABS is its high glass transition temperature, which is responsible for dimensional instability and limits its application. The three components polystyrene, butadiene, acrylonitriles impart a specific set of properties as an amorphous and stiff structure, toughness, and resistance to environmental degradation, respectively.

High-impact polystyrene (HIPS) is composed of styrene and butadiene monomers and does not have a nitrile group similar to ABS. This distinct composition provides better impact resistance. The material can be dissolved in the differential solvents, then the solvents used for routinely used materials, e.g., ABS, and allow its use as a support material for other printing processes.

HIPS can be usually dissolved in terpene chemicals liked-limonene and even in some biodegradable solvent combinations, e.g., acetone. Most of the properties profile is similar to ABS, as they largely share a similar composition.

### Thermoplastic Polyurethane (TPU) Elastomer

Thermoplastic polyurethane is a flexible material, composite of long nonpolar regions and short polar regions. Differential polarity provides a combination of flexibility and a composed set structure. This co-polymeric molecular arrangement simulates a



spring, which is responsible for an elastomeric, rubbery, consistency of the material. The material is applied widely as has a workable melting temperature range (around 230 °C) and shows resistance to abrasion and organic solvents.

### Polyethylene Terephthalate (PET) Plastic

Polyethylene terephthalate is another common, particularly, in fabric and bottle industry. The appearance of the material varies with the cooling conditions, as on rapid cooling, it becomes amorphous and appears transparent. The surface of the printed PET is carefully treated with fumed acetone to enhance smoothness. The material can be dissolved by organic solvents such as acetone and gasoline, etc. A distinct advantage offered by the material is good moisture resistance, which makes the material amenable to easy storage and workability. Temperature range for workability is same, i.e., 230 °C, as for rest of FDM printable materials.

### Nylon

The characteristics of the class are the presence of at least one monomer with carboxylic acid groups at its ends and another with amines at its ends. These are polyamide compounds with an amide group  $-(C=O)-(NH)-$  at the place of monomer units joining in the chain. Owing to the immense variability in the molecular structure, this class of polymers offers an enormous range of properties. High toughness and stiffness, flexibility, resistance to fatigue, heat and wear and strong adhesion between Z-layers are few to mention to make them a material of immense application. Major issues with nylon are high cost, dimensional instability, and easy moisture contamination. Gasoline, acetone, and benzene like solvents do not affect nylon, but it can be degraded with acids. Workable temperature range for the material is higher than the usual thermoplastic materials (240–270 °C) depending on the specific formulation.

Nylons exhibit a high degree of crystallinity owing to the aliphatic backbone and polar amide groups, whereas the amorphous regions have good mobility which provides the material good flexibility, in addition to high strength.

### Polycarbonate (PC)

Polycarbonates which are amenable to 3D printing are largely polymeric forms of bisphenol A. As only one defined repeat unit, i.e., polycarbonate (PC) is basic backbone structure of the compound, and the properties are affected by the differential lengths of chains rather than compositional differences. Salient merits are its high strength and very high Z-layer adhesion, good impact resistance and toughness, immense deformability, high-temperature stability, smooth texture, and optical clarity. A high temperature, viz. 315 °C is needed for extrusion, so specific printer devices are required for polycarbonates. The surface of the material is easily

scratched. It can be solvated by petroleum chemicals like gasoline and kerosene but is resistant to most acids. Exceptionally, acetone embrittles the material. Polycarbonate has a highly amorphous microstructure due to the pendant groups and aromatic rings. These features are also responsible for PC's high strength, optical transparency, and high  $T_g$  and processing temperatures. The material discolors over a period of time from initial transparent appearance to yellowish tinge, due to oxidation of aromatic rings [20].

### 15.2.1.2 Ceramics

Few aluminas reinforced and zirconia-based ceramic materials have been utilized for fabrication of dental prosthesis, especially for crown and bridgework by AM process. Still there exist many issues like anisotropic shrinkage and staircase effect in the final product (owing to layering) for this category of materials pose a concern for their widest scope of application. Most of the current 3D printing methods need an elaborate workflow in terms of pre- and post-processing treatment for ceramics, which limits their expansion from prototype to a final manufacturing stage. FDM and the use of a jetted binder to bind specially coated ceramic powders together need additional sintering procedures after an initial reaction to achieve the full strength of the material [21]. Use of SLS technology to produce ceramics involves either ceramic powder or a pre-sintered ceramic. To date, however, direct SLS of ceramic powder has only yielded porous structures difficult to post-process to high density, so it has been mainly used to produce modified glass-ceramics for the fabrication of bioactive tissue scaffolds [22] (discussed in detail in the next section). With recent innovations, many composite materials are becoming more and more workable. However, powder-bed inkjet 3D printing and vacuum infiltration have been found to produce a dense alumina-reinforced-ceramic structure with high density and satisfactory strength [23, 24]. Crude zirconia prostheses have also been produced using a similar method [21, 25].

### 15.2.1.3 Metals

Titanium, Co-Cr, and nickel alloys have been utilized primarily in the field of dentistry. Nowadays, the use of nickel-containing alloys is almost obsolete in dental prostheses due to the risk of nickel allergy. However, research on titanium structures fabricated using additive techniques has documented a favorable yield strength, ultimate tensile strength, and ductility, albeit with some surface roughness [26]. Titanium is much widely used as this has biocompatible, bioinert properties to be used for intraoral use, especially as implantable devices. Many clinical studies have documented the successful workability of such implants [27, 28]. In fact, intrinsic surface roughness, osseointegration and functional integration of these implants with adjacent living tissues is a salient advantage [29, 30]. Many well-designed studies on the properties of titanium alloy (particularly Ti6Al4V) fabricated using SLS have also

been documented [26]. With novel methods such as DMLS technology, where there is a passive fabrication of the material without energy and minimal material wastage, other precious metals such as Co-Cr have also been workable. This has expanded the range of materials for 3D printing, yet remains an expensive option only [25, 31, 32].

### ***15.2.2 Material Updates from Tissue Engineering Perspectives***

In recent years, tissue engineering has gained a prime place in the regenerative therapeutic choices. Dentistry has also witnessed a similar surge in regenerative approaches based on tissue engineering principles applied to restore the lost bone around teeth as well as for maxillofacial prosthesis. The pivotal functional triad for successful regeneration involves the formative cells, signal molecules, and biologic scaffolds to keep these in place and provide the environment to recapitulate the development of the tissues as happened during the embryonic stage. The structure of the scaffolds is critical to simulate biologic environment for cellular infiltration and proliferation, space creation for the growth of extracellular matrix, biochemical signals to guide the populating cells for healing, and physical networking of different components, including nutrient transport, and cell–matrix interactions [33–35]. Additive manufacturing allows the development of complex 3D printed parts to replace the patient or organ-specific anatomic part (macrostructure), with the microstructure simulating tissue architecture in terms of porosity and spatial orientation compatible for in the growth of new cells and associated vascular and extracellular substances. The selection of biomaterials for such applications is very challenging as each material has different physical and chemical properties, processing methods and FDA approval. Generally speaking, polymers, ceramics, and metals all have been tried, alone as well as in combinations, in tissue engineering. The selection of the fabrication technique depends upon that which material is being worked upon, characteristics of the printing machine and the specific requirements of the final scaffold in terms of physical strength and chemical behavior.

Various SFF techniques were introduced to build objects with controlled macro as well as microstructures for biomedical tissue engineering applications. The freedom in form, coupled with a suitable material choice allows a controlled development of a product adhering to tissue engineering triad by directing the cells, signals, and scaffolding substrates in a desired orientation simultaneously fabrication. These technologies used in conjunction with case-based imaging data enabled the aseptic and customized manufacturing of tissue engineering grafts according to individual clinical situation. Multi-functional scaffolds for tissue engineering meeting the specific requirements can be developed based on best simulating models of the patient's defect [36]. Precision injection molding technique is another innovative addition, which can utilize most of the existing thermoplastic materials without pretreatment to make a customizable patient device as it offers a mold-free printing [37].

In particular, 3DP offers a huge choice of printable material to be worked with and many biological agents such as peptides, proteins, polysaccharides, DNA plasmids, and living cells have been utilized in combination with existing materials. FDM, on the other hand, utilizes materials based on heat transfer and flow behavior. Materials with low melting temperatures such as nylon, ABS, and investment casting wax have been utilized most often. PLGA also have been utilized, but high glass transition (40–60 °C) of the material limits its application via FDM [38, 39]. Combinations of the materials are also utilized in FDM, e.g., poly (ethylene glycol) terephthalate/poly (butylene terephthalate) or polypropylene/TCP [40, 41], PCL/HA or PCL/TCP [42]. Acrylics and epoxies are mostly utilized with stereolithographic techniques, but as during photopolymerization, very few materials retain their dimensional stability. So, the choice of materials is quite limited for tissue engineering. Complex 3D scaffolds have been developed by utilizing photocrosslinkable poly (propylene fumarate) (PPF) and investigated in animal studies [43, 44]. Resins with and without bio-ceramic dispersions have also been processed by SLA for similar applications. SLS mostly utilized PCL and a combination of materials (PEEK + HA) [45–47]. An elaborate technical workflow is needed for biomaterial fabrication, as the coated particles are to sinter together with the elimination of the coating during the process and even post-processing aimed at enhancing the strength of the printed parts is required [48]. Another combination of (PVA) and (HA) was also used for biologic applications [49]. SLS techniques coupled with computational design data utilization have allowed the fabrication of complex tissue engineering matrices with desired micro and macro three-dimensional structural organization. PCL scaffolds for tissue engineering applications were first developed by Williams et al. [50]. Lately, FDA has provided approval for the use of SLS to process medical-grade polyether ether ketone (PEEK) for construction of personalized craniofacial implants. More recently, first patient-specific, implantable titanium mandible that accepts dental implants have been developed with SLM [51]. The key strength of SLS/SLM/EBM technique is the ability to direct translation of implant designs into metallic implants capable of allowing vital bone in growth and regeneration.

3D plotting/direct-write bioprinting is the technique exclusively meant for natural polymers for various biologic applications. Two approaches for fabrication have been commonly utilized, viz. extruding heated natural polymers (agar or gelatin) into a cooler environment (gelatin or silicone oil) so as to solidify quickly [52, 53] or into a liquid medium containing reactants for cross-linking (gelatin into calcium reservoir) for microvasculature build up [54]. TCP, on the other hand, is lyophilized to remove the liquid after extrusion from a syringe [55, 56]. Recent advances in materials utilized with specific AM techniques have been summarized in Table 15.1 for a quick review.

**Table 15.1** Recent material and technology advances in different additive manufacturing processes for tissue engineering applications

3D Printing	Fused deposition modelling	Stereolithography	Selective laser sintering	3d plotting/direct write bioprinting
Calcium polyphosphate &PVA	PVC	PEG-DMA and PEG-DA with fluorescently labeled dextran, fluorescently labeled bioactive PEG or bioactive PEG	PCL & HA	PLGA
HA and TCP	Nylon	PCL (three-armed hydroxyl-terminated) or poly (D,L-lactide)	PCL and $\beta$ -TCP with collagen coating	TCP
TCP, ( $Mg_3(PO_4)_2$ )	ABS	Photo-curable poly (D,L-lactide) (PLA) resin without the use of reactive diluents	Ca-P/PHBV	Collagen & chitosan
TCP with SrO and MgO doping	Investment casting wax	Acrylate or methacrylate	CHAp/PLLA	Chitosan
HA and apatite–Wollastonite		PPF-DEF	PVA	Collagen alginate silica
Glass ceramic with water-based binder	PCL	PPF-DEF with BMP-2 loaded PLGA microspheres	BSA encapsulated in Ca-P/PHBV microparticles	Composites coated with HA
Calcium phosphate with collagen in binder	PLGA	PPF-DEF or PPF-DEF with HA		Soy protein
PLGA	Polypropylene/TCP	Poly(trimethylene Carbonate)		Agarose with gelatin
Farringtonite powder	PCL/HA, PCL/TCP			

Source Adapted from [56]

### 15.2.3 Emerging Materials for Novel Applications

This section summarizes the new materials that can be specifically 3D printed for a defined application. It is an emerging field aimed at optimizing the material for an application by a 3D fabrication process, with retained or enhanced original properties of the material [57]. Though there are diverse novel materials coming up, in context of oral health care, only advanced materials with biologic applicability will

be discussed: (1) Smart materials; (2) Ceramic materials; (3) Electronic materials; (4) Biomaterials; (5) Composite materials.

### 15.2.3.1 Smart Materials

These are defined as those materials, which are able to change their internal geometry under the effect of external stimuli [58–60]. Due to this inherent ability of the material, the 3D fabricated portions can develop in a planned way over a period of time during the intended application [61–63]. A new term called ‘4D printing’ has emerged out of such material usage [63]. ‘Smart’ behavior such as environment sensing, actuating on its own, and shape changing are essential requirements to be termed as a 4D printed product, in addition to being a component of vital tissue [64–66]. They are classified according to the number of materials used for printing. Much research has been carried out regarding enhanced smart nanocomposites [67], shape memory alloys (SMA) [68–70], 3D printing of shape memory polymers (SMPs), actuators for soft robotics [71], self-evolving structures [72], anti-counterfeiting system [73], active origami and controlled sequential folding [61, 74, 75]. Nickel-titanium (NiTi) SMA is a unique class of materials that can exhibit both SME (thermal memory) and superelasticity (mechanical memory) [69, 70]. It has been extensively utilized in biomedical implants and root canal instrumentation in dentistry [76, 77]. NiTi exhibits excellent parameters such as shape recovery and stress associated with it, high superelastic strain [78]. However, it is a difficult material in terms of processing via traditional methods [68, 77]. NiTi parts have been documented to be produced by SLM (SLM NiTi) also by Meier et al. [68], which could reduce the number of manufacturing cycles and associated processes as machining and thermomechanical treatments [66, 68, 79].

### 15.2.3.2 Composites

Composite materials, i.e., approach to use more than one material in one product attained great attention from researchers due to the diversity added to a range of application. Production of tailor-made gradient multi-phase materials is one of the salient features of AM processes. As a result of composites, different properties could be achieved within one single integrated part [80]. Furthermore, in making a component with composite materials, the required properties of included materials can be combined while compensating for some of their restrictions [81]. Such materials were focused on to improve the clinical performance in terms of better mechanical properties including resistance to corrosion and wear, design flexibility. Usually, first-generation composites were made by a hybrid process in which the combination of different materials can be performed before or after AM as a previous or subsequent stage of production of a component. But the problem encountered was an abrupt change in the properties, where two different materials contacted, which increased

the susceptibility of component failure by the layer dislodgement. This paved the way for the development of functionally graded materials.

### 15.2.3.3 Functionally Graded Materials (FGMs)

These are the second generation of composite materials, categorized based on their graded structure. An FGM typically consists of a composite material with variant properties across the structure to optimize the material performance based on the differential distributed specific property. The differential grade may exist for any aspects, viz. physical or chemical composition and associated parameters from layer to layer. The change over in the material properties across the junction of the materials used is turned subtle and gentle, so as to avoid the delamination across the layers of product. Thus, these materials exhibit superior mechanical properties when compared to basic (monolithic) and composite materials. Such materials were so much needed in order to replace the oral tissues as in nature most of living tissues such as bones, teeth, human skin are functionally graded to perform the specialized functions in the human body [80].

Earliest materials included at least one metal phase in an FGM, but lately, ceramic-ceramic and glass-ceramic systems are being worked at [82]. Ceramic materials are inherently designed to withstand high temperatures, corrosive liquids and gases, abrasion, and mechanical and thermal-induced stresses, so serve as value additions to the FGM for biologic applicability. Functionally graded ceramic compositions can be classified into:

1. Ceramic/metal—(Ti-TiB<sub>2</sub>) (Ni/Al<sub>2</sub>O<sub>3</sub>) FGC—used as an armor material [83, 84].
2. Ceramic/ceramic and glass/ceramic—Alumina/zirconia—biomedical applications,
  - Mullite/alumina—as a protective coating in chemically susceptible environments [85, 86].
  - Zirconia-mullite/alumina FGCs—refractory materials in high temperature.
3. Ceramic/polymer  
Boron carbide/polymer—ceramic filters supports, artificial bones.

A nine-layer laminated and functionally graded HA/yttria-stabilized zirconia (Y-TZP) for orthopedic applications was developed. In addition, Zhou C presented a novel FGC with both micro-grain and nano-grain HA crystals meeting the mechanical and biological requisites of bone implants [87–89]. Other functionally graded ceramics that are used in biomedical applications are ZrO<sub>2</sub>/AIS1316L as artificial joints and hip prostheses, and ZrO<sub>2</sub>/Al<sub>2</sub>O<sub>3</sub> FGCs as teeth implants [90].

#### 15.2.3.4 Biomaterials

Bioprinting technique is usually referred to as a hybrid process that allows printing of tailored structures including multiple cells and biomaterials in a single part [91, 92]. IJP, extrusion-based printing and laser-aided printing are the most common methods used for bioprinting applications. Bioprinting allows for the production of a wide variety of practical biomedical tissues with different shapes and material compositions [57, 81, 93–95]. Bioprinting can be defined as ‘the use of material transfer processes for patterning and assembling biologically relevant materials—molecules, cells, tissues, and biodegradable biomaterials—with a prescribed organization to accomplish one or more biological functions [96].’ The main advantages of bioprinting include large scale production of tissue engineering scaffolds with a great accuracy and highly dense cellular structures [96, 97]. The development of biomaterials for tissue engineering has added a new dimension to the existing periodontal regenerative therapies aimed at reconstruction of bone around teeth. Ceramics and polymers are extensively worked on for enhancing the outcomes of regenerative therapies. Calcium phosphate (e.g., tricalcium phosphate and hydroxyapatite), calcium sulfate and bioactive glass, etc., both in natural and synthetic forms have been utilized as scaffold materials. The natural polymers include modified polysaccharide (e.g., chitosan) and polypeptides (collagen and gelatin), whereas poly (glycolic acid), poly (L-lactic acid)] are the main synthetic polymers. Generally, all these materials have osteogenic, osteoconductive, and osteoinductive properties to act as tissue scaffolds. Polymers have been more used as a barrier material in guided tissue regeneration (GTR). They intend to guide the healing tissue for more regeneration by excluding epithelial growth in the bone defects [98]. Synthetic polymers such as PLGA and PLA are the materials of choice as these offer the many essential requisites of biocompatibility, biodegradability, ample availability, and cost-effectiveness. A large number of determinants such as composition, structural organization, impending stresses, and residual monomer content affect the degradation rate of the biomaterials [99]. Bioprinting is a new emerging technology and PLA along with its combinations with other biomaterials (such as glass, ceramics, metals, fibers, and polymers offer great opportunities to fabricate living biological 3D structures such as tissues, organs, nutrients, and cells [97, 100].

### 15.3 Conclusion and Critical Issues Concerning the Use of Materials for Additive Manufacturing

As their exist discrete differences in the workflow and manufacturing process in different techniques of 3D printing, the characteristics of a specific material are to be optimized in terms of its suitability to be used with a particular technique and provide a workable product form for the intended use. Materials used in AM require careful pre- and post-processing. In addition to the inherent chemical constitution, many



physical and chemical properties are important considerations. Extrinsic properties that require special considerations are the process of manufacturing of feed, shape, and surface of the feed, colloidal properties and flow through the feeding system at the feeding conditions. The state of the art 3D printing, especially for the production of implantable biomedical devices, is very restricted by the limited choice of printable materials. Therefore, novel alternative machining and processing methods are necessarily need to researched and brought in place for materials difficult to be workable with contemporary techniques. 3D printing is particularly advantageous for the production of customized complex devices that are generally not so cost-effective, when conventional manufacturing methods such as injection molding are utilized.

With the ongoing advancements, industrial 3D printers can now reach extremely small build layers such as 16  $\mu\text{m}$  layer thickness for SLA (Polyjet, Stratasys), 178  $\mu\text{m}$  layer thickness for FDM (Fortus 900mc, Stratasys), 80  $\mu\text{m}$  layer thickness for SLS (sPro 230HS, 3D systems) and 75  $\mu\text{m}$  resolution for SLA (3D systems). These systems, are yet not, really optimized for biomaterials of interest for in vitro and in vivo applications. Though some new macromers with biodegradable moieties have been developed, but FDA approval and other regulatory demands are pending, before the clinical applications. FDM, SLS, and 3DP are able to use polymers such as PLGA, PLLA, and PCL without chemical modification which will help expedite future FDA approval for biomedical devices. Although macro and microarchitecture have showed immense growth in past some time, but additional efforts are needed to develop nanoarchitecture biomolecules. Improvised strategies to incorporate biochemical molecules directly into scaffolds for prolonged release will be needed. A better understanding of the degradation kinetics and byproducts of the materials is required to tackle the issues related to mass transport limitations within thick scaffolds. Novel methods to control the release of acidic degradation products and their associated adverse effects during 3D printing process to seeded cells and/or the surrounding wound healing area for better clinical outcomes should be developed [1, 56, 66, 96].

## References

1. Tofail SAM, Koumoulos EP, Bandyopadhyay A, Bose S, O'Donoghue L, Charitidis C (2018) Additive manufacturing: scientific and technological challenges, market uptake and opportunities. *Mater Today* 21(1):22–37
2. Emilia M, Marek M, Łukasz Z, Sonia S, Patryk K, Dariusz M (2014) 3D printing technologies in rehabilitation engineering (Technologiedruku 3D w in'zynieriiirehabilitacyjnej). *J Health Sci* 4(12):78–83
3. Dawood A, Marti B, Sauret-Jackson V, Darwood A (2015) 3D printing in dentistry. *Br Dent J* 219:521–529
4. Bhushan J, Grover V (2019) Additive manufacturing: current concepts, methods, and applications in oral health care. In: Prakash C, Singh S, Singh R, Ramakrishna S, Pabla BS, Puri S, Uddin MS (eds) *Biomanufacturing*. Springer, Cham, pp 103–123
5. Quan Z et al (2016) *Addit Manuf Mech Eng Annu Rep Mater Today* 18:503–512

6. Additive Manufacturing: Strategic Research Agenda. <http://www.rmplatform.com/linkdoc/AM%20SRA%20-%20February%202014.pdf>
7. Additive Manufacturing Tackling Standards & Certification. <http://knowledge.ulprospector.com/3740/pe-additive-manufacturing-tackling-standardscertification/>
8. See CV, Meindorfer M (2016) 3D printing: additive processes in dentistry
9. Turner BN, Strong R, Gold SA (2014) Rapid Prototyp J 20(3):192–204
10. Turner BN, Gold SA (2015) Rapid Prototyp J 21(3):250–261
11. Wendel B et al (2008) Macromol Mater Eng 293:799–809
12. Metal additive manufacturing/3D printing: an introduction. <http://www.metalam.com/introduction-to-metal-additive-manufacturing-and-3d-printing/>
13. Gu DD, Meiners W, Wissenbach K, Poprawe R (2012) Laser additive manufacturing of metallic components: materials, processes and mechanisms. Int Mater Rev 57(3):133–164
14. Vayre B, Vignat F, Villeneuve F (2012) Metallic additive manufacturing: state-of-the-art review and prospects. Mech Ind 139(2):89–96
15. King WE, Anderson AT, Ferencz RM, Hodge NE, Kamath C, Khairallah SA, Rubenchik AM (2015) Laser powder bed fusion additive manufacturing of metals; physics, computational, and materials challenges. Appl Phys Rev 2(4):041304
16. Zocca A, Colombo P, Gomes CM et al (2015) Additive manufacturing of ceramics: issues, potentialities, and opportunities. J Am Ceram Soc 98(7):1983–2001
17. Travitzky N, Bonet A (2014) Additive manufacturing of ceramic-based materials. Adv Eng Mater 16:729–754
18. Mühler T, Gomes CM, Heinrich J, Günster J (2015) Slurry-based additive manufacturing of ceramics. Int J Appl Ceram Technol 12:18–25
19. Doreau F, Chaput C, Chartier T (2000) Stereolithography for manufacturing ceramic parts. Adv Eng Mater 2:493–496
20. Callister WD, Rethwisch D (2014) Materials science and engineering: an introduction, 9th edn. Wiley, Hoboken, NJ
21. Ebert J, Ozkol E, Zeichner A et al (2009) Direct inkjet printing of dental prostheses made of zirconia. J Dent Res 88:673–676
22. Scheithauer U, Schwarzer E, Richter H-J et al (2015) Thermoplastic 3D printing—an additive manufacturing method for producing dense ceramics. Int J Appl Ceram Technol 12:26–31
23. Tian X, Gunster J, Melcher J et al (2009) Process parameters analysis of direct laser sintering and post-treatment of porcelain components using Taguchi's method. J Eur Ceram Soc 29:1903–1915
24. Maleksaeedi S, Eng H, Wiria FE et al (2014) Property enhancement of 3D-printed alumina ceramics using vacuum infiltration. J Mater Process Technol 214:1301–1306
25. Barazanchi A, Li KC, Al-Amleh B, Lyons K, Waddell JN (2017) Additive technology: update on current materials and applications in dentistry. J Prosthodont 26:156–163
26. Frazier WE (2014) Metal additive manufacturing: a review. J Mater Eng Perform 23:1917–1928
27. Jardini AL, Larosa MA, de Carvalho Zavaglia CA et al (2014) Customised titanium implant fabricated in additive manufacturing for craniomaxillofacial surgery. Virtual Phys Prototyp 9:115–125
28. Jardini AL, Larosa MA, Maciel Filho R et al (2014) Cranial reconstruction: 3D bio model and custom-built implant created using additive manufacturing. J Cranio Maxillofac Surg 42:1877–1884
29. Figliuzzi M, Mangano F, Mangano C (2012) A novel root analogue dental implant using CT scan and CAD/CAM: selective laser melting technology. Int J Oral Maxillofac Surg 41:858–862
30. Mangano FG, De Franco M, Caprioglio A et al (2014) Immediate, non-submerged, root-analogue direct laser metal sintering (DLMS) implants: a 1-year prospective study on 15 patients. Laser Med Sci 29:1321–1328
31. Abduo J, Lyons K, Bennamoun M (2014) Trends in computer-aided manufacturing in prosthodontics: a review of the available streams. Int J Dent 2014:783948

32. Berman B (2012) 3-D printing: the new industrial revolution. *Bus Horiz* 55:155–162
33. Karande TS, Ong JL, Agrawal CM (2004) Diffusion in musculoskeletal tissue engineering scaffolds: design issues related to porosity, permeability, architecture, and nutrient mixing. *Ann Biomed Eng* 32:1728–1743
34. Hollister SJ (2005) Porous scaffold design for tissue engineering. *Nat Mater* 4:518–524
35. Stevens MM, George JH (2005) Exploring and engineering the cell surface interface. *Science* 310:1135–1138
36. Hollister S, Maddox R, Taboas J (2002) Optimal design and fabrication of scaffolds to mimic tissue properties and satisfy biological constraints. *Biomaterials* 23:4095–4103
37. Arburg. 3D printing with freeform from ARBURG. <http://www.arburg-injection-moulding-machine.com/3d-printing.html>
38. Park SH, Park DS, Shin JW, Kang YG, Kim HK, Yoon TR et al (2012) Scaffolds for bone tissue engineering fabricated from two different materials by the rapid prototyping technique: PCL versus PLGA. *J Mater Sci Mater Med* 23:2671–2678
39. Kim J, McBride S, Tellis B, Alvarez-Urena P, Song Y-H, Dean DD et al (2012) Rapid-prototyped PLGA/ $\beta$ -TCP/hydroxyapatite nanocomposite scaffolds in a rabbit femoral defect model. *Biofabrication* 4:025003
40. Woodfield TB, Malda J, De Wijn J, Peters F, Riesle J, van Blitterswijk CA (2004) Design of porous scaffolds for cartilage tissue engineering using a three-dimensional fiber-deposition technique. *Biomaterials* 25:4149–4161
41. Kalita SJ, Bose S, Hosick HL, Bandyopadhyay A (2003) Development of controlled porosity polymer-ceramic composite scaffolds via fused deposition modeling. *Mater Sci Eng* 23:611–620
42. Rai B, Teoh SH, Ho KH, Huttmacher DW, Cao T, Chen F et al (2004) The effect of rhBMP-2 on canine osteoblasts seeded onto 3D bioactive polycaprolactone scaffolds. *Biomaterials* 25:5499–5506
43. Lee K-W, Wang S, Fox BC, Ritman EL, Yaszemski MJ, Lu L (2007) Poly (propylene fumarate) bone tissue engineering scaffold fabrication using stereolithography: effects of resin formulations and laser parameters. *Biomacromol* 8:1077–1084
44. Fisher JP, Dean D, Mikos A (2002) Photocrosslinking characteristics and mechanical properties of diethyl fumarate/poly (propylene fumarate) biomaterials. *Biomaterials* 23:4333–4343
45. Lohfeld S, Tyndyk M, Cahill S, Flaherty N, Barron V, McHugh P (2010) A method to fabricate small features on scaffolds for tissue engineering via selective laser sintering. *J Biomed Sci Eng* 3:138–147
46. Wiria FE, Leong KF, Chua CK, Liu Y (2007) Poly- $\epsilon$ -caprolactone/hydroxyapatite for tissue engineering scaffold fabrication via selective laser sintering. *Acta Biomater* 3:1–12
47. Tan K, Chua C, Leong K, Cheah C, Cheang P, Abu Bakar M et al (2003) Scaffold development using selective laser sintering of polyetheretherketone–hydroxyapatite biocomposite blends. *Biomaterials* 24:3115–3123
48. Singh S, Prakash C, Ramakrishna S (2019, 26 February) 3D printing of polyether-ether-ketone for biomedical applications. *Euro Polym J*. <https://doi.org/10.1016/j.eurpolymj.2019.02.035>
49. Chua C, Leong K, Tan K, Wiria F, Cheah C (2004) Development of tissue scaffolds using selective laser sintering of polyvinyl alcohol/hydroxyapatite biocomposite for craniofacial and joint defects. *J Mater Sci Mater Med* 15:1113–1121
50. Williams JM, Adewunmi A, Schek RM, Flanagan CL, Krebsbach PH, Feinberg SE et al (2005) Bone tissue engineering using polycaprolactone scaffolds fabricated via selective laser sintering. *Biomaterials* 26:4817–4827
51. Nickels L (2012) World's first patient-specific jaw implant. *Met Powder Rep* 67:12–14
52. Landers R, Hübner U, Schmelzeisen R, Mülhaupt R (2002) Rapid prototyping of scaffolds derived from thermoreversible hydrogels and tailored for applications in tissue engineering. *Biomaterials* 23:4437–4447
53. Maher P, Keatch R, Donnelly K, Paxton J (2009) Formed 3D bio-scaffolds via rapid prototyping technology. In: 4th European conference of the international federation for medical and biological engineering. Springer, pp 2200–2204

54. Pataky K, Braschler T, Negro A, Renaud P, Lutolf MP, Brugger J (2012) Microdrop printing of hydrogel bio inks into 3D tissue-like geometries. *Adv Mater* 24:391–396
55. Haberstroh K, Ritter K, Kuschnierz J, Bormann KH, Kaps C, Carvalho C et al (2010) Bone repair by cell-seeded 3D-plotted composite scaffolds made of collagen treated tricalcium phosphate or tricalcium phosphate-chitosan-collagen hydrogel or PLGA in ovine critical-sized calvarial defects. *J Biomed Mater Res B Appl Biomater* 93:520–530
56. Chia HN, Wu BM (2015) Recent advances in 3D printing of biomaterials. *J Biol Eng* 9:4
57. Lee JY, An J, Chua CK (2017) Fundamentals and applications of 3D printing for novel materials. *Appl Mater Today* 7:120–133
58. Khoo ZX, Teoh JEM, Liu Y, Chua CK, Yang S, An J, Leong KF, Yeong WY (2015) 3D printing of smart materials: a review on recent progresses in 4D printing. *Virtual Phys Prototyp* 10:103–122
59. Leist SK, Zhou J (2016) Current status of 4D printing technology and the potential of light-reactive smart materials as 4D printable materials. *Virtual Phys Prototyp* 11:249–262
60. An J, Chua CK, Mironov V (2016) A perspective on 4D bioprinting. *Int J Bioprint* 2:3–5
61. Ge Q, Qi HJ, Dunn ML (2013) Active materials by four-dimension printing. *Appl Phys Lett* 103:131901
62. Pei E (2014) 4D printing – revolution or fad? *Assem Autom* 34:123–127
63. Tibbits S (2014) 4D printing: multi-material shape change. *Archit Des* 84:116–121
64. Bogue R (2014) Smart materials: a review of capabilities and applications. *Assem Autom* 34:3–7
65. Pei E (2014) 4D printing: dawn of an emerging technology cycle. *Assem Autom* 34:310–314
66. Varadan VK, Vinoy KJ, Gopalakrishnan S (2006) Smart material systems and MEMS: design and development methodologies. Wiley, Chichester
67. Kim K et al (2014) 3D optical printing of piezoelectric nanoparticle-polymer composite materials. *ACS Nano* 8:9799–9806
68. Meier H et al (2009) Selective laser melting of NiTi shape memory components. Presented at the Advanced Research in Virtual and Rapid Prototyping, Leiria, Portugal
69. Meier H, Haberland C, Frenzel J (2012) Structural and functional properties of NiTi shape memory alloys produced by Selective Laser Melting. *Innovative Developments in Virtual and Physical Prototyping*, London, pp 291–296
70. Dadbakhsh S et al (2014) Effect of SLM parameters on transformation temperatures of shape memory nickel-titanium parts. *Adv Eng Mater* 16:1140–1146
71. Rossiter J, Walters P, Stoimenov B (2009) Printing 3D dielectric elastomers actuators for soft robotics. *Proc SPIE* 7287
72. Raviv D et al (2014) Active printed materials for complex self evolving deformations. *Sci Rep* 4:Article Id-7422
73. Ivanova O et al (2014) Unclonable security features for additive manufacturing. *Addit Manuf* 1–4:24–31
74. Ge Q et al (2014) Active origami by 4D printing. *Smart Mater Struct* 23:1–15
75. Yu K et al (2015) Controlled sequential shape changing components by 3D printing of shape memory polymer multi-materials. *Procedia IUTAM* 12:193–203
76. Bormann T et al (2012) Tailoring selective laser melting process parameters for NiTi implants. *J Mater Eng Perform* 21:2519–2524
77. Elahinia MH et al (2012) Manufacturing and processing of NiTi implants: a review. *Prog Mater Sci* 57:911–946
78. Van Humbeeck J (2009) Shape memory alloys in smart materials. CRC Press, Taylor & Francis Group, Boca Raton, FL
79. Zhang B, Chen J, Coddet C (2013) Microstructure and transformation behavior of in-situ shape memory alloys by Selective Laser Melting Ti-Ni mixed powder. *J Mater Sci Technol* 29:863–867
80. Zhang N, Khan T, Guo H, Shi S, Zhong W, Zhang W (2019) Functionally graded materials: an overview of stability, buckling, and free vibration analysis. *Adv Mater Sci Eng Article ID* 1354150:18 p

81. Toursangsaraki M (2018) A review of multi-material and composite parts production by modified additive manufacturing methods. *J Mater Res*
82. Besisa DHA, Ewais EMM (2016) Advances in functionally graded ceramics—processing. Sintering properties and applications. Intech open
83. Pettersson A, Magnusson P, Lundberg P, Nygren M (2005) Titanium-titanium di-boride composites as Part of a gradient armour material. *Int J Impact Eng* 32:387–399
84. Panda KB, Chandran KSR (2007) Titanium-titanium boride (Ti-TiB) functionally graded materials through reaction sintering: synthesis, microstructure, and properties. *Metall Mater Trans A* 34(9):1993–2003
85. Kaya C (2003) Al<sub>2</sub>O<sub>3</sub>-Y-TZP/Al<sub>2</sub>O<sub>3</sub> functionally graded composites of tubular shape from nano-sols using double-step electrophoretic deposition. *J Eur Ceram Soc* 23:1655–1660
86. Sotirchos SV (1999) Functionally graded alumina/mullite coatings for protection of silicon carbide ceramic components from corrosion. Semi-annual report provided by University of Rochester, Department of Chemical Engineering, Rochester, New York. Special contribution to the book “Functionally graded materials; design, processing and applications”
87. Maruno S, Imamura K, Hanaichi T, Ban S, Iwata H, Itoh H (1994) Characterization and stability of bioactive HA-G-Ti composite materials and bonding to bone. *Bio-ceramics* 7:249–254
88. Maruno S, Itoh H, Ban S, Iwata H, Ishikawa T (1991) Micro-observation and characterization of bonding between bone and Ha-glass-titanium functionally gradient composite. *Biomaterials* 12:225–230
89. Zhou C, Deng C, Chena X, Zhao X, Chena Y, Fana Y, Zhang X (2015) Mechanical and biological properties of the micro-/nano-grain functionally graded hydroxyapatite bioceramics for bone tissue engineering. *J Mech Behav Biomed Mater* 4(8):1–11
90. Leong KF, Chuna CK, Sudaramadji N, Yeong W (2008) Engineering functionally graded tissue engineering scaffolds. *J Mech Behav Biomed Mater* 1:140–152
91. Seol YJ et al (2014) Bioprinting technology and its applications. *Eur J Cardiothorac Surg* 46(3):342–348
92. Visser J et al (2013) Biofabrication of multi-material anatomically shaped tissue constructs. *Biofabrication* 5(3):035007
93. Murphy SV, Atala A (2014) 3D bioprinting of tissues and organs. *Nat Biotechnol* 32(8):773–785
94. Lee VK et al (2014) Creating perfused functional vascular channels using 3D bioprinting technology. *Biomaterials* 35(28):8092–8102
95. Kumar A et al (2016) Low temperature additive manufacturing of three dimensional scaffolds for bone-tissue engineering applications: processing related challenges and property assessment. *Mater Sci Eng R* 103:1–39
96. Chua CK, Yeong WY (2015) Bioprinting: principles and applications. World Scientific Publishing Co., Pte. Ltd., Singapore
97. An J et al (2015) Design and 3D printing of scaffolds and tissues. *Engineering* 1:261–268
98. Shue L, Yufeng Z, Mony U (2012) Biomaterials for periodontal regeneration. A review of ceramics and polymers. *Biomatter* 2(4):271–277
99. Singh M, Mann GS, Gupta MK, Singh R, Ramakrishna S (2019) Poly-lactic-acid: potential material for bio-printing applications. In: Prakash C, Singh S, Singh R, Ramakrishna S, Pabla BS, Puri S, Uddin MS (eds) *Biomanufacturing*. Springer, Cham, pp 69–87
100. Seliktar D, Dikovskiy D, Napadensky (2013) Bioprinting and tissue engineering: recent advances and future perspectives. *Isr J Chem* 53:795–804

**Dr. Anoop Kapoor** is Professor and Head, Sri Sukhmani Dental College and Hospital, Dera Bassi, Punjab, India. He is working on the area of application of 3D Printing in dentistry.

**Dr. Priyanka Chopra** is Professor, Sri SGT Dental College and Hospital, SGT University Gurugram. She is working on the area of application of 3D Printing in dentistry.

**Dr. Komal Sehgal** is working as Associate professor in the Department of Prosthodontics, Dr. H.S.J. Institute of Dental Sciences, Panjab University Chandigarh. She is working on the area of application of 3D Printing in dentistry.

**Dr. Shaveta Sood** is working as Assistant Professor in the Department of Periodontology and Oral Implantology, Dr. H.S.J. Institute of Dental Sciences, Panjab University Chandigarh. She is working on the area of application of 3D Printing in dentistry.

**Dr. Ashish Jain** is Professor and Head, Department of Periodontology and Oral Implantology, Dr. H.S.J. Institute of Dental Sciences, Panjab University Chandigarh. He is working on the area of application of 3D Printing in dentistry.

**Dr. Vishakha Grover** is working as Associate Professor, Department of Periodontology and Oral Implantology, Dr. H.S.J. Institute of Dental Sciences, Panjab University Chandigarh. She is working on the area of application of 3D Printing in dentistry.